

SEQUENCED PHENYLENE-VINYLENE OLIGOMERS AND COPOLYMERS

by

Benjamin Nathaniel Norris

Bachelor of Science in Chemistry, Frostburg State University, 2004

Submitted to the Graduate Faculty of
Arts and Sciences in partial fulfillment
of the requirements for the degree of
Doctor of Philosophy in Chemistry

University of Pittsburgh

2011

UNIVERSITY OF PITTSBURGH

ARTS AND SCIENCES

This dissertation was presented

by

Benjamin Nathaniel Norris

It was defended on

January 18, 2011

and approved by

Tara Y. Meyer, Associate Professor, Chemistry

Toby M. Chapman, Associate Professor, Chemistry

Geoff R. Hutchison, Assistant Professor, Chemistry

Tracy Cui, Associate Professor, Bioengineering

Dissertation Advisor: Tara Y. Meyer, Associate Professor, Chemistry

SEQUENCED PHENYLENE-VINYLENE OLIGOMERS AND COPOLYMERS

Benjamin Nathaniel Norris, PhD

University of Pittsburgh, 2011

Copyright © by Benjamin Nathaniel Norris

2011

SEQUENCED PHENYLENE-VINYLENE OLIGOMERS AND COPOLYMERS

Benjamin Nathaniel Norris, PhD

University of Pittsburgh, 2011

ABSTRACT

The role of sequence in determining the properties of oligomers and polymers is poorly understood despite Nature's formidable examples of libraries of macromolecules whose function is determined by monomer order. A series of oligomers and copolymers bearing poly(*para*-phenylene-vinylene) sequences was prepared and the dependence of both optoelectronic and thermal properties on monomer order was determined. The optoelectronic properties of three series (dimers, trimers, and tetramers) of *oligo*(phenylene-vinylenes) OPVs were found to depend on the sequence of donor and acceptor units. These oligomers were prepared using a simple and robust homologation based on Horner-Wadsworth-Emmons (HWE) reactions. Increased donor content was important, and the best sequences (highest absorption and emission maxima, earliest first oxidation potentials, and smallest HOMO-LUMO gaps) contained two adjacent donors without having two adjacent acceptors. Sequences with low donor content or donors with acceptors spaced between them exhibited less desirable properties. The thermal

properties of these OPVs are also sequence dependent. The observed trends suggest design principles that could be utilized to prepare specific longer oligomers with attractive properties.

Sequenced OPVs were also prepared by a novel iterative olefin cross-metathesis (CM) strategy. The synthesis relies on assembly of orthogonal monomers in a selective CM reaction. The key coupling step proceeded in fair to good yields, and OPVs with 2-5 phenyl units with alternating substitution patterns were prepared. The orthogonal end groups were exploited to prepare donor-acceptor complexes and repeating sequence copolymers. Olefin metathesis was also exploited to prepare fully-substituted symmetric OPVs.

Rod-coil copolymers containing well-defined phenylene-vinylene chromophores separated by flexible linkers of precise length have been prepared by acyclic diene metathesis (ADMET) or by HWE polycondensation. The ADMET polymerizations proceeded in good to quantitative yields with moderate molecular weights. The HWE polycondensation route allowed us to prepare rod-coil polymers with varying oxygen content and placement in the linkers in good to excellent yields with high molecular weights. The physical properties of these copolymers varied significantly with composition.

TABLE OF CONTENTS

ABSTRACT.....	IV
TABLE OF CONTENTS	VI
LIST OF TABLES	XI
LIST OF SCHEMES	XIII
LIST OF FIGURES	XV
SYMBOLS AND ABBREVIATIONS.....	XXVI
PREFACE.....	XXXIII
1.0 INTRODUCTION.....	1
1.1 SEQUENCE IN POLYMER CHEMISTRY.....	1
1.2 CONJUGATED POLYMERS AS PHOTOVOLTAIC MATERIALS	6
1.3 SEQUENCED CONJUGATED POLYMERS AS THE NEXT PARADIGM IN PHOTOVOLTAIC MATERIALS	12
1.4 OLIGO(PHENYLENE-VINYLENE)S AS PROBES OF THE EFFECTS OF SEQUENCE ON OPTOELECTRONIC PROPERTIES	17
2.0 SYNTHESIS OF SEQUENCED OLIGO(PHENYLENE-VINYLENE)S USING HORNER-WADSWORTH-EMMONS HOMOLOGATION – THE EFFECTS OF SEQUENCE ON OPTOELECTRONIC AND THERMAL PROPERTIES	21
2.1 OVERVIEW.....	21

2.2	SYNTHETIC APPROACH	23
2.3	RESULTS	25
2.3.1	Monomer synthesis	25
2.3.2	HWE optimization.....	29
2.3.3	Oligomer synthesis by the nitrile approach	31
2.3.4	Optical spectroscopy.....	33
2.3.5	Electrochemistry	37
2.3.6	DFT calculations	40
2.3.7	Thermal properties.....	41
2.4	DISCUSSION.....	43
2.4.1	Optoelectronic properties	43
2.4.1.1	Sequence dependence of optoelectronic properties.....	44
2.4.1.2	Sequence dependence of HOMO-LUMO gap	48
2.4.1.3	Design principles and predictions.....	51
2.4.1.4	Comparison of experimental and theoretical data.....	52
2.4.1.5	Absorption Profile.....	54
2.4.2	Thermal properties.....	56
2.4.3	HWE optimization.....	58
2.5	CONCLUSIONS	60
2.6	EXPERIMENTAL SECTION.....	60
2.6.1	General methods	60
2.6.2	Monomer synthesis	62
2.6.3	HWE optimization.....	75

2.6.4	Synthesis of oligomers	78
3.0	SYNTHESIS OF HETEROTELECHELIC AND SYMMETRIC OLIGO(PHENYLENE-VINYLENE)S USING OLEFIN METATHESIS	105
3.1	OVERVIEW.....	105
3.1.1	Homologation approach.....	106
3.1.2	Dimerization approach.....	108
3.2	RESULTS AND DISCUSSION	109
3.2.1	Monomer synthesis	109
3.2.2	Synthesis of heterotelechelic OPVs using cross-metathesis	111
3.2.3	Modification of heterotelechelic OPVs	113
3.2.4	Optical spectroscopy.....	116
3.2.5	Progress toward more complex sequences by CM	118
3.2.6	Synthesis of symmetric OPVs using homometathesis	122
3.3	CONCLUSIONS	124
3.4	EXPERIMENTAL SECTION.....	124
3.4.1	General methods	124
3.4.2	Monomer synthesis	125
3.4.3	Synthesis of OPVs by iterative cross metathesis.....	129
3.4.4	Synthesis of modified OPVs.....	138
3.4.5	Progress toward more complex sequences	144
3.4.6	Synthesis of OPVs by dimerization	146
4.0	SYNTHESIS AND CHARACTERIZATION OF MISCELLANEOUS ROD-COIL POLY(PHENYLENE-VINYLENE) REPEAT-SEQUENCE COPOLYMERS	150

4.1	INTRODUCTION	150
4.2	RESULTS AND DISCUSSION	153
4.2.1	Rod-coil copolymers prepared by ADMET	153
4.2.1.1	Segmer synthesis	154
4.2.1.2	ADMET polymerization and hydrogenation.....	156
4.2.1.3	Thermal and optical properties of p29 and p32	159
4.2.1.4	Conclusions	160
4.2.2	Rod-coil copolymers prepared by HWE polycondensation.....	161
4.2.2.1	Polymer synthesis.....	161
4.2.2.2	Thermal properties	163
4.2.2.3	Conclusions	164
4.3	EXPERIMENTAL SECTION.....	165
4.3.1	General methods	165
4.3.2	Rod-coil copolymers prepared by ADMET	166
4.3.3	Rod-coil copolymers prepared by HWE	183
APPENDIX A : CHAPTER 2		188
A.1	¹H AND ¹³C NMR SPECTRA OF NEW COMPOUNDS	188
A.2	ABSORPTION AND EMISSION SPECTRA.....	231
A.3	CYCLIC AND DIFFERENTIAL PULSE VOLTAMMOGRAMS	239
A.4	DIFFERENTIAL SCANNING CALORIMOGRAMS	255
A.5	TRENDS IN OPTOELECTRONIC PROPERTIES.....	271
APPENDIX B : CHAPTER 3		278
B.1	¹H AND ¹³C NMR SPECTRA OF NEW COMPOUNDS	278

B.2	ABSORPTION AND EMISSION SPECTRA.....	299
APPENDIX C : CHAPTER 4	303
C.1	¹H AND ¹³C NMR SPECTRA OF NEW COMPOUNDS	303
C.2	ABSORPTION AND EMISSION SPECTRA OF 29, 32, P29 AND P32 ...	324
C.3	DIFFERENTIAL CALORIMOGRAMS OF THE PV-O_xT_y SERIES.....	325
REFERENCES.....	326

LIST OF TABLES

Table 1. Optoelectronic and photovoltaic parameters of polymers from refs. 52 and 49.....	15
Table 2. Optoelectronic and photovoltaic parameters of polymers from ref. 71.....	17
Table 3. HWE optimization	30
Table 4. Oligomers prepared by HWE oligomerization	33
Table 5. Optical properties of the OPVs.....	34
Table 6. Electrochemical Properties of OPVs from DPV.....	39
Table 7. Frontier orbital energy levels predicted using DFT (B3LYP/6-31G*).....	41
Table 8. Thermal properties of OPVs.....	42
Table 9. Optoelectronic properties of the OPVs ordered by increasing absorption maximum and sorted by oligomer length	46
Table 10. ΔE_g data ordered by decreasing optical ΔE_g and sorted by oligomer length	50
Table 11. Thermal properties of the OPVs ordered by increasing melting point and sorted by oligomer length.	57
Table 12. Head-to-Tail polymerization of OPV2e	116
Table 13. Optoelectronic properties of the OPVs ^a	117
Table 14. Optical properties of 29, p29, 32, and p32. ^a	160
Table 15. Yields and properties of rod-coil copolymers.....	163
Table 16. Sequences with A on the outside.	271

Table 17. Sequences with D on the outside.	271
Table 18. Alternating sequences with A on the bromo end.	271
Table 19. Alternating sequences with D on the bromo end.	272
Table 20. Alternating sequences with A on the nitrile end.	272
Table 21. Alternating sequences with D on the nitrile end.	272
Table 22. Blocky sequences with A on the bromo end and D on the nitrile end.	272
Table 23. Blocky sequences with D on the bromo end and A on the nitrile end.	273
Table 24. Sequences with two adjacent A units.	273
Table 25. Sequences with two adjacent D units.	273
Table 26. Sequences in the synthesis of Br-AADD-CN.	273
Table 27. Sequences in the synthesis of Br-ADAD-CN.	274
Table 28. Sequences in the synthesis of Br-ADDA-CN.	274
Table 29. Sequences in the synthesis of Br-DDAA-CN.	274
Table 30. Sequences in the synthesis of Br-DADA-CN.	274
Table 31. Sequences in the synthesis of Br-DAAD-CN.	275

LIST OF SCHEMES

Scheme 1. Sequenced radical polymerizations.....	3
Scheme 2. Examples of RSCs prepared by the Meyer group.....	6
Scheme 3. Syntheses of sequenced oligo(phenylene-vinylenes) by a) Maddux, <i>et al</i> , ⁷⁶ b) Jørgensen and Krebs, ⁷² c) Jian and Tour, ⁷⁷ and Iwadate, and Suginome. ⁷⁸	18
Scheme 4. Synthetic approach to OPVs.....	24
Scheme 5. Synthesis of Br-D-CHO.....	26
Scheme 6. Synthesis of P-A-acetal.....	27
Scheme 7. Synthesis of P-D-acetal.....	28
Scheme 8. Synthesis of nitrile monomers P-A-CN and P-D-CN.....	29
Scheme 9. Representative synthesis of OPVs - synthesis of Br-AD-CN, Br-ADD-CN, and Br-ADDA-CN.....	32
Scheme 10. Pathways leading to <i>Z</i> and <i>E</i> stilbenes in a HWE reaction.....	59
Scheme 11. Proposed role of Li ⁺ in the stereoselectivity of the HWE reaction.....	59
Scheme 12. Homologation approach to OPVs by CM.....	106
Scheme 13. Olefin metathesis outcomes of Type I and Type II vinylbenzaldehydes.....	107
Scheme 14. Synthetic approaching to alternating OPVs by metathesis homologation.....	108
Scheme 15. Dimerization approach to OPVs using metathesis.....	109
Scheme 16. Synthesis of monomers 12 and 13.....	110

Scheme 17. Synthesis of OPVs by CM homologation.	112
Scheme 18. Synthesis of donor-acceptor chromophores by orthogonal functionalization of OPV2a.....	113
Scheme 19. Synthesis of head-to-tail copolymer.....	115
Scheme 20. Synthesis of ADMET monomers from styrene 13 and OPV1b.....	116
Scheme 21. Possible products in a CM reaction between two Type II olefins.....	119
Scheme 22. Optimized Type II + Type II CM reaction.....	119
Scheme 23. Preparation of OPVs by metathesis dimerization	123
Scheme 24. Synthesis of rod-coil phenylene-vinylene copolymers from refs 100 and 101.....	151
Scheme 25 HWE preparation of rod-coil phenylene-vinylene copolymers.	153
Scheme 26. Synthesis of ADMET segmers.....	155
Scheme 27. Synthesis of bisphosphonate 22.	155
Scheme 28. Synthesis of aldehydes 23, 24, and 25.	156
Scheme 29. Synthesis of aldehydes 26, 27, and 28.	156
Scheme 30. Synthesis of ADMET polymers p29 and p32. M_n s and PDIs determined by SEC in THF relative to polystyrene standards.	157
Scheme 31. Synthesis of ADMET polymers p30, p31, and p34. M_n s and PDIs determined by SEC in THF relative to polystyrene standards.....	158
Scheme 32. Synthesis of dialdehyde linkers.....	162

LIST OF FIGURES

Figure 1. Examples of polymer microstructures – filled and open circles represent different monomers.....	2
Figure 2. Top: Structures of PCBM, PEDOT, and PSS. Bottom: Construction of a BHJ photovoltaic cell.....	7
Figure 3. Mechanism of current generation in a polymer/PCBM photovoltaic cell.....	8
Figure 4. Definitions of relevant energy differences relative to frontier orbitals of the polymer donor and PCBM.	10
Figure 5. Optimal frontier molecular orbital energy levels for an ideal polymer donor compared to PCBM.	11
Figure 6. a) Localized orbital model for frontier molecular orbitals of donor-acceptor polymers. b) Orbital mixing model for frontier molecular orbitals of donor-acceptor polymers.	13
Figure 7. a) Polymers from ref. 52. b) Polymers from ref. 49.....	15
Figure 8. Polymers from ref. 76.....	16
Figure 9. Examples of OPV oligomer nomenclature.....	19
Figure 10. Sequenced OPVs prepared.	22
Figure 11. Further examples of OPV nomenclature.	23

Figure 12. a) Benzaldehyde monomers common to both the acetal and nitrile approaches. b) Phosphonate monomers for the acetal approach. c) Phosphonate monomers for the nitrile approach.....	25
Figure 13. Overlaid absorption spectra of OPV dimers.....	35
Figure 14. Overlaid absorption spectra of OPV trimers.	36
Figure 15. Overlaid absorption spectra of OPV tetramers.....	37
Figure 16. Ranges of λ_{\max} data from optical spectroscopy.....	45
Figure 17. Ranges of the first oxidation potential of the OPVs.....	45
Figure 18. Correlation of optical and electrochemical HOMO-LUMO gaps of the oligomers....	49
Figure 19. Correlations between predicted and experimental properties. Top left: correlation between predicted HOMO energies and first oxidation potentials. Top right: correlation between predicted LUMO energies and first reduction potentials. Middle left: correlation between predicted ΔE_g and optical ΔE_g . Middle right: correlation between predicted ΔE_g and electrochemical ΔE_g . Bottom left: correlation between predicted HOMO energies and optical ΔE_g . Bottom right: Correlation between predicted HOMO energies and electrochemical ΔE_g . ..	53
Figure 20. Normalized absorption spectra of the OPV trimers.	55
Figure 21. Range of melting points as a function of oligomer composition and length.....	58
Figure 22. Common metathesis monomers	109
Figure 23. ^1H NMR spectra of the head-to-tail polymerization as a function of time. A) At 0 h (OPV2e); B) After 24 h; C) After 48 h; D) After 96 h. Labels ($\text{H}_{\text{A-H}}$) refer to labeled protons in Scheme 5. Head-head protons ($\delta \sim 7.2$) are not assignable due to overlap.	115
Figure 24. ^1H NMR spectra of CM between styrene 13 and vinylbenzaldehyde 12 after 30 min and 5 h. Labels refer to compound numbers.....	120

Figure 25. Relative concentrations of the components of the CM reaction (From ^1H NMR) between styrene 3 and vinylbenzaldehyde 1 as a function of time.....	121
Figure 26. Schematic representation of the ADMET preparation of rod-coil phenylene-vinylene copolymers.....	152
Figure 27. Differential scanning calorimograms of p29 and p32.	159
Figure 28. Correlation of thermal properties of the PV-O _x T _y series to composition: T_g (open circles) and T_m (closed circles).	164
Figure 29. ^1H and ^{13}C NMR spectra of compound 1.	189
Figure 30. ^1H and ^{13}C NMR spectra of compound 2.	190
Figure 31. ^1H and ^{13}C NMR spectra of Br-D-CHO.	191
Figure 32. ^1H and ^{13}C NMR spectra of compound 3.	192
Figure 33. ^1H and ^{13}C NMR spectra of compound 4.	193
Figure 34. ^1H and ^{13}C NMR spectra of compound 5.	194
Figure 35. ^1H and ^{13}C NMR spectra of P-A-acetal.	195
Figure 36. ^1H and ^{13}C NMR spectra of compound 6.	196
Figure 37. ^1H spectrum of compound 7.	197
Figure 38. ^1H and ^{13}C NMR spectra of compound 8.	198
Figure 39. ^1H and ^{13}C NMR spectra of P-D-acetal.	199
Figure 40. ^1H and ^{13}C NMR spectra of P-A-CN.....	200
Figure 41. ^1H and ^{13}C NMR spectra of compound 9.	201
Figure 42. ^1H and ^{13}C NMR spectra of compound 10.	202
Figure 43. ^1H and ^{13}C NMR spectra of compound 11.	203
Figure 44. ^1H and ^{13}C NMR spectra of P-D-CN.....	204

Figure 45. ^1H , ^{13}C , and DEPT 135 NMR spectra of Br-AA-CN.	205
Figure 46. ^1H , ^{13}C , and DEPT 135 NMR spectra of Br-AD-CN.	206
Figure 47. ^1H , ^{13}C , and DEPT 135 NMR spectra of Br-DA-CN.	207
Figure 48. ^1H , ^{13}C , and DEPT 135 NMR spectra of Br-DD-CN.	208
Figure 49. ^1H , ^{13}C , and DEPT 135 NMR spectra of Br-AA-CHO.	209
Figure 50. ^1H , ^{13}C , and DEPT 135 NMR spectra of Br-AD-CHO.	210
Figure 51. ^1H , ^{13}C , and DEPT 135 NMR spectra of Br-DA-CHO.	211
Figure 52. ^1H , ^{13}C , and DEPT 135 NMR spectra of Br-DD-CHO.	212
Figure 53. ^1H , ^{13}C , and DEPT 135 NMR spectra of Br-AAD-CN.	213
Figure 54. ^1H , ^{13}C , and DEPT 135 NMR spectra of Br-ADD-CN.	214
Figure 55. ^1H , ^{13}C , and DEPT 135 NMR spectra of Br-ADA-CN.	215
Figure 56. ^1H , ^{13}C , and DEPT 135 NMR spectra of Br-DAA-CN.	216
Figure 57. ^1H , ^{13}C , and DEPT 135 NMR spectra of Br-DAD-CN.	217
Figure 58. ^1H , ^{13}C , and DEPT 135 NMR spectra of Br-DDA-CN.	218
Figure 59. ^1H , ^{13}C , and DEPT 135 NMR spectra of Br-AAD-CHO.....	219
Figure 60. ^1H , ^{13}C , and DEPT 135 NMR spectra of Br-ADD-CHO.....	220
Figure 61. ^1H , ^{13}C , and DEPT 135 NMR spectra of Br-ADA-CHO.....	221
Figure 62. ^1H , ^{13}C , and DEPT 135 NMR spectra of Br-DAA-CHO.....	222
Figure 63. ^1H , ^{13}C , and DEPT 135 NMR spectra of Br-DAD-CHO.....	223
Figure 64. ^1H , ^{13}C , and DEPT 135 NMR spectra of Br-DDA-CHO.....	224
Figure 65. ^1H , ^{13}C , and DEPT 135 NMR spectra of Br-AADD-CN.....	225
Figure 66. ^1H , ^{13}C , and DEPT 135 NMR spectra of Br-ADDA-CN.....	226
Figure 67. ^1H , ^{13}C , and DEPT 135 NMR spectra of Br-ADAD-CN.....	227

Figure 68. ^1H , ^{13}C , and DEPT 135 NMR spectra of Br-DAAD-CN.....	228
Figure 69. ^1H , ^{13}C , and DEPT 135 NMR spectra of Br-DADA-CN.....	229
Figure 70. ^1H , ^{13}C , and DEPT 135 NMR spectra of Br-DDAA-CN.....	230
Figure 71. Absorption and emission spectra of Br-AA-CN.	231
Figure 72. Absorption and emission spectra of Br-DD-CN.	231
Figure 73. Absorption and emission spectra of Br-AD-CN.	232
Figure 74. Absorption and emission spectra of Br-DA-CN.	232
Figure 75. Absorption and emission spectra of Br-AAD-CN.....	233
Figure 76. Absorption and emission spectra of Br-DAA-CN.....	233
Figure 77. Absorption and emission spectra of Br-ADA-CN.....	234
Figure 78. Absorption and emission spectra of Br-DAD-CN.....	234
Figure 79. Absorption and emission spectra of Br-ADD-CN.....	235
Figure 80. Absorption and emission spectra of Br-DDA-CN.....	235
Figure 81. Absorption and emission spectra of Br-AADD-CN.....	236
Figure 82. Absorption and emission spectra of Br-AADD-CN.....	236
Figure 83. Absorption and emission spectra of Br-ADAD-CN.....	237
Figure 84. Absorption and emission spectra of Br-DADA-CN.....	237
Figure 85. Absorption and emission spectra of Br-ADDA-CN.....	238
Figure 86. Absorption and emission spectra of Br-DAAD-CN.....	238
Figure 87. Cyclic voltammograms of Br-AA-CN.	239
Figure 88. Differential pulse voltammograms of Br-AA-CN. Left: reduction. Right: oxidation.	239
Figure 89. Cyclic voltammograms of Br-AD-CN.	240

Figure 90. Differential pulse voltammograms of Br-AD-CN. Left: reduction. Right: oxidation.	240
Figure 91. Cyclic voltammograms of Br-DA-CN.	241
Figure 92. Differential pulse voltammograms of Br-DA-CN. Left: reduction. Right: oxidation.	241
Figure 93. Cyclic voltammograms of Br-DD-CN.	242
Figure 94. Differential pulse voltammograms of Br-DD-CN. Left: reduction. Right: oxidation.	242
Figure 95. Cyclic voltammograms of Br-AAD-CN.	243
Figure 96. Differential pulse voltammograms of Br-AAD-CN. Left: reduction. Right: oxidation.	243
Figure 97. Cyclic voltammograms of Br-ADA-CN.	244
Figure 98. Differential pulse voltammograms of Br-ADA-CN. Left: reduction. Right: oxidation.	244
Figure 99. Cyclic voltammograms of Br-AA-CN.	245
Figure 100. Differential pulse voltammograms of Br-ADD-CN. Left: reduction. Right: oxidation.	245
Figure 101. Cyclic voltammograms of Br-DAA-CN.	246
Figure 102. Differential pulse voltammograms of Br-DAA-CN. Left: reduction. Right: oxidation.	246
Figure 103. Cyclic voltammograms of Br-DAD-CN.	247
Figure 104. Differential pulse voltammograms of Br-DAD-CN. Left: reduction. Right: oxidation.	247

Figure 105. Cyclic voltammograms of Br-DDA-CN.	248
Figure 106. Differential pulse voltammograms of Br-DDA-CN. Left: reduction. Right: oxidation.	248
Figure 107. Cyclic voltammograms of Br-AADD-CN.....	249
Figure 108. Differential pulse voltammograms of Br-AADD-CN. Left: reduction. Right: oxidation.	249
Figure 109. Cyclic voltammograms of Br-ADAD-CN.....	250
Figure 110. Differential pulse voltammograms of Br-ADAD-CN. Left: reduction. Right: oxidation.	250
Figure 111. Cyclic voltammograms of Br-ADDA-CN.....	251
Figure 112. Differential pulse voltammograms of Br-ADAD-CN. Left: reduction. Right: oxidation.	251
Figure 113. Cyclic voltammograms of Br-DAAD-CN.....	252
Figure 114. Differential pulse voltammograms of Br-DAAD-CN. Left: reduction. Right: oxidation.	252
Figure 115. Cyclic voltammograms of Br-DADA-CN.....	253
Figure 116. Differential pulse voltammograms of Br-DAAD-CN. Left: reduction. Right: oxidation.	253
Figure 117. Cyclic voltammograms of Br-DDAA-CN.....	254
Figure 118. Differential pulse voltammograms of Br-DDAA-CN. Left: reduction. Right: oxidation.	254
Figure 119. Differential scanning calorimograms of Br-AA-CN.....	255
Figure 120. Differential scanning calorimograms of Br-AD-CN.....	256

Figure 121. Differential scanning calorimograms of Br-DA-CN.....	257
Figure 122. Differential scanning calorimograms of Br-DD-CN.....	258
Figure 123. Differential scanning calorimograms of Br-AAD-CN.....	259
Figure 124. Differential scanning calorimograms of Br-ADA-CN.....	260
Figure 125. Differential scanning calorimograms of Br-ADD-CN.....	261
Figure 126. Differential scanning calorimograms of Br-DAA-CN.....	262
Figure 127. Differential scanning calorimograms of Br-DAD-CN.....	263
Figure 128. Differential scanning calorimograms of Br-DDA-CN.....	264
Figure 129. Differential scanning calorimograms of Br-AADD-CN.....	265
Figure 130. Differential scanning calorimograms of Br-ADAD-CN.....	266
Figure 131. Differential scanning calorimograms of Br-ADDA-CN.....	267
Figure 132. Differential scanning calorimograms of Br-DAAD-CN.....	268
Figure 133. Differential scanning calorimograms of Br-DADA-CN.....	269
Figure 134. Differential scanning calorimograms of Br-DDAA-CN.....	270
Figure 135. Ordering of the OPVs according to increasing λ_{maxabs} , disregarding oligomer length.....	275
Figure 136. Ordering of the OPVs according to increasing solution λ_{maxem} , disregarding oligomer length.....	276
Figure 137. Ordering of the OPVs according to increasing Δ_{gopt} disregarding oligomer length.....	276
Figure 138. Ordering of the OPVs according to increasing Δ_{gec} disregarding oligomer length.....	277
Figure 139. Sequence dependent trends in optoelectronic properties.....	277

Figure 140. ^1H and ^{13}C NMR spectra of compound 15.	279
Figure 141. ^1H and ^{13}C NMR spectra of compound 16.	280
Figure 142. ^1H and ^{13}C NMR spectra of compound 13.	281
Figure 143. ^1H and ^{13}C NMR spectra of compound 12.	282
Figure 144. ^1H , ^{13}C , and DEPT 135 NMR spectra of OPV1a.....	283
Figure 145. ^1H , ^{13}C , and DEPT 135 NMR spectra of OPV1b.	284
Figure 146. ^1H , ^{13}C , and DEPT 135 NMR spectra of OPV2a.....	285
Figure 147. ^1H , ^{13}C , and DEPT 135 NMR spectra of OPV2b.	286
Figure 148. ^1H , ^{13}C , and DEPT 135 NMR spectra of OPV3a.....	287
Figure 149. ^1H , ^{13}C , and DEPT 135 NMR spectra of OPV3b.	288
Figure 150. ^1H , ^{13}C , and DEPT 135 NMR spectra of OPV4a.....	289
Figure 151. ^1H , ^{13}C , and DEPT 135 NMR spectra of OPV4b.	290
Figure 152. ^1H , ^{13}C , and DEPT 135 NMR spectra of OPV2c.....	291
Figure 153. ^1H , ^{13}C , and DEPT 135 NMR spectra of OPV2d.	292
Figure 154. ^1H , ^{13}C , and DEPT 135 NMR spectra of OPV2e.....	293
Figure 155. ^1H , and ^{13}C NMR spectra of p(OPV2e).....	294
Figure 156. ^1H , ^{13}C , and DEPT 135 NMR spectra of compound 17.	295
Figure 157. ^1H , ^{13}C , and DEPT 135 NMR spectra of OPV1c.....	296
Figure 158. ^1H and ^{13}C NMR spectra of compound 18.	297
Figure 159. ^1H and ^{13}C NMR spectra of compound 19.	298
Figure 160. Normalized absorption spectra of OPV1a, OPV2a, OPV3a, and OPV4a (10^{-6} M in CHCl_3).....	299

Figure 161. Normalized emission spectra of OPV1a, OPV2a, OPV3a, and OPV4a (10^{-6} M in CHCl_3).....	299
Figure 162. Normalized absorption spectra of OPV1b, OPV2b, OPV3b, and OPV4b (10^{-6} M in CHCl_3).....	300
Figure 163. Normalized emission spectra of OPV1b, OPV2b, OPV3b, and OPV4b (10^{-6} M in CHCl_3).....	300
Figure 164. Normalized absorption spectra of OPV2a, OPV2b, OPV2c, and OPV2d (10^{-6} M in CHCl_3).....	301
Figure 165. Emission spectra of OPV2a, OPV2b, OPV2c, (10^{-6} M in CHCl_3) and OPV2d (10^{-3} M in CHCl_3).....	301
Figure 166. Absorption (solid lines) and emission (dashed lines) spectra of OPV2e and p(OPV2e) (10^{-5} M in CHCl_3).....	302
Figure 167. ^1H and ^{13}C NMR spectra of compound 35.	304
Figure 168. ^1H and ^{13}C NMR spectra of compound 22.	305
Figure 169. ^1H and ^{13}C NMR spectra of compound 23.	306
Figure 170. ^1H and ^{13}C NMR spectra of compound 24.	307
Figure 171. ^1H spectrum of compound 37.	308
Figure 172. ^1H spectrum of compound 38.	308
Figure 173. ^1H spectrum of compound 39.	309
Figure 174. ^1H and ^{13}C NMR spectra of compound 26.	310
Figure 175. ^1H and ^{13}C NMR spectra of compound 27.	311
Figure 176. ^1H and ^{13}C NMR spectra of compound 28.	312
Figure 177. ^1H and ^{13}C NMR spectra of compound 29.	313

Figure 178. ^1H and ^{13}C NMR spectra of compound 30.	314
Figure 179. ^1H and ^{13}C NMR spectra of compound 31.	315
Figure 180. ^1H spectrum of compound 32.	316
Figure 181. ^1H and ^{13}C NMR spectra of compound 33.	317
Figure 182. ^1H and ^{13}C NMR spectra of compound 34.	318
Figure 183. ^1H and ^{13}C NMR spectra of p29.	319
Figure 184. ^1H and ^{13}C NMR spectra of p32.	320
Figure 185. ^1H and ^{13}C NMR spectra of compound O.	321
Figure 186. ^1H and ^{13}C NMR spectra of $(\text{TsOCH}_2\text{CH}_2\text{OCH}_2)_2$	322
Figure 187. ^1H and ^{13}C NMR spectra of compound T.	323
Figure 188. Normalized absorption and emission spectra of 29, 32, p29, p32 (10^{-6} M in CH_2Cl_2)	324
Figure 189. Differential calorimograms of the PV-O _X T _Y series.	325

SYMBOLS AND ABBREVIATIONS

Å	angstrom
A	electron-accepting unit, particularly an unsubstituted phenylene
Abs	absorption
Ac	acetyl
Ac ₂ O	acetic anhydride
ADMET	acyclic diene metathesis
AIBN	azobis(isobutyronitrile)
aq	aqueous
Ar	aryl
atm	atmosphere
AU	arbitrary unit
BBN	borabicyclo[3.3.1]nonane
BHJ	bulk heterojunction
brine	saturated aqueous NaCl
ⁿ Bu	<i>n</i> -butyl
^t Bu	<i>tert</i> -butyl
°C	degrees Celsius

calcd	calculated
cm	centimeter
CM	cross metathesis
CV	cyclic voltammetry/voltammogram
Cy	cyclohexyl
d	day
d	doublet (NMR signal)
δ	chemical shift
D	electron-donating unit, particularly a dialkoxyphenylene
DCE	1,2-dichloroethane
DCM	dichloromethane
dd	doublet of doublets (NMR signal)
ddt	doublet of doublets of triplets (NMR signal)
DFT	density functional theory
DIBAL-H	diisobutylaluminum hydride
DMF	<i>N,N</i> -dimethylformamide
DPV	differential pulse voltammetry/voltammograms
DSC	differential scanning calorimetry
dt	doublet of triplets (NMR signal)
<i>e</i>	an electron, fundamental unit of charge
ε	extinction coefficient, molar absorptivity
<i>E</i>	energy

E_{HOMO}	HOMO energy
E_{LUMO}	LUMO energy
ΔE	energy difference
ΔE_{d}	energy difference between the LUMO of a polymer donor and the LUMO of a fullerene acceptor
ΔE_{g}	HOMO-LUMO gap or bandgap
ΔE_{off}	offset energy between the HOMO of a polymer donor and the LUMO of a fullerene acceptor
EI	electron impact ionization
em	emission
eq	equivalent
ESI	electrospray ionization
Et	ethyl
Et_2O	diethyl ether
EtOAc	ethyl acetate
eV	electron volt
FF	fill factor
g	gram
h	hour
η	power conversion efficiency
HOMO	highest occupied molecular orbital
HRMS	high resolution mass spectrometry
HWE	Horner-Wadsworth-Emmons

Hz	hertz
I	irradiance
ITO	indium tin oxide
J	coupling constant (NMR signal)
J	current density
J_{sc}	short-circuit current density
kDa	kilodalton
λ	wavelength
λ_{max}	wavelength at maximum absorption or emission
L	liter
LUMO	lowest unoccupied molecular orbital
μ_h	hole mobility
M	molar (moles per liter)
M^+	molecular ion
mA	milliamp
Me	methyl
MeCN	acetonitrile
MeOH	methanol
meV	millielectron volt
mg	milligram
MHz	megahertz
min	minute
mL	milliliter

μL	microliter
μm	micrometer
mmol	millimole
μmol	micromole
M_n	number average molecular weight
mol	mole
MP	melting point
MS	mass spectrometry
mult	multiplet (NMR signal)
M_w	weight average molecular weight
m/z	mass/charge ratio
NBS	<i>N</i> -bromosuccinimide
nm	nanometer
NMR	nuclear magnetic resonance
OAc	acetate
OLED	organic light-emitting diode
OPV	oligo(phenylene-vinylene)
OPVC	organic photovoltaic cell
<i>p</i>	para
<i>P</i>	power
PCBM	phenyl- C_{61} -butyric acid methyl ester
PDI	polydispersity index
PEDOT	poly(ethylenedioxythiophene)

pent	pentet (NMR signal)
Ph	phenyl
Ph ₂ O	diphenyl ether
PhH	benzene
PhMe	toluene
PLA	poly(lactic acid)
PLGA	poly(lactic- <i>co</i> -glycolic acid)
pm	picometer
ppm	parts per million
PPV	poly(<i>p</i> -phenylene-vinylene)
psi	pounds per square inch
PSS	polystyrene sulfonate
Pyr	pyridine
q	quartet (NMR signal)
quat	quaternary carbon
RAFT	reversible addition-fragmentation transfer
rbf	round-bottom flask
ref.	reference
ROMP	ring-opening metathesis polymerization
ROP	ring-opening polymerization
RSC	repeat-sequence copolymer
rt	room temperature
s	second

s	singlet (NMR signal)
sat	saturated
SEC	size exclusion chromatography
t	triplet (NMR signal)
T	temperature
T_c	crystallization transition temperature
T_g	glass transition temperature
T_m	melting transition temperature
TBAB	tetrabutylammonium bromide
THF	tetrahydrofuran
TLC	thin-layer chromatography
TOF	time of flight
Ts	<i>p</i> -toluenesulfonyl
TsCl	<i>p</i> -toluenesulfonyl chloride
TsOH	<i>p</i> -toluenesulfonic acid
tt	triplet of triplets (NMR signal)
UV/VIS	ultraviolet/visible
V	volt (unit)
V	voltage (potential difference)
V_{OC}	open-circuit voltage
V_{ox}	oxidation potential
V_{red}	reduction potential

PREFACE

In the fall of 2004, I came to the University of Pittsburgh seeking my PhD in chemistry. I was uncertain at the time in which division of chemistry I would specialize, but I knew that I wanted to take what I would be learning during my experiences at Pitt and use them to train the next generation of chemists. My road to my PhD was long and hard, but it was full of good people and good experiences that have shaped the scientist and teacher that I have become. The teaching and research that I have done at Pitt helped me find employment doing what I love, teaching undergraduate chemistry at Frostburg State University.

First and foremost, I want to thank Prof. Tara Y. Meyer for being my research advisor and for being supportive of me while I completed my PhD. She has helped me in innumerable ways over the last six years, and I have enjoyed the work I have done as a part of her research group. She has been supportive of my passion for teaching and allowed me to accept extraordinary teaching opportunities. She instilled in me strong convictions on what constitutes good science and what constitutes good scientific communication. She has always provided a good ear for my problems, both in and out of lab.

I want to thank the members of the Meyer group for their help along the way. Ryan Stayshich helped me stay on track and helped me stay sane at times. Dr. Rob Walters was a willing collaborator in some of my crazier ideas, especially those we weren't quite ready to pitch to Tara. I want to thank Dr. James Copenhafer for giving me perspective on my priorities, even if

I didn't understand it at the time. Dr. Percy Calvo-Marzal provided great help with the electrochemistry portions of my project. Tianqi Pan helped solve some of the more difficult synthetic problems in the metathesis project. Jian Li, Ryan Weiss, Xiao Jin, and Ken Cutler made my time in the Meyer group enjoyable and interesting. I also want to thank the many undergraduate researchers who worked in the Meyer group, particularly Mark Ringenberger and Matt Deklava, whom I had the privilege of supervising.

The faculty, students, and staff of the Chemistry Department have always been helpful to me. I want to thank Dr. George Bandik and Dr. Ericka Huston for providing me with excellent teaching experiences and with good examples, good advice, and good conversations about teaching chemistry. I would also like to thank Peter Bell and Matt Davis for being sounding boards for some of my unusual ideas. I want to thank the facilities directors, Dr. Damodaran Krishnan Avary (NMR), Dr. John Williams (mass spec), and Joel Gillespie (MCL) for helping collect the data I needed. The staff of the Chemistry Department made many aspects of being a graduate student simpler. In particular, I want to thank Fran Nagy for helping me navigate the bureaucracy of graduate school, Lori Neu for fixing all of the glassware I broke, Debbie Hunt for helping me get my teaching materials in order, Josh Jones for running a tight ship in the undergraduate stockroom, Darlene Lanz for making ordering easy, and Michelle Monaco and Michael Pater for doing all kinds of things for me that were outside their job descriptions.

I want to thank Professors Geoff Hutchison, Toby Chapman, and Tracy Cui for serving on my dissertation defense committee. I would also like to thank Professors Hutchison and Chapman for serving on my proposal committee and for many helpful discussions. I want to thank Professor Joe Grabowski for being my proposal mentor and Professors Kay Brummond

and Paul Floreancig for serving on my comprehensive exam committee. Your input and advice have been most helpful.

I want to extend a special thank you to my colleagues in the Chemistry Department at FSU: Dr. Mary Mumper, Dr. Robert Larivee, Dr. Jerald Simon, Dr. Fred Senese, and Dr. Peggy Biser. Not all that long ago, you were my teachers, instilling in me a love of chemistry. As colleagues, you have been very supportive of me as I started my career in academia while preparing and defending my thesis. I especially want to thank Dr. Don Weser for being an outstanding undergraduate advisor and for encouraging me to explore chemistry and to seek excellence.

Finally, I wish to thank my family and friends for sticking with me through the years. I want to thank my wife, Teresa, for being there for me, and putting up with me, for six years of a long distance relationship and six months of stressful preparation for my defense. I want to thank Mom, Dad, Natalie, Grandma, and Grandpap for being supportive of everything I do and pushing me to be successful. I want to thank my good friends Tom, Lacy, and Meagan for everything they have done and everything they have put up with. Thank you, everyone.

1.0 INTRODUCTION

1.1 SEQUENCE IN POLYMER CHEMISTRY

There is a growing sense that sequence is important for macromolecular materials.¹⁻³ The ability to prepare precisely sequenced copolymers would provide an opportunity to access novel architectures and create materials with properties that can be exquisitely fine-tuned. Synthetic polymer chemistry is far behind Nature² in this endeavor. By using sequences of just four monomers, Nature can encode the genome of trillions of species. Nature also demonstrates mastery of converting sequence into structure and function through the synthesis of hundreds of thousands of precisely sequenced peptides from a library of more than 20 monomers. The primary structures of these peptides encode the ultimate secondary, tertiary, and quaternary structures of the resulting proteins, which creates a specific function.

Sequence control in polymers has not been a main focus in synthetic polymer chemistry.² Research in the last two decades has instead focused on the development of novel macromolecular architectures and topologies, i.e. macrostructure.^{3, 4} Sequence control, i.e. microstructure, primarily remains limited to alternating, random, diblock, and segmented multiblock copolymers (Figure 1). However, several synthetic approaches exist that have been utilized to prepare sequenced polymers: template assisted synthesis, control of monomer addition

by kinetics or catalyst manipulation, step growth polymerization of orthogonal monomers, and polymerization of sequenced segments.

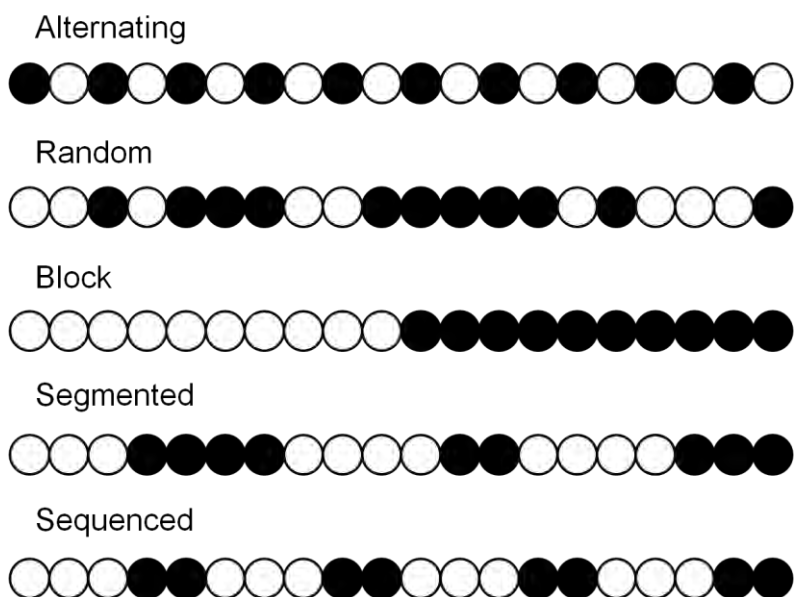
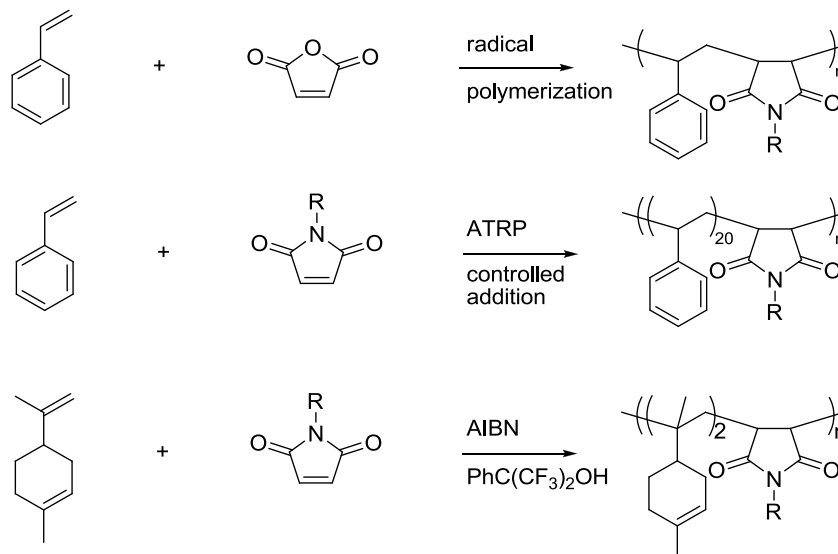


Figure 1. Examples of polymer microstructures – filled and open circles represent different monomers.

Sequenced natural and artificial biopolymers can be prepared using a template process, similar to the method that Nature uses.⁵ Synthetic step- and chain-growth polymers can also be prepared from templates.⁶ In a recent example, Sawamoto and coworkers developed a templated macroinitiator with recognition sites for anionic⁷ and cationic⁸ monomers. However, the template approach is limited in that the template generally needs to be as complex as the desired complexity in the polymer.

Control over polymerization kinetics, particularly the relative rates of homopolymerization vs. copolymerization (reactivity ratios), can influence sequence in chain growth polymers (Scheme 1). In particular, predominantly alternating copolymers are possible for the special case when both reactivity ratios are approximately zero, e.g. styrene and maleic anhydride.^{9, 10} This approach has been utilized by Pfeifer and Lutz^{11, 12} to prepare polystyrenes with regularly spaced functionalized maleimides, though these polymers do not display precise

sequence control so much as precision insertion of maleimides in living polystyrene. A recent example from Satoh, *et al.*,¹³ demonstrates that sequenced copolymers of maleimide and limonene are possible using reversible addition-fragmentation transfer (RAFT) polymerization. The addition of a perfluoroalcohol promotes the formation of an AAB copolymer (maleimide-maleimide-limonene) even when the feed ratio of monomers contains 50% limonene.



Scheme 1. Sequenced radical polymerizations.

Kinetic control of monomer insertion can also be achieved using selective catalysis. Primarily this approach has been used to prepare homopolymers of controlled stereosequence, an important subset of sequenced polymers given the dependence of properties on tacticity. The control of tacticity of polyolefins using Zeigler-Natta type catalysts¹⁴ represents some of the earliest work in the preparation of sequenced materials. In the last two decades, this approach has been extended to ring-opening polymerization (ROP) of lactones to produce polyesters.¹⁵ Particularly noteworthy are the efforts of the Coates and coworkers in the development of catalysts that generate syndiotactic,¹⁶ heterotactic,¹⁷ and stereo-complexed^{18, 19} poly(lactic acid) (PLA). Thomas and coworkers have extended this methodology to produced syndiotactic poly(3-

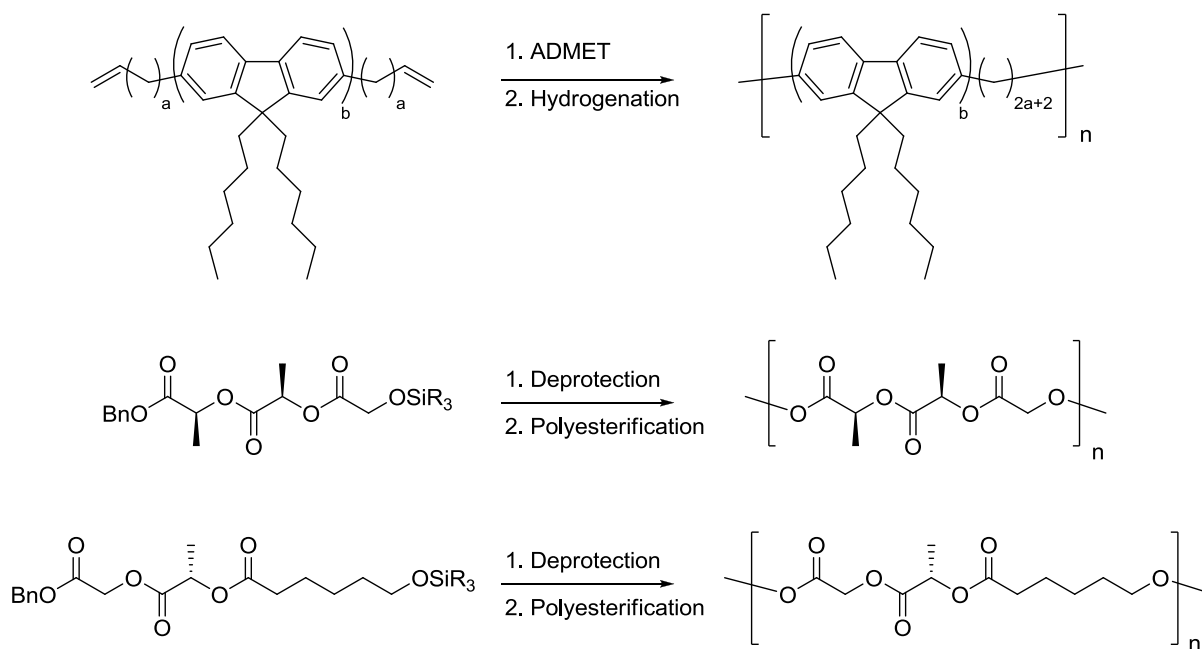
hydroxybutyrate)²⁰ and alternating copolymers of different enantiopure β -lactones of opposite configuration.²¹

Sequence can be controlled in step-growth polymerization by using monomers with orthogonal or variable reactivity. High polymers with simple sequences can be prepared through the reaction of AA and BB type monomers.²² More complex sequences require partial protection or deactivation of the monomer and are usually limited to the preparation of oligomers. The vast number of solid phase syntheses of linear and dendritic monodisperse sequenced synthetic biopolymers and “unnatural” biopolymers follow this motif.²³ Alternatively, sequenced copolymers could be rapidly assembled by iterative alternation of orthogonal chemistry, i.e. AB + CD, without protecting groups, although this approach is rarer. In an impressive recent example, Malkoch, Hawker, and coworkers used alternating thiol-ene reactions and Cu catalyzed Huisgen 1,3-dipolar cycloadditions to prepare a 6th generation dendrimer in just over six hours total reaction time.²⁴

The approach to producing sequenced polymers which gives the greatest control is the polymerization of sequenced segments—monomers in which the desired sequence is preassembled—to produce repeating sequence copolymers (RSCs). This approach has been used to assemble short peptide sequences through native ligation to produce longer peptides.²⁵ Similarly, the Huisgen cycloaddition²⁶ and other “click” reactions²⁷ have become popular for the rapid assembly of short oligomers into more complex sequenced materials. The group of Wagener has also employed this strategy to produce sequenced analogues of polyolefins by acyclic-diene metathesis (ADMET) polymerizations of sequenced α,ω -diolefins.²⁸⁻³⁰ Another approach to sequenced polyolefin analogues was recently reported by Satoh, *et al.*³¹ They

prepared short segments containing the equivalent of styrene and acrylate units and polymerized them by a Cu catalyzed step-growth radical polymerization.

Research in the Meyer group has recently focused on using the segment approach to systematically prepare sequenced copolymers with the aim of investigating the effects of sequence on properties (Scheme 2). Ward and Meyer reported the synthesis of polyaniline containing regularly spaced *o*-phenylene units,³² with the goal of improving the processibility of the material. Copenhafer, Walters, and Meyer have systematically prepared a series of rod-coil fluorene RSCs by ADMET to examine the effects of sequence on optical and thermal properties.³³ Stayshich and Meyer have prepared sequenced and stereosequenced poly(lactic-co-glycolic acid)s (PLGAs) based on segments of up to six repeat units.^{34, 35} The sequenced PLGAs demonstrated a profound dependence of NMR chemical shifts on both the monomer sequence and the stereosequence of the PLGAs. The work on PLGA is being extended to the preparation of polymers containing ϵ -hydroxycaproic acid³⁶ and functional monomers,³⁷ and the effects of sequence on hydrolysis rate and bulk mechanical properties are also under investigation.



Scheme 2. Examples of RSCs prepared by the Meyer group.

1.2 CONJUGATED POLYMERS AS PHOTOVOLTAIC MATERIALS

Conjugated polymers represent an important class of materials since their optoelectronic and thermal properties make them ideal candidates for organic light-emitting diodes (OLEDs)³⁸ and organic photovoltaic cells (OPVCs),³⁹ with the former application being more well developed.

In a polymer-fullerene bulk heterojunction (BHJ) solar cell a composite blend containing a conjugated polymer donor, such a polythiophene or poly(*p*-phenylene-vinylene) (PPV), and a fullerene acceptor, such as phenyl-C61-butyric acid methyl ester (PCBM) is layered between a transparent electrode, such as poly(ethylenedioxythiophene) (PEDOT)-polystyrene sulfonate (PSS) coated on indium tin oxide (ITO) and a metal electrode (usually aluminum) (Figure 2).⁴⁰ Upon irradiation, an electron is promoted from the valence band (HOMO) to the conductance band (LUMO) of the polymer (Figure 3). This exciton migrates to the polymer-fullerene

interface, where electron transfer to the fullerene creates a charge transfer state. Finally, the electrons and holes are transported to the electrodes to generate a current.

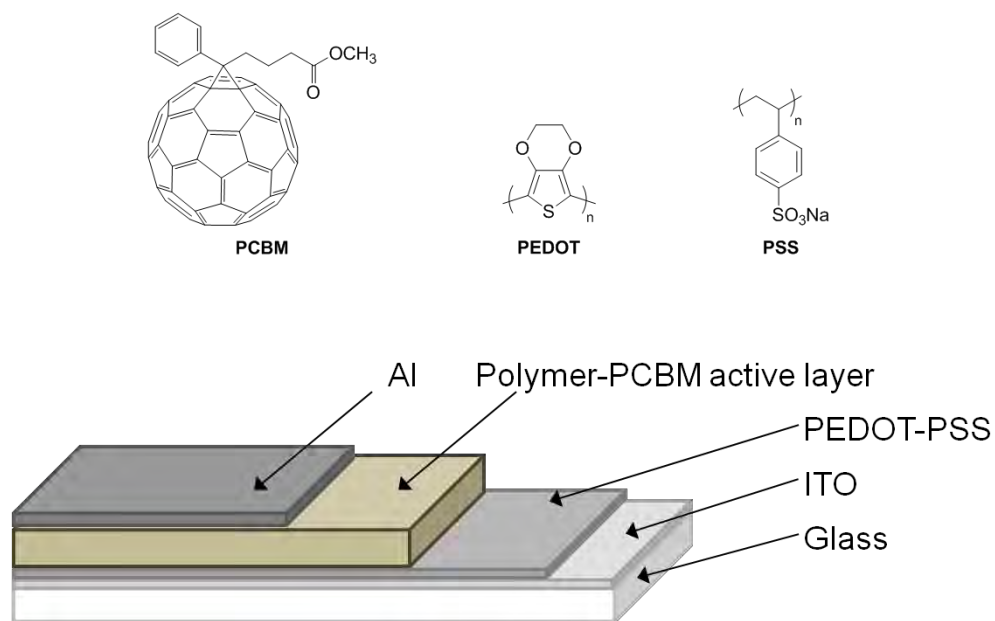
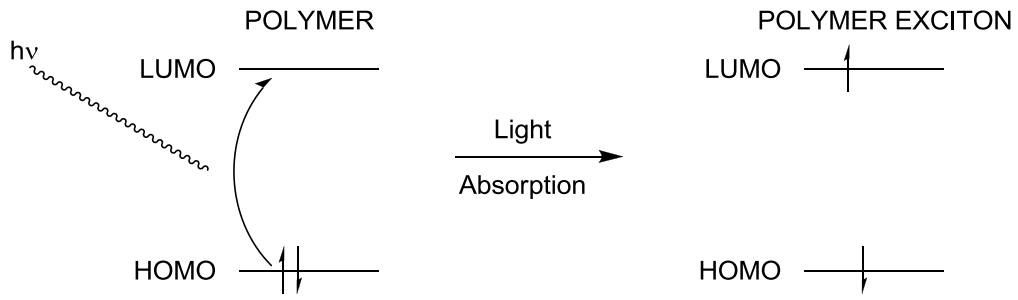
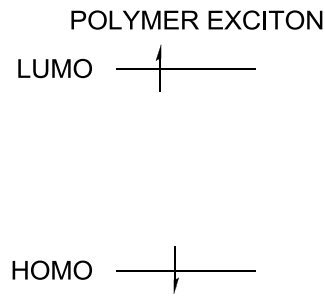


Figure 2. Top: Structures of PCBM, PEDOT, and PSS. Bottom: Construction of a BHJ photovoltaic cell.

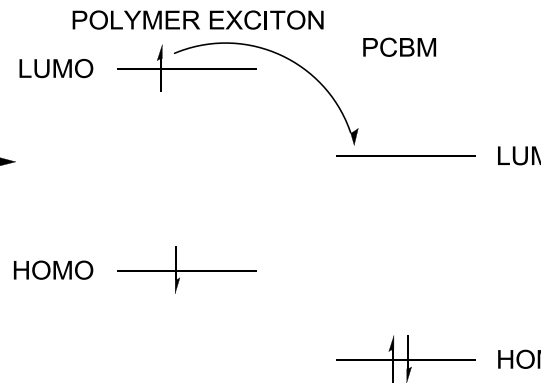
1. Exciton Formation



2. Exciton Migration



3. Charge Transfer



4. Charge Transport - Current Generation

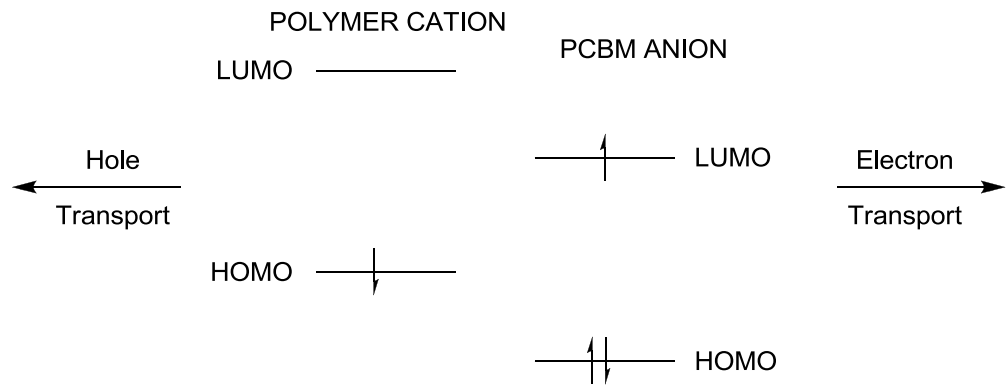


Figure 3. Mechanism of current generation in a polymer/PCBM photovoltaic cell.

Fullerene derivatives are generally accepted as the optimal acceptor material in a BHJ solar cell because they have low lying LUMOs (~ 4.2 eV) and high electron mobilities (~ 1 cm² V⁻¹ s⁻¹).⁴⁰ Thus, all efforts to improve the performance of OPVCs focus on the polymer donor. Bredas, *et al.*,⁴¹ noted in 2004 that the majority of synthetic efforts were empirical in nature and not based on well-defined design principles. A review of recent syntheses by Cheng, *et al.*,³⁹ in 2009 suggests the state of the art to be no different now. Nevertheless, power conversion efficiencies (PCEs) as high as 7% have been achieved.^{42, 43} The predominant approach to developing materials for OPVCs is bandgap engineering, the practice of decreasing the bandgap of the polymer to harvest more of the solar spectrum. Initially put forth by Havinga, *et al.*,⁴⁴ the alternation of electron-donating (D) and electron-accepting (A) units can lead to very low band gaps. The donor-acceptor approach has become popular^{39, 45-52} in both the preparation of alternating and random copolymers.

Achievement of the lowest possible bandgap is a limited approach, especially given that Chen and Cao⁴⁵ recently demonstrated no statistical correlation between HOMO-LUMO gap, ΔE_g and PCE. PCE, η , is calculated as $\eta = P_{max}/P_{in} \times 100\% = (|J_{max}|V_{max})/I_L \times 100\%$,⁵³ where P_{max} is the maximum output power, P_{in} is the input power, J_{max} is the current density at maximum power, V_{max} is the voltage at maximum power, and I_L is the irradiance of the source. PCE can be reformulated in terms of the short-circuit current density ($|J_{SC}|$), the current density when the voltage across the device is zero, and the open-circuit voltage (V_{OC}), the voltage across the device when the current density is zero: $\eta = (FF|J_{SC}|V_{OC})/I_L \times 100\%$, where FF is the fill factor, defined as $FF = (|J_{max}|V_{max})/(|J_{SC}|V_{OC})$. It is generally well accepted^{39-42, 45, 47, 53-56} that $|J_{SC}|$ has a negative correlation with the bandgap, ΔE_g , of the polymer, while V_{OC} has a positive correlation

with the energy offset, ΔE_{off} , between the HOMO of the polymer donor and the LUMO of the fullerene acceptor (Figure 4).

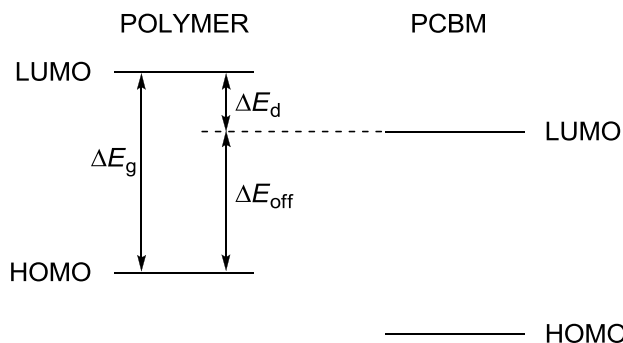


Figure 4. Definitions of relevant energy differences relative to frontier orbitals of the polymer donor and PCBM.

The sense then is that there is an optimal combination of bandgap and offset energy that should yield high PCE. Scharber, *et al.*,⁵⁶ developed a model predicting PCE based on the bandgap of the polymer donor and the energy difference, ΔE_d , between the LUMO of the polymer and the LUMO of the fullerene ($\Delta E_d = \Delta E_g - \Delta E_{\text{off}}$). They predict a region of high PCE (>10%) centered at $\Delta E_d = 0.3$ eV and $\Delta E_g = 1.5$ eV, which corresponds to a donor HOMO of -5.5 eV and LUMO of -4.0 eV if PCBM is the acceptor. Rand, *et al.*,⁵⁴ have examined the relationship between ΔE_g and ΔE_{off} using Marcus theory to model the J - V profile of several OPVC materials. They find that $|J_{\text{SC}}|$ has a maximum centered at $\Delta E_g = 1.4$ eV and $\Delta E_{\text{off}} = 0.8$ eV, while V_{OC} has a maximum centered at $\Delta E_g = 1.8$ eV and $\Delta E_{\text{off}} = 1.6$ eV. Combining these findings, they predict a region of high PCE (>7%) centered at $\Delta E_g = 1.5$ eV and $\Delta E_{\text{off}} = 1.1$ eV, which corresponds to a donor HOMO of -5.4 eV and LUMO of -3.9 eV when PCBM is taken to be the acceptor. In addition to predicting a ΔE_g and ΔE_{off} that will maximize $|J_{\text{SC}}|V_{\text{OC}}$, these models conveniently place the LUMO energy of the polymer the required 0.3 eV above the LUMO of PCBM to ensure a driving force for the formation of a charge transfer state.^{39, 40} Recently Zhou, *et al.*,⁵¹ have proposed that copolymers containing weakly electron-donating and

strongly electron-accepting units can realize these ideal energy levels. Figure 5 illustrates the ideal energy levels of a conjugated polymer compared to PCBM.

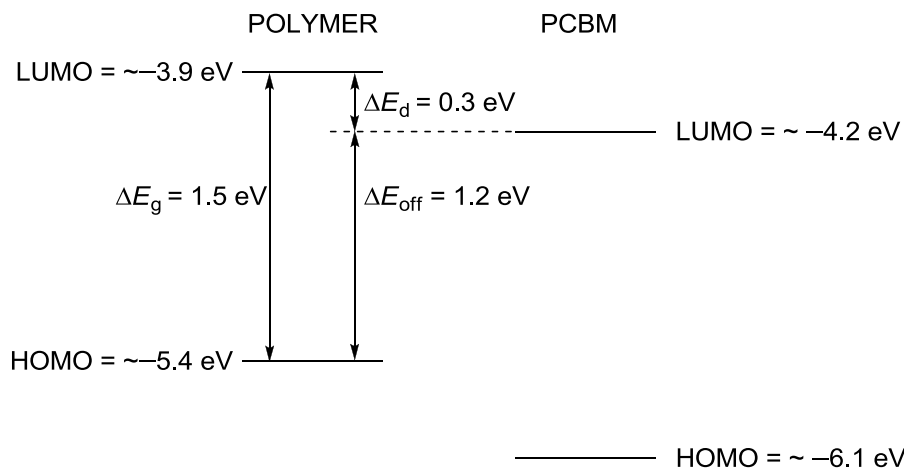


Figure 5. Optimal frontier molecular orbital energy levels for an ideal polymer donor compared to PCBM.

Other important parameters include the shape of the absorption spectrum and the extinction coefficient, to ensure a better absorption of the solar spectrum,^{47, 48} and hole mobility, μ_h , to maximize charge transport over recombination.^{45, 47} These properties are dependent on the same π -conjugation that controls the HOMO and LUMO levels, but in a less obvious way. Likely, they influence the fill factor parameter, which has not been rigorously studied. Hole mobility is an especially troubling parameter in that it is also dependent of the methods of film casting and device fabrication as well as polymer morphology.^{41, 57, 58}

Given the clear frontier molecular orbital requirements, the use of theory, as advocated by Bredas, *et al*,⁴¹ should refine and focus the search for the optimal polymer donor. However, with the exception of Bredas and collaborators,⁵⁹⁻⁶⁷ there are few examples of theory guiding synthesis. In one example, Blouin, *et al*,⁶⁸ used density functional theory (DFT) to predict the frontier orbitals of carbazole containing polymers. They found that the calculated energy levels correlated well with the experimental measurements, but their PCEs did not fit with Scharber's model due to lower than expected hole mobilities. In another example, Mondal, *et al*,⁶¹ found

that removing thiophene spacers from a thienopyrazene-*alt*-fluorene copolymer increased ΔE_g by lowering the HOMO energy, as predicted using DFT calculations, which also increased $|J_{SC}|$, V_{OC} , and PCE.

1.3 SEQUENCED CONJUGATED POLYMERS AS THE NEXT PARADIGM IN PHOTOVOLTAIC MATERIALS

The effects of sequence in conjugated polymers are easy to underestimate. The frontier molecular orbitals of donor-acceptor polymers are commonly depicted as localized orbitals:⁵¹ the HOMO of the polymer derives principally from the HOMO of the donor and the LUMO of the polymer derives principally from the acceptor (Figure 6a). If this is the case, only the type and number of donors and acceptors will determine the HOMO-LUMO gap of the polymer; the relative arrangement of donors and acceptors in a polymer should not matter. However, this model is overly simplistic. It only applies at the limit of no electronic communication between the donors and acceptors along the polymer chain, which is unlikely. If the donors and acceptors are in conjugation, then the frontier orbitals of the donors and acceptors should mix to form new frontier orbitals for the polymer³⁹ (Figure 6b). In this model, the relative placement, or sequence, of donors and acceptors along the polymer chain must affect the ways in which the frontier orbitals of the monomers can mix to form the new frontier orbitals of the polymer.

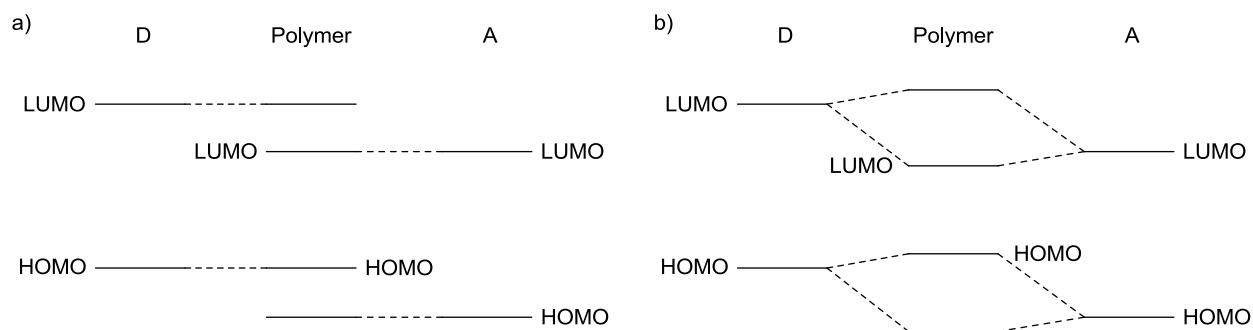


Figure 6. a) Localized orbital model for frontier molecular orbitals of donor-acceptor polymers. b) Orbital mixing model for frontier molecular orbitals of donor-acceptor polymers.

Sequence is thus the logical tool to provide the fine tuning necessary to optimize the energy levels of conjugated polymers for OPVCs. However, the majority of polymers used in OPVCs are alternating copolymers or random copolymers, and more complex sequences are rarely prepared. In particular, the fortuitously good properties of a random copolymer may be attributable to a statistically small number of ideal sequences in the chain. In the most significant example, Beaujuge, *et al.*,⁴⁸ recently reported on the absorption behavior of copolymers as a function of the exact number of electron-donating units between each electron-accepting units, finding that sequence drastically affects the shape of the absorption spectrum and the extinction coefficients. However, the effects of having multiple electron-accepters together, as must happen in a random copolymer, have not been examined.

The group of Bao has also examined sequence, comparing the properties of alternating⁶¹ and random⁶² copolymers containing or lacking thiophene spacer units. They found that removing the thiophene spacers increased ΔE_g for the alternating copolymer, but decreased ΔE_g for the random copolymers. The loss of the thiophene from the random polymers also led to a lower hole mobility. Studies detailing the systematic change of electron-acceptor unit, e.g. reports by Blouin, *et al.*,⁶⁸ and Mondal, *et al.*,⁶³ also represent limited sequence modification.

An interesting subset of sequence investigations consists of those that focus on the position of the alkyl side-chains. Side-chains, which are added to increase solubility and processibility and occasionally to impart other functionality,⁶⁹ are often overlooked as an influence on optoelectronic properties. Side-chain placement can create small perturbations of the energy levels of the conjugated backbone.⁷⁰ Additionally, the side-chains influence planarity of the polymer and the interchain packing, which can have dramatic effects on the optoelectronic properties and the hole mobility of the polymer.

Recent reports have examined the effects of side-chain placement on the optoelectronic and photovoltaic properties of alternating copolymers. Zhou, *et al*,⁵² and Biniek, *et al*,⁴⁹ prepared alternating copolymers containing benzothiadiazole as an electron-accepter unit and electron-donor units based on thiophene (Figure 7, Table 1). Zhou, *et al*, found that placement of an alkyl group on the β -position (PBDT-4DTBT) of their thiophene spacer led to the highest PCE, enough though this polymer had less optimal energy levels than the unsubstituted polymer (PBDT-DTBT). Nevertheless, PBDT-4DTBT exhibited slightly higher V_{OC} , $|J_{SC}|$, and FF and a noticeably higher hole mobility than PBDT-DTBT. Placement of the alkyl group on the α -position (PBDT-3DTBT) of the thiophene spacer or on the benzothiadiazole unit (PBDT-DTsolBT) led to higher bandgaps, lower $|J_{SC}|$, lower FF, and dramatically reduced PCE, even though PBDT-3DTBT exhibited the best ΔE_{off} and V_{OC} . Biniek, *et al*, reported no difference between PTBzT²-C12 α and PTBzT²-C12 β ; however, PTBzT²-CEH β exhibited the highest hole mobility, $|J_{SC}|$, and PCE. Zhou and Biniek attribute the differences in photovoltaic behavior to differences in planarity caused by the substitution patterns. Calculations performed by both groups using DFT (B3LYP/6-311+G^{*}) indicate that substitution on the benzothiadiazole or at the α -position on the thiophene spacer induces large deviations from planarity, while substitution at

the β -position on the thiophene spacer does not. However, this explanation is clearly insufficient, as PBDT-DTBT is predicted to be more planar than PBDT-4DTBT, and there was no significant difference between PTBzT²-C12 α and PTBzT²-C12 β . Both Zhou and Biniek note that their best materials (PBDT-4DTBT and PTBzT²-CEH β , respectively), were more soluble, and thus easier to process. The increased processibility would have led to better films, which would explain the marked increase in hole mobility.

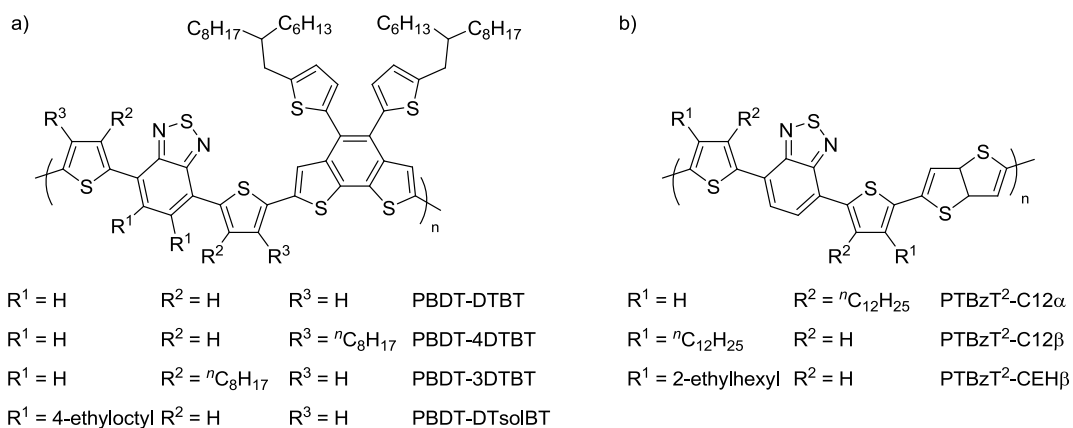


Figure 7. a) Polymers from ref. 52. b) Polymers from ref. 49.

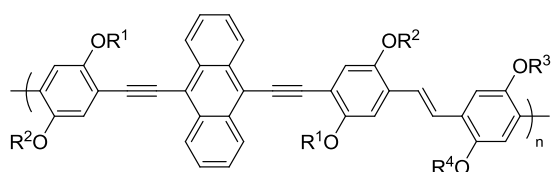
Table 1. Optoelectronic and photovoltaic parameters of polymers from refs. 52 and 49.

Polymer	$\Delta E_g^a /$ eV	$\Delta E_{off}^b /$ eV	$\mu_h^c /$ $cm^2 V^{-1} s^{-1}$	$V_{OC} /$ V	$ J_{SC} /$ $mA cm^{-2}$	FF / %	PCE / %	Ref.
PBDT-DTBT	1.63	1.07	3.94×10^{-6}	0.55	3.53	36.8	0.72	52
PBDT-4DTBT	1.69	1.01	9.20×10^{-6}	0.75	5.92	41.3	1.83	52
PBDT-3DTBT	1.97	1.18	N.D.	0.89	0.94	24.7	0.01	52
PBDT-DTsolBT	2.35	1.49	N.D.	0.43	0.12	26.4	0.21	52
PTBzT ² -C12 α	1.88	1.0	1×10^{-4}	0.67	2.17	32	0.46	49
PTBzT ² -C12 β	1.56	0.7	1×10^{-5}	0.55	1.88	41	0.42	49
PTBzT ² -CEH β	1.56	0.7	1×10^{-3}	0.55	5.67	40	1.24	49

^a Optical Bandgap determined at the onset of thin film absorption; ^b $\Delta E_{off} = \text{LUMO (PCBM)} - \text{HOMO (polymer)}$;

^c Hole mobility

Egbe, *et al.*,⁷¹ prepared alternating copolymers containing diethynyl anthracene units and phenylene-vinylene units with variable substitutions on the phenylenes (Figure 8, Table 2). Their best polymer, AnE-PV-ab, exhibited the best energy level match to the optimal values and the best $|J_{SC}|$, FF, and PCE. Egbe, *et al.*, attribute the poorer performance of their other polymers to smaller π - π stacking distances (380 pm vs. 386 pm for AnE-PV-ab). However, they note that some π - π stacking is necessary; the two polymers that showed no inclination to stack, AnE-PV-ba and AnE-PV-bb, have the lowest PCEs. Nevertheless, these two polymers have the highest hole mobilities. In fact, from the work of Biniek, *et al.*,⁴⁹ and of Egbe, *et al.*,⁷¹ the polymers with the highest hole mobilities contained disorder inducing 2-ethylhexyl groups.



$R^1 = nC_8H_{17}$	$R^2 = nC_8H_{17}$	$R^3 = 2\text{-ethylhexyl}$	$R^4 = 2\text{-ethylhexyl}$	AnE-PV-ab
$R^1 = nC_8H_{17}$	$R^2 = nC_8H_{17}$	$R^3 = nC_{10}H_{21}$	$R^4 = nC_{10}H_{21}$	AnE-PV-ad
$R^1 = nC_8H_{17}$	$R^2 = nC_8H_{17}$	$R^3 = nC_{12}H_{25}$	$R^4 = nC_{12}H_{25}$	AnE-PV-ae
$R^1 = 2\text{-ethylhexyl}$	$R^2 = 2\text{-ethylhexyl}$	$R^3 = nC_8H_{17}$	$R^4 = nC_8H_{17}$	AnE-PV-ba
$R^1 = 2\text{-ethylhexyl}$	$R^2 = 2\text{-ethylhexyl}$	$R^3 = 2\text{-ethylhexyl}$	$R^4 = 2\text{-ethylhexyl}$	AnE-PV-bb
$R^1 = CH_3$	$R^2 = 2\text{-ethylhexyl}$	$R^3 = CH_3$	$R^4 = 2\text{-ethylhexyl}$	AnE-PV-cc

Figure 8. Polymers from ref. 76.

Table 2. Optoelectronic and photovoltaic parameters of polymers from ref. 71.

Polymer	ΔE_g^a / eV	ΔE_{off}^b / eV	μ_h^c / $\text{cm}^2 \text{V}^{-1} \text{s}^{-1}$	V_{OC} / V	$ J_{\text{sc}} $ / mA cm^{-2}	FF / %	PCE / %	$d_{\pi\pi}^d$ / pm
AnE-PV-ab	1.80	0.97	2.57×10^{-5}	0.69	7.14	55.7	3.14	386
AnE-PV-ad	1.91	0.95	1.69×10^{-5}	0.68	6.75	48.4	2.22	380
AnE-PV-ae	1.98	0.94	3.39×10^{-5}	0.62	4.97	39.8	1.23	380
AnE-PV-ba	1.95	0.96	4.52×10^{-4}	0.93	3.44	34.7	1.11	— ^e
AnE-PV-bb	2.02	0.99	1.53×10^{-4}	0.83	4.22	34.8	1.22	— ^e
AnE-PV-cc	1.84	0.95	9.22×10^{-5}	0.91	5.86	36.9	1.90	379

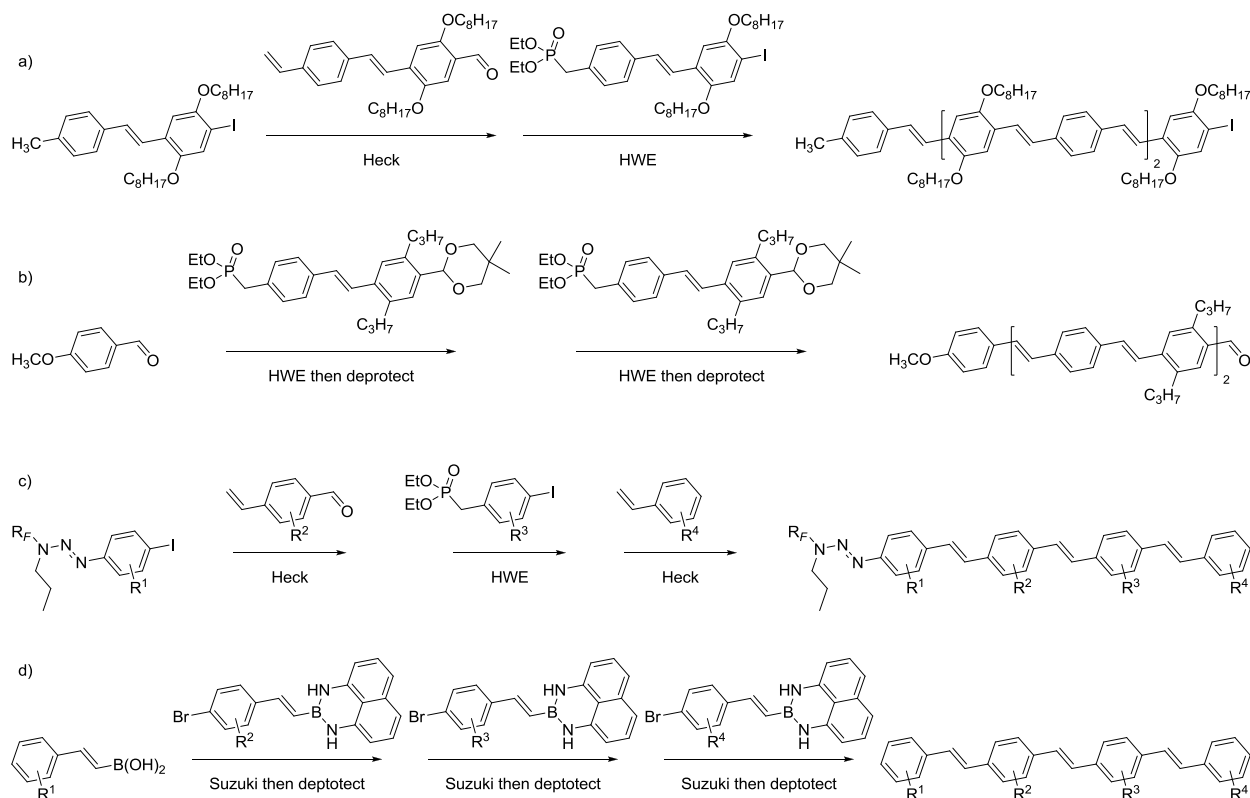
^a Optical Bandgap determined at the onset of thin film absorption; ^b $\Delta E_{\text{off}} = \text{LUMO}(\text{PCBM}) - \text{HOMO}(\text{polymer})$; ^c Hole mobility; ^d π - π stacking distance; ^e Polymers showed no inclination to stack

1.4 OLIGO(PHENYLENE-VINYLENE)S AS PROBES OF THE EFFECTS OF SEQUENCE ON OPTOELECTRONIC PROPERTIES

We are interested in extending the study of optoelectronic properties of conjugated materials as a function of sequence to more complicated sequences than have been previously reported. We have chosen oligo(phenylene-vinylene)s (OPVs) as our model system for this research. Poly(phenylene-vinylene)s (PPVs) are among the popular materials⁴⁰ for photovoltaic applications. OPVs are also one of the few conjugated materials that can be prepared without palladium catalysts.⁷²⁻⁷⁴ Residual palladium has been found by Krebs, *et al.*,⁷⁵ to dramatically decrease both V_{OC} and J_{SC} .

Several syntheses of sequenced OPVs have been reported (Scheme 3). In one of the earliest syntheses of conjugated oligomers, Maddux, Li, and Yu⁷⁶ prepared OPVs with alternating substitution patterns from AC and BD type stilbenes (A reacts with B; C reacts with D) using alternating Heck and Horner-Wadsworth-Emmons (HWE) reactions. Tour and

coworkers expanded the syntheses of OPVs using fluororous mixture synthesis to prepare more complex syntheses.⁷⁷ Other syntheses of OPVs include the work of Jørgensen and Krebs^{72, 73} to incorporate various heterocycles using only the Horner-Wadsworth-Emmons reaction, and the use of protected styryl boronates in iterative Suzuki reactions by Iwadate and Sugimoto.⁷⁸



Scheme 3. Syntheses of sequenced oligo(phenylene-vinylenes) by a) Maddux, *et al.*⁷⁶ b) Jørgensen and Krebs,⁷² c) Jian and Tour,⁷⁷ and Iwadate, and Sugimoto.⁷⁸

We have chosen to refer to our OPVs as dimers, trimers, tetramers, etc. based on the number of phenylene units in the oligomer, despite the oligomers containing less than the requisite number of complete (*viz.* a phenylene unit and a vinylene unit) repeat units. Thus monomers are substituted phenylenes, dimers are substituted stilbenes, trimers are distyrylbenzenes, etc. (Figure 9). The convention of referring to these oligomers as 1½-mers, 2½-mers, 3½-mers, etc. is awkward and ambiguous. We derive our nomenclature from the well-

established convention, which has also been used by Jian and Tour⁷⁷ for their OPVs, based on the number of monomers, which are all substituted phenylenes, used to prepare the oligomer.

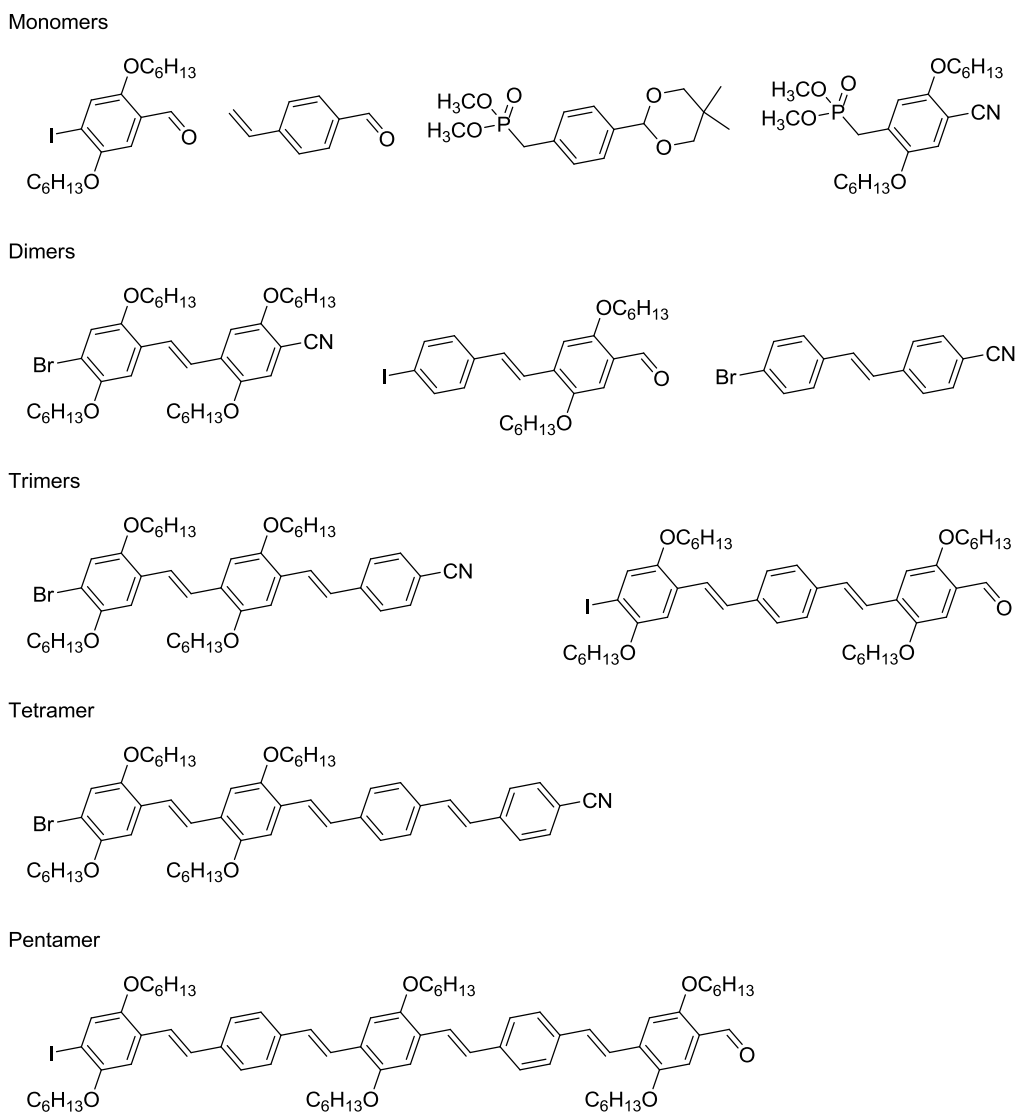


Figure 9. Examples of OPV oligomer nomenclature.

Herein we describe our synthesis of sequenced OPVs using HWE chemistry (Chapter 2). These OPVs display sequence-dependent optoelectronic and thermal properties. We were able to derive principles from these studies that could be used to guide further synthesis.

We also report on our progress toward sequenced OPVs using olefin cross metathesis (CM) (Chapter 3). The methodology lends itself to the preparation of alternating OPVs. The

preparation of more complex sequences suffers from a lack of stereoselectivity in the CM reaction. Examination of this reaction by NMR suggests that optimization could be possible.

Finally, we report our progress on the preparation of well-defined phenylene-vinylene rod-coil copolymers by HWE or ADMET polycondensations (Chapter 4). The physical properties of the copolymers depend strongly on the content and placement of oxygen atoms in the flexible linker between the phenylene-vinylene chromophores. The optical properties, however, are independent of the linker composition.

2.0 SYNTHESIS OF SEQUENCED OLIGO(PHENYLENE-VINYLENE)S USING HORNER-WADSWORTH-EMMONS HOMOLOGATION – THE EFFECTS OF SEQUENCE ON OPTOELECTRONIC AND THERMAL PROPERTIES

2.1 OVERVIEW

In order to develop design principles based upon sequence for OPVs, we have prepared three series of OPVs containing two different phenylene substitutions: all four possible dimers, six out of eight trimers (the homotrimers were omitted), and the set of six constitutionally isomeric tetramers containing two substituted phenylene rings and two unsubstituted rings (Figure 10). We have utilized an operationally simple iterative approach to these OPVs using HWE chemistry. We report the sequence-dependent optoelectronic and thermal properties of these OPVs, and we use these sequence-property relationships to derive principles to guide further synthesis.

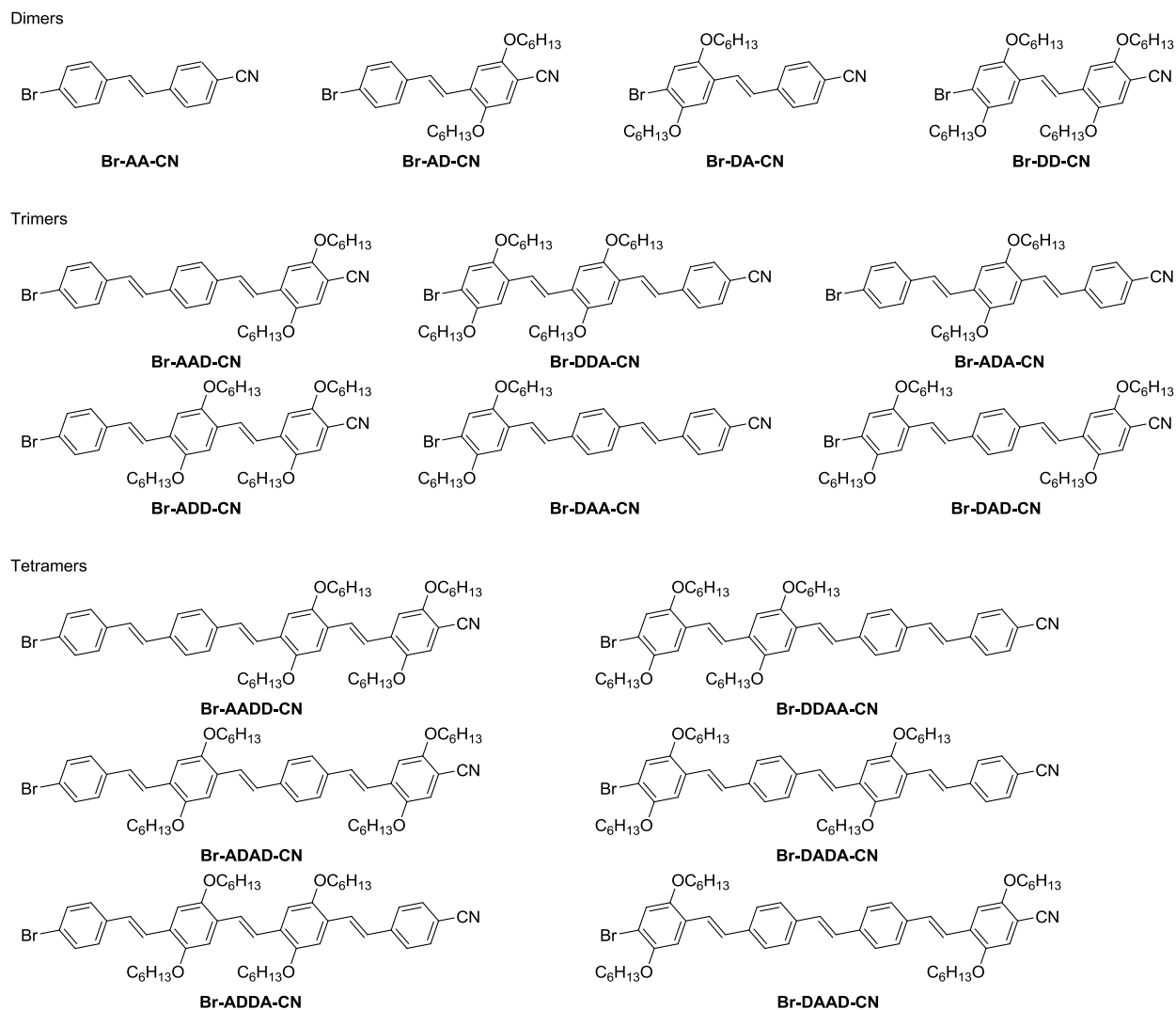


Figure 10. Sequenced OPVs prepared.

The sequences that we are examining are simple variations of substitution. On each phenylene unit an electron donating alkoxy group is either present or absent. Based on the reports by Zhou, *et al*,⁵² and Biniek, *et al*,⁴⁹ we believe that sequence differences as simple as ours should produce variations in the optoelectronic properties. The phenylene units with alkoxy substituents will serve as the donors (**D**) in our sequences. The unsubstituted units will be designated as acceptors (**A**), since they are weakly electron-accepting by comparison. Our nomenclature refers to each material by its sequence of donors and acceptors, with the appropriate end groups indicated. Examples are shown in Figures 10 & 11.

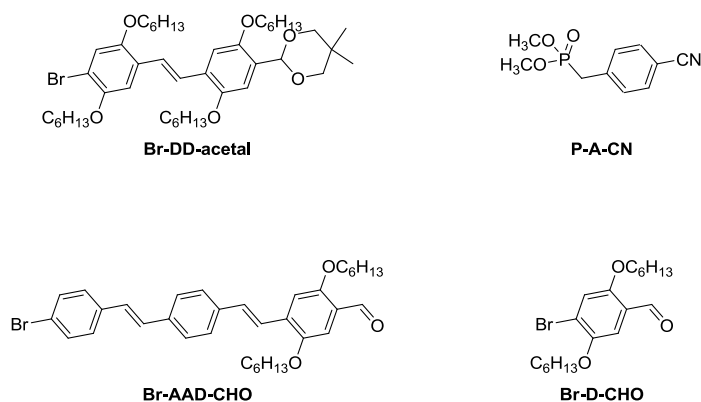


Figure 11. Further examples of OPV nomenclature.

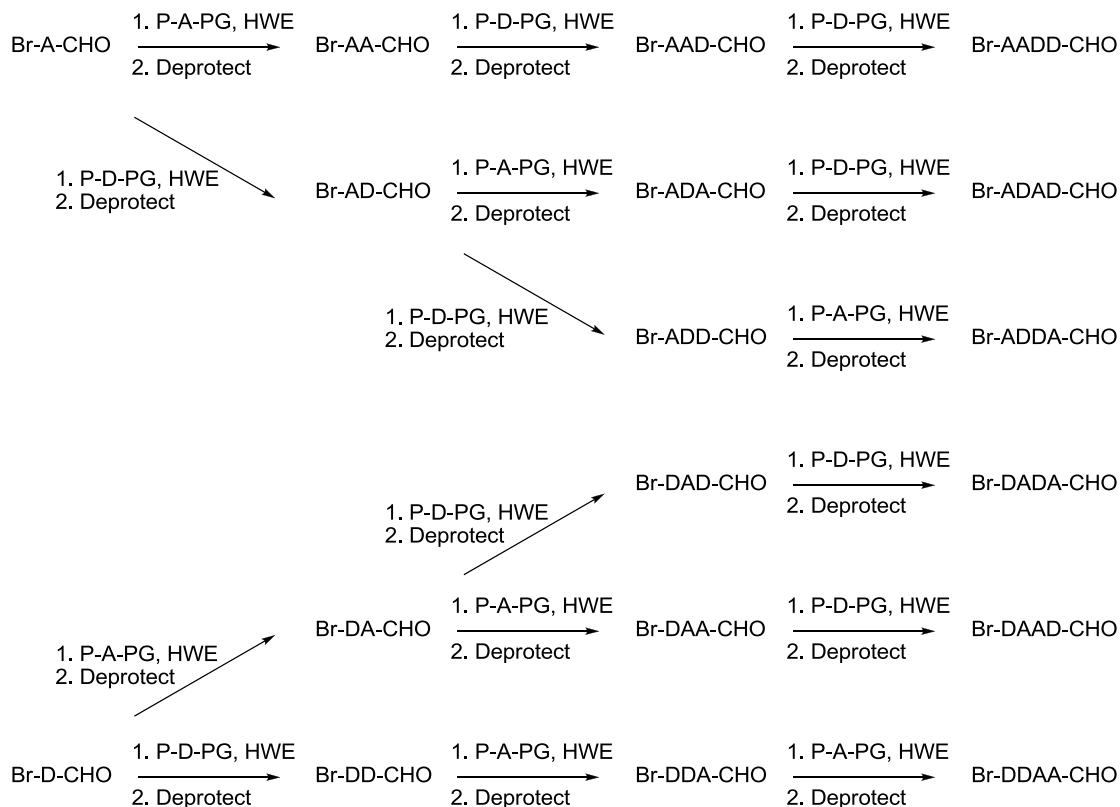
2.2 SYNTHETIC APPROACH

Our approach to preparation of OPVs using HWE chemistry was inspired by the work of Maddux, *et al*,⁷⁶ of Jian and Tour,⁷⁹ and of Jørgensen and Krebs.⁷² Maddux's approach utilized orthogonally reactive stilbene monomers: one with a vinyl group and a formyl group and a second with an aryl iodide and a phosphonate. The monomers were assembled into oligomers via alternating HWE and Heck reactions. Jian and Tour expanded on this approach by using fluororous mixture synthesis to prepare more complex sequences. The approach by Jørgensen and Krebs likewise uses a stilbene monomer with orthogonally reactive groups, in this case a phosphonate and a protected aldehyde. The oligomers were assembled by HWE reactions followed by deprotection of the acetal.

These approaches have limitations. In the work of Maddux, *et al*, and of Jørgensen and Krebs, the length of the oligomers was increased by two phenylene units each step. As a consequence, the substitution pattern is limited. In both approaches, only an alternating substitution pattern was achieved. Jian and Tour increased their oligomer lengths one phenylene

unit at a time, and were thus able to produce more complex sequences, but their monomer set did not allow them to place the same substituents at all positions.

We desired to fully control substitution pattern at each phenylene unit, which required us to develop a new synthesis of OPVs. Our synthetic strategy involves the use of partially masked AB-type phenylene monomers; ether substituted (**P-D-PG**) or unsubstituted (**P-A-PG**). These monomers are coupled with a *p*-bromobenzaldehyde, also either substituted (**Br-D-CHO**) or unsubstituted (**Br-A-CHO**) to produce dimers. The dimers are deprotected to unmask the aldehydes, which are reacted with another AB monomer to produce trimers, and so on. In this way we are able to prepare any substitution pattern on any length oligomer. This assembly approach is depicted in Scheme 4.



Scheme 4. Synthetic approach to OPVs

We examined two versions of this approach: one in which the aldehyde was protected as an acetal and one in which the aldehyde was masked as a nitrile precursor. The “deprotection” step in the nitrile version is a DIBAL-H reduction, which converts nitriles to aldehydes after aqueous workup. Each approach requires only a small set of monomers to prepare all possible sequences: two benzaldehydes and two phosphonates (Figure 12). The nitrile approach proved to be the better of the two methods; we were unable to achieve high *E*-selectivity in the HWE reactions of the acetal monomers.

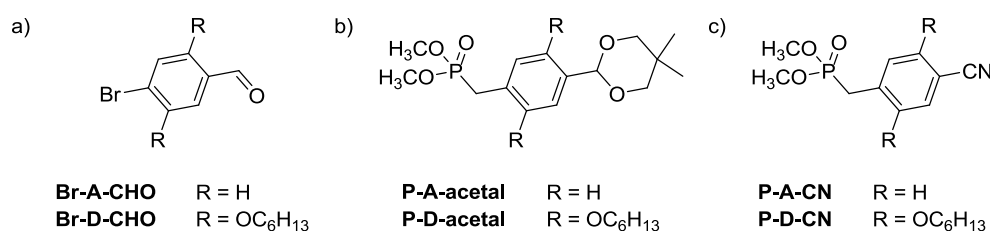


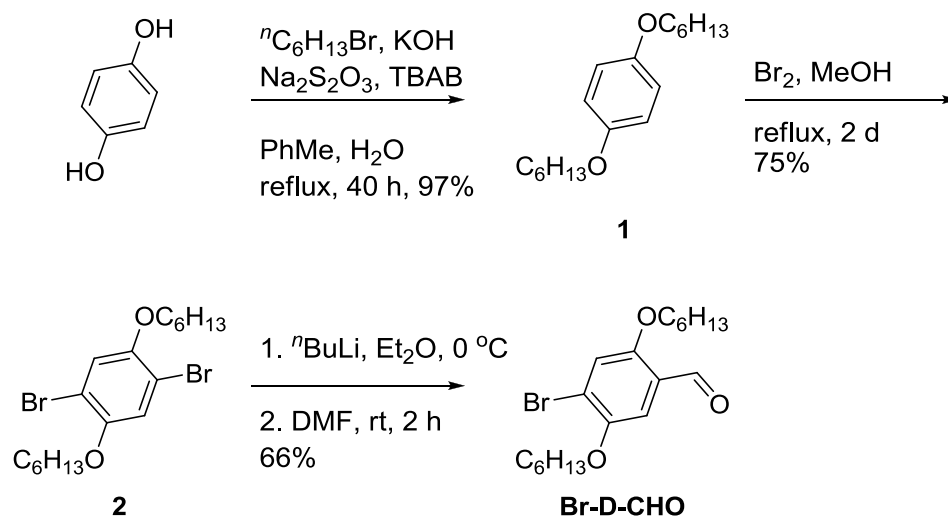
Figure 12. a) Benzaldehyde monomers common to both the acetal and nitrile approaches. b) Phosphonate monomers for the acetal approach. c) Phosphonate monomers for the nitrile approach.

2.3 RESULTS

2.3.1 Monomer synthesis

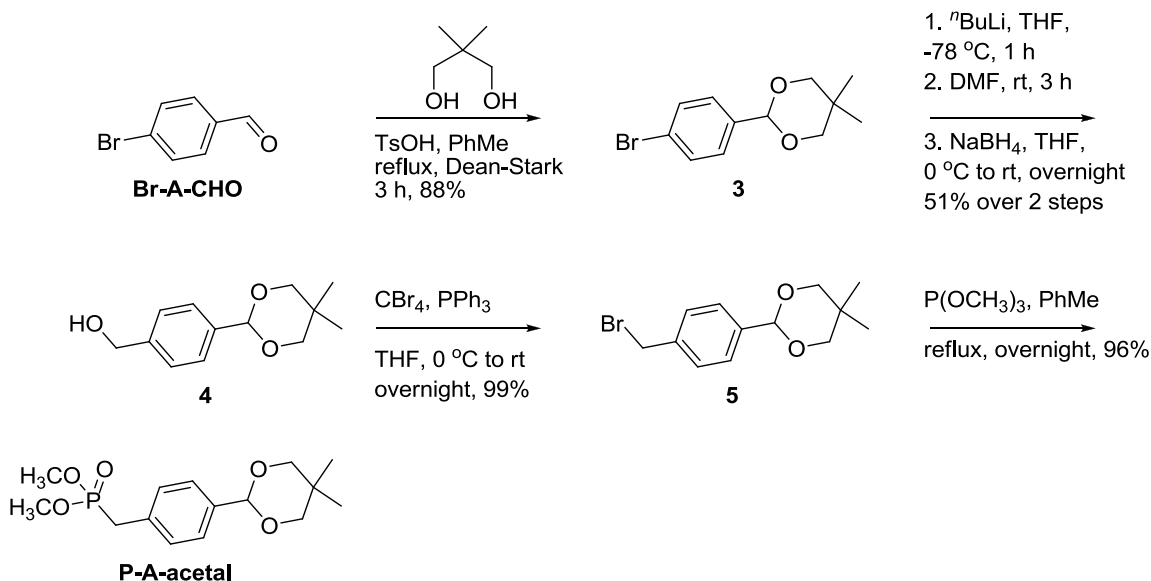
The two common bromobenzaldehyde monomers were either purchased (**Br-A-CHO**) or prepared in good yields using well established chemistry (**Br-D-CHO**). Donor benzaldehyde **Br-D-CHO** was prepared in three steps from hydroquinone in 48% overall yield (Scheme 5). Hydroquinone was alkylated with 1-bromohexane and KOH in a water/toluene biphasic system using TBAB as a phase transfer catalyst. The addition of 1 equivalent of Na₂S₂O₃ increased the yield from 20-30% to 91-97%. Ether **1** was brominated with Br₂ in refluxing methanol in a 75% yield. Finally, dibromide **2** was lithiated with ⁿBuLi in Et₂O at 0 °C, followed by quenching with

DMF to give benzaldehyde **Br-D-CHO** in 66% yield. Common bromobenzaldehyde monomer **Br-A-CHO** is commercially available 4-bromobenzaldehyde.



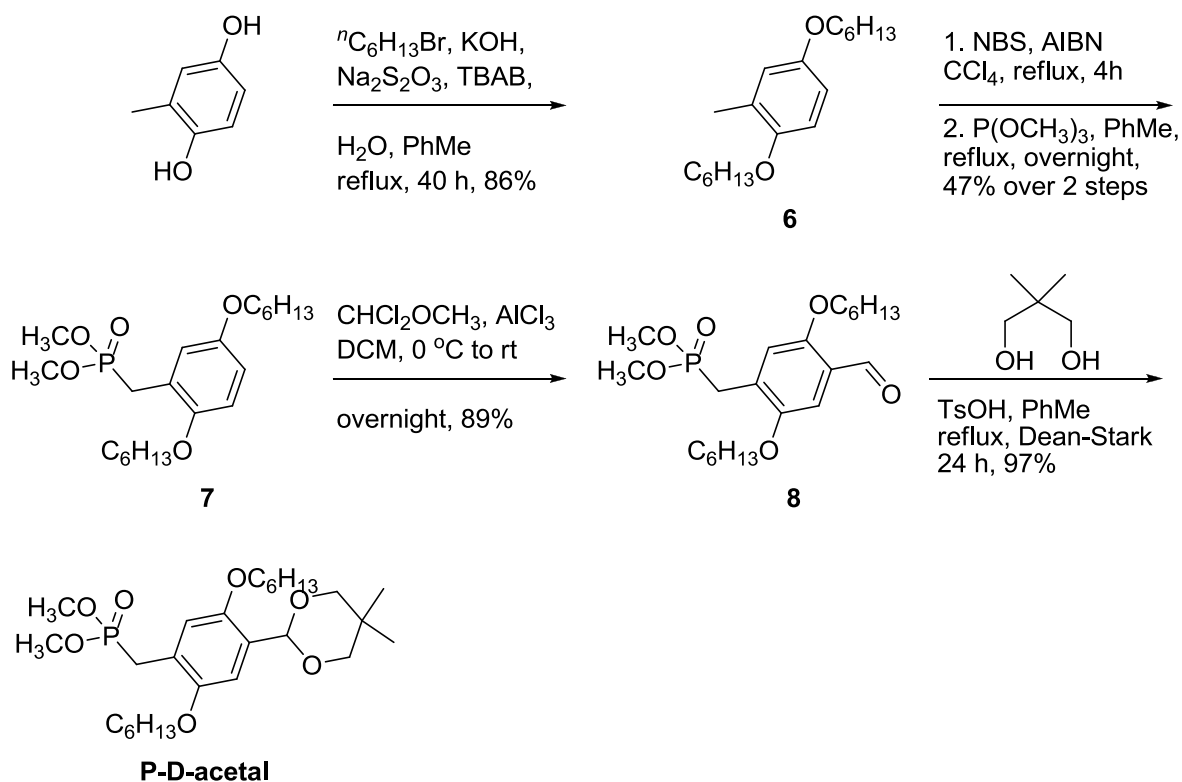
Scheme 5. Synthesis of **Br-D-CHO**

The two phosphonate monomers required for the acetal approach were prepared using well-established chemistry. Acetal monomer **P-A-acetal** was prepared from 4-bromobenzaldehyde in five steps with 43% overall yield (Scheme 6). The aldehyde was initially protected as the neopentylene acetal **3** in 88% yield. Lithiation with $n\text{BuLi}$ in THF, followed by quenching with DMF gave an aldehyde which was immediately reduced with NaBH_4 in THF to give benzyl alcohol **4** in 51% yield over 2 steps. Bromination with CBr_4 and PPh_3 in THF gave benzyl bromide **5** in 99% yield. Bromide **5** was converted to phosphonate **P-A-acetal** with $\text{P}(\text{OCH}_3)_3$ in refluxing PhMe in 96% yield.



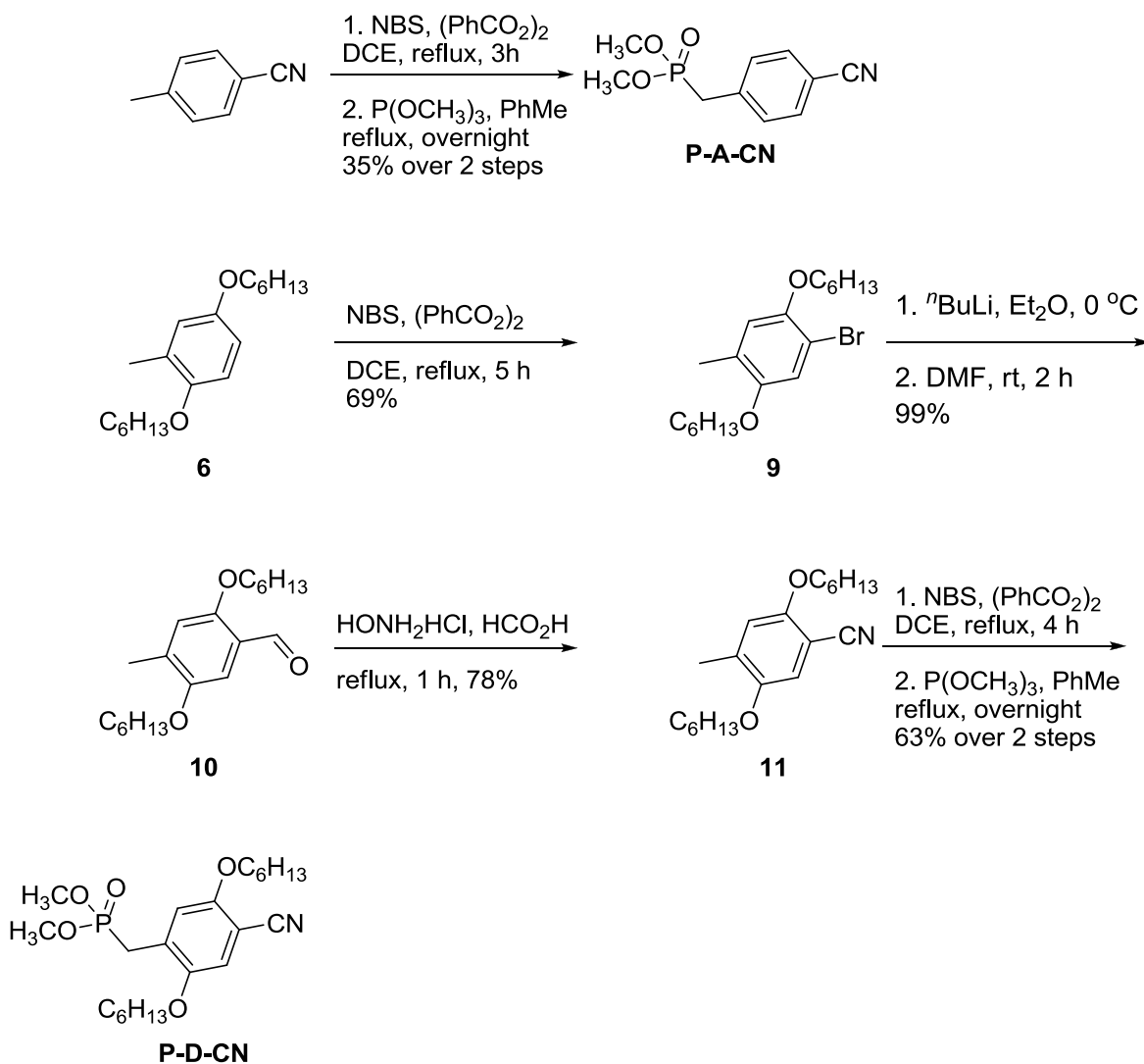
Scheme 6. Synthesis of **P-A-acetal**.

Acetal monomer **P-D-acetal** was prepared from 2-methylhydroquinone in five steps in 36% overall yield (Scheme 7). 2-Methylhydroquinone was alkylated in 86% yield with 1-bromohexane, KOH, and $\text{Na}_2\text{S}_2\text{O}_3$ in a water/toluene biphasic mixture with TBAB as a phase transfer catalyst. Ether **6** was brominated with NBS and AIBN in CCl_4 to give a 3:2 mixture of benzyl bromide to aryl bromide regioisomers. In other solvents, only the aryl bromide was formed. The two regioisomers were difficult to separate, so the mixture of isomers was subjected to an Arbusov reaction with $\text{P(OCH}_3)_3$ in refluxing PhMe to give phosphonate **7** in 47% over 2 steps. The unreacted aryl bromide is easily separated from the more polar phosphonate. Phosphonate **7** was formylated with $\text{CHCl}_2\text{OCH}_3$ and AlCl_3 in DCM in 89% yield followed by conversion to the acetal, **P-D-acetal**, with neopentylene glycol and TsOH in refluxing toluene in 97% yield.



Scheme 7. Synthesis of **P-D-acetal**.

The two phosphonate monomers for the nitrile approach were also prepared using well established chemistry. Nitrile monomer **P-A-CN** was prepared in two steps from *p*-tolunitrile in 35% yield (Scheme 8). *p*-Tolunitrile was brominated with NBS in DCE, followed by an Arbusov reaction with P(OCH₃)₃ in PhMe to give monomer **P-A-CN** in 35% yield over 2 steps. Nitrile monomer **P-D-CN** was prepared from ether **6** in 5 steps, with an overall yield of 34% (Scheme 8). Ether **6** was brominated with NBS in DCE to give bromide **9** in 69% yield, followed by lithiation with ⁿBuLi in Et₂O and quenching with DMF to give benzaldehyde **10** in 99% yield. A modified Hofmann rearrangement⁸⁰ gave benzonitrile **11** in 78% yield. Bromination with NBS in DCE, followed by an Arbusov reaction with P(OCH₃)₃ in PhMe gave nitrile monomer **P-D-CN** in 63% yield over 2 steps.



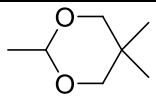
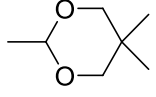
Scheme 8. Synthesis of nitrile monomers **P-A-CN** and **P-D-CN**.

2.3.2 HWE optimization

HWE couplings of nitrile-functionalized monomers gave better stereoselectivity and yields than those observed for those monomers bearing acetal-protected aldehydes. The addition of LiCl further improved stereoselectivity. Our first attempt involved the coupling between benzaldehyde **Br-D-CHO** and acetal monomer **Br-D-acetal** using KO^tBu in THF (Table 3, entry 1). The reaction gave the dimer in quantitative yield. However, ¹H NMR showed the product to

be a 2:1 mixture of the *E* and *Z* isomers, which we were unable to separate. We were perplexed at this result, given that the stereoselectivity of the HWE reaction has not been well addressed in the synthesis of OPVs,^{70, 72, 73, 76, 77} leading us to anticipate high *E* selectivity. The stereoselectivity of the HWE reaction has been well studied, and the presence of Li⁺ in the reaction mixture has been shown to increase *E* selectivity.^{81, 82} The addition of LiCl to the HWE reaction between aldehyde **Br-D-CHO** and acetal monomer **Br-D-acetal** (Table HWE, entry 2) increased the selectivity to 4:1 *E:Z* at the expense of conversion.

Table 3. HWE optimization

#	R	Additive	Yield	<i>E:Z</i> ^a
1		None	100%	2:1
2		LiCl	55% (85% BRSM)	4:1
3	H	None	98%	5:1
4	H	LiCl	60%	6:1
5	CN	None	70%	5:1
6	CN	LiCl	100%	10:1

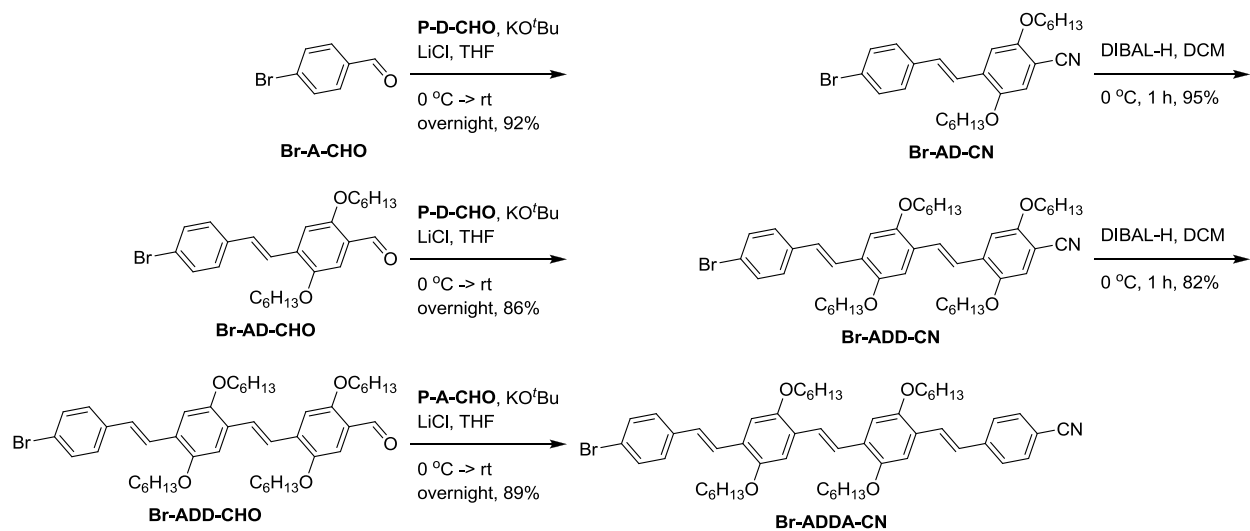
^a Estimated from ¹H NMR spectroscopy

We examined the effects of the structure of the phosphonate on the *E:Z* ratio (Table HWE). The HWE reaction of phosphonate **91** with benzaldehyde **Br-D-CHO** (entry 3) gave 5:1 *E:Z* in 98% yield. The addition of LiCl (entry 4) only marginally increased the *E:Z* ratio at the expense of yield. The HWE reaction between phosphonate **P-D-CN** and benzaldehyde **Br-D-CHO** (entry 5) also gave 5:1 *E:Z*, but with a lower yield compared to the other phosphonates.

The addition of LiCl (entry 6) increased the *E:Z* ratio to 10:1 and the yield to 100%. Based on these results, we abandoned the acetal approach and focused on the nitrile approach.

2.3.3 Oligomer synthesis by the nitrile approach

OPVs were prepared in an iterative fashion from either **Br-A-CHO** or **Br-D-CHO** by successive HWE reactions with either **P-A-CN** or **Br-D-CN** followed by reductions with DIBAL-H. For example, the synthesis **Br-ADDA-CN** (Scheme 9) began with the HWE reaction of **Br-A-CHO** and **P-D-CN** to give **Br-AD-CN** in 92% yield, followed by a DIBAL-H reduction to give **Br-AD-CHO** in 95%. The next HWE reaction with **P-D-CN** gave **Br-ADD-CN** in 86% yield, followed by DIBAL-H reduction to give **Br-ADD-CHO** in 82% yield. Finally, the HWE reaction of **Br-ADD-CHO** with **P-A-CN** gave **Br-ADDA-CN** in 89% yield. The other oligomers were synthesized similarly (Table 4). Yields were generally good to excellent. Use of 1.5 equivalents of the phosphonate monomer ensured high conversion of the aldehyde, which facilitated separation. We attribute the conspicuously low yield of **Br-AA-CN** to the limited solubility of this dimer. The tetramers were not reduced to the aldehydes as they were our desired final product in this study.



Scheme 9. Representative synthesis of OPVs - synthesis of **Br-AD-CN**, **Br-ADD-CN**, and **Br-ADDA-CN**

Table 4. Oligomers prepared by HWE oligomerization

Br-X-CHO	+ P-Y-CN	$\xrightarrow[\text{THF, 0 }^{\circ}\text{C to rt overnight}]{\text{KO}^t\text{Bu, LiCl}}$	Br-XY-CN	$\xrightarrow[\text{DCM, 0 }^{\circ}\text{C, 1h}]{\text{DIBAL-H}}$	Br-XY-CHO
Br-X-CHO	P-Y-CN		Br-XY-CN		Br-XY-CHO
Br-A-CHO	P-A-CN		Br-AA-CN (55%)		Br-AA-CHO (93%)
Br-A-CHO	P-D-CN		Br-AD-CN (92%)		Br-AD-CHO (95%)
Br-D-CHO	P-A-CN		Br-DA-CN (96%)		Br-DA-CHO (92%)
Br-D-CHO	P-D-CN		Br-DD-CN (99%)		Br-DD-CHO (94%)
Br-AA-CHO	P-D-CN		Br-AAD-CN (84%)		Br-AAD-CHO (82%)
Br-AD-CHO	P-A-CN		Br-ADA-CN (92%)		Br-ADA-CHO (81%)
Br-AD-CHO	P-D-CN		Br-ADD-CN (86%)		Br-ADD-CHO (82%)
Br-DA-CHO	P-A-CN		Br-DAA-CN (99%)		Br-DAA-CHO (91%)
Br-DA-CHO	P-D-CN		Br-DAD-CN (95%)		Br-DAD-CHO (85%)
Br-DD-CHO	P-A-CN		Br-DDA-CN (86%)		Br-DDA-CHO (90%)
Br-AAD-CHO	P-D-CN		Br-AADD-CN (97%)		—
Br-ADA-CHO	P-D-CN		Br-ADAD-CN (88%)		—
Br-ADD-CHO	P-A-CN		Br-ADDA-CN (89%)		—
Br-DAA-CHO	P-D-CN		Br-DAAD-CN (89%)		—
Br-DAD-CHO	P-A-CN		Br-DADA-CN (100%)		—
Br-DDA-CHO	P-A-CN		Br-DDAA-CN (100%)		—

2.3.4 Optical spectroscopy

We examined the effects of sequence on the optical properties of our OPVs, which are of prime importance to photovoltaic applications. Absorption spectra of the nitrile-terminated OPVs were obtained in CHCl_3 ($\sim 10^{-5}$ M), and emission spectra were obtained in CHCl_3 ($\sim 10^{-5}$ M) and as films drop cast from CHCl_3 onto quartz slides (Table 5). The absorption and emission maxima

generally increase with oligomer length, with the exception of **Br-DAAD-CN**. Within the dimer series, the absorption and emission maxima increase with increasing donor content, although **Br-AD-CN** and **Br-DA-CN** are slightly different. The trimers do not show an obvious trend in their absorption and emission maxima based on donor/acceptor content. The tetramers all have the same donor/acceptor content, so no analysis based on content is possible. The trimers and tetramers exhibit higher molar absorptivities than the dimers. The emission maxima of the films are redshifted compared to the solution values, with the conspicuous exception of **Br-DA-CN**. Full absorption and emission spectra can be found in Appendix A.

Table 5. Optical properties of the OPVs

OPV	$\lambda_{\max}^{\text{abs } a} / \text{nm}$	$\varepsilon^b / 10^3 \text{ cm}^{-1} \text{ M}^{-1}$	$\lambda_{\max}^{\text{em } a} / \text{nm}$	$\lambda_{\max}^{\text{em } c} / \text{nm}$	$\Delta_g^{\text{optd}} / \text{eV}$
Br-AA-CN	327	54.5	379	463	3.44
Br-AD-CN	316, 364	29.4, 24.9	418	443, 469	2.99
Br-DA-CN	309, 362	28.1, 29.2	450	460	2.97
Br-DD-CN	303, 380	16.9, 26.6	450	519	2.89
Br-AAD-CN	385	93.2	433, 461	507	2.86
Br-ADA-CN	334, 406	37.9, 50.2	477	514	2.65
Br-DAA-CN	383	73.2	476	497	2.84
Br-ADD-CN	329, 412	34.0, 53.8	478	524	2.63
Br-DAD-CN	396	72.4	474	504	2.77
Br-DDA-CN	333, 412	29.4, 53.9	488	522	2.62
Br-AADD-CN	360, 425	47.9, 83.7	492	547	2.55
Br-ADAD-CN	422	73.9	499	549	2.58
Br-ADDA-CN	337, 437	35.3, 78.3	511	541, 568	2.47
Br-DAAD-CN	408	93.3	485	512	2.72
Br-DADA-CN	425	89.9	492	534	2.56
Br-DDAA-CN	366, 424	41.4, 86.2	515	553	2.56

^a $\sim 10^{-5}$ M in CHCl_3 ; ^b calculated at $\lambda_{\max}^{\text{abs}}$; ^c Thin film; ^d Δ_g^{opt} determined at the onset of the absorption spectrum

The HOMO-LUMO gaps of the nitrile-terminated OPVs were estimated from the onset of absorption spectra. The HOMO-LUMO gaps decreased as oligomer length increased, with the exception of **Br-DAAD-CN**. Only the dimers exhibited variation based on composition, with the HOMO-LUMO gaps decreasing with increasing donor content.

Many of our oligomers exhibited two absorption bands, as do many donor-acceptor polymers.⁴⁸ The absorption profile (shape of the absorption spectrum) of a conjugated material will define how much of the solar spectrum can be absorbed. The absorption spectra of each series of oligomers (dimers, trimers, and tetramers) are presented below (Figures 13, 14, and 15).

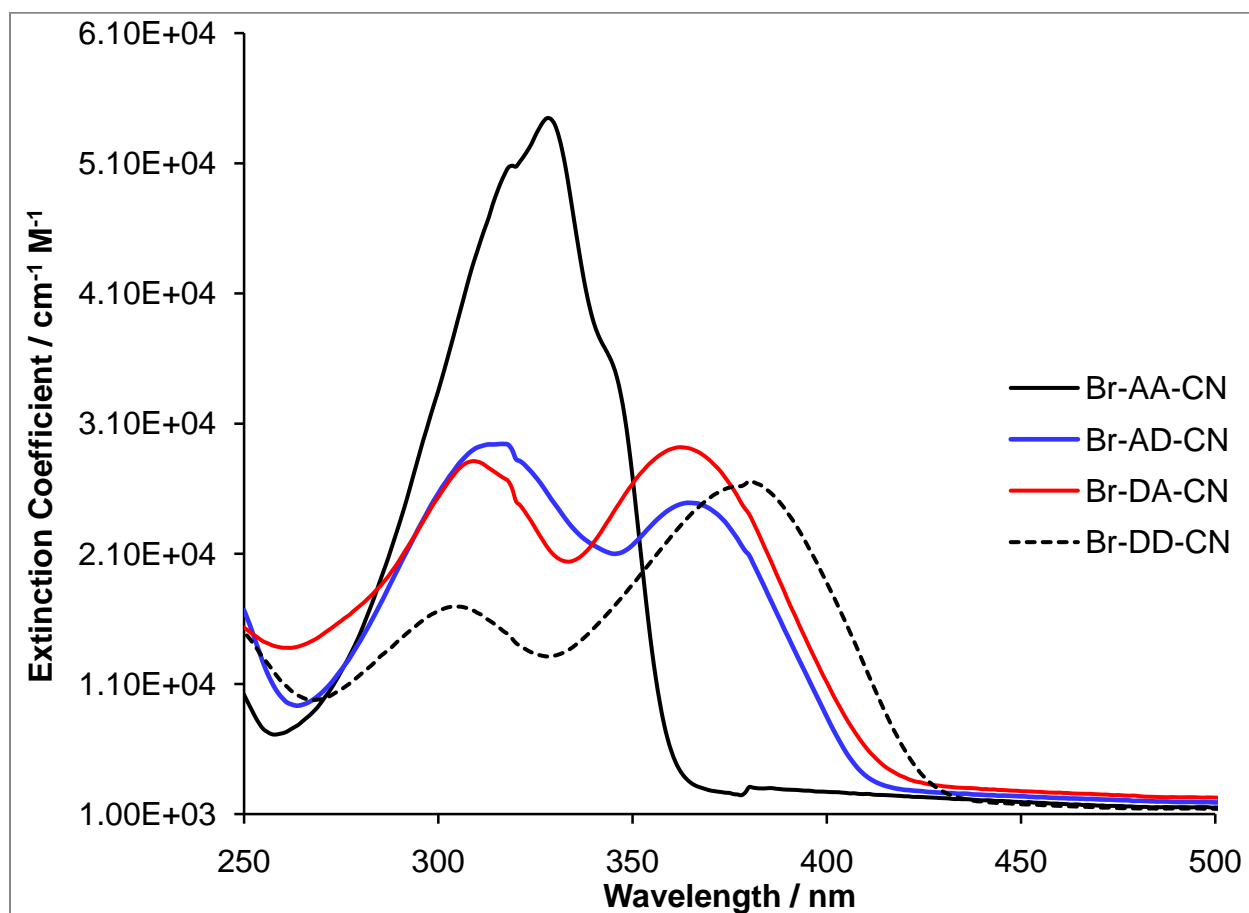


Figure 13. Overlaid absorption spectra of OPV dimers.

Three dimers show two distinct absorbance bands: **Br-AD-CN**, **Br-DA-CN**, and **Br-DD-CN** (Figure 13). The position and relative intensity of the two bands appears to be dependent on

donor composition. The bands of **Br-DD-CN** are more widely spaced than those of **Br-AD-CN** and **Br-DA-CN**. The high energy band of **Br-DD-CN** is noticeably smaller than the low energy band, while the bands of **Br-AD-CN** and **Br-DA-CN** are similar in intensity. **Br-AA-CN** exhibits only a single absorbance band, but its molar absorptivity at the absorbance maximum is twice that of the other three dimers.

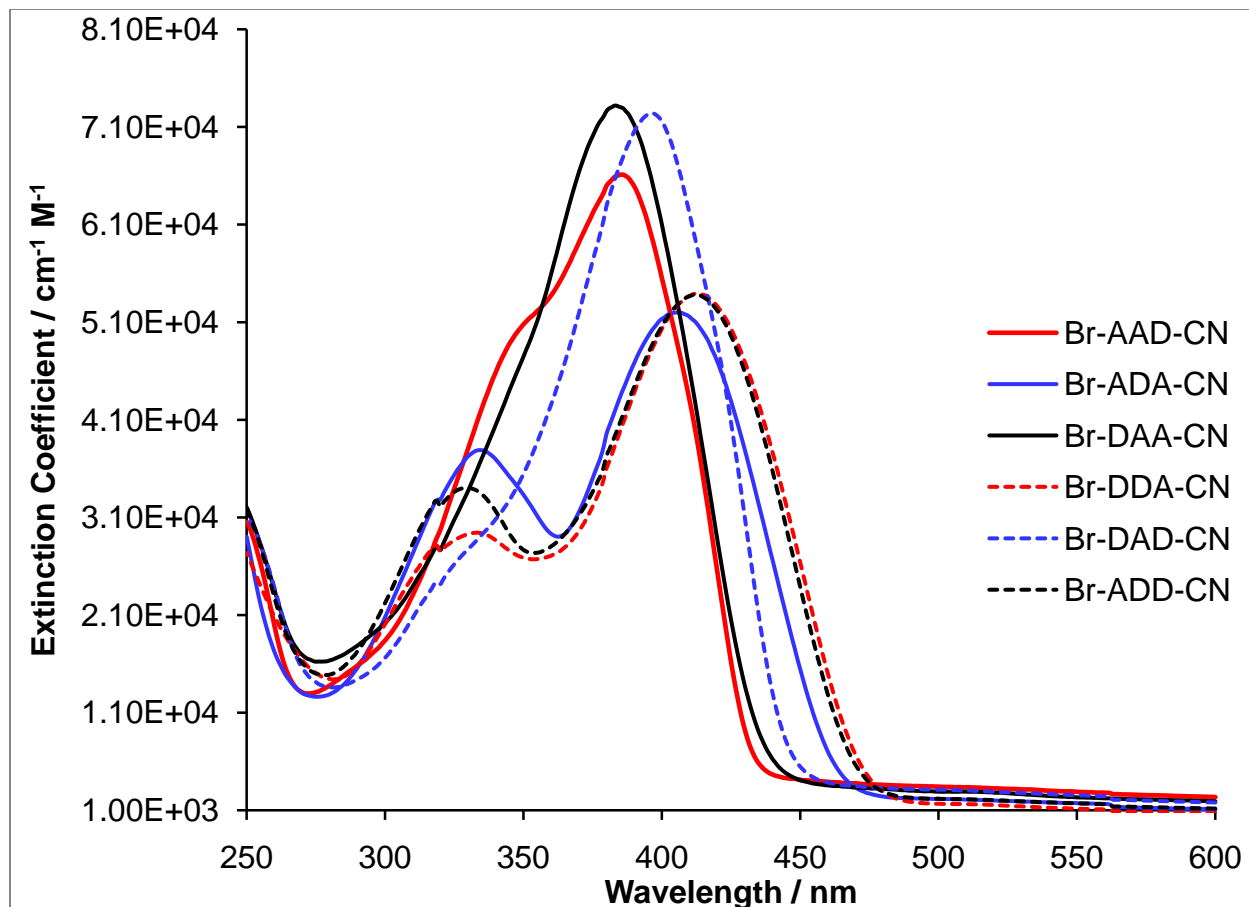


Figure 14. Overlaid absorption spectra of OPV trimers.

Three trimers show two distinct absorbance bands: **Br-ADA-CN**, **Br-DDA-CN**, and **Br-ADD-CN** (Figure 14) In all three trimers, the low energy band is larger. Two trimers, **Br-AAD-CN** and **Br-DAD-CN**, appear to have the remnants of a second absorbance band as a shoulder on the high energy side. **Br-DAA-CN** only shows one absorbance band. The three trimers without two distinct absorbance bands have higher molar absorptivities at their absorbance maxima.

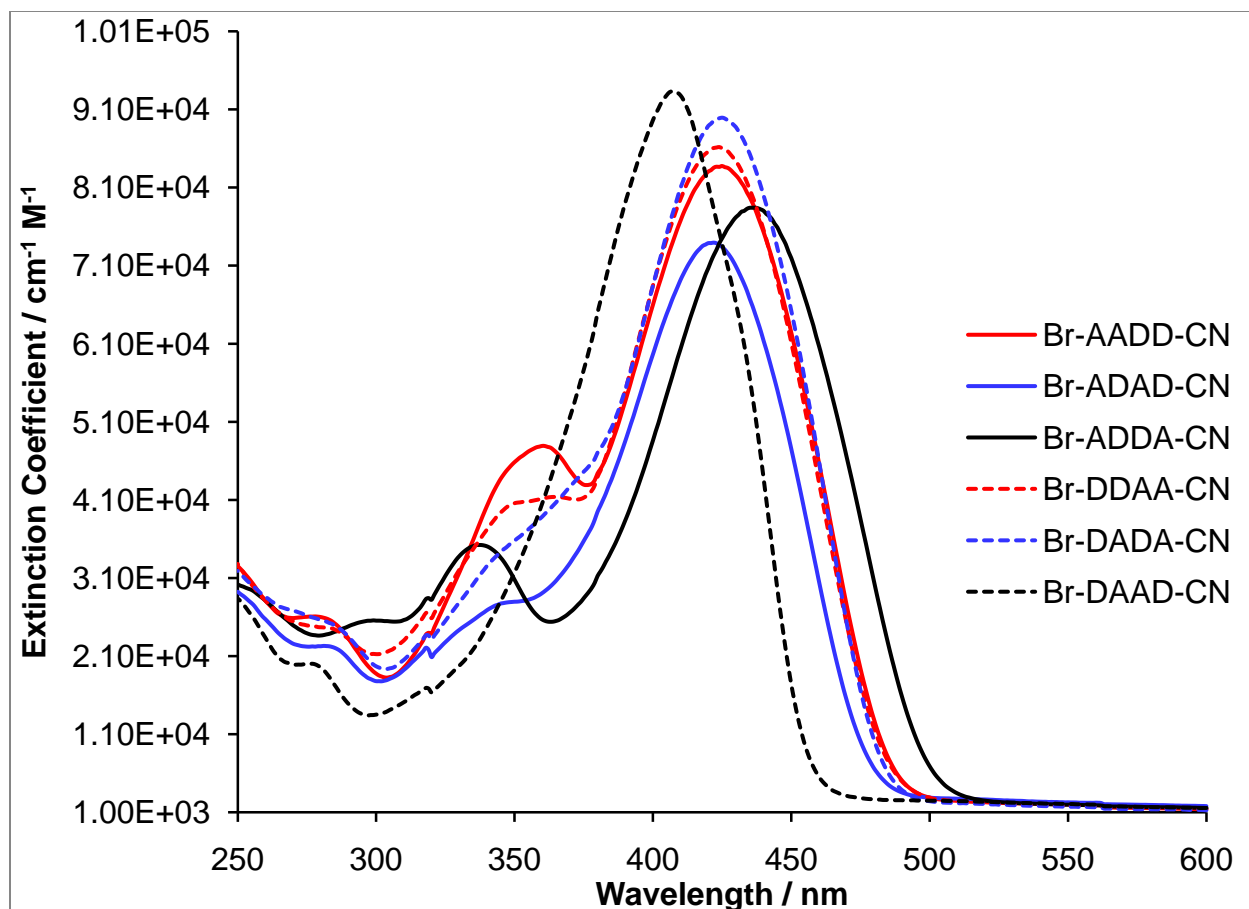


Figure 15. Overlaid absorption spectra of OPV tetramers.

Three tetramers exhibit a small second high energy absorbance band: **Br-AADD-CN**, **Br-ADDA-CN**, and **Br-DDAA-CN** (Figure 15). Two tetramers, **Br-ADAD-CN** and **Br-DADA-CN**, exhibit a small high energy shoulder. **Br-DAAD-CN** only has one distinct absorbance band. All six tetramers have similar molar absorptivities at their absorbance maxima.

2.3.5 Electrochemistry

Electrochemical data, particularly oxidation and reduction potentials, are necessary to estimate the relative HOMO and LUMO energies of the OPVs. Cyclic voltammograms (CVs) and differential pulse voltammograms (DPVs) of the nitrile-terminated OPVs were obtained in

Bu₄NPF₆/CH₃CN by Dr. Percy Calvo-Marzal. The peak oxidation and reduction potentials vs. Ag/Ag⁺ obtained from DPV are presented here for comparison to the optical spectroscopy data (Table 6). Only the distinct peaks are listed. Several oligomers, notably the tetramers, also displayed indistinct peaks that could not be assigned. The voltammograms can be found in Appendix A.

All oligomers exhibited reversible oxidation and reduction processes in their CVs over three cycles. DPVs showed distinct transitions for all oligomers except **Br-ADDA-CN**, due to its limited solubility in CH₃CN. Only the one oxidation peak is distinct for **Br-ADDA-CN**. However, a strong correlation between the optical and electrochemical HOMO-LUMO gaps allowed the estimation of the position of the first oxidation peak for **Br-ADDA-CN** at 0.63 V, and a strong correlation between first oxidation potential and calculated HOMO energies allowed for the estimation of **Br-ADDA-CN** at 0.55 eV (vide infra). All oligomers exhibited multiple oxidation processes except **Br-AA-CN**. Most oligomers exhibited two reduction transitions. **Br-DADA-CN**, **Br-ADAD-CN**, and **Br-ADDA-CN** each exhibited a single reduction transition, while **Br-DD-CN** and **Br-DDAA-CN** exhibited three reduction transitions.

Table 6. Electrochemical Properties of OPVs from DPV

OPV	E_{ox}^a / V	E_{red}^a / V	ΔE_g^{ecb} / eV
Br-AA-CN	1.36	-1.94, -2.07	3.30
Br-AD-CN	1.12, 1.26, 1.41	-1.91, -2.04	3.03
Br-DA-CN	0.95, 1.05, 1.26	-1.91, -2.04	2.86
Br-DD-CN	0.91, 1.03, 1.26, 1.41	-1.90, -1.98, -2.12	2.81
Br-AAD-CN	0.92, 1.13, 1.29, 1.41	-1.94, -2.15	2.86
Br-ADA-CN	0.74, 1.12, 1.42, 1.54	-1.91, -2.11	2.65
Br-DAA-CN	0.85, 1.08, 1.42, 1.56	-1.92, -2.16	2.77
Br-ADD-CN	0.71, 0.79, 0.91, 1.12, 1.40	-1.93, -2.04	2.64
Br-DAD-CN	0.83, 1.13, 1.28, 1.43	-1.91, -2.15	2.74
Br-DDA-CN	0.57, 0.71, 0.95, 1.13, 1.24	-1.89, -2.05	2.46
Br-AADD-CN	0.72, 1.11, 1.30	-1.77, -1.90	2.49
Br-ADAD-CN	0.63, 1.14, 1.42	-1.92	2.55
Br-ADDA-CN	(0.55 ^c), (0.63 ^d), 1.14	-1.91	(2.46 ^c)
Br-DAAD-CN	0.70, 1.18	-1.90, -2.03	2.60
Br-DADA-CN	0.65, 0.96, 1.11, 1.45	-1.89	2.54
Br-DDAA-CN	0.61, 0.81, 1.00, 1.12, 1.23	-1.80, -1.90, -2.04	2.41

^a Potential vs. Ag/Ag⁺, 240 μ M in 0.1 M Bu₄NPF₆ in CH₃CN - only distinct peaks are listed; ^b $\Delta E_g^{\text{ecb}} = -e(E_{\text{red}} - E_{\text{ox}})$;

^c Estimated based on correlation to HOMO energies calculated using DFT (B3LYP/6-31G*); ^d Estimated based on correlation to optical spectroscopy

The position of the first oxidation peaks generally decreased with oligomer length, with the exception of **Br-DDA-CN** exhibiting a lower first oxidation peak than all six tetramers. Only the dimers exhibited composition dependent behavior, with the potential of the first oxidation peak decreasing with donor content. The number of observable oxidation peaks also increased for the dimers with increasing donor content. The position and number of the oxidation peaks is not dependent on composition in the trimers and tetramers. The position of the reduction peaks

shows little variation over all 16 OPVs, with only **Br-AADD-CN** and **Br-DDAA-CN** showing a first reduction peak lower than the others.

The HOMO-LUMO gaps of the OPVs were estimated based on the energy difference between the first oxidation (HOMO) and first reduction (LUMO) peaks. The HOMO-LUMO gaps generally decrease with increasing oligomer length, with the exception of **Br-DDA-CN**, which has the second smallest optical HOMO-LUMO gap. The HOMO-LUMO gaps of the dimers decrease with increasing donor content.

2.3.6 DFT calculations

The optoelectronic properties of these OPVs were modeled using Gaussian 09 by Casey Campbell and Professor Geoff Hutchison at the University of Pittsburgh. The HOMO and LUMO energies were predicted using DFT with the B3LYP hybrid functional and the 6-31G* basis set with the Polarizable Continuum Model for acetonitrile. The results of these predictions are included for comparison (Table 7).

Table 7. Frontier orbital energy levels predicted using DFT (B3LYP/6-31G*).

OPV	E_{HOMO} / eV	E_{LUMO} / eV	$\Delta E_{\text{g}}^{\text{a}}$ / eV
Br-AA-CN	-5.914	-0.613	5.301
Br-AD-CN	-5.631	-0.580	5.051
Br-DA-CN	-5.526	-0.623	4.903
Br-DD-CN	-5.404	-0.591	4.813

Br-AAD-CN	-5.354	-1.335	4.020
Br-ADA-CN	-5.200	-1.330	3.870
Br-DAA-CN	-5.395	-1.316	4.080
Br-ADD-CN	-5.134	-1.254	3.880
Br-DAD-CN	-5.201	-1.329	3.872
Br-DDA-CN	-5.115	-1.313	3.802

Br-AADD-CN	-5.029	-1.686	3.343
Br-ADAD-CN	-5.013	-1.724	3.289
Br-ADDA-CN	-5.101	-1.650	3.451
Br-DAAD-CN	-5.164	-1.675	3.489
Br-DADA-CN	-5.063	-1.687	3.376
Br-DDAA-CN	-5.090	-1.709	3.381

$$^{\text{a}} \Delta E_{\text{g}} = E_{\text{LUMO}} - E_{\text{HOMO}}$$

2.3.7 Thermal properties

Thermal properties, most importantly melting point, are important for device performance. The thermal properties of the oligomers were investigated using differential scanning calorimetry (DSC) with a 10 °C/min scan rate (Table 8). Melting transition temperatures (T_{m} s) were noted as endotherms on the heating curves. Crystallization transition temperatures (T_{c} s) were noted as exotherms on both heating and cooling cycles. The DSC traces can be found in Appendix A.

Table 8. Thermal properties of OPVs

OPV	$T_m / ^\circ\text{C}$	$T_c^a / ^\circ\text{C}$	$T_c^b / ^\circ\text{C}$
Br-AA-CN	197.3	— ^d	151.3, 167.0
Br-AD-CN	74.7 ^c	—	—
Br-DA-CN	83.2	66.8	30.6
Br-DD-CN	96.3	—	68.8
Br-AAD-CN	104.6	—	41.6
Br-ADA-CN	184.9	—	79.5, 85.3, 92.7
Br-DAA-CN	125.1 ^c	—	—
Br-ADD-CN	114.2	81.2	43.2
Br-DAD-CN	104.5	—	77.8
Br-DDA-CN	109.2	46.0	—
Br-AADD-CN	144.0	—	113.8, 121.4
Br-ADAD-CN	122.8	85.0	41.7
Br-ADDA-CN	190.9	—	123.9
Br-DAAD-CN	119.4	81.2	—
Br-DADA-CN	93.8	75.4	—
Br-DDAA-CN	110.8, 116.3	—	57.5

^a Exothermic transition observed on second heating scan; ^b Exothermic transition observed on second cooling scan; ^c Transition observed in first scan only; ^d Not observed.

All oligomers exhibited endothermic transitions upon heating (T_m s). The symmetrical oligomers with unsubstituted units on the outsides (**Br-AA-CN**, **Br-ADA-CN**, and **Br-ADDA-CN**) have the highest melting points. In the dimers and trimers there is no clear dependence of the melting temperatures on composition.

All oligomers except **Br-AD-CN** and **Br-DAA-CN** exhibited exothermic transitions (T_c s) either upon the cooling cycles or the second heating cycles or both. If an exothermic transition was observed in both the heating and cooling cycles, the transition on the heating cycle occurred at a higher temperature than the transition on the cooling cycle. In general, the symmetric

oligomers have higher crystallization temperatures than the less symmetric oligomers. The dimers and trimers do not exhibit any clear dependence of the crystallization temperature on composition.

2.4 DISCUSSION

2.4.1 Optoelectronic properties

The optoelectronic properties of the OPVs, which are of primary importance for photovoltaic applications, are sequence dependent. In general having two adjacent donors contributes to the oligomers exhibiting low energy absorption and emission maxima, early first oxidation potentials, and smaller HOMO-LUMO gaps. Having two adjacent acceptors leads to higher energy absorption and emission maxima, later first oxidation potentials, and larger HOMO-LUMO gaps, although this effect can be attenuated or negated if there are also two adjacent donors in a tetramer. The oligomers with alternating sequences tend to have intermediate properties. In the pairs of dissymmetric oligomers with reverse sequence (e.g. **Br-DAA-CN** and **Br-AAD-CN**), the oligomer which has the sequence beginning with the donor tends to have lower energy absorption and emission maxima, earlier first oxidation potentials, and smaller HOMO-LUMO gaps than the oligomer with an acceptor first sequence. These principles suggest that longer oligomers with optimal properties could be chosen by design, rather than selected empirically after exhaustive synthesis.

Before discussing the properties in detail, we need to define two relationships between sequences. Two oligomers with *reverse* sequences are a pair of oligomers which contain the

same content of donors and acceptors but in exactly reverse order, e.g. **Br-DDA-CN** and **Br-ADD-CN**. Two oligomers with *inverse* sequences are a pair of oligomers in which each acceptor in the sequence is systematically switched with a donor and each donor switched with an acceptor, e.g. **Br-DDA-CN** and **Br-AAD-CN**. Symmetric oligomers, such as **Br-ADA-CN**, are their own reverse. For the even oligomers, the inverse and reverse sequences may be identical, e.g. **Br-ADAD-CN** and **Br-DADA-CN** are both inverse and reverse sequences.

2.4.1.1 Sequence dependence of optoelectronic properties

The absorption and emission maxima and the first oxidation potentials are sequence dependent within each series of OPVs. Selected data from Tables 5 and 6 have been reordered in Table 9 to highlight the sequence dependent trends. There is some dependence of these properties on oligomer length and donor content, but significant overlap in the ranges observed for these properties, especially between the trimers and tetramers and between the two sets of trimers, (Figures 16 and 17) indicates that oligomer length and content are not the sole predictors of the properties of OPVs. Indeed, the range of optoelectronic properties exhibited by the tetramers (absorption maxima: 29 nm; solution emission maxima: 30 nm; film emission maxima: 41 nm; and first oxidation potential: 0.17 V) clearly demonstrates that sequence is important. Conversely, the first reduction potentials show little variation with oligomer length, donor content, or sequence. The first reduction potentials of all 16 OPVs fall within a 0.17 V range, with the first reduction potentials of all but two OPVs falling in a 0.05 V range between -1.89 V and -1.94 V.

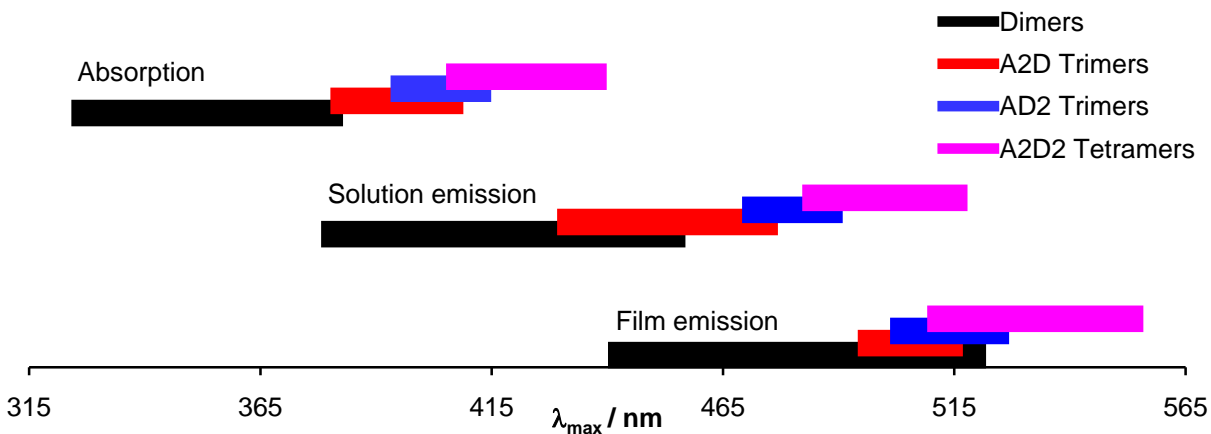


Figure 16. Ranges of λ_{\max} data from optical spectroscopy.

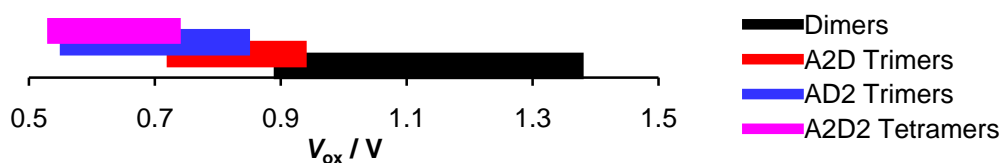


Figure 17. Ranges of the first oxidation potential of the OPVs.

The optoelectronic properties of the dimers depend on both sequence and donor-acceptor content (Table 9, earlier optical and electrochemical data tabulated together to facilitate comparison). In general, the first oxidation potentials decrease and the first reduction potentials and absorption and emission maxima increase with increasing donor content. The differences between **Br-AD-CN** and **Br-DA-CN** highlight the sequence dependence of certain properties. **Br-DA-CN** exhibits a higher emission maximum and an earlier first oxidation peak than **Br-AD-CN**. The first reduction potentials and absorption maxima are not sequence dependent for the dimers. The small difference in absorption maxima between **Br-DA-CN** and **Br-AD-CN** is attributable to the error in the measurement.

Table 9. Optoelectronic properties of the OPVs ordered by increasing absorption maximum and sorted by oligomer length

OPV	$\lambda_{\max}^{\text{abs}}$ ^a / nm	$\lambda_{\max}^{\text{em}}$ ^b / nm	$\lambda_{\max}^{\text{em}}$ ^c / nm	E_{ox} ^d / V	E_{red} ^e / V
Br-AA-CN	327	379	463	1.36	-1.94
Br-DA-CN	362	450	460	0.95	-1.91
Br-AD-CN	364	418	443	1.12	-1.91
Br-DD-CN	380	450	519	0.91	-1.90

Br-DAA-CN	383	476	507	0.85	-1.92
Br-AAD-CN	385	433	497	0.92	-1.94
Br-DAD-CN	396	474	504	0.83	-1.91
Br-ADA-CN	406	477	514	0.74	-1.91
Br-ADD-CN	412	478	522	0.71	-1.93
Br-DDA-CN	412	488	524	0.57	-1.89

Br-DAAD-CN	408	485	512	0.70	-1.90
Br-ADAD-CN	422	499	549	0.63	-1.92
Br-DDAA-CN	424	515	553	0.61	-1.80
Br-DADA-CN	425	492	534	0.65	-1.89
Br-AADD-CN	425	492	547	0.72	-1.77
Br-ADDA-CN	437	511	541	(0.55) ^f	-1.91

^a Lower energy absorption band; ^d (~10⁻⁵ M in CHCl₃); ^c thin film; ^d First oxidation peak; ^e First reduction peak; ^f Estimated based on correlation to HOMO energies calculated by DFT (B3LYP/613G*)

The sequence dependence of the optoelectronic properties is more evident in the trimer series (Table 9). The oligomers with dissymmetric sequences do exhibit properties that vary with donor-acceptor content. For example, **Br-ADD-CN** and **Br-DDA-CN** exhibit higher absorption and emission maxima and lower first oxidation peaks than **Br-AAD-CN** and **Br-DAA-CN**. However, this dependence on content is reversed in the two OPVs with symmetric sequences: **Br-ADA-CN** has a higher absorption maximum and a lower first oxidation peak than **Br-DAD-CN**. The pairs of dissymmetric trimers that have identical donor-acceptor content exhibit do

show sequence dependence in some properties. Trimers **Br-DAA-CN** and **Br-DDA-CN** have earlier first oxidation potentials and higher emission maxima than their reverse sequences **Br-AAD-CN** and **Br-ADD-CN**, respectively. However, there is no significant difference in absorption maximum between **Br-AAD-CN** and **Br-DAA-CN** or between **Br-ADD-CN** and **Br-DDA-CN**.

All variation in the optoelectronic properties of the tetramers is dependent on sequence since all six tetramers are constitutionally isomeric, i.e. there is no variation of donor-acceptor content. The greatest sequence effects are evident for the tetramers with symmetric sequences. Similar to the trend observed for the trimers, the symmetric sequence with acceptors on the outside (**Br-ADDA-CN**) has the higher absorption and emission maxima and the earlier first oxidation peak than the inverse sequence with donors on the outside (**Br-DAAD-CN**). However, the dissymmetric sequences only show significant sequence dependence in the first reduction potentials, a property that has generally been independent of sequence. The two blocky sequences **Br-AADD-CN** and **Br-DDAA-CN** first oxidation potentials at -1.77 and -1.80 V, respectively, when all other OPVs have first reduction potentials between -1.89 V and -1.94 V. There is no significant difference in the absorption maxima of the four dissymmetric sequences: **Br-ADAD-CN**, **Br-DADA-CN**, **Br-AADD-CN**, and **Br-DDAA-CN**. These four OPVs also have similar solution emission maxima, except for **Br-DDAA-CN**, which has a higher maximum than the others. The film emission maxima vary, but there is no pattern to the variation. **Br-ADAD-CN** has a higher film emission maximum than **Br-DADA-CN**, but **Br-AADD-CN** has a lower film emission maximum than **Br-DDAA-CN**. The first oxidation potentials are also similar, with the exception of **Br-AADD-CN** having a noticeably later first oxidation.

While donor-acceptor content matters, the position of the donors and acceptors in the sequence is equally important. Sequences with two adjacent donors (e.g. **Br-ADDA-CN**, **Br-ADD-CN**, and **Br-DDA-CN**) tend to have higher absorption and emission maxima and earlier first oxidation potentials. Sequences with two adjacent acceptors (e.g. **Br-DAAD-CN**, **Br-AAD-CN**, and **Br-DAA-CN**) tend to have lower absorption and emission maxima. Alternating sequences (e.g. **Br-ADAD-CN**, **Br-DADA-CN**, **Br-ADA-CN**, and **Br-DAD-CN**) and those sequences containing both two adjacent donors and two adjacent acceptors (**Br-AADD-CN**, and **Br-DDAA-CN**) have intermediate properties with a few exceptions. For the dimers and trimers, the donor-first dissymmetric sequences exhibited higher emission maxima and earlier first oxidation potentials than the corresponding acceptor-first reverse sequences. This trend was not observed for the tetramers.

2.4.1.2 Sequence dependence of HOMO-LUMO gap

The HOMO-LUMO gaps, ΔE_{gs} , of our OPVs are sequence dependent. The optical and electrochemical ΔE_{gs} from tables 5 and 6 have been reordered in Table 10 to highlight the sequence dependent trends. The electrochemical HOMO-LUMO gaps of the oligomers correlate strongly with the optical HOMO-LUMO gaps ($R^2 = 0.925$, Figure 18). From this correlation, the electrochemical ΔE_g of **Br-ADDA-CN** (which could not be assigned due to indistinct oxidation peaks) is estimated to be 2.54 eV, which would place the first oxidation peak at 0.63 V.

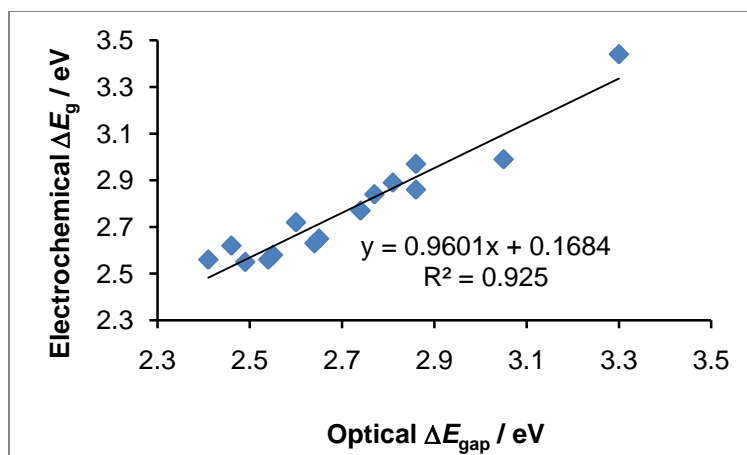


Figure 18. Correlation of optical and electrochemical HOMO-LUMO gaps of the oligomers.

The HOMO-LUMO gaps show moderate sequence dependence, with the observed trends mirroring those for the dependence of the absorption and emission maxima and first oxidation potentials on sequence (Table 10). Donor content is important. In each series, the smallest ΔE_g s were observed for the OPVs containing two adjacent donors and lacking two adjacent acceptors (**Br-DD-CN**, **Br-ADD-CN**, **Br-DDA-CN**, and **Br-ADDA-CN**). The symmetric trimers disrupt the donor-dependent trend, with **Br-ADA-CN** ΔE_g than **Br-DAD-CN**. The OPVs with the largest ΔE_g s in each series were those sequences containing two acceptors without two adjacent donors (**Br-AA-CN**, **Br-AAD-CN**, **Br-DAA-CN**, and **Br-DAAD-CN**). The alternating sequences (**Br-AD-CN**, **Br-DA-CN**, **Br-ADA-CN**, **Br-DAD-CN**, **Br-ADAD-CN**, and **Br-DADA-CN**) and the blocky tetramers containing both two adjacent donors and two adjacent acceptors (**Br-AADD-CN** and **Br-DDAA-CN**) displayed intermediate ΔE_g s. It is worth noting that the range of ΔE_g s for the tetramers (optical: 0.25 eV; electrochemical: 0.19 eV) is comparable to the difference in ΔE_g between the polymers exhibiting the best and worst power conversion efficiencies in several recent reports.^{49, 68, 71}

Table 10. ΔE_g data ordered by decreasing optical ΔE_g and sorted by oligomer length

Oligomer	$\Delta_g^{\text{opta}} / \text{eV}$	$\Delta_g^{\text{ecb}} / \text{eV}$
Br-AA-CN	3.44	3.30
Br-AD-CN	2.99	3.03
Br-DA-CN	2.97	2.86
Br-DD-CN	2.89	2.81

Br-AAD-CN	2.86	2.86
Br-DAA-CN	2.84	2.77
Br-DAD-CN	2.77	2.74
Br-ADA-CN	2.65	2.65
Br-ADD-CN	2.63	2.64
Br-DDA-CN	2.62	2.46

Br-DAAD-CN	2.72	2.60
Br-ADAD-CN	2.58	2.55
Br-DADA-CN	2.56	2.54
Br-DDAA-CN	2.56	2.41
Br-AADD-CN	2.55	2.49
Br-ADDA-CN	2.47	(2.46) ^c

^a Δ_g^{opt} determined at the onset of the absorption. ^b $\Delta_g^{\text{ec}} = -e(\epsilon_{\text{red}} - \epsilon_{\text{ox}})$; ^c Estimated based on correlation to HOMO energies calculated using DFT (B3LYP/6-31G*).

In general, the optical and electrochemical HOMO-LUMO gaps were similar. The dissymmetric sequences, however, display interesting sequence dependent differences between their optical and electrochemical ΔE_g s. The optical ΔE_g s for each dissymmetric sequence and its reverse sequence are with 0.02 eV of each other. However, with one exception, the oligomer with the donor-first sequence has a lower electrochemical ΔE_g by 70-160 meV than its optical ΔE_g , while the acceptor-first reverse sequence has similar optical and electrochemical ΔE_g s. Only **Br-DADA-CN** does not show this decrease from its optical ΔE_g to its electrochemical ΔE_g . The

difference in behavior for the optical and electrochemical ΔE_{gs} is likely dependent on the solvent: optical spectroscopy was performed in chloroform and electrochemistry was performed in acetonitrile.

2.4.1.3 Design principles and predictions

The sequence dependent trends suggest two principles for the design of OPVs desired optoelectronic properties. First, for series of oligomers with identical donor-acceptor content, the lowest ΔE_{gs} and highest absorption and emission maxima occur in the sequences that maximize adjacent donors while minimizing adjacent acceptors. For example, we predict that two hexamers, **Br-AADDDA-CN** and **Br-ADDDAA-CN**, out of the set of hexamers containing three donors and three acceptors will likely exhibit the lowest ΔE_{gs} and the highest absorption and emission maxima. The two sequences that maximize adjacent acceptors while minimizing adjacent donors, **Br-DDAAAD-CN** and **Br-DAAADD-CN** should have the highest ΔE_{gs} and the lowest absorption and emission maxima. The blocky hexamers (**Br-AAADDD-CN** and **Br-DDDAAA-CN**), the perfectly alternating hexamers (**Br-ADADAD-CN** and **Br-DADADA-CN**), and the pseudorandom hexamers (**Br-AADADD-CN**, **Br-AADDAD-CN**, **Br-ADADDA-CN**, **Br-ADDAAD-CN**, **Br-ADDADA-CN**, **Br-DDADAA-CN**, **Br-DDAADA-CN**, **Br-DADAAD-CN**, **Br-DAADDA-CN**, and **Br-DAADAD-CN**) will have intermediate properties.

Second, increasing the adjacent donor content leads to lower HOMO-LUMO gaps and first oxidation potentials and higher absorption and emission maxima. For example, we predict that the two tetramers with three adjacent donors and one acceptor (**Br-ADDD-CN** and **Br-DDDA-CN**) will have lower ΔE_{gs} and higher absorption and emission maxima than the six tetramers we have already prepared. These two molecules should have similar properties,

although **Br-DDDA-CN** may have a lower electrochemical ΔE_g and a higher emission maximum than **Br-ADDD-CN**. Similarly, we predict that the two tetramers with three adjacent acceptors and one donor (**Br-AAAD-CN** and **Br-DAAA-CN**) will have higher ΔE_g s and lower absorption and emission maxima than the six tetramers we have prepared.

2.4.1.4 Comparison of experimental and theoretical data

Successful modeling of the frontier orbital energies of sequenced materials could guide synthetic efforts, especially if the model correlates well to empirical trends. Our OPVs display strong correlation between the first oxidation potentials (electrochemical HOMO) and the HOMO energies predicted by DFT (Figure 19, top left). The strong correlation between predicted HOMO energies and first oxidation potentials was used to estimate the first oxidation potential of **Br-ADDA-CN** (which was indistinct). The first oxidation potential of **Br-ADDA-CN** was thus estimated as 0.55 V.

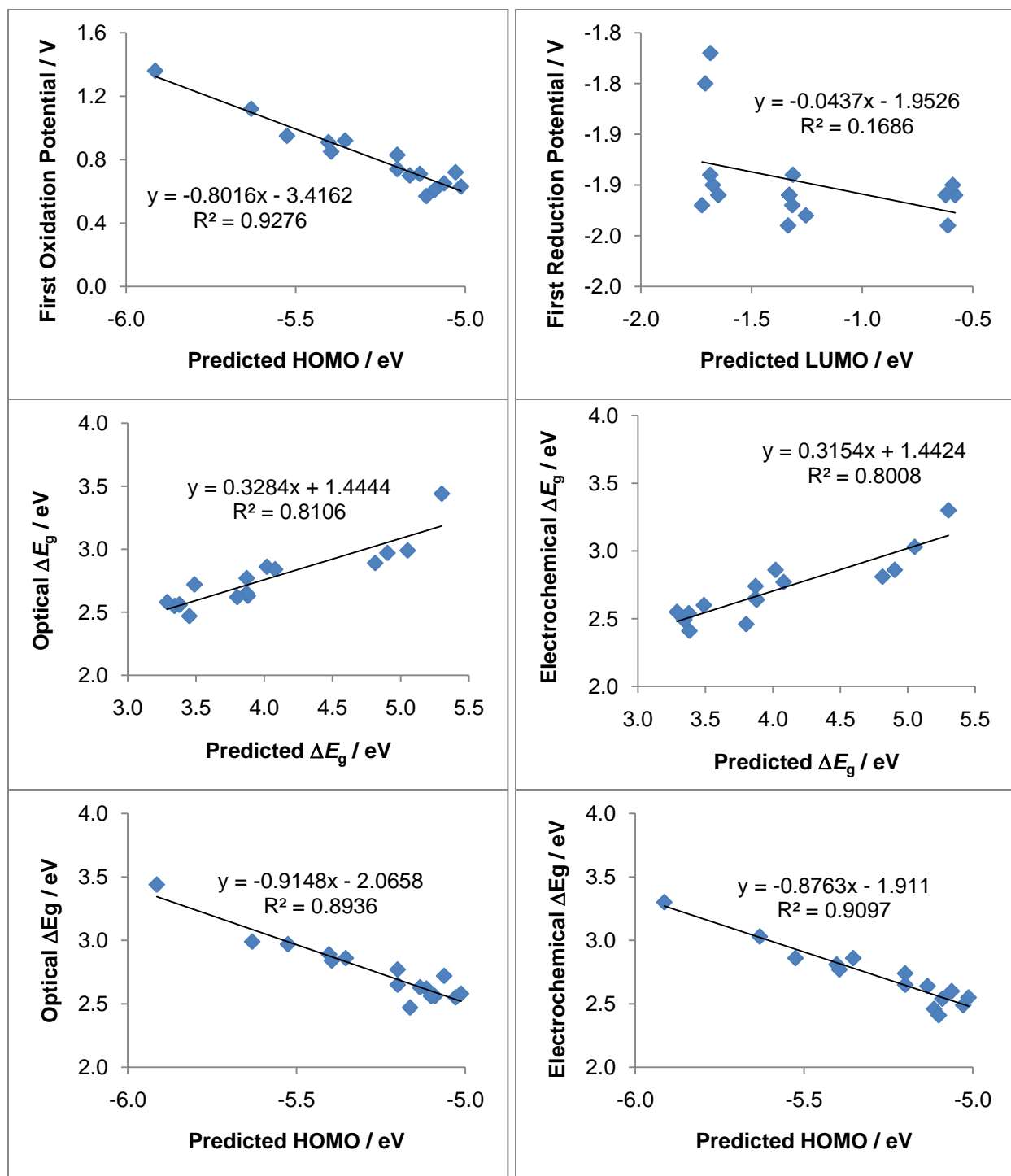


Figure 19. Correlations between predicted and experimental properties. Top left: correlation between predicted HOMO energies and first oxidation potentials. Top right: correlation between predicted LUMO energies and first reduction potentials. Middle left: correlation between predicted ΔE_g and optical ΔE_g . Middle right: correlation between predicted ΔE_g and electrochemical ΔE_g . Bottom left: correlation between predicted HOMO energies and optical ΔE_g . Bottom right: Correlation between predicted HOMO energies and electrochemical ΔE_g .

There is no correlation between first reduction potential (electrochemical LUMO) and predicted LUMO energies (Figure 19, top right). The predicted LUMO energies show a larger variation than is observed. This lack of correlation weakens the correlation between the predicted and experimental ΔE_{gs} (Figure 19, middle). However, the experimental ΔE_{gs} depend mostly on the first oxidation potential, since the first reduction potentials do not vary significantly. Thus, predicted HOMO energies have a stronger correlation with the experimental ΔE_{gs} than the predicted ΔE_{gs} (Figure 19, bottom).

2.4.1.5 Absorption Profile

Several of our OPVs exhibit two absorption bands. Beaujuge, *et al*, have also examined the dual absorption band phenomenon in donor-acceptor polymers with distinct sequences.⁴⁸ They found that increasing the donor content caused the two bands to coalesce: the lower energy band decreased in intensity, the high energy band increased in intensity, and the two bands moved closer together. Beaujuge, *et al*, discuss three possible explanations for the behavior of the dual absorption bands in donor-acceptor polymers: the presence of separate donor-rich and acceptor-rich chromophores on the chain, the formation of intramolecular charge-transfer states between the donors and acceptors, and the presence of the low-lying acceptor LUMO between the valence and conductance bands of the conjugated polymer. Decreasing population of the acceptor LUMO, and thus the low-lying state (be it a localized acceptor LUMO, charge-transfer state, etc.), as donor content increases leads to the decreasing intensity of the low energy band and the coalescence of the two bands.

For our OPVs, the presence or absence of two absorption bands, and the relative intensities of the bands, is strongly dependent on sequence and not on donor-acceptor content.

This behavior is especially noticeable in the trimers (Figure 20). Three trimers (**Br-ADA-CN**, **Br-ADD-CN**, and **Br-DDA-CN**) exhibit two absorption bands, and **Br-AAD-CN** exhibits the remnants of a high energy band as a shoulder. The relative intensity of the high energy band increases with *decreasing* donor content: **Br-DDA-CN** to **Br-ADD-CN** to **Br-ADA-CN** to **Br-AAD-CN**. Again, in the dimers, the most donor-rich sequence (**Br-DD-CN**) has the least intense high energy band, while in **Br-AD-CN**, the intensity of the high energy band exceeds that of the low energy band. For the tetramers, the order of increasing intensity of the high energy band or shoulder (**Br-ADAD-CN**, **Br-DADA-CN**, **Br-ADDA-CN**, **Br-DDAA-CN**, and **Br-AADD-CN**) is entirely sequence dependent.

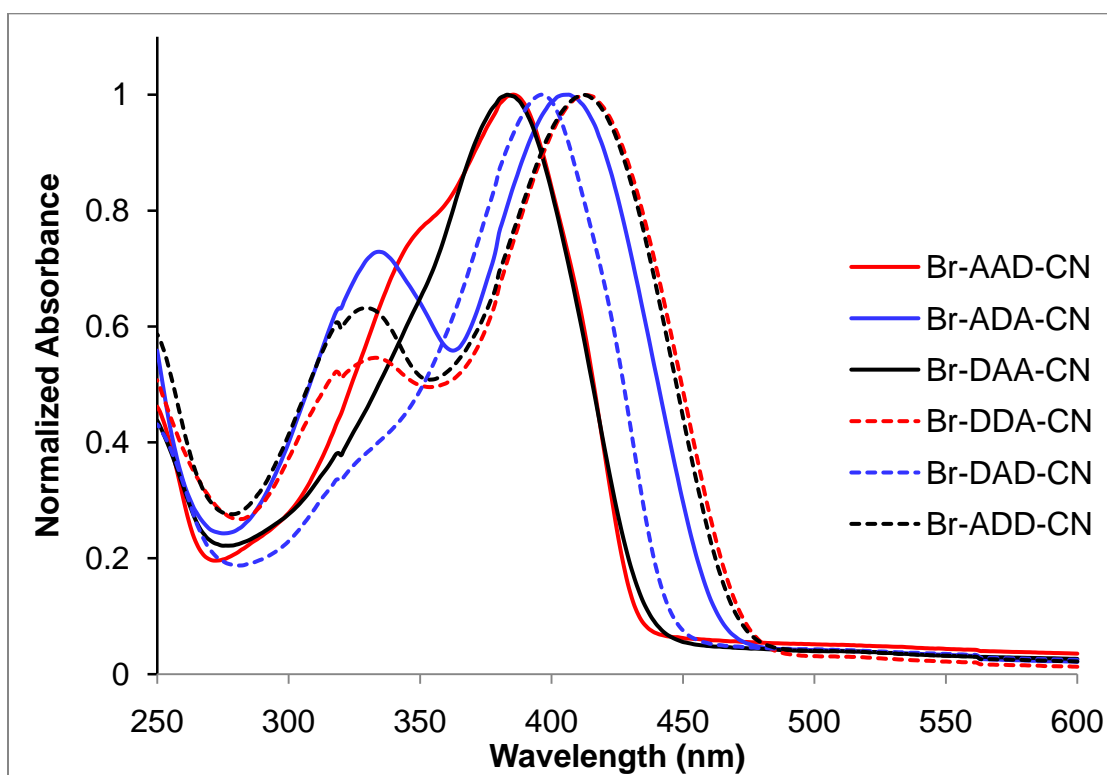


Figure 20. Normalized absorption spectra of the OPV trimers.

The charge transfer explanation is the most reasonable of the explanations offered by Beaujuge because it is the only explanation that does not rely on localized orbitals. Given that our OPVs contain weak acceptors, it is also unlikely that the LUMO is localized while the

HOMO is delocalized. Also, since we are studying short, well-defined oligomers, it is unlikely that the electronics of the donors and acceptors are isolated enough to create multiple chromophores in molecules with just two, three, or four repeat units. Beaujuge suggests that strong acceptors are necessary for the formation of a charge transfer state. However, the promotion of an electron from the HOMO to the LUMO of any conjugated molecule necessarily creates charge separation: an extra electron in the LUMO (negative) and a hole in the HOMO (positive). We hypothesize that the presence of two absorption bands derives from the accessibility of two different charge-separated excited states, which is controlled by sequence.

Predictions

2.4.2 Thermal properties

The thermal properties of the OPVS are also sequence dependent, but there are fewer predictive principles that can be derived from this variation. A high melting point is beneficial for photovoltaic applications so that the material is solid over a large temperature range. Generally, the symmetric sequences with acceptors on the outside have the highest melting points on heating and crystallization points on cooling. There are no other significant patterns to the data. However, the significant variation in the melting and crystallization transitions within each set of oligomers demonstrates that sequence is important. The data from Table 8 has been reordered to list the OPVs in order of increasing melting point by oligomer length (Table 11).

Table 11. Thermal properties of the OPVs ordered by increasing melting point and sorted by oligomer length.

OPV	$T_m / ^\circ\text{C}$	$T_c^a / ^\circ\text{C}$	$T_c^b / ^\circ\text{C}$
Br-AD-CN	74.7 ^c	— ^d	—
Br-DA-CN	83.2	66.8	30.6
Br-DD-CN	96.3	—	68.8
Br-AA-CN	197.3	—	151.3, 167.0
Br-DAD-CN	104.5	—	77.8
Br-AAD-CN	104.6	—	41.6
Br-DDA-CN	109.2	46.0	—
Br-ADD-CN	114.2	81.2	43.2
Br-DAA-CN	125.1 ^c	—	—
Br-ADA-CN	184.9	—	79.5, 85.3, 92.7
Br-DADA-CN	93.8	75.4	—
Br-DDAA-CN	110.8, 116.3	—	57.5
Br-DAAD-CN	119.4	81.2	—
Br-ADAD-CN	122.8	85.0	41.7
Br-AADD-CN	144.0	—	113.8, 121.4
Br-ADDA-CN	190.9	—	123.9

^a Exothermic transition observed on second heating scan; ^b Exothermic transition observed on second cooling scan; ^c Transition observed in first scan only; ^d Not observed.

Figure 21 shows the range of melting points as a function of oligomer composition and length. From the graph, it is clear that there can be exceptional variation in the melting points of oligomers with the same composition, but different sequence. This effect is pronounced in the A_2D trimers, with a melting point span of 80 °C, and in the A_2D_2 tetramers, with a melting point span of 97 °C. The AD_2 trimers, with a melting point span of only 10 °C, do not show any sequence-specific behavior in their melting points. Other than the symmetric oligomers with acceptors on the outside (**Br-AA-CN**, **Br-ADA-CN**, **Br-ADDA-CN**) having the highest melting points, there is no obvious correlation between sequence and melting point.

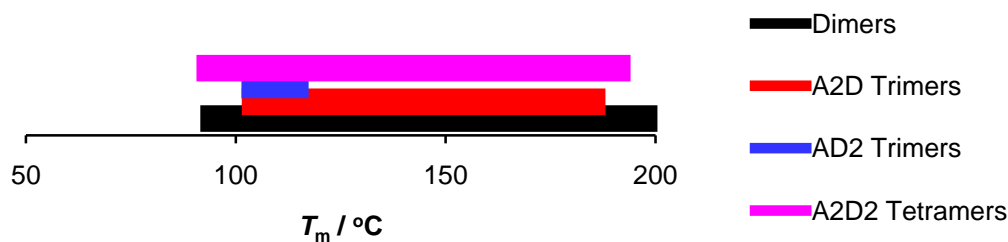


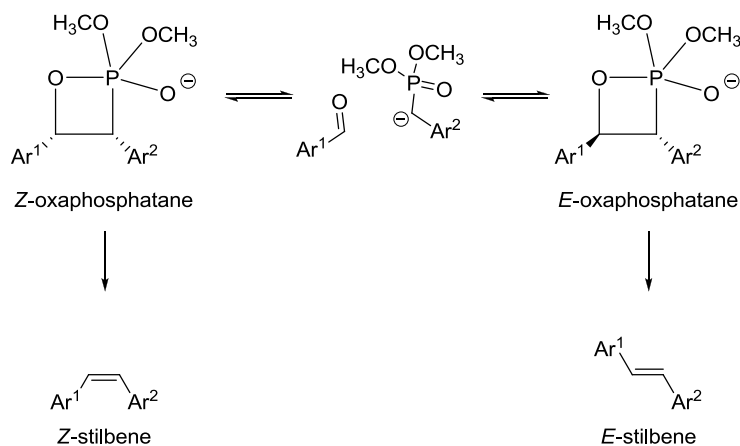
Figure 21. Range of melting points as a function of oligomer composition and length.

The crystallization data show some sequence dependence in a predictive way. In particular, the presence of a crystallization transition on heating seems to be sequence dependent. The trimers that exhibit a crystallization transition upon heating both contain two adjacent donors. However, the three tetramers that exhibit a crystallization morphology change upon heating are those three that lack two adjacent donors. Other than the symmetric oligomers with acceptors on the outside (**Br-AA-CN**, **Br-ADA-CN**, **Br-ADDA-CN**) exhibiting the highest crystallization points on cooling, there is no pattern to the crystallization transitions on cooling.

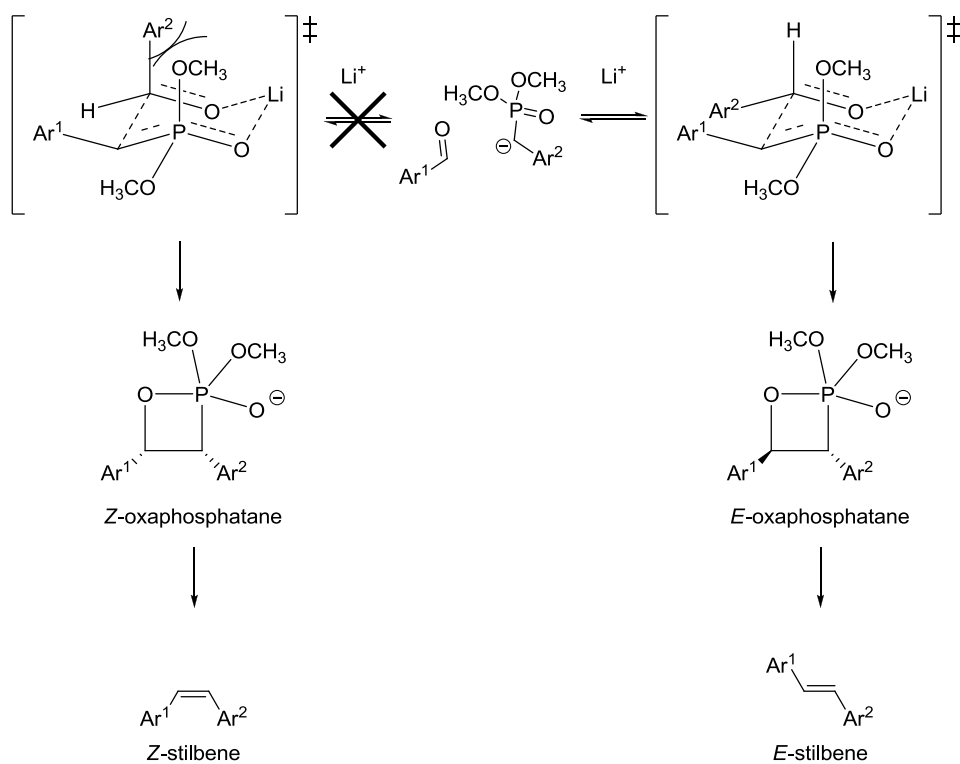
2.4.3 HWE optimization

Stereoselectivity in the HWE relies on equilibration between the *E* and *Z* oxaphosphatanes (Scheme 10). We believe that acetal group in monomer **P-D-acetal**, which is slightly electron-donating, increases the nucleophilicity of the phosphonate anion by destabilizing the negative charge, which increases the rate of the addition step and makes the addition less reversible. Equilibrium is likely not established before the reaction proceeds to the irreversible elimination step, limiting the selectivity. The electron-withdrawing nitrile stabilizes the phosphonate anion, decreasing nucleophilicity and the rate of addition, while increasing the reversibility of the addition, all of which favor the formation of equilibrium and the formation of the thermodynamically more stable *E* product. Despite the reported positive influence of Li^+ on

the stereoselectivity, a mechanistic explanation has not been proposed.^{81, 82} We hypothesize that Li^+ promotes a favorable arrangement leading to the *E* oxaphosphatane, similar to the Zimmerman-Traxler transition state proposed for the aldol reaction (Scheme 11).



Scheme 10. Pathways leading to *Z* and *E* stilbenes in a HWE reaction.



Scheme 11. Proposed role of Li^+ in the stereoselectivity of the HWE reaction.

2.5 CONCLUSIONS

The optoelectronic properties of three series (dimers, trimers, and tetramers) of *oligo*(phenylene-vinylenes) OPVs depend on the sequence of donor and acceptor units. Increased donor content is important, and the best sequences (highest absorption and emission maxima, earliest first oxidation potentials, and smallest HOMO-LUMO gaps) maximize the number of adjacent donors while minimizing adjacent acceptors. Sequences with low donor content or donors with acceptors spaced between them exhibited less desirable properties. The observed trends suggest design principles that could be utilized to prepare specific longer oligomers with attractive properties. In particular, the emission maxima and first oxidation potentials, of these OPVs show strong dependence on sequence. The absorption maxima and HOMO-LUMO gaps show moderate sequence dependence, and the first reduction potentials show minimal sequence dependence. The thermal properties of these OPVs are also sequence dependent. These oligomers can be rapidly prepared using a simple and robust homologation centered on Horner-Wadsworth-Emmons (HWE) reactions.

2.6 EXPERIMENTAL SECTION

2.6.1 General methods

Materials. Anhydrous DMF, ⁿBuLi (1.6 M in hexanes), and DIBAL-H (1.0 M in hexanes) were purchased from Aldrich and dispensed using air-sensitive techniques. Benzoyl peroxide, AIBN, and NBS were stored at -20 °C. KO^tBu was stored in a desiccator over anhydrous CaSO₄. LiCl

was dried at 120 °C for at least 24 h. Anhydrous diethyl ether for lithiation reactions was opened immediately prior to use. When necessary, THF was dried by passing over a column of activated alumina. Reagent grade THF was used for most reactions; notably the HWE reactions used reagent grade THF. DCM for reactions was dried by refluxing with CaH₂. All other reagents and solvents were used as received. Column chromatography was carried out on standard grade silica gel (60 Å pore size, 40-63 µm particle size), which was purchased and used as received. Hexanes, dichloromethane, and ethyl acetate used for column chromatography were purchased and used as received.

NMR Spectroscopy. ¹H (300 and 400 MHz) and ¹³C (75 and 100 MHz) NMR spectra were recorded on Bruker spectrometers. Chemical shifts were referenced to residual ¹H or ¹³C signals in deuterated solvents (7.27 and 77.0 ppm, respectively, for CHCl₃ and 5.32 and 54.0 ppm, respectively, for CH₂Cl₂).

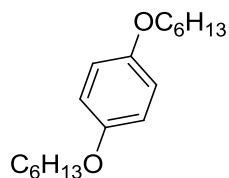
Mass Spectrometry. HRMS were recorded on EI-quadrupole or ESI-TOF instruments in the Mass Spectrometry Facility of the University of Pittsburgh.

Optical Spectroscopy. UV/VIS absorption spectra were recorded in CHCl₃ on a Perkin Elmer Lambda 9 UV/VIS/NIR spectrometer. Solution (CHCl₃) and film emission spectra were recorded on a Varian Cary Eclipse fluorimeter. Films were drop cast on quartz slides from CHCl₃.

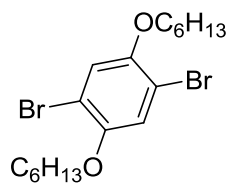
Thermal Analysis. DSC was performed on a Perkin Elmer Pyris 6 with a heating and cooling rate of 10 °C/min.

Electrochemistry. DPV and CV were performed on a CH Electrochemistry workstation (in acetonitrile with Bu₄NPF₆ as the supporting electrolyte using a glassy carbon working electrode, a Ag/Ag⁺ reference electrode, and a Pt wire counter electrode).

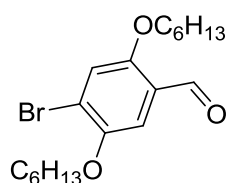
2.6.2 Monomer synthesis



1,4-Bis(hexyloxy)benzene (1). KOH (40.0 g, 713 mmol), and Na₂S₂O₃·5H₂O (86.0 g, 346 mmol) were dissolved in water (200 mL) in a 1 L round-bottom flask with stirring. The flask was cooled on an ice bath. Then, hydroquinone (38.0 g, 345 mmol) and TBAB (5.0 g, 16 mmol) were added. The mixture was stirred until most of the solid had dissolved. Then, 1-bromohexane (100 mL, 712 mmol) and toluene (100 mL) were added, and the flask was equipped with a water-cooled condenser. The mixture was brought to rt, and then refluxed with vigorous stirring for 24 – 48 h (until complete by TLC analysis). Once complete, the mixture was allowed to cool to rt. The aqueous layer was extracted once with toluene (100 mL). The combined organic layers were washed with water (200 mL) and brine (200 mL) and dried over MgSO₄. The solvent was removed under reduced pressure until the residue solidified. The residue was recrystallized from methanol to give the title compound as white flaky crystals (78.1 g – 93.0 g, 81 – 97%). MP 42.0 – 43.0 °C. ¹H NMR (CDCl₃, 300 MHz), δ 0.93 (6H, t, *J* = 6.8 Hz, CH₃), 1.25-1.40 (8H, mult), 1.40-1.50 (4H, mult), 1.78 (4H, tt, *J* = 6.6, 6.8 Hz), 3.92 (4H, t, *J* = 6.6 Hz, OCH₂), 6.85 (4H, s, ArH) ppm. ¹³C NMR (CDCl₃, 75 MHz) δ 14.0 (CH₃), 22.6 (CH₂), 25.7 (CH₂), 29.4 (CH₂), 31.6 (CH₂), 68.6 (OCH₂), 115.3 (Ar CH), 153.2 (ArO quat) ppm. MS(EI) 278 (M⁺, base), 255, 207, 194, 151, 123, 111, 109, 93, 85, 81, 65, 57 m/z. HRMS calcd for C₁₈H₃₀O₂: 278.2246 g/mol. Found: 278.2244 g/mol.

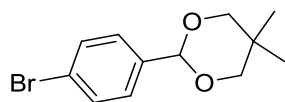


1,4-dibromo-2,5-bis(hexyloxy)benzene (2, vi35). Bromine (70.0 mL, 1.36 mol) was added dropwise to methanol (650 mL) in a round-bottom flask cooled on ice. **1** (75.0 g, 269 mmol) was added and the mixture was refluxed for 48 h. The reaction mixture was extracted with hexanes (4x 250 mL). The combined organic layers were washed with 20% aq. NaHSO₃ (2x 200 mL), water (200 mL), and brine (200 mL). The solution was dried over MgSO₄, and the solvent was removed *in vacuo*. The residue was recrystallized (9:1 methanol:CH₂Cl₂) to give the title compound as a white solid (88.5 g, 75%). ¹H NMR (CDCl₃, 300 MHz) δ 0.93 (6H, t, *J* = 6.8 Hz), 1.30-1.40 (8H, mult), 1.40-1.55 (4H, mult), 1.81 (4H, tt *J* = 6.8, 6.4 Hz), 3.95 (4H, t, *J* = 6.4 Hz), 7.09 (2H, s) ppm. ¹³C NMR (CDCl₃) δ 14.00 (CH₃), 22.56 (CH₂), 25.59 (CH₂), 29.06 (CH₂), 31.46 (CH₂), 70.26 (OCH₂), 111.09 (ArBr quat), 118.41 (Ar CH), 150.04 (ArO quat) ppm.

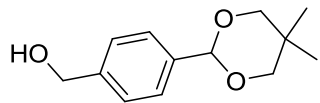


4-bromo-2,5-bis(hexyloxy)benzaldehyde (Br-D-CHO, vi39). Based on the methods of Peng,⁸³ two batches of **2** (34.9 g, 80.0 mmol each) were each dissolved in Et₂O (150 mL) and cooled to 0 °C under N₂. ⁿBuLi (1.6 M in hexanes, 50 mL, 80 mmol) diluted with 100 mL Et₂O was added to each batch dropwise over 30 min. Then, anhydrous DMF (10.0 mL, 130 mmol) in Et₂O (35 mL) was added rapidly to each batch. The mixtures were removed from the cold bath and stirred at room temperature for 2 h. The reactions were quenched into water (300 mL). The aqueous layers

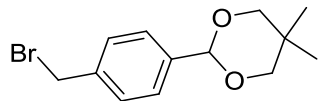
were extracted thrice with ether (100 mL). The organic layers were washed with brine (100 mL) and dried over MgSO₄. The solvent was removed *in vacuo*. The residues of both batches were combined and recrystallized from hexanes and then methanol to give the title compound as a white solid (40.5 g, 66%). ¹H NMR (CDCl₃, 300 MHz) δ 0.80-0.95 (6H,mult), 1.30-1.40 (8H, mult), 1.40-1.55 (4H, mult), 1.75-1.90 (mult, 4H), 4.00 (2H, t, *J* = 6.4 Hz), 4.02 (2H, t, *J* = 6.4 Hz), 7.22 (1H, s), 7.30 (1H, s), 10.41 (1H, s) ppm. ¹³CNMR (CDCl₃) δ 13.95 (CH₃), 13.97 (CH₃), 22.51 (CH₂), 22.53 (CH₂), 25.57 (CH₂), 25.62 (CH₂), 28.94 (CH₂), 28.98 (CH₂), 31.42 (CH₂), 69.76 (OCH₂), 69.76 (OCH₂), 110.52 (Ar CH), 118.39 (Ar CH), 120.89 (ArBr quat), 124.20 (Ar quat), 149.80 (ArO quat), 155.71 (ArO quat), 188.86 (CHO) ppm.



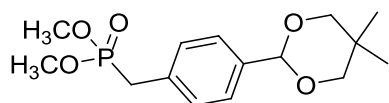
2-(4-bromophenyl)-5,5-dimethyl-1,3-dioxane (3, v70a,b). Neopentylene glycol (15.0 g, 144 mmol), 4-bromobenzaldehyde (20.35 g, 110 mmol), and TsOH (0.80 g, 5.7 mmol) were refluxed in PhMe (400 mL) with a Dean-Stark trap for 3 h. The reaction mixture was washed with H₂O (100 mL) and brine (100 mL) and dried over MgSO₄. The solvent was removed *in vacuo*. The crude product was recrystallized from hexanes to give white needles (25.36 g, 88%). ¹H NMR (CDCl₃, 300 MHz) δ 0.81 (3H, s, *axial* CH₃), 1.29 (3H, s, *equatorial* CH₃), 3.65 (2H, d, *J* = 11.0 Hz, *axial* CH), 3.78 (2H, d, *J* = 11.0 Hz, *equatorial* CH), 5.36 (1H, s, ArCH(O)₂), 7.40 (2H, d, *J* = 8.4 Hz, *p*-C₆H₄), 7.52 (2H, d, *J* = 8.4 Hz, *p*-C₆H₄) ppm. ¹³C NMR (CDCl₃, 75 MHz) δ 21.8 (*axial* CH₃), 22.9 (*equatorial* CH₃), 30.1 (quat), 77.5 (OCH₂), 100.8 (ArCH(O)₂), 122.8 (ArBr quat), 127.9 (Ar CH), 131.3 (Ar CH), 135.7 (Ar quat) ppm.



2-(4-(hydroxymethyl)phenyl)-5,5-dimethyl-1,3-dioxane (4, v73a). **3** (25.0 g, 92.2 mmol) was dissolved in dry THF (500 mL), and cooled to $-78\text{ }^{\circ}\text{C}$. $n\text{BuLi}$ (1.6 M in hexanes, 65.0 mL, 104 mmol) was added dropwise over 15 min. The reaction mixture was stirred at $-78\text{ }^{\circ}\text{C}$ for 1 h. DMF (10.0 mL, 129 mmol) was added rapidly. The mixture was stirred at rt for 1 h and quenched with brine (100 mL). The organic layer was dried over MgSO_4 , and the solvent was removed *in vacuo*. The crude product was redissolved in THF (200 mL) and cooled to $0\text{ }^{\circ}\text{C}$. NaBH_4 (5.23 g, 138 mmol) was added portionwise over 15 min. The reaction was stirred at rt overnight and then quenched into water (200 mL). The mixture was extracted with ethyl acetate (4x 100 mL). The combined organic layers were washed with H_2O (100 mL) and brine (100 mL) and dried over MgSO_4 . The solvent was removed *in vacuo*. The crude product was recrystallized from hexanes to give a white crystalline solid (10.43 g, 51% over 2 steps). NMR (CDCl_3 , 300 MHz) δ 0.81 (3H, s, *axial* CH_3), 1.30 (3H, s, *equatorial* CH_3), 2.18 (1H, t, $J = 5.6\text{ Hz}$, OH), 3.65 (2H, d, $J = 11.0\text{ Hz}$, *axial* CH), 3.77 (2H, d, $J = 11.0\text{ Hz}$, *equatorial* CH), 4.62 (2H, d, $J = 5.6\text{ Hz}$, ArCH_2O), 5.39 (1H, s, $\text{ArCH}(\text{O})_2$), 7.38 (2H, d, $J = 8.0\text{ Hz}$, *p*- C_6H_4), 7.48 (2H, d, $J = 8.0\text{ Hz}$, *p*- C_6H_4) ppm. ^{13}C NMR (CDCl_3 , 75 MHz) δ 21.8 (*axial* CH_3), 23.0 (*equatorial* CH_3), 30.1 (quat), 64.7 (ArCH_2O), 77.6 (OCH_2), 101.5 ($\text{ArCH}(\text{O})_2$), 126.2 (Ar CH), 126.6 (Ar CH), 137.7 (Ar quat) 141.6 (Ar quat) ppm.

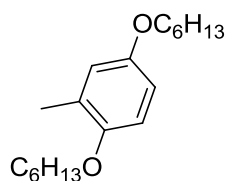


2-(4-(bromomethyl)phenyl)-5,5-dimethyl-1,3-dioxane (5, v95a). **4** (7.5 g, 32.3 mmol) was dissolved in dry THF (200 mL) under N₂ and cooled to 0 °C. Then CBr₄ (16.06 g, 48.4 mmol) and PPh₃ (12.69 g, 48.4 mmol) were added and the mixture was allowed to come to rt overnight with stirring. The reaction mixture was poured into H₂O (250 mL) and extracted with Et₂O (4x 100 mL). The organic layers were washed with brine (100 mL) and dried over MgSO₄. The solvent was removed *in vacuo*. The crude product was purified by column chromatography (silica gel, 1:1 hexanes:DCM) to give the title compound as a white solid (9.1 g, 99%). NMR (CDCl₃, 300 MHz) δ 0.81 (3H, s, *axial* CH₃), 1.29 (3H, s, *equatorial* CH₃), 3.66 (2H, d, J = 11.0 Hz, *axial* CH), 3.78 (2H, d, J = 11.0 Hz, *equatorial* CH), 4.49 (2H, s, ArCH₂Br), 5.49 (1H, s, ArCH(O)₂), 7.41 (2H, d, J = 8.0 Hz, *p*-C₆H₄), 7.50 (2H, d, J = 8.0 Hz, *p*-C₆H₄) ppm. ¹³C NMR (CDCl₃, 75 MHz) δ 21.8 (*axial* CH₃), 23.0 (*equatorial* CH₃), 30.2 (quat), 33.1 (ArCH₂Br), 77.6 (OCH₂), 101.1 (ArCH(O)₂), 126.6 (Ar CH), 129.0 (Ar CH), 138.3 (Ar quat) 138.7 (Ar quat) ppm.



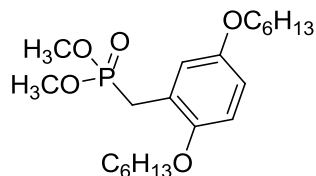
2-(4-(dimethoxyphosphorylmethyl)phenyl)-5,5-dimethyl-1,3-dioxane (P-A-acetal, v97a). **5** (9.0 g, 31.6 mmol) and P(OCH₃)₃ (13 mL, 110 mmol) were refluxed in PhMe (100 mL) overnight. The volatiles were removed *in vacuo* to give the title compound as a waxy white solid (9.50 g, 96%). ¹H NMR (CDCl₃, 400 MHz) δ 0.76 (3H, s, *axial* CH₃), 1.25 (3H, s, *equatorial* CH₃), 3.13 (2H, d, ² $J_{\text{H-P}}$ = 21.6 Hz), 3.61 (2H, d, ² $J_{\text{H-H}}$ = 11.6 Hz, *axial* CH), 3.61 (6H, d, ³ $J_{\text{H-P}}$ =

10.8 Hz), 3.71 (2H, d, $^2J_{\text{H-H}} = 11.6$ Hz, *equatorial* CH), 5.33 (1H, s, ArCH(O)₂), 7.41 (2H, d, $^3J_{\text{H-H}} = 8.0$ Hz, *p*-C₆H₄), 7.50 (2H, d, $^3J_{\text{H-H}} = 8.0$ Hz, *p*-C₆H₄) ppm. ¹³C NMR (CDCl₃, 75 MHz) δ 21.7 (*axial* CH₃), 22.9 (*equatorial* CH₃), 30.0 (quat), 32.5 (d, $^1J_{\text{C-P}} = 137$ Hz, ArCH₂P), 52.7 (d, $^2J_{\text{C-P}} = 6$ Hz), 77.5 (OCH₂), 101.3 (ArCH(O)₂), 126.3 (d, $^4J_{\text{C-P}} = 3$ Hz, Ar CH), 129.4 (d, $^3J_{\text{C-P}} = 13$, Hz Ar CH), 131.7 (d, $^2J_{\text{C-P}} = 10$ Hz, Ar quat) 137.2 (d, $^6J_{\text{C-P}} = 4$ Hz Ar quat) ppm.

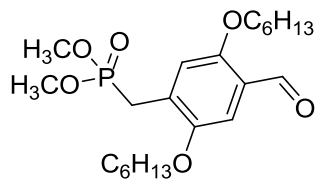


2-methyl-1,4-bis(hexyloxy)benzene (6, iv89). KOH (40.0 g, 713 mmol) and Na₂S₂O₃ (86.0 g, 346 mmol) were dissolved in water (200 mL) in a 1 L round-bottom flask and cooled on ice. 2-Methylhydroquinone (42.8 g, 345 mmol), TBAB (5.0 g, 16 mmol), 1-bromohexane (100 mL, 712 mmol), and PhMe (100 mL) were added in that order. The mixture was refluxed with vigorous stirring for 40 h. The aqueous layer was extracted with PhMe (2x 100 mL). The combined organic layers were washed with water (100 mL) and brine (100 mL) and dried over MgSO₄. The solvent was removed *in vacuo*. The residue was purified by column chromatography (silica gel, 17:3 hexanes:CH₂Cl₂) to give the title compound as a yellow liquid (86.3 g, 86%). ¹H NMR (CDCl₃) δ 0.90-1.00 (6H, mult), 1.30-1.45 (8H, mult), 1.45-1.60 (4H, mult), 1.75-1.90 (4H, mult), 3.94 (2H, t, $J = 6.4$ Hz), 3.95 (2H, t, $J = 6.4$ Hz), 6.71 (1H, dd, $J = 9.0$ Hz, 3.0 Hz), 6.77 (1H, d, $J = 9.0$ Hz), 6.79 (1H, d, $J = 3.0$ Hz) ppm. ¹³C NMR (CDCl₃) δ 13.99 (CH₃), 16.34 (CH₃), 22.60 (CH₂), 25.75 (CH₂), 25.83 (CH₂), 29.39 (CH₂), 29.45 (CH₂), 31.59 (CH₂), 31.61 (CH₂), 68.41 (OCH₂), 68.68 (OCH₂), 111.46 (Ar CH), 112.11 (Ar CH), 117.56 (Ar CH), 128 (Ar quat), 151.39 (ArO quat), 152.78 (ArO quat) ppm. MS(EI): 292 (M⁺),

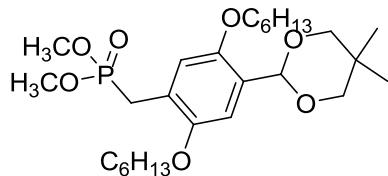
234, 221, 208, 165, 150, 124 (base), 107, 95, 84, 77, 67, 55 m/z. HRMS calcd for C₁₉H₃₂O₂: 292.2402 g/mol. Found: 292.2406 g/mol.



1,4-bis(hexyloxy)-2-(dimethoxyphosphorylmethyl)benzene (7, vi37a). 6 (109.7 g, 375 mmol) was dissolved in CCl₄ (500 mL). NBS (33.7 g, 189 mmol) and AIBN (3.48 g, 37.8 mmol) were added, and the mixture was refluxed for 1.5 h. More NBS (33.7 g, 189 mmol) and AIBN (3.48 g, 37.8 mmol) were added, and the mixture was refluxed for another 1.5 h. The mixture was returned to rt and the succinimide was removed by filtration. The mixture was washed with H₂O (100 mL) and brine (100 mL) and dried over MgSO₄. The MgSO₄ was removed by filtration through a silica plug, which was washed with 3:1 hexanes:DCM. The combined filtrates were reduced *in vacuo* to give a mixture of regioisomers (3:2 benzyl:aryl bromide) (132 g, 95%). This mixture was dissolved in PhMe (250 mL). P(OCH₃)₃ (100 mL, 848 mmol) was added and the mixture was refluxed for 24 h. The volatiles were removed *in vacuo*. The crude product was purified by column chromatography (silica gel, 9:1 DCM:acetone) to give the title compound as a viscous yellow liquid (71.0 g, 47% over 2 steps). ¹H NMR (CDCl₃, 300 MHz) δ 0.80-0.90 (6H, mult), 1.15-1.45 (14H, mult), 1.60-1.75 (4H, mult), 3.18 (2H, d, ²J_{H-P} = 21.6 Hz), 3.61 (6H, d, ³J_{H-P} = 11.7 Hz) 3.81 (2H, d, ³J_{H-H} = 6.6 Hz), 3.86 (2H, d, ³J_{H-H} = 6.9 Hz), 6.66 (1H, d, ³J_{H-H} = 8.7 Hz), 6.71 (1H, d, ³J_{H-H} = 9.0 Hz), 6.84 (1H, s) ppm.

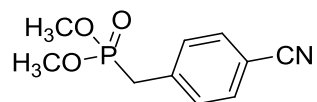


2-(2,5-bis(hexyloxy)-4-(dimethoxyphosphorylmethyl)benzaldehyde (8, vi40a). 7 (65.0 g, 162 mmol) was dissolved in 1.5 L of dry DCM in a 3-neck round-bottom flask under N₂ and cooled to 0 °C. AlCl₃ (43.3 g, 324 mmol) was added portionwise with vigorous stirring over 15 min. The dark green mixture was stirred at 0 °C for another 15 min. A solution of CHCl₂OCH₃ (29 mL, 327 mmol) in dry DCM (300 mL) was added dropwise. The mixture was allowed to come to rt overnight with stirring. The dark red mixture was quenched by adding 1000 g of ice rapidly with vigorous stirring. The aqueous layer was extracted with DCM (4x 200 mL). The combined organic layer divided into two portions and washed with H₂O (300 mL) and brine (300 mL). The organic layers were dried over MgSO₄, and the solvent was removed *in vacuo*. The crude product was purified by column chromatography (silica gel, 19:1 DCM:acetone) to give 2,5-bis(hexyloxy)-4-(dimethoxyphosphorylmethyl)benzaldehyde as 62.3 g of an orange liquid (89%). ¹H NMR (CDCl₃, 300 MHz) δ 0.80-0.90 (6H, mult), 1.20-1.50 (14H, mult), 1.65-1.80 (4H, mult), 3.23 (2H, d, ²J_{H-P} = 22.5 Hz), 3.62 (6H, d, ³J_{H-P} = 10.8 Hz), 3.91 (2H, t, ³J_{H-H} = 6.5 Hz), 3.97 (2H, t, ³J_{H-H} = 6.5 Hz), 6.97 (1H, d, ⁴J_{H-P} = 2.7 Hz), 7.21 (1H, s), 10.36 (1H, s) ppm. ¹³C NMR (CDCl₃, 75 MHz) δ 13.8 (CH₃), 22.3 (CH₂), 22.4 (CH₂), 25.5 (CH₂), 25.2 and 27.1 (d, ¹J_{C-P} = 142.5 Hz PCH₂), 28.9 (CH₂), 29.0 (CH₂), 31.3 (CH₂), 52.5 (d, ²J_{C-P} = 6.5 Hz POCH₃), 68.6 (OCH₂), 68.9 (OCH₂), 108.9 (d, ⁴J_{C-P} = 2.9 Hz, Ar CH), 115.9 (d, ³J_{C-P} = 5.6 Hz, Ar CH), 123.7 (d, ⁵J_{C-P} = 3.5 Hz, Ar quat), 128.8 (d, ²J_{C-P} = 9.5 Hz, Ar quat), 150.4 (d, ³J_{C-P} = 7.1 Hz, ArO quat), 155.6 (d, ⁴J_{C-P} = 3.7 Hz, ArO quat), 189.0 (d, ⁶J_{C-P} = 1.1 Hz, CHO) ppm.

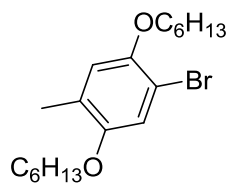


2-(2,5-bis(hexyloxy)-4-(dimethoxyphosphorylmethyl)phenyl)-5,5-dimethyl-1,3-dioxane

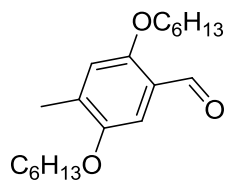
(P-D-acetal, vi41a). 8 (62.3 g, 144 mmol) was dissolved in PhMe (500 mL). Neopentylene glycol (22.5 g, 145 mmol) and TsOH (1.0 g, 7.13 mmol) were added and the mixture was refluxed for 24 h. The mixture was washed with H₂O (100 mL) and brine (100 mL) and dried over MgSO₄. The solvent was removed *in vacuo*. The crude product was purified by column chromatography (silica gel, 9:1 DCM:acetone) to give the title compound as an orange liquid (72.3 g, 97%). ¹H NMR (CDCl₃, 300 MHz) δ 0.75 (3H, s, *axial* CH₃), 0.88-0.91 (6H, mult), 1.25-1.40 (11H, mult), 1.42-1.50 (4H, mult), 1.72-1.78 (4H, mult), 3.23 (2H, d, ²J_{H-P} = 22.5 Hz), 3.62 (6H, d, ³J_{H-P} = 10.8 Hz), 3.63 (2H, d, ²J_{H-H} = 11.1 Hz, *axial* CH), 3.73 (2H, d, ²J_{H-H} = 11.1 Hz, *equatorial* CH), 3.92 (2H, t, ³J_{H-H} = 6.3 Hz, OCH₂), 3.97 (2H, t, ³J_{H-H} = 6.3 Hz, OCH₂), 6.89 (1H, d, ⁴J_{H-P} = 2.7 Hz), 7.13 (1H, s) ppm. ¹³C NMR (CDCl₃, 75 MHz) δ 13.9 (CH₃), 14.0 (CH₃), 21.8 (CH₃), 22.50 (CH₂), 22.54 (CH₂), 23.1 (CH₃), 25.6 (CH₂), 25.7 (CH₂), 25.1 (d, ¹J_{C-P} = 138.1 Hz, ArCH₂P), 29.2 (CH₂), 29.3 (CH₂), 30.2 (quat), 31.5 (CH₂), 52.5 (d, ²J_{C-P} = 6.6 Hz, POCH₃), 68.8 (OCH₂), 69.4 (OCH₂), 77.8 (OCH₂), 97.0 (ArCHO₂), 110.3 (d, ⁴J_{C-P} = 3.0 Hz, Ar CH), 115.8 (d, ³J_{C-P} = 5.1 Hz, Ar CH), 121.2 (d, ⁴J_{C-P} = 9.5 Hz, Ar quat), 126.5 (d, ⁵J_{C-P} = 4.1.0 Hz, Ar quat), 149.7 (d, ⁴J_{C-P} = 3.7 Hz, ArO quat), 150.8 (d, ³J_{C-P} = 7.3 Hz, ArO quat) ppm. MS (ESI): 537 (M+Na, base), 515, 497 m/z. HRMS calcd for C₂₇H₄₇O₇P+Na: 537.2957 g/mol. Found: 537.2954 g/mol.



4-(dimethoxyphosphorylmethyl)benzonitrile (P-A-CN, vi98 + vi99). *p*-Tolunitrile (25.0 mL, 209 mmol) was added to 1,2-dichloroethane (400 mL) in a round-bottom flask with stirring. NBS (18.8 g, 105 mmol), and benzoyl peroxide (2.55 g, 10.5 mmol) were added, and the mixture was refluxed until the orange color disappeared (1.5 h). NBS (18.8 g, 105 mmol), and benzoyl peroxide (2.55 g, 10.5 mmol) were added, and the mixture was refluxed for a second 1.5 h. The reaction mixture was allowed to stand overnight. The succinimide precipitate was removed by filtration. The filtrate was washed successively with water (200 mL), sat. aq. NaHCO₃ (200 mL), and brine (200 mL). The organic solution was dried over MgSO₄, and the solvent was removed *in vacuo*. The crude product was dissolved in toluene (100 mL). Trimethyl phosphite (60.0 mL, 508 mmol) was added, and the mixture was refluxed overnight. The solvent was removed *in vacuo*, and the crude product was purified by column chromatography (silica gel, 4:1 CH₂Cl₂:acetone) and then by recrystallization (1:1 ethyl acetate:hexanes) to give the title compound as an off-white crystalline solid (16.7 g, 35% over 2 steps). MP 79.0-81.0 °C. ¹H NMR (CDCl₃) δ 3.17 (2H, d, ²J_{H-P} = 22.4), 3.66 (6H, d, ³J_{H-P} = 11.2 Hz), 7.37 (2H, dd, J_{H-H} = 8.4 Hz, J_{H-P} = 2.0 Hz), 7.58 (d, 2H, J_{H-H} = 8.0 Hz) ppm. ¹³CNMR (CDCl₃, 300 MHz) δ 32.92 (d, ¹J_{C-P} = 137 Hz, CH₂), 52.82 (d, ²J_{C-P} = 7 Hz, OCH₃), 110.84 (d, ⁵J_{C-P} = 3 Hz, Ar quat), 118.45 (d, ⁶J_{C-P} = 2 Hz, CN), 130.31 (d, ³J_{C-P} = 6 Hz, Ar CH), 132.14 (d, ⁴J_{C-P} = 3 Hz, Ar CH), 137.02 (d, ²J_{C-P} = 10 Hz, Ar quat) ppm. MS (EI) 225 (M⁺), 129, 116, 109 (base) m/z. HRMS calcd for C₁₀H₁₂NO₃P: 225.0556 g/mol. Found: 225.0555 g/mol.

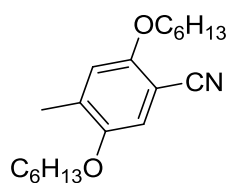


1-bromo-2,5-bis(hexyloxy)-4-methylbenzene (9, vi104). **6** (37.5 g, 128 mmol) was dissolved in 1,2-dichloroethane (375 mL). NBS (23.0 g, 129 mmol) and benzoyl peroxide (1.56 g, 6.44 mmol) were added and the mixture was refluxed for 5h. Hexanes (100 mL) was added to precipitate succinimide. The filtrate was washed with water (3x 100 mL), sat. aq. NaHCO₃ (100 mL), and brine (100 mL). The solution was dried over MgSO₄, and the solvent was removed *in vacuo*. The residue was recrystallized from methanol to give the title compound as a white solid (33.0 g, 69%). ¹H NMR (CDCl₃) δ 0.90-1.00 (6H, mult), 1.30-1.40 (8H, mult), 1.45-1.55 (4H, mult), 1.75-1.90 (4H, mult), 2.19 (3H, s), 3.90 (2H, t, *J* = 6.4 Hz), 3.96 (2H, t, *J* = 6.4 Hz), 6.76 (1H, s), 6.99 (1H, s) ppm. ¹³C NMR (CDCl₃, 300 MHz) δ 13.98 (CH₃), 14.00 (CH₃), 16.22 (CH₃), 22.58 (CH₂), 25.65 (CH₂), 25.74 (CH₂), 29.26 (CH₂), 29.29 (CH₂), 31.52 (CH₂), 68.84 (OCH₂), 70.28 (OCH₂), 108.88 (ArBr quat), 116.28 (Ar CH), 116.90 (Ar CH), 126.28 (Ar quat), 149.15 (ArO quat), 151.72 (ArO quat) ppm. MS (EI): 372 (M+2), 370 (M⁺), 288, 286, 204, 202 (base), 164, 124, 94, 84, 77, 69 m/z. HRMS calcd for C₁₉H₃₁O₂Br: 370.1507 g/mol. Found: 370.1500 g/mol.



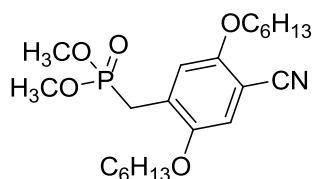
2,5-bis(hexyloxy)-4-methylbenzaldehyde (10, vii19). **9** (30.0 g, 80.1 mmol) was dissolved in Et₂O (150 mL) and cooled to 0 °C under N₂. ⁿBuLi (1.6 M in hexanes, 55 mL, 88 mmol) diluted

with 100 mL Et₂O was added dropwise over 30 min. Then, DMF (10.0 mL, 130 mmol) in Et₂O (35 mL) was added rapidly. The mixture was removed from the cold bath and stirred at room temperature for 2 h. The reaction was quenched into water (300 mL). The aqueous layer was extracted with ether (3x 100 mL). The organic layers were washed with brine (100 mL) and dried over MgSO₄. The solvent was removed *in vacuo*. The residue was purified by column chromatography (silica gel, 19:1 hexanes:EtOAc) to give the title compound as an off-white solid (25.7 g, 99%). ¹H NMR (CDCl₃, 300 MHz) δ 0.85-0.95 (6H, mult), 1.30-1.40 (8H, mult), 1.40-1.50 (4H, mult), 1.75-1.85 (4H, mult), 2.27 (3H, s), 3.94 (2H, t, *J* = 6.4 Hz), 4.01 (2H, t, *J* = 6.4 Hz), 6.79 (1H, s), 7.22 (1H, s), 10.41 (1H, s) ppm. ¹³C NMR (CDCl₃) δ 13.95 (CH₃), 17.21 (CH₃), 22.53 (CH₂), 22.55 (CH₂), 25.69 (CH₂), 25.72 (CH₂), 29.16 (CH₂), 31.47 (CH₂), 31.49 (CH₂), 68.40 (OCH₂), 69.10 (OCH₂), 108.19 (Ar CH), 115.58 (Ar CH), 122.96 (Ar quat), 136.71 (Ar quat), 151.32 (ArO quat), 156.12 (ArO quat), 189.31 (CHO) ppm. MS (EI): 320 (M⁺), 292, 236, 152 (base), 124, 91, 84 m/z. HRMS calcd for C₂₀H₃₂O₃: 320.2351 g/mol. Found: 320.2349 g/mol.



2,5-bis(hexyloxy)-4-methylbenzonitrile (11, vii23). Based on the methods of Olah,⁸⁰ **10** (23.3 g, 73.6 mmol) and hydroxylamine hydrochloride (6.57 g, 94.5 mmol) were added to formic acid (100 mL) in a round-bottom flask and refluxed for 1 h. The dark mixture was poured into ice water (200 mL). The aqueous mixture was extracted thrice with ether (50 mL). The combined organic layers were washed with brine (50 mL) and dried over MgSO₄. The solvent was removed

in vacuo, and the residue was purified by column chromatography (silica gel, 99:1 hexanes:EtOAc) to give the title compound as an orange liquid (17.1 g, 78%). ^1H NMR (CDCl_3 , 300 MHz) δ 0.85-0.95 (6H, mult), 1.30-1.40 (8H, mult), 1.40-1.50 (4H, mult), 1.75-1.85 (4H, mult), 2.24 (3H, s), 3.87 (2H, t, $J = 6.4$ Hz), 3.98 (2H, t, $J = 6.4$ Hz), 6.75 (1H, s), 6.88 (1H, s) ppm. ^{13}C NMR (CDCl_3) δ 13.87 (CH_3), 16.99 (CH_3), 22.43 (CH_2), 22.46 (CH_2), 25.43 (CH_2), 25.62 (CH_2), 28.94 (CH_2), 29.03 (CH_2), 31.38 (CH_2), 31.40 (CH_2), 68.63 (OCH_2), 69.44 (OCH_2), 98.53 (CN quat), 114.41 (Ar CH), 115.33 (Ar CH), 116.83 (Ar quat), 134.64 (Ar quat), 150.76 (ArO quat), 154.97 (ArO quat) ppm.

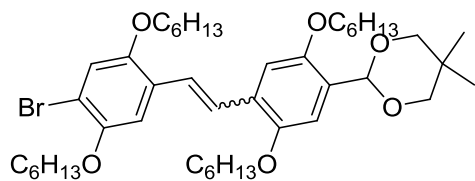


2,5-bis(hexyloxy)-4-(dimethoxyphosphorylmethyl)benzonitrile (P-D-CN, vii26 + vii27). 11 (13.8 g, 43.5 mmol) was dissolved in 1,2-dichloroethane (70 mL). NBS (3.90 g, 43.8 mmol), and benzoyl peroxide (0.540 g, 4.45 mmol) were added, and the mixture was refluxed until the orange color disappeared (2 h). NBS (3.90 g, 43.8 mmol), and benzoyl peroxide (0.540 g, 4.45 mmol) were added, and the mixture was refluxed for a second 2 h. The reaction mixture was allowed to stand overnight. The reaction mixture was filtered through a plug of silica and the solvent was removed *in vacuo*. The crude product was dissolved in PhMe (30 mL). Trimethyl phosphate (16.0 mL, 136 mmol) was added, and the mixture was refluxed overnight. The solvent was removed *in vacuo*, and the crude product was purified by column chromatography (silica gel, 1:1 hexanes:EtOAc) to give the title compound as a viscous orange liquid (11.7 g, 63% over 2 steps). ^1H NMR (CDCl_3 , 300 MHz) δ 0.80-0.90 (6H, mult), 1.25-1.35 (8H, mult), 1.40-1.50

(4H, mult), 1.70-1.80 (4H, mult), 3.24 (2H, d, $^2J_{\text{H-P}}=22.4$ Hz), 3.66 (6H, d $^3J_{\text{H-P}} = 11.2$ Hz), 3.89 (2H, t, $J = 6.4$ Hz), 3.98 (2H, t, $J = 6.4$ Hz), 6.94 (1H, s), 6.96 (1H, d $^4J_{\text{H-P}} = 2.8$ Hz) ppm. ^{13}C NMR (CDCl_3) δ 13.83 (CH_3), 22.37 (CH_2), 22.41 (CH_2), 25.35 (CH_2), 25.50 (CH_2), 26.14 (d, $^1J_{\text{C-P}} = 138$ Hz, CH_2) 28.78 (CH_2), 28.97 (CH_2), 31.33 (CH_2), 31.34 (CH_2), 52.69 (d, $^2J_{\text{C-P}} = 7$ Hz, OCH_3) 69.08 (OCH_2), 69.45 (OCH_2), 100.24 (d, $^6J_{\text{C-P}} = 3$ Hz, CN quat), 115.36 (d, $^4J_{\text{C-P}} = 3$ Hz, Ar CH), 115.33 (d, $^3J_{\text{C-P}} = 5$ Hz, Ar CH), 116.31 (d, $^5J_{\text{C-P}} = 2$ Hz, Ar quat), 127.36 (d, $^2J_{\text{C-P}} = 9$ Hz, Ar quat), 150.06 (d, $^3J_{\text{C-P}} = 7$ Hz, ArO quat), 154.75 (d, $^4J_{\text{C-P}} = 3$ Hz, ArO quat) ppm.

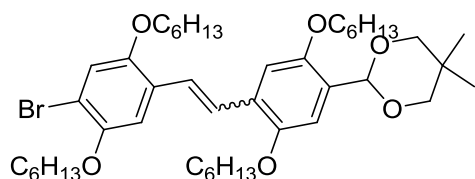
2.6.3 HWE optimization

General procedure for HWE optimization (TABLE 3). Aldehyde (1 eq) and benzyolphosphonate (1.5 eq), with or without and LiCl (2.3 eq), were dissolved in THF (12 mL per mmol aldehyde) and cooled to 0 °C under N_2 . KO^tBu (2.3 eq) was added portionwise over 5 minutes, and the reactions were allowed to come to rt overnight with stirring. The reaction mixtures were poured into saturated aqueous NH_4Cl (2.5 mL per mL THF). The aqueous layers were extracted thrice with EtOAc (equal volume). The combined organic layers were dried over MgSO_4 , and the solvent was removed *in vacuo*. The residues were purified by column chromatography. The E/Z ratio was determined by ^1H NMR spectroscopy.

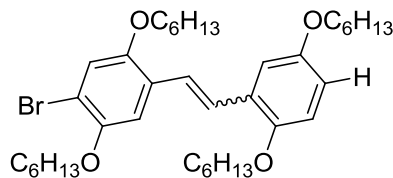


2-(4-(4-bromo-2,5-bis(hexyloxy)styryl)-2,5-bis(hexyloxy)phenyl)-5,5-dimethyl-1,3-dioxane, (Table 3 Line 1, vi85). According to the general HWE optimization procedure (Table 3), **Br-D-**

CHO (0.20 g, 0.519 mmol) and **P-D-acetal** (0.40 g, 0.777 mmol) were dissolved in THF (5 mL) and cooled to 0 °C under N₂. KO^tBu (125 mg, 1.11 mmol) was added portionwise over 5 minutes, and the reactions were allowed to come to rt overnight with stirring. After workup, column chromatography (silica gel, 3:1 hexanes:DCM) gave the title compound as yellow solid (401 mg, 100%). E/Z ratio by ¹H NMR: 2:1.

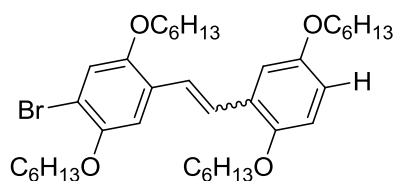


2-(4-(4-bromo-2,5-bis(hexyloxy)styryl)-2,5-bis(hexyloxy)phenyl)-5,5-dimethyl-1,3-dioxane, (Table 3 Line 2, vi85). According to the general HWE optimization procedure (Table 3), **Br-D-CHO** (0.20 g, 0.519 mmol), **7** (0.40 g, 0.777 mmol), and LiCl (50 mg, 1.18 mmol) were dissolved in THF (10 mL) and cooled to 0 °C under N₂. KO^tBu (125 mg, 1.11 mmol) was added portionwise over 5 minutes, and the reactions were allowed to come to rt overnight with stirring. After workup, column chromatography (silica gel, 3:1 hexanes:DCM) gave the title compound as yellow solid (221 mg, 55%). E/Z ratio by ¹H NMR: 4:1.



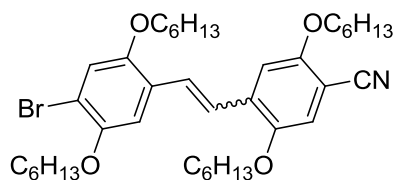
1-(4-bromo-2,5-bis(hexyloxy)styryl)-2,5-bis(hexyloxy)benzene, (Table 3 Line 3, vi92). According to the general HWE optimization procedure (Table 3), **Br-D-CHO** (0.20 g, 0.519 mmol) and **7** (0.311 g, 0.777 mmol) were dissolved in THF (5 mL) and cooled to 0 °C under N₂. KO^tBu (125 mg, 1.11 mmol) was added portionwise over 5 minutes, and the reactions were

allowed to come to rt overnight with stirring. After workup, column chromatography (silica gel, 3:1 hexanes:DCM) gave the title compound as yellow solid (338 mg, 98%). E/Z ratio by ^1H NMR: 83:17.



1-(4-bromo-2,5-bis(hexyloxy)styryl)-2,5-bis(hexyloxy)benzene, (Table 3 Line 4, vi92).

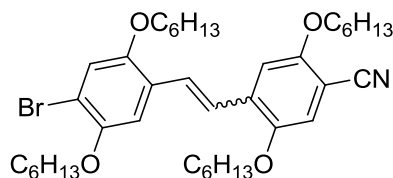
According to the general HWE optimization procedure (Table 3), **Br-D-CHO** (0.20 g, 0.519 mmol), **7** (0.311 g, 0.777 mmol), and LiCl (50 mg, 1.18 mmol) were dissolved in THF (5 mL) and cooled to 0 °C under N₂. KO^tBu (125 mg, 1.11 mmol) was added portionwise over 5 minutes, and the reactions were allowed to come to rt overnight with stirring. After workup, column chromatography (silica gel, 3:1 hexanes:DCM) gave the title compound as yellow solid (338 mg, 98%). E/Z ratio by ^1H NMR: 87:13.



4-(4-bromo-2,5-bis(hexyloxy)styryl)-2,5-bis(hexyloxy)benzonitrile, (Table 3 Line 5, vi95).

According to the general HWE optimization procedure (Table 3), **Br-D-CHO** (0.150 g, 0.389 mmol) and **P-D-CN** (0.250 g, 0.587 mmol) were dissolved in THF (5 mL) and cooled to 0 °C under N₂. KO^tBu (100 mg, 0.891 mmol) was added portionwise over 5 minutes, and the reactions were allowed to come to rt overnight with stirring. After workup, column

chromatography (silica gel, 3:1 hexanes:DCM) gave the title compound as yellow solid (187 mg, 70%). E/Z ratio by ^1H NMR: 5:1.



4-(4-bromo-2,5-bis(hexyloxy)styryl)-2,5-bis(hexyloxy)benzonitrile, (Table 3 Line 6, vi95).

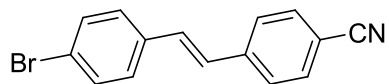
According to the general HWE optimization procedure (Table 3), **Br-D-CHO** (0.150 g, 0.389 mmol), **P-D-CN** (0.250 g, 0.587 mmol), and LiCl (38 mg, 0.896 mmol) were dissolved in THF (5 mL) and cooled to 0 °C under N₂. KO^tBu (100 mg, 0.891 mmol) was added portionwise over 5 minutes, and the reactions were allowed to come to rt overnight with stirring. After workup, column chromatography (silica gel, 3:1 hexanes:DCM) gave the title compound as yellow solid (297 mg, 100%). E/Z ratio by ^1H NMR: 10:1.

2.6.4 Synthesis of oligomers

General HWE procedure. Aldehyde (**Br-A-CHO**, **Br-D-CHO**, or **OPV-CHO**) (1 eq), 4-cyanobenzylphosponate (**P-A-CN** or **P-D-CN**) (1.5 eq), and LiCl (2.3 eq) were dissolved in THF (12 mL per mmol aldehyde) and cooled to 0 °C under N₂. KO^tBu (2.3 eq) was added portionwise over 5 minutes, and the reactions were allowed to come to rt overnight with stirring. The reaction mixtures were poured into saturated aqueous NH₄Cl (2.5 mL per mL THF). The aqueous layers were extracted thrice with EtOAc (equal volume). The combined organic layers were dried over

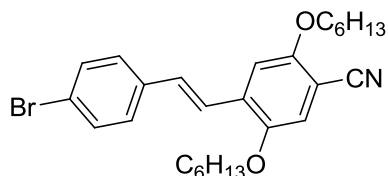
MgSO₄, and the solvent was removed *in vacuo*. The residues were purified by column chromatography.

General DIBAL-H reduction procedure. OPV nitriles (1 eq.) were dissolved in dry DCM (5 mL per mmol nitrile) and cooled to 0 °C. DIBAL-H (1.0M in hexanes, 1.1 eq) was added dropwise. The reaction mixtures were stirred at 0 °C for 1 h. Wet silica (0.4 mL H₂O and 1.3 g SiO₂ per mmol nitrile) was added and the mixture was stirred at 0 °C for 1 h. Then, K₂CO₃ (0.5 g per mmol nitrile) and MgSO₄ (0.5 g per mmol nitrile) were added. The mixtures were filtered and the solids washed with DCM. The combined filtrate and washes were reduced *in vacuo*, and the residues were purified by column chromatography, except as noted.

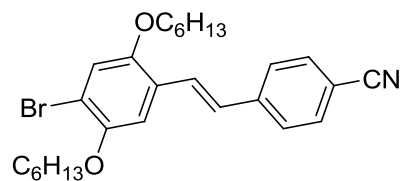


4-(4-bromostyryl)benzonitrile (Br-AA-CN, vii36). According to the general HWE procedure, **Br-A-CHO** (611 mg, 3.30 mmol), **P-A-CN** (1.115 g, 4.95 mmol), and LiCl (321 mg, 7.57 mmol) were dissolved in THF (40 mL) and cooled to 0 °C under N₂. KO^tBu (850 mg, 7.57 mmol) was added portionwise over 5 minutes, and the reaction was allowed to come to rt overnight with stirring. After workup, column chromatography (silica gel, 1:1 hexanes:DCM) gave the title compound as a white solid (517.3 mg, 55%). ¹H NMR (CD₂Cl₂, 400 MHz) δ 7.11 (1H, d, *J* = 16.4 Hz, *trans* CH=CH), 7.18 (1H, d, *J* = 16.4 Hz, *trans* CH=CH), 7.42 (2H, d, *J* = 8.8 Hz, *p*-C₆H₄), 7.52 (2H, d, *J* = 8.8 Hz, *p*-C₆H₄), 7.59 (2H, d, *J* = 8.4 Hz, *p*-C₆H₄), 7.65 (2H, d, *J* = 8.4 Hz, *p*-C₆H₄) ppm. ¹³C NMR (CD₂Cl₂, 100 MHz) δ 111.39 (Ar quat), 119.41 (CN), 122.81 (ArBr quat), 127.45 (Ar CH), 127.99 (vinylene CH), 128.92 (Ar CH), 131.39 (vinylene CH), 132.46 (Ar CH), 133.06 (Ar CH), 135.97 (Ar quat), 141.96 (Ar quat) ppm. MS (EI) 285 (M+2), 283

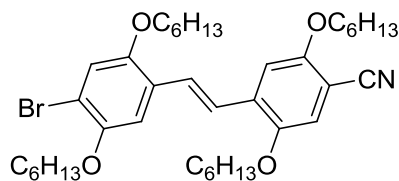
(M⁺), 204, 203 (base), 177, 176, 151, 127, 103 m/z. HRMS calcd for C₁₅H₁₀NBr 282.9995 g/mol. Found: 282.9997 g/mol.



4-(4-bromostyryl)-2,5-bis(hexyloxy)benzonitrile (Br-AD-CN, vii39). According to the general HWE procedure, **Br-A-CHO** (611 mg, 3.30 mmol), **P-D-CN** (2.106 g, 4.95 mmol), and LiCl (321 mg, 7.57 mmol) were dissolved in THF (40 mL) and cooled to 0 °C under N₂. KO^tBu (850 mg, 7.57 mmol) was added portionwise over 5 minutes, and the reaction was allowed to come to rt overnight with stirring. After workup, column chromatography (silica gel, 9:1 hexanes:CHCl₃) gave the title compound as a pale yellow solid (1.414 g, 92%). ¹H NMR (CD₂Cl₂, 400 MHz) δ 0.85-1.00 (6H, mult), 1.30-1.45 (8H, mult), 1.45-1.55 (4H, mult), 1.70-1.80 (4H, mult), 3.97 (2H, t, *J* = 6.4 Hz, OCH₂), 4.09 (2H, t, *J* = 6.4 Hz, OCH₂), 7.04 (1H, s), 7.158 (1H, s), 7.18 (1H, d, *J* = 17.2 Hz, *trans* CH=CH), 7.43 (2H, d, *J* = 8.0 Hz, *p*-C₆H₄), 7.44 (1H, d, *J* = 17.2 Hz, *trans* CH=CH), 7.51 (2H, d, *J* = 8.0 Hz, *p*-C₆H₄) ppm. ¹³C NMR (CD₂Cl₂, 100 MHz) δ 14.36 (CH₃), 14.37 (CH₃), 23.15 (CH₂), 23.18 (CH₂), 26.11 (CH₂), 26.36 (CH₂), 29.61 (CH₂), 29.68 (CH₂), 32.07 (CH₂), 32.10 (CH₂), 70.11 (OCH₂), 70.24 (OCH₂), 101.18 (Ar quat), 110.76 (Ar CH), 117.04 (Ar CH), 117.15 (CN), 122.50 (ArBr quat), 123.60 (vinylene CH), 128.87 (Ar CH), 132.34 (vinylene CH), 132.43 (Ar CH), 132.81 (Ar quat), 136.69 (Ar quat), 150.79 (ArO quat), 155.66 (ArO quat) ppm.

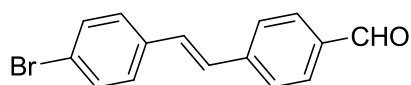


4-(4-bromo-2,5-bis(hexyloxy)styryl)benzonitrile (Br-DA-CN, vii35). According to the general HWE procedure, **Br-D-CHO** (1.272 g, 3.30 mmol), **P-A-CN** (1.115 g, 4.95 mmol), and LiCl (321 mg, 7.57 mmol) were dissolved in THF (40 mL) and cooled to 0 °C under N₂. KO^tBu (850 mg, 7.57 mmol) was added portionwise over 5 minutes, and the reaction was allowed to come to rt overnight with stirring. After workup, column chromatography (silica gel, 4:1 hexanes:DCM) gave the title compound as a pale yellow solid (1.480 g, 96%). ¹H NMR (CD₂Cl₂, 400 MHz) δ 0.85-1.00 (6H, mult), 1.30-1.45 (8H, mult), 1.45-1.55 (4H, mult), 1.70-1.80 (4H, mult), 3.97 (2H, t, *J* = 6.4 Hz, OCH₂), 4.03 (2H, t, *J* = 6.4 Hz, OCH₂), 7.13 (1H, s), 7.13 (1H, s), 7.16 (1H, d, *J* = 16.4 Hz, *trans* CH=CH), 7.52 (1H, d, *J* = 16.4 Hz, *trans* CH=CH), 7.60 (2H, d, *J* = 8.4 Hz, *p*-C₆H₄), 7.64 (2H, d, *J* = 8.4 Hz, *p*-C₆H₄) ppm. ¹³C NMR (CD₂Cl₂, 100 MHz) δ 14.36 (CH₃), 14.39 (CH₃), 23.18 (CH₂), 26.24 (CH₂), 26.39 (CH₂), 29.76 (CH₂), 29.81 (CH₂), 32.11 (CH₂), 70.18 (OCH₂), 70.72 (OCH₂), 111.04 (ArBr quat), 112.12 (Ar CH), 113.40 (Ar quat), 118.35 (Ar CH), 119.35 (CN), 125.93 (Ar quat), 127.15 (vinylene CH), 127.36 (Ar CH), 127.88 (vinylene CH), 133.03 (Ar CH), 142.75 (Ar quat), 150.34 (ArO quat), 151.95 (ArO quat) ppm.

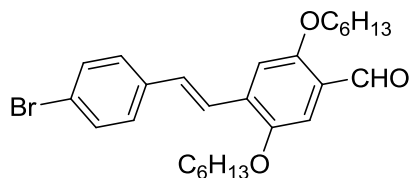


4-(4-bromo-2,5-bis(hexyloxy)styryl)-2,5-bis(hexyloxy)benzonitrile (Br-DD-CN, vii42).

According to the general HWE procedure, **Br-D-CHO** (1.272 g, 3.30 mmol), **P-D-CN** (2.106 g, 4.95 mmol), and LiCl (321 mg, 7.57 mmol) were dissolved in THF (40 mL) and cooled to 0 °C under N₂. KO^tBu (850 mg, 7.57 mmol) was added portionwise over 5 minutes, and the reaction was allowed to come to rt overnight with stirring. After workup, column chromatography (silica gel, 4:1 hexanes:DCM) gave the title compound as a bright yellow solid (2.240 g, 96%). ¹H NMR (CD₂Cl₂, 400 MHz) δ 0.85-1.00 (12H, mult), 1.30-1.45 (16H, mult), 1.45-1.55 (8H, mult), 1.70-1.80 (8H, mult), 3.97 (4H, t, *J* = 6.4 Hz, OCH₂), 4.02 (2H, t, *J* = 6.4 Hz, OCH₂), 4.10 (2H, t, *J* = 6.4 Hz, OCH₂), 7.04 (1H, s), 7.13 (1H, s), 7.15 (1H, s), 7.18 (1H, s), 7.45 (1H, d, *J* = 16.8 Hz, *trans* CH=CH), 7.51 (1H, d, *J* = 16.8 Hz, *trans* CH=CH) ppm. ¹³C NMR (CD₂Cl₂, 100 MHz) δ 14.38 (CH₃), 14.397 (CH₃), 23.16 (CH₂), 23.19 (CH₂), 23.21 (CH₂), 26.13 (CH₂), 26.26 (CH₂), 26.37 (CH₂), 29.64 (CH₂), 29.72 (CH₂), 29.79 (CH₂), 29.84 (CH₂), 32.09 (CH₂), 32.13 (CH₂), 70.04 (OCH₂), 70.11 (OCH₂), 70.18 (OCH₂), 70.69 (OCH₂), 100.82 (Ar quat), 110.73 (Ar CH), 112.26 (Ar CH), 113.06 (ArBr quat), 116.97 (Ar CH), 117.25 (CN), 118.28 (Ar CH), 123.56 (vinylene CH), 126.69 (Ar quat), 127.16 (vinylene CH), 133.66 (Ar quat), 150.34 (ArO quat), 150.73 (ArO quat), 151.89 (ArO quat), 155.70 (ArO quat) ppm. MS (EI): 685 (M+2, base), 683 (M⁺), 605, 349, 347, 267, 205, 85 m/z. HRMS calcd for C₃₉H₅₈NO₄Br: 683.3549 g/mol. Found: 683.3540 g/mol.

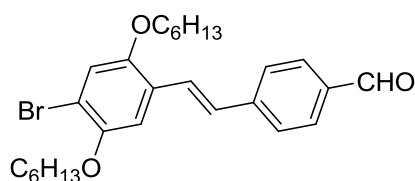


4-(4-bromostyryl)benzaldehyde (Br-AA-CHO, vii48). According to the general DIBAL-H procedure, **Br-AA-CN** (448 mg, 1.80 mmol) was dissolved in DCM (10 mL) and cooled to 0 °C. DIBAL-H (1.0M in hexanes, 1.9 mL, 1.9 mmol) was added dropwise. After workup, the solvent was removed *in vacuo* to give the title compound as a white solid (423 mg, 93%). ¹H NMR (CD₂Cl₂, 400 MHz) δ 7.17 (1H, d, *J* = 16.4 Hz, *trans* CH=CH), 7.24 (1H, d, *J* = 16.4 Hz, *trans* CH=CH), 7.45 (2H, d, *J* = 8.4 Hz, *p*-C₆H₄), 7.53 (2H, d, *J* = 8.4 Hz, *p*-C₆H₄), 7.68 (2H, d, *J* = 8.4 Hz, *p*-C₆H₄), 7.87 (2H, d, *J* = 8.4 Hz, *p*-C₆H₄), 9.99 (1H, s, CHO) ppm. ¹³C NMR (CD₂Cl₂, 100 MHz) δ 122.62 (ArBr quat), 127.52 (vinylene CH), 128.61 (Ar CH), 128.93 (vinylene CH), 130.63 (vinylene CH), 131.20 (Ar CH), 132.47 (Ar CH), 136.20 (Ar quat), 136.20 (Ar quat), 143.49 (Ar quat), 191.97 (CHO) ppm. MS (EI) 288 (M+2), 286 (M⁺), 178 (base), 152, 131, 107, 102, 89, 84, 76, 57 m/z. HRMS calcd for C₁₅H₁₁BrO: 285.9984 g/mol. Found: 285.9993 g/mol.



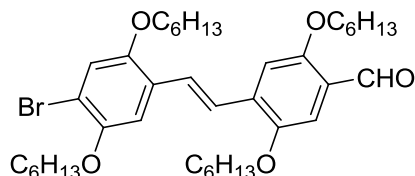
4-(4-bromostyryl)-2,5-bis(hexyloxy)benzaldehyde (Br-AD-CHO, vii50). According to the general DIBAL-H procedure, **Br-AD-CN** (2.154 g, 4.446 mmol) was dissolved in DCM (25 mL) and cooled to 0 °C. DIBAL-H (1.0M in hexanes, 4.5 mL, 4.5 mmol) was added dropwise. After workup, column chromatography (silica gel, 3:2 hexanes:DCM) gave the title compound as a yellow oil that crystallized on standing (2.095 g, 95%). ¹H NMR (CD₂Cl₂, 400 MHz) δ 0.85-1.00 (6H, mult), 1.30-1.45 (8H, mult), 1.45-1.55 (4H, mult), 1.70-1.80 (4H, mult), 4.02 (2H, t, *J* = 6.4 Hz, OCH₂), 4.12 (2H, t, *J* = 6.4 Hz, OCH₂), 7.20 (1H, s), 7.30 (1H, s), 7.22 (1H, d, *J* = 16.4 Hz, *trans* CH=CH), 7.44 (2H, d, *J* = 8.4 Hz, *p*-C₆H₄), 7.49 (1H, d, *J* = 16.4 Hz, *trans* CH=CH), 7.51

(2H, d, $J = 8.4$ Hz, p -C₆H₄), 10.43 (1h, s, CHO) ppm. ¹³C NMR (CD₂Cl₂, 100 MHz) δ 14.37 (CH₃), 23.17 (CH₂), 23.19 (CH₂), 26.32 (CH₂), 26.42 (CH₂), 29.76 (CH₂), 29.78 (CH₂), 32.13 (CH₂), 32.14 (CH₂), 69.75 (OCH₂), 69.85 (OCH₂), 110.50 (Ar CH), 111.26 (Ar CH), 122.38 (ArBr quat), 124.14 (vinylene CH), 125.06 (Ar quat), 128.86 (Ar CH), 131.28 (vinylene CH), 132.40 (Ar CH), 134.13 (Ar quat), 136.89 (Ar quat), 151.33 (ArO quat), 156.68 (ArO quat), 189.25 (CHO) ppm. MS (EI): 488 (M+2), 486 (M⁺, base), 402, 374, 320, 318, 234, 206, 181, 165, 152, 119 m/z. HRMS calcd for C₂₇H₃₅O₃Br: 486.1770 g/mol. Found: 486.1763 g/mol.



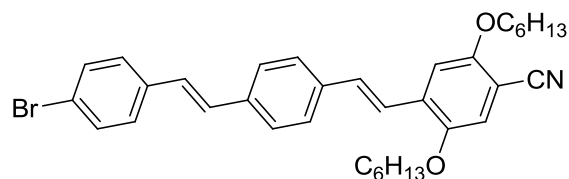
4-(4-bromo-2,5-bis(hexyloxy)styryl)benzaldehyde (Br-DA-CHO, vi59). According to the general DIBAL-H procedure, **Br-DA-CN** (2.560 g, 5.28 mmol) was dissolved in DCM (30 mL) and cooled to 0 °C. DIBAL-H (1.0M in hexanes, 5.3 mL, 5.3 mmol) was added dropwise. After workup, column chromatography (silica gel, 3:2 hexanes:DCM) gave the title compound as a yellow solid (2.420 g, 94%). ¹H NMR (CD₂Cl₂, 400 MHz) δ 0.85-1.00 (6H, mult), 1.30-1.45 (8H, mult), 1.45-1.55 (4H, mult), 1.70-1.80 (4H, mult), 3.98 (2H, t, $J = 6.4$ Hz, OCH₂), 4.04 (2H, t, $J = 6.4$ Hz, OCH₂), 7.13 (1H, s), 7.16 (1H, s), 7.21 (1H, d, $J = 16.4$ Hz, *trans* CH=CH), 7.57 (1H, d, $J = 16.4$ Hz, *trans* CH=CH), 7.68 (2H, d, $J = 8.4$ Hz, p -C₆H₄), 7.86 (2H, d, $J = 8.4$ Hz, p -C₆H₄), 9.98 (1H, s, CHO) ppm. ¹³C NMR (CD₂Cl₂, 100 MHz) δ 14.37 (CH₃), 14.39 (CH₃), 23.19 (CH₂), 26.25 (CH₂), 26.41 (CH₂), 29.79 (CH₂), 29.83 (CH₂), 32.13 (CH₂), 70.20 (OCH₂), 70.73 (OCH₂), 112.10 (Ar CH), 113.25 (ArBr quat), 118.36 (Ar CH), 126.19 (Ar quat), 126.93

(vinylene CH), 127.41 (Ar CH), 128.46 (vinylene CH), 130.62 (Ar CH), 135.96 (Ar quat), 144.27 (Ar quat), 150.35 (ArO quat), 151.95 (ArO quat), 191.95 (CHO) ppm.

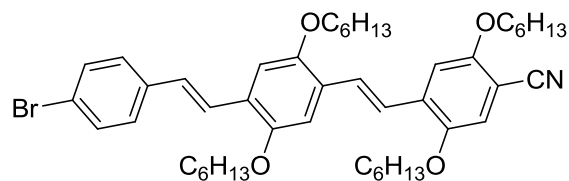


4-(4-bromo-2,5-bis(hexyloxy)styryl)-2,5-bis(hexyloxy)benzaldehyde (Br-DD-CHO, vii57).

According to the general DIBAL-H procedure, **Br-DD-CN** (2.00 g, 2.92 mmol) was dissolved in DCM (20 mL) and cooled to 0 °C. DIBAL-H (1.0M in hexanes, 3.0 mL, 3.0 mmol) was added dropwise. After workup, column chromatography (silica gel, 4:1 hexanes:DCM) gave the title compound as a yellow solid (1.843 g, 92%). ¹H NMR (CD₂Cl₂, 400 MHz) δ 0.85-1.00 (12H, mult), 1.30-1.45 (16H, mult), 1.45-1.55 (8H, mult), 1.70-1.80 (8H, mult), 3.98 (2H, t, *J* = 6.4 Hz, OCH₂), 4.03 (2H, t, *J* = 6.4 Hz, OCH₂), 4.04 (2H, t, *J* = 6.4 Hz, OCH₂), 4.11 (2H, t, *J* = 6.4 Hz, OCH₂), 7.13 (1H, s), 7.17 (1H, s), 7.23 (1H, s), 7.30 (1H, s), 7.50 (1H, d, *J* = 16.8 Hz, *trans* CH=CH), 7.58 (1H, d, *J* = 16.8 Hz, *trans* CH=CH), 10.43 (1H, s, CHO) ppm. ¹³C NMR (CD₂Cl₂, 100 MHz) δ 14.40 (CH₃), 23.19 (CH₂), 23.24 (CH₂), 26.28 (CH₂), 26.35 (CH₂), 26.40 (CH₂), 29.42 (CH₂), 29.81 (CH₂), 29.83 (CH₂), 29.85 (CH₂), 32.14 (CH₂), 32.17 (CH₂), 32.18 (CH₂), 69.68 (OCH₂), 69.78 (OCH₂), 70.13 (OCH₂), 70.68 (OCH₂), 110.41 (Ar CH), 111.17 (Ar CH), 112.19 (Ar CH), 112.94 (ArBr quat), 118.29 (Ar CH), 124.05 (vinylene CH), 124.84 (Ar quat), 126.92 (Ar quat), 127.07 (vinylene CH), 135.02 (Ar quat), 150.35 (ArO quat), 151.28 (ArO quat), 151.89 (ArO quat), 156.75 (ArO quat), 189.25 (CHO) ppm. MS (ESI): 711 (M+Na+2, base), 709 (M+Na), 631, 527, 365 m/z. HRMS calcd for C₃₉H₅₉O₅Br+Na: 709.3444 g/mol. Found: 709.3455 g/mol.

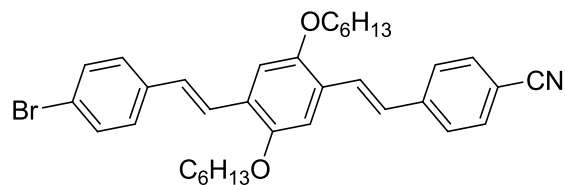


4-(4-(4-bromostyryl)styryl)-2,5-bis(hexyloxy)benzonitrile (Br-AAD-CN, vii52). According to the general HWE procedure, **Br-AA-CHO** (700 mg, 2.44 mmol), **P-D-CN** (1.557 g, 3.66 mmol), and LiCl (237 mg, 5.59 mmol) were dissolved in THF (30 mL) and cooled to 0 °C under N₂. KO^tBu (627 mg, 5.59 mmol) was added portionwise over 5 minutes, and the reaction was allowed to come to rt overnight with stirring. After workup, column chromatography (silica gel, 7:3 hexanes:DCM) gave the title compound as a yellow solid (1.166 g, 84%). ¹H NMR (CD₂Cl₂, 400 MHz) δ 0.93 (6H, t, *J* = 7.0 Hz), 1.30-1.40 (8H, mult), 1.50-1.60 (4H, mult), 1.86 (4H, pent, *J* = 7.3 Hz), 3.98 (2H, t, *J* = 6.4 Hz, OCH₂), 4.11 (2H, t, *J* = 6.4 Hz, OCH₂), 7.05 (1H, s), 7.09 (1H, d, *J* = 16.4 Hz, *trans* CH=CH), 7.14 (1H, d, *J* = 16.4 Hz, *trans* CH=CH), 7.19 (1H, s), 7.25 (1H, d, *J* = 16.4 Hz, *trans* CH=CH), 7.42 (2H, d, *J* = 8.8 Hz, *p*-C₆H₄), 7.48 (1H, d, *J* = 16.4 Hz, *trans* CH=CH), 7.50 (2H, d, *J* = 8.8 Hz, *p*-C₆H₄), 7.53 (2H, d, *J* = 8.8 Hz, *p*-C₆H₄), 7.56 (2H, d, *J* = 8.8 Hz, *p*-C₆H₄) ppm. ¹³C NMR (CD₂Cl₂, 100 MHz) δ 14.38 (CH₃), 23.16 (CH₂), 23.18 (CH₂), 26.13 (CH₂), 26.39 (CH₂), 29.64 (CH₂), 29.73 (CH₂), 32.09 (CH₂), 32.13 (CH₂), 70.15 (OCH₂), 70.27 (OCH₂), 100.95 (ArCN quat), 110.66 (Ar CH), 117.07 (Ar CH), 117.23 (CN), 121.89 (ArBr quat), 122.83 (vinylene CH), 127.52 (Ar CH), 127.81 (Ar CH), 128.13 (vinylene CH), 128.60 (Ar CH), 129.35 (vinylene CH), 132.16 (vinylene CH), 132.36 (Ar CH), 133.22 (Ar quat), 136.86 (Ar quat), 137.28 (Ar quat), 137.59 (Ar quat), 150.80 (ArO quat), 155.72 (ArO quat) ppm. MS (ES): 587 (M+2), 585 (M⁺), 419, 420, 251, 228, 181, 169, 131, 119, 100, 69 (base), 55 m/z. HRMS calcd for C₃₅H₄₀NO₂Br: 585.2242 g/mol. Found: 585.2240 g/mol.

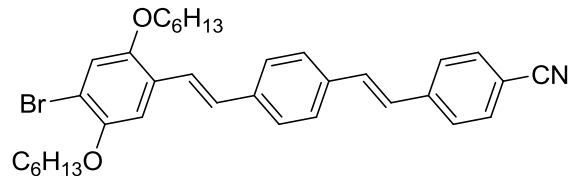


4-(4-(4-bromostyryl)-2,5-bis(hexyloxy)styryl)-2,5-bis(hexyloxy)benzonitrile (Br-ADD-CN, vii53).

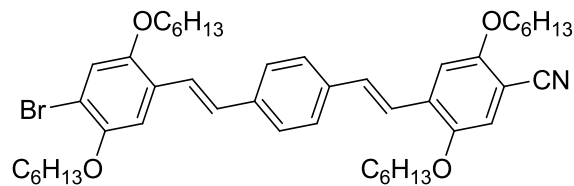
According to the general HWE procedure, **Br-AD-CHO** (850 mg, 1.74 mmol), **P-D-CN** (1.11 g, 2.61 mmol), and LiCl (170 mg, 4.01 mmol) were dissolved in THF (25 mL) and cooled to 0 °C under N₂. KO^tBu (450 mg, 4.01 mmol) was added portionwise over 5 minutes, and the reaction was allowed to come to rt overnight with stirring. After workup, column chromatography (silica gel, 4:1 hexanes:DCM) gave the title compound as a yellow solid (1.181 g, 86%). ¹H NMR (CD₂Cl₂, 400 MHz) δ 0.85-0.95 (12H, mult), 1.30-1.45 (16H, mult), 1.45-1.60 (8H, mult), 1.80-1.95 (8H, mult), 3.98 (2H, t, *J* = 6.4 Hz, OCH₂), 4.05 (2H, t, *J* = 6.4 Hz, OCH₂), 4.07 (2H, t, *J* = 6.4 Hz, OCH₂), 4.10 (2H, t, *J* = 6.4 Hz, OCH₂), 7.04 (1H, s), 7.13 (1H, d, *J* = 16.4 Hz, *trans* CH=CH), 7.14 (1H, s), 7.15 (1H, s), 7.20 (1H, s), 7.42 (2H, d, *J* = 8.4 Hz, *p*-C₆H₄), 7.46-7.51 (4H, mult) 7.59 (1H d, *J* = 16.8 Hz, *trans* CH=CH) ppm. ¹³C NMR (CD₂Cl₂, 100 MHz) δ 14.37 (CH₃), 14.39 (CH₃), 23.16 (CH₂), 23.23 (CH₂), 23.25 (CH₂), 26.15 (CH₂), 26.39 (CH₂), 26.48 (CH₂), 26.54 (CH₂), 29.66 (CH₂), 29.75 (CH₂), 30.00 (CH₂), 32.10 (CH₂), 32.16 (CH₂), 32.16 (CH₂), 69.96 (OCH₂), 70.02 (OCH₂), 70.08 (OCH₂), 70.19 (OCH₂), 100.64 (ArCN quat), 110.59 (Ar CH), 110.91 (Ar CH), 111.31 (Ar CH), 117.07 (Ar CH), 117.32 (CN), 121.62 (ArBr quat), 122.99 (vinylene CH), 124.59 (vinylene CH), 127.22 (Ar quat), 127.50 (vinylene CH), 127.70 (Ar quat), 128.33 (vinylene CH), 128.56 (Ar CH), 132.31 (Ar CH) 133.97 (Ar quat), 137.50 (Ar quat), 150.74 (ArO quat), 151.66 (ArO quat), 151.94 (ArO quat), 155.72 (ArO quat) ppm. MS (ESI): 810 (M+Na+2, base), 808 (M+Na), 788, 786, 776, 685 (base)\m/z. HRMS calcd for C₄₇H₆₄NO₄Br+Na: 808.3916 g/mol. Found: 808.3965 g/mol.



4-(4-(4-bromostyryl)-2,5-bis(hexyloxy)styryl)benzonitrile (Br-ADA-CN, vii54). According to the general HWE procedure, **Br-AD-CHO** (850 mg, 1.74 mmol), **P-A-CN** (588 mg, 2.61 mmol), and LiCl (170 mg, 4.01 mmol) were dissolved in THF (25 mL) and cooled to 0 °C under N₂. KO^tBu (450 mg, 4.01 mmol) was added portionwise over 5 minutes, and the reaction was allowed to come to rt overnight with stirring. After workup, column chromatography (silica gel, 2:3 hexanes:DCM) gave the title compound as a yellow solid (950 mg, 92%). ¹H NMR (CD₂Cl₂, 400 MHz) δ 0.93 (6H, t, *J* = 7.0 Hz), 1.30-1.45 (8H, mult), 1.45-1.60 (4H, mult), 1.86 (4H, pent, *J* = 6.7 Hz), 4.06 (2H, t, *J* = 6.4 Hz, OCH₂), 4.07 (2H, t, *J* = 6.4 Hz, OCH₂), 7.13 (1H, d, *J* = 16.4 Hz, *trans* CH=CH), 7.135 (1H, s), 7.138 (1H, s), 7.18 (1H, d, *J* = 16.4 Hz, *trans* CH=CH), 7.42 (2H, d, *J* = 8.4 Hz, *p*-C₆H₄), 7.48 (1H, d, *J* = 16.4 Hz, *trans* CH=CH), 7.50 (2H, d, *J* = 8.4 Hz, *p*-C₆H₄), 7.61 (1H, d, *J* = 16.4 Hz, *trans* CH=CH), 7.61 (2H, d, *J* = 8.8 Hz, *p*-C₆H₄), 7.65 (2H, d, *J* = 8.8 Hz, *p*-C₆H₄) ppm. ¹³C NMR (CD₂Cl₂, 100 MHz) δ 14.39 (CH₃), 23.23 (CH₂), 26.51 (CH₂), 29.98 (CH₂), 32.20 (CH₂), 70.02 (OCH₂), 70.06 (OCH₂), 110.83 (ArCN quat), 110.95 (Ar CH), 111.23 (Ar CH), 119.61 (CN), 121.66 (ArBr quat), 124.55 (vinylene CH), 126.44 (Ar quat), 127.57 (Ar CH), 127.39 (vinylene CH), 127.57 (vinylene CH), 127.98 (Ar quat) 128.48 (vinylene CH), 128.58 (Ar CH), 132.30 (vinylene CH), 133.02 (Ar CH), 137.45 (Ar quat), 143.03 (Ar quat), 151.64 (ArO quat), 152.02 (ArO quat) ppm. MS (ES): 587 (M+2), 585 (M⁺), 485, 483, 419, 417, 401, 317, 315, 290, 235, 206, 169, 152, 131, 116, 85, 69, 55 (base) m/z. HRMS calcd for C₃₅H₄₀NO₂Br: 585.2242 g/mol. Found: 585.2237 g/mol.

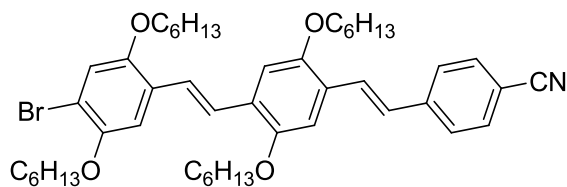


4-(4-(4-bromo-2,5-bis(hexyloxy)styryl)styryl)benzonitrile (Br-DAA-CN, vii62). According to the general HWE procedure, **Br-DA-CHO** (1.10 g, 2.26 mmol), **P-A-CN** (761 mg, 3.38 mmol), and LiCl (220 mg, 4.01 mmol) were dissolved in THF (40 mL) and cooled to 0 °C under N₂. KO^tBu (583 mg, 5.19 mmol) was added portionwise over 5 minutes, and the reaction was allowed to come to rt overnight with stirring. After workup, column chromatography (silica gel, 2:3 hexanes:DCM) gave the title compound as a yellow solid (1.305 g, 99%). ¹H NMR (CD₂Cl₂, 400 MHz) δ 0.93 (6H, t, *J* = 6.4 Hz), 1.30-1.45 (8H, mult), 1.50-1.60 (4H, mult), 1.83 (2H, pent, *J* = 6.8 Hz), 1.85 (2H, pent, *J* = 6.8 Hz), 3.97 (2H, t, *J* = 6.4 Hz, OCH₂), 4.04 (2H, t, *J* = 6.4 Hz, OCH₂), 7.12 (1H, s), 7.14 (1H, d, *J* = 16.0 Hz, *trans* CH=CH), 7.16 (1H, s), 7.16 (1H, d, *J* = 16.4 Hz, *trans* CH=CH), 7.25 (1H, d, *J* = 16.0 Hz, *trans* CH=CH), 7.46 (1H, d, *J* = 16.4 Hz, *trans* CH=CH), 7.55 (4H, br s, *p*-C₆H₄), 7.61 (2H, d, *J* = 8.8 Hz, *p*-C₆H₄), 7.65 (2H, d, *J* = 8.8 Hz, *p*-C₆H₄) ppm. ¹³C NMR (CD₂Cl₂, 100 MHz) δ 14.39 (CH₃), 23.21 (CH₂), 26.26 (CH₂), 26.42 (CH₂), 29.84 (CH₂), 29.86 (CH₂), 32.14 (CH₂), 32.15 (CH₂), 70.22 (OCH₂), 70.74 (OCH₂), 110.10 (ArCN quat), 110.93 (Ar CH), 112.41 (ArBr quat), 118.35 (Ar CH), 119.52 (CN), 123.97 (vinylene CH), 126.87 (Ar quat), 127.06 (vinylene CH), 127.38 (Ar CH), 127.47 (Ar CH), 127.85 (Ar CH), 129.15 (vinylene CH), 132.34 (vinylene CH), 133.06 (Ar CH), 136.27 (Ar quat), 138.62 (Ar quat), 142.40 (Ar quat), 150.38 (ArO quat), 151.73 (ArO quat) ppm. MS (ESI): 610 (M+Na+2), 608 (M+Na), 527, 365 (base)\m/z. HRMS calcd for C₃₅H₄₀NO₂Br+Na: 608.2140 g/mol. Found: 608.2094 g/mol.



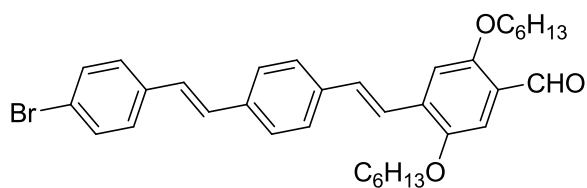
4-(4-(4-bromo-2,5-bis(hexyloxy)styryl)styryl)-2,5-bis(hexyloxy)styrylbenzonitrile (Br-DAD-CN, vii61). According to the general HWE procedure, **Br-DA-CHO** (1.10 g, 2.26 mmol), **P-D-CN** (1.44 g, 3.38 mmol), and LiCl (220 mg, 4.01 mmol) were dissolved in THF (30 mL) and cooled to 0 °C under N₂. KO^tBu (583 mg, 5.19 mmol) was added portionwise over 5 minutes, and the reaction was allowed to come to rt overnight with stirring. After workup, column chromatography (silica gel, 7:3 hexanes:DCM) gave the title compound as a yellow solid (1.687 g, 95%). ¹H NMR (CD₂Cl₂, 400 MHz) δ 0.85-0.95 (12H, mult), 1.30-1.45 (16H, mult), 1.45-1.60 (8H, mult), 1.80-1.95 (8H, mult), 3.97 (2H, t, *J* = 6.4 Hz, OCH₂), 3.98 (2H, t, *J* = 6.4 Hz, OCH₂), 4.04 (2H, t, *J* = 6.4 Hz, OCH₂), 4.11 (2H, t, *J* = 6.4 Hz, OCH₂), 7.04 (1H, s), 7.12 (1H, s), 7.16 (1H, d, *J* = 16.4 Hz, *trans* CH=CH), 7.16(1H, s), 7.19 (1H, s), 7.25 (1H, d, *J* = 16.4 Hz, *trans* CH=CH), 7.46 (1H, d, *J* = 16.4 Hz, *trans* CH=CH), 7.48 (1H, d, *J* = 16.4 Hz, *trans* CH=CH), 7.55 (4H, br s, *p*-C₆H₄) ppm. ¹³C NMR (CD₂Cl₂, 100 MHz) δ 14.39 (CH₃), 23.18 (CH₂), 23.21 (CH₂), 26.14 (CH₂), 26.27 (CH₂), 26.41 (CH₂), 26.44 (CH₂), 29.66 (CH₂), 29.74 (CH₂), 29.86 (CH₂), 29.87 (CH₂), 32.11 (CH₂), 32.15 (CH₂), 32.17 (CH₂), 70.15 (OCH₂), 70.23 (OCH₂), 70.26 (OCH₂), 70.75 (OCH₂), 100.88 (ArCN quat), 110.60 (Ar CH), 111.89 (Ar CH), 112.35 (ArBr quat), 117.05 (Ar CH), 117.25 (CN), 118.35 (Ar CH), 122.60 (vinylene CH), 123.77 (vinylene CH), 126.92 (Ar quat), 127.45 (Ar CH), 127.79 (Ar CH), 129.21 (vinylene CH), 133.27 (vinylene CH) 133.27 (Ar quat), 136.99 (Ar quat), 138.36 (Ar quat), 150.38 (ArO quat), 150.78 (ArO quat), 151.72 (ArO quat), 155.73 (ArO quat) ppm. MS (ESI): 810 (M+Na+2), 808

(M+Na), 788, 786, 711, 709, 691, 527 (base)\m/z. HRMS calcd for C₄₇H₆₄NO₄Br+Na: 808.3916 g/mol. Found: 808.4011 g/mol.



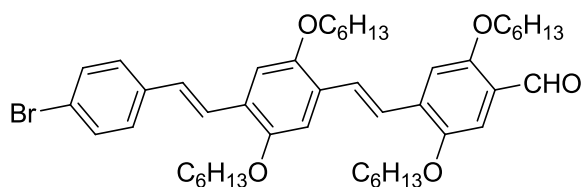
4-(4-(4-bromo-2,5-bis(hexyloxy)styryl)-2,5-bis(hexyloxy)styrylstyryl)benzonitrile (Br-DDA-CN, vii60). According to the general HWE procedure, **Br-DD-CHO** (1.64 g, 2.39 mmol), **P-A-CN** (807 mg, 3.58 mmol),-were dissolved in THF (30 mL) and cooled to 0 °C under N₂. KO^tBu (618 mg, 5.50 mmol) was added portionwise over 5 minutes, and the reaction was allowed to come to rt overnight with stirring. After workup, column chromatography (silica gel, 1:1 hexanes:DCM) gave the title compound as a yellow solid (1.610 g, 86%). ¹H NMR (CD₂Cl₂, 400 MHz) δ 0.85-0.95 (12H, mult), 1.30-1.45 (16H, mult), 1.45-1.60 (8H, mult), 1.80-1.95 (8H, mult), 3.98 (2H, t, *J* = 6.4 Hz, OCH₂), 4.04 (2H, t, *J* = 6.4 Hz, OCH₂), 4.06 (2H, t, *J* = 6.4 Hz, OCH₂), 4.07 (2H, t, *J* = 6.4 Hz, OCH₂), 7.11 (1H, s), 7.14 (1H, s), 7.17 (1H, s), 7.18 (1H, d, *J* = 16.4 Hz, *trans* CH=CH), 7.18 (1H, s), 7.45 (1H, d, *J* = 16.8 Hz, *trans* CH=CH), 7.50 (1H, d, *J* = 16.8 Hz, *trans* CH=CH), 7.62 (1H, d, *J* = 16.4 Hz, *trans* CH=CH), 7.62 (2H, d, *J* = 8.8 Hz, *p*-C₆H₄), 7.65 (2H, d, *J* = 8.8 Hz, *p*-C₆H₄) ppm. ¹³C NMR (CD₂Cl₂, 100 MHz) δ 14.40 (CH₃), 14.42 (CH₃), 14.43 (CH₃), 23.20 (CH₂), 23.24 (CH₂), 23.26 (CH₂), 26.29 (CH₂), 26.42 (CH₂), 26.50 (CH₂), 26.54 (CH₂), 29.88 (CH₂), 30.00 (CH₂), 30.02 (CH₂), 32.15 (CH₂), 32.19 (CH₂), 32.21 (CH₂), 32.24 (CH₂), 69.97 (OCH₂), 70.00 (OCH₂), 70.15 (OCH₂), 70.69 (OCH₂), 110.78 (Ar CH), 110.95 (Ar CH), 111.17 (ArCN quat), 111.95 (Ar CH), 112.13 (ArBr quat), 118.28 (Ar CH), 119.62 (CN), 124.15 (vinylene CH), 124.42 (vinylene CH), 126.14 (Ar quat), 127.21

(vinylene CH), 127.30 (Ar CH), 127.55 (Ar quat), 127.64 (vinylene CH), 128.81 (Ar quat), 133.03 (Ar CH), 143.10 (Ar quat), 150.37 (ArO quat), 151.58 (ArO quat), 151.68 (ArO quat), 152.05 (ArO quat) ppm. MS (ESI): 810 (M+Na+2), 808 (M+Na), 788, 786, 711, 709, 691, 527 (base)\m/z. HRMS calcd for C₄₇H₆₄NO₄Br+Na: 808.3916 g/mol. Found: 808.4011 g/mol. MS (ESI): 810 (M+Na+2), 808 (M+Na), 786, 776, 707, 527, 365 (base)\m/z. HRMS calcd for C₄₇H₆₄NO₄Br+Na: 808.3916 g/mol. Found: 808.3856 g/mol.



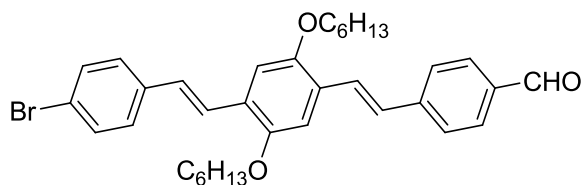
4-(4-(4-bromostyryl)styryl)-2,5-bis(hexyloxy)benzaldehyde (Br-AAD-CHO, vii69). According to the general DIBAL-H procedure, **Br-AAD-CN** (375 mg, 0.635 mmol) was dissolved in DCM (5 mL) and cooled to 0 °C. DIBAL-H (1.0M in hexanes, 0.75 mL, 0.75 mmol) was added dropwise. After workup, column chromatography (silica gel, 7:3 hexanes:DCM) gave the title compound as a yellow solid (308 mg, 82%). ¹H NMR (CD₂Cl₂, 400 MHz) δ 0.93 (6H, t, *J* = 7.0 Hz), 1.30-1.40 (8H, mult), 1.50-1.60 (4H, mult), 1.86 (4H, pent, *J* = 7.1 Hz), 4.04 (2H, t, *J* = 6.4 Hz, OCH₂), 4.12 (2H, t, *J* = 6.4 Hz, OCH₂), 7.09 (1H, d, *J* = 16.4 Hz, *trans* CH=CH), 7.14 (1H, d, *J* = 16.4 Hz, *trans* CH=CH), 7.22 (1H, s), 7.28 (1H, d, *J* = 16.4 Hz, *trans* CH=CH), 7.30 (1H, s), 7.41 (2H, d, *J* = 8.8 Hz, *p*-C₆H₄), 7.50 (2H, d, *J* = 8.8 Hz, *p*-C₆H₄), 7.53 (1H, d, *J* = 16.4 Hz, *trans* CH=CH), 7.54 (2H, d, *J* = 8.8 Hz, *p*-C₆H₄), 7.57 (2H, d, *J* = 8.4 Hz, *p*-C₆H₄), 10.44 (1H, s, CHO) ppm. ¹³C NMR (CD₂Cl₂, 100 MHz) δ 14.39 (CH₃), 23.16 (CH₂), 23.18 (CH₂), 23.21 (CH₂), 26.33 (CH₂), 26.44 (CH₂), 29.79 (CH₂), 32.13 (CH₂), 32.17 (CH₂), 69.76 (OCH₂), 69.84 (OCH₂), 110.47 (Ar CH), 111.07 (Ar CH), 121.85 (ArBr quat), 123.35 (vinylene CH), 124.89

(Ar quat), 127.51 (Ar CH), 127.79 (Ar CH), 128.03 (vinylene CH), 128.58 (Ar CH), 129.37 (vinylene CH), 132.11 (vinylene CH), 132.34 (Ar CH), 133.53 (Ar quat), 136.87 (Ar quat), 137.47 (Ar quat), 151.32 (ArO quat), 156.73 (ArO quat) 189.24 (CHO) ppm. MS (ES): 590 (M+2), 588 (M⁺), 420, 288, 286, 178 (base), 152, 131, 102, 90, 77, 69, 55 m/z. HRMS calcd for C₃₅H₄₁O₃Br: 588.2239 g/mol. Found: 588.2239 g/mol.



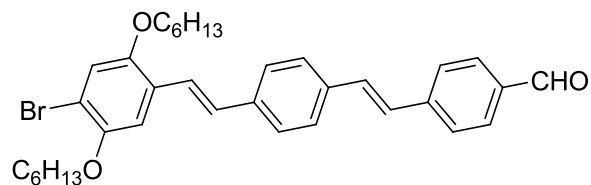
4-(4-(4-bromostyryl)-2,5-bis(hexyloxy)styryl)-2,5-bis(hexyloxy)benzaldehyde (Br-ADD-CHO, vii68). According to the general DIBAL-H procedure, **Br-ADD-CN** (500 mg, 0.635 mmol) was dissolved in DCM (5 mL) and cooled to 0 °C. DIBAL-H (1.0M in hexanes, 0.75 mL, 0.75 mmol) was added dropwise. After workup, column chromatography (silica gel, 7:3 hexanes:DCM) gave the title compound as a yellow solid (409 mg, 82%). ¹H NMR (CD₂Cl₂, 400 MHz) δ 0.85-0.95 (12H, mult), 1.30-1.45 (16H, mult), 1.45-1.60 (8H, mult), 1.80-1.95 (8H, mult), 4.05 (2H, t, *J* = 6.4 Hz, OCH₂), 4.06 (2H, t, *J* = 6.4 Hz, OCH₂), 4.07 (2H, t, *J* = 6.4 Hz, OCH₂), 7.04 (1H, s), 4.14 (2H, t, *J* = 6.4 Hz, OCH₂), 7.13 (1H, d, *J* = 16.4 Hz, *trans* CH=CH), 7.15 (1H, s), 7.17 (1H, s), 7.25 (1H, s), 7.30 (1H, s), 7.43 (2H, d, *J* = 8.4 Hz, *p*-C₆H₄), 7.50 (2H, d, *J* = 8.4 Hz, *p*-C₆H₄), 7.50 (1H d, *J* = 16.4 Hz, *trans* CH=CH), 7.53 (1H d, *J* = 16.8 Hz, *trans* CH=CH), 7.63 (1H d, *J* = 16.8 Hz, *trans* CH=CH), 10.43 (1H, s, CHO) ppm. ¹³C NMR (CD₂Cl₂, 100 MHz) δ 14.38 (CH₃), 14.41 (CH₃), 23.18 (CH₂), 23.24 (CH₂), 23.26 (CH₂), 26.35 (CH₂), 26.44 (CH₂), 26.50 (CH₂), 26.53 (CH₂), 29.81 (CH₂), 30.00 (CH₂), 32.14 (CH₂), 32.19 (CH₂), 32.20 (CH₂), 32.23 (CH₂), 69.70 (OCH₂), 69.78 (OCH₂), 69.96 (OCH₂), 69.99 (OCH₂), 110.40

(Ar CH), 110.90 (Ar CH), 110.99 (Ar CH), 111.22 (Ar CH), 121.59 (ArBr quat), 123.49 (vinylene CH), 124.61 (vinylene CH), 124.72 (Ar quat), 127.43 (Ar quat), 127.43 (vinylene CH), 127.57 (Ar quat), 128.24 (vinylene CH), 128.55 (Ar CH), 132.30 (Ar CH) 135.31 (Ar quat), 137.51 (Ar quat), 151.27 (ArO quat), 151.67 (ArO quat), 151.92 (ArO quat), 156.79 (ArO quat), 189.25 (CHO) ppm.



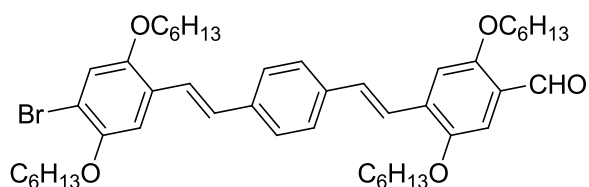
4-(4-(4-bromostyryl)-2,5-bis(hexyloxy)styryl)benzaldehyde (Br-ADA-CHO, vii70). According to the general DIBAL-H procedure, **Br-ADA-CN** (375 mg, 0.635 mmol) was dissolved in DCM (5 mL) and cooled to 0 °C. DIBAL-H (1.0M in hexanes, 0.75 mL, 0.75 mmol) was added dropwise. After workup, column chromatography (silica gel, 2:3 hexanes:DCM) gave the title compound as a yellow solid (302 mg, 81%). ¹H NMR (CD₂Cl₂, 400 MHz) δ 0.94 (6H, t, *J* = 6.8 Hz), 1.30-1.45 (8H, mult), 1.45-1.60 (4H, mult), 1.80-1.95 (4H, mult), 4.06 (2H, t, *J* = 6.4 Hz, OCH₂), 4.07 (2H, t, *J* = 6.4 Hz, OCH₂), 7.13 (1H, d, *J* = 16.4 Hz, *trans* CH=CH), 7.14 (1H, s), 7.15 (1H, s), 7.23 (1H, d, *J* = 16.8 Hz, *trans* CH=CH), 7.42 (2H, d, *J* = 8.4 Hz, *p*-C₆H₄), 7.49 (1H, d, *J* = 16.4 Hz, *trans* CH=CH), 7.50 (2H, d, *J* = 8.4 Hz, *p*-C₆H₄), 7.60 (1H, d, *J* = 16.8 Hz, *trans* CH=CH), 7.69 (2H, d, *J* = 8.4 Hz, *p*-C₆H₄), 7.86 (2H, d, *J* = 8.4 Hz, *p*-C₆H₄), 9.98 (CHO) ppm. ¹³C NMR (CD₂Cl₂, 100 MHz) δ 14.41 (CH₃), 23.24 (CH₂), 26.53 (CH₂), 30.00 (CH₂), 32.21 (CH₂), 70.04 (OCH₂), 110.93 (Ar CH), 111.16 (Ar CH), 121.63 (ArBr quat), 124.57 (vinylene CH), 126.69 (Ar quat), 127.36 (Ar CH), 127.36 (vinylene CH), 127.84 (Ar quat), 127.96 (vinylene CH), 128.38 (vinylene CH), 128.57 (Ar CH), 130.62 (Ar CH), 132.30 (Ar CH),

135.83 (Ar quat), 137.47 (Ar quat) 144.56 (Ar quat), 151.65 (ArO quat), 152.00 (ArO quat), 191.94 (CHO) ppm. MS (ES): 590 (M+2), 588 (M⁺), 504, 476, 420, 422, 340, 265, 149, 131, 127, 91, 85, 69 (base) m/z. HRMS calcd for C₃₅H₄₁O₃Br: 588.2239 g/mol. Found: 588.2231 g/mol.



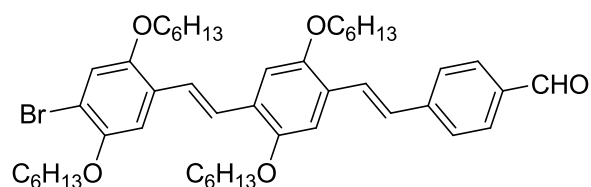
4-(4-(4-bromo-2,5-bis(hexyloxy)styryl)styryl)benzaldehyde (Br-DAA-CHO, vii71). According to the general DIBAL-H procedure, **Br-DAA-CN** (375 mg, 0.635 mmol) was dissolved in DCM (5 mL) and cooled to 0 °C. DIBAL-H (1.0M in hexanes, 0.75 mL, 0.75 mmol) was added dropwise. After workup, column chromatography (silica gel, 7:3 hexanes:DCM) gave the title compound as a yellow solid (348 mg, 93%). ¹H NMR (CD₂Cl₂, 400 MHz) δ 0.95 (6H, t, *J* = 6.0 Hz), 1.30-1.45 (8H, mult), 1.50-1.60 (4H, mult), 1.83 (2H, pent, *J* = 6.8 Hz), 1.85 (2H, pent, *J* = 6.8 Hz), 3.97 (2H, t, *J* = 6.4 Hz, OCH₂), 4.04 (2H, t, *J* = 6.4 Hz, OCH₂), 7.12 (1H, s), 7.16 (1H, d, *J* = 16.8 Hz, *trans* CH=CH), 7.16 (1H, s), 7.19 (1H, d, *J* = 16.4 Hz, *trans* CH=CH), 7.29 (1H, d, *J* = 16.4 Hz, *trans* CH=CH), 7.46 (1H, d, *J* = 16.8 Hz, *trans* CH=CH), 7.56 (4H, br s, *p*-C₆H₄), 7.68 (2H, d, *J* = 8.4 Hz, *p*-C₆H₄), 7.87 (2H, d, *J* = 8.4 Hz, *p*-C₆H₄), 9.98 (1H, s, CHO) ppm. ¹³C NMR (CD₂Cl₂, 100 MHz) δ 14.40 (CH₃), 23.20 (CH₂), 23.22 (CH₂), 26.26 (CH₂), 26.42 (CH₂), 29.84 (CH₂), 29.86 (CH₂), 32.14 (CH₂), 32.15 (CH₂), 70.20 (OCH₂), 70.72 (OCH₂), 111.88 (Ar CH), 112.35 (ArBr quat), 118.32 (Ar CH), 123.87 (vinylene CH), 126.87 (Ar quat), 127.41 (Ar CH), 127.46 (Ar CH), 127.63 (vinylene CH), 127.83 (Ar CH), 129.18 (vinylene CH), 130.63 (Ar CH), 132.34 (vinylene CH), 135.98 (Ar quat), 136.49 (Ar quat), 138.49 (Ar quat), 143.89 (Ar

quat), 150.35 (ArO quat), 151.70 (ArO quat), 191.92 (CHO) ppm. MS (ES): 590 (M+2), 588 (M⁺), 422, 420, 221, 181, 131, 119, 100, 85, 69 (base) m/z. HRMS calcd for C₃₅H₄₁O₃Br: 588.2239 g/mol. Found: 588.2230 g/mol.



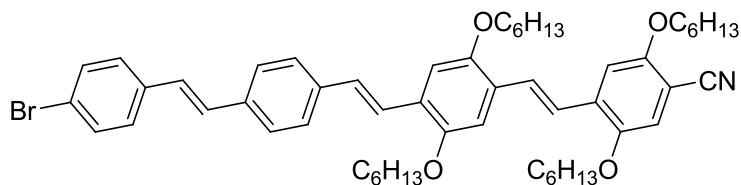
4-(4-(4-bromo-2,5-bis(hexyloxy)styryl)styryl)-2,5-bis(hexyloxy)styrylbenzaldehyde (Br-DAD-CHO, vii67). According to the general DIBAL-H procedure, **Br-DAD-CN** (500 mg, 0.635 mmol) was dissolved in DCM (5 mL) and cooled to 0 °C. DIBAL-H (1.0M in hexanes, 0.75 mL, 0.75 mmol) was added dropwise. After workup, column chromatography (silica gel, 2:3 hexanes:DCM) gave the title compound as a yellow solid (426 mg, 85%). ¹H NMR (CD₂Cl₂, 400 MHz) δ 0.85-0.95 (12H, mult), 1.30-1.45 (16H, mult), 1.45-1.60 (8H, mult), 1.80-1.95 (8H, mult), 3.97 (2H, t, *J* = 6.4 Hz, OCH₂), 4.04 (4H, t, *J* = 6.4 Hz, OCH₂), 4.12 (2H, t, *J* = 6.4 Hz, OCH₂), 7.12 (1H, s), 7.16 (1H, s), 7.17 (1H, d, *J* = 16.4 Hz, *trans* CH=CH), 7.23 (1H, s), 7.29 (1H, d, *J* = 16.4 Hz, *trans* CH=CH), 7.31 (1H, s), 7.46 (1H, d, *J* = 16.4 Hz, *trans* CH=CH), 7.53 (1H, d, *J* = 16.4 Hz, *trans* CH=CH), 7.56 (4H, br s, *p*-C₆H₄), 10.44 ppm (1H, s, CHO) ppm. ¹³C NMR (CD₂Cl₂, 100 MHz) δ 14.41 (CH₃), 23.23 (CH₂), 26.29 (CH₂), 26.36 (CH₂), 26.45 (CH₂), 26.47 (CH₂), 29.83 (CH₂), 29.87 (CH₂), 32.16 (CH₂), 32.18 (CH₂), 32.20 (CH₂), 69.78 (OCH₂), 69.85 (OCH₂), 70.22 (OCH₂), 70.73 (OCH₂), 110.49 (Ar CH), 111.03 (Ar CH), 111.97 (Ar CH), 112.32 (ArBr quat), 118.35 (Ar CH), 123.16 (vinylene CH), 123.70 (vinylene CH), 124.88 (Ar quat) 126.95 (Ar quat), 127.44 (Ar CH), 127.78 (Ar CH), 129.25 (vinylene CH), 133.20 (vinylene CH) 134.61 (Ar quat), 137.21 (Ar quat), 138.26 (Ar quat), 150.38 (ArO quat), 151.33

(ArO quat), 151.71 (ArO quat), 156.76 (ArO quat), 189.22 (CHO) ppm. MS (ESI): 813 (M+Na+2), 811 (M+Na), 527, 365 (base)\m/z. HRMS calcd for C₄₇H₆₄NO₄Br+Na: 811.3913 g/mol. Found: 811.3898 g/mol.



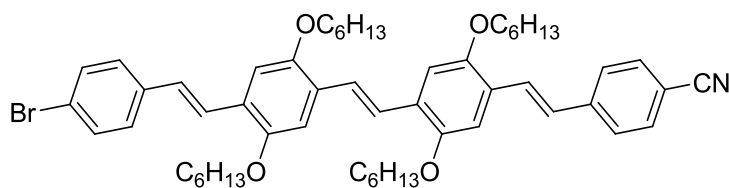
4-(4-(4-bromo-2,5-bis(hexyloxy)styryl)-2,5-bis(hexyloxy)styryl)benzaldehyde (Br-DDA-CHO, vii66). According to the general DIBAL-H procedure, **Br-DDA-CN** (500 mg, 0.635 mmol) was dissolved in DCM (5 mL) and cooled to 0 °C. DIBAL-H (1.0M in hexanes, 0.75 mL, 0.75 mmol) was added dropwise. After workup, column chromatography (silica gel, 7:3 hexanes:DCM) gave the title compound as a yellow solid (490 mg, 98%). ¹H NMR (CD₂Cl₂, 400 MHz) δ 0.85-0.95 (12H, mult), 1.30-1.45 (16H, mult), 1.45-1.60 (8H, mult), 1.80-1.95 (8H, mult), 3.98 (2H, t, *J* = 6.4 Hz, OCH₂), 4.04 (2H, t, *J* = 6.4 Hz, OCH₂), 4.07 (2H, t, *J* = 6.4 Hz, OCH₂), 4.08 (2H, t, *J* = 6.4 Hz, OCH₂), 7.11 (1H, s), 7.16 (1H, s), 7.17 (1H, s), 7.18 (1H, s), 7.24 (1H, d, *J* = 16.4 Hz, *trans* CH=CH), 7.45 (1H, d, *J* = 16.8 Hz, *trans* CH=CH), 7.50 (1H, d, *J* = 16.8 Hz, *trans* CH=CH), 7.67 (1H, d, *J* = 16.4 Hz, *trans* CH=CH), 7.69 (2H, d, *J* = 8.0 Hz, *p*-C₆H₄), 7.86 (2H, d, *J* = 8.0 Hz, *p*-C₆H₄), 9.98 (1H, s, CHO) ppm. ¹³C NMR (CD₂Cl₂, 100 MHz) δ 14.42 (CH₃), 23.20 (CH₂), 23.24 (CH₂), 23.26 (CH₂), 26.28 (CH₂), 26.41 (CH₂), 26.50 (CH₂), 26.55 (CH₂), 29.87 (CH₂), 30.02 (CH₂), 32.15 (CH₂), 32.18 (CH₂), 32.22 (CH₂), 32.23 (CH₂), 70.00 (OCH₂), 70.16 (OCH₂), 70.69 (OCH₂), 110.97 (Ar CH), 111.15 (Ar CH), 111.94 (Ar CH), 112.10 (ArBr quat), 118.29 (Ar CH), 124.07 (vinylene CH), 124.45 (vinylene CH), 126.41 (Ar quat), 127.43 (vinylene CH), 127.34 (Ar CH), 127.59 (Ar quat), 127.81 (vinylene CH), 128.68

(Ar quat), 130.63 (Ar CH), 144.63 (Ar quat), 150.37 (ArO quat), 151.59 (ArO quat), 151.67 (ArO quat), 152.05 (ArO quat), 191.94 (CHO) ppm. MS (ESI): 813 (M+Na+2), 811 (M+Na), 776, 711, 709, 691, 527, 365 (base) m/z. HRMS calcd for C₄₇H₆₅O₅Br+Na: 811.3913 g/mol. Found: 811.3935 g/mol.



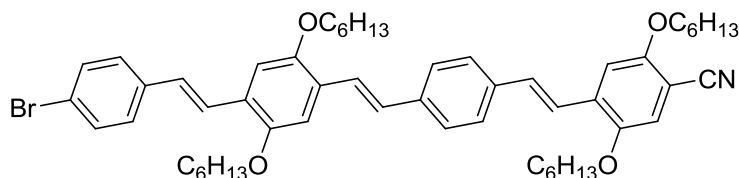
4-(4-(4-(4-bromostyryl)styryl)-2,5-bis(hexyloxy)styryl)-2,5-bis(hexyloxy)benzonitrile (Br-AADD-CN, vii75). According to the general HWE procedure, **Br-AAD-CHO** (200 mg, 0.341 mmol), **P-D-CN** (220 mg, 0.517 mmol), and LiCl (34.0 mg, 0.802 mmol) were dissolved in THF (5 mL) and cooled to 0 °C under N₂. KO^tBu (88.0 mg, 0.784 mmol) was added portionwise over 5 minutes, and the reaction was allowed to come to rt overnight with stirring. After workup, column chromatography (silica gel, 13:7 hexanes:DCM) gave the title compound as an orange solid (293 mg, 97%). ¹H NMR (CD₂Cl₂, 400 MHz) δ 0.85-1.00 (12H, mult), 1.30-1.45 (16H, mult), 1.45-1.60 (8H, mult), 1.80-1.95 (8H, mult), 3.99 (2H, t, *J* = 6.4 Hz, OCH₂), 4.06 (2H, t, *J* = 6.4 Hz, OCH₂), 4.08 (2H, t, *J* = 6.4 Hz, OCH₂), 4.11 (2H, t, *J* = 6.4 Hz, OCH₂), 7.04 (1H, s), 7.08 (1H, d, *J* = 16.4 Hz, *trans* CH=CH), 7.14 (1H, d, *J* = 16.4 Hz, *trans* CH=CH), 7.16 (1H, s), 7.17 (1H, s), 7.20 (1H, d, *J* = 16.4 Hz, *trans* CH=CH), 7.21 (1H, s), 7.42 (2H, d, *J* = 8.4 Hz, *p*-C₆H₄), 7.47-7.57 (8H, mult), 7.60 (1H, d, *J* = 16.4 Hz, *trans* CH=CH) ppm. ¹³C NMR (CD₂Cl₂, 100 MHz) δ 14.38 (CH₃), 14.42 (CH₃), 23.17 (CH₂), 23.23 (CH₂), 23.25 (CH₂), 23.27 (CH₂), 26.15 (CH₂), 26.39 (CH₂), 26.50 (CH₂), 26.55 (CH₂), 29.66 (CH₂), 29.76 (CH₂), 30.01 (CH₂), 30.03 (CH₂), 32.10 (CH₂), 32.17 (CH₂), 32.23 (CH₂), 69.92 (OCH₂), 70.01 (OCH₂), 70.05

(OCH₂), 70.16 (OCH₂), 100.56 (ArCN, quat), 110.51 (Ar CH), 110.74 (Ar CH), 111.28 (Ar CH), 116.95 (Ar CH), 117.34 (CN), 121.73 (ArBr quat), 122.82 (vinylene CH), 123.84 (vinylene CH), 126.98 (Ar quat), 127.43 (Ar CH), 128.43 (Ar CH), 128.52 (vinylene CH), 127.63 (vinylene CH), 128.05 (Ar quat), 128.05 (Ar CH), 128.55 (vinylene CH), 129.51 (vinylene CH), 132.32 (Ar CH), 133.98 (Ar quat), 136.83 (Ar quat), 136.97 (Ar quat), 138.11 (Ar quat), 150.72 (ArO quat), 151.63 (ArO quat), 151.96 (ArO quat), 155.72 (ArO quat) ppm.



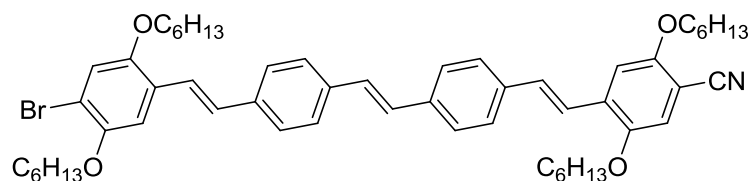
4-(4-(4-(4-bromostyryl)-2,5-bis(hexyloxy)styryl)-2,5-bis(hexyloxy)styryl)benzonitrile (Br-ADDA-CN, vii74). According to the general HWE procedure, **Br-ADD-CHO** (300 mg, 0.380 mmol), **P-A-CN** (130 mg, 0.577 mmol), and LiCl (37.0 mg, 0.873 mmol) were dissolved in THF (40 mL) and cooled to 0 °C under N₂. KO^tBu (98.0 mg, 0.873 mmol) was added portionwise over 5 minutes, and the reaction was allowed to come to rt overnight with stirring. After workup, column chromatography (silica gel, 4:1 hexanes:DCM) gave the title compound as an orange solid (300 mg, 89%). ¹H NMR (CD₂Cl₂, 400 MHz) δ 0.85-1.00 (12H, mult), 1.30-1.45 (16H, mult), 1.45-1.60 (8H, mult), 1.80-1.95 (8H, mult), 4.05-4.10 (8H, mult), 7.11-7.19 (6H, mult), 7.42 (2H, d, *J* = 8.4 Hz, *p*-C₆H₄), 7.48-7.52 (5H, mult), 7.61-7.66 (5H, mult) ppm. ¹³C NMR (CD₂Cl₂, 100 MHz) δ 13.83 (CH₃), 13.87 (CH₃), 22.67 (CH₂), 22.70 (CH₂), 25.95 (CH₂), 25.98 (CH₂), 29.44 (CH₂), 29.47 (CH₂), 31.65 (CH₂), 31.68 (CH₂), 69.38 (OCH₂), 69.42 (OCH₂), 69.46 (OCH₂), 110.18 (ArCN, quat), 110.21 (Ar CH), 110.32 (Ar CH), 110.36 (Ar CH), 110.35 (Ar CH), 119.07 (CN), 120.91 (ArBr quat), 123.33 (vinylene CH), 123.93 (vinylene CH), 126.73 (Ar

CH quat), 126.83 (Ar quat), 126.99 (vinylene CH), 127.41 (Ar quat), 127.53 (Ar quat), 127.96 (vinylene CH), 128.01 (vinylene CH), 128.51 (Ar quat), 131.71 (Ar CH), 132.47 (Ar CH), 136.88 (Ar quat), 137.04 (Ar quat), 151.07 (ArO quat), 151.16 (ArO quat), 151.45 (ArO quat), 151.51 (ArO quat) ppm.



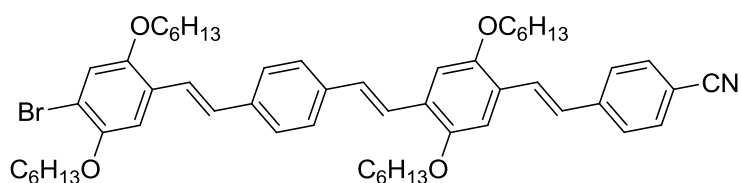
4-(4-(4-(4-bromostyryl)-2,5-bis(hexyloxy)styryl)styryl)-2,5-bis(hexyloxy)benzonitrile (Br-ADAD-CN, vii76). According to the general HWE procedure, **Br-ADA-CHO** (200 mg, 0.341 mmol), **P-D-CN** (220 mg, 0.517 mmol), and LiCl (34.0 mg, 0.802 mmol) were dissolved in THF (5 mL) and cooled to 0 °C under N₂. KO^tBu (88.0 mg, 0.784 mmol) was added portionwise over 5 minutes, and the reaction was allowed to come to rt overnight with stirring. After workup, column chromatography (silica gel, 2:3 hexanes:DCM) gave the title compound as an orange solid (268 mg, 88%). ¹H NMR (CD₂Cl₂, 400 MHz) δ 0.85-1.00 (12H, mult), 1.30-1.45 (16H, mult), 1.45-1.60 (8H, mult), 1.80-1.95 (8H, mult), 3.99 (2H, t, *J* = 6.4 Hz, OCH₂), 4.07 (4H, t, *J* = 6.4 Hz, OCH₂), 4.11 (2H, t, *J* = 6.4 Hz, OCH₂), 7.05 (1H, s), 7.05 (1H, d, *J* = 16.4 Hz, *trans* CH=CH), 7.15 (1H, s), 7.16 (1H, s), 7.19 (1H, s), 7.19 (1H, d, *J* = 16.4 Hz, *trans* CH=CH), 7.26 (1H, d, *J* = 16.4 Hz, *trans* CH=CH), 7.42 (2H, d, *J* = 8.4 Hz, *p*-C₆H₄), 7.48 (1H, d, *J* = 16.4 Hz, *trans* CH=CH), 7.49 (1H, d, *J* = 16.4 Hz, *trans* CH=CH), 7.49 (2H, d, *J* = 8.4 Hz, *p*-C₆H₄), 7.50 (1H, d, *J* = 16.4 Hz, *trans* CH=CH), 7.56 (4H, br s, *p*-C₆H₄), ppm. ¹³C NMR (CD₂Cl₂, 100 MHz) δ 14.39 (CH₃), 14.41 (CH₃), 23.17 (CH₂), 23.20 (CH₂), 23.25 (CH₂), 26.13 (CH₂), 26.40 (CH₂), 26.54 (CH₂), 29.64 (CH₂), 29.74 (CH₂), 30.02 (CH₂), 30.04 (CH₂), 32.10 (CH₂), 32.15

(CH₂), 32.22 (CH₂), 32.23 (CH₂), 70.04 (OCH₂), 70.05 (OCH₂), 70.13 (OCH₂), 70.23 (OCH₂), 100.81 (ArCN, quat), 110.54 (Ar CH), 110.85 (Ar CH), 110.97 (Ar CH), 117.03 (Ar CH), 117.27 (CN), 121.50 (ArBr quat), 122.47 (vinylene CH), 124.17 (vinylene CH), 124.67 (vinylene CH), 127.05 (Ar quat), 127.41 (Ar CH), 127.78 (Ar CH), 127.96 (vinylene CH), 128.52 (Ar CH), 128.75 (vinylene CH), 132.27 (Ar CH), 133.29 (Ar quat), 136.83 (Ar quat), 137.57 (Ar quat), 138.60 (Ar quat), 150.76 (ArO quat), 151.71 (ArO quat), 151.72 (ArO quat), 155.71 (ArO quat) ppm.



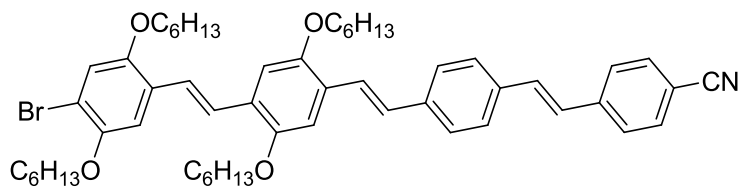
4-(4-(4-(4-bromo-2,5-bis(hexyloxy)styryl)styryl)styryl)-2,5-bis(hexyloxy)benzonitrile (Br-DAAD-CN, vii77). According to the general HWE procedure, **Br-DAA-CHO** (200 mg, 0.341 mmol), **P-D-CN** (220 mg, 0.517 mmol), and LiCl (34.0 mg, 0.802 mmol) were dissolved in THF (5 mL) and cooled to 0 °C under N₂. KO^tBu (88.0 mg, 0.784 mmol) was added portionwise over 5 minutes, and the reaction was allowed to come to rt overnight with stirring. After workup, column chromatography (silica gel, 7:3 hexanes:DCM) gave the title compound as an orange solid (270 mg, 89%). ¹H NMR (CD₂Cl₂, 400 MHz) δ 0.85-1.00 (12H, mult), 1.30-1.45 (16H, mult), 1.45-1.60 (8H, mult), 1.80-1.95 (8H, mult), 3.97 (2H, t, *J* = 6.4 Hz, OCH₂), 3.99 (2H, t, *J* = 6.4 Hz, OCH₂), 4.04 (2H, t, *J* = 6.4 Hz, OCH₂), 4.11 (2H, t, *J* = 6.4 Hz, OCH₂), 7.04 (1H, s), 7.11 (1H, s), 7.16 (1H, d, *J* = 16.4 Hz, *trans* CH=CH), 7.16 (1H, s), 7.17 (2H, br s, *trans* CH=CH), 7.19 (1H, s), 7.25 (1H, d, *J* = 16.4 Hz, *trans* CH=CH), 7.44 (1H, d, *J* = 16.4 Hz, *trans* CH=CH), 7.48 (1H, d, *J* = 16.4 Hz, *trans* CH=CH), 7.54 (4H, br s, *p*-C₆H₄), 7.56 (4H, br s, *p*-

C₆H₄) ppm. ¹³C NMR (CD₂Cl₂, 100 MHz) δ 14.40 (CH₃), 23.17 (CH₂), 23.21 (CH₂), 23.22 (CH₂), 26.13 (CH₂), 26.27 (CH₂), 26.40 (CH₂), 26.43 (CH₂), 29.65 (CH₂), 29.73 (CH₂), 29.85 (CH₂), 29.86 (CH₂), 32.10 (CH₂), 32.15 (CH₂), 32.17 (CH₂), 70.13 (OCH₂), 70.22 (OCH₂), 70.24 (OCH₂), 70.72 (OCH₂), 100.85 (ArCN, quat), 110.59 (Ar CH), 111.85 (Ar CH), 112.21 (ArBr quat), 117.02 (Ar CH), 117.26 (CN), 118.32 (Ar CH), 122.63 (vinylene CH), 122.43 (vinylene CH), 127.05 (Ar quat), 127.44 (Ar CH), 127.80 (Ar CH), 128.43 (vinylene CH), 129.04 (vinylene CH), 129.32 (vinylene CH), 132.21 (vinylene CH), 133.24 (Ar quat), 137.02 (Ar quat), 137.16 (Ar quat), 137.81 (Ar quat), 137.98 (Ar quat), 150.36 (ArO quat), 150.77 (ArO quat), 151.67 (ArO quat), 155.71 (ArO quat) ppm.



4-(4-(4-(4-bromo-2,5-bis(hexyloxy)styryl)styryl)-2,5-bis(hexyloxy)styryl)benzonitrile (Br-DADA-CN, vii73). According to the general HWE procedure, **Br-DAD-CHO** (300 mg, 0.380 mmol), **P-A-CN** (130 mg, 0.577 mmol), and LiCl (37.0 mg, 0.873 mmol) were dissolved in THF (5 mL) and cooled to 0 °C under N₂. KO^tBu (98.0 mg, 0.873 mmol) was added portionwise over 5 minutes, and the reaction was allowed to come to rt overnight with stirring. After workup, column chromatography (silica gel, 1:1 hexanes:DCM) gave the title compound as an orange solid (337 mg, 100%). ¹H NMR (CD₂Cl₂, 400 MHz) δ 0.85-1.00 (12H, mult), 1.30-1.45 (16H, mult), 1.45-1.60 (8H, mult), 1.80-1.95 (8H, mult), 3.97 (2H, t, *J* = 6.4 Hz, OCH₂), 4.04 (2H, t, *J* = 6.4 Hz, OCH₂), 4.07 (2H, t, *J* = 6.4 Hz, OCH₂), 4.08 (2H, t, *J* = 6.4 Hz, OCH₂), 7.11 (1H, s), 7.14 (1H, s), 7.16 (1H, d, *J* = 16.4 Hz, *trans* CH=CH), 7.17 (1H, s), 7.18 (1H, d, *J* = 16.4 Hz,

trans CH=CH), 7.18 (1H, s), 7.20 (1H, d, $J = 16.4$ Hz, *trans* CH=CH), 7.44 (1H, d, $J = 16.4$ Hz, *trans* CH=CH), 7.53 (1H, d, $J = 16.4$ Hz, *trans* CH=CH), 7.55 (4H, br s, *p*-C₆H₄), 7.62 (2H, s, $J = 8.8$ Hz, *p*-C₆H₄), 7.62 (1H, d, $J = 16.4$ Hz, *trans* CH=CH), 7.65 (2H, s, $J = 8.8$ Hz, *p*-C₆H₄) ppm. ¹³C NMR (CD₂Cl₂, 100 MHz) δ 14.40 (CH₃), 23.21 (CH₂), 23.25 (CH₂), 26.27 (CH₂), 26.43 (CH₂), 26.53 (CH₂), 26.54 (CH₂), 29.86 (CH₂), 29.99 (CH₂), 30.03 (CH₂), 32.14 (CH₂), 32.17 (CH₂), 32.21 (CH₂), 32.23 (CH₂), 70.00 (OCH₂), 70.08 (OCH₂), 70.22 (OCH₂), 70.71 (OCH₂), 110.75 (Ar CH), 111.21 (Ar CH), 111.81 (Ar CH), 112.15 (ArBr quat, ArCN quat), 118.33 (Ar CH), 119.62 (CN), 123.28 (vinylene CH), 123.57 (vinylene CH), 126.16 (Ar quat), 127.03 (Ar quat), 127.21 (vinylene CH), 127.30 (Ar CH), 127.40 (Ar CH), 127.43 (Ar CH), 127.61 (vinylene CH), 128.41 (Ar quat), 129.36 (vinylene CH), 133.02 (Ar CH), 137.62 (Ar quat), 137.77 (Ar quat), 150.36 (ArO quat), 151.60 (ArO quat), 151.66 (ArO quat), 152.06 (ArO quat) ppm.



4-(4-(4-(4-bromo-2,5-bis(hexyloxy)styryl)-2,5-bis(hexyloxy)styryl)styryl)benzonitrile (Br-DDAA-CN, vii72). According to the general HWE procedure, **Br-DDA-CHO** (300 mg, 0.380 mmol), **P-A-CN** (130 mg, 0.577 mmol), and LiCl (37.0 mg, 0.873 mmol) were dissolved in THF (5 mL) and cooled to 0 °C under N₂. KO^tBu (98.0 mg, 0.873 mmol) was added portionwise over 5 minutes, and the reaction was allowed to come to rt overnight with stirring. After workup, column chromatography (silica gel, 1:1 hexanes:DCM) gave the title compound as an orange solid (338 mg, 100%). ¹H NMR (CD₂Cl₂, 400 MHz) δ 0.85-1.00 (12H, mult), 1.30-1.45 (16H,

mult), 1.45-1.60 (8H, mult), 1.80-1.95 (8H, mult), 3.97 (2H, t, $J = 6.4$ Hz, OCH₂), 4.04 (2H, t, $J = 6.4$ Hz, OCH₂), 4.07 (4H, t, $J = 6.4$ Hz, OCH₂), 7.11 (1H, s), 7.14 (1H, d, $J = 16.0$ Hz, *trans* CH=CH), 7.16 (2H, br s), 7.18 (1H, d, $J = 16.4$ Hz, *trans* CH=CH), 7.18 (1H, s), 7.25 (1H, d, $J = 16.0$ Hz, *trans* CH=CH), 7.44 (1H, d, $J = 16.8$ Hz, *trans* CH=CH), 7.50 (1H, d, $J = 16.8$ Hz, *trans* CH=CH), 7.54 (1H, d, $J = 16.4$ Hz, *trans* CH=CH), 7.56 (4H, br s, *p*-C₆H₄), 7.61 (2H, s, $J = 8.4$ Hz, *p*-C₆H₄), 7.65 (2H, s, $J = 8.4$ Hz, *p*-C₆H₄) ppm. ¹³C NMR (CD₂Cl₂, 100 MHz) δ 14.40 (CH₃), 14.42 (CH₃), 14.43 (CH₃), 23.20 (CH₂), 23.23 (CH₂), 23.25 (CH₂), 23.26 (CH₂), 26.28 (CH₂), 26.41 (CH₂), 26.50 (CH₂), 26.55 (CH₂), 29.86 (CH₂), 30.04 (CH₂), 32.14 (CH₂), 32.18 (CH₂), 32.24 (CH₂), 70.00 (OCH₂), 69.96 (OCH₂), 69.97 (OCH₂), 70.13 (OCH₂), 70.65 (OCH₂), 110.83 (Ar CH), 110.96 (Ar CH), 111.03 (ArCN quat), 111.85 (Ar CH), 111.93 (ArBr quat), 118.25 (Ar CH), 119.53 (CN), 123.61 (vinylene CH), 124.42 (vinylene CH), 124.52 (vinylene CH), 126.91 (vinylene CH), 127.07 (Ar quat), 127.36 (Ar CH), 127.41 (Ar CH), 127.66 (Ar quat), 127.85 (Ar CH), 127.89 (Ar quat), 128.51 (vinylene CH), 132.38 (vinylene CH), 136.06 (Ar quat), 138.92 (Ar quat), 142.43 (Ar quat), 150.33 (ArO quat), 151.62 (ArO quat), 151.73 (ArO quat) ppm.

3.0 SYNTHESIS OF HETEROTELECHELIC AND SYMMETRIC OLIGO(PHENYLENE-VINYLENE)S USING OLEFIN METATHESIS

Portions of this chapter (primarily sections 3.1.1, 3.2.2, 3.2.3, and 3.2.4) have been reproduced with permission from Norris, B. N.; Pan, T.; Meyer, T. Y., "Iterative synthesis of heterotelechelic *oligo*(phenylene-vinylene)s by olefin cross-metathesis" *Org. Lett.* **2010**, *12* (23), 5514-5517.⁸⁴

Copyright © 2010 American Chemical Society.

3.1 OVERVIEW

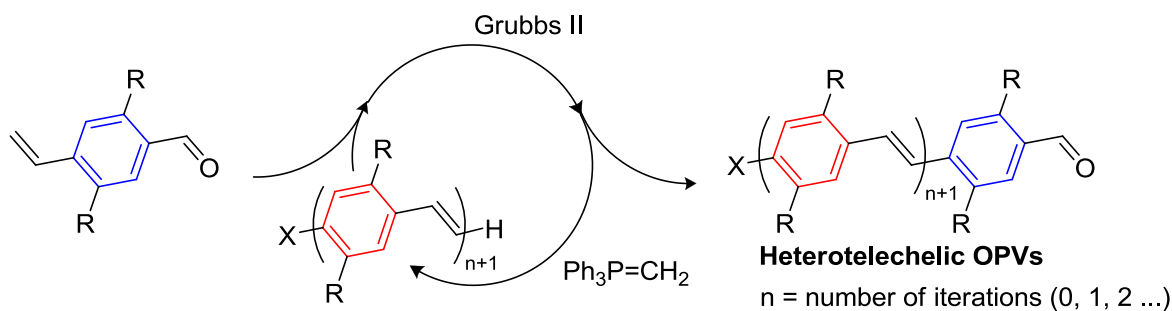
We present two approaches for the synthesis of OPVs using olefin metathesis – a homologation approach that yields heterotelechelic, alternating oligomers and a dimerization approach that yields symmetric, fully-substituted oligomers. This work represents the first use of olefin metathesis to produce well defined OPVs. Previous metathesis approaches to produce OPVs, particularly the work of Thorn-Csányi and coworkers,⁸⁵⁻⁸⁸ have instead used abortive ADMET processes to produce oligomers, which were then separated.

Olefin metathesis provides an attractive approach to the synthesis of OPVs due to its 1) *simplicity*: the coupling of vinyl groups to give internal olefins avoids the need for complex functionality in the monomer, 2) *generality*: the Grubbs II catalyst is highly tolerant; and 3)

utility: the resultant oligomers exhibit reactive endgroups that can be elaborated into more complex materials. Further functionalization of OPVs permits the physical and electronic properties of the material to be adjusted to meet the needs of various applications.^{89, 90}

3.1.1 Homologation approach

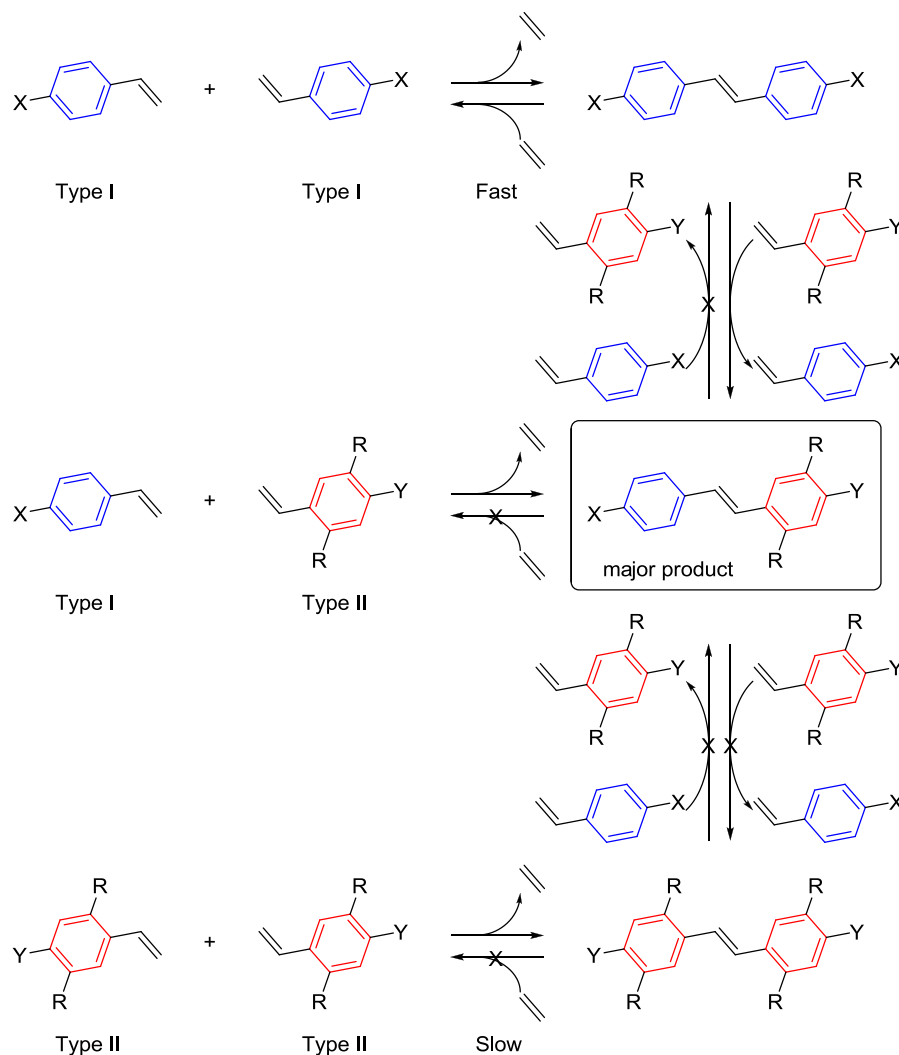
Our strategy for the synthesis of heterotelechelic OPVs involves the sequential coupling of phenyl monomers (Scheme 12). End-to-end homologation allows for the creation of oligomers of any desired length. The key step is a cross-metathesis (CM) reaction between olefin-terminated growing oligomers and a vinylbenzaldehyde. The aldehyde endgroup of the $n+1$ oligomer product can then be converted into a metathesis-ready vinyl moiety or exploited for further functionalization.



Scheme 12. Homologation approach to OPVs by CM

In order to promote CM over homometathesis, we exploit the known reactivity difference between *ortho*-substituted and *ortho*-unsubstituted styrenes.⁹¹ Styrenes lacking *ortho*-substituents, which are Type I olefins with the Grubbs II catalyst, undergo rapid and reversible homodimerization (Scheme 13), and the homodimer is capable of engaging in further metathesis. Styrenes with *ortho*-substituents, which are Type II olefins, are slow to homodimerize and the

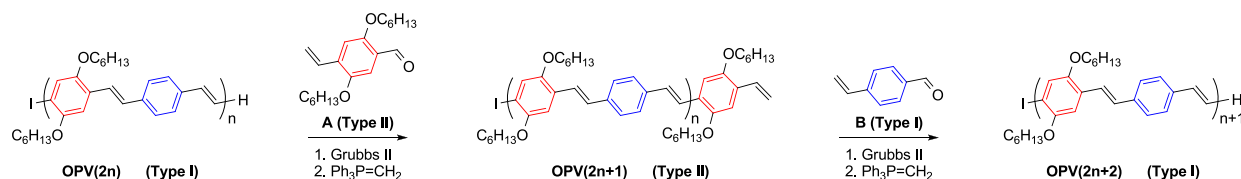
coupling reaction, which produces a Type IV olefin, is nearly irreversible. The reaction of a Type I olefin with a Type II olefin is driven toward the desired CM product, which, in our case is a Type IV olefin and unreactive towards further metathesis.



Scheme 13. Olefin metathesis outcomes of Type I and Type II vinylbenzaldehydes

Alternation between Type I and Type II vinylbenzaldehydes allows for stepwise growth of the oligomer (Scheme 14). An OPV terminated with a Type I olefin can undergo selective homologation with a Type II monomer, 2,5-bis(hexyloxy)-4-vinylbenzaldehyde, **A**. This new OPV will be terminated with a Type II olefin and can undergo homologation with a Type I monomer, 4-vinylbenzaldehyde, **B**, to give another OPV terminated with a Type I olefin, and so

on. Since all of the CM products are internal olefins of Type IV, scrambling of extant vinylene groups is suppressed. The only caveat to this approach is that we can only produce alternating OPVs. More complex sequences would require the CM of two Type II olefins to extend the chain.

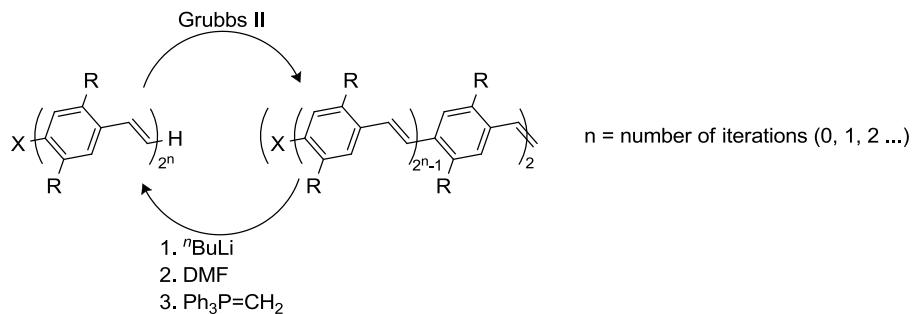


Scheme 14. Synthetic approaching to alternating OPVs by metathesis homologation

This approach is not unlike past approaches that utilize orthogonally reactive or orthogonally protected monomers to produce dissymmetric oligomers,^{72, 73, 76-78} which have been highlighted in Chapter 1.

3.1.2 Dimerization approach

Our strategy for the preparation of symmetric, fully substituted OPVs involves the dimerization of a Type II olefin by homometathesis to produce an oligomer, which is then desymmetrized. This newly dissymmetric oligomer can then be dimerized to produce a new, longer, oligomer (Scheme 15). This approach is limited in that it can only produce symmetric oligomers. However, since we are using homometathesis, there is no selectivity issue and we can prepare the fully substituted oligomers.



Scheme 15. Dimerization approach to OPVs using metathesis

3.2 RESULTS AND DISCUSSION

3.2.1 Monomer synthesis

Type II vinylbenzaldehyde **12** and its precursor 2,5-bis(hexyloxy)-4-iodostyrene **13** are common monomers for both metathesis approaches (Figure 22). These compounds were prepared from hydroquinone using well known chemistry. 4-Vinylbenzaldehyde **14**, required for the homologation approach, was prepared as previously reported.⁹²

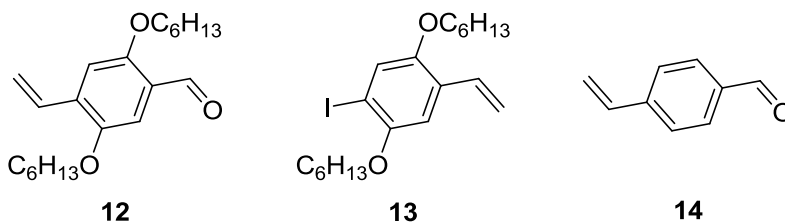
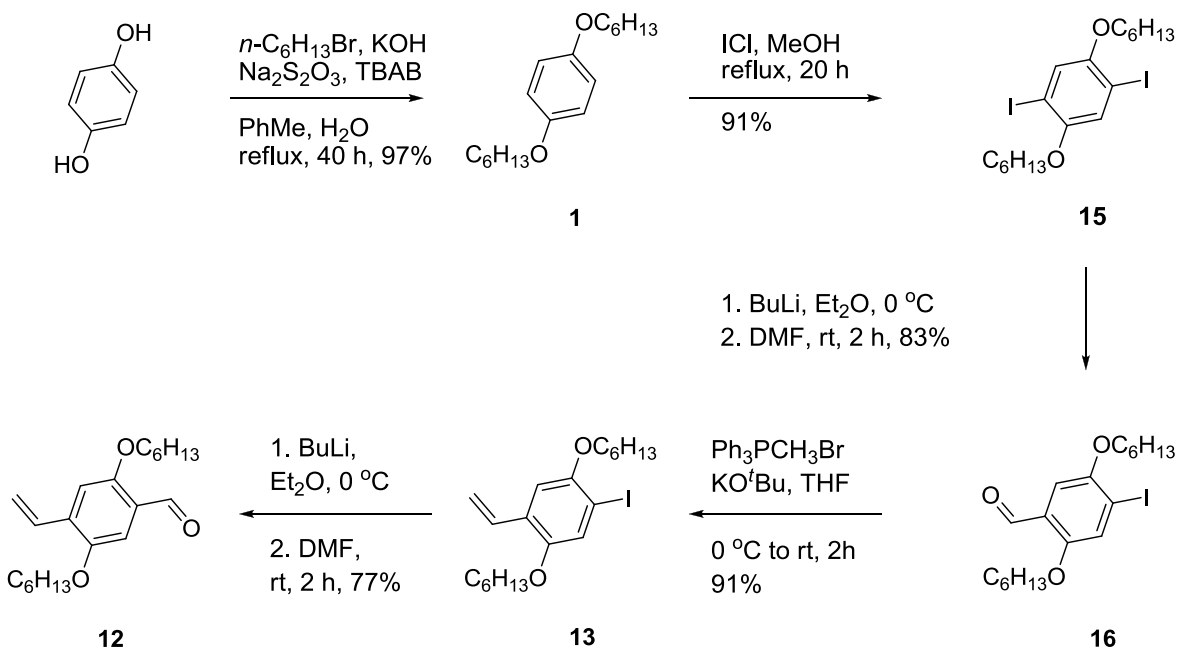


Figure 22. Common metathesis monomers

Monomer **13** was prepared from hydroquinone in 4 steps with an overall yield of 67% (Scheme 16). Monomer **12** was prepared in one step from monomer **13**. Hydroquinone was alkylated with 1-bromohexane and KOH in a water/toluene biphasic system using TBAB as a

phase transfer catalyst. The addition of 1 equivalent of $\text{Na}_2\text{S}_2\text{O}_3$ increased the yield from 20-30% to 91-97%. Ether **1** was then iodated with ICl in MeOH to give diiodo arene **15**, which was lithiated with $n\text{-BuLi}$ in Et_2O ⁸³ and quenched with DMF to give benzaldehyde **16**. Lithiation of **15** in THF , followed by quenching with DMF , led to low yields due to preferential formation of the dialdehyde, even when $n\text{-BuLi}$ is the limiting reagent. We hypothesized that the increased Lewis basicity of THF over Et_2O increases the dissociation of the $n\text{-BuLi}$ clusters in THF relative to Et_2O , increasing the reactivity of $n\text{-BuLi}$, even at lower temperatures. Benzaldehyde **16** was converted to styrene **13** using a Wittig reaction with $\text{Ph}_3\text{P}=\text{CH}_2$. Styrene **13** was converted to vinylbenzaldehyde **12** by lithiation with $n\text{-BuLi}$ in Et_2O and quenching with DMF . All reactions proceed with good to excellent yields. The conversion of hydroquinone to **13** was regularly performed on a 30+ gram scale and the conversion of **13** to **12** was regularly performed on a 10+ gram scale.

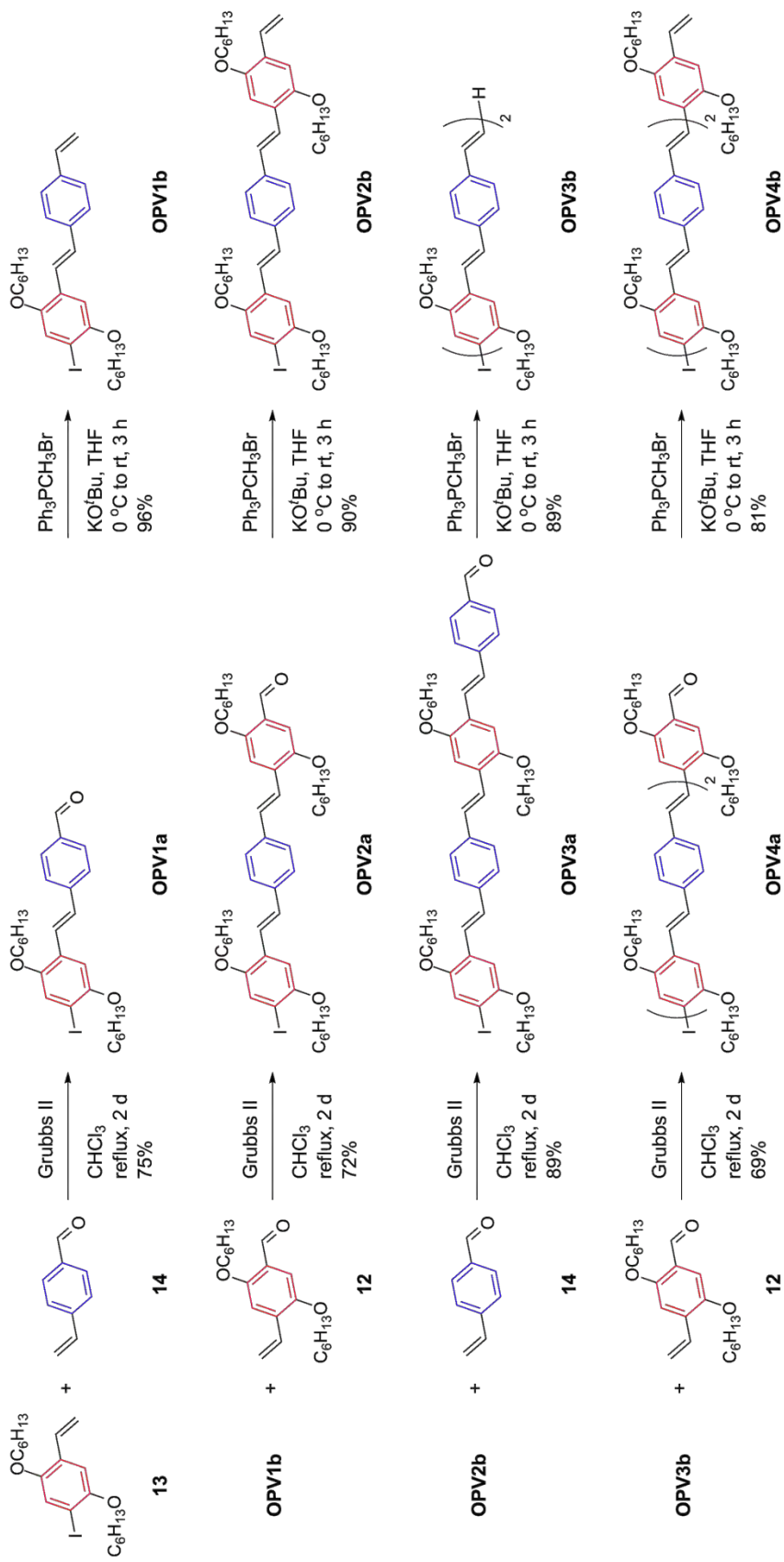


Scheme 16. Synthesis of monomers **12** and **13**

3.2.2 Synthesis of heterotelechelic OPVs using cross-metathesis

A series of heterotelechelic OPVs was prepared by cross-metathesis. The first homologation involved CM between styrene **13** (Type II) and monomer **14** (Type I) to give aldehyde terminated **OPV1a** in 71-81% yield (Scheme 17). This CM requires very low catalyst loading (7.5×10^{-3} eq.) and can be performed on multigram scales. The use of a two-fold excess of monomer **14** improved the yield of the crosscoupled product. The homologation is *E*-specific; the ^1H NMR spectrum bears no peaks between δ 6.5 and 7.0, the characteristic range for *Z*-phenylene-vinylenes.⁹³ The homologation was completed by a Wittig olefination with $\text{Ph}_3\text{P}=\text{CH}_2$, which gave vinyl terminated **OPV1b** in a 96% yield.

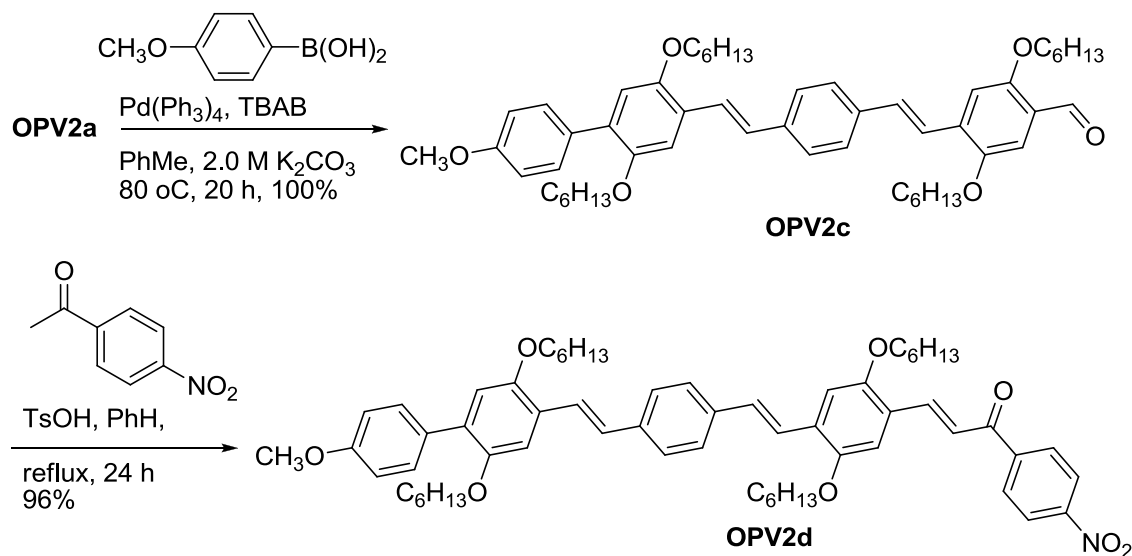
Subsequent homologations followed an alternating pattern. Each CM reaction used three equivalents or less of the vinylbenzaldehyde, 0.01 equivalents or less of Grubbs II catalyst, proceeded in moderate to good yields, and was *E*-specific. The Wittig reactions all proceeded in good to excellent yields. The excess vinylbenzaldehyde, especially monomer **12**, complicated the isolation and purification of the oligomers, leading to lower isolated yields of **OPV2a** and **OPV4a** compared to those of **OPV1a** and **OPV3a**. The OPVs are soluble in a wide range of organic solvents, including hexane, dichloromethane, chloroform, ethyl acetate, acetone, toluene, tetrahydrofuran, and isopropanol.



Scheme 17. Synthesis of OPVs by CM homologation.

3.2.3 Modification of heterotelechelic OPVs

To highlight the ability of our heterotelechelic OPVs to serve as modular platforms for orthogonal functionalization by we elaborated upon **OPV2a** (Scheme 18). Phenylboronic acid was coupled to the bromo endgroup of **OPV2a** using a Suzuki coupling to produce donor-acceptor chromophore **OPV2c**, which was further functionalized at the aldehyde endgroup by an aldol condensation with 4'-nitroacetophenone to give **OPV2d**. Both reactions are simple, robust, and proceed in excellent yields. To the best of our knowledge, this is the first example of an aldol reaction being utilized to functionalize OPVs.

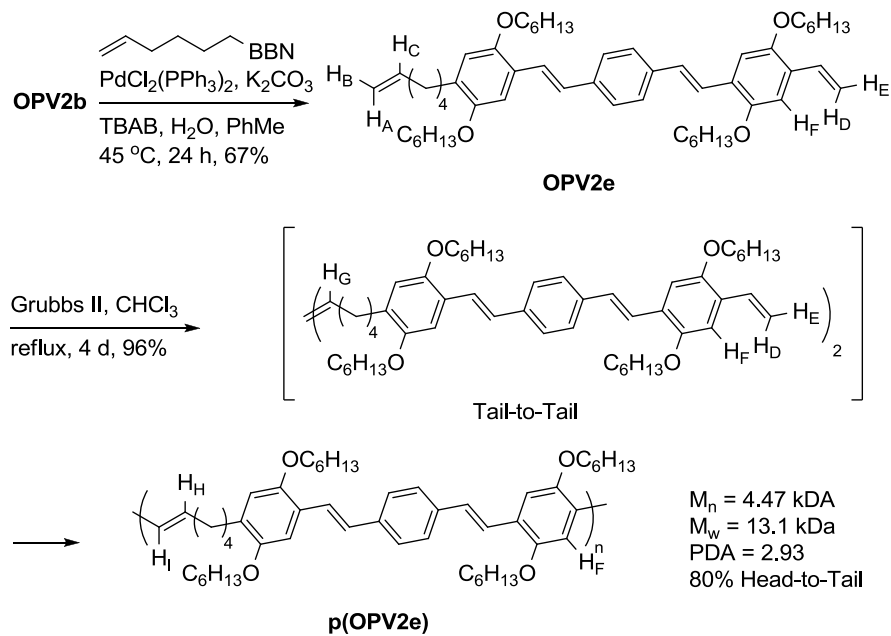


Scheme 18. Synthesis of donor-acceptor chromophores by orthogonal functionalization of **OPV2a**

Heterotelechelic OPVs can also be used to prepare head-to-tail sequenced polymers. As an initial demonstration of the types of complex copolymers that could be prepared from heterotelechelic OPVs, we have converted **OPV2b** to **OPV2e** and onward to copolymer **p(OPV2e)** (Scheme 19), using a Suzuki-Miyaura coupling followed by acyclic diene metathesis

(ADMET) polymerization, chemistry amenable to producing a family of such RSCs.³³ We believe **P(OPV2e)** should exhibit a high degree of head-to-tail regioregularity because **OPV2e** is an AB monomer containing a Type II styrenyl olefin (head) and a Type I aliphatic olefin (tail). Selective metathesis has previously been used to prepare AABB alternating copolymers,^{94,95} but, to the best of our knowledge, there is only one example of a head-to-tail polymer prepared in this fashion.⁹⁴ The incorporation of a flexible unit into the backbone of a highly conjugated structure can lead to improved solubilities, interesting liquid crystal behavior and/or modulated physical properties,³³ and the inherent dissymmetry of the AB copolymer could lead to enhanced optoelectronic properties.⁹⁶

OPV2e was polymerized using Grubbs II catalyst in CHCl_3 . The polymerization was monitored using ^1H NMR spectroscopy by observing the disappearance of the signals for the aliphatic alkenyl group (H_A , $\delta \sim 5.2$, H_B , $\delta \sim 5.1$, and H_C , $\delta \sim 5.9$) and the styrenyl group (H_D , $\delta \sim 5.3$, and H_E , $\delta \sim 5.8$) and the appearance of the signals for the tail-to-tail (H_G , $\delta \sim 5.5$) and head-to-tail (H_H , $\delta \sim 6.7$ and H_I , $\delta \sim 6.3$) connections. We estimated the % head-to-tail based on conversion of styrenyl groups to head-to-tail groups (Figure 23, Table 12). After 24 h, no **OPV2e** remains, having been converted first to the tail-to-tail intermediate followed by further metathesis to give head-to-tail connections. At longer reaction times there is decrease in % head-to-tail couplings which can be attributed to head-to-head couplings, which are improbable but accumulate slowly.



Scheme 19. Synthesis of head-to-tail copolymer

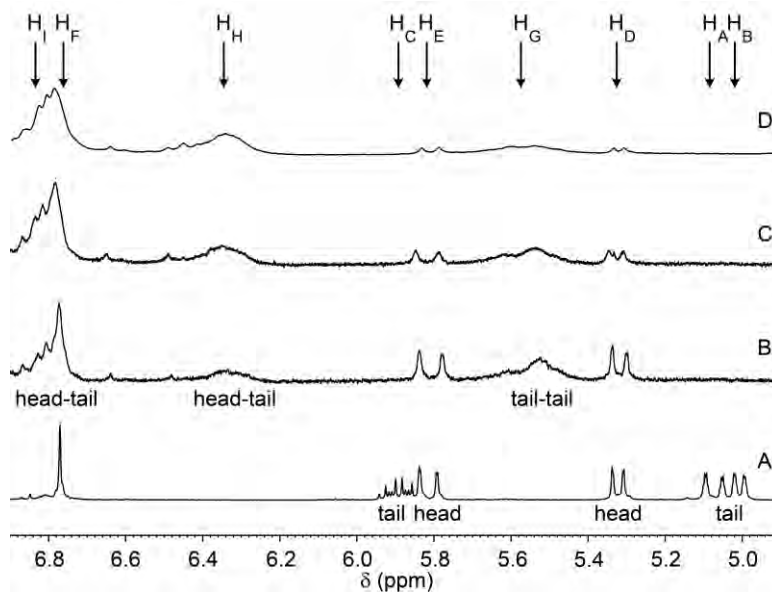


Figure 23. ^1H NMR spectra of the head-to-tail polymerization as a function of time. A) At 0 h (**OPV2e**); B) After 24 h; C) After 48 h; D) After 96 h. Labels ($\text{H}_{\text{A-H}}$) refer to labeled protons in Scheme 5. Head-head protons ($\delta \sim 7.2$) are not assignable due to overlap.

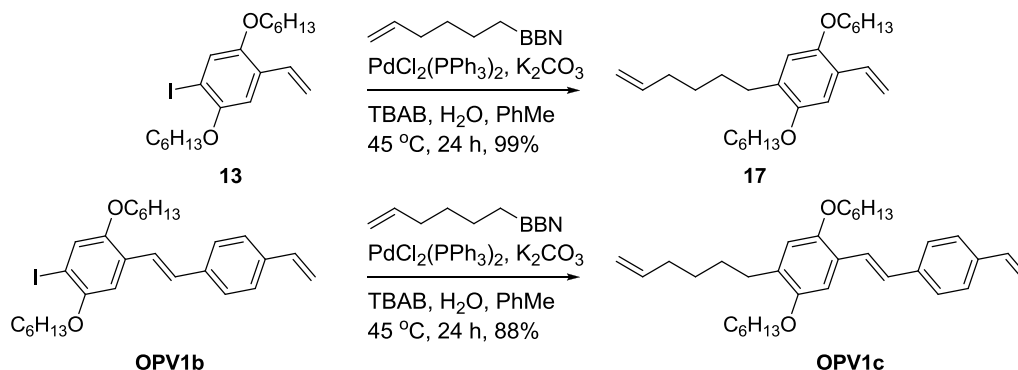
Table 12. Head-to-Tail polymerization of **OPV2e**

Time / h	Conversion of headgroups ^a	Conversion of tailgroups ^b	head-to-tail ^c	head-to-head ^d	tail-to-tail ^e
24	50%	100%	50%	0%	50%
48	80%	100%	60%	20%	20%
96	90%	100%	72%	18%	10%

^a Based on the integration of H_D; ^b Based on the integration of H_A and H_B, and H_C; ^c Based on the integration of H_H;

^d Based on difference between integration of H_D and H_H; ^e Based on the integration of H_G.

We also attempted to prepare head-to-tail polymers from styrene **13** and **OPV1b**, but were unsuccessful. We were able to convert styrene **13** into ADMET monomer **17** and **OPV1b** into monomer **OPV1c** (Scheme 20) using Suzuki couplings. However, after ADMET polymerization, we were only able to isolate insoluble gels.

**Scheme 20.** Synthesis of ADMET monomers from styrene **13** and **OPV1b**.

3.2.4 Optical spectroscopy

The optoelectronic properties of the OPVs depend on the oligomer length and on the endgroup (aldehyde vs. vinyl). Within each series (**OPVa** and **OPVb**), the absorption and emission maxima and molar extinction coefficients increase with increasing conjugation, while the HOMO-LUMO gap, ΔE_g , decreases (Table 13). The absorption and emission spectra of the

OPVa series are red-shifted relative to the **OPVb** series, and the HOMO-LUMO gaps of the **OPVa** series are smaller than those of the **OPVb** series. These effects are most pronounced in the **OPV1** oligomers and become progressively smaller with increasing conjugation. The extinction coefficients of the **OPVb** series are higher than those of the **OPVa** series, with the difference most pronounced in the **OPV2** and **OPV4** oligomers.

Table 13. Optoelectronic properties of the OPVs^a

OPV	$\lambda_{\max}^{\text{abs}} / \text{nm}$	$\lambda_{\max}^{\text{em}} / \text{nm}$	$\epsilon^{\text{b}} / \text{M}^{-1} \text{cm}^{-1}$	$\Delta E_{\text{g}}^{\text{c}} / \text{eV}$
OPV1a	376	492	29,100	2.89
OPV2a	411	503	35,300	2.69
OPV3a	427	519	82,800	2.51
OPV4a	443	548	77,500	2.48
OPV1b	360	423	40,500	3.06
OPV2b	399	473	70,900	2.76
OPV3b	419	480	94,400	2.58
OPV4b	437	496	118,000	2.52
OPV2c	417	542	62,100	2.63
OPV2d	456	530	62,500	2.31

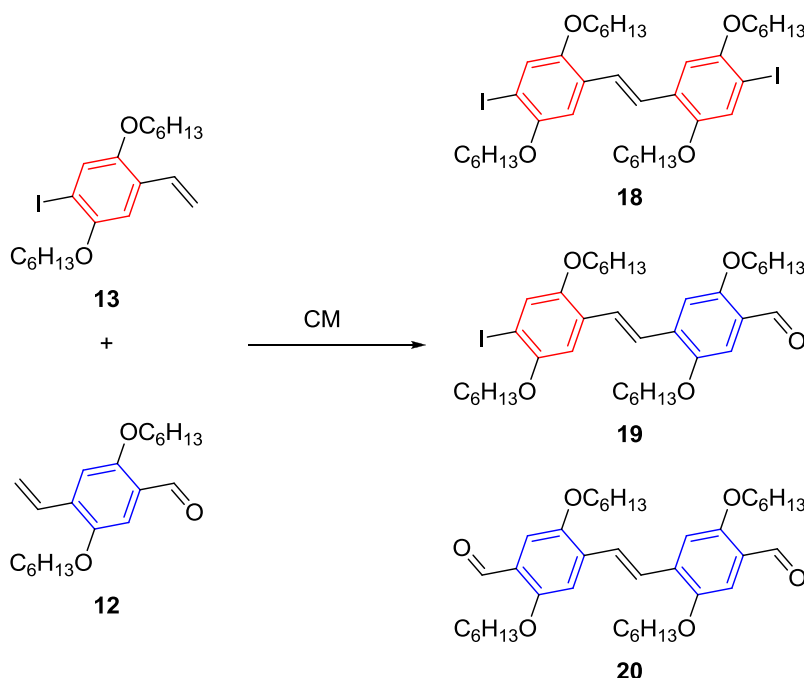
^a Obtained in CHCl₃ (~10⁻⁵ M); ^b Calculated at absorption maximum ^c HOMO-LUMO gap estimated as the onset of absorption.

Modified trimers **OPV2c** and **OPV2d** exhibited modulated optical properties in comparison to **OPV2a** and **OPV2b**. The absorption and emission maxima of **OPV2c** and **OPV2d** are redshifted relative to **OPV2a** and **OPV2b**. The HOMO-LUMO gaps of the modified OPVs are lower than those of **OPV2a** and **OPV2b**. The molar absorption coefficients of the modified OPVs are intermediate between those of **OPV2a** and **OPV2b**. Interestingly, **OPV2d** exhibited a much weaker emission than any other OPV.

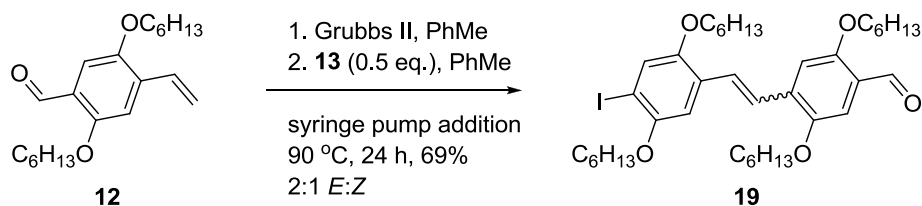
3.2.5 Progress toward more complex sequences by CM

Our attempts to prepare more complex sequences by the homologation approach were not successful. Preparation of more complex sequences would require CM between two type II olefins, which is predicted to generate a statistical mixture of homo- and cross-metathesis products.⁹¹ We were able to optimize conditions that led to moderate isolable yields of CM product, but the *E*-selectivity was low, and we were unable to efficiently separate the isomers.

Our model reaction for this study was the CM between styrene **13** and vinylbenzaldehyde **12** (both Type II olefins), which can produce three possible products (Scheme 21): the desired cross-metathesis product, stilbene **19**, and the undesired homometathesis products, stilbenes **18** and **20**. The initial optimization study was completed by Tianqi Pan. We determined that a 1:2 ratio of styrene **13** to vinylbenzaldehyde **12** gave the best conversion to desired stilbene **19** (Scheme 22). Addition of vinylbenzaldehyde **12** slowly by syringe pump allowed us to achieve isolated yields as high as 69%. However, ¹H NMR spectroscopy revealed that the *E* selectivity was low. The highest *E* selectivity achieved was 2:1 *E*:*Z*. The mixture can be recrystallized from MeOH to give exclusively *E*-**19**, although the recovery of *E*-**19** from the mixture was as low as 18%.



Scheme 21. Possible products in a CM reaction between two Type II olefins.



Scheme 22. Optimized Type II + Type II CM reaction.

We conducted a series of NMR experiments to investigate the potential to increase the *E:Z* selectivity of our cross metathesis reaction. Ritter, *et al.*,⁹⁷ have noted that that *E* selectivity in cross metatheses between two Type I olefins increases as a function of conversion to cross metathesis product. They attribute this increase to secondary metathesis leading to a thermodynamic control of the *E:Z* ratio. To assess the selectivity of the CM between styrenes **12** and **13**, we followed the progress of our optimal conditions in CDCl₃ periodically by ¹H NMR over 45 hours. Figure 24 illustrates the resonances in the ¹H NMR spectra that were followed. Concentrations were determined relative to DMF (δ 8.0 ppm) as an internal standard. Distinct

vinyl peaks are observable for both **12** ($\delta \sim 5.4$ and ~ 5.9) and **13** ($\delta \sim 5.25$ and 5.75). Characteristic aryl singlets are observable for *E*-**19** ($\delta \sim 7.5$) and *E*-**20** ($\delta \sim 7.6$). Stilbene **18** exhibits no distinct peaks. Since styrene **13** is converted only to stilbene **18** or to stilbene **19**, the concentration of stilbene **18** can be estimated based on the difference between total conversion of styrene **13** and the concentration of stilbene **19**. Although the ethylene resonance ($\delta \sim 5.4$) can also be quantified by integration, it represents only dissolved ethylene and does not include vapor phase ethylene in the NMR tube headspace. Interestingly, at no time was a significant peak for *Z*-stilbenes ($\delta \sim 6.7 - 6.8$) observed.

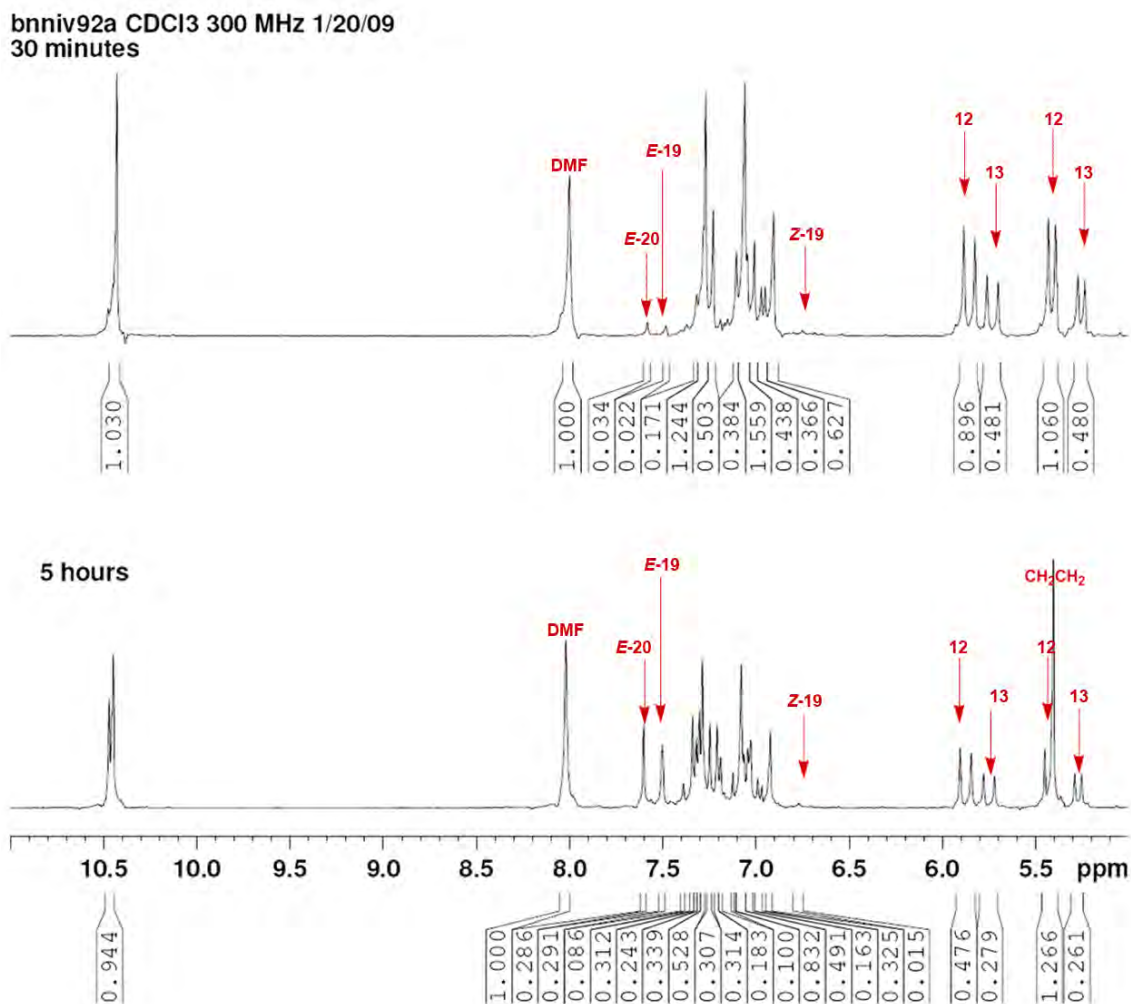


Figure 24. ¹H NMR spectra of CM between styrene **13** and vinylbenzaldehyde **12** after 30 min and 5 h. Labels refer to compound numbers.

We also followed the rate of the reaction between styrenes **12** and **13** to form stilbenes **18**, **19**, and **20**. A plot of relative concentration of the reaction components (initial concentration of styrene **12** is set to 1.0) as a function of time (Figure 25) shows that the reaction rate begins to decrease after three hours and significantly levels off after five hours. No significant change in composition was observed after five hours.

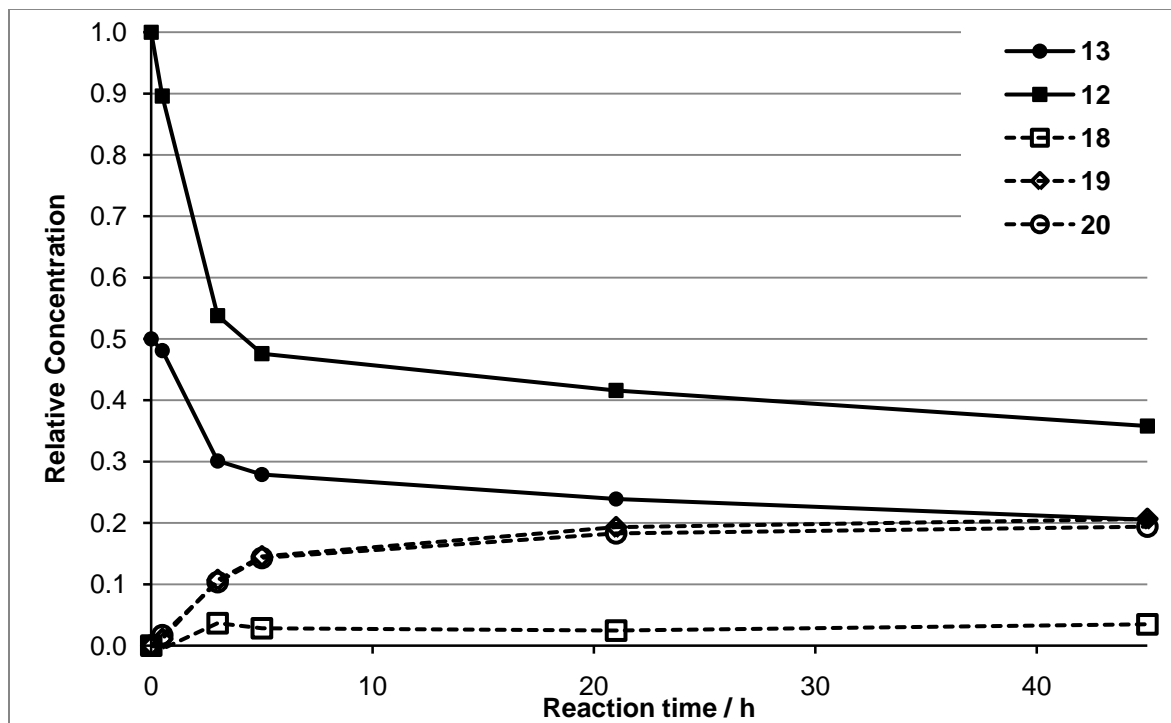


Figure 25. Relative concentrations of the components of the CM reaction (From ^1H NMR) between styrene **3** and vinylbenzaldehyde **1** as a function of time.

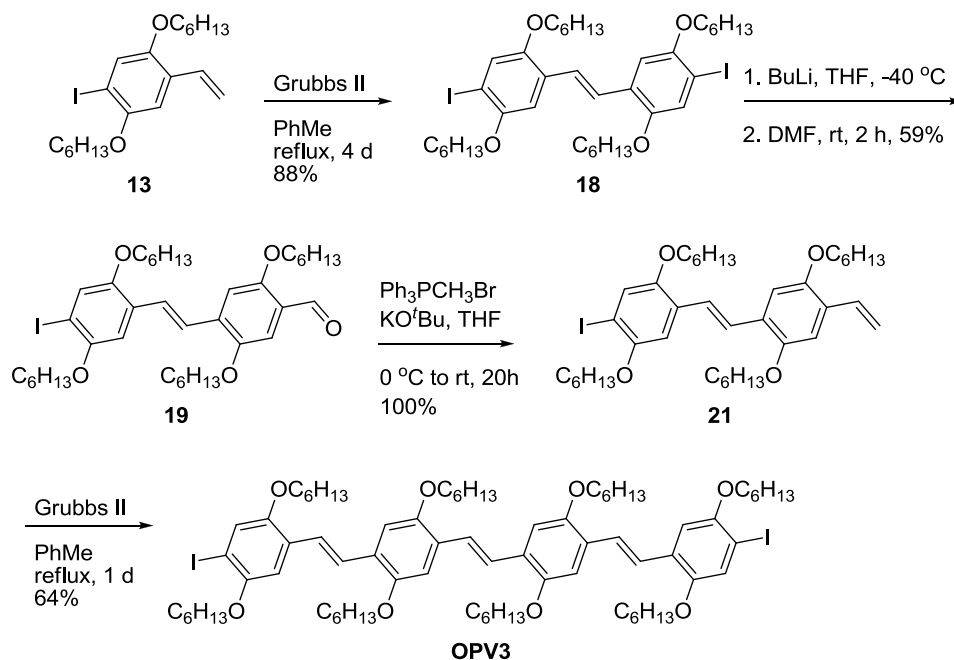
The lack of significant concentration of *Z* isomers was unexpected. We attribute this observation to the presence of ethylene, which would increase the reversibility of initial reactions between the styrene substrates and the ruthenium alkylidene catalyst. This reversibility promotes equilibrium, which will favor the thermodynamic products, the *E* stilbenes. Conventional scale reactions are performed in an open system to encourage ethylene loss and thereby increase yield. In this closed system, in contrast, the reaction is slower and does not proceed past 60% completion.

We performed a second NMR experiment to rule out secondary metathesis, which should be unlikely with Type II olefins, as a factor in the *E* selectivity of our CM reaction. A 9:1 mixture of stilbene *E*-**19** to styrene **13** with Grubbs II was heated in CDCl₃ for 24 h. No secondary metathesis products were observable by ¹H NMR.

The results of the NMR studies are encouraging. The *E* selectivity increases dramatically in the presence of ethylene, but reaction rate and conversion decrease. Conditions that maintain a low level of ethylene, but prevent it from accumulating, might lead to high conversion and high *E* selectivity.

3.2.6 Synthesis of symmetric OPVs using homometathesis

The dimerization approach allowed us to prepare symmetric OPVs up to four phenylene units in length. However, the low solubility of the symmetric OPVs prevented us from progressing farther. The synthesis of the symmetric OPVs began with the dimerization of styrene **13** to give stilbene **18**. This reaction proceeds in 84-88% yields using less than 0.01 equiv of Grubbs II in refluxing toluene on 10-20 gram scales (Scheme 23). The reaction also proceeds in moderate yields (72-79%) with shorter reaction times (24 h) if the Grubbs II catalyst is generated *in situ* from Grubbs I, bis(mesityl)imidazolium chloride, and potassium *t*-pentoxide. ¹H NMR spectroscopy reveals stilbene **18** to be 100% *E*.



Scheme 23. Preparation of OPVs by metathesis dimerization

Desymmetrization of stilbene **18** is required to produce vinylstilbene **21**, which can be dimerized by homometathesis to give a tetrameric OPV (Scheme 23). Despite the success of Et₂O as a solvent for the desymmetrization of **15**, lithiation of stilbene **18** in Et₂O led to decomposition. Lithiation with *n*BuLi in THF, followed by quenching with DMF gives stilbene **19** in 40-59% yield, although the reaction is unreliable. The low solubility of **18** in THF at subambient temperatures leads to low conversion after short reaction times, while decomposition occurs at longer reaction times and higher temperatures. The best yield (59%) was achieved by lithiation at -40 °C for one hour, following by quenching with DMF. Stilbene **19** was then converted to vinylstilbene **21** in quantitative yield by a Wittig reaction with Ph₃P=CH₂. Finally, homometathesis of **22** using 0.01 equiv Grubbs II in refluxing toluene gave tetramer **OPV3** in 67% yield. The limited solubility of **OPV3**, presumably due to its symmetry, halted the dimerization approach after just two dimerizations.

3.3 CONCLUSIONS

We have developed two approaches to well-defined *oligo*(phenylene-vinylene)s using CM. The iterative homologation approach was more successful, allowing us to prepare heterotelechelic, alternating OPVs up to five phenylene units in length. The CM reactions proceed in moderate to good yields and are *E* specific. This approach, however, suffers from long reaction times and potentially difficult separations. The dimerization approach, which could yield longer oligomers more rapidly, is less attractive due to the low solubility of the symmetric OPVs.

We have also investigated the possibility of producing more complex sequences by the iterative approach. We developed conditions for CM reaction between two Type II olefins with the potential for moderate yields of the CM product without using a large excess of one substrate. NMR studies show that the stereoselectivity may be controllable with the presence of a small amount of ethylene – just enough to enforce the equilibrium which promotes high *E* selectivity, but not so much as to drastically retard the rate of the reaction.

3.4 EXPERIMENTAL SECTION

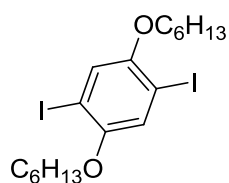
3.4.1 General methods

Materials. Anhydrous DMF was purchased from Aldrich and dispensed using air-sensitive techniques. Anhydrous diethyl ether was purchased from Fisher and opened immediately prior to use. KO^tBu was stored in a desiccator over CaSO₄. 4-Vinylbenzaldehyde, **14**,⁹² and 9-(hex-5-en-1-yl)-9-borabicyclo[3.3.1]nonane⁹⁸ were prepared according to literature procedures. All other

reagents and solvents were purchased and used as received. Column chromatography was carried out on standard grade silica gel (60 Å pore size, 40-63 µm particle size), which was purchased and used as received. Hexanes, dichloromethane, and ethyl acetate used for column chromatography were purchased and used as received.

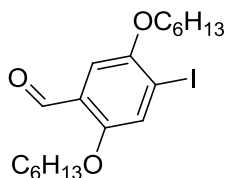
Instrumentation. ^1H (300 and 400 MHz) and ^{13}C (75 and 100 MHz) NMR spectra were recorded on Bruker spectrometers. Chemical shifts were referenced to residual ^1H or ^{13}C signals in deuterated solvents (7.27 and 77.0 ppm, respectively, for CHCl_3 and 5.32 and 54.0 ppm, respectively, for CH_2Cl_2). UV/VIS absorption spectra were recorded on a Perkin Elmer Lambda 9 UV/VIS/NIR spectrometer. Emission spectra were recorded on a Varian Cary Eclipse fluorimeter. HRMS were recorded on a Fison VG Autospec in the Mass Spectral Facility of the University of Pittsburgh. Elemental analysis was performed independently by Atlantic Microlabs.

3.4.2 Monomer synthesis



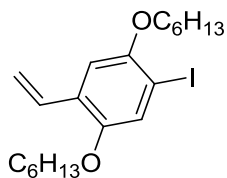
1,4-Bis(hexyloxy)-2,5-diiodobenzene (15). Methanol (600 mL) was added to a 2 L round-bottom flask equipped with a magnetic stirbar and cooled on an ice bath. Iodine monochloride (80 mL, 1.60 mol) was added slowly with rapid stirring. Then, **1** (84.0 g, 302 mmol) was added. The mixture was returned to rt, and then refluxed for 24 h. The mixture was cooled to rt, and sodium metabisulfite was added portionwise with vigorous stirring until the dark color is gone. The reaction mixture is then portioned between hexanes and water (500 mL each). The aqueous layer

was extracted with hexanes (3x 300 mL). The combined organic layers were washed with water (2x 300 mL) and brine (1x 300 mL), and dried over MgSO₄. The solvent was removed under reduced pressure. The residue was recrystallized from a mixture of methanol and dichloromethane by evaporation of the dichloromethane to give the title compound as off-white orthorhombic crystals (145.7 g, 91%). ¹H NMR (CDCl₃, 300 MHz) δ 0.92 (6H, t, *J* = 6.8 Hz, CH₃), 1.33 – 1.39 (8H, mult), 1.40-1.60 (4H, mult), 1.80 (4H, tt, *J* = 6.5, 6.8 Hz), 3.93 (4H, t, *J* = 6.5 Hz, OCH₂) 7.18 (2H, s, ArH) ppm. ¹³C NMR (CDCl₃, 75 MHz) δ 14.0 (CH₃), 22.6 (CH₂), 25.7 (CH₂), 29.1 (CH₂), 31.4 (CH₂), 70.3 (OCH₂), 86.3 (ArI quat), 122.7 (Ar CH), 152.8 (ArO quat) ppm. MS (EI) 530 (M⁺), 446, 361, 270, 248, 236, 189, 149, 135, 108, 85, 55 (base) m/z. HRMS calcd for C₁₈H₂₈I₂O₂: 530.0179 g/mol. Found: 530.0175 g/mol.



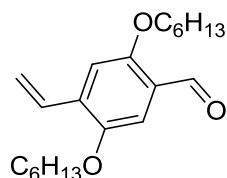
2,5-Bis(hexyloxy)-4-iodobenzaldehyde (16). Based on the methods of Peng, et al,⁸³ **5** (42.4 g, 80.0 mmol) was dissolved in anhydrous diethyl ether (150 mL) under N₂ in an oven-dried 1 L 3-neck rbf equipped with a magnetic stirbar, a gas adapter, an addition funnel containing ⁿBuLi (1.6 M in hexanes, 50 mL, 80 mmol) dissolved in anhydrous diethyl ether (100 mL), and a second addition funnel containing anhydrous DMF (10 mL, 130mmol) dissolved in anhydrous diethyl ether (35 mL). The rbf was cooled to 0 °C on an ice bath. The ⁿBuLi solution was added dropwise over 45 min (~2-3 drops/sec) with stirring. Once addition of ⁿBuLi was complete, the DMF solution was added at a rapid dropwise rate. The mixture was stirred at room temperature for 2 h. The reaction was quenched into 400 mL of water cooled on an ice bath. The aqueous layer was extracted three times with diethyl ether (100 mL). The combined organic layers were

washed three times with water (100 mL) and once with brine (100 mL). The organic layer was dried over MgSO₄, and the solvent was removed under reduced pressure. The residue was recrystallized by dissolution into 100 mL of hexanes and cooling to -20 °C. The title compound was isolated as pale yellow crystals (28.8 g, 83%). $\lambda_{\text{max}} = 356 \text{ nm}$. ¹H NMR (CDCl₃, 300 MHz) δ 0.94 (6H, t, $J = 7.0 \text{ Hz}$, CH₃), 1.34 – 1.37 (8H, mult), 1.50 (4H, mult), 1.82 (4H, mult), 4.00 (2H, t, $J = 6.6 \text{ Hz}$, OCH₂), 4.02 (2H, t, $J = 6.6 \text{ Hz}$, OCH₂), 7.19 (1H, s), 7.46 (1H, s), 10.43 (1H, s, CHO) ppm. ¹³C NMR (CDCl₃, 75 MHz) δ 13.99 (CH₃), 14.02 (CH₃), 22.54 (CH₂), 22.56 (CH₂), 25.65 (CH₂), 26.69 (CH₂), 28.96 (CH₂), 29.03 (CH₂), 31.44 (CH₂), 69.43 (OCH₂), 69.88 (OCH₂), 86.97 (ArI quat), 108.80 (Ar CH), 124.50 (Ar CH), 125.11 (Ar quat), 152.11 (ArO quat), 155.76 (Ar quat), 189.25 (CHO) ppm. MS (EI) 432 (M⁺), 348, 264 (base), 138, 84 m/z. HRMS calcd for C₁₉H₂₉IO₃: 432.1161 g/mol. Found: 432.1152 g/mol.



2,5-Bishexyloxy-4-iodostyrene (13). KO^tBu (30.0 g, 267 mmol) was added portionwise to a slurry of Ph₃PCH₃Br (100 g, 280 mmol) in THF (600 mL) at 0 °C under N₂ in an oven-dried 2 L 2-neck rbf equipped with a gas adapter and a septum. The resulting yellow suspension was stirred at rt for 30 min. The flask was cooled to 0 °C, and a solution of **6** (50 g, 116 mmol) in THF (600 mL) was added dropwise via cannula. The mixture was stirred overnight at rt. The reaction mixture was quenched with 100 mL saturated aqueous NH₄Cl. Approximately 800 mL of solvent were removed by vacuum distillation at room temperature. The remaining mixture was proportioned between hexanes (200 mL) and saturated NH₄Cl (200 mL). The aqueous layer was

extracted with hexanes (200 mL). The combined organic layers were washed twice with water (200 mL) and once with brine (200 mL) and dried over MgSO₄. The solvent was removed under reduced pressure. The residue was purified by column chromatography (silica gel, 9:1 hexanes:CH₂Cl₂) to give the title compound as a pale yellow amorphous solid (45.2 g, 91%). $\lambda_{\text{max}} = 328 \text{ nm}$. ¹H NMR (CDCl₃, 300 MHz) δ 0.90-1.10 (6H, mult, CH₃), 1.43-1.49 (8H, mult), 1.50-1.65 (4H, mult), 1.88-2.00 (4H, mult), 4.02 (2H, t, $J = 6.5 \text{ Hz}$, OCH₂), 4.07 (2H, t, $J = 6.5 \text{ Hz}$, OCH₂), 5.37 (1H, dd, $J = 11.1, 1.2 \text{ Hz}$, ArCH=CH₂), 5.84 (1H, dd, $J = 17.7, 1.2 \text{ Hz}$, ArCH=CH₂), 7.02 (1H, s), 7.08 (1H, dd, $J = 17.7, 11.1 \text{ Hz}$, ArCH=CH₂), 7.35 (1H, s) ppm. ¹³C NMR (CDCl₃, 75 MHz) δ 14.00 (CH₃), 14.03 (CH₃), 22.55 (CH₂), 22.57 (CH₂), 25.72 (CH₂), 25.74 (CH₂), 29.21 (CH₂), 29.23 (CH₂), 31.50 (CH₂), 69.37 (OCH₂), 70.12 (OCH₂), 85.97 (ArI quat), 110.03 (Ar CH), 114.65 (vinyl CH₂), 123.41 (Ar CH), 127.66 (Ar quat), 131.28 (vinyl CH), 151.04 (ArO quat), 152.06 (ArO quat) ppm. MS (EI) 430 (base, M⁺), 362, 346, 262, ,13, 143, 107, 77, 55 m/z. HRMS calcd for C₃₀H₃₁O₂ 430.1369 g/mol. Found 430.1367 g/mol.



2,5-Bis(hexyloxy)-4-vinylbenzaldehyde (12). **3** (10 g, 23.2 mmol) was dissolved in anhydrous diethyl ether (40 mL) under N₂ in an oven dried 3-neck 250 mL rbf equipped with a gas adapter, an addition funnel containing ⁿBuLi (1.6 M in hexanes, 15 mL, 24 mmol) dissolved in anhydrous diethyl ether (30 mL), and a second addition funnel containing anhydrous DMF (3 mL, 39 mmol) dissolved in anhydrous diethyl ether (10 mL). The flask was cooled to 0 °C, and the ⁿBuLi solution was added dropwise (~1 drop/s). Once addition of ⁿBuLi was complete, the DMF

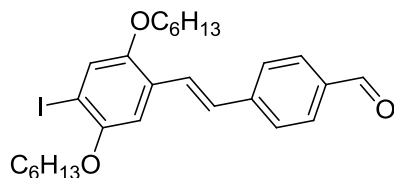
solution was added rapidly. The mixture was stirred at rt for 2 h and quenched into 100 mL of water cooled on an ice bath. The aqueous layer was extracted three times with ether (50 mL). The combined organic layers were washed three times with water (100 mL) and once with brine (100 mL). The solution was dried over MgSO₄, and the solvent was removed under reduced pressure. The residue was purified by column chromatography (silica gel, 99:1 hexanes:ethyl acetate) to give the title compound as a yellow amorphous solid (5.97 g, 77%). $\lambda_{\text{max}} = 288, 375$ nm. ¹H NMR (CDCl₃, 300 MHz) δ 0.90-1.10 (6H, mult, CH₃), 1.32-1.38 (8H, mult), 1.40-1.50 (4H, mult), 1.75-1.84 (4H, mult), 3.96 (2H, t, $J = 6.5$ Hz, OCH₂), 4.04 (2H, t, $J = 6.5$ Hz, OCH₂), 5.41 (1H, d, $J = 11.1$ Hz, ArCH=CH₂), 5.85 (1H, d, $J = 17.7$ Hz, ArCH=CH₂), 7.05 (1H, s), 7.06 (1H, dd, $J = 17.7, 11.1$ Hz, ArCH=CH₂), 7.27 (1H, s), 10.43 (1H, s, CHO) ppm. ¹³C NMR (CDCl₃, 75 MHz) δ 13.92 (CH₃), 22.50 (CH₂), 25.68 (CH₂), 29.09 (CH₂), 29.10 (CH₂), 31.45 (CH₂), 31.46 (CH₂), 68.80 (OCH₂), 69.01 (OCH₂), 109.78 (CH), 110.62 (CH), 117.37 (vinyl CH₂), 124.36 (quat), 131.24 (vinyl CH), 134.22 (quat), 150.38 (ArO quat), 155.98 (ArO quat), 189.07 (CHO) ppm. MS (EI) 332 (M⁺), 248, 164 (base), 135, 107, 91, 68 m/z. HRMS calcd for C₂₁H₃₂O₃: 332.2351 g/mol. Found 332.2349 g/mol.

3.4.3 Synthesis of OPVs by iterative cross metathesis

General Cross Metathesis Procedure: Cross metathesis substrates (ratios of reagents are outlined in individual entries below) were dissolved in CHCl₃ (0.3 M olefin concentration) Grubbs catalyst II (0.0075 eq) was added, and the flask was equipped with a water-cooled condenser. The mixture was refluxed under N₂ for 24-48 h until TLC indicated the reaction is complete. If the reaction was not complete after 24 h, more Grubbs catalyst II (0.0075

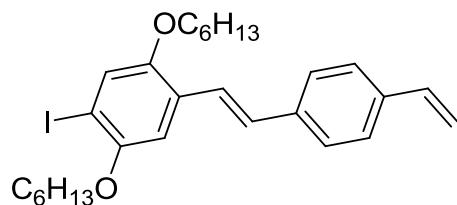
equivalents) was added. Upon completion, the solvent was removed under reduced pressure, and the residue is purified by column chromatography (silica gel, hexanes:EtOAc or hexanes:DCM).

General Wittig Procedure: KO^tBu (2.4 eq) was added portionwise to a slurry of Ph₃PCH₃Br (2.5 eq) in THF (6 mL per g phosphonium salt) under N₂ at 0 °C in a flame-dried Schlenk flask. The yellow mixture was stirred for 30 min at rt and then returned to 0 °C. Aldehyde (1.0 eq) in THF (equal volume) was added dropwise, and the mixture was stirred at rt for 2-3 h until TLC indicated the reaction was complete. The reaction was quenched into saturated aqueous NH₄Cl (0.5 mL per mL THF). The aqueous layer was extracted twice with EtOAc (equal volume). The combined organic layers were washed with brine (0.25 mL per mL organic solution), and dried over MgSO₄. The solvent was removed under reduced pressure, and the residue was purified by column chromatography (silica gel, hexanes:CH₂Cl₂).



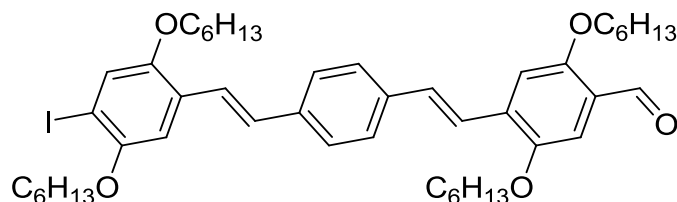
4-(2,5-bis(hexyloxy)-4-iodostyryl)benzaldehyde (OPV1a). Following the general CM procedure, **7** (4.30 g, 9.99 mmol) and **2** (2.0 M in benzene, 10 mL, 20 mmol), and Grubbs catalyst II (200 mg, 0.236 mmol) were dissolved in CHCl₃ (100 mL) and refluxed for 40 h. Column chromatography (silica gel, 49:1 – 19:1 hexanes:ethyl acetate) gave the title compound as a fluorescent, yellow, amorphous solid (4.00 g, 75%). λ_{\max} = 376 nm. ¹H NMR (CDCl₃, 300 MHz) δ 0.80-1.00 (6H, mult, CH₃), 1.26-1.43 (8H, mult), 1.45-1.60 (4H, mult), 1.80-1.90 (4H, mult), 3.98 (2H, t, J = 6.6 Hz OCH₂), 4.03 (2H, t, J = 6.6 Hz, OCH₂), 7.03 (1H, s), 7.32 (1H, s),

7.18 and 7.55 (2H, 2d, $J = 16.5$ Hz, *trans* CH=CH), 7.66 and 7.88 (4H, 2 d, $J = 8.1$ Hz, *p*-C₆H₄), 10.00 (1H, s, CHO) ppm. ¹³C NMR (CDCl₃, 75 MHz) δ 14.00 (CH₃), 14.05 (CH₃), 22.60 (CH₂), 25.77 (CH₂), 25.82 (CH₂), 29.23 (CH₂), 31.51 (CH₂), 69.57 (OCH₂), 70.23 (OCH₂), 87.24 (ArI quat), 110.09 (CH), 123.71 (CH), 126.55 (quat), 126.73 (CH), 126.88 (CH), 127.96 (CH), 130.21 (CH), 135.22 (quat), 143.77 (quat), 151.60 (quat), 152.22 (quat), 191.59 (CHO) ppm. MS (EI) 534 (M⁺), 432, 393, 366, 322, 264, 208, 179, 153 (base), 125, 115, 91, 77 m/z. HRMS calcd for C₂₇H₃₅IO₃: 534.1631 g/mol. Found: 534.1631 g/mol.



4-(2,5-bis(hexyloxy)-4-iodostyryl)styrene (OPV1b). Following the general Wittig procedure, KO^tBu (1.83 g, 16.3 mmol) was added to Ph₃PCH₃Br (5.85 g, 16.4 mmol) in THF (30 mL). Then **OPV1a** (3.50 g, 6.54 mmol) in THF (30 mL) was added and stirred for 2 h. Column chromatography (silica gel, 4:1 hexanes:CH₂Cl₂) gave the title compound as a fluorescent, yellow, amorphous solid (3.34 g, 96%). $\lambda_{\text{max}} = 360$ nm. ¹H NMR (CD₂Cl₂, 300 MHz) δ 0.90-1.10 (6H, mult, CH₃), 1.30-1.45 (8H, mult), 1.45-1.60 (4H, mult), 1.75-1.90 (4H, mult), 3.96 (2H, t, $J = 6.5$ Hz, OCH₂), 4.02 (2H, t, $J = 6.5$ Hz, OCH₂), 5.26 (1H, dd, $J = 10.8, 1.2$ Hz, ArCH=CH₂), 5.79 (1H, dd, $J = 17.4, 1.2$ Hz, ArCH=CH₂), 6.74 (1H, dd, $J = 17.4, 10.8$ Hz, ArCH=CH₂), 7.06 (1H, s), 7.31 (1H, s), 7.16 and 7.42 (2H, 2 d, $J = 16.4$ Hz, *trans* CH=CH), 7.42 and 7.50 (4H, 2 d, $J = 8.3$ Hz, *p*-C₆H₄) ppm. ¹³C NMR (CD₂Cl₂, 75 MHz) δ 14.39 (CH₃), 14.42 (CH₃), 23.21 (CH₂), 26.36 (CH₂), 26.42 (CH₂), 29.85 (CH₂), 32.12 (CH₂), 32.15 (CH₂), 70.26 (OCH₂), 70.72 (OCH₂), 86.14 (ArI quat), 110.30 (CH), 114.10 (CH₂), 123.50 (CH), 124.25

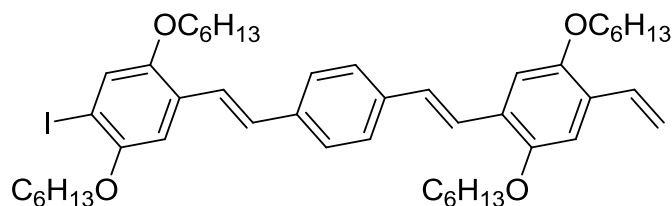
(CH), 127.07 (CH), 127.23 (CH), 127.99 (quat), 129.44 (CH), 136.96 (CH), 137.49 (quat), 137.78 (quat), 151.93 (ArO quat), 152.82 (ArO quat) ppm. MS (EI) 532 (base, M⁺), 448, 364, 236, 117 m/z. HRMS calcd for C₂₈H₃₇IO₂ 532.1838 g/mol. Found 532.1834 g/mol.



4-(4-(2,5-bis(hexyloxy)-4-iodostyryl)-styryl)-2,5-bis(hexyloxy)benzaldehyde (OPV2a).

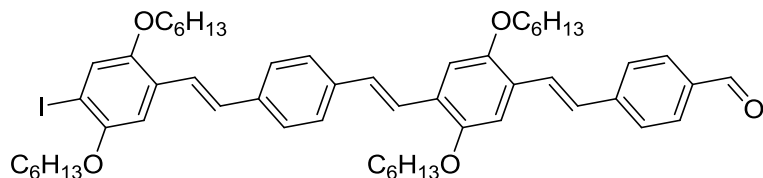
Following the general CM procedure, **OPV1b** (100 mg, 0.187 mmol), **1** (250 mg, 0.752 mmol), and Grubbs II catalyst (10 mg, 11.8 μ mol) were dissolved in CHCl₃ (2 mL) in a 5 mL rbf and refluxed for 40 h. Column chromatography (silica gel, 7:3 hexanes:CH₂Cl₂) gave the title compound as a fluorescent, yellow-orange, amorphous solid (112.2 mg, 72%). $\lambda_{\text{max}} = 411$ nm. ¹H NMR (CD₂Cl₂, 300 MHz) δ 0.85-1.00 (12H, mult, CH₃), 1.30-1.45 (16H, mult), 1.45-1.60 (8H, mult), 1.75-1.90 (8H, mult), 3.97 (2H, t, $J = 6.3$ Hz, OCH₂), 4.03 (2H, t, $J = 6.3$ Hz, OCH₂), 4.05 (2H, t, $J = 6.3$ Hz, OCH₂), 4.13 (2H, t, $J = 6.3$ Hz, OCH₂), 7.07 (1H, s), 7.18 (1H, d, $J = 16.5$ Hz, *trans* CH=CH), 7.27 (1H, s), 7.29 (1H, d, $J = 16.5$ Hz, *trans* CH=CH), 7.31 (1H, s), 7.32 (1H, s), 7.46 (1H, d, $J = 16.5$ Hz, *trans* CH=CH), 7.53 (1H, d, $J = 16.5$ Hz, *trans* CH=CH), 7.56 (4H, br s, *p*-C₆H₄), 10.44 (1H, s, CHO) ppm. ¹³C NMR (CD₂Cl₂) δ 14.42 (CH₃), 23.20 (CH₂), 23.23 (CH₂), 26.35 (CH₂), 26.38 (CH₂), 26.45 (CH₂), 29.81 (CH₂), 29.87 (CH₂), 29.89 (CH₂), 32.14 (CH₂), 32.15 (CH₂), 32.18 (CH₂), 69.74 (OCH₂), 69.81 (OCH₂), 70.23 (OCH₂), 70.71 (OCH₂), 86.32 (ArI quat), 110.23 (CH), 110.44 (CH), 110.97 (CH), 123.13 (CH), 123.80 (CH), 124.22 (CH), 124.83 (quat), 127.46 (CH), 127.77 (CH), 127.88 (quat), 129.28 (CH), 132.17 (CH), 134.57 (quat), 137.21 (quat), 138.21 (quat), 151.29 (ArO quat), 151.96 (ArO quat), 152.81 (ArO quat),

156.73 (ArO quat), 189.21 (CHO) ppm. MS (EI) 836 (M^+ , base), 734 m/z. HRMS calcd for $C_{47}H_{65}IO_5$: 836.3877 g/mol. Found: 836.3899 g/mol.



4-(4-(2,5-bis(hexyloxy)-4-iodostyryl)-styryl)-2,5-bis(hexyloxy)styrene (OPV2b). Following the general Wittig procedure, KO^tBu (0.55 g, 4.95 mmol), was added to Ph_3PCH_3Br (1.77 g, 4.95 mmol) in THF (10 mL). Then **OPV2a** (1.17 g, 1.39 mmol) in THF (25 mL) was added and stirred for 3 h. Column chromatography (silica gel, 1:1 hexanes: CH_2Cl_2) gave the title compound as a fluorescent, yellow, tacky solid (1.04 g, 90%). $\lambda_{max} = 399$ nm. 1H NMR (CD_2Cl_2 , 300 MHz) δ 0.85-1.00 (12H, mult, CH_3), 1.30-1.45 (16H, mult), 1.45-1.60 (8H, mult), 1.75-1.90 (8H, mult), 3.97 (2H, t, $J = 6.4$ Hz, OCH_2), 4.03 (2H, t, $J = 6.4$ Hz, OCH_2), 4.04 (2H, t, $J = 6.4$ Hz, OCH_2), 4.12 (2H, t, $J = 6.4$ Hz, OCH_2), 5.27 (1H, d, $J = 11.4$ Hz, $ArCH=CH_2$), 5.78 (1H, d, $J = 17.7$ Hz, $ArCH=CH_2$), 7.05 (1H, s), 7.07 (1H, dd, $J = 17.7, 11.4$ Hz, $ArCH=CH_2$), 7.08 (1H, s), 7.16 (1H, d, $J = 16.5$ *trans* $CH=CH$), 7.18 (1H, d, $J = 16.5$ Hz, *trans* $CH=CH$), 7.32 (1H, s), 7.44 (1H, d, $J = 16.5$ $CH=CH$), 7.52 (1H, d, $J = 16.5$, *trans* $CH=CH$), 7.54 (4H, br s, *p*- C_6H_4) ppm. ^{13}C NMR (CD_2Cl_2 , 75 MHz) δ 14.41 (CH_3), 23.22 (CH_2), 23.24 (CH_2), 26.37 (CH_2), 26.42 (CH_2), 26.44 (CH_2), 26.52 (CH_2), 29.86 (CH_2), 29.89 (CH_2), 30.02 (CH_2), 32.13 (CH_2), 32.17 (CH_2), 32.21 (CH_2), 32.23 (CH_2), 69.86 (OCH_2), 70.05 (OCH_2), 70.28 (OCH_2), 70.74 (OCH_2), 86.10 (ArI quat), 110.26 (CH), 110.68 (CH), 111.06 (CH), 114.38 (CH_2), 123.30 (CH), 123.81 (CH), 124.27 (CH), 127.34 (CH), 127.40 (CH), 127.54 (quat), 128.07 (quat), 128.75 (CH), 129.49 (CH), 132.04 (CH), 137.41 (quat), 137.95 (quat), 151.35 (ArO quat), 151.54 (ArO quat), 151.94 (ArO

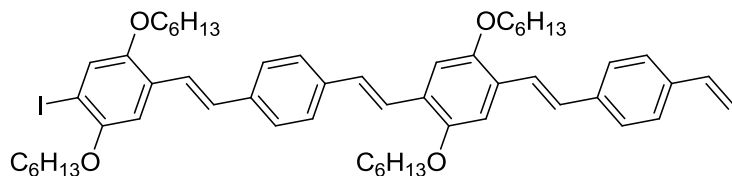
quat), 152.84 (ArO quat) ppm. MS (EI) 834 (M^+), 711, 589, 497, 417, 369, 306, 278, 254, 212, 155 (base), 138, 128 m/z. HRMS calcd for $C_{48}H_{67}IO_4$: 834.4084 g/mol. Found: 834.4077 g/mol.



4-(4-(4-(2,5-bis(hexyloxy)-4-iodostyryl)-styryl)-2,5-bis(hexyloxy)styryl)benzaldehyde

(OPV3a). Following the general CM procedure, **OPV2b** (890 mg, 1.06 mmol), **2** (2.0 M in benzene, 1.6 mL, 3.2 mmol), and Grubbs II catalyst (25 mg, 29.4 μ mol) were dissolved in $CHCl_3$ (20 mL) in a 50 mL rbf and refluxed for 48 h. Column chromatography (silica gel, 3:2 hexanes: CH_2Cl_2) gave the title compound as a fluorescent, orange, amorphous solid (888 mg, 89%). $\lambda_{max} = 427$ nm. 1H NMR (CD_2Cl_2 , 300 MHz) δ 0.85-1.00 (12H, mult $-CH_3$), 1.20-1.50 (16H, mult), 1.50-1.70 (8H, mult), 1.80-2.00 (8H, mult), 3.97 (3H, t, $J = 6.4$ Hz), 4.03 (3H, t, $J = 6.4$ Hz), 4.08 (3H, t, $J = 6.4$ Hz), 4.09 (3H, t, $J = 6.4$ Hz), 7.07 (1H, s), 7.17 (1H, s), 7.18 (1H, s), 7.18 (1H, d, $J = 16.2$ Hz, *trans* CH=CH), 7.20 (1H, d, $J = 16.2$ Hz, *trans* CH=CH), 7.23 (1H, d, $J = 16.2$ Hz, *trans* CH=CH), 7.32 (1H, s), 7.45 (1H, d, $J = 16.5$ Hz, *trans* CH=CH), 7.54 (1H, d, $J = 16.2$ Hz, *trans* CH=CH), 7.56 (4H, br s, *p*- C_6H_4), 7.68 (1H, d, $J = 16.5$ Hz, *trans* CH=CH), 7.69 and 7.86 (4H, 2 d, $J = 7.9$ Hz, *p*- C_6H_4), 9.98 (1H, s, $-CHO$) ppm. ^{13}C NMR (CD_2Cl_2 , 75 MHz) δ 14.42 (CH_3), 23.21 (CH_2), 23.25 (CH_2), 26.35 (CH_2), 26.43 (CH_2), 26.53 (CH_2), 29.84 (CH_2), 29.99 (CH_2), 30.03 (CH_2), 30.26 (CH_2), 32.11 (CH_2), 32.16 (CH_2), 32.21 (CH_2), 69.97 (OCH_2), 70.03 (OCH_2), 70.22 (OCH_2), 70.69 (OCH_2), 86.13 (ArI quat), 110.18 (CH), 110.69 (CH), 111.11 (CH), 123.36 (CH), 123.58 (CH), 124.20 (CH), 126.39 (quat), 127.32 (CH), 127.40 (CH), 127.76 (CH), 127.82 (CH), 127.97 (quat), 128.24 (quat), 129.26 (CH), 129.41 (CH),

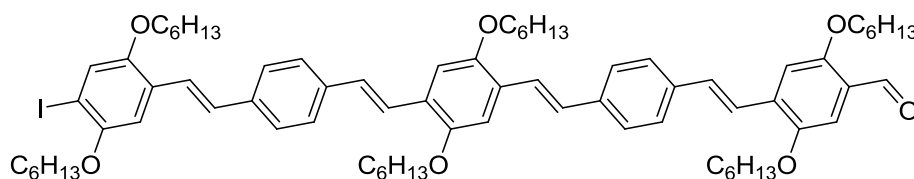
130.62 (CH), 135.75 (quat), 135.94 (quat), 137.54 (quat), 137.80 (quat), 144.59 (quat), 151.58 (ArO quat), 151.91 (ArO quat), 152.01 (ArO quat), 152.78 (ArO quat), 191.96 (CHO) ppm. MS (EI) 938 (M^+), 836, 381, 181, 131 (base) m/z. HRMS calcd for $C_{55}H_{71}IO_5$: 938.4346 g/mol. Found 938.4302 g/mol



4-(4-(4-(2,5-bis(hexyloxy)-4-iodostyryl)-styryl)-2,5-bis(hexyloxy)styryl)styrene (OPV3b).

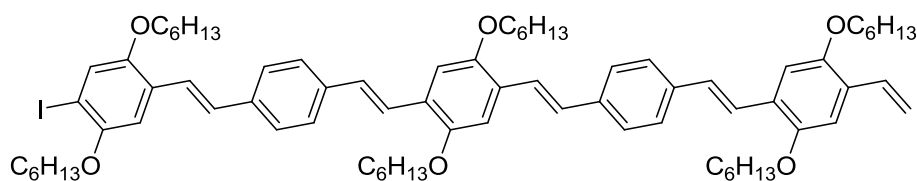
Following the general Wittig procedure, KO^tBu (53 mg, 472 μmol), was added to Ph_3PCH_3Br (170 mg, 476 μmol) in THF (2 mL). Then OPV3a (180 mg, 192 μmol) in THF (10 mL) was added and stirred for 3 h. Column chromatography (silica gel, 1:1 hexanes: CH_2Cl_2) gave the title compound as a fluorescent, orange solid (160 mg, 89%). $\lambda_{\text{max}} = 419 \text{ nm}$. 1H NMR (CD_2Cl_2 , 300 MHz) δ 0.85-1.00 (12H, mult, CH_3), 1.20-1.50 (16H, mult), 1.50-1.70 (8H, mult), 1.80-2.00 (8H, mult), 3.97 (2H, t, $J = 6.5 \text{ Hz}$, OCH_2), 4.04 (2H, t, $J = 6.5 \text{ Hz}$, OCH_2), 4.07 (2H, t, $J = 6.5 \text{ Hz}$, OCH_2), 4.09 (2H, t, $J = 6.5 \text{ Hz}$, OCH_2), 5.28 (1H, d, $J = 10.8 \text{ Hz}$, $ArCH=CH_2$), 5.81 (1H, d, $J = 17.7 \text{ Hz}$, $ArCH=CH_2$), 6.78 (1H, dd, $J = 10.8, 17.7 \text{ Hz}$, $ArCH=CH_2$), 7.09 (1H, s), 7.10-7.20 (5H, mult), 7.33 (1H, s), 7.40-7.60 (11H, mult) ppm. ^{13}C NMR (CD_2Cl_2 , 75 MHz) δ 14.46 (CH_3), 23.25 (CH_2), 23.29 (CH_2), 26.39 (CH_2), 26.46 (CH_2), 26.57 (CH_2), 29.89 (CH_2), 29.91 (CH_2), 30.08 (CH_2), 30.31 (CH_2), 32.16 (CH_2), 32.20 (CH_2), 32.27 (CH_2), 70.04 (OCH_2), 70.25 (OCH_2), 70.72 (OCH_2), 86.12 (ArI quat), 110.23 (CH), 110.80 (CH), 110.85 (CH), 113.96 (CH_2), 123.31 (CH), 123.79 (CH), 123.85 (CH), 124.23 (CH), 127.08 (CH), 127.18 (CH), 127.32 (quat), 127.36 (CH), 127.43 (CH), 128.06 (quat), 128.77 (CH), 129.48 (CH), 137.02 (CH),

137.29 (quat), 137.43 (quat), 137.98 (quat), 138.14 (quat), 151.69 (ArO quat), 151.95 (ArO quat), 152.83 (ArO quat) ppm. MS (EI) 936 (M^+), 834, 813, 634 (base), 466, 338, 254, 219, 128 m/z. HRMS calcd for $C_{56}H_{73}IO_4$: 936.4554 g/mol. Found 936.4519 g/mol.



4-(4-(4-(4-(2,5-bis(hexyloxy)-4-iodostyryl)-styryl)-2,5-bis(hexyloxy)styryl)styryl)-2,5-bis(hexyloxy)benzaldehyde (OPV4a). Following the general CM procedure, OPV3b (200 mg, 213 μ mol), 1 (250 mg, 752 μ mol), were dissolved in $CHCl_3$ (20 mL), and Grubbs II catalyst (20 mg, 23.5 μ mol) were dissolved in $CHCl_3$ (2 mL) in a 50 mL rbf and refluxed for 40 h. Column chromatography (silica gel, 7:3 hexanes: CH_2Cl_2) gave the title compound as a fluorescent, orange, amorphous solid (181.7 mg, 69%). λ_{max} = 443 nm. 1H NMR (CD_2Cl_2 , 400 MHz) δ 0.85-1.00 (18H, mult, CH_3), 1.20-1.50 (24H, mult), 1.50-1.70 (12H, mult), 1.80-2.00 (12H, mult), 3.97 (2H, t, J = 6.4 Hz, OCH_2), 4.03 (2H, t, J = 6.4 Hz, OCH_2), 4.05 (2H, t, J = 6.4 Hz, OCH_2), 4.09 (4H, t, J = 6.4 Hz, OCH_2), 4.13 (H, t, J = 6.4 Hz, OCH_2), 7.08 (1H, s), 7.15-7.22 (5H, mult), 7.24 (1H, s), 7.28-7.32 (3H, mult), 7.44 (1H, d, J = 16.8 Hz, *trans* $CH=CH$), 7.52-7.57 (11H, mult), 10.44 (1H, s, CHO) ppm. ^{13}C NMR (CD_2Cl_2 , 100 MHz) δ 14.40 (CH_3), 14.42 (CH_3), 23.19 (CH_2), 23.22 (CH_2), 23.26 (CH_2), 26.34 (CH_2), 26.37 (CH_2), 26.44 (CH_2), 26.46 (CH_2), 26.56 (CH_2), 29.81 (CH_2), 29.86 (CH_2), 29.89 (CH_2), 30.06 (CH_2), 30.27 (CH_2), 32.13 (CH_2), 32.14 (CH_2), 32.17 (CH_2), 32.25 (CH_2), 69.79 (OCH_2), 69.86 (OCH_2), 70.07 (OCH_2), 70.28 (OCH_2), 70.74 (OCH_2), 86.12 (ArI, quat), 110.26 (CH), 110.49 (CH), 110.83 (CH), 110.87 (CH), 111.02 (CH), 123.01 (CH), 123.32 (CH), 123.75 (CH), 124.15 (CH), 124.28 (CH), 124.84 (quat),

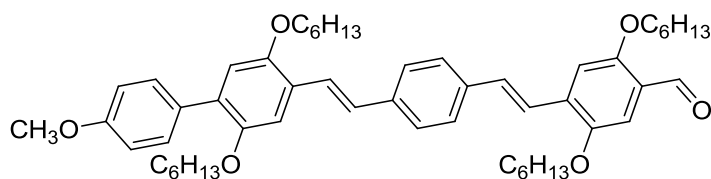
127.24 (quat), 127.37 (CH), 127.40 (CH), 127.40 (CH), 127.42 (CH), 127.47 (quat), 127.78 (CH), 128.07 (quat), 128.66 (CH), 128.85 (CH), 129.49 (CH), 132.27 (CH), 134.68 (quat), 137.01 (quat), 137.45 (quat), 137.95 (quat), 138.56 (quat), 151.32 (ArO quat), 151.70 (ArO quat), 151.75 (ArO quat), 151.95 (ArO, quat), 152.84 (ArO, quat), 156.78 (ArO quat), 189.26 (CHO) ppm. Analysis calcd for C₇₅H₁₀₁IO₇: C, 72.56; H, 8.20; I, 10.22; O, 9.02. Found: C, 72.67; H, 8.48.



4-(4-(4-(4-(2,5-bis(hexyloxy)-4-iodostyryl)-styryl)-2,5-bis(hexyloxy)styryl)styryl)-2,5-bis(hexyloxy)styrene (OPV4b). Following the general Wittig procedure, KO^tBu (26 mg, 232 μmol), was added to Ph₃PCH₃Br (83 mg, 323 μmol) in THF (1 mL). Then **OPV4a** (115 mg, 92.6 μmol) in THF (5 mL) was added and stirred for 3 h. Column chromatography (silica gel, 3:1 hexanes:CH₂Cl₂) gave the title compound as a fluorescent, orange solid (93.3 mg, 81%). λ_{max} = 437 nm. ¹H NMR (CD₂Cl₂, 400 MHz) δ 0.85-1.00 (18H, mult, CH₃), 1.20-1.50 (24H, mult), 1.50-1.70 (12H, mult), 1.80-2.00 (12H, mult), 3.97 (2H, t, *J* = 6.4 Hz, OCH₂), 4.04 (6H, t, *J* = 6.4 Hz, OCH₂), 4.10 (4H, t, *J* = 6.4 Hz, OCH₂), 5.29 (1H, dd, *J* = 11.2, 1.2 Hz, ArCH=CH₂), 5.80 (1H, dd, *J* = 17.6, 1.2 Hz, ArCH=CH₂), 7.05-7.10 (3H, mult), 7.13-7.22 (7H, mult), 7.33 (1H, s), 7.46 (1H, d, *J* = 16.4 Hz, *trans* CH=CH), 7.51-7.58 (11H, mult) ppm. ¹³C NMR (CD₂Cl₂, 100 MHz) δ 14.46 (CH₃), 23.24 (CH₂), 23.29 (CH₂), 26.39 (CH₂), 26.45 (CH₂), 26.47 (CH₂), 26.56 (CH₂), 26.58 (CH₂), 29.89 (CH₂), 29.92 (CH₂), 30.05 (CH₂), 30.07 (CH₂), 30.10 (CH₂), 30.30 (CH₂), 32.16 (CH₂), 32.20 (CH₂), 32.24 (CH₂), 32.26 (CH₂), 32.28 (CH₂), 69.86 (OCH₂), 70.06

(OCH₂), 70.26 (OCH₂), 70.73 (OCH₂), 86.12 (ArI quat), 110.24 (CH), 110.67 (CH), 110.82 (CH), 111.06 (CH), 114.36 (CH₂), 123.31 (CH), 123.65 (CH), 123.68 (CH), 123.81 (CH), 124.24 (CH), 127.31 (quat), 127.36 (CH), 127.41 (CH), 127.43 (CH), 127.50 (quat), 128.74 (CH), 128.82 (CH), 129.49 (CH), 132.08 (CH), 137.43 (quat), 137.76 (quat), 138.00 (quat), 151.37 (ArO quat), 151.54 (ArO quat), 151.70 (ArO quat), 151.72 (ArO quat), 151.96 (ArO quat), 152.84 (ArO quat) ppm. Analysis calcd for C₇₆H₁₀₃IO₆: C, 73.64; H, 8.38; I, 10.24; O, 7.74. Found: C, 73.66; H, 8.55.

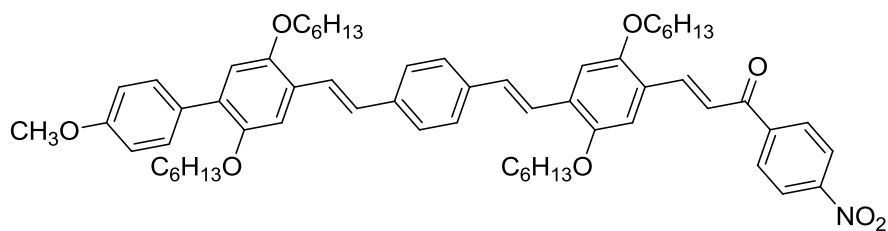
3.4.4 Synthesis of modified OPVs



4-(4-(2,5-bis(hexyloxy)-4-(4-methoxyphenyl)styryl)-styryl)-2,5-bis(hexyloxy)benzaldehyde

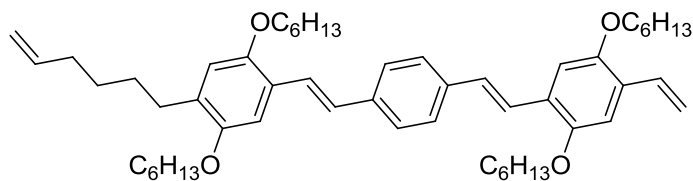
(OPV2c). In a nitrogen filled glovebox, OPV2a (100 mg, 119 μ mol), 4-methoxyphenylboronic acid (35 mg, 230 μ mol), Pd(PPh₃)₄ (10 mg, 8.7 μ mol), and TBAB (5 mg, 14 μ mol) were dissolved in PhMe (5 mL) in a flame-dried Schlenk flask. The flask was fitted with a septum and removed from the glovebox. The flask was charged with 2.0 M K₂CO₃ (aq) (5 mL) that had been sparged with N₂ for 10 min. The mixture was stirred at 80 °C under N₂ for 20 h. After cooling to rt, the layers were separated, and the aqueous layer was extracted with EtOAc (3x 5 mL). The combined organic layers were dried over MgSO₄ and reduced *in vacuo*. The residue was purified by silica gel chromatography (1:1 hexanes:DCM) to give the title compound as an orange amorphous solid (100 mg, 100%). λ_{\max} 418 nm. ¹H NMR (CD₂Cl₂, 400 MHz) δ 0.85-1.00 (12H, mult), 1.30-1.50 (18H, mult), 1.50-1.60 (6H, mult), 1.75 (2H, pent, *J* = 6.8 Hz), 1.80-1.90 (6H,

mult), 3.86 (3H, s), 3.99 (2H, t, $J=6.4$ Hz), 4.05 (2H, t, $J=6.4$ Hz), 4.06 (2H, t, $J=6.4$ Hz), 4.14 (2H, t, $J=6.4$ Hz), 6.93 (1H, s), 6.97 (2H, d, $J=8.8$ Hz, p -C₆H₄), 7.22 (1H, d, $J=16.4$ Hz, *trans* CH=CH), 7.24 (1H, s), 7.32 (1H, d, $J=16.4$ Hz, *trans* CH=CH), 7.33 (2H, br s, p -C₆H₄), 7.55 (1H, d, $J=16.4$ Hz, *trans* CH=CH), 7.56 (2H, d, $J=8.8$ Hz, p -C₆H₄), 7.57 (1H, s), 7.59 (1H, s), 7.59 (2H, br s, p -C₆H₄), 7.59 (1H, d, $J=16.4$ Hz, *trans* CH=CH), 10.46 (1H, s, CHO) ppm. ¹³C NMR (CD₂Cl₂, 100 MHz) δ 14.43 (CH₃), 14.45 (CH₃), 23.23 (CH₂), 23.26 (CH₂), 23.28 (CH₂), 26.38 (CH₂), 26.42 (CH₂), 26.50 (CH₂), 26.56 (CH₂), 29.85 (CH₂), 29.98 (CH₂), 30.09 (CH₂), 32.14 (CH₂), 32.19 (CH₂), 32.23 (CH₂), 32.26 (CH₂), 55.78 (OCH₃), 69.77 (OCH₂), 69.83 (OCH₂), 69.94 (OCH₂), 70.13 (OCH₂), 110.47 (CH), 110.99 (CH), 111.43 (CH), 113.88 (CH), 115.83 (CH), 122.98 (CH), 124.26 (CH), 124.83 (quat), 126.10 (quat), 127.38 (CH), 127.79 (CH), 128.46 (CH), 131.12 (CH), 131.35 (quat), 131.56 (quat), 132.30 (CH), 134.70 (quat), 136.95 (quat), 138.66 (quat), 150.81 (ArO quat), 151.32 (ArO quat), 151.75 (ArO quat), 156.78 (ArO quat), 159.43 (ArO quat), 189.24 (CHO) ppm. MS (EI) 817 (M⁺, base), 715, 636, 514 m/z. HRMS calcd for C₅₄H₇₂O₆: 816.5329 g/mol. Found: 816.5320 g/mol.



3-(4-(4-(2,5-bis(hexyloxy)-4-(4-methoxyphenyl)styryl)-styryl)-2,5-bis(hexyloxy)phenyl)-1-(4-nitrophenyl)-2-propen-1-one (OPV2d). *p*-Nitroacetophenone (40 mg, 242 μ mol), OPV2c (50 mg, 61.2 μ mol), and TsOH (10 mg, 52.6 μ mol) were dissolved in benzene (10 mL) and refluxed in a Dean-Stark apparatus for 24 h. The deep red solution was concentrated *in vacuo* and the residue was purified by silica gel chromatography (1:1 hexanes:DCM) to give the title compound

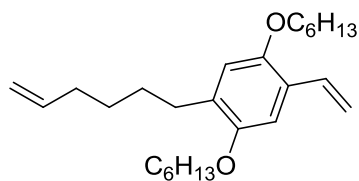
as a red amorphous solid (56.6 mg, 96%). λ_{\max} 456 nm. $^1\text{H NMR}$ (CD_2Cl_2 , 400 MHz) δ 0.85-1.00 (12H, mult, CH_3), 1.30-1.50 (18H, mult), 1.50-1.60 (6H, mult), 1.73 (2H, pent, $J=6.8$ Hz), 1.80-1.95 (6H, mult), 3.85 (3H, s OCH_3), 3.97 (2H, t, $J=6.4$ Hz, OCH_2), 4.04 (2H, t, $J=6.4$ Hz, OCH_2), 4.07 (2H, t, $J=6.4$ Hz, OCH_2), 4.13 (2H, t, $J=6.4$ Hz, OCH_2), 6.91 (1H, s), 6.95 (2H, d, $J=8.4$ Hz, $p\text{-C}_6\text{H}_4$), 7.16-7.22 (mult, 4H), 7.28 (1H, d, $J=16.8$ Hz, *trans* $\text{CH}=\text{CH}$), 7.52-7.57 (8H, mult), 7.67 (1H, d, $J=15.6$ Hz, *trans* $\text{CH}=\text{CH}$), 8.05 (1H, d, $J=16.0$ Hz, *trans* $\text{CH}=\text{CH}$), 8.13 (2H, d, $J=8.8$ Hz, $p\text{-C}_6\text{H}_4$), 8.33 (2H, d, $J=8.8$ Hz, $p\text{-C}_6\text{H}_4$) ppm. $^{13}\text{C NMR}$ (CD_2Cl_2 , 100 MHz) δ 14.38 (CH_3), 14.41 (CH_3), 23.19 (CH_2), 23.24 (CH_2), 26.37 (CH_2), 26.51 (CH_2), 26.54 (CH_2), 29.94 (CH_2), 29.95 (CH_2), 29.98 (CH_2), 30.05 (CH_2), 30.26 (CH_2), 32.09 (CH_2), 32.21 (CH_2), 55.87 (OCH_3), 69.75 (OCH_2), 69.91 (OCH_2), 70.09 (OCH_2), 70.13 (OCH_2), 110.32 (CH), 111.37 (CH), 113.85 (CH), 114.14 (CH), 115.84 (CH), 122.40 (CH), 123.02 (CH), 123.64 (quat), 124.07 (CH), 124.24 (CH), 126.09 (quat), 127.34 (CH), 127.62 (CH), 128.47 (CH), 129.87 (CH), 130.98 (CH), 131.09 (CH), 131.30 (quat), 131.49 (quat), 131.49 (quat), 137.15 (quat), 138.39 (quat), 142.52 (CH), 144.27 (quat), 150.42 (ArO quat), 150.78 (ArO quat), 151.30 (ArO quat), 151.69 (ArO quat), 154.01 (ArNO₂ quat), 159.39 (ArO quat), 189.92 (C=O, quat) ppm. HRMS calcd for $\text{C}_{62}\text{H}_{77}\text{NO}_8+\text{Na}$: 986.5547 g/mol. Found: 986.5554 g/mol.



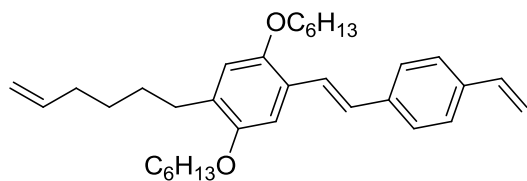
4-(4-(2,5-bis(hexyloxy)-4-(hex-5-enyl)styryl)-styryl)-2,5-bis(hexyloxy)styrene (OPV2e). In a nitrogen filled glovebox, **OPV2b** (250 mg, 299 μmol), 9-(hex-5-en-1-yl)-9-BBN (183 mg, 896 μmol), $\text{PdCl}_2(\text{PPh}_3)_2$ (15 mg, 21 μmol), and TBAB (7.5 mg, 23 μmol), were dissolved in PhMe

(5 mL) in a Schlenk flask. The flask was removed from the glove box, and charged with 2.0 M aq K₂CO₃ (5 mL) that had been sparged with N₂ for 10 minutes. The mixture was stirred at 45 °C under N₂ for 20 h. After cooling, the layers were separated, and the aqueous layer was extracted thrice with EtOAc. The combined organic layers were dried over MgSO₄ and reduced *in vacuo*. The residue was purified via silica gel chromatography (49:1 hexanes:ethyl acetate) to give the title compound as an amorphous yellow solid (158.8 mg, 67%). λ_{max} 397 nm. ¹H NMR (CDCl₃, 400 MHz) δ 0.95-1.05 (12H, mult), 1.35-1.50 (18H, mult), 1.50-1.70 (14H, mult), 1.80-1.95 (8H, mult), 2.16 (2H, q, $J = 7.2$ Hz, CH₂CH=CH₂), 2.68 (2H, t, $J = 7.6$ Hz, ArCH₂), 4.00-4.10 (8H, mult, OCH₂), 5.01 (1H, dd, $J = 10.0, 2.0$ Hz, CH₂CH=CH₂), 5.07 (1H, dd, $J = 17.2, 2.0$ Hz, CH₂CH=CH₂), 5.32 (1H, dd, $J = 11.2, 1.2$ Hz, ArCH=CH₂), 5.81 (1H, dd, $J = 17.6, 1.2$ Hz, ArCH=CH₂), 5.89 (1H, ddt, $J = 17.2, 10.0, 7.2$ Hz, CH₂CH=CH₂), 6.77 (1H, s), 7.08 (1H, s), 7.12 (1H, s), 7.13 (1H, dd, $J = 17.6, 11.2$ Hz, ArCH=CH₂), 7.16 (1H, d, $J = 16.4$ Hz, *trans* CH=CH), 7.16 (1H, s), 7.18 (1H, d, $J = 17.2$ Hz, *trans* CH=CH), 7.55 (1H, d, $J = 17.2$ Hz, *trans* CH=CH), 7.56 (1H, d, $J = 16.4$ Hz, *trans* CH=CH) 7.57 (4H, br s, *p*-C₆H₄) ppm. ¹³C NMR (CDCl₃, 100 MHz) δ 14.02 (CH₃), 22.60 (CH₂), 22.63 (CH₂), 25.83 (CH₂), 25.93 (CH₂), 28.81 (CH₂), 29.42 (CH₂), 29.43 (CH₂), 29.50 (CH₂), 29.61 (CH₂), 30.36 (CH₂), 31.58 (CH₂), 31.61 (CH₂), 33.68 (CH₂), 68.57 (OCH₂), 69.26 (OCH₂), 69.46 (OCH₂), 69.65 (OCH₂), 109.08 (CH), 110.21 (CH), 110.64 (CH), 113.87 (CH₂), 114.20 (CH₂), 115.29 (CH₂), 123.01 (CH₂), 123.59 (CH₂), 124.53 (quat), 126.62 (CH), 126.72 (CH), 126.91 (quat), 127.04 (quat), 127.35 (CH), 128.39 (CH), 131.59 (CH), 132.29 (quat), 136.83 (quat), 137.35 (quat), 138.98 (CH), 150.57 (ArO quat), 150.77 (ArO quat), 150.90 (ArO, quat), 151.22 (ArO, quat) ppm. HRMS calcd for C₅₄H₇₈O₄+K: 829.5537 g/mol. Found 829.5574 g/mol.

Poly(OPV2e). OPV2e (150 mg, 0.189 mmol) and Grubbs II catalyst (3.0 mg, 3.5 μ mol) were refluxed in CHCl_3 (10 mL) under N_2 . After 24 h, the solvent was removed *in vacuo* and a ^1H NMR was taken of the reaction mixture. Another portion of Grubbs II catalyst was added (3.0 mg, 3.5 μ mol) along with more CHCl_3 (10 mL). The reaction was monitored in the same way after 48 h and 96 h. After 96 h, the reaction mixture was quenched with ethyl vinyl ether (1 mL) and precipitated into methanol. The resulting polymer was an orange tacky material (139.0 mg, 96%). $\lambda_{\text{max}} = 399$ nm. Molecular weight determination by SEC: $M_n = 4.47$ kDa, $M_w = 13.1$ kDa, PDI = 2.93. ^1H NMR (400 MHz, CD_2Cl_2) δ 0.80-1.00 (17H, mult), 1.20-1.60 (37.5H, mult), 1.80-2.00 (8H, mult), 2.20-2.35 (0.9H, mult), 2.35-2.50 (0.4H, mult), 2.60-2.75 (1.3H, mult), 3.90-4.20 (8H, mult), 5.27 (0.06H, d, $J = 12.8$ Hz), 5.40-5.70 (0.53H, mult), 5.78 (0.06H, d, $J = 17.2$ Hz), 6.20-6.50 (0.6H, mult), 6.60-6.85 (1.6H, mult), 6.90-7.30 (4.7H, mult), 7.40-7.80 (5.6H, mult) ppm. ^{13}C NMR (100 MHz, CD_2Cl_2) δ 14.45, 23.28, 26.38, 26.49, 26.52, 26.58, 29.85, 29.98, 30.13, 30.30, 32.18, 32.25, 32.28, 32.55, 61.18, 63.66, 64.59, 65.68, 69.21, 69.31, 69.84, 69.91, 69.95, 70.04, 70.09, 70.16, 70.19, 70.22, 70.24, 109.58, 109.66, 109.67, 110.56, 110.87, 110.92, 111.08, 111.19, 112.12, 114.41, 115.82, 115.85, 115.91, 123.94, 123.96, 124.05, 124.10, 124.15, 124.88, 124.91, 124.95, 125.19, 126.43, 126.43, 126.45, 126.47, 126.56, 126.59, 127.03, 127.23, 127.27, 127.35, 127.78, 127.81, 127.92, 128.04, 128.06, 128.36, 128.39, 128.79, 128.82, 128.94, 129.03, 129.10, 129.25, 129.96, 130.20, 130.23, 130.30, 130.33, 130.58, 130.64, 131.80, 132.11, 132.34, 132.38, 133.07, 134.80, 136.79, 137.59, 137.92, 138.02, 138.57, 150.98, 151.01, 151.27, 151.36, 151.32, 151.69, 151.72, 151.76, 151.92, 151.96, 156.83, 189.23, 192.21 ppm.

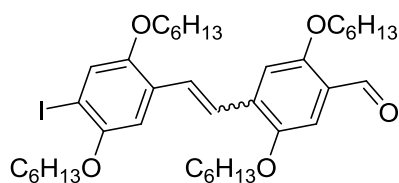


2,5-bis(hexyloxy)-4-(hex-5-enyl)styrene (17, bnnvii3a). In a nitrogen filled glovebox, **3** (86.8 mg, 202 μmol), 9-(hex-5-en-1-yl)-9-BBN (123 mg, 603 μmol), $\text{PdCl}_2(\text{PPh}_3)_2$ (10 mg, 14 μmol), and TBAB (5 mg, 14 μmol), were dissolved in PhMe (5 mL) in a Schlenk flask. The flask was removed from the glove box, and charged with 2.0 M aq K_2CO_3 (5 mL) that had been sparged with N_2 for 10 minutes. The mixture was stirred at 45 $^\circ\text{C}$ under N_2 for 24 h. After cooling, the layers were separated, and the aqueous layer was extracted thrice with EtOAc. The combined organic layers were dried over MgSO_4 and reduced *in vacuo*. The residue was purified via silica gel chromatography (19:1 hexanes:ethyl acetate) to give the title compound as a pale yellow oil (77.3 mg, 99%). ^1H NMR (CDCl_3 , 300 MHz) δ 0.85-1.00 (6H, mult), 1.25-1.70 (16H, mult), 1.80-1.95 (4H, mult), 2.12 (2H, q, $J = 7.2$ Hz, $\text{CH}_2\text{CH}=\text{CH}_2$), 2.62 (2H, t, $J = 7.5$ Hz, Ar CH_2), 3.95 (2H, t, $J = 6.3$ Hz O CH_2), 3.96 (2H, t, $J = 6.4$ Hz O CH_2), 4.96 (1H, d, $J = 10.2$ Hz, $\text{CH}_2\text{CH}=\text{CH}_2$), 5.02 (1H, d, $J = 17.1$ Hz, $\text{CH}_2\text{CH}=\text{CH}_2$), 5.22 (1H, d, $J = 12.0$ Hz, Ar $\text{CH}=\text{CH}_2$), 5.70 (1H, d, $J = 17.7$ Hz, Ar $\text{CH}=\text{CH}_2$), 5.85 (1H, ddt, $J = 17.1$ 10.2, 7.2 Hz, $\text{CH}_2\text{CH}=\text{CH}_2$), 6.70 (1H, s), 6.97 (1H, s), 7.06 (1H, dd, $J = 17.7$, 12.0 Hz, Ar $\text{CH}=\text{CH}_2$), ppm. ^{13}C NMR (CDCl_3 , 75 MHz) δ 14.02 (CH_3), 22.60 (CH_2), 22.63 (CH_2), 25.82 (CH_2), 25.88 (CH_2), 29.48 (CH_2), 29.64 (CH_2), 30.30 (CH_2), 31.57 (CH_2), 31.60 (CH_2), 33.68 (CH_2), 68.58 (O CH_2), 69.46 (CH_2), 109.26 (Ar CH), 112.90 (vinyl CH_2), 114.20 (vinyl CH_2), 115.09 (vinyl CH), 124.72 (Ar quat), 131.75 (Ar CH), 132.29 (Ar quat), 139.02 (vinyl CH), 150.21 (ArO quat), 151.07 (ArO quat) ppm.

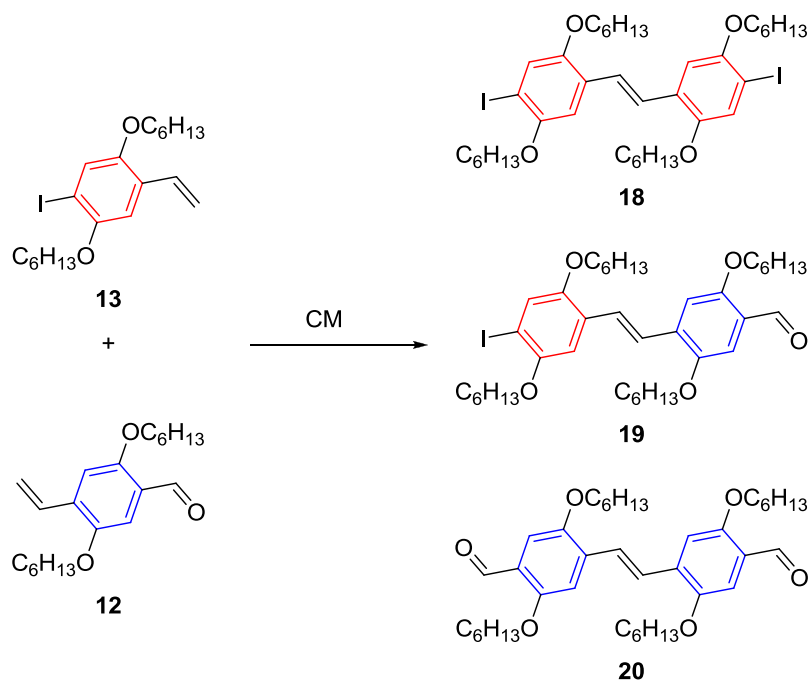


4-(2,5-bis(hexyloxy)-4-(hex-5-enyl)styryl)-styrene (OPV1c, bnnvii16a). In a nitrogen filled glovebox, **OPV1b** (425 mg, 795 μmol), 9-(hex-5-en-1-yl)-9-BBN (550 mg, 2.69 mmol), $\text{PdCl}_2(\text{PPh}_3)_2$ (50 mg, 71 μmol), and TBAB (25 mg, 77 μmol), were dissolved in PhMe (25 mL) in a Schlenk flask. The flask was removed from the glove box, and charged with 2.0 M aq K_2CO_3 (25 mL) that had been sparged with N_2 for 10 minutes. The mixture was stirred at 45 $^\circ\text{C}$ under N_2 for 20 h. After cooling, the layers were separated, and the aqueous layer was extracted thrice with EtOAc. The combined organic layers were dried over MgSO_4 and reduced *in vacuo*. The residue was purified via silica gel chromatography (9:1 hexanes: CH_2Cl_2) to give the title compound as an amorphous yellow solid (308 mg, 88%). $^1\text{H NMR}$ (CDCl_3 , 400 MHz) δ 0.95

3.4.5 Progress toward more complex sequences

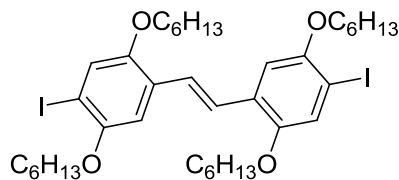


Optimized Type II + Type II cross metathesis (iv70 or iv68). **12** (166 mg, 0.499 mmol) and Grubbs II (6.4 mg, 7.54 μmol) were dissolved in PhMe (2 mL) and heated to 90 $^\circ\text{C}$ under N_2 with stirring. **13** (167 mg, 0.248 mmol) in PhMe (1 mL) was added over 2 h by syringe pump. After 24 h, the solvent was removed *in vacuo* and the residue purified by column chromatography (silica gel, 3:2 hexanes: DCM) to give the CM product as 106 mg of an amorphous yellow solid (69%) that is 2:1 *E:Z* by $^1\text{H NMR}$.

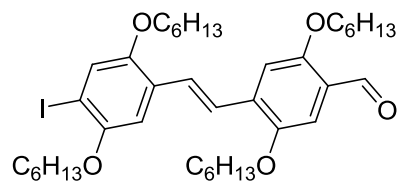


Following Type II + Type II cross-metathesis by NMR (iv90). **12** (83 mg, 0.250 mmol), **13** (53 mg, 0.123 mmol), and Grubbs II (6.4 mg, 7.5 μ mol) were dissolved in CDCl_3 (1 mL). DMF (20 μ L, 0.259 mmol) was added as an internal standard. The mixture was transferred to an NMR tube sealed with a J Young valve and heated at 75 $^\circ\text{C}$. Within 10 minutes, the solution changed color from purple to green, signaling the initial reaction of styrene **12** or **13** with Grubbs II, and ethylene bubbles were observed. ^1H NMR spectra were taken at 30 min, 3 h, 5 h, 21 h, and 45 h.

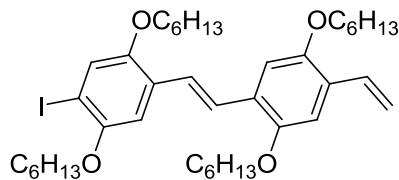
3.4.6 Synthesis of OPVs by dimerization



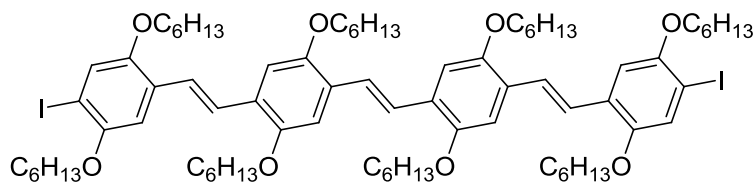
2,2',5,5'-tetrakis(hexyloxy)-4,4'-diiodo-E-stilbene (18, iv36a). **13** (21.0 g, 48.8 mmol) and Grubbs II (0.10 g, 0.12 mmol), were refluxed in PhMe (100 mL) for 4 d. Small amounts of additional Grubbs II (ca. 5 mg) were added after each day of reflux. The solvent was removed *in vacuo*, and the crude product was purified by column chromatography (silica gel, 4:1 DCM:hexanes) to give the title compound as a pale yellow solid (17.8 g, 88%). Alternatively, *N,N*-bis(mesityl)imidazolium chloride (170 mg, 0.50 mmol) was added to a Schlenk flask under N₂ with PhMe (5 mL). Potassium pentoxide (1.7 M in PhMe, 0.3 mL, 0.51 mmol) was added and the mixture was stirred at rt for 1 h. Grubbs I (380 mg, 0.46 mmol) was added and the mixture was stirred at rt for 1.5 h. **13** (20.0 g, 46.4 mmol) was added with more PhMe (100 mL) and the mixture was refluxed for 48 h. The solvent was removed *in vacuo*, and the crude product was purified by column chromatography (silica gel, 4:1 DCM:hexanes) to give the title compound as a pale yellow solid (13.4 g, 72%). ¹H NMR (CD₂Cl₂, 300 MHz) δ 0.80-0.90 (12H, mult), 1.35-1.45 (16H, mult), 1.45-1.60 (8H, mult), 1.83 (8H, pent, *J* = 6.9 Hz), 3.96 (4H, t, *J* = 6.3 Hz), 4.02 (4H, t, *J* = 6.3 Hz), 7.06 (2H, s), 7.32 (2H, s), 7.42 (2H, s) ppm. ¹³C NMR (CD₂Cl₂, 74 MHz) δ 14.22 (CH₃), 23.02 (CH₂), 23.04 (CH₂), 26.20 (CH₂), 26.22 (CH₂), 29.70 (CH₂), 31.94 (CH₂), 31.99 (CH₂), 70.04 (OCH₂), 70.55 (OCH₂), 85.97 (ArI quat), 110.33 (Ar CH), 124.07 (Ar CH), 124.24 (vinylene CH), 128.24 (Ar quat), 151.78 (ArO quat), 152.68 (ArO quat) ppm.



4-(2,5-bis(hexyloxy)-4-iodostyryl)-2,5-bis(hexyloxy)benzaldehyde (19, iv49a). **18** (1.0 g, 1.2 mmol) was dissolved in THF (30 mL) and cooled to $-40\text{ }^{\circ}\text{C}$ under N_2 . $n\text{-BuLi}$ (1.6 M in hexanes, 0.75 mL, 1.2 mmol) was added and the mixture was stirred at $-40\text{ }^{\circ}\text{C}$ for 1 h. DMF (0.15 mL) was added and the reaction mixture was stirred at rt for 1 h. The reaction mixture was poured into a mixture of 50 mL ice and 50 mL brine. The organic layer was dried over MgSO_4 , and the solvent was removed *in vacuo*. The crude product was purified by column chromatography (silica gel, 1:1 DCM:hexanes) to give the title compound as a yellow solid (518 mg, 59%). ^1H NMR (CD_2Cl_2 , 300 MHz) δ 0.80-0.90 (12H, mult), 1.35-1.45 (16H, mult), 1.45-1.60 (8H, mult), 1.83 (8H, pent, $J = 6.9$ Hz), 3.98 (2H, t, $J = 6.3$ Hz), 4.02 (2H, t, $J = 6.3$ Hz), 4.04 (2H, t, $J = 6.3$ Hz), 4.12 (2H, t, $J = 6.3$ Hz), 7.07 (1H, s), 7.23 (1H, s), 7.31 (1H, s), 7.33 (1H, s), 7.53 (2H, br s), 10.44 (1H, s, CHO) ppm. ^{13}C NMR (CD_2Cl_2 , 74 MHz) δ 14.21 (CH_3), 23.00 (CH_2), 23.02 (CH_2), 23.05 (CH_2), 26.17 (CH_2), 26.20 (CH_2), 26.23 (CH_2), 26.25 (CH_2), 29.64 (CH_2), 29.69 (CH_2), 31.94 (CH_2), 31.96 (CH_2), 32.00 (CH_2), 69.56 (OCH_2), 69.67 (OCH_2), 70.05 (OCH_2), 70.58 (OCH_2), 86.92 (ArI quat), 110.33 (Ar CH), 110.51 (Ar CH), 111.08 (Ar CH), 123.98 (Ar CH), 124.13 (vinylene CH), 124.76 (Ar quat) 126.06 (vinylene CH), 127.79 (Ar quat), 134.85 (Ar quat), 151.16 (ArO quat), 152.01 (ArO quat), 152.70 (ArO quat), 156.59 (ArO quat), 189.07 (CHO) ppm.



4-(2,5-bis(hexyloxy)-4-iodostyryl)-2,5-bis(hexyloxy)styrene (21, iv50a). KO^tBu (550 mg, 4.90 mmol) was added portionwise to a slurry of Ph₃PCH₃Br (1.85 g, 5.18 mmol) in THF (10 mL) under N₂ at 0 °C in a flame-dried Schlenk flask. The yellow mixture was stirred for 30 min at rt and then returned to 0 °C. **19** (1.50 g, 2.05 mmol) in THF (10 mL) was added dropwise, and the mixture was stirred at rt overnight. The reaction was quenched into saturated aqueous NH₄Cl (20 mL). The aqueous layer was extracted twice with EtOAc (20 mL). The combined organic layers were washed with brine (20 mL), and dried over MgSO₄. The solvent was removed *in vacuo*, and the residue was purified by column chromatography (silica gel, 9:1 hexanes:DCM) to give the title compound as a yellow solid (1.50 g, 100%). ¹H NMR (CD₂Cl₂, 300 MHz) δ 0.80-0.90 (12H, mult), 1.35-1.45 (16H, mult), 1.45-1.60 (8H, mult), 1.83 (8H, pent, *J* = 6.9 Hz), 3.97 (2H, t, *J* = 6.3 Hz), 4.00-4.10 (6H, mult), 7.07 (1H, s), 5.26 (1H, dd, *J* = 12.6, 1.5 Hz), 5.77 (1H, dd, *J* = 17.7, 1.5 Hz), 7.04 (1H, s), 7.07 (1H, dd, *J* = 17.7, 12.6 Hz), 7.08 (1H, s), 7.12 (1H, s), 7.31 (1H, s), 7.40 (1H, d, *J* = 16.5 Hz), 7.50 (1H, d, *J* = 16.5 Hz) ppm.



4,4'-bis(4-(2,5-bis(hexyloxy)-4-iodostyryl))-2,2',5,5'-tetrakis(hexyloxy)stilbene (OPV3, iv55a). **21** (1.00 g, 1.36 mmol) and Grubbs II (12 mg, 13.6 μmol) were refluxed in PhMe (5 mL) for 24 h. The hot reaction mixture was precipitated into MeOH (50 mL). The product was

isolated by filtration to give the title compound as a red solid (654 mg, 67%). NMR spectra were not collected due to low solubility.

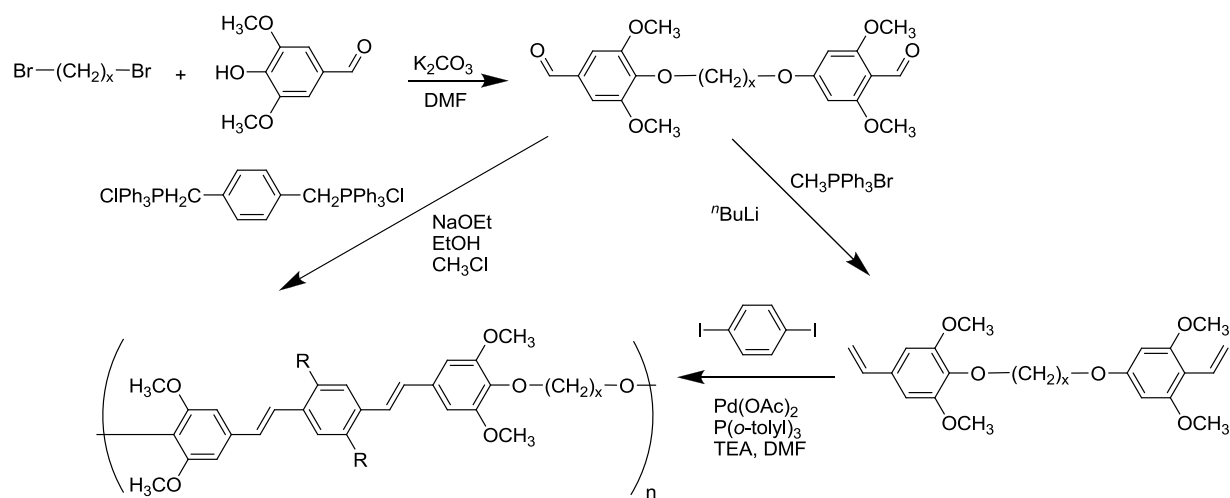
4.0 SYNTHESIS AND CHARACTERIZATION OF MISCELLANEOUS ROD-COIL POLY(PHENYLENE-VINYLENE) REPEAT-SEQUENCE COPOLYMERS

4.1 INTRODUCTION

We explored the preparation of well-defined, segmented, rod-coil copolymers containing phenylene-vinylene segments separated by nonconjugated flexible linker segments in which all segments were of precisely controlled length. We desired to probe the effects of sequence on the optical and thermal properties of these copolymers by systematically varying the lengths of the conjugated and nonconjugated segments as well as varying the composition of the nonconjugated segments. We intended this work to serve as a complement to our analogous studies on fluorene-containing rod-coil copolymers.³³

Well-defined rod-coil copolymers containing phenylene-vinylene segments have been previously reported. The introduction of a nonconjugated flexible spacer into the backbone of phenylene-vinylene has many benefits:⁹⁹ increasing solubility, modulating physical properties, and isolating the chromophore to control optical properties. Karasz and coworkers have prepared many copolymers of this type by Heck¹⁰⁰ or Wittig¹⁰¹ polymerizations in which the phenylene-vinylene chromophore was assembled in the polymerization (Scheme 24). They reported that the optical properties of their polymers did not significantly change with the length of the linker^{100, 101} or if an *oligo*(ethylene oxide) linker was used instead of an alkyl linker.¹⁰² However, these

studies do not represent systematic treatment of sequence effects, especially on the thermal properties of the copolymers.



Scheme 24. Synthesis of rod-coil phenylene-vinylene copolymers from refs 100 and 101.

Our initial goal was to study the effect of chromophore length on the optical and thermal properties of phenylene-vinylene rod-coil copolymers. We prepared six copolymers containing trimeric phenylene-vinylene cores with varying linker lengths, but we were unable to prepare polymers containing longer phenylene-vinylene units. Our approach to these materials was to synthesize and polymerize a segment containing the intact phenylene-vinylene chromophore and the precursors to the flexible linkers. This approach is in contrast to the more common method of assembling the chromophore in the polymerization. This convergent approach would allow us easy access to chromophores of different lengths, while avoiding the potential of imperfect chromophores in our polymers. We chose to use HWE reactions between bisphosphonate cores and aldehyde arms terminated in long chain aliphatic ω -olefins to assemble the segments (Figure 26). These segments could then be polymerized using a tandem ADMET/hydrogenation process developed by Wagener and coworkers.^{29, 103}

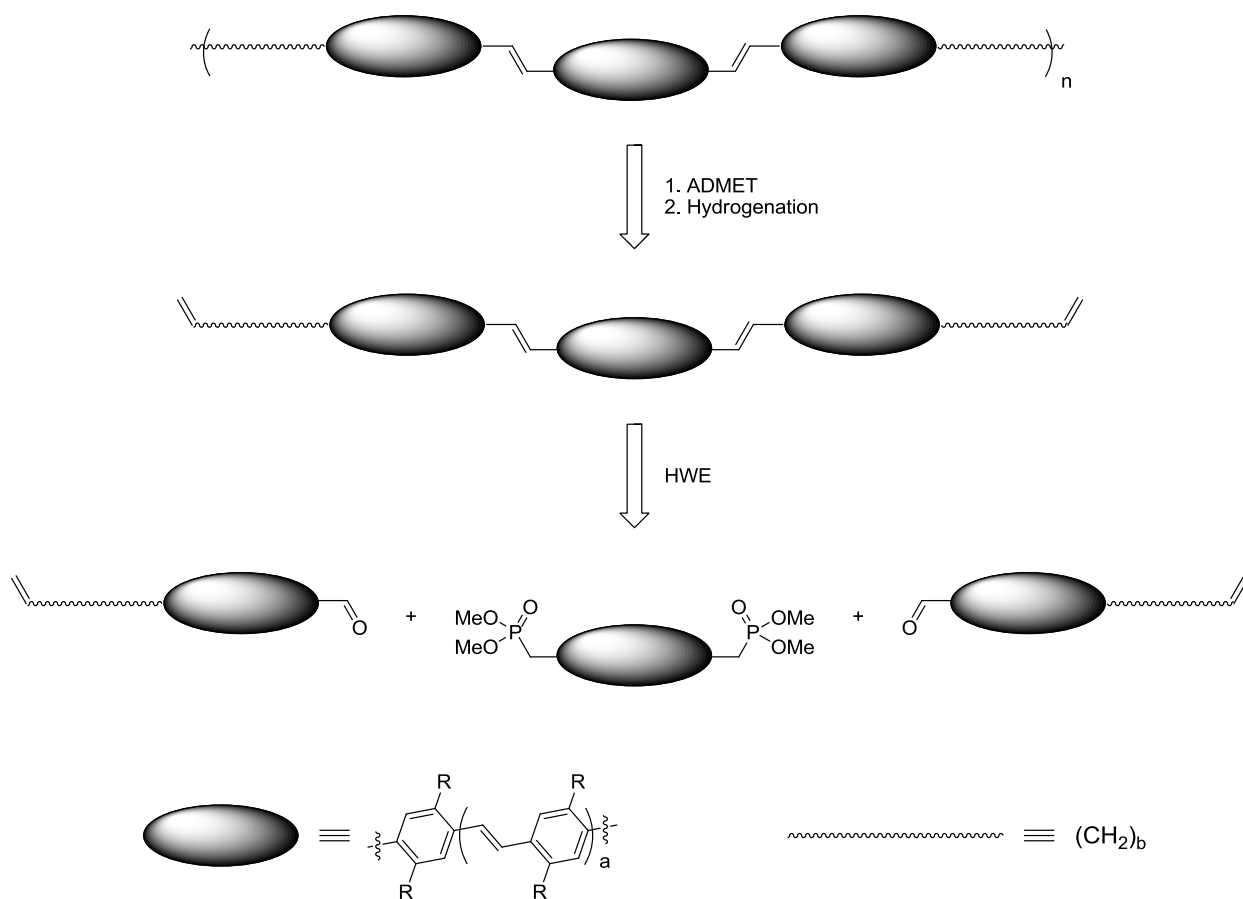
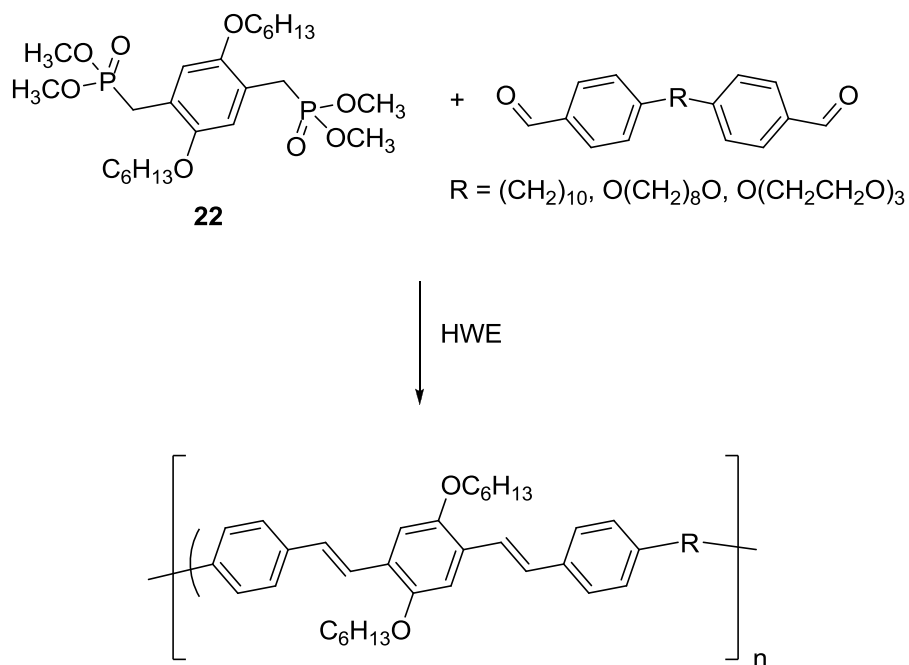


Figure 26. Schematic representation of the ADMET preparation of rod-coil phenylene-vinylene copolymers.

We were also interested in assessing the effects of linker composition on the thermal properties of phenylene-vinylene containing rod-coil copolymers. To investigate the effects of oxygen content and placement in the linker on the thermal properties of the polymer, we inverted our synthesis, assembling the linker first, followed by formation of the chromophore during a condensation polymerization (Scheme 25). We chose three linkers: decimethylene, $(\text{CH}_2)_{10}$, 1,8-octanedioxy, $\text{O}(\text{CH}_2)_8\text{O}$, and triethylene glycoxy, $\text{O}(\text{CH}_2\text{CH}_2\text{O})_3$. Since these three linkers have the same number of backbone atoms (10), the only variable is the number and placement of the oxygen atoms. Additionally, the HWE polymerization provided higher MW polymers while being more robust and operationally simpler than the ADMET polymerization. This approach also allowed us to prepare polymers containing mixtures of linkers in different ratios to further

probe the effects of linker composition on the properties of the polymers. This investigation is still in its preliminary stages.



Scheme 25 HWE preparation of rod-coil phenylene-vinylene copolymers.

4.2 RESULTS AND DISCUSSION

4.2.1 Rod-coil copolymers prepared by ADMET

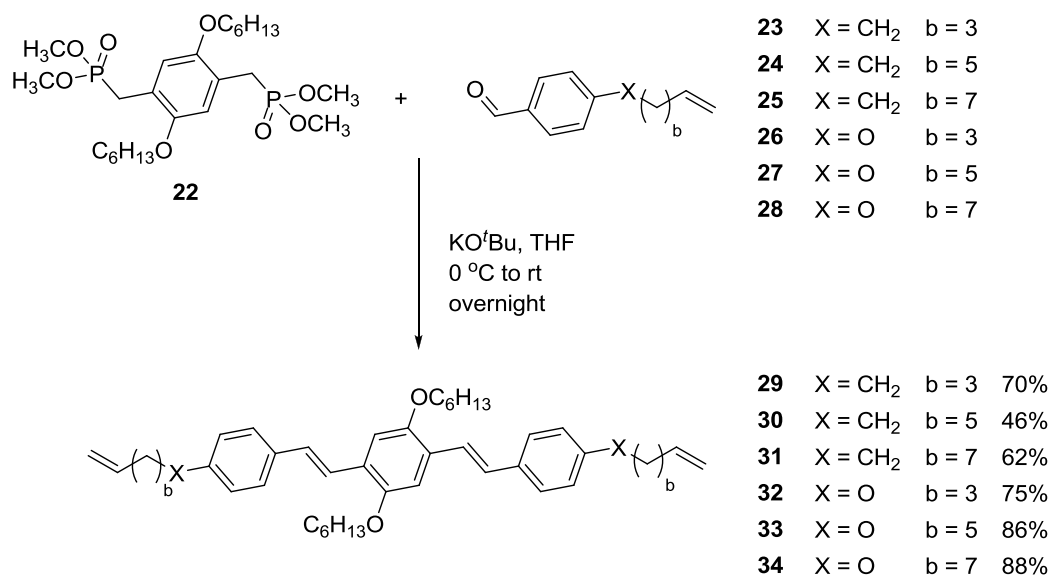
Six segmers were assembled by HWE reactions in moderate to good yields. The segmers were polymerized by an ADMET polymerization with Grubbs I in good to quantitative yields. The polymers displayed modest number average molecular weights (M_n s) of 13-30 kDa and low polydispersity indices (PDIs) of 1.66-2.05, as determined by size exclusion chromatography (SEC) to relative to polystyrene standards. The tandem ADMET/hydrogenation procedure was

complex and required long reaction times, but we were unable to find replacement hydrogenation conditions that did not also result in partial reduction of the vinylene groups in the chromophore.

We investigated thermal and optical properties of the two copolymers that retained the greatest chromophore fidelity after hydrogenation. The melting transition temperatures (T_m s) varied significantly with linker content. The polymer with oxygen atoms in the linker exhibited a significantly higher T_m than the polymer with a linker containing only methylenes. The optical properties of the polymers were identical to those of the segmer precursors and did not vary significantly based on the linker composition.

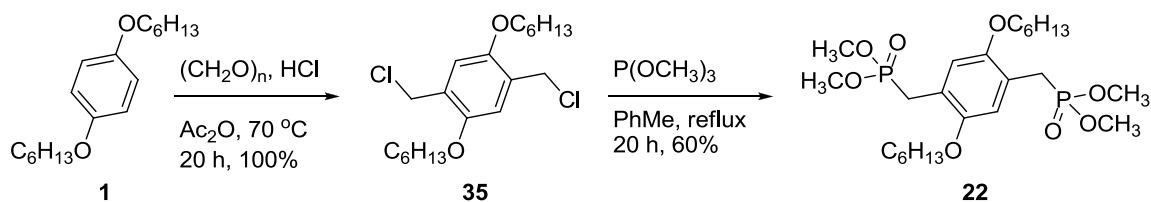
4.2.1.1 Segmer synthesis

We have prepared six segmers based around a trimeric OPV core by the HWE reaction of bisphosphonate **22** and six different benzaldehydes, **23** – **28** (Scheme 26). The reactions proceeded in moderate to good yields. The segmers contained small *cis* impurities by ^1H NMR. These six segmers (**29** – **34**) contain the precursors for six different linkers: decimethylene, $(\text{CH}_2)_{10}$ (**29**), tetradecimethylene, $(\text{CH}_2)_{14}$ (**30**), octadecimethylene, $(\text{CH}_2)_{18}$ (**31**), 1,8-octanedioxy, $\text{O}(\text{CH}_2)_8\text{O}$ (**32**), 1,12-dodecanedioxy, $\text{O}(\text{CH}_2)_{12}\text{O}$ (**33**), and 1,16-hexadecanedioxy, $\text{O}(\text{CH}_2)_{16}\text{O}$ (**34**). Attempts to prepare pentameric segmers were unsuccessful due to the low solubility of the pentamers inhibiting isolation and purification.



Scheme 26. Synthesis of ADMET segmers

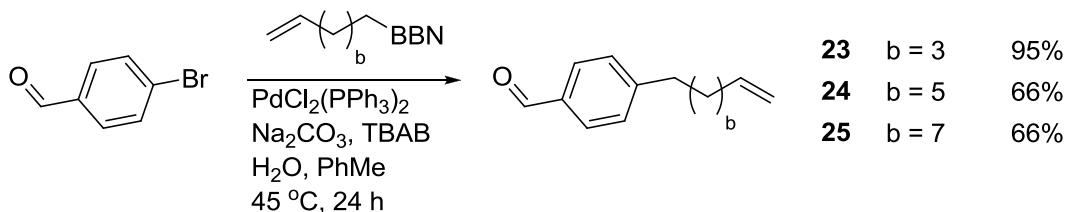
The syntheses of all segmers require bisphosphonate **22**, which was prepared from hydroquinone ether **1** in 60% yield over 2 steps (Scheme 27). Ether **1** was chloromethylated with concentrated HCl and paraformaldehyde in acetic anhydride in quantitative yield. The chloromethyl compound **35** was converted into the bisphosphonate via an Arbusov reaction with P(OMe)₃ in refluxing toluene in 60% yield. These reactions were regularly performed on 25+ g scales.



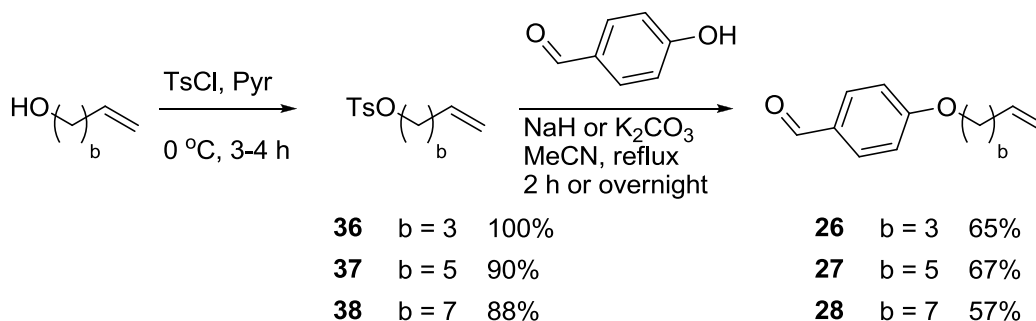
Scheme 27. Synthesis of bisphosphonate **22**.

The aldehyde components were prepared in one or two steps using conventional chemistry. Three of the benzaldehydes (**23**, **24**, and **25**) were prepared from 4-bromobenzaldehyde by Suzuki reactions with 9-(alk- ω -enyl)-9-borabicyclonanes (Scheme 28). Yields were typically around 65-70%, although we were able to optimize the yield of **23**. The

other three benzaldehydes (**26**, **27**, and **28**) were prepared from 4-hydroxybenzaldehyde and the tosylates of alk- ω -en-1-ols (Scheme 29). Conversion of the alcohols to tosylates proceeded in excellent yields, and the alkylations of 4-hydroxybenzaldehyde proceeded in moderate yields.



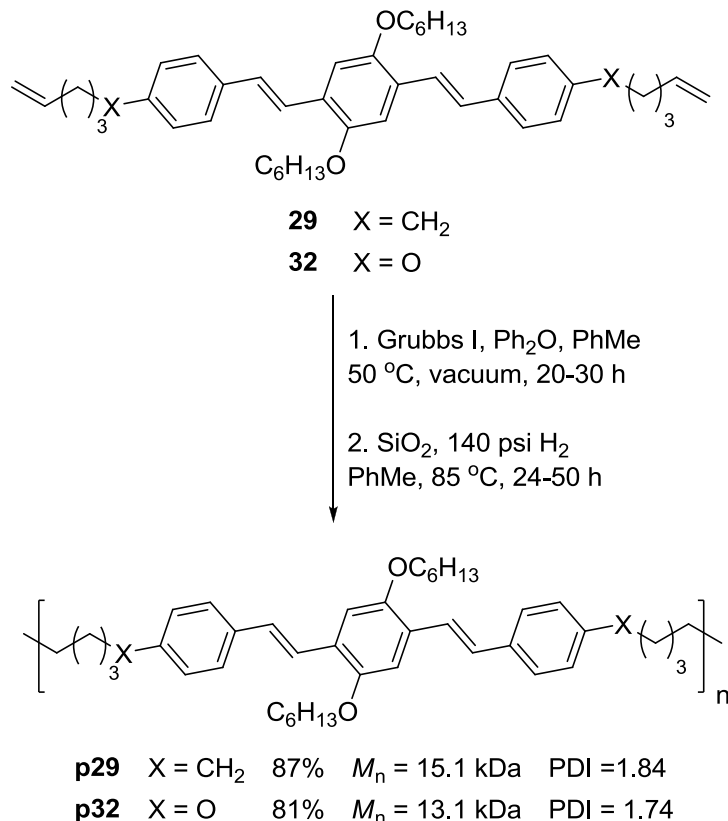
Scheme 28. Synthesis of aldehydes **23**, **24**, and **25**.



Scheme 29. Synthesis of aldehydes **26**, **27**, and **28**.

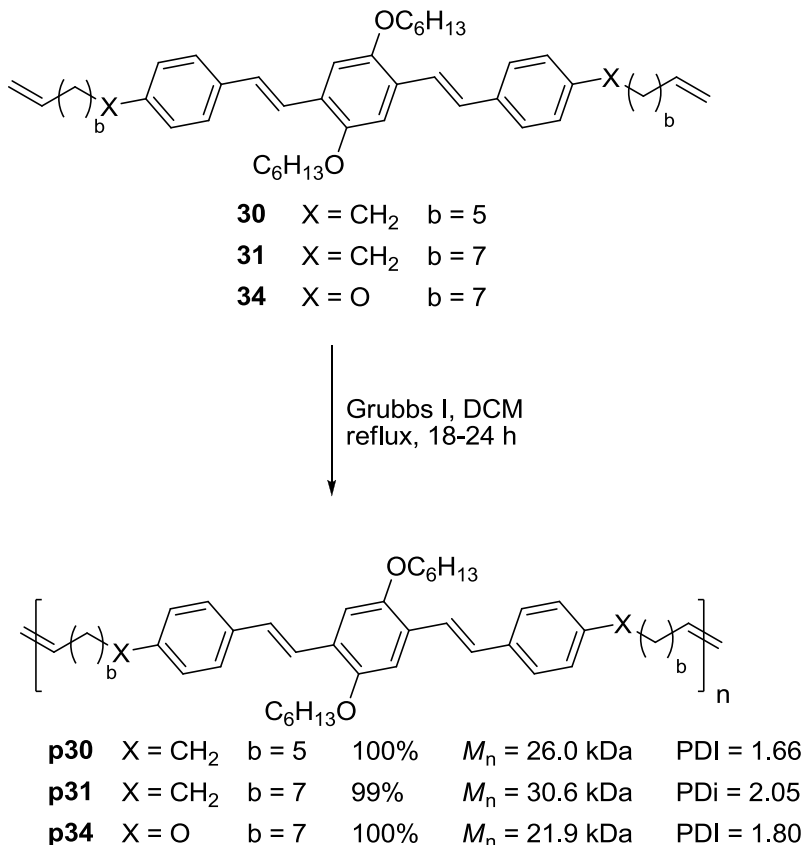
4.2.1.2 ADMET polymerization and hydrogenation

We polymerized two segmers, **29** and **32**, using the tandem ADMET/hydrogenation procedure. Segmers **29** and **32** were polymerized in PhMe/Ph₂O under vacuum at 50 °C (Scheme 30). The resulting polymers were hydrogenated immediately using residual Grubbs I catalyst in PhMe under 140 psi H₂ at 80 °C, with SiO₂ added as a solid support. Long hydrogenation times, 24-48 hours, were required to fully reduce the aliphatic olefin. After precipitation, the polymers were isolated in good yields. The polymers displayed modest *M_ns* (13-15 kDa) with low PDIs (1.7-1.8).



Scheme 30. Synthesis of ADMET polymers **p29** and **p32**. M_n s and PDIs determined by SEC in THF relative to polystyrene standards.

Given the long hydrogenation times necessary in the tandem ADMET/hydrogenation methodology, we chose to isolate the remainder of our polymers after the ADMET step in the interest of investigating alternative methods of hydrogenation. Segmers **30**, **31**, and **34** were polymerized by Grubbs I in refluxing DCM (Scheme 31). ADMET polymerization in refluxing DCM proved an improvement over the PhMe/Ph₂O procedure. First, it was operationally simpler. Second, the ADMET polymers **p30**, **p31**, and **p34** were isolated in quantitative yield, with higher M_n s (22 – 30 kDa) and similar PDIs when compared to **p29** and **p32**.



Scheme 31. Synthesis of ADMET polymers **p30**, **p31**, and **p34**. *M_n*s and PDIs determined by SEC in THF relative to polystyrene standards.

We examined three alternative procedures to reduce the aliphatic olefins in the flexible segments of **p30**, **p31**, and **p34**. However, we were unable to prevent partial reduction of the vinylene olefins in the chromophore. Reduction of **p31** and **p34** by RuHCl(CO)(PCy₃)₂ and SiO₂, which mimics the hydrogenation conditions using residual Grubbs I, under 180 psi H₂ in PhMe at 80 °C was selective for the aliphatic olefin. However, by the time the aliphatic olefin was completely reduced (48 h), 25% of the vinylene olefins were also reduced. Reduction of **p34** by Pd/C under 1 atm of H₂ in THF was unselective. After 10 min, equal proportions of all olefins were reduced. Reduction of **p31** by Raney Ni under 1 atm of H₂ in THF was selective for the vinylene olefins in the chromophore. After 15 min, partial reduction of the vinylene olefins was observed with minimal aliphatic olefin reduction.

4.2.1.3 Thermal and optical properties of p29 and p32

We investigated the thermal and optical properties of **p29** and **p32**, the two copolymers with the greatest chromophore fidelity after hydrogenation. The oxygen atoms in the linker of **p32** dramatically increase the T_m of **p32** over that of **p29**. However, there is no significant difference in the optical properties of the two polymers. These two polymers represent an interesting subset of the ADMET polymers since they are identical except for two positions in their linkers. The chromophores in **p29** are linked by decimethylene groups, $-(CH_2)_{10}-$, while the chromophores in **p32** are linked by 1,8-octanedioxy groups, $-O(CH_2)_8O-$.

We report the surprising result that replacing two methylene units with oxygen atoms in the flexible linker of our rod-coil copolymers dramatically increases the T_m of the polymer. Both copolymers **p29** and **p30** exhibit two T_m s, but the transitions for **p32** are 60-70 °C higher than those of **p29** (Figure 27). Additionally, **p32** exhibits a crystallization transition on cooling, while **p29** does not. These differences in thermal properties cannot be attributed to molecular weight differences; both polymers have similar M_n s. The presence of the oxygen atoms must enhance the crystallinity of the polymer.

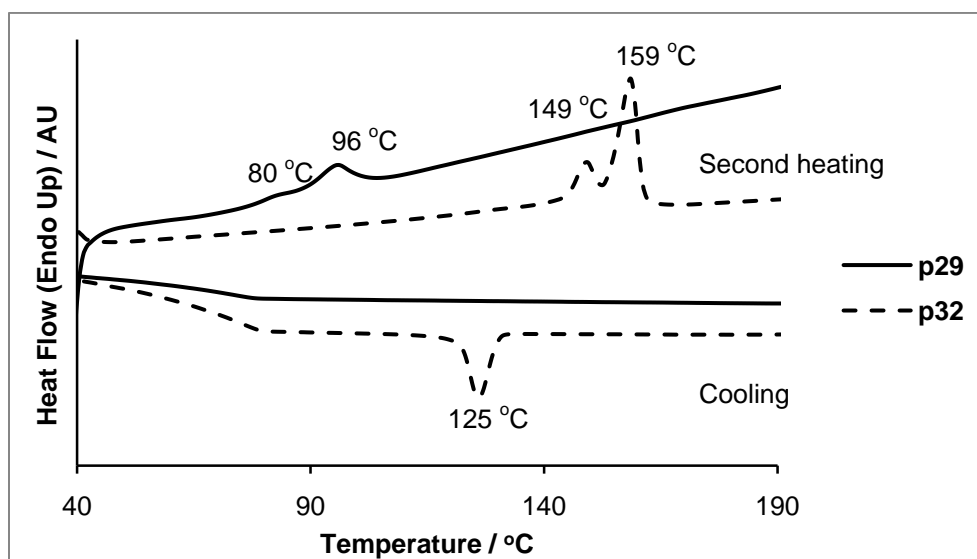


Figure 27. Differential scanning calorimograms of **p29** and **p32**.

The optical properties of the copolymers are not affected by the presence or absence of oxygen atoms in the linker. Copolymers **p29** and **p32** have nearly identical absorption maxima, emission maxima, and optical ΔE_g s (Table 14). The only difference is in molar absorptivity; the molar absorptivity of **p29** is nearly twice that of **p32**. The segment precursors, **29** and **32** also have nearly identical optical properties, including molar absorptivity.

Table 14. Optical properties of **29**, **p29**, **32**, and **p32**.^a

Compound	$\lambda_{\max}^{\text{abs}} / \text{nm}$	$\lambda_{\max}^{\text{em}} / \text{nm}$	$\epsilon^b / \text{M}^{-1} \text{cm}^{-1}$	$\Delta E_g^c / \text{eV}$
29	392	446, 468	59,500	2.79
p29	391	445, 469	78,400	2.79
32	395	446, 471	56,100	2.78
p32	393	447, 475	40,700	2.76

^a Obtained in DCM ($\sim 10^{-6}$ M); ^b Calculated at absorption maximum ^c HOMO-LUMO gap estimated as the onset of absorption.

The absorption and emission maxima and HOMO-LUMO gap do not change after polymerization, indicating the success of our methodology. By assembling the chromophore before the polymerization, we ensure that the polymer chains do not contain incomplete chromophores, which would detract from the optical properties. Additionally, the linkers isolate any potential defects, preventing them from detracting from the optical properties.

4.2.1.4 Conclusions

We have examined an ADMET/hydrogenation route for the preparation of well-defined phenylene-vinylene rod-coil copolymers. The ADMET polymerization produced modest molecular weight polymers in good to quantitative yields. The tandem ADMET/hydrogenation procedure, while operationally more complex, yielded polymers without noticeable chromophore

reduction. Alternative hydrogenation procedures were not selective for the aliphatic olefins in the linkers.

The two copolymers with the greatest chromophore fidelity, **p29** and **p32**, exhibited interesting thermal and optical properties. The T_m s of **p32**, the copolymer with oxygen atoms in the linker, were 60-70 °C higher than those of **p29**, the copolymer with only methylenes in its linker. However, the optical properties of the two copolymers were nearly identical. The similarity between the optical properties of the polymers and their segment precursors indicates that the chromophore fidelity is maintained in the polymerization.

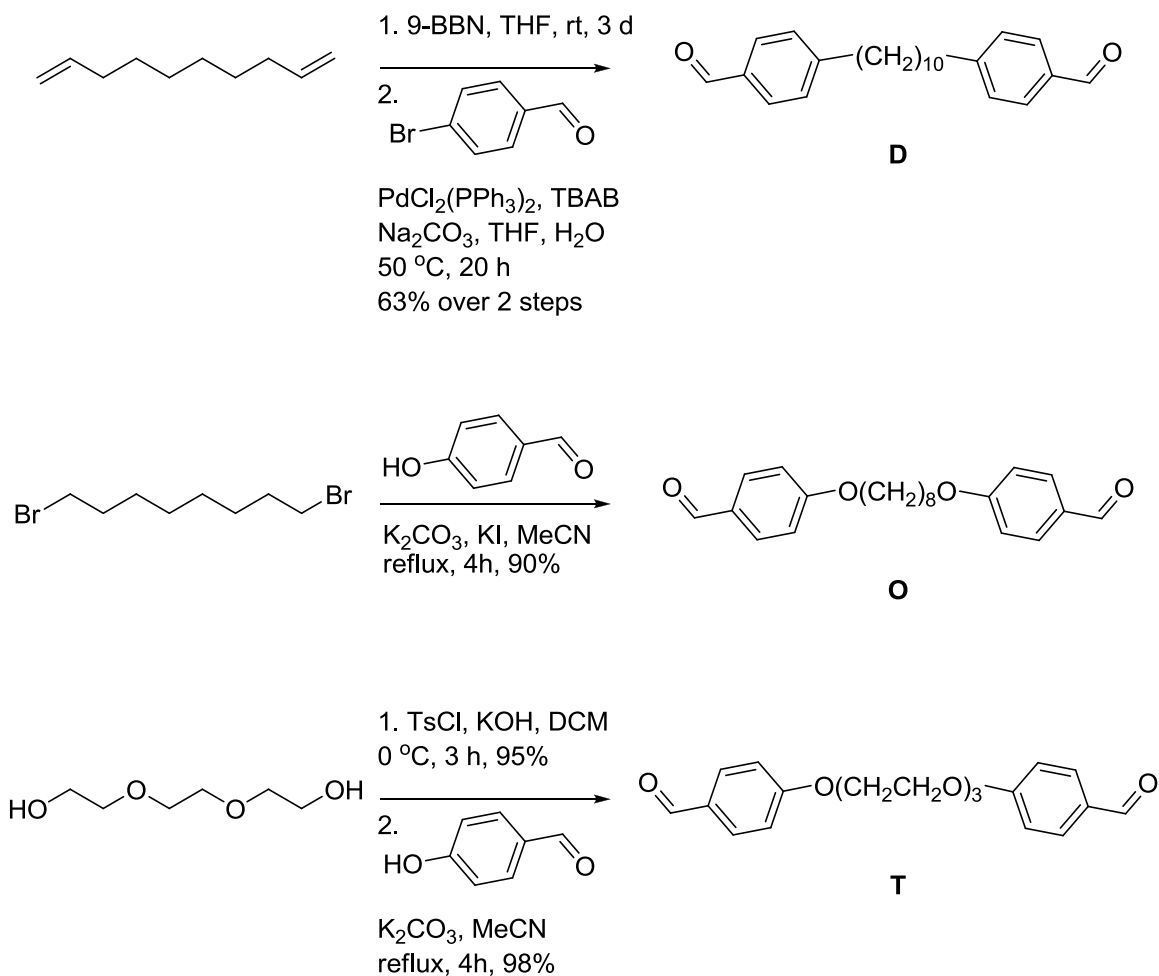
4.2.2 Rod-coil copolymers prepared by HWE polycondensation

We have prepared a series of rod-coil copolymers containing varying oxygen content and placement in the linker. The polymers display a wide range of thermal properties based on the linker composition. The thermal properties of the random copolymers are intermediate between the thermal properties of the respective homopolymers and display a linear relationship with respect to composition.

4.2.2.1 Polymer synthesis

The three dialdehyde linkers were prepared in one or two steps from commercially available compounds (Scheme 32). 1,9-Decadiene was converted to dialdehyde **D** by first hydroboration with 9-BBN to produce a 1,10-decane-diborane followed by a Suzuki reaction with 4-bromobenzaldehyde in 63% yield over 2 steps. 1,8-Dibromooctane and 4-hydroxybenzaldehyde were converted to dialdehyde **O** by an S_N2 reaction with K_2CO_3 and catalytic KI in refluxing MeCN in 90% yield. Triethylene glycol was converted into the

bis(tosylate) using TsCl and KOH in DCM in 95%. The bis(tosylate) was then reacted with 4-hydroxybenzaldehyde and K₂CO₃ in refluxing MeCN to give dialdehyde **T** in 98% yield.



Scheme 32. Synthesis of dialdehyde linkers.

One series of copolymers was prepared by HWE polycondensations between dialdehydes **O** and **T** and bis(phosphonate) **22**. Varying ratios of dialdehydes **O** and **T** were condensed with one equivalent of bis(phosphonate) **22** (based on total dialdehyde). The polymerizations proceeded in good to excellent yields, with *M_n*s ranging from 36.5 kDa to 57.8 kDa (Table 15). The PDIs (1.28 – 1.42) were low for polycondensations. Polymers containing dialdehyde **D** have not yet been prepared.

Table 15. Yields and properties of rod-coil copolymers

Polymer	x:y	Yield	M_n^a / kDa	M_w^a / kDa	PDI ^a	T_g^b / °C	T_m^b / °C
PV-O	10:0	89%	48.7	69.0	1.42	40	141
PV-O₉T₁	9:1	92%	51.8	71.1	1.38	39	134
PV-O₅T₅	5:5	81%	57.8	74.0	1.28	36	109
PV-O₁T₉	1:9	82%	41.1	53.7	1.31	32	N.O. ^c
PV-T	0:10	94%	36.5	49.3	1.35	31	62

^a Determined by SEC relative to polystyrene standards; ^b Determined by DSC, 10 °C/min scan rate; ^c not observed

4.2.2.2 Thermal properties

The thermal properties of the copolymers vary with oxygen content in the linker. The T_m of **PV-O** is nearly 80 °C higher than that of **PV-T**, even though **PV-T** contains more oxygen atoms in its linker. **PV-O** also has a higher T_g than **PV-T**, though the difference in T_g is smaller. The optimal number and placement of oxygen atoms in the linker appears to be two oxygen atoms, one at each end of the linker. This arrangement leads to a higher T_m than either an all methylene linker (vide supra) or a linker with four regularly spaced oxygen atoms. Based on the data collected for our ADMET polymers, we expect **PV-D**, the copolymer containing only the all methylene linker, will exhibit a T_m intermediate between those of **PV-O** and **PV-T**.

The thermal properties of the rod-coil copolymers can be fine-tuned by preparing copolymers containing varying ratios of **O** and **T** linkers. The thermal properties of these **PV-O_xT_y** copolymers vary linearly with composition between the properties of the parent polymers **PV-O** and **PV-T** (Table 15, Figure 28), with the exception of **PV-O₁T₉**, which anomalously does

not exhibit a melting transition. We expect that copolymers containing various ratios of linkers **D** and **O** or **D** and **T** will exhibit similar behavior.

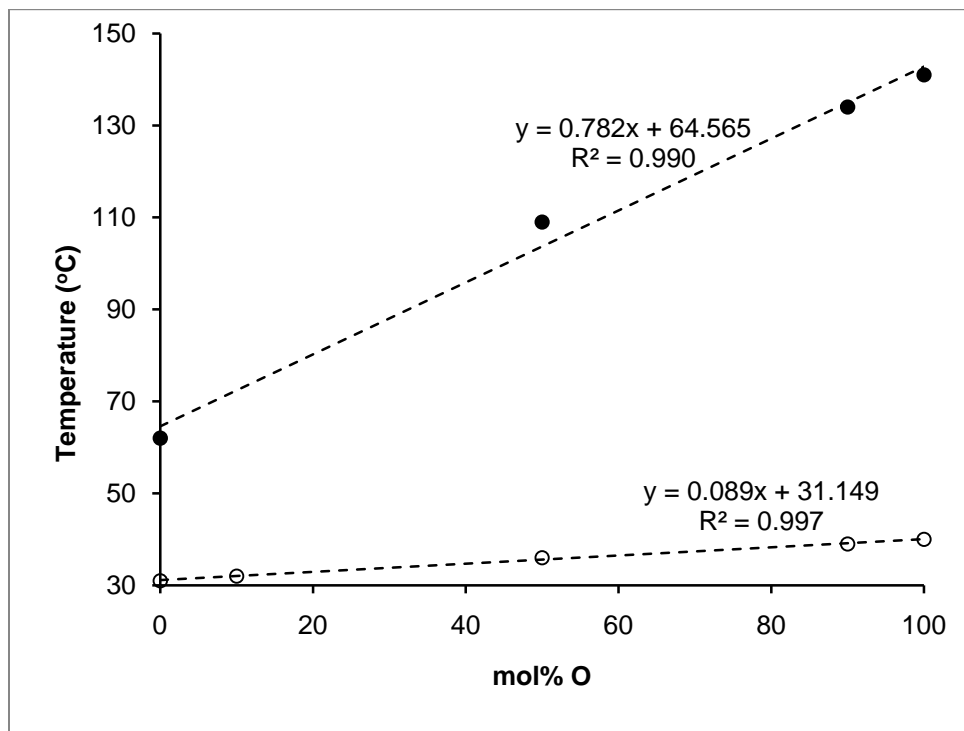


Figure 28. Correlation of thermal properties of the $PV-O_xT_y$ series to composition: T_g (open circles) and T_m (closed circles).

4.2.2.3 Conclusions

The thermal properties of a series of rod-coil phenylene-vinylene copolymers vary significantly with changes in the oxygen content and placement within the linker group. The copolymers with linkers containing two oxygen atoms, one at either end of the linker, have the highest T_m s and T_g s. The thermal properties can be fine-tuned by incorporating varying ratios of two linkers. The thermal properties of these copolymers vary linearly between the properties of the parent polymers. These polymers are prepared by an HWE polycondensation that proceeds in good to excellent yields and generates polymers with moderate M_n s and low PDIs.

We will investigate the optical properties of these copolymers. Based on previous reports¹⁰⁰⁻¹⁰² and our own results with the ADMET polymers we believe these copolymers will have similar absorption and emission profiles. If so, these polymers would represent an example of fine-tuning thermal properties of conjugated polymers without disrupting optical properties.

4.3 EXPERIMENTAL SECTION

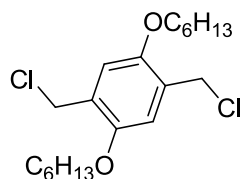
4.3.1 General methods

Materials. Pyridine and MeCN were dried over CaH₂ and distilled. Anhydrous DMF, 9-H-9-borabicyclo[3.3.1]nonane (0.5 M in THF) and ⁿBuLi (1.6 M in hexanes) were purchased from Aldrich and dispensed using air-sensitive techniques. KO^tBu was stored in a desiccator over anhydrous CaSO₄. PdCl₂(PPh₃)₂ was stored in a nitrogen-filled glovebox. When necessary, THF was dried by passing over a column of activated alumina. 9-(hex-5-en-1-yl)-9-borabicyclo[3.3.1]nonane, 9-(oct-7-en-1-yl)-9-borabicyclo[3.3.1]nonane, and 9-(dec-9-en-1-yl)-9-borabicyclo[3.3.1]nonane were according to a literature procedure. All other reagents and solvents were used as received. Column chromatography was carried out on standard grade silica gel (60 Å pore size, 40-63 µm particle size), which was purchased and used as received. Hexanes, dichloromethane, ethyl acetate, and diethyl ether used for column chromatography were purchased and used as received.

Instrumentation. ¹H (300 and 400 MHz) and ¹³C (75 and 100 MHz) NMR spectra were recorded on Bruker spectrometers. Chemical shifts were referenced to residual ¹H or ¹³C signals in deuterated solvents (7.27 and 77.0 ppm, respectively, for CHCl₃ and 5.32 and 54.0 ppm,

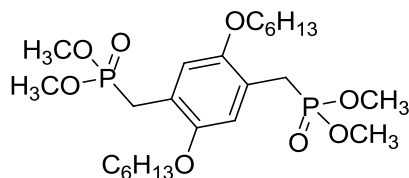
respectively, for CH₂Cl₂). UV/VIS absorption spectra were recorded on a Perkin Elmer Lambda 9 UV/VIS/NIR spectrometer. Emission spectra were recorded on a Varian Cary Eclipse fluorimeter. DSC was performed on a Perkin Elmer Pyris 6 with a heating and cooling rate of 10 °C/min. HRMS were recorded on a Fison VG Autospec in the Mass Spectral Facility of the University of Pittsburgh. Elemental analysis was performed independently by Atlantic Microlabs.

4.3.2 Rod-coil copolymers prepared by ADMET

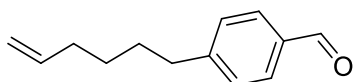


1,4-bis(chloromethyl)-2,5-bis(hexyloxy)benzene (35, vi15a). Based on the methods of Severen, *et al.*,¹⁰⁴ **1** (25.0 g, 89.8 mmol), paraformaldehyde (8.0 g, 265 mmol), and HCl (12 M, 53 mL, 636 mmol) were added to a round-bottom flask equipped with a water-cooled condenser and a thermometer and heated to 60 °C with stirring. Ac₂O (90 mL, 958 mmol) was added dropwise down the condenser at a slow rate to prevent the temperature from rising above 70 °C. The mixture was stirred at 60 °C overnight, by which time the product had precipitated. The mixture was poured into ice cold H₂O (500 mL) and extracted with DCM (3x 250 mL). The combined organic layers were washed with sat. NaHCO₃ (100 mL), water (2x 100 mL), and brine (100 mL). The organic solution was dried over MgSO₄ and the solvent was removed *in vacuo* to give 1,4-bis(chloromethyl)-2,5-bis(hexyloxy)benzene as a white solid (32.8 g, 100%). ¹H NMR (CDCl₃, 300 MHz) δ 0.89 (6H, t, *J* = 6.8 Hz), 1.33 (8H, mult), 1.47 (4H, mult), 1.78 (6H, pent, *J*

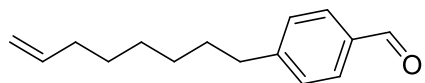
= 6.7 Hz), 3.96 (4H, t, $J = 6.4$ Hz), 4.61 (4H, s), 6.89 (2H) ppm. ^{13}C NMR (CDCl_3 , 75 MHz) δ 14.0, 22.6, 25.7, 29.3, 31.5, 41.4, 69.1, 114.3, 127.0, 150.6 ppm. MS (EI) 376 ($\text{M}+2$), 374 (M^+), 339, 255, 208, 206 (base), 172, 158, 122, 107, 91, 84, 77, 69, 57, 55 m/z. HRMS calcd for $\text{C}_{20}\text{H}_{32}\text{Cl}_2\text{O}_2$ 374.1782 g/mol. Found: 374.1779 g/mol.



1,4-bis(dimethoxyphosphorylmethyl)-2,5-bis(hexyloxy)benzene (22, vi17a). **35** (31.0 g, 87.2 mmol) and $\text{P}(\text{OCH}_3)_3$ (25 mL, 212 mmol) were dissolved in PhMe (200 mL) and refluxed for 24 h. The volatiles were removed *in vacuo*. The crude product was triturated with cold hexanes and filtered to give the title compound as a white solid (27.8 g, 60%). MP 68.0-69.0 °C. ^1H NMR (CDCl_3 , 300 MHz) δ 0.88 (6H, t, $^3J_{\text{H-H}} = 6.6$ Hz), 1.32 (8H, mult), 1.43 (4H, mult), 1.75 (4H, pent, $^3J_{\text{H-H}} = 7.3$ Hz), 3.21 (4H, d, $^2J_{\text{H-P}} = 20.5$ Hz), 3.65 (12H, d, $^3J_{\text{H-P}} = 10.4$ Hz), 3.91 (4H, d, $^3J_{\text{H-H}} = 6.6$ Hz), 6.87 (2H, s) ppm. ^{13}C NMR (CDCl_3) δ 14.0 (CH_3), 22.6 (CH_2), 25.6 (d, $^1J_{\text{C-P}} = 141.9$ Hz, PCH_2Ar), 25.7 (CH_2), 29.5 (CH_2), 31.6 (CH_2), 52.6 (2d, $^2J_{\text{C-P}} = 3.1$ Hz, $\text{P}(\text{OCH}_3)_2$), 69.0 (OCH_2), 114.9 (Ar CH), 119.2 (t, $^2J_{\text{C-P}} = 2.5$ Hz, Ar quat), 150.4 (ArO quat) ppm. FT-IR (thin film) 2950 (m), 2869 (m), 1515 (m), 1474 (w), 1423 (w), 1395 (w), 1275 (m), 1224 (s), 1058 (m), 1032 (s), 901 (m), 871 (m), 859 (m), 834 (m) cm^{-1} . MS (EI) 522 (M^+ , base), 438, 400, 354, 322, 316, 278, 245, 232, 213, 110, 93, 57 m/z. HRMS calcd for $\text{C}_{24}\text{H}_{44}\text{O}_8\text{P}_2$: 522.2511 g/mol. Found: 522.2514 g/mol.

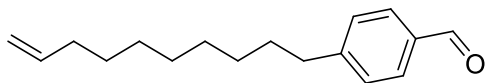


4-(hex-5-enyl)benzaldehyde (23, iii28a). Based on the methods of Thiem, *et al.*,¹⁰⁵ *p*-bromobenzaldehyde (2.60 g, 14.1 mmol) and tetra-*N*-butylammonium bromide (90 mg, 0.28 mmol) were dissolved in toluene (50 mL) in a Schlenk flask equipped with a stirbar. Aqueous sodium carbonate (2.0 M, 20 mL) was added and the mixture was degassed and taken into a nitrogen-filled glovebox. 9-(hex-5-enyl)-9-BBN (4.1 mL, 18 mmol) and PdCl₂(PPh₃)₂ (196 mg, 0.28 mmol) were added quickly and the reaction mixture was removed from the glovebox. The reaction mixture was stirred under nitrogen at 50 °C for 24 h. After cooling to RT, the layers separated. The aqueous layer was extracted with DCM (2x 30 mL). The combined organic layers were then washed with brine (50 mL), dried over MgSO₄, and reduced *in vacuo*. The crude product was purified column chromatography (silica gel, 19:1 hexanes:Et₂O) to give the title compound as a colorless oil (2.50 g, 95%). ¹H NMR (CDCl₃, 300 MHz) δ 1.39 (2H, pent, *J* = 7.2 Hz), 1.64 (2H, pent, *J* = 7.5 Hz), 2.07 (2H, q, *J* = 7.2 Hz), 2.68 (2H, t, *J* = 7.7 Hz), 4.85-5.00 (2H, mult), 5.70-5.85 (1H, mult), 7.31 (2H, d, *J* = 8.0 Hz, *p*-C₆H₄), 7.78 (2H, d, *J* = 8.0 Hz, *p*-C₆H₄), 9.95 (s, 1H) ppm. ¹³C NMR (CDCl₃, 75 MHz) δ 28.2 (CH₂), 30.3 (CH₂), 33.3 (CH₂), 35.8 (CH₂), 114.5 (vinyl CH₂), 128.9 (Ar CH), 129.7 (Ar CH), 134.3 (Ar quat), 138.3 (vinyl CH), 150.0 (Ar quat), 191.7 (CHO) ppm. FT-IR (neat) 3076 (s), 2932 (s), 2857 (s), 2732 (s), 1705 (s), 1640 (s), 1607 (s), 1576 (s), 1461 (s), 1388 (s), 1306 (s), 1213 (s), 1168 (s), 1114 (w), 993 (s), 912 (s), 826 (s), 779 (s) cm⁻¹. MS (EI) 188 (M⁺), 159, 145, 132, 117, 105, 91 (base), 77, 65 m/z. HRMS calcd for C₁₃H₁₆O: 188.1201 g/mol. Found: 188.1202 g/mol.



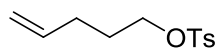
4-(oct-7-enyl)benzaldehyde (24, iii24a). Based on the methods of Thiem, *et al.*,¹⁰⁵ *p*-bromobenzaldehyde (3.00 g, 16.2 mmol) and tetra-*N*-butylammonium bromide (100 mg, 0.32

mmol) were dissolved in toluene (30 mL) in a Schlenk flask equipped with a stirbar. Aqueous sodium carbonate (2.0 M, 20 mL) was added and the mixture was degassed and taken into a nitrogen-filled glovebox. 9-(oct-7-enyl)-9-BBN (5.64 g, 24.3 mmol) and PdCl₂(PPh₃)₂ (225 mg, 0.28 mmol) were added quickly and the reaction mixture was removed from the glovebox. The reaction mixture was stirred under nitrogen at 50 °C for 24 h. After cooling to RT, the layers separated. The aqueous layer was extracted with DCM (2x 30 mL). The combined organic layers were then washed with brine (50 mL), dried over MgSO₄, and reduced *in vacuo*. The crude product was purified column chromatography (silica gel, 19:1 hexanes:Et₂O) to give the title compound as a colorless oil (2.30, 66%). ¹H NMR (CDCl₃, 300 MHz) δ 1.35-1.45 (6H, mult), 1.62 (2H, pent, *J* = 6.9 Hz), 1.95-2.05 (2H, mult), 2.67 (2H, t, *J* = 7.5 Hz), 4.85-5.00 (2H, mult), 5.70-5.85 (1H, mult), 7.31 (2H, d, *J* = 8.1 Hz, *p*-C₆H₄), 7.78 (2H, d, *J* = 8.1 Hz, *p*-C₆H₄), 9.95 (1H, s, CHO). ¹³C NMR (CDCl₃, 75 MHz) δ 28.79 (CH₂), 28.90 (CH₂), 29.08 (CH₂), 31.02 (CH₂), 33.74 (CH₂), 36.20 (CH₂), 114.30 (vinyl CH₂), 128.09 (Ar CH), 129.91 (Ar CH), 134.42 (Ar quat), 139.03 (vinyl CH), 150.43 (Ar quat), 192.06 (CHO) ppm. MS (EI): 216 (M⁺) 145, 132, 120, 105, 91 (base), 77, 65, 55 m/z. HRMS calcd for C₁₅H₂₀O: 216.514 g/mol. Found: 216.1514 g/mol.



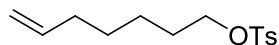
4-(dec-9-enyl)benzaldehyde (25, iii25a). Based on the methods of Thiem, *et al.*,¹⁰⁵ *p*-bromobenzaldehyde (3.00 g, 16.2 mmol) and tetra-*N*-butylammonium bromide (100 mg, 0.32 mmol) were dissolved in toluene (30 mL) in a Schlenk flask equipped with a stirbar. Aqueous sodium carbonate (2.0 M, 20 mL) was added and the mixture was degassed and taken into a nitrogen-filled glovebox. 9-(dec-9-enyl)-9-BBN (6.32 g, 24.3 mmol) and PdCl₂(PPh₃)₂ (225 mg,

0.28 mmol) were added quickly and the reaction mixture was removed from the glovebox. The reaction mixture was stirred under nitrogen at 50 °C for 24 h. After cooling to RT, the layers separated. The aqueous layer was extracted with DCM (2x 30 mL). The combined organic layers were then washed with brine (50 mL), dried over MgSO₄, and reduced *in vacuo*. The crude product was purified column chromatography (silica gel, 19:1 hexanes:Et₂O) to give the title compound as a colorless oil (2.61 g, 66%). ¹H NMR (CDCl₃, 300 MHz) δ 1.35-1.45 (10H, mult), 1.62 (2H, mult), 2.01 (2H, q, *J* = 6.6 Hz), 2.66 (2H, t, *J* = 7.8 Hz), 4.85-5.00 (2H, mult), 5.70-5.85 (1H, mult), 7.31 (2H, d, *J* = 8.1 Hz, *p*-C₆H₄), 7.78 (2H, d, *J* = 8.1 Hz, *p*-C₆H₄), 9.95 (1H, s, CHO). ¹³C NMR (CDCl₃, 75 MHz) δ 28.90 (CH₂), 29.10 (CH₂), 29.24 (CH₂), 29.38 (CH₂), 31.09 (CH₂), 33.80 (CH₂), 36.23 (CH₂), 114.50 (vinyl CH₂), 129.09 (Ar CH), 129.91 (Ar CH), 134.41 (Ar quat), 139.19 (vinyl CH), 150.50 (Ar quat), 192.06 (CHO) ppm. MS (EI:) 244 (M⁺), 159, 146, 132, 120, 91 (base), 77, 69, 55 m/z. HRMS calcd for C₁₇H₂₄O: 244.1827 g/mol. Found: 244.1829 g/mol.

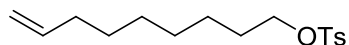


Pent-4-enyl tosylate (36, ii91a). 4-penten-1-ol (4.72 g, 54.8 mmol) and TsCl (14.2 g, 74.3 mmol) were dissolved in dry pyridine (40 mL) at 0 °C and stirred for 3.5 h. The reaction was quenched into a mixture of 100 g of ice and 100 mL of 1 M HCl. The mixture was extracted with Et₂O (3x 100 mL). The combined organic layers were washed with sat. NaHCO₃ (100 mL), water (100 mL), and brine (100 mL). The solution was dried over MgSO₄ and the solvent was removed *in vacuo* to give the title compound as a pale yellow oil that crystallized into thin needles (13.2 g, 100%). ¹H NMR (CHCl₃, 300 MHz) δ 1.75 (2H, pent, *J* = 6.9 Hz), 2.09 (2H, q, *J*

= 6.9 Hz), 2.46 (3H, s), 4.04 (2H, t, $J = 6.3$ Hz), 4.90-5.00 (2H, mult), 5.60-5.75 (1H, mult), 7.36 (2H, d, $J = 8.1$ Hz, p -C₆H₄), 7.80 (2H, d, $J = 8.1$ Hz, p -C₆H₄) ppm.

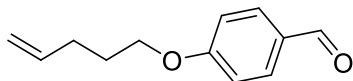


Hept-6-enyl tosylate (37, iii39a). 6-hepten-1-ol (5.0 mL, 37.2 mmol) and TsCl (10.6 g, 55.5 mmol) were dissolved in dry pyridine (40 mL) at 0 °C and stirred for 3.5 h. The reaction was quenched into a mixture of 100 g of ice and 100 mL of 1 M HCl. The mixture was extracted with Et₂O (3x 100 mL). The combined organic layers were washed with sat. NaHCO₃ (100 mL), water (100 mL), and brine (100 mL). The solution was dried over MgSO₄ and the solvent was removed *in vacuo* to give the title compound as a pale yellow oil (8.97, 90%). ¹H NMR (CHCl₃, 300 MHz) δ 1.25-1.35 (4H, mult), 1.65 (2H, pent, $J = 6.3$ Hz), 1.95-2.05 (2H, mult), 2.46 (3H, s), 4.03 (2H, t, $J = 6.3$ Hz), 4.90-5.00 (2H, mult), 5.65-5.75 (1H, mult), 7.35 (2H, d, $J = 8.1$ Hz, p -C₆H₄), 7.80 (2H, d, $J = 8.1$ Hz, p -C₆H₄) ppm.

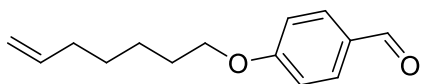


Non-8-enyl tosylate (38, iii39a). 8-nonen-1-ol (5.0 mL, 29.9 mmol) and TsCl (10.6 g, 55.5 mmol) were dissolved in dry pyridine (40 mL) at 0 °C and stirred for 3.5 h. The reaction was quenched into a mixture of 100 g of ice and 100 mL of 1 M HCl. The mixture was extracted with Et₂O (3x 100 mL). The combined organic layers were washed with sat. NaHCO₃ (100 mL), water (100 mL), and brine (100 mL). The solution was dried over MgSO₄ and the solvent was removed *in vacuo* to give the title compound as a pale yellow oil (7.59 g, 86%). ¹H NMR (CHCl₃, 300 MHz) δ 1.15-1.40 (8H, mult), 1.55-1.70 (2H, mult), 2.02 (2H, pent, $J = 7.0$ Hz),

2.46 (3H, s), 4.03 (2H, t, $J = 6.3$ Hz), 4.90-5.05 (2H, mult), 5.60-5.75 (1H, mult), 7.35 (2H, d, $J = 8.4$ Hz, p -C₆H₄), 7.80 (2H, d, $J = 8.4$ Hz, p -C₆H₄) ppm.

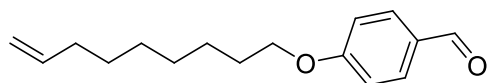


4-(pent-4-enyloxy)benzaldehyde (26, ii92a). p -Hydroxybenzaldehyde (5.00 g, 40.9 mmol) was dissolved in dry MeCN (50 mL). K₂CO₃ (6.00 g, 43.4 mmol) was added, followed by **36** (10.0 g, 41.6 mmol). The dark pink mixture was refluxed for 2.5 h. The mixture was poured into H₂O (100 mL) and extracted with Et₂O (3x 100 mL). The combined organic layers were washed with brine (100 mL) and dried over MgSO₄. The solvent was removed *in vacuo*. The crude product was purified by column chromatography (silica gel, 4:1 hexanes:Et₂O) gave the title compound as a colorless oil (5.07 g, 65%). ¹H NMR (CHCl₃, 300 MHz) δ 1.93 (2H, pent, $J = 6.9$ Hz), 2.27 (2H, q, $J = 7.0$ Hz), 4.06 (2H, t, $J = 6.3$ Hz), 4.95-5.15 (2H, mult), 5.75-5.95 (1H, mult), 7.00 (2H, d, $J = 8.7$ Hz, p -C₆H₄), 7.84 (2H, d, $J = 8.7$ Hz, p -C₆H₄), 9.89 (1H, s, CHO) ppm. ¹³C NMR (CDCl₃, 75 MHz) δ 28.14 (CH₂), 29.92 (CH₂), 67.49 (OCH₂), 114.71 (Ar CH), 115.44 (vinyl CH₂), 129.82 (Ar quat), 131.92 (Ar CH), 137.39 (vinyl CH), 164.10 (ArO quat), 190.69 (CHO) ppm. MS (EI): 190 (M⁺), 119, 81 (base), 65 m/z. HRMS calcd for C₁₂H₁₄O₂: 190.0994 g/mol. Found: 190.1001 g/mol.



4-(hept-6-enyloxy)benzaldehyde (27, iii58a). p -Hydroxybenzaldehyde (3.30 g, 27.0 mmol) was dissolved in dry MeCN (60 mL). K₂CO₃ (3.75 g, 26.8 mmol) was added, followed by **37** (30.0 g, 11.2 mmol). The dark pink mixture was refluxed for 24 h. The mixture was poured into H₂O

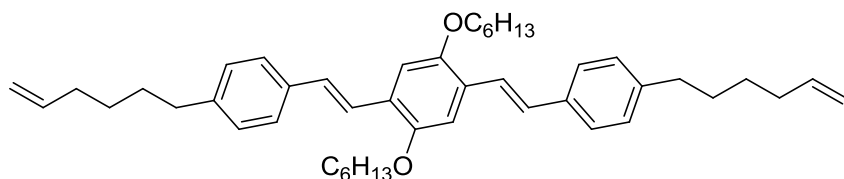
(100 mL) and extracted with Et₂O (3x 100 mL). The combined organic layers were washed with brine (100 mL) and dried over MgSO₄. The solvent was removed *in vacuo*. The crude product was purified by column chromatography (silica gel, 9:1 hexanes:Et₂O) gave the title compound as a colorless oil (2.44 g, 90%). ¹H NMR (CHCl₃, 300 MHz) δ 1.40-1.50 (4H, mult), 1.70-1.85 (2H, mult), 2.00-2.10 (2H, mult), 4.00 (2H, t, *J* = 6.3 Hz), 4.90-5.05 (2H, mult), 5.75-5.90 (1H, mult), 6.95 (2H, d, *J* = 8.7 Hz, *p*-C₆H₄), 7.79 (2H, d, *J* = 8.7 Hz, *p*-C₆H₄), 9.84 (1H, s, CHO) ppm. ¹³C NMR (CDCl₃, 75 MHz) δ 25.26 (CH₂), 28.37 (CH₂), 28.72 (CH₂), 33.46 (CH₂), 68.10 (OCH₂), 114.19 (vinyl CH₂), 114.55 (Ar CH), 129.59 (Ar quat), 131.76 (Ar CH), 138.46 (vinyl CH), 164.01 (ArO quat), 190.50 (CHO) ppm.



4-(non-8-enyloxy)benzaldehyde (28, iii46a). *p*-Hydroxybenzaldehyde (2.50 g, 20.5 mmol) was dissolved in dry MeCN (30 mL). NaH (60% in mineral oil, 0.86 g, 21.5 mmol) was added, followed by **38** (6.20 g, 20.9 mmol). The dark pink mixture was refluxed for 2.0 h. Further aliquots of NaH (60% in mineral oil, 0.86 g, 21.5 mmol) and *p*-hydroxybenzaldehyde (2.50 g, 20.5 mmol) were added and the mixture was refluxed for another 2 h. The mixture was poured into H₂O (100 mL) and extracted with Et₂O (3x 100 mL). The combined organic layers were washed with brine (100 mL) and dried over MgSO₄. The solvent was removed *in vacuo*. The crude product was purified by column chromatography (silica gel, 49:1 hexanes:Et₂O) gave the title compound as a colorless oil (2.89 g, 57%). ¹H NMR (CHCl₃, 300 MHz) δ 1.25-1.50 (8H, mult), 1.80 (2H, pent, *J* = 7.1 Hz), 2.03 (2H, q, *J* = 7.2 Hz), 4.02 (2H, t, *J* = 6.6 Hz), 4.85-5.05 (2H, mult), 5.70-5.90 (1H, mult), 6.97 (2H, d, *J* = 8.7 Hz, *p*-C₆H₄), 7.81 (2H, d, *J* = 8.7 Hz, *p*-C₆H₄), 9.86 (1H, s, CHO) ppm. ¹³C NMR (CDCl₃, 75 MHz) δ 25.92 (CH₂), 28.30 (CH₂), 29.00

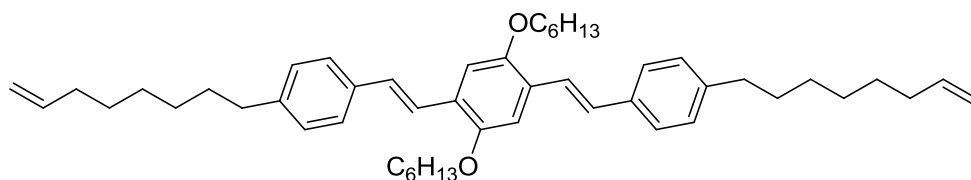
(CH₂), 29.05 (CH₂), 29.18 (CH₂), 33.76 (CH₂), 68.41 (OCH₂), 114.27 (vinyl CH₂), 114.76 (Ar CH), 129.79 (Ar quat), 132.00 (Ar CH), 139.07 (vinyl CH), 190.81 (CHO) ppm. MS (EI): 246 (M⁺), 135, 123, 122, 121, 110, 105, 95, 83, 77, 69, 55 (base) m/z. HRMS calcd for C₁₆H₂₂O₂: 246.1620 g/mol. Found: 246.1615 g/mol.

General HWE procedure to produce segmers. 22 (1 eq) was dissolved in THF (20 mL per g) and cooled to 0 °C under N₂. KO^tBu (4 eq) was added portionwise over 2 min, and the mixture was stirred at 0 °C for 5 min. A solution of aldehyde (2.5 eq) in THF (10 mL per g) was added dropwise, and the mixture was allowed to come to rt overnight with stirring. The reaction mixture was poured into 100 mL H₂O and 100 mL of sat. NH₄Cl and extracted with DCM (5x 100 mL) and hexanes (100 mL). The combined organic layers were washed with brine (100 mL) and dried over MgSO₄. The solvent was removed *in vacuo*. The crude product was purified using column chromatography.



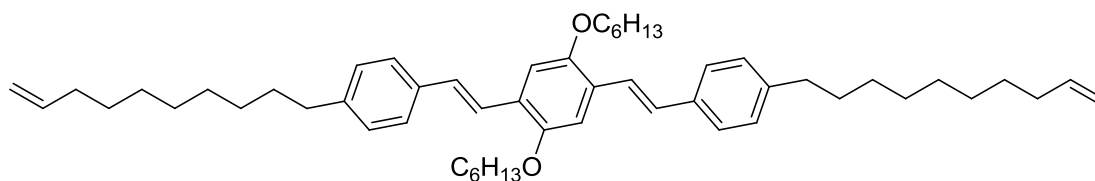
1,4-bis(4-(hex-5-enyl)styryl)-2,5-bis(hexyloxy)benzene (29, ii68a). According to the general procedure, **22** (0.925 g, 1.77 mmol) was dissolved in THF (20 mL) and cooled to 0 °C under N₂. KO^tBu (0.800 g, 7.13 mmol) was added portionwise over 2 min, and the mixture was stirred for 5 min. To the orange mixture, as solution of **23** (0.800 g, 4.25 mmol) in THF (10 mL) was added dropwise. The reaction mixture was allowed to come to rt overnight with stirring. After workup, the crude product was purified using column chromatography (silica gel, 99:1 hexanes:Et₂O) to give the title compound as a yellow solid (0.80 g, 70%). ¹H NMR spectroscopy showed a small

cis impurity (δ 6.7) that could not be removed. ^1H NMR (CD_2Cl_2 , 300 MHz) δ 0.94 (6H, t, $J = 6.9$ Hz), 1.27 – 1.70 (20H, mult), 1.88 (4H, t, $J = 6.9$ Hz), 2.10 (4H, q, $J = 6.9$ Hz), 2.63 (4H, t, $J = 7.5$ Hz), 4.06 (4H, t, $J = 6.6$ Hz), 4.90 – 5.05 (4H, mult), 5.80 – 5.90 (2H, mult), 7.10 – 7.20 (8H, mult), 7.40 – 7.50 (6H, mult) ppm. ^{13}C NMR (CD_2Cl_2 , 75 MHz) δ 14.4 (CH_3), 23.3 (CH_2), 26.6 (CH_2), 29.2 (CH_2), 30.1 (CH_2), 31.5 (CH_2), 32.3 (CH_2), 34.2 (CH_2), 36.1 (CH_2), 70.2 (OCH_2), 111.0 (Ar CH), 114.7 (vinyl CH_2), 123.0 (vinylene CH), 126.9 (Ar CH), 127.4 (Ar quat), 129.1 (vinylene CH), 129.3 (Ar CH), 136.0 (Ar quat), 139.6 (vinyl CH), 143.0 (Ar quat), 151.6 (ArO quat) ppm. MS (EI) 646 (M^+), 462 (base), 377, 294, 225, 223, 187, 173, 141, 129, 117, 91, 83, 69, 55 m/z. HRMS calcd for $\text{C}_{42}\text{H}_{62}\text{O}_2$: 646.4750. Found: 646.4756.



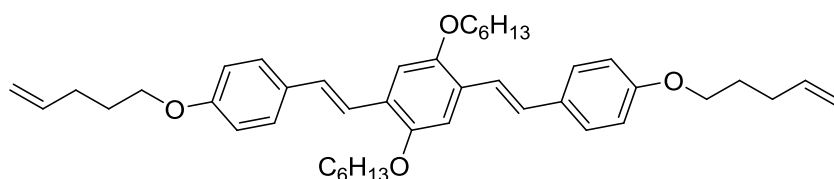
1,4-bis(4-(oct-7-enyl)styryl)-2,5-bis(hexyloxy)benzene (30, iii49a). According to the general procedure, **22** (1.15 g, 2.20 mmol) was dissolved in THF (20 mL) and cooled to 0 °C under N_2 . KO^tBu (1.00 g, 8.91 mmol) was added portionwise over 2 min, and the mixture was stirred for 5 min. To the orange mixture, as solution of **24** (0.970 g, 4.48 mmol) in THF (10 mL) was added dropwise. The reaction mixture was allowed to come to rt overnight with stirring. After workup, the crude product was purified using column chromatography (silica gel, 99:1 hexanes: Et_2O) to give the title compound as a yellow solid (0.711 g, 46%). ^1H NMR (CD_2Cl_2 , 300 MHz) δ 0.94 (6H, mult), 1.27 – 1.50 (20H, mult), 1.50-1.70 (8H, mult), 1.89 (4H, t, $J = 6.6$ Hz), 2.00-2.10 (4H, mult), 2.62 (4H, t, $J = 7.5$ Hz), 4.06 (4H, t, $J = 6.6$ Hz), 4.90 – 5.05 (4H, mult), 5.75 – 5.90 (2H, mult), 7.10 – 7.20 (8H, mult), 7.40 – 7.50 (6H, mult) ppm. ^{13}C NMR (CD_2Cl_2 , 75 MHz)

δ 14.24 (CH₃), 23.06 (CH₂), 26.35 (CH₂), 29.27 (CH₂), 29.36 (CH₂), 29.51 (CH₂), 29.88 (CH₂), 31.78 (CH₂), 31.93 (CH₂), 32.05 (CH₂), 34.15 (CH₂), 36.01 (CH₂), 70.26 (OCH₂), 110.81 (Ar CH), 114.27 (vinyl CH₂), 122.77 (vinylene CH), 126.73 (Ar CH), 127.20 (Ar quat), 128.96 (vinylene CH), 129.13 (Ar CH), 135.81 (Ar quat), 139.65 (vinyl CH), 142.96 (Ar quat), 151.46 (ArO quat) ppm. MS (EI) 702 (M⁺, base), 534, 504, 490, 369, 239, 129, 117, 97, 83, 69, 53 m/z. HRMS calcd for C₅₀H₇₀O₂: 702.5376 g/mol. Found: 702.5355 g/mol.

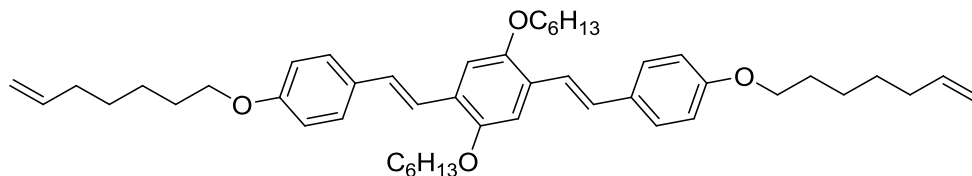


1,4-bis(4-(dec-9-enyl)styryl)-2,5-bis(hexyloxy)benzene (31, iii53a). According to the general procedure, **22** (1.00 g, 1.91 mmol) was dissolved in THF (20 mL) and cooled to 0 °C under N₂. KO^tBu (0.886 g, 7.90 mmol) was added portionwise over 2 min, and the mixture was stirred for 5 min. To the orange mixture, as solution of **25** (0.965 g, 3.95 mmol) in THF (10 mL) was added dropwise. The reaction mixture was allowed to come to rt overnight with stirring. After workup, the crude product was purified using column chromatography (silica gel, 49:1 hexanes:Et₂O) to give the title compound as a yellow solid (0.899 g, 62%). ¹H NMR (CD₂Cl₂, 300 MHz) δ 0.94 (6H, mult), 1.27 – 1.50 (28H, mult), 1.50-1.70 (8H, mult), 1.88 (4H, t, *J* = 6.6 Hz), 2.04 (4H, q, *J* = 7.5 Hz), 2.61 (4H, t, *J* = 7.5 Hz), 4.04 (4H, t, *J* = 6.6 Hz), 4.90 – 5.05 (4H, mult), 5.75 – 5.90 (2H, mult), 7.10 – 7.20 (8H, mult), 7.40 – 7.50 (6H, mult) ppm. ¹³C NMR (CD₂Cl₂, 75 MHz) δ 14.05 (CH₃), 22.64 (CH₂), 25.94 (CH₂), 28.91 (CH₂), 29.11 (CH₂), 29.28 (CH₂), 29.40 (CH₂), 29.44 (CH₂), 29.48 (CH₂), 31.42 (CH₂), 31.63 (CH₂), 31.91 (CH₂), 33.78 (CH₂), 35.70 (CH₂), 69.58 (OCH₂), 110.50 (Ar CH), 114.01 (vinyl CH₂), 122.47 (vinylene CH), 126.37 (Ar CH),

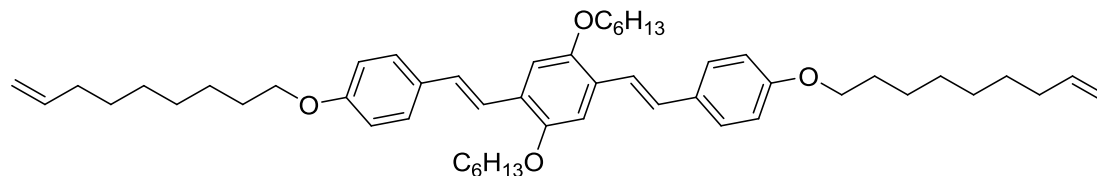
126.85 (Ar quat), 128.56 (vinylene CH), 128.69 (Ar CH), 135.38 (Ar quat), 139.25 (vinyl CH), 142.43 (Ar quat), 151.01 (ArO quat) ppm. MS (EI) 759 (M^+), 702, 551, 518, 368, 334, 256, 149, 129 (base) m/z. HRMS calcd for $C_{54}H_{78}O_2$: 758.6002 g/mol. Found: 758.6023 g/mol



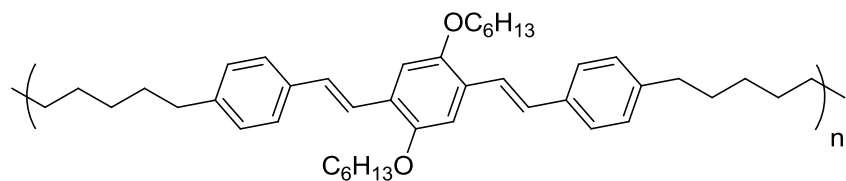
1,4-bis(4-pent-4-enyloxy)styryl)-2,5-bis(hexyloxy)benzene (32, ii80a). According to the general procedure, **22** (1.15 g, 2.20 mmol) was dissolved in THF (20 mL) and cooled to 0 °C under N_2 . n BuLi (1.6 M in hexanes, 2.8 mL, 4.5 mmol) was added dropwise over 2 min, and the mixture was stirred for 5 min. To the orange mixture, as solution of **26** (1.00 g, 5.25 mmol) in THF (10 mL) was added dropwise. The reaction mixture was allowed to come to rt overnight with stirring. After workup, the crude product was purified using column chromatography (silica gel, 1:1 hexanes:PhMe) to give the title compound as a yellow solid (1.07 g, 75%). 1H NMR spectroscopy showed a small cis impurity (δ 6.7) that could not be removed. 1H NMR (CD_2Cl_2 , 300 MHz) δ 0.93 (6H, t, $J = 6.9$ Hz), 1.25 – 1.45 (8H, mult), 1.45-1.60 (4H, mult), 1.80-1.95 (8H, mult), 2.25 (4H, q, $J = 6.6$ Hz), 4.00 (4H, t, $J = 6.6$ Hz), 4.05 (4H, t, $J = 6.6$ Hz), 4.95 – 5.15 (4H, mult), 5.80 – 5.95 (2H, mult), 6.89 (4H, d, $J = 8.7$ Hz, p - C_6H_4), 7.10 (1H, d, $J = 16.5$ Hz, *trans* CH=CH), 7.12 (1H, s), 7.34 (1H, d, $J = 16.5$ Hz, *trans* CH=CH), 7.46 (4H, d, $J = 8.7$ Hz, p - C_6H_4) ppm. MS (EI): 650 (M^+ , base), 464, 420, 379, 228, 211, 183, 107, 95, 83, 69, 55 m/z. HRMS calcd for $C_{44}H_{58}O_4$: 650.4335 g/mol. Found: 650.4357 g/mol.



1,4-bis(4-(hept-6-enyloxy)styryl)-2,5-bis(hexyloxy)benzene (33, iii62a). According to the general procedure, **22** (1.00 g, 1.91 mmol) was dissolved in THF (20 mL) and cooled to 0 °C under N₂ KO^tBu (0.886 g, 7.90 mmol) was added portionwise over 2 min, and the mixture was stirred for 5 min. To the orange mixture, as solution of **27** (0.860 g, 3.94 mmol) in THF (10 mL) was added dropwise. The reaction mixture was allowed to come to rt overnight with stirring. After workup, the crude product was purified using column chromatography (alumina, 1:1 hexanes:DCM) to give the title compound as a yellow solid (1.16 g, 86%). ¹H NMR spectroscopy showed a small cis impurity (δ 6.7) that could not be removed. ¹H NMR (CD₂Cl₂, 300 MHz) δ 0.94 (6H, t, *J* = 6.9 Hz), 1.25 – 1.65 (20H, mult) 1.75-1.95 (8H, mult), 2.05-2.15 (4H, mult), 3.99 (4H, t, *J* = 6.6 Hz), 4.06 (4H, t, *J* = 6.6 Hz), 4.90 – 5.10 (4H, mult), 5.80 – 5.95 (2H, mult), 6.89 (4H, d, *J* = 8.7 Hz, *p*-C₆H₄), 7.12 (1H, d, *J* = 16.5 Hz, *trans* CH=CH), 7.13 (1H, s), 7.36 (1H, d, *J* = 16.5 Hz, *trans* CH=CH), 7.47 (4H, d, *J* = 8.7 Hz, *p*-C₆H₄) ppm. ¹³C NMR (CD₂Cl₂, 75 MHz) δ 14.43 (CH₃), 23.27 (CH₂), 26.57 (CH₂), 26.50 (CH₂), 29.66 (CH₂), 29.83 (CH₂), 29.87 (CH₂), 30.12 (CH₂), 32.27 (CH₂), 34.36 (CH₂), 68.70 (OCH₂), 70.17 (OCH₂), 110.84 (Ar CH), 114.47 (vinyl CH₂), 115.25 (Ar CH), 121.66 (vinylene CH), 127.31 (Ar quat), 128.18 (Ar CH), 128.69 (vinylene CH), 131.15 (Ar quat), 139.85 (vinyl CH), 151.54 (ArO quat), 159.51 (ArO quat) ppm. MS (EI) 707 (M⁺), 429, 307, 293, 167, 149 (base), 129 m/z. HRMS calcd for C₄₈H₆₆O₄: 706.4961 g/mol. Found: 706.4955

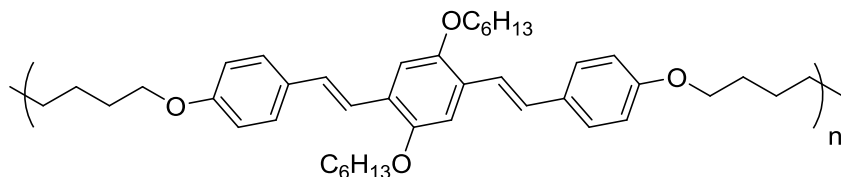


1,4-bis(4-(non-8-enyloxy)styryl)-2,5-bis(hexyloxy)benzene (34, iii54a). According to the general procedure, **22** (0.846 g, 1.62 mmol) was dissolved in THF (20 mL) and cooled to 0 °C under N₂ KO^tBu (0.752 g, 6.70 mmol) was added portionwise over 2 min, and the mixture was stirred for 5 min. To the orange mixture, as solution of **28** (0.825 g, 3.35 mmol) in THF (10 mL) was added dropwise. The reaction mixture was allowed to come to rt overnight with stirring. After workup, the crude product was purified using column chromatography (silica gel, 19:1 hexanes:Et₂O) to give the title compound as a yellow solid (1.24 g, 88%). ¹H NMR spectroscopy showed a small cis impurity (δ 6.7) that could not be removed. ¹H NMR (CD₂Cl₂, 300 MHz) δ 0.94 (6H, t, *J* = 6.9 Hz), 1.25 – 1.65 (28H, mult), 1.79 (4H, pent, *J* = 7.0 Hz), 1.88 (4H, pent, *J* = 7.2 Hz), 2.05-2.15 (4H, mult), 3.98 (4H, t, *J* = 6.6 Hz), 4.05 (4H, t, *J* = 6.6 Hz), 4.90 – 5.05 (4H, mult), 5.75 – 5.90 (4H, mult), 6.90 (4H, d, *J* = 8.7 Hz, *p*-C₆H₄), 7.11 (1H, d, *J* = 16.5 Hz, *trans* CH=CH), 7.13 (1H, s), 7.35 (1H, d, *J* = 16.5 Hz, *trans* CH=CH), 7.47 (4H, d, *J* = 8.7 Hz, *p*-C₆H₄) ppm. ¹³C NMR (CD₂Cl₂, 75 MHz) δ 14.40 (CH₃), 23.24 (CH₂), 26.10 (CH₂), 26.53 (CH₂), 29.25 (CH₂), 29.69 (CH₂), 30.06 (CH₂), 30.25 (CH₂), 32.23 (CH₂), 34.26 (CH₂), 68.54 (OCH₂), 70.07 (OCH₂), 110.71 (Ar CH), 114.6 (vinyl CH₂), 115.17 (Ar CH), 121.57 (vinylene CH), 127.21 (Ar quat), 128.14 (Ar CH), 128.60 (vinylene CH), 131.08 (Ar quat), 139.55 (vinyl CH), 151.45 (ArO quat), 159.41 (ArO quat) ppm. MS (EI) 763 (M⁺, base), 565, 535, 107 m/z. HRMS calcd for C₅₂H₇₄O₄: 762.5587 g/mol. Found: 762.5621 g/mol.



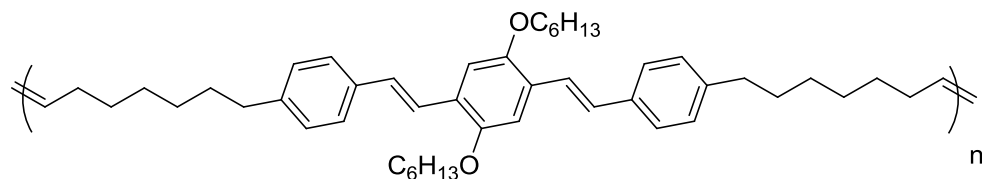
Tandem ADMET polymerization/hydrogenation – p29 (ii70). In a nitrogen-filled glovebox, **29** (0.50 g, 0.77 mmol) was dissolved in toluene (10 mL), in a pear-shaped flask equipped with a stirbar. Grubbs catalyst I (15 mg, 19 μ mol) and diphenyl ether (200 mg, 1.2 mmol) were added, and the reaction mixture was removed from the glovebox. While stirring, the toluene was slowly removed under vacuum. Once all toluene had been removed, the reaction mixture was heated to 50 °C under vacuum. After 24 h, the stirbar became immobilized, and the reaction mixture was cooled to RT and returned to the glovebox. ^1H NMR spectroscopy revealed no remaining terminal olefin. The reaction mixture was transferred to a stainless steel bomb with toluene (7 mL). Silica (250 mg) was added, and the bomb was sealed. The bomb was removed from the glovebox, pressurized to 140 psi H_2 and heated to 80 °C. After 72 h, the bomb was cooled to rt and degassed. The silica was removed by filtration through a plug of celite. The filtrate was reduced *in vacuo*, and the residue was dissolved in a small amount of DCM and precipitated into MeOH to give the polymer as a yellow-green solid (0.42 g, 88%). $M_w = 27.8$ kDa, $M_n = 15.1$ kDa, PDI = 1.84. ^1H NMR (CD_2Cl_2 , 300 MHz) δ 0.93 (6H, mult), 1.27 – 1.40 (28H, mult), 1.52 – 1.59 (10H, mult), 1.87 (4H, mult), 2.61 (4H, t, $J = 7.5$ Hz), 4.05 (4H, t, $J = 6.6$ Hz), 7.07 – 7.19 (8H, mult), 7.42 – 7.46 (6H, mult) ppm. ^{13}C NMR (CD_2Cl_2 , 75 MHz) δ 14.2 (CH_3), 23.1 (CH_2), 26.4 (CH_2), 29.7 (CH_2), 29.9 (CH_2), 30.0 (CH_2), 31.9 (CH_2), 32.1 (CH_2), 36.1 (CH_2), 70.0 (OCH_2), 110.8 (Ar CH), 122.7 (vinylene CH), 126.7 (Ar CH), 127.2 (Ar quat), 129.0 (vinylene CH), 129.1 (Ar CH), 135.8 (Ar quat), 143.0 (Ar quat), 151.4 ppm (ArO quat). UV/VIS

absorbance (6.19×10^{-6} M, DCM) $\lambda_{\text{max}} = 391$ nm, $\epsilon = 78,400$. Fluorescent emission (6.19×10^{-6} M, DCM) $\lambda_{\text{max}} = 445, 469$ nm. Analysis Calcd: C, 85.12; H, 9.84. Found: C, 81.46; H, 9.62.

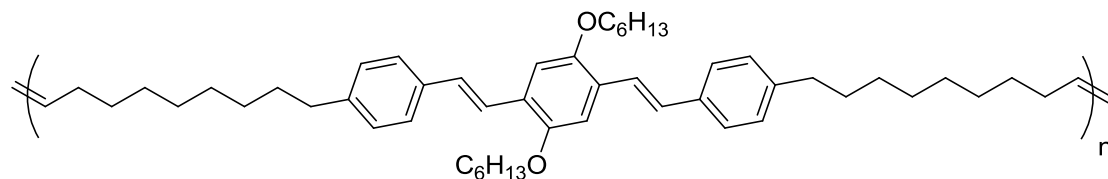


Tandem ADMET polymerization/hydrogenation – p32 (ii95). In a nitrogen-filled glovebox, **32** (0.50 g, 0.77 mmol) was dissolved in toluene (10 mL), in a pear-shaped flask equipped with a stirbar. Grubbs catalyst I (29 mg, 24 μmol) and diphenyl ether (200 mg, 1.2 mmol) were added, and the reaction mixture was removed from the glovebox. While stirring, the toluene was slowly removed under vacuum. Once all toluene had been removed, the reaction mixture was heated to 50 °C under vacuum. After 30 h, the stirbar became immobilized, and the reaction mixture was cooled to RT and returned to the glovebox. ^1H NMR spectroscopy revealed no remaining terminal olefin. The reaction mixture was transferred to a stainless steel bomb with toluene (7 mL). Silica (250 mg) was added, and the bomb was sealed. The bomb was removed from the glovebox, pressurized to 140 psi H_2 and heated to 80 °C. After 30 h, the bomb was cooled to rt and degassed. Continuous extraction of the reaction mixture with DCM over 72 h followed by removal of the solvent gave the polymer as a yellow-green solid (0.39 g, 81%). $M_w = 22.8$ kDa, $M_n = 13.1$ kDa, PDI = 1.74. ^1H NMR (CD_2Cl_2 , 300 MHz) δ 0.93 (6H, mult), 1.25-1.65 (36H, mult), 1.70-1.90 (8H, mult), 3.98 (4H, t, $J = 6.6$ Hz), 4.04 (4H, t, $J = 6.6$ Hz), 6.89 (4H, d, $J = 8.7$ Hz, *p*- C_6H_4), 7.09 (1H, d, $J = 16.5$ Hz, *trans* CH=CH), 7.11 (1H, s), 7.34 (1H, d, $J = 16.5$ Hz, *trans* CH=CH), 7.46 (4H, d, $J = 8.7$ Hz, *p*- C_6H_4) ppm. ^{13}C NMR (CD_2Cl_2 , 75 MHz) δ 14.40 (CH_3), 23.25 (CH_2), 26.54 (CH_2), 29.86 (CH_2), 29.92 (CH_2), 30.09 (CH_2), 30.26 (CH_2), 32.24

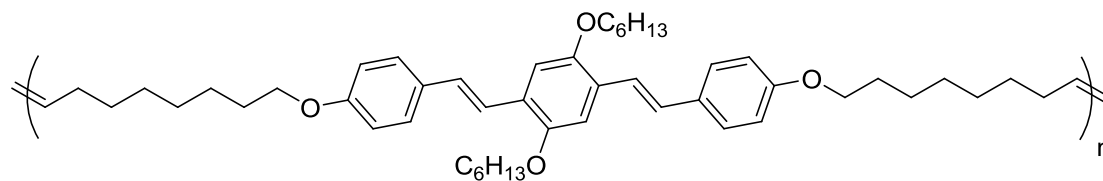
(CH₂), 68.67 (OCH₂), 70.14 (OCH₂), 110.82 (Ar CH), 115.25 (Ar CH), 121.64 (vinylene CH), 127.29 (Ar quat), 128.17 (Ar CH), 128.67 (vinylene CH), 131.14 (Ar quat), 151.52 (ArO quat), 159.48 (ArO quat) ppm. UV/VIS absorbance (DCM) $\lambda_{\text{max}} = 393$ nm, $\epsilon = 40,700$. Fluorescent emission (DCM) $\lambda_{\text{max}} = 447, 475$ nm.



ADMET polymerization in DCM without hydrogenation – p30 (iii69). **30** (200 mg, 0.284 mmol) and Grubbs I (5.0 mg, 6.1 μmol) were dissolved in DCM (4 mL) and refluxed for 24 h under N₂. The reaction mixture was precipitated into MeOH and the polymer was isolated by filtration as 192 mg (100%) of a yellow solid. $M_w = 43.3$ kDa, $M_n = 20.6$ kDa, PDI = 1.66.

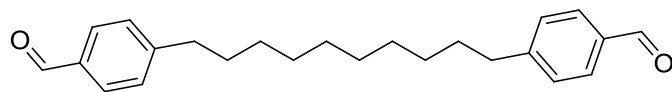


ADMET polymerization in DCM without hydrogenation – p31 (iii74). **31** (200 mg, 0.263 mmol) and Grubbs I (5.0 mg, 6.1 μmol) were dissolved in DCM (4 mL) and refluxed for 24 h under N₂. The reaction mixture was precipitated into MeOH and the polymer was isolated by filtration as 190 mg (99%) of a yellow solid. $M_w = 62.5$ kDa, $M_n = 30.6$ kDa, PDI = 2.05.



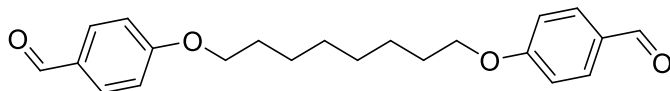
ADMET polymerization in DCM without hydrogenation – p34 (iii67). **34** (210 mg, 0.275 mmol) and Grubbs I (5.0 mg, 6.1 μ mol) were dissolved in DCM (4 mL) and refluxed for 24 h under N_2 . The reaction mixture was precipitated into MeOH and the polymer was isolated by filtration as 204 mg (100%) of a yellow solid. $M_w = 39.4$ kDa, $M_n = 21.9$ kDa, PDI = 1.80.

4.3.3 Rod-coil copolymers prepared by HWE

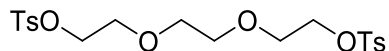


1,10-bis(4-formylphenyl)decane (D, ii104). A solution of 9-H-9-BBN in THF (0.5 M, 26 mL, 13 mmol) was added dropwise to 1,9-decadiene (1.2 mL, 6.51 mmol) under N_2 with stirring. The mixture was stirred for 48 h at rt and 20 h at 45 $^{\circ}C$. Then, $PdCl_2(PPh_3)_2$ (390 mg, 0.56 mmol), 4-bromobenzaldehyde 5.00 g, 27.0 mmol), and 2.0 M Na_2CO_3 (20 mL) were added. The reaction mixture was stirred at 45 $^{\circ}C$ under N_2 for 72 h. The mixture was cooled to rt. The aqueous layer was extracted with DCM (2x 30 mL). The combined organic layers were then washed with brine (50 mL), dried over $MgSO_4$, and reduced *in vacuo*. The crude product was purified column chromatography (silica gel, 3:1 hexanes:Et₂O) to give the title compound as a white solid (1.44 g, 63%). 1H NMR ($CDCl_3$, 300 MHz) δ 1.35-1.45 (12H, mult), 1.62 (4H, pent, $J = 6.9$ Hz), 2.67 (4H, t, $J = 7.5$ Hz), 7.31 (4H, d, $J = 8.1$ Hz), 7.78 (4H, d, $J = 8.1$ Hz), 9.95 (1H, s, CHO). ^{13}C NMR ($CDCl_3$, 75 MHz) δ 28.79 (CH_2), 28.90 (CH_2), 29.08 (CH_2), 31.02 (CH_2), 36.20 (CH_2), 128.09 (Ar CH), 129.91 (Ar CH), 134.42 (Ar quat), 150.43 (Ar quat), 192.06 (CHO) ppm. MS

(EI): 350 (M^+), 181, 161, 133, 120, 91 (base), 82, 67, 55 m/z. HRMS calcd for $C_{24}H_{30}O_2$: 350.2246 g/mol. Found: 350.2250 g/mol.



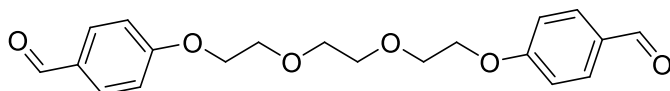
1,8-bis(4-formylphenoxy)octane (O, vi70a). 1,8-dibromooctane (4.80 g, 17.6 mmol), 4-hydroxybenzaldehyde (8.60 g, 70.4 mmol), K_2CO_3 (10.0 g, 72.4 mmol), and KI (2.90 g, 17.5 mmol) were added to dry MeCN (100 mL) and refluxed for 4 h. The reaction mixture was poured into 3 M NaOH (200 mL) and extracted into Et_2O (3x 100 mL). The combined ether layers were washed with 3 M NaOH (200 mL) and dried over $MgSO_4$. The solvent was removed *in vacuo* to give the title compound as a white solid (5.6 g, 90%). 1H NMR ($CDCl_3$, 300 MHz) δ 1.35 – 1.55 (8H, mult), 1.83 (4H, pent, $J = 6.6$ Hz), 4.05 (4H, t, $J = 6.6$ Hz), 6.99 (4H, d, $J = 8.7$ Hz), 7.83 (4H, d, $J = 8.7$ Hz), 9.88 (1H, s, CHO) ppm. ^{13}C NMR ($CDCl_3$, 75 MHz) δ 25.9 (CH_2), 29.0 (CH_2), 29.2 (CH_2), 68.3 (OCH_2), 114.7 (Ar CH), 129.7 (Ar quat), 132.0 (Ar CH), 164.2 (ArO quat), 190.8 (CHO) ppm. MS (EI) 354 (M^+), 326, 250, 233, 135, 123, 121, 105, 94, 81, 77, 69, 65, 55 (base) m/z. HRMS calcd for $C_{22}H_{26}O_4$: 354.1831 g/mol. Found: 354.1824.



2,2'-(ethane-1,2-diylbis(oxy))bis(ethane-2,1-diyl) bis(4-methylbenzenesulfonate) (vi68a).

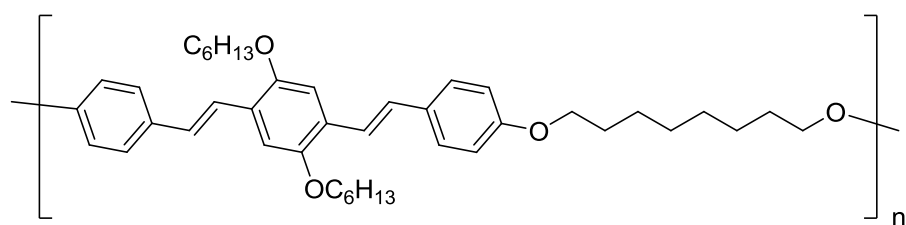
According to the methods of Bonger, *et al.*,¹⁰⁶ triethylene glycol (2.5 mL, 18.3 mmol) and TsCl (6.96 g, 36.6 mmol) were dissolved in DCM (20 mL) and cooled to 0 °C. Powdered KOH (8.21 g, 141 mmol) was added portionwise over 10 min, and the reaction mixture was stirred at 0 °C for 3 h. The mixture was proportioned between water (50 mL) and DCM (50 mL). The aqueous

layer was extracted with DCM (2x 50 mL). The combined organic layers were washed with water (50 mL) and brine (50 mL) and dried over MgSO₄. The solvent was removed *in vacuo* to give the title compound as a white solid (8.0 g, 95%). ¹H NMR (CDCl₃, 300 MHz) δ 2.31 (6H, s), 3.53 (4H, s), 3.66 (4H, t, *J* = 4.8 Hz), 4.14 (4H, t, *J* = 4.8 Hz), 7.34 (4H, dd, *J* = 6.6, 1.8 Hz), 7.79 (4H, dd, *J* = 6.6, 1.8 Hz) ppm. ¹³C NMR (CDCl₃, 75 MHz) δ 21.6 (ArCH₃), 68.7 (OCH₂), 69.1 (OCH₂), 70.6 (OCH₂), 127.9 (Ar CH), 129.8 (Ar CH), 132.7 (Ar quat), 144.8 (ArSO₂ quat) ppm.

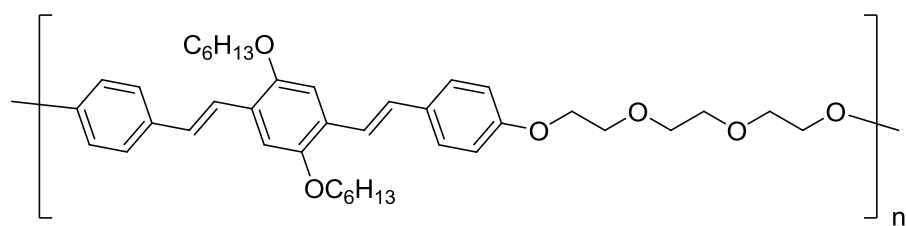


1,2-bis(2-(4-formylphenoxy)ethoxy)ethane (T, vi69a). **vi68a** (8.0 g, 17.4 mmol), 4-hydroxybenzaldehyde (8.60 g, 70.4 mmol), and K₂CO₃ (10.0 g, 72.4 mmol), were added to dry MeCN (100 mL) and refluxed for 4 h. The reaction mixture was poured into 3 M NaOH (200 mL) and extracted into Et₂O (3x 100 mL). The combined ether layers were washed with 3 M NaOH (200 mL) and dried over MgSO₄. The solvent was removed *in vacuo* to give the title compound as a white solid (6.1 g, 98%). ¹H NMR (CDCl₃, 300 MHz) 3.76 (4H, s), 3.89 (4H, t, *J* = 4.8 Hz), 4.20 (4H, t, *J* = 4.8 Hz), 6.99 (4H, dd, *J* = 6.9, 1.8 Hz), 7.80 (4H, dd, *J* = 6.9, 1.8 Hz), 9.87 (1H, s, CHO) ppm. ¹³C NMR (CDCl₃, 75 MHz) δ 67.6 (OCH₂), 69.5 (OCH₂), 70.8 (OCH₂), 114.0 (Ar CH), 130.0 (Ar quat), 131.4 (Ar CH), 163.7 (ArO quat), 190.7 (CHO) ppm. MS (EI): 358 (M⁺), 254, 224, 210, 193, 181, 149 (base), 131, 121, 105 m/z. HRMS calcd for C₂₀H₂₂O₆: 358.1416 g/mol. Found 358.1433 g/mol.

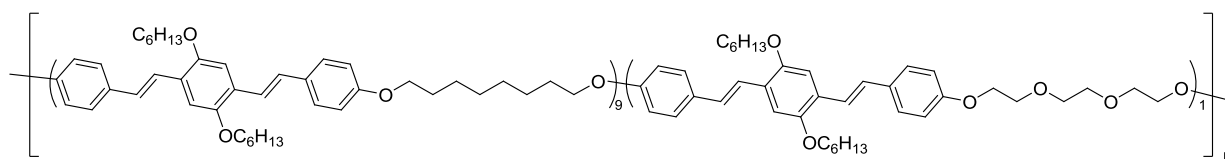
General HWE polycondensation procedure (vi72). A solution of **22** in THF (0.10 M, 10 mL, 1 mmol) and various ratios of solutions of dialdehyde linkers in THF (0.10 M, 10 mL total, 1 mmol, total) were added to an oven-dried rbf and cooled to 0 °C under N₂. KO^tBu (450 mg, 4.01 mmol) was added portionwise over 5 min and the mixtures were allowed to come to rt overnight with stirring. The mixture was poured into cold MeOH (150 mL), and the polymers were isolated by filtration.



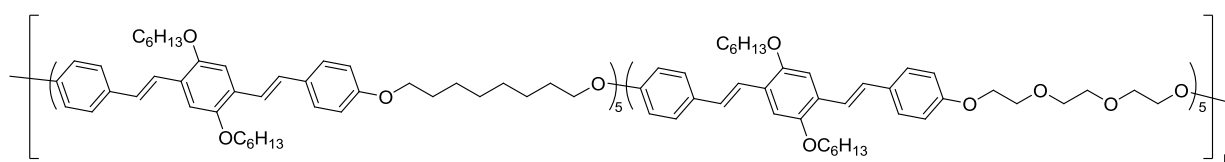
PV-O (vi73). Following the general HWE polycondensation procedure, **O** (0.1 M in THF, 10 mL, 1 mmol) was copolymerized with **22** (0.1 M in THF, 10 mL, 1 mmol). The polymer was isolated as 554 mg (89%) of a yellow-orange solid. $M_w = 69.0$ kDa, $M_n = 48.7$ kDa, PDI = 1.42.



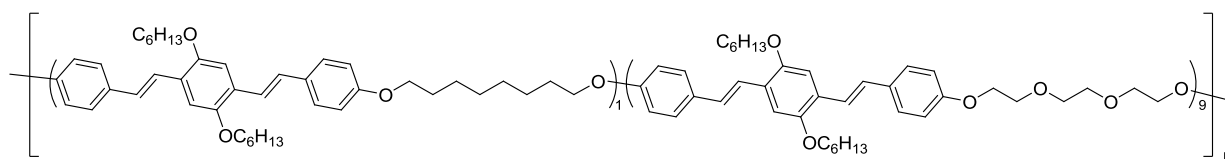
PV-T (vi74). Following the general HWE polycondensation procedure, **T** (0.1 M in THF, 10 mL, 1 mmol) was copolymerized with **22** (0.1 M in THF, 10 mL, 1 mmol). The polymer was isolated as 590 mg (94%) of a yellow-orange solid. $M_w = 49.3$ kDa, $M_n = 36.5$ kDa, PDI = 1.35.



PV-O₉T₁ (vi75). Following the general HWE polycondensation procedure, **O** (0.1 M in THF, 9 mL, 0.9 mmol) and **T** (0.1 M in THF, 1 mL, 0.1 mmol) were copolymerized with **22** (0.1 M in THF, 10 mL, 1 mmol). The polymer was isolated as 575 mg (92%) of a yellow-orange solid. $M_w = 71.1$ kDa, $M_n = 51.8$ kDa, PDI = 1.38.



PV-O₅T₅ (vi77). Following the general HWE polycondensation procedure, **O** (0.1 M in THF, 5 mL, 0.5 mmol) and **T** (0.1 M in THF, 5 mL, 0.5 mmol) were copolymerized with **22** (0.1 M in THF, 10 mL, 1 mmol). The polymer was isolated as 509 mg (81%) of a yellow-orange solid. $M_w = 74.0$ kDa, $M_n = 57.8$ kDa, PDI = 1.28.



PV-O₁T₉ (vi76). Following the general HWE polycondensation procedure, **O** (0.1 M in THF, 1 mL, 0.1 mmol) and **T** (0.1 M in THF, 9 mL, 0.9 mmol) were copolymerized with **22** (0.1 M in THF, 10 mL, 1 mmol). The polymer was isolated as 505 mg (82%) of a yellow-orange solid. $M_w = 74.0$ kDa, $M_n = 57.8$ kDa, PDI = 1.28.

APPENDIX A: CHAPTER 2

A.1 ^1H AND ^{13}C NMR SPECTRA OF NEW COMPOUNDS

Figure 29. ^1H and ^{13}C NMR spectra of compound 1.

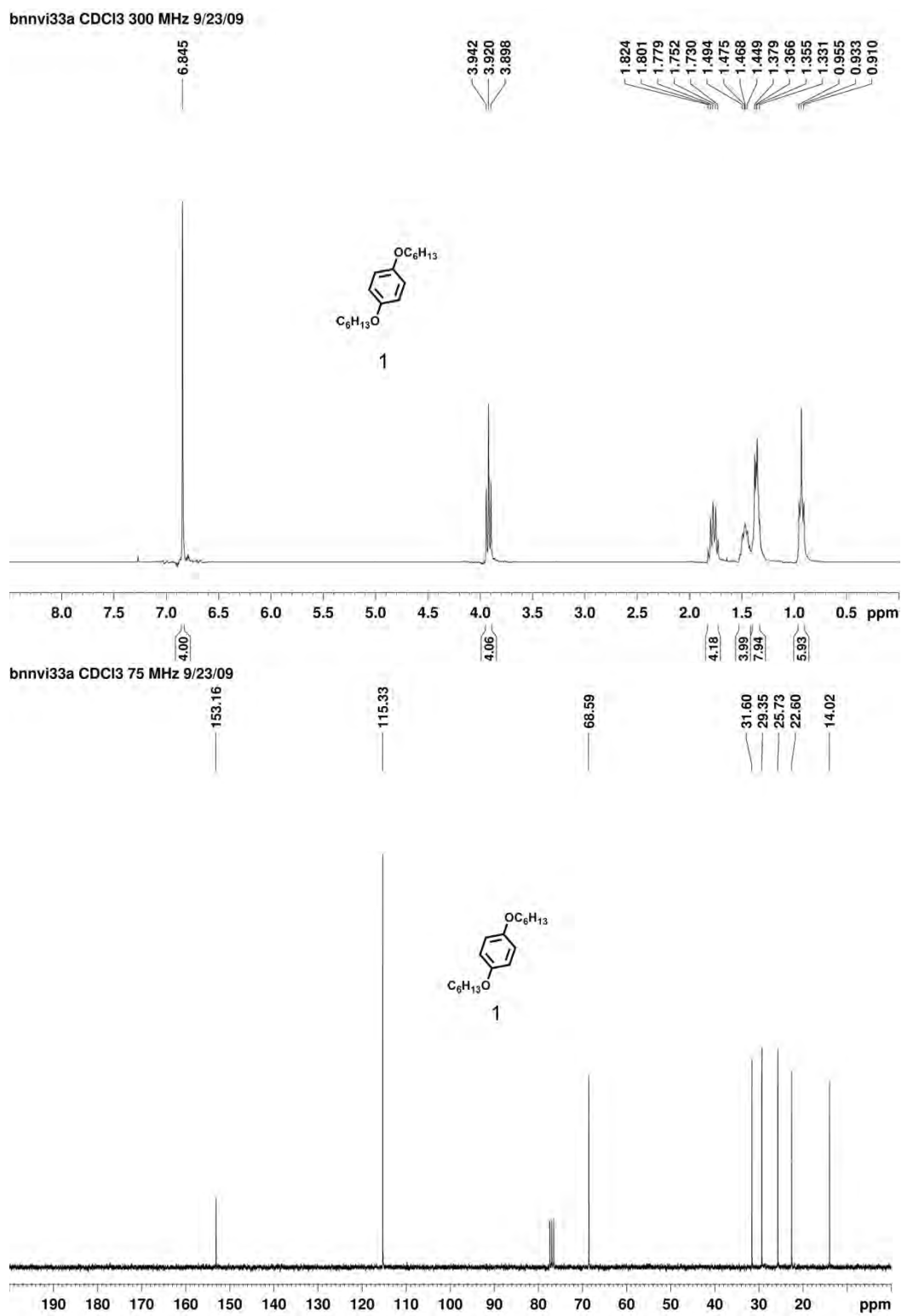
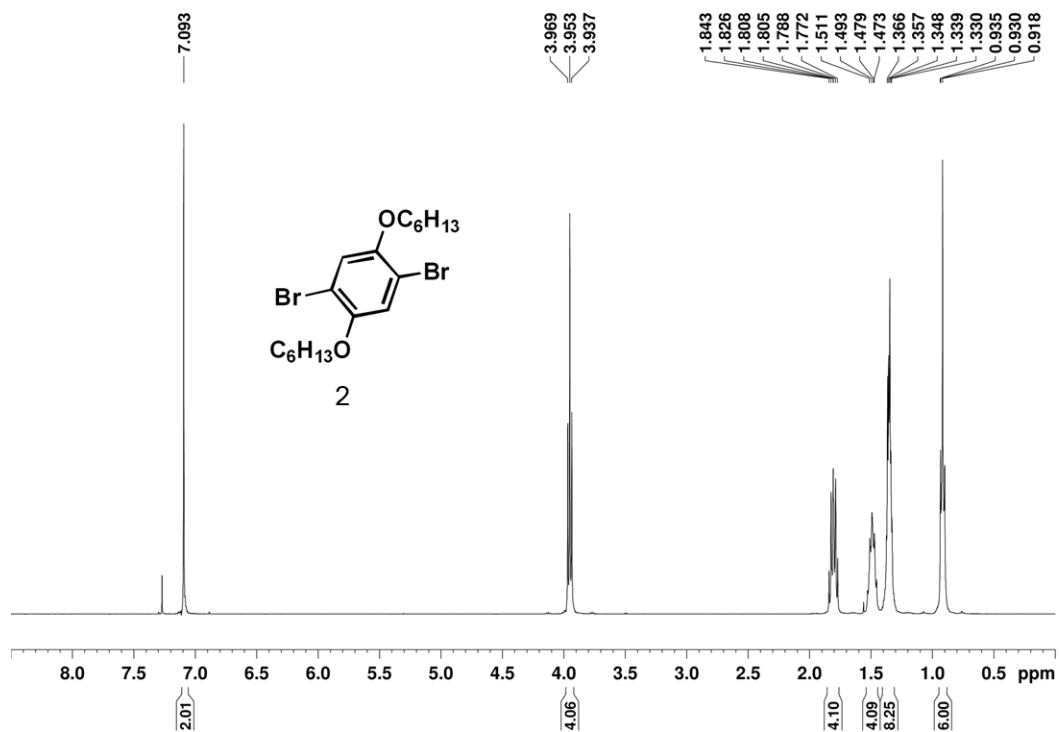


Figure 30. ^1H and ^{13}C NMR spectra of compound 2.

bnnvi35a CDCl₃ 400 MHz 9/5/10



bnnvi35a CDCl₃ 100 MHz 9/5/10

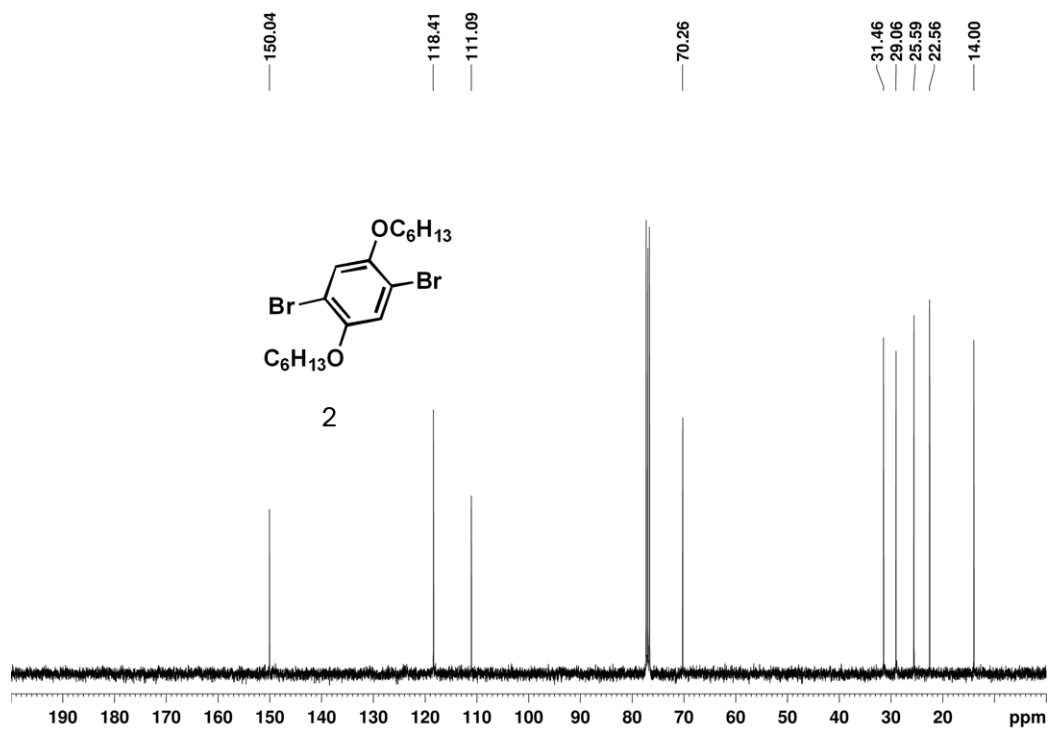
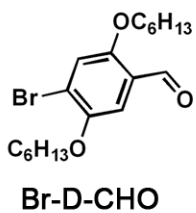
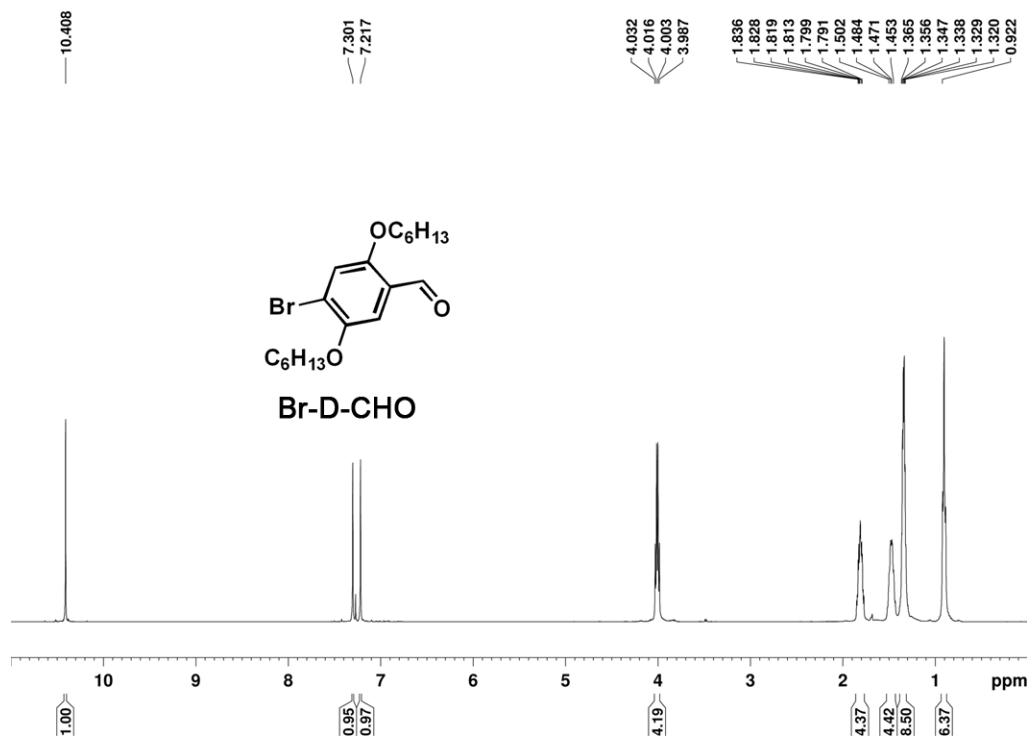


Figure 31. ^1H and ^{13}C NMR spectra of Br-D-CHO.

bnnvi39a CDCl₃ 400 MHz 9/5/10



bnnvi39a CDCl₃ 100 MHz 9/5/10

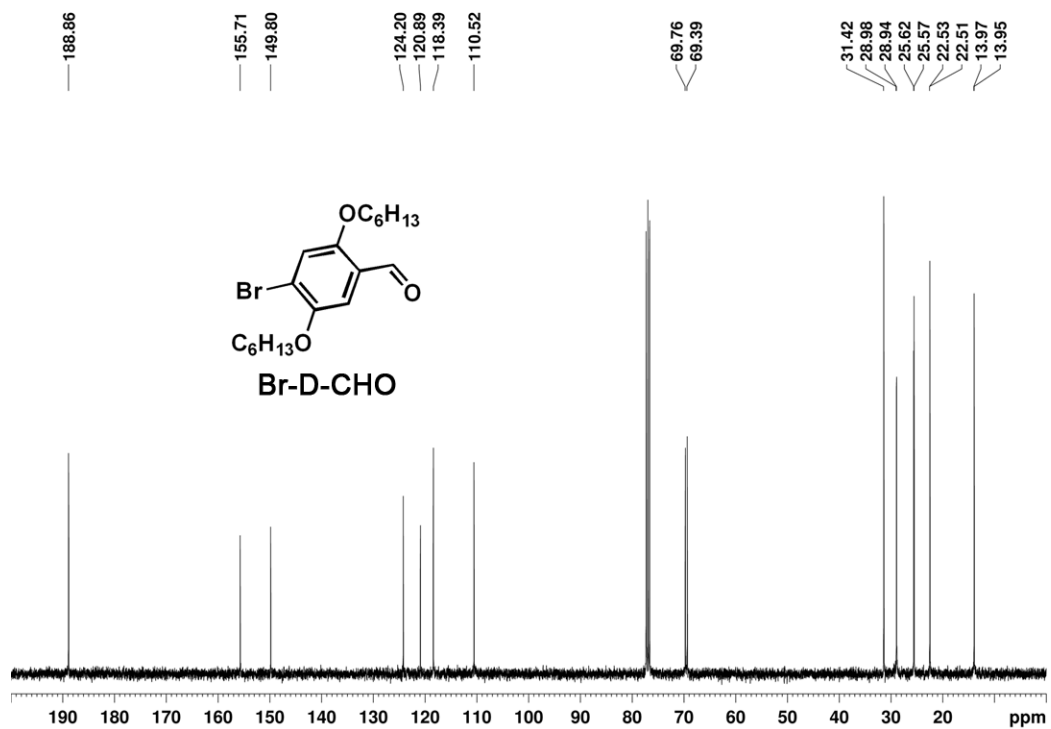
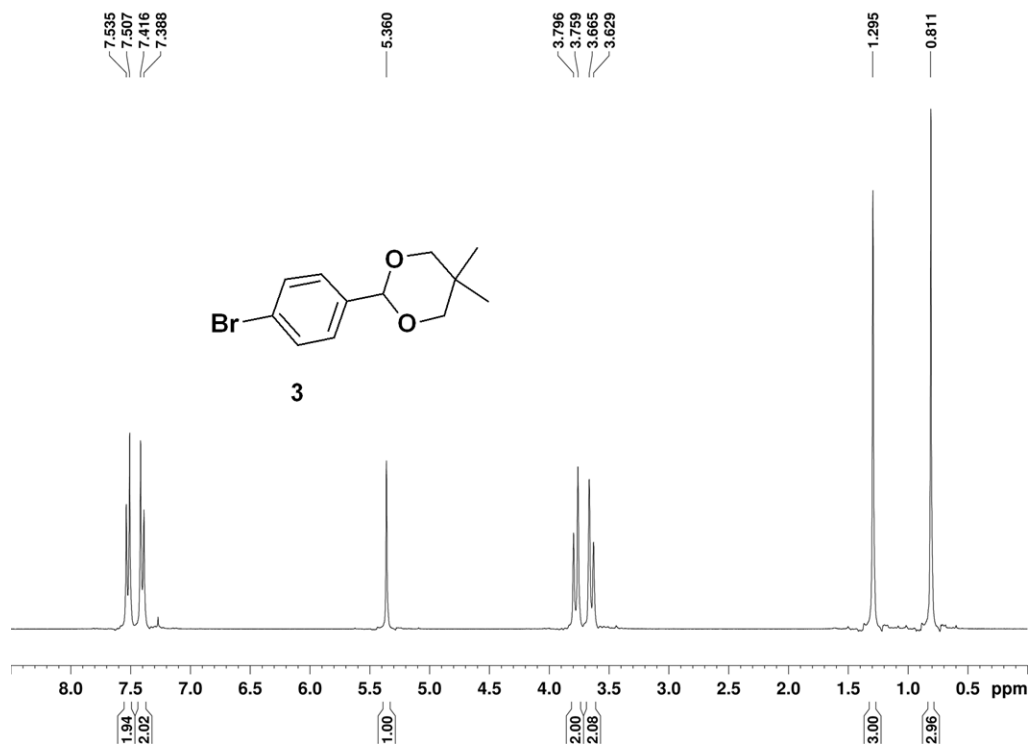


Figure 32. ^1H and ^{13}C NMR spectra of compound 3.

bnnv70b CDCl₃ 300 MHz 6/2/09



bnnv70b CDCl₃ 75 MHz 6/2/09

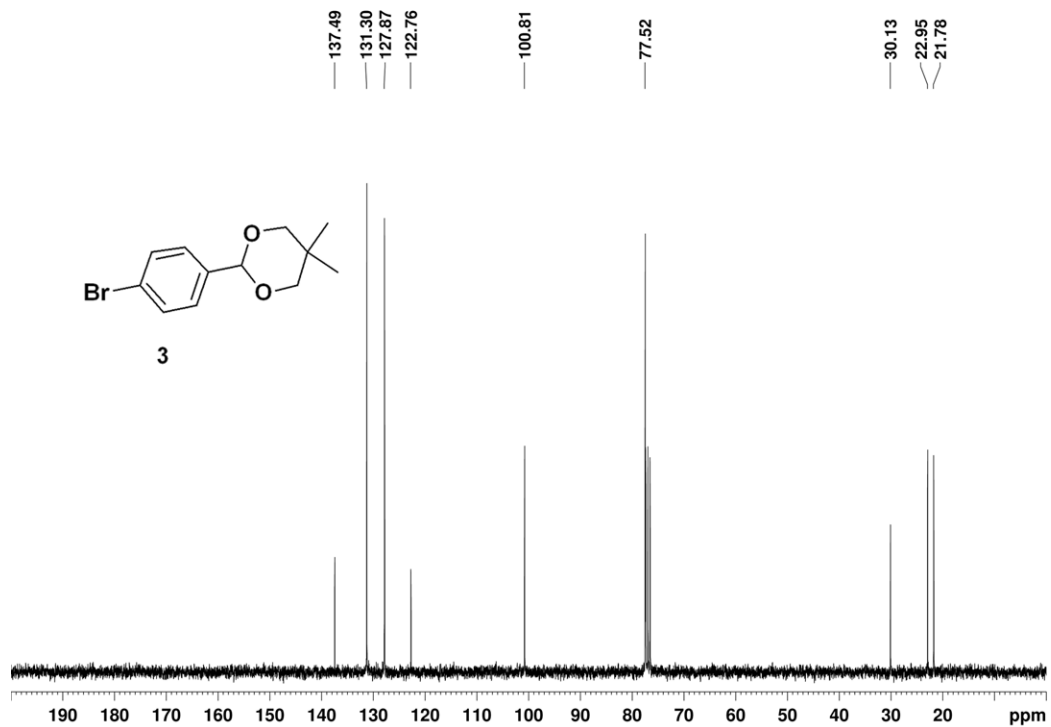


Figure 33. ^1H and ^{13}C NMR spectra of compound 4.

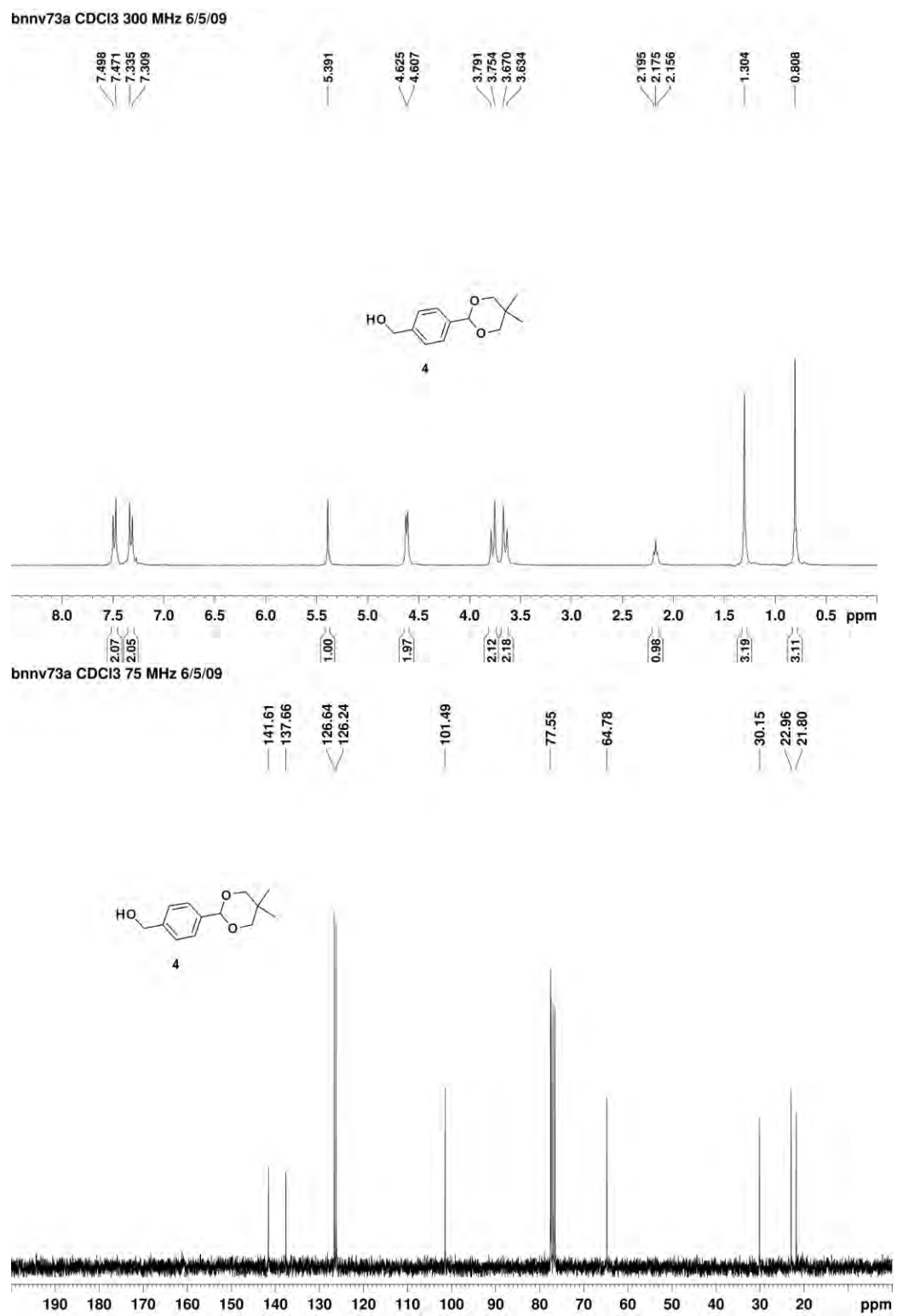


Figure 34. ^1H and ^{13}C NMR spectra of compound 5.

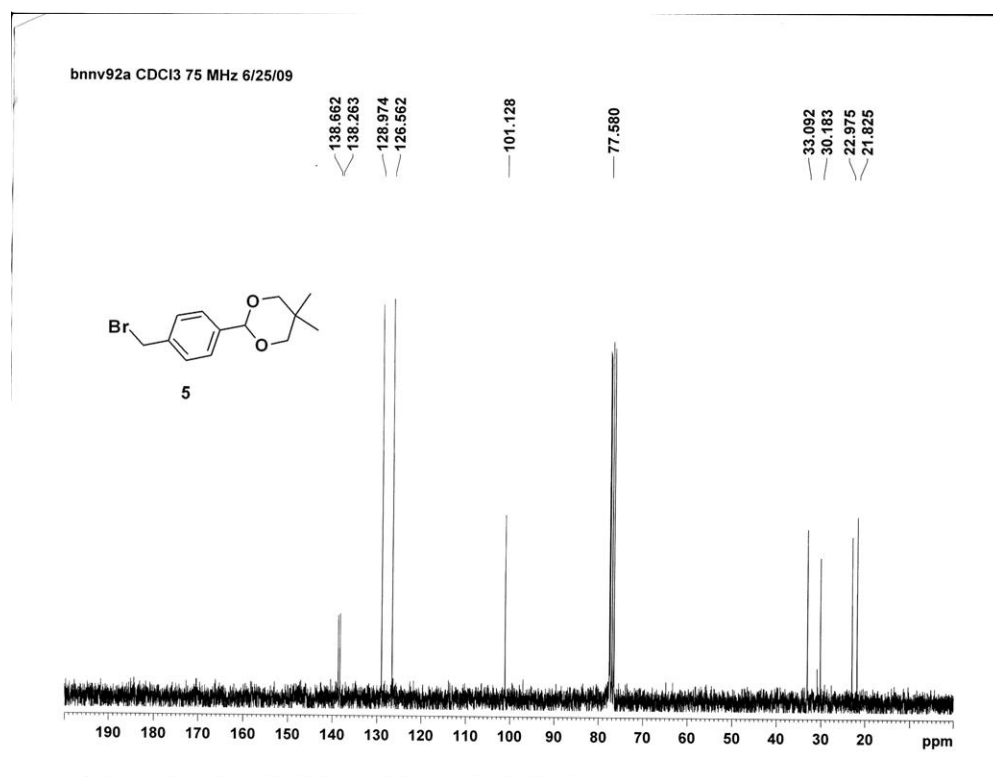
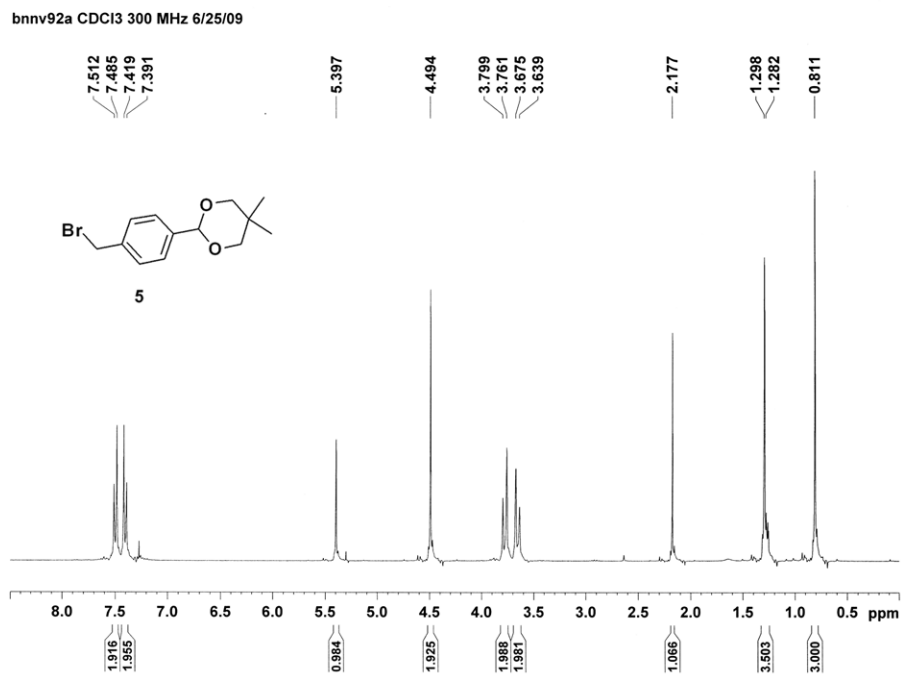
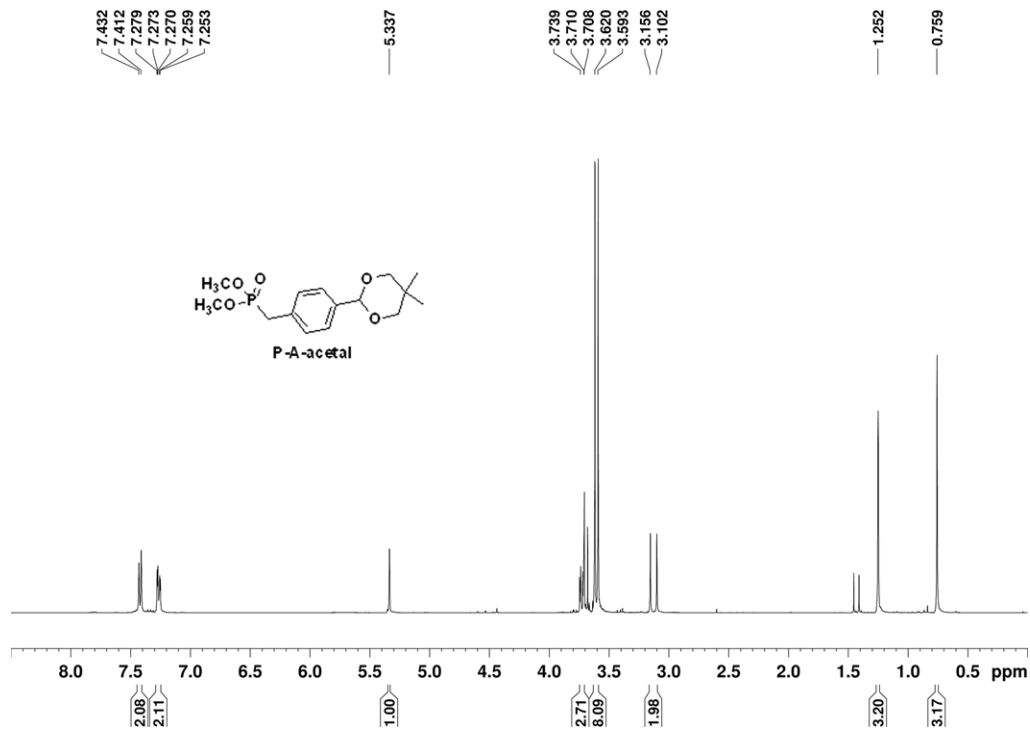


Figure 35. ^1H and ^{13}C NMR spectra of P-A-acetal.

bnnv97a CDCl₃ 400 MHz 12/28/10



bnnv97a CDCl₃ 100 MHz 12/28/10

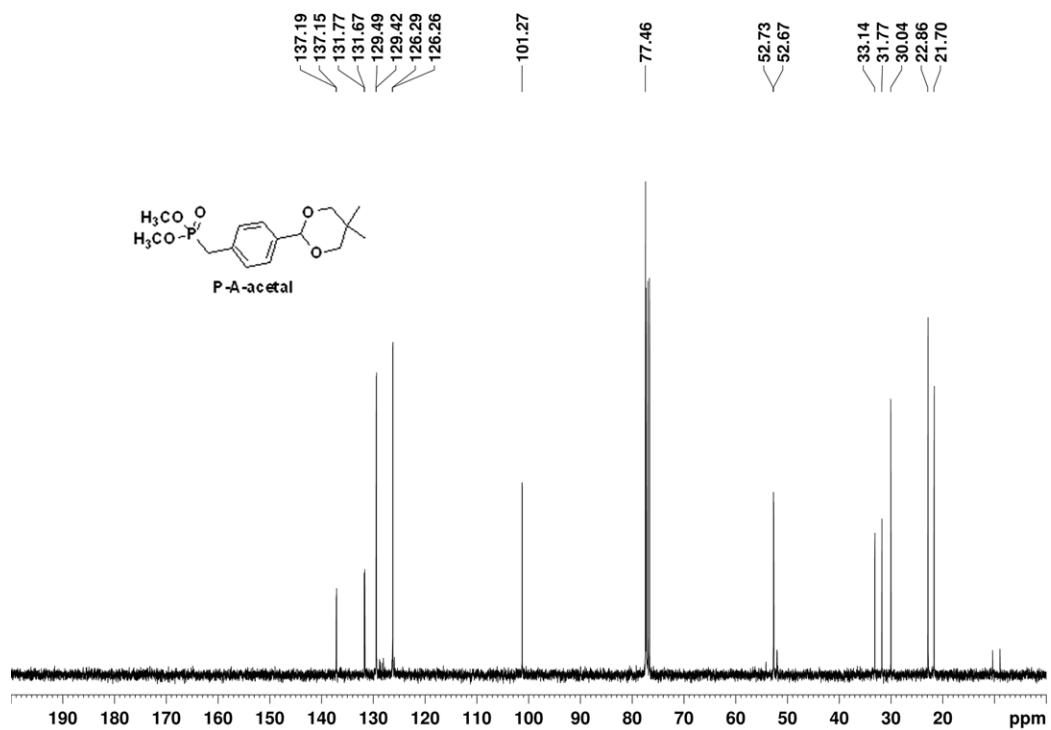
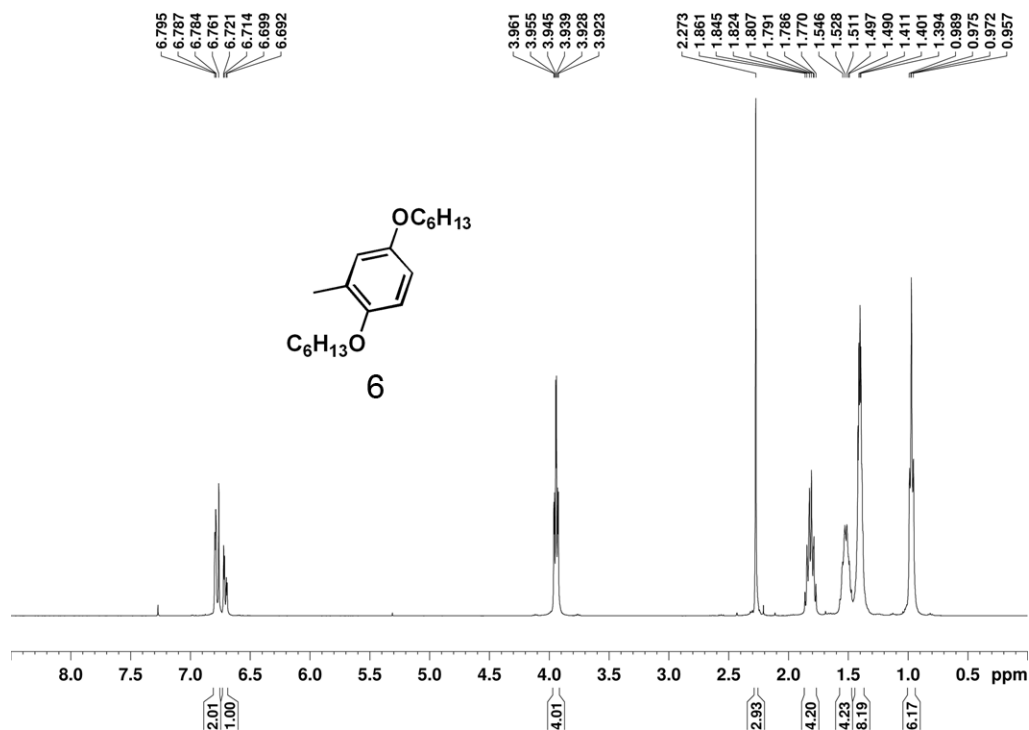


Figure 36. ^1H and ^{13}C NMR spectra of compound 6.

bnniv89a CDCl₃ 400 MHz 9/5/10



bnniv89a CDCl₃ 400 MHz 9/5/10

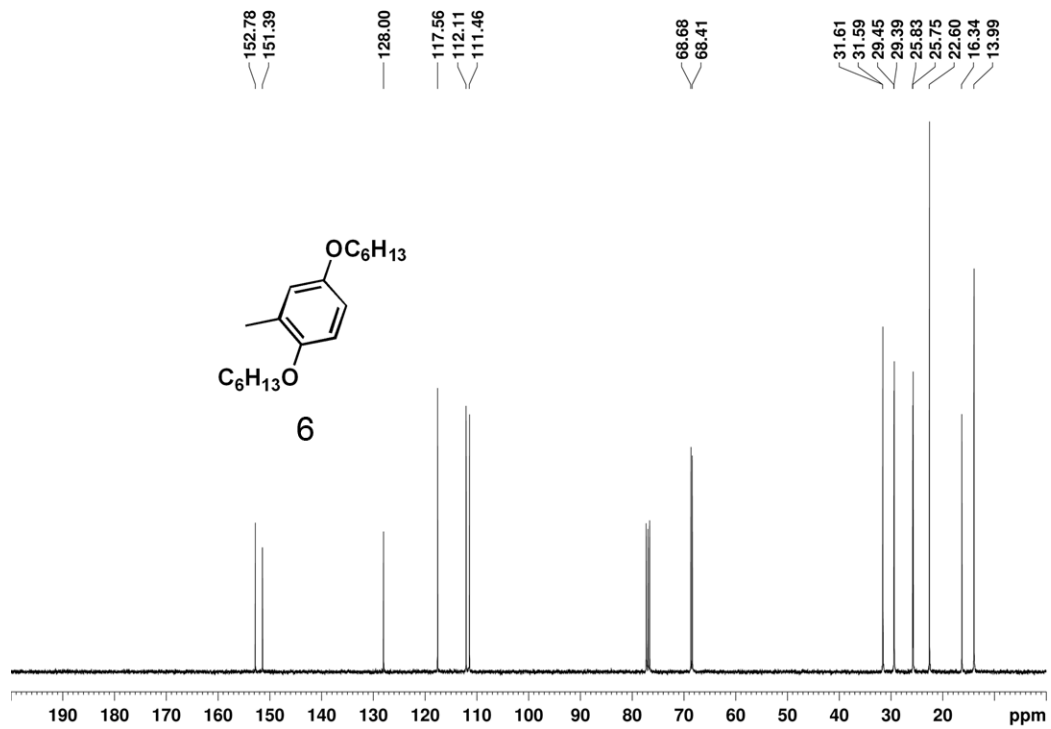


Figure 37. ^1H spectrum of compound 7.

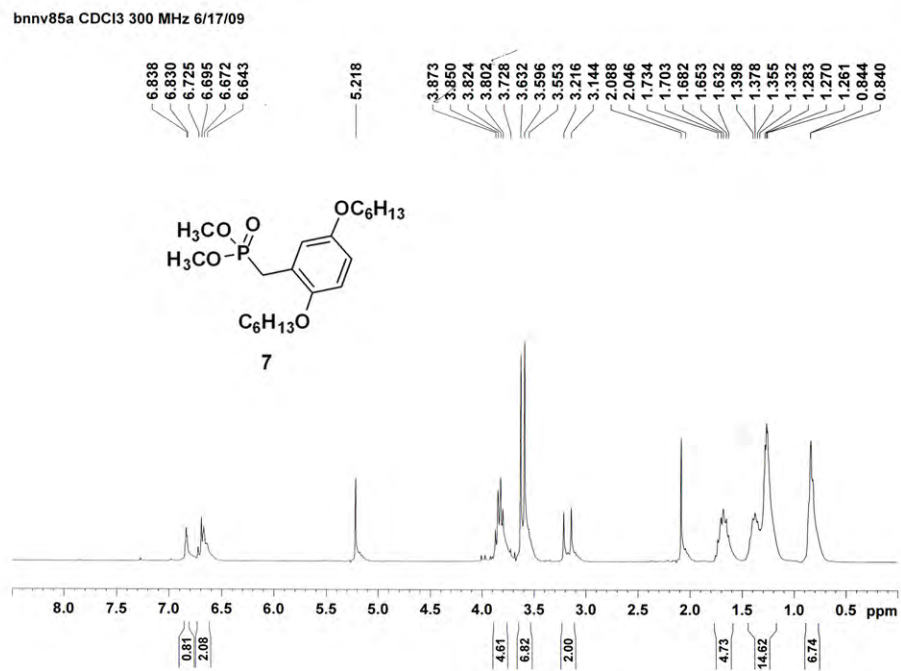


Figure 38. ^1H and ^{13}C NMR spectra of compound **8**.

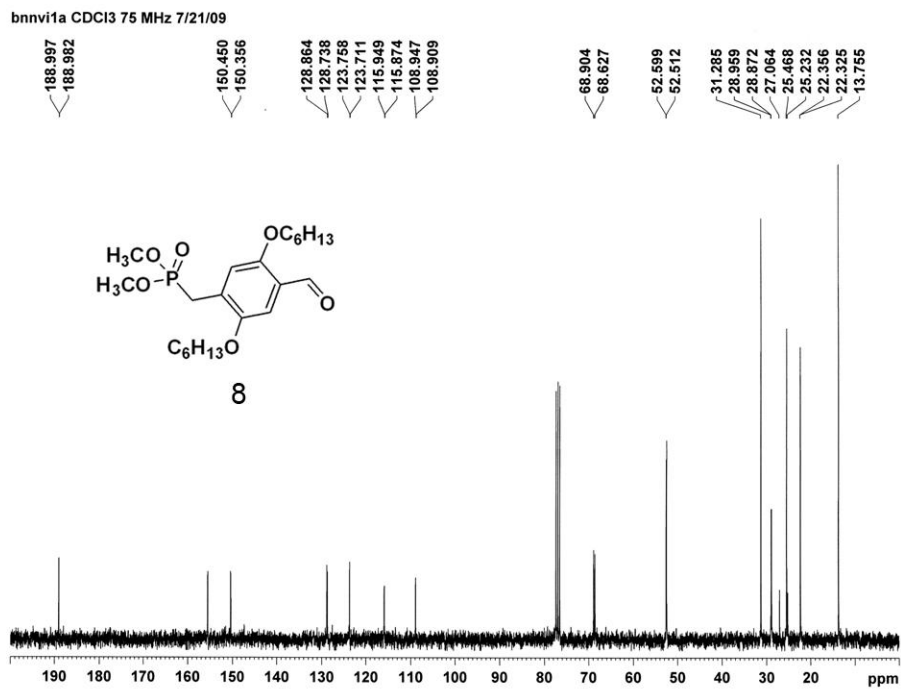
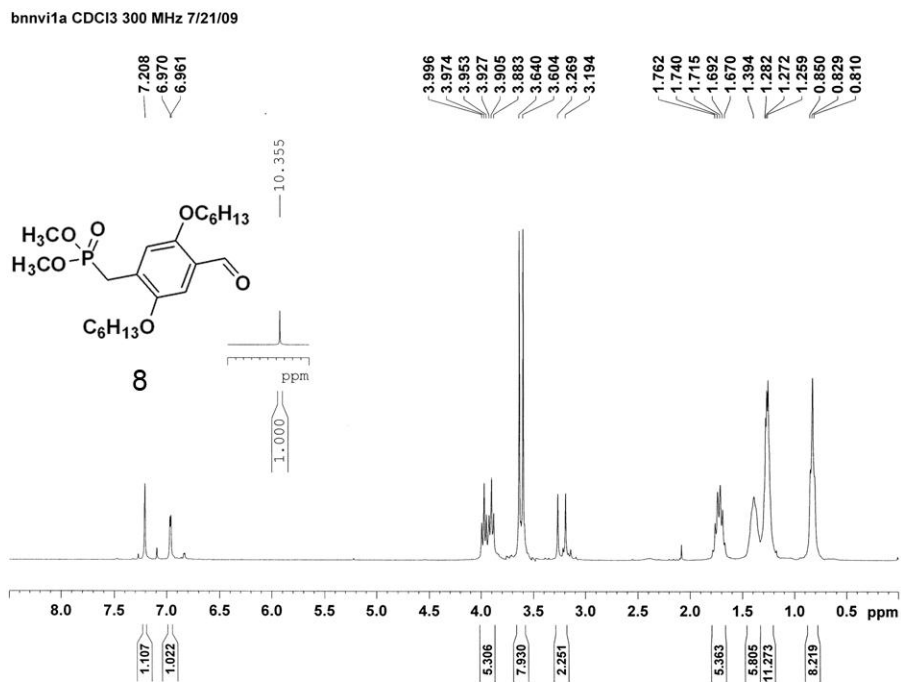


Figure 39. ^1H and ^{13}C NMR spectra of P-D-acetal.

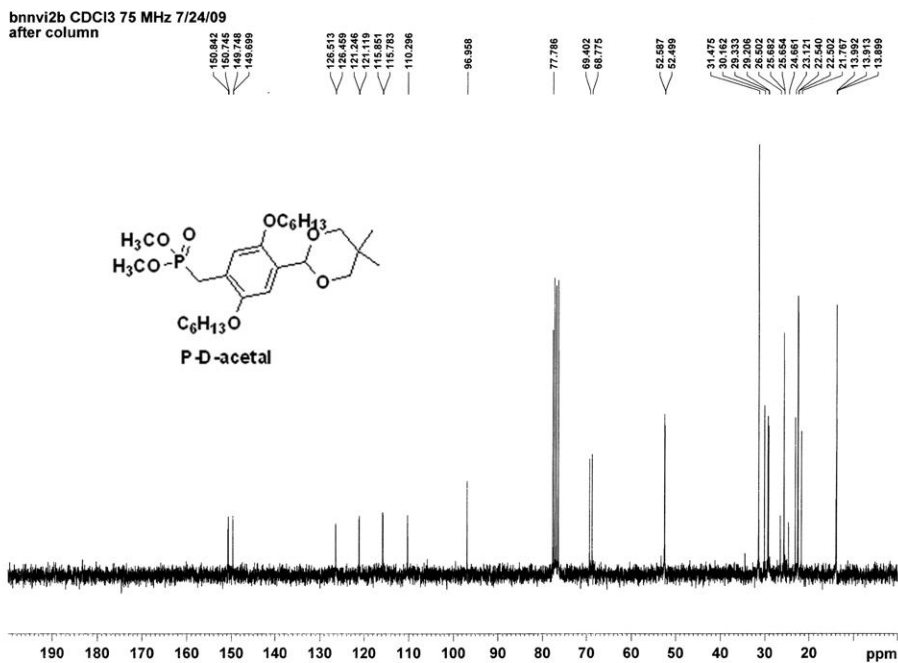
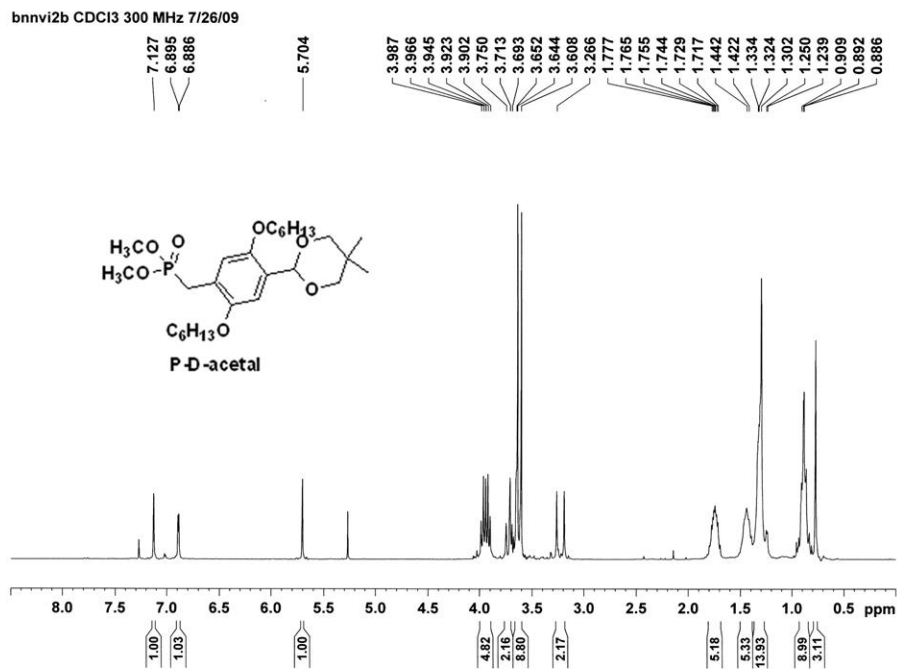
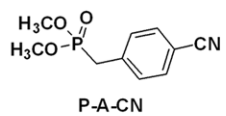
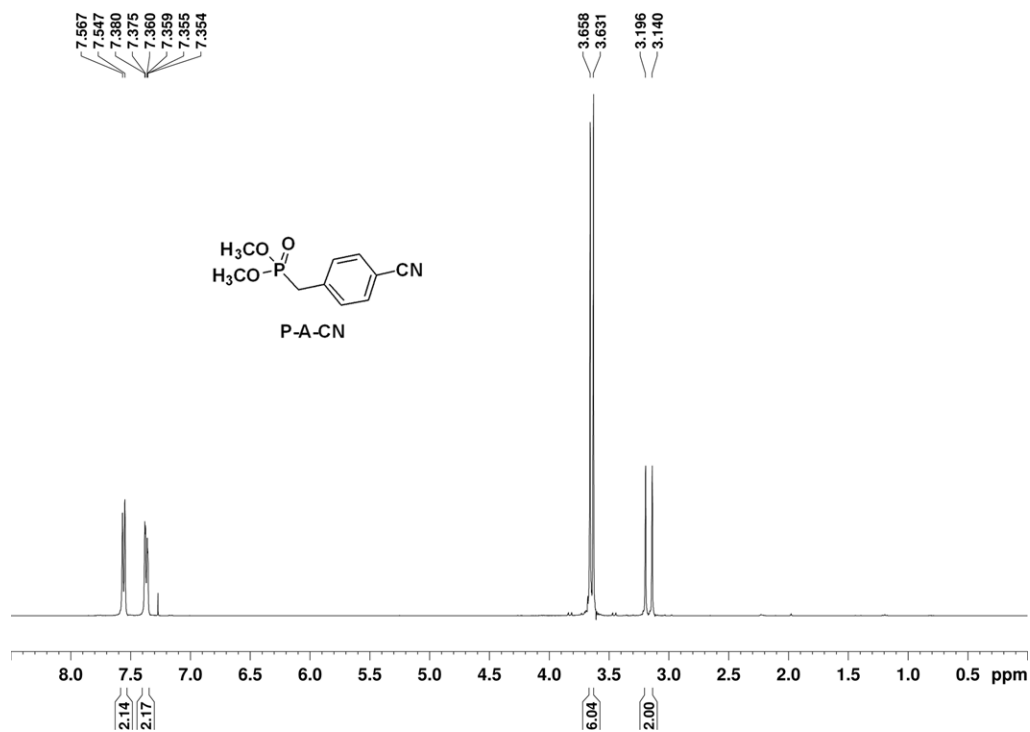


Figure 40. ^1H and ^{13}C NMR spectra of P-A-CN.

bnnvi99a CDCl₃ 400 MHz 9/5/10



bnnvi99a CDCl₃ 100 MHz 9/5/10

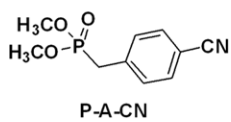
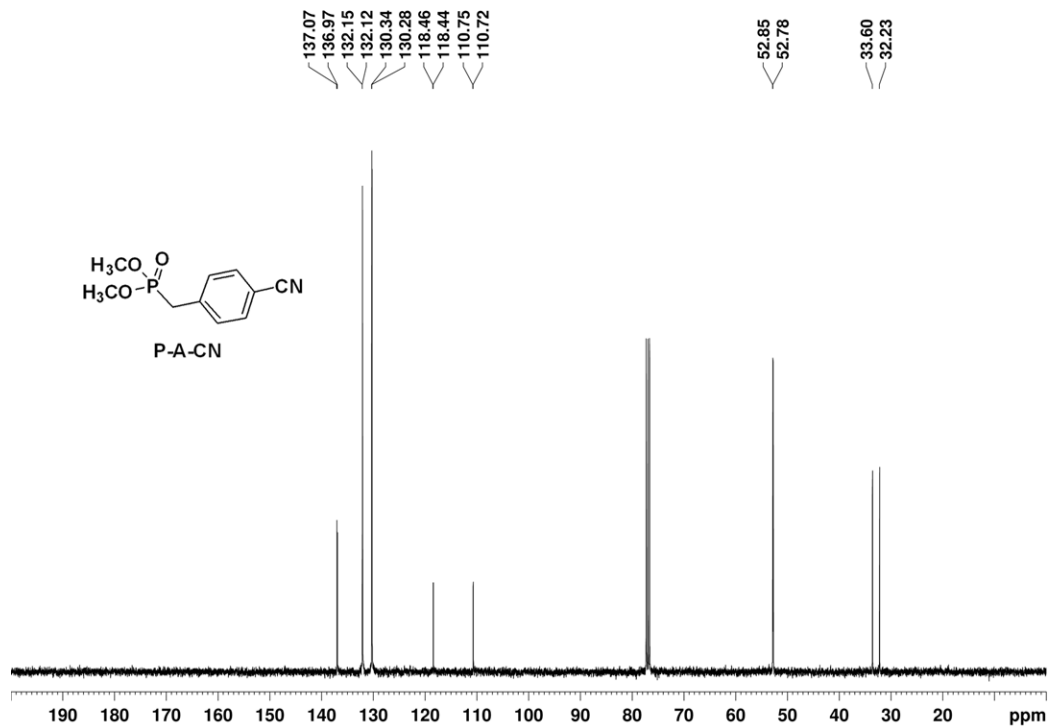
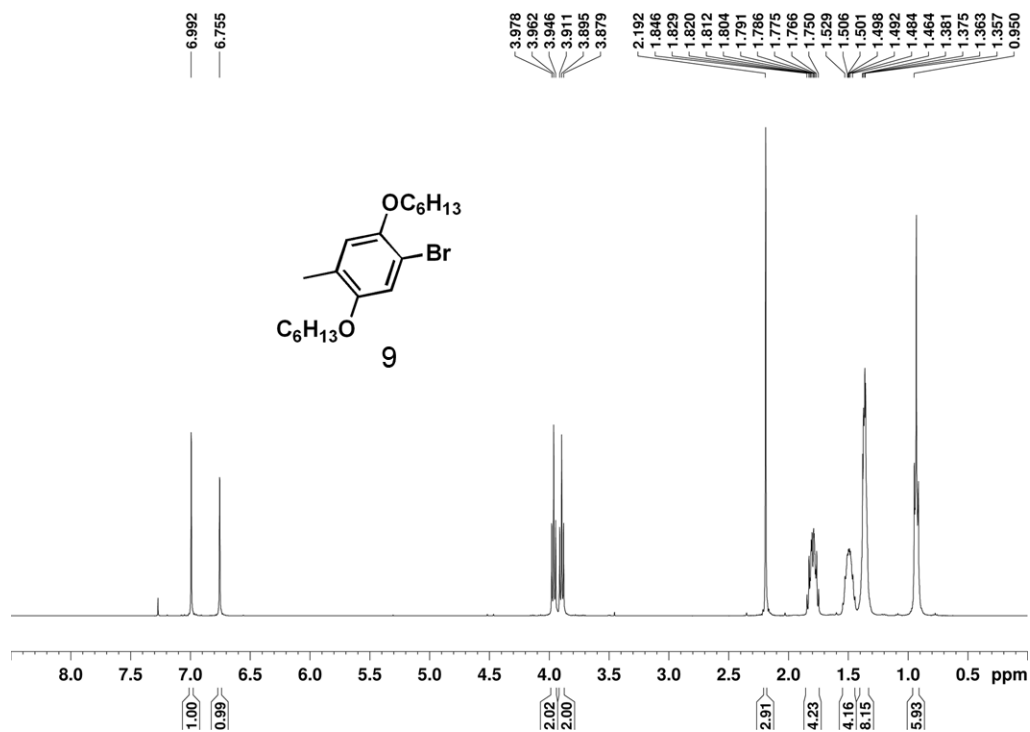


Figure 41. ^1H and ^{13}C NMR spectra of compound **9**.

bnnvi104a CDCl₃ 400 MHz 9/5/10



bnnvi104a CDCl₃ 100 MHz 9/5/10

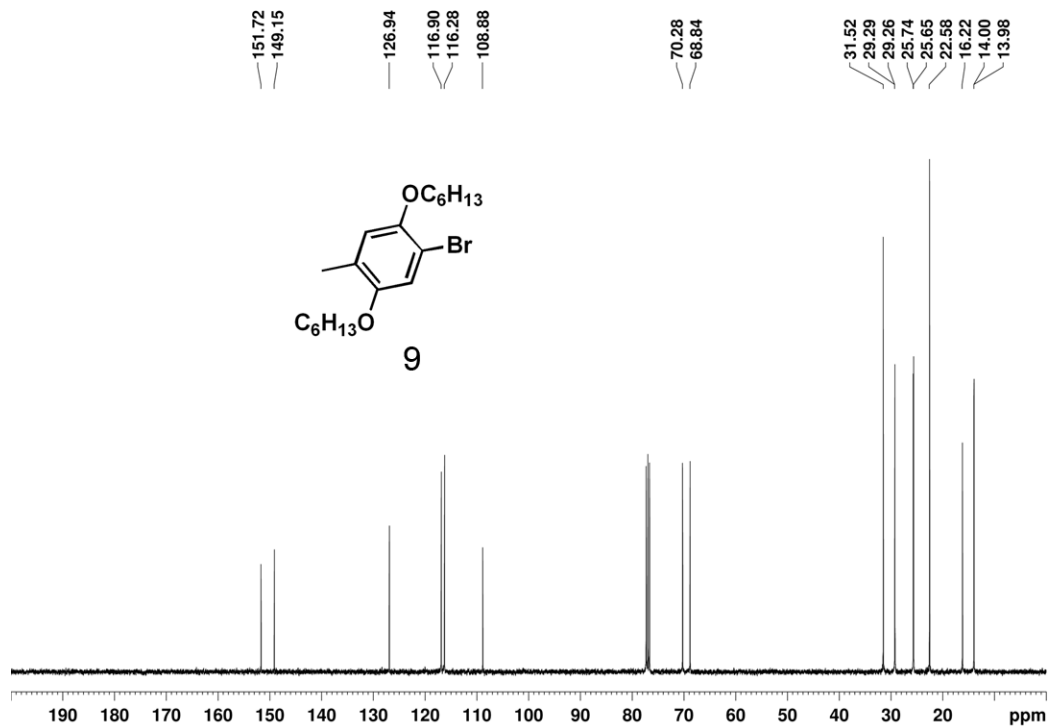
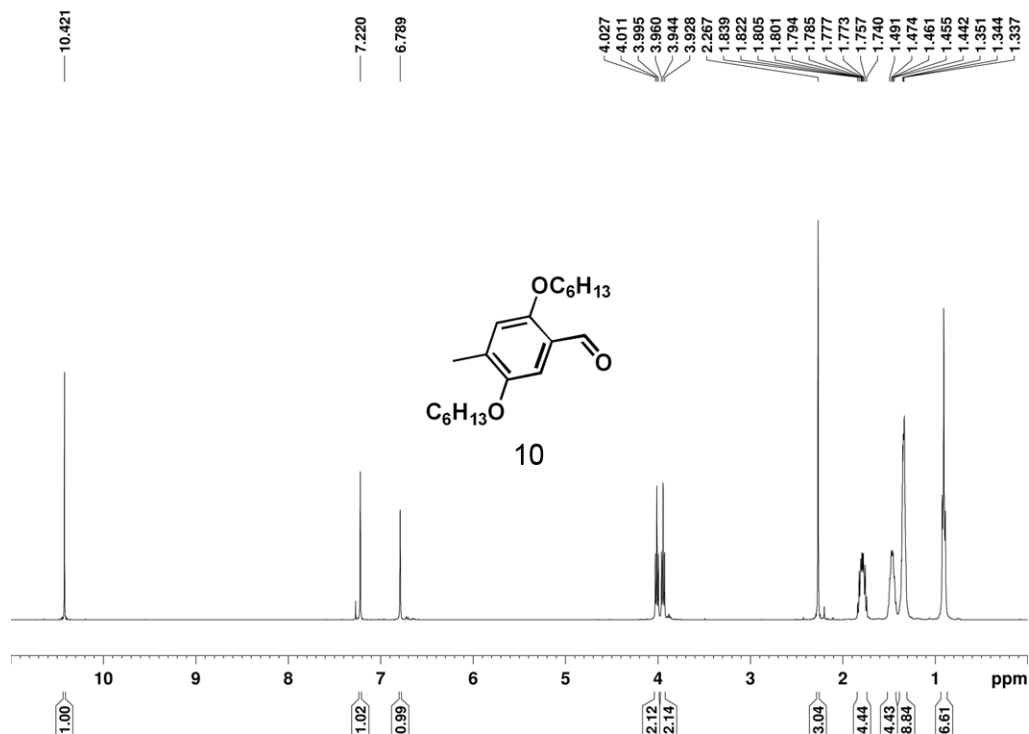


Figure 42. ^1H and ^{13}C NMR spectra of compound 10.

bnnvii19a CDCl₃ 400 MHz 9/5/10



bnnvii19a CDCl₃ 100 MHz 9/5/10

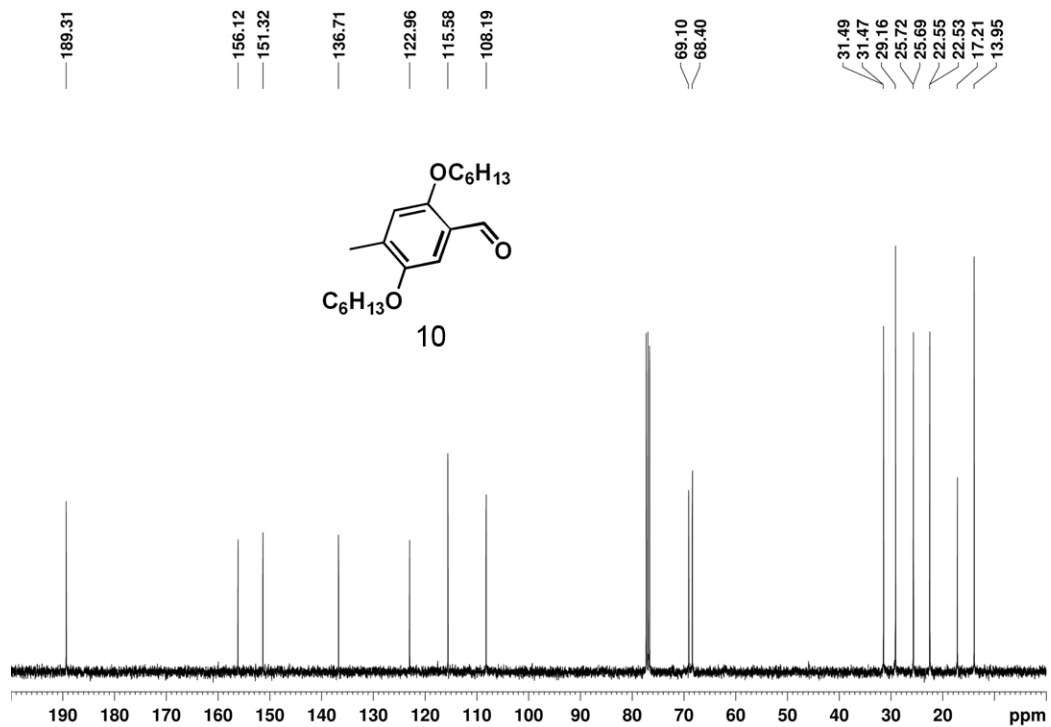
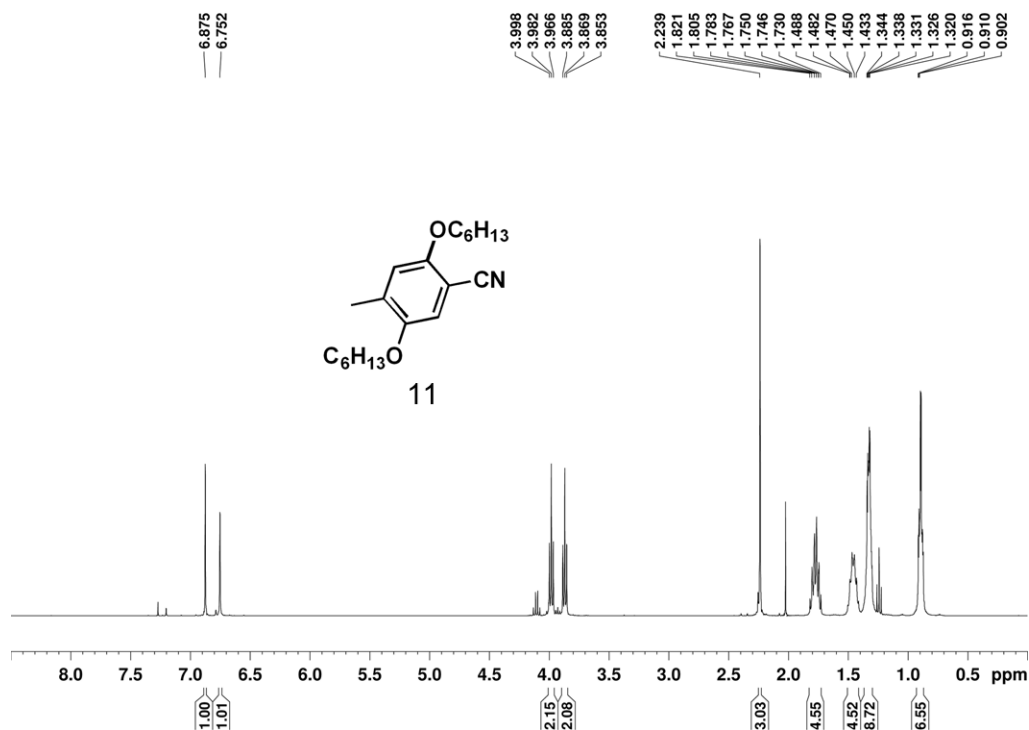


Figure 43. ^1H and ^{13}C NMR spectra of compound **11**.

bnnvii23a CDCl₃ 400 MHz 9/5/10



bnnvii23a CDCl₃ 100 MHz 9/5/10

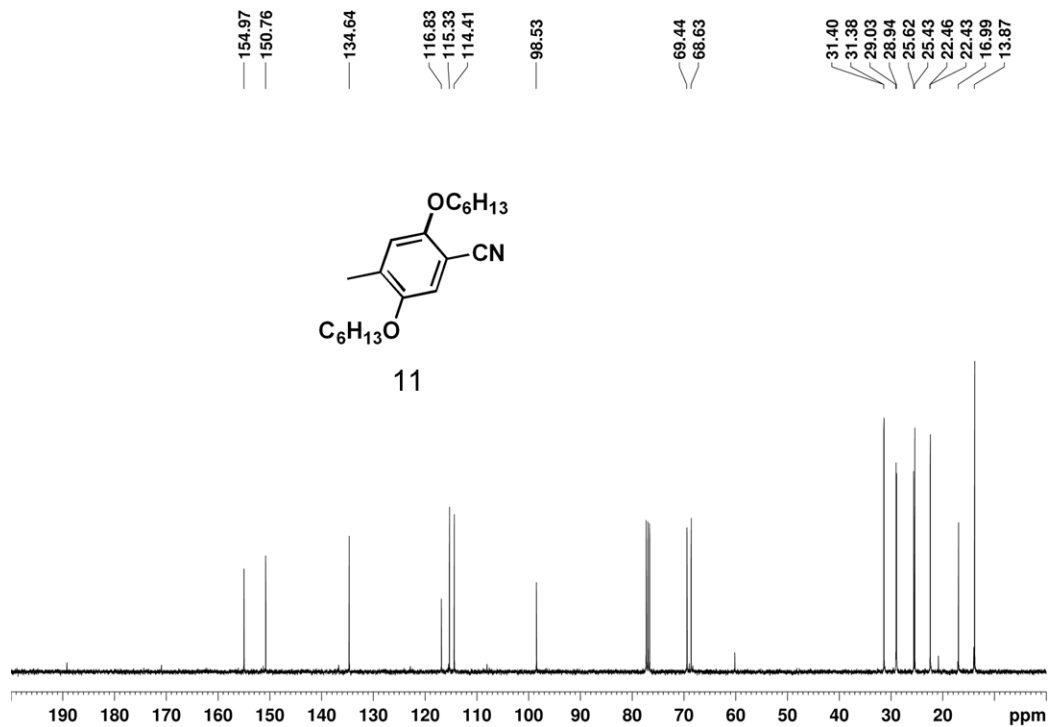
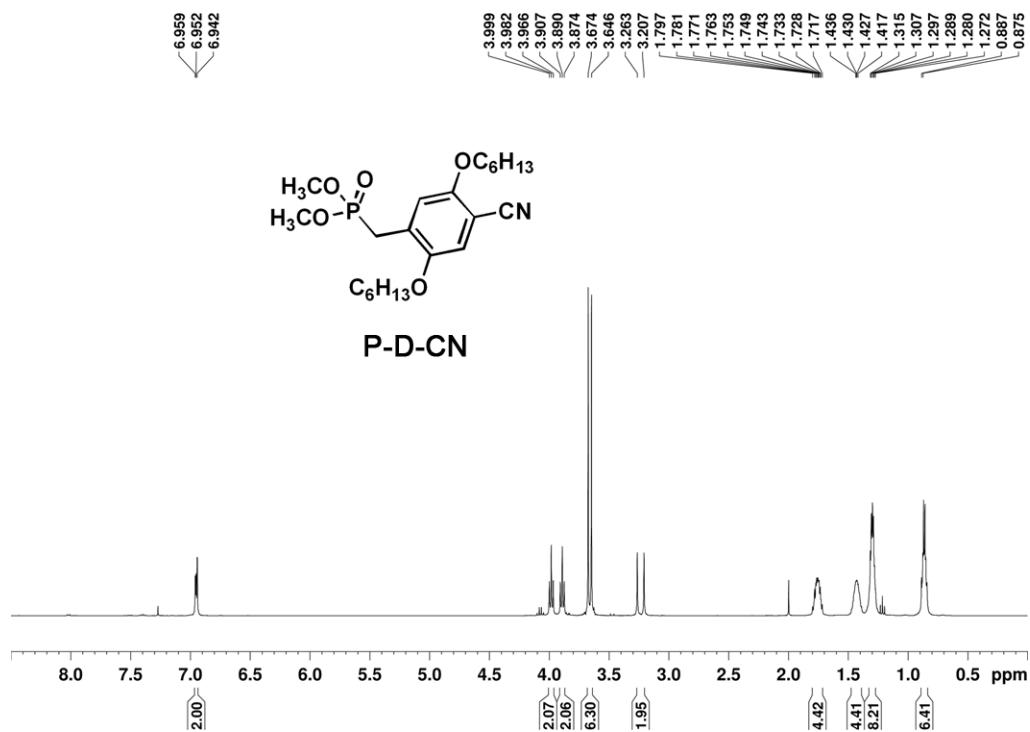


Figure 44. ^1H and ^{13}C NMR spectra of P-D-CN

bnnvii27a CDCl₃ 400 MHz 9/5/10



bnnvii27a CDCl₃ 100 MHz 9/5/10

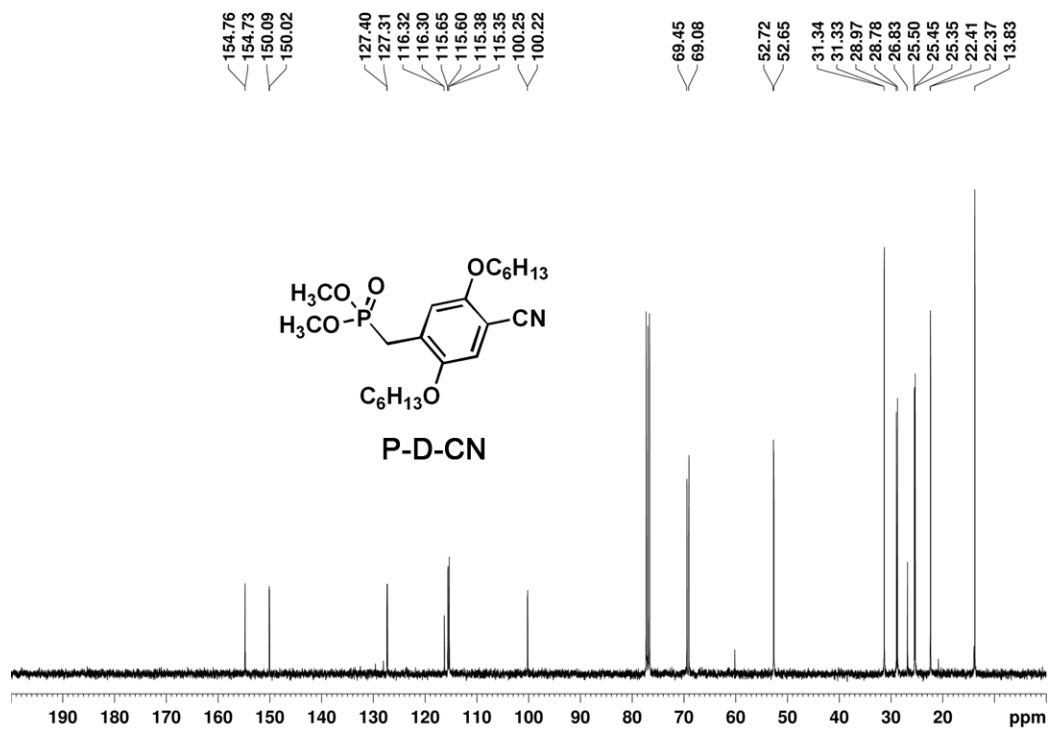
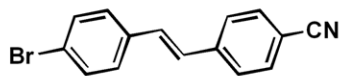
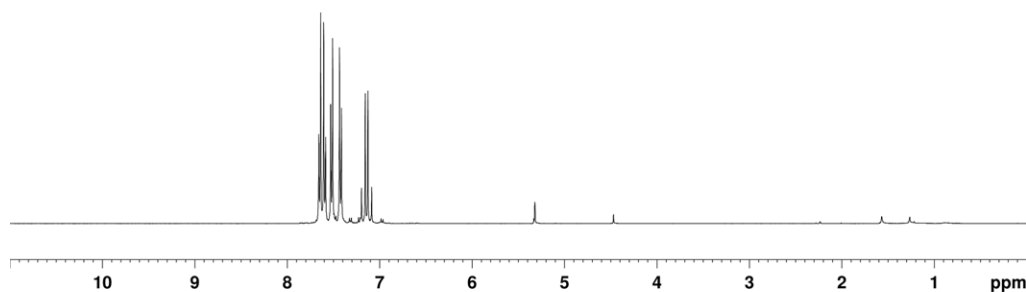


Figure 45. ^1H , ^{13}C , and DEPT 135 NMR spectra of Br-AA-CN.

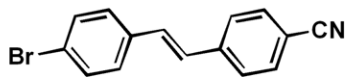
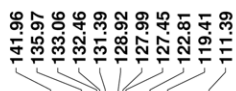
bnnvii36a CD2Cl2 400 MHz 9/5/10



Br-AA-CN



bnnvii36a CD2Cl2 100 MHz 9/5/10



Br-AA-CN

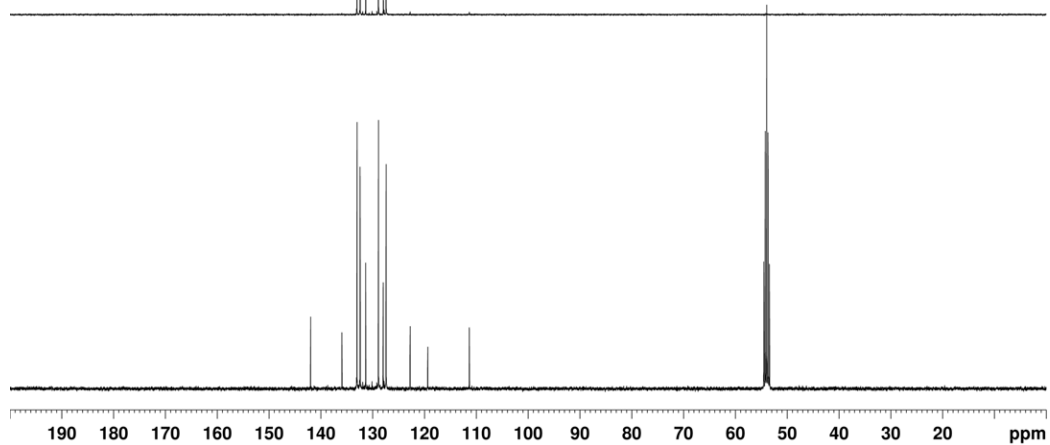
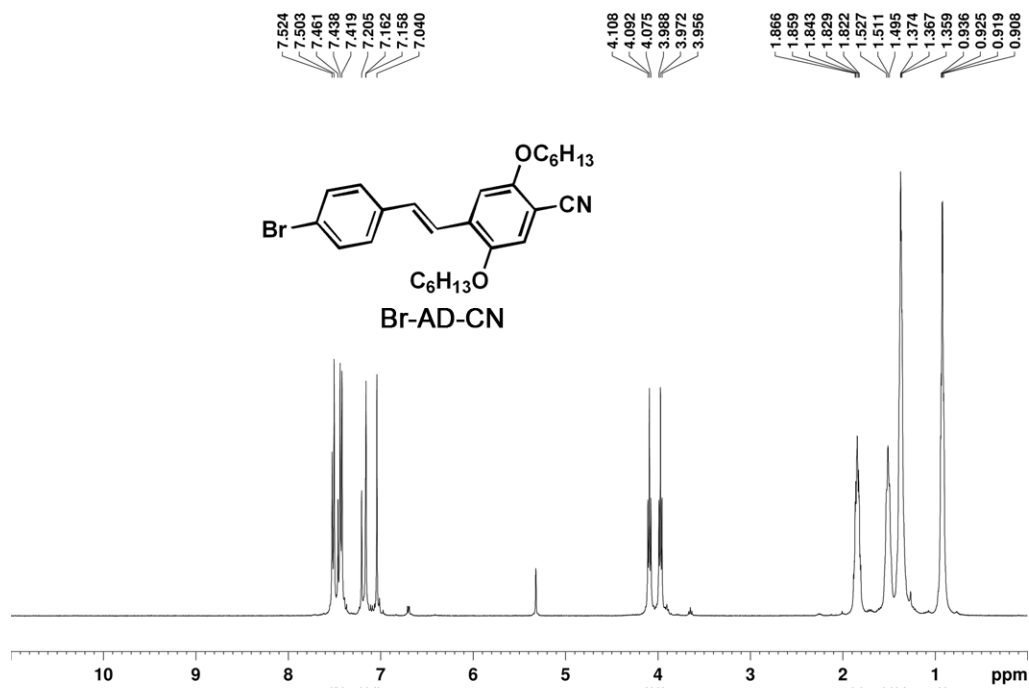


Figure 46. ^1H , ^{13}C , and DEPT 135 NMR spectra of Br-AD-CN.

bnnvii39a CD2Cl2 400 MHz 9/5/10



bnnvii39a CD2Cl2 100 MHz 9/5/10

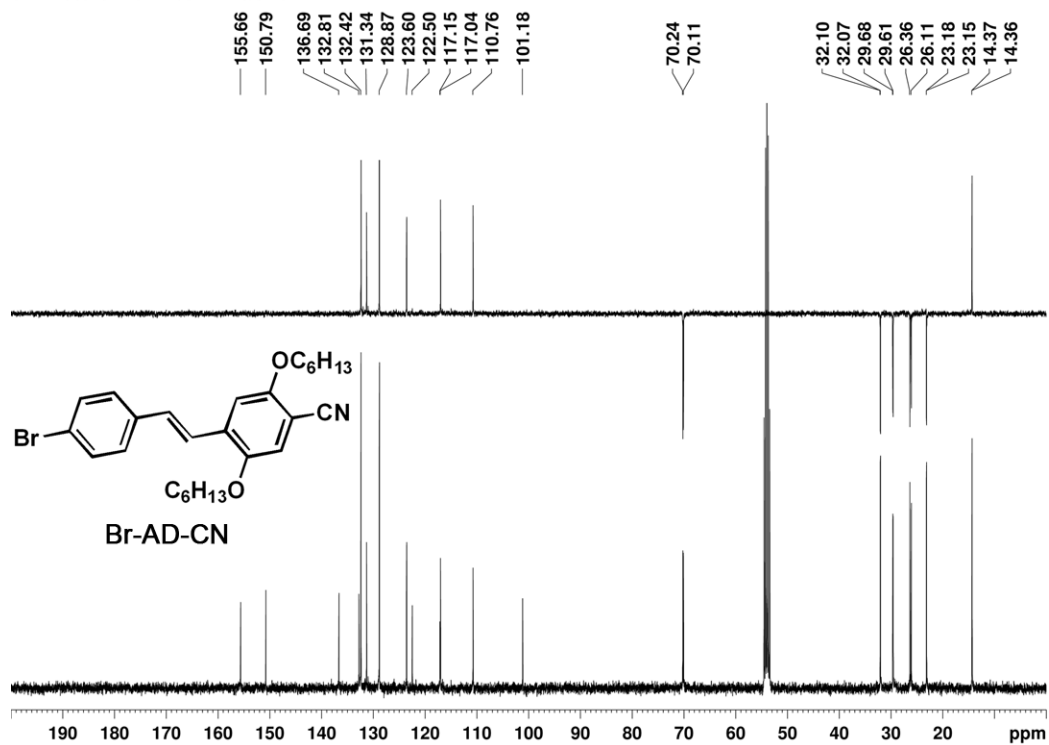
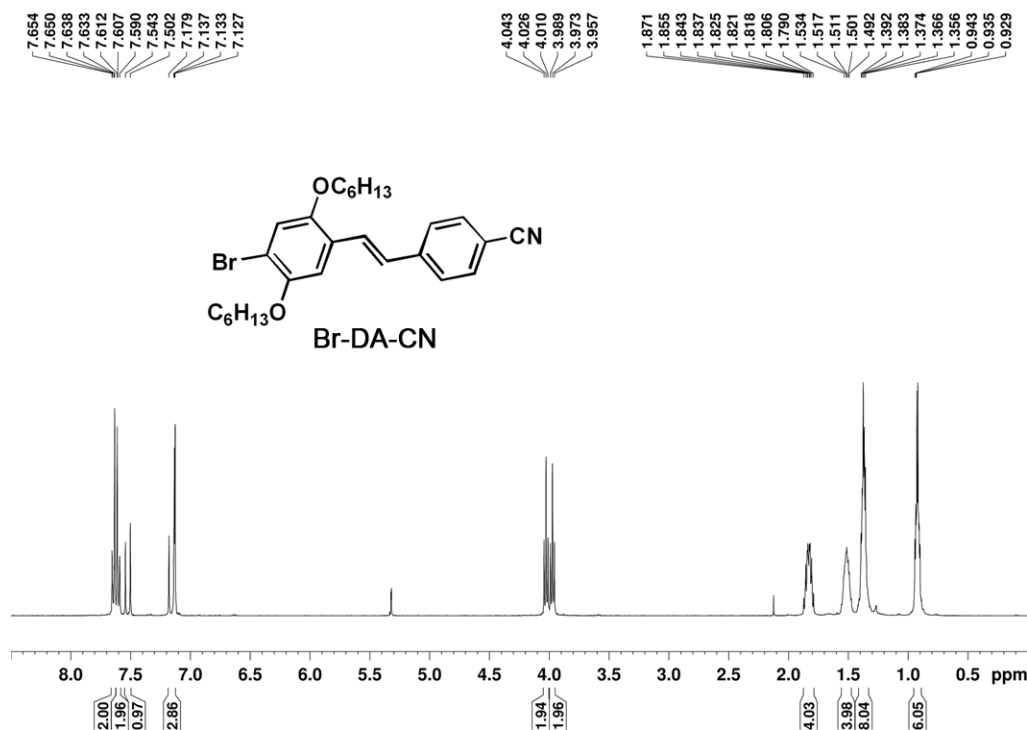


Figure 47. ^1H , ^{13}C , and DEPT 135 NMR spectra of Br-DA-CN.

bnnvii35a CD2Cl2 400 MHz 9/5/10



bnnvii35a CD2Cl2 100 MHz 9/5/10

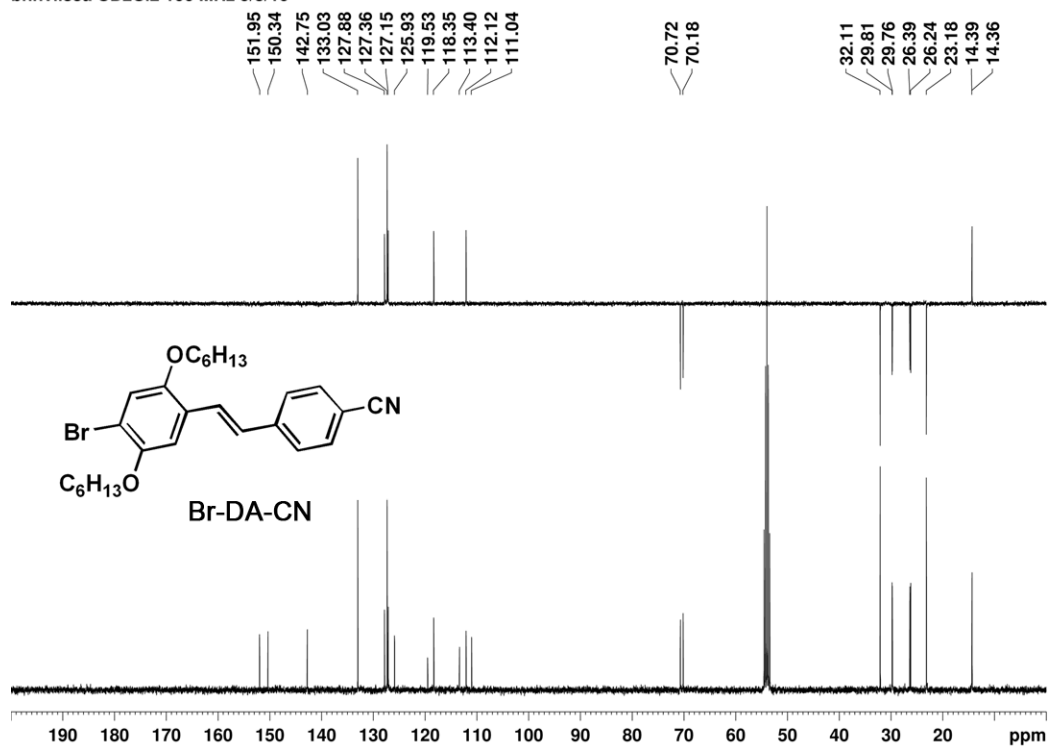
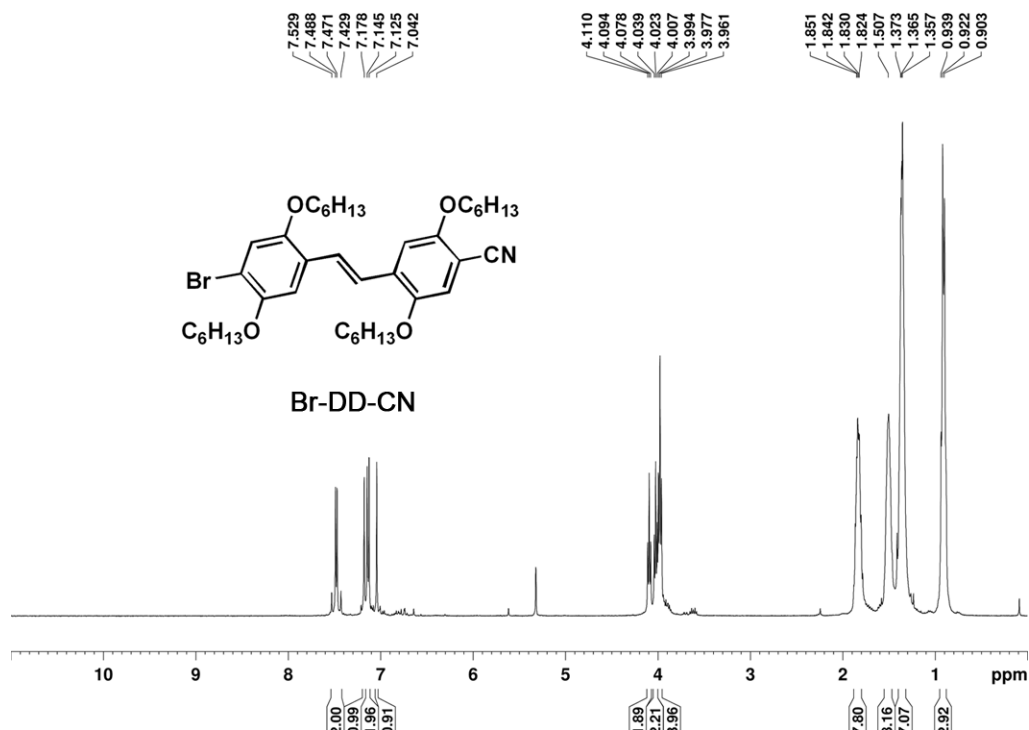


Figure 48. ^1H , ^{13}C , and DEPT 135 NMR spectra of **Br-DD-CN**.

bnnvii42a CD2Cl2 400 MHz 9/5/10



bnnvii42a CD2Cl2 100 MHz 9/5/10

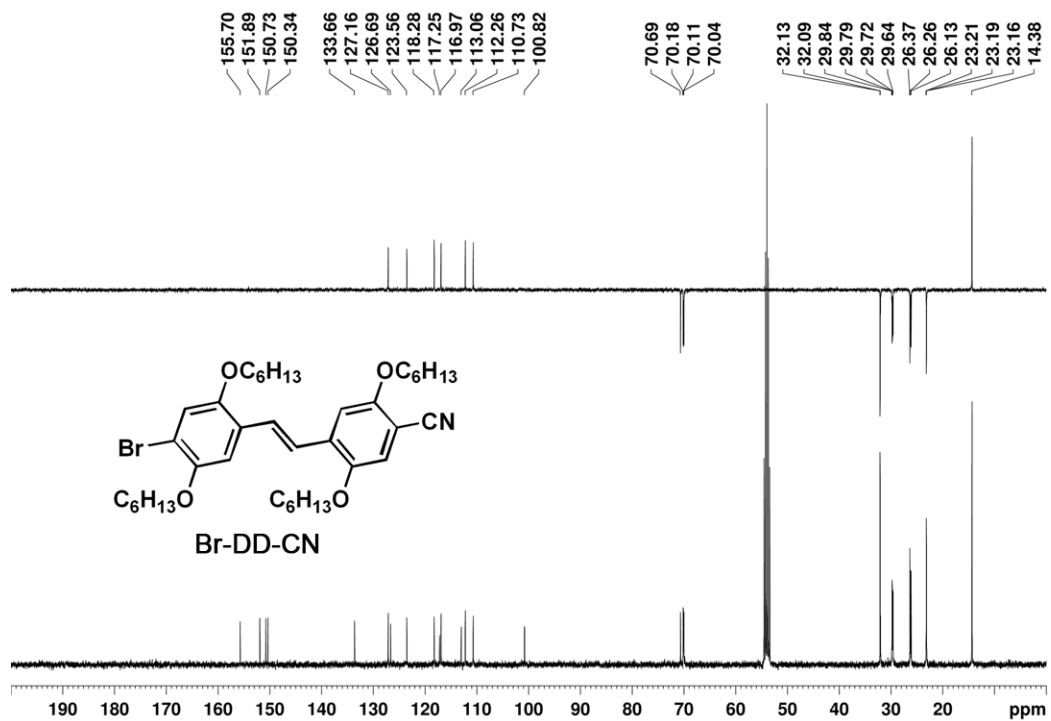
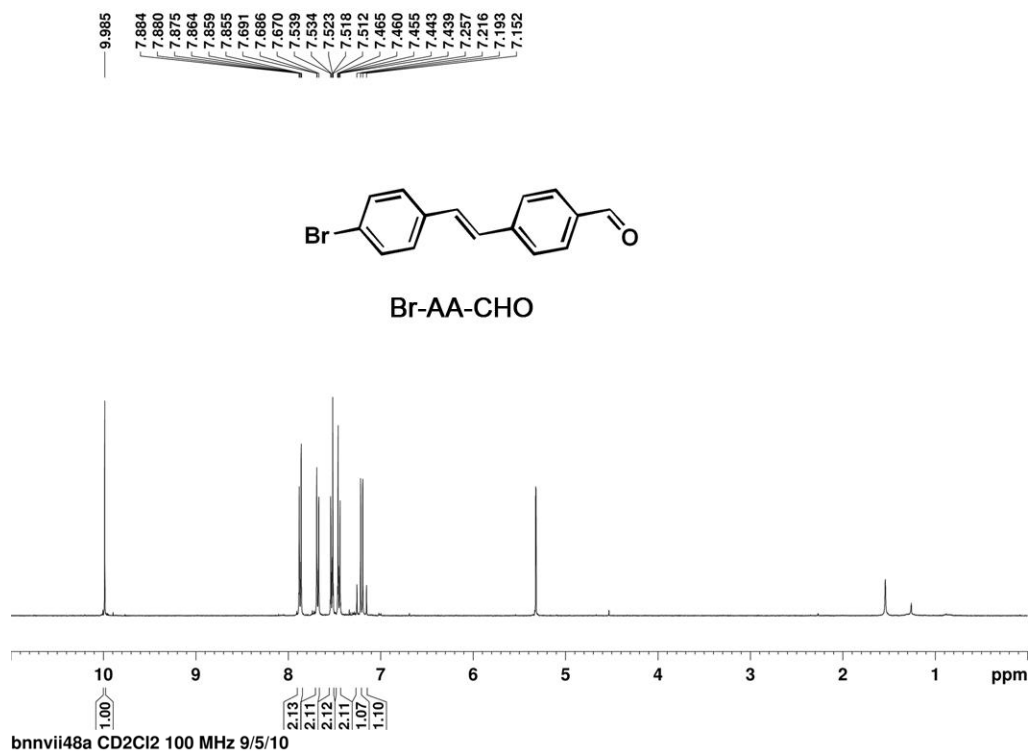


Figure 49. ^1H , ^{13}C , and DEPT 135 NMR spectra of Br-AA-CHO.

bnnvii48a CD₂Cl₂ 400 MHz 9/5/10



bnnvii48a CD₂Cl₂ 100 MHz 9/5/10

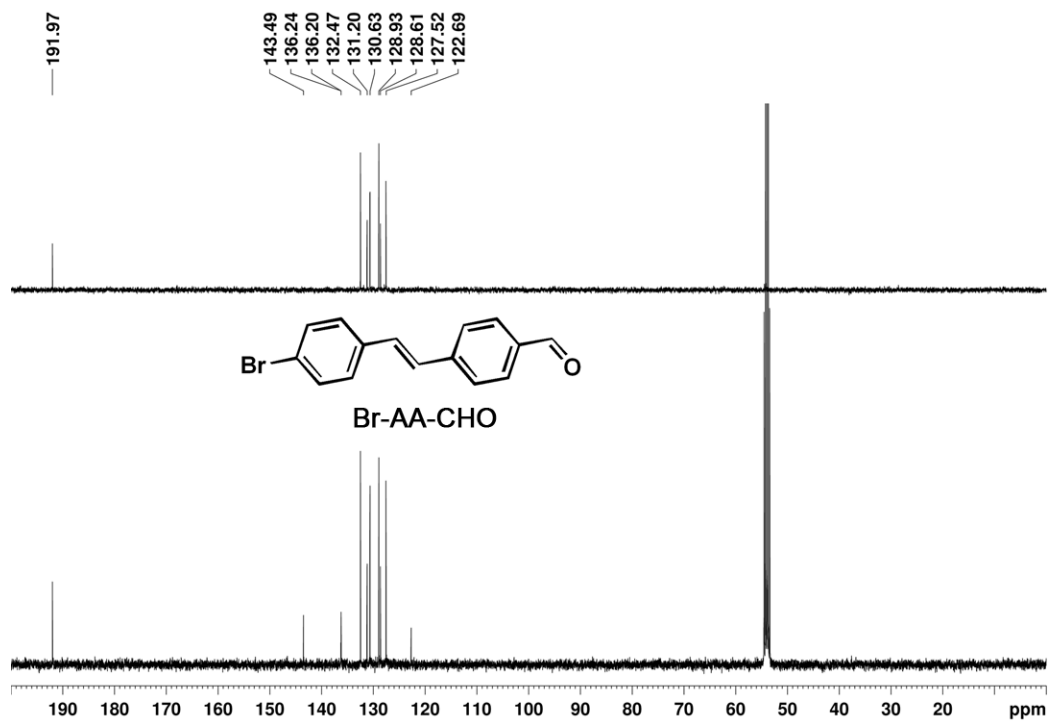
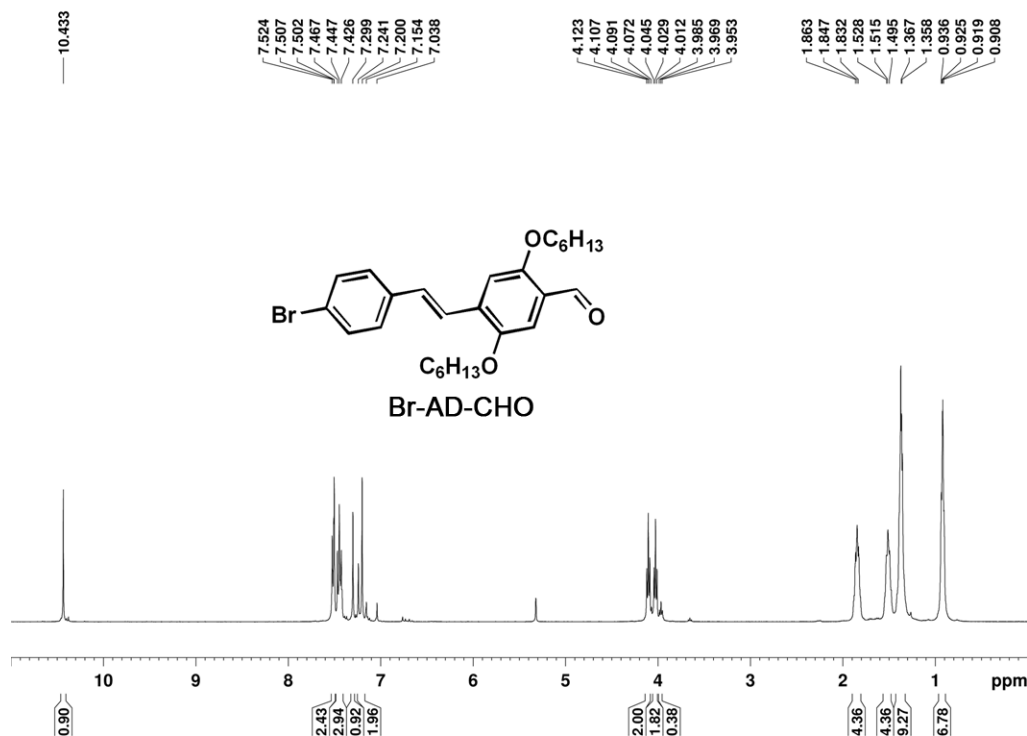


Figure 50. ^1H , ^{13}C , and DEPT 135 NMR spectra of Br-AD-CHO.

bnnvii50a CD2Cl2 400 MHz 9/5/10



bnnvii50a CD2Cl2 100 MHz 9/5/10

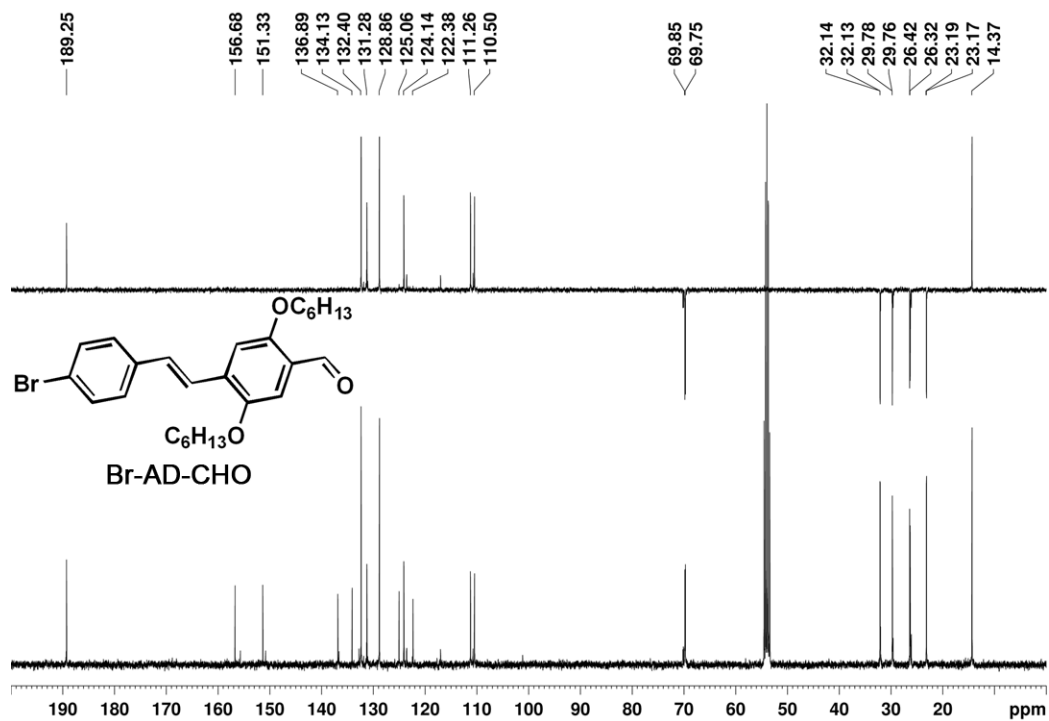
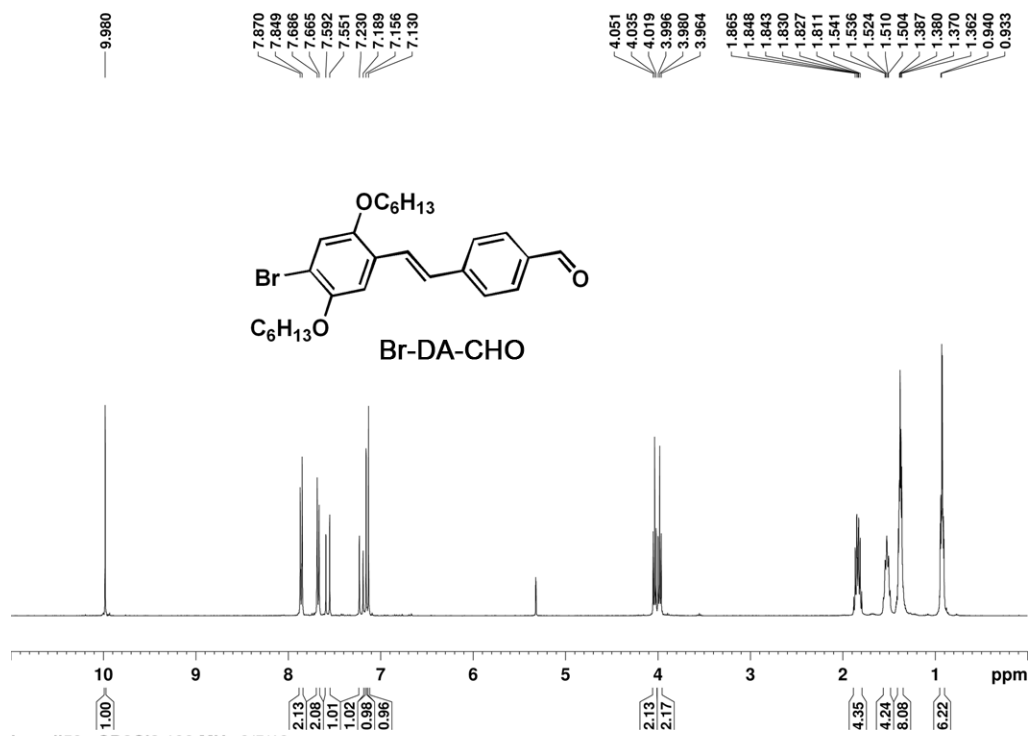


Figure 51. ^1H , ^{13}C , and DEPT 135 NMR spectra of Br-DA-CHO.

bnnvii59a CD2Cl2 400 MHz 9/5/10



bnnvii59a CD2Cl2 100 MHz 9/5/10

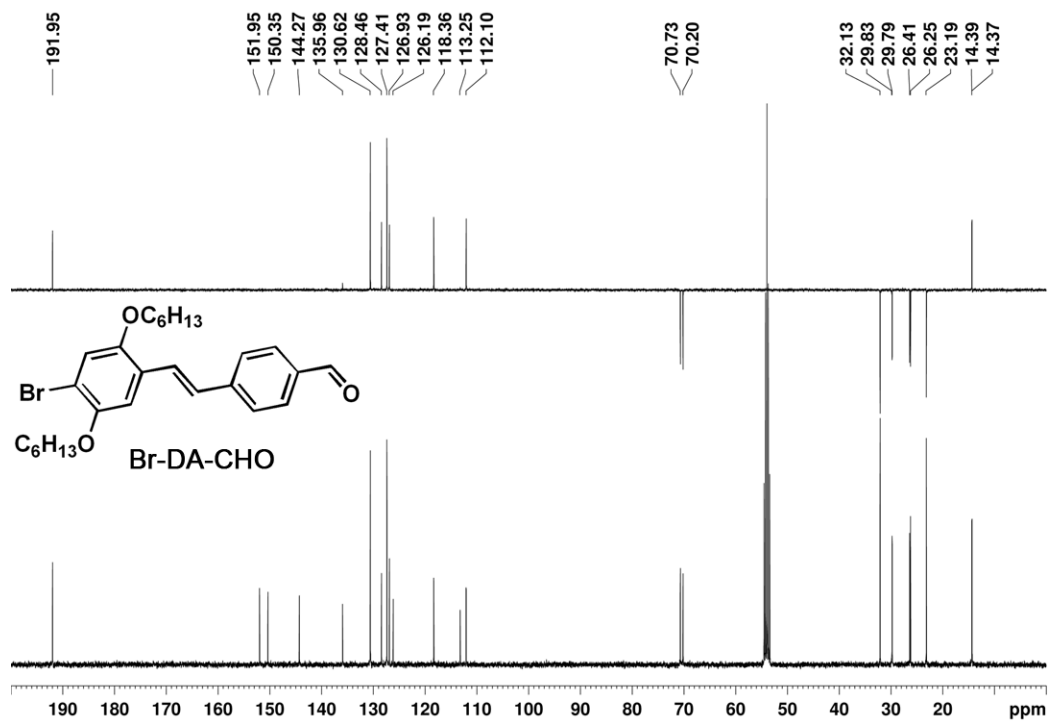
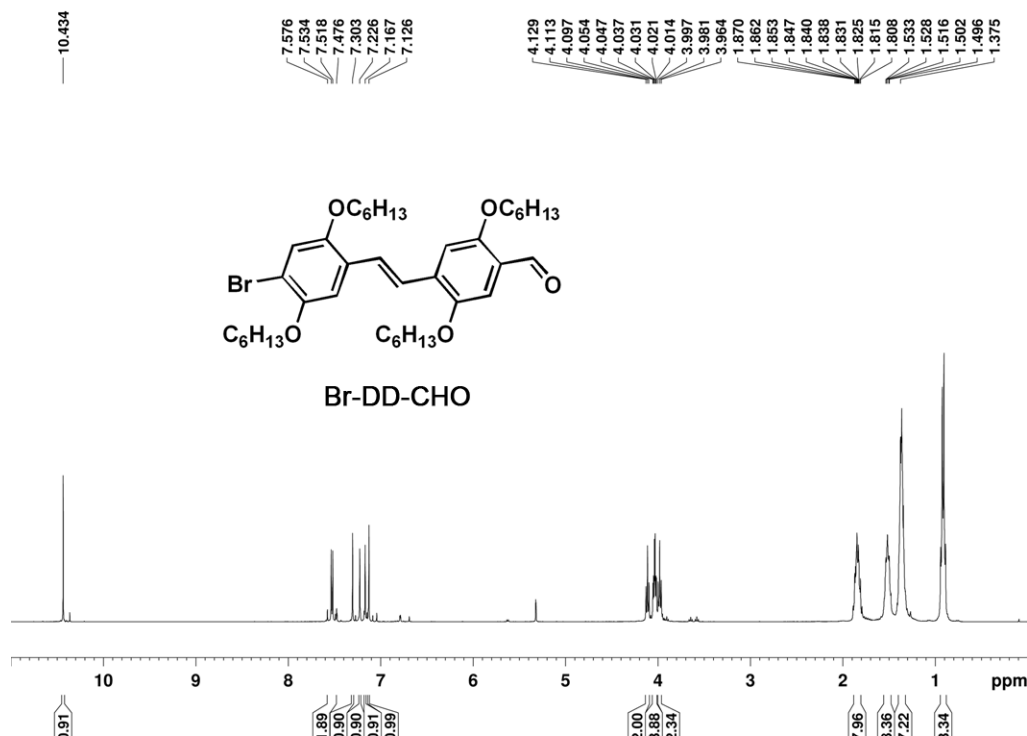


Figure 52. ^1H , ^{13}C , and DEPT 135 NMR spectra of Br-DD-CHO.

bnnvii57a CD2Cl2 400 MHz 9/5/10



bnnvii57a CD2Cl2 100 MHz 9/5/10

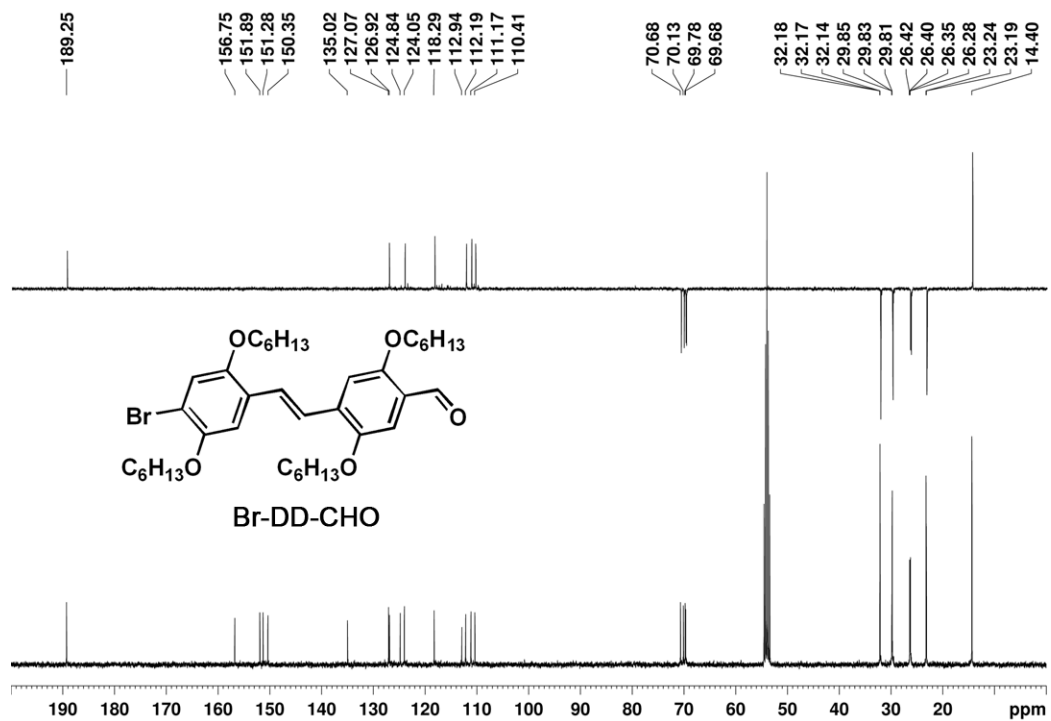
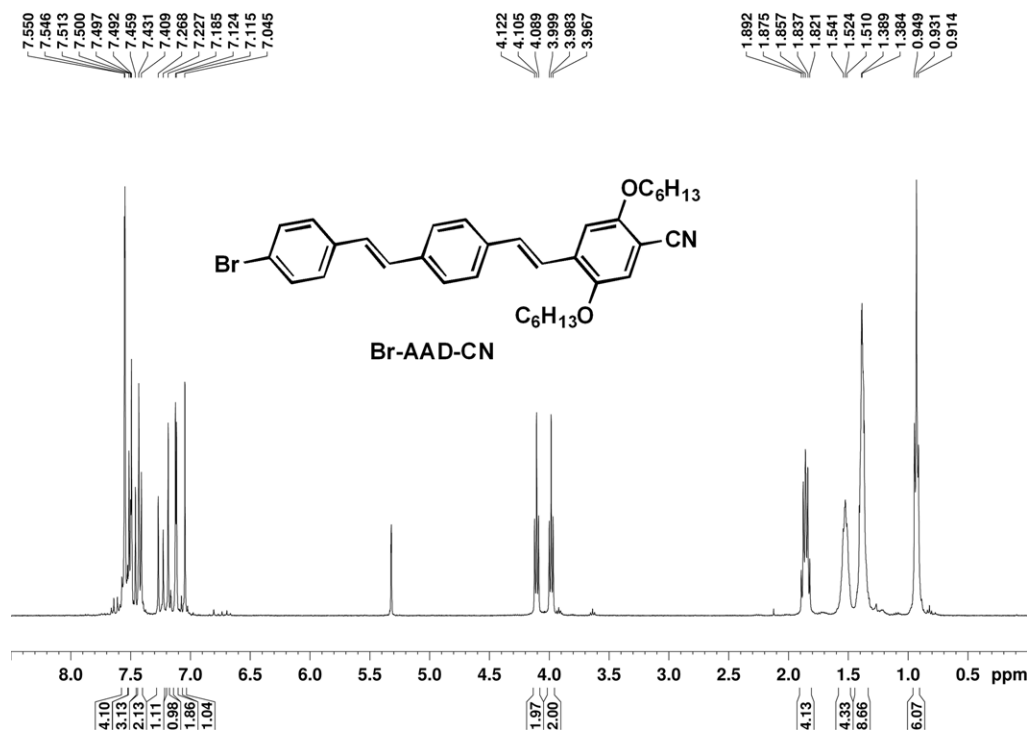


Figure 53. ^1H , ^{13}C , and DEPT 135 NMR spectra of Br-AAD-CN.

bnnvii52a CD2Cl2 400 MHz 9/19/20
BrAADCN



bnnvii52a CD2Cl2 100 MHz 9/19/20
BrAADCN

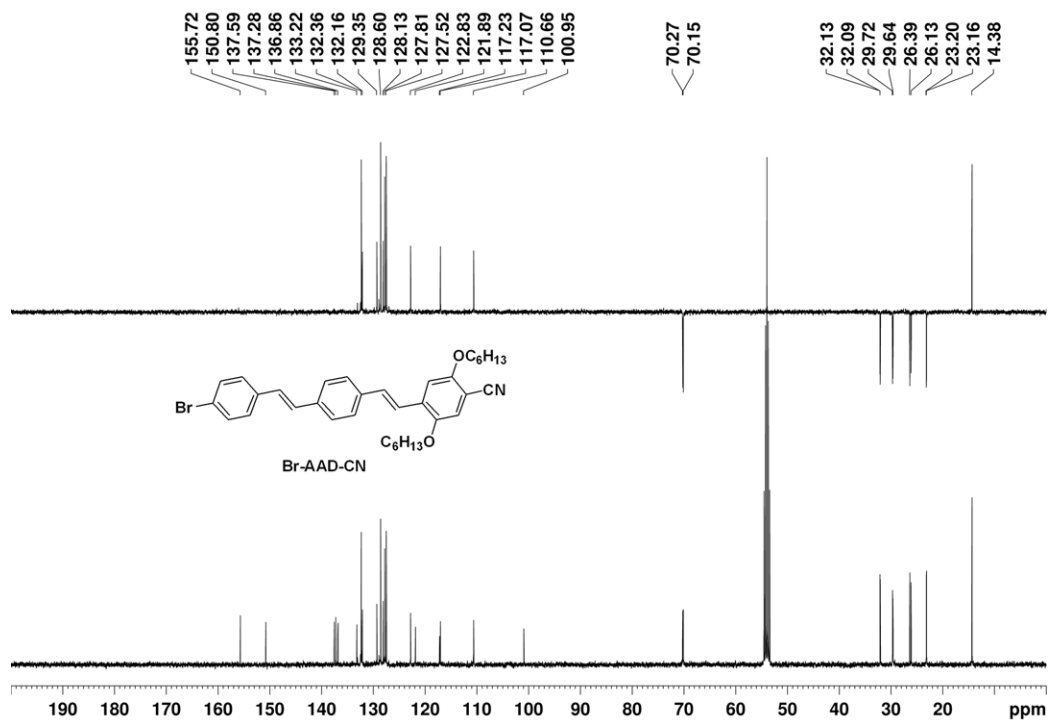
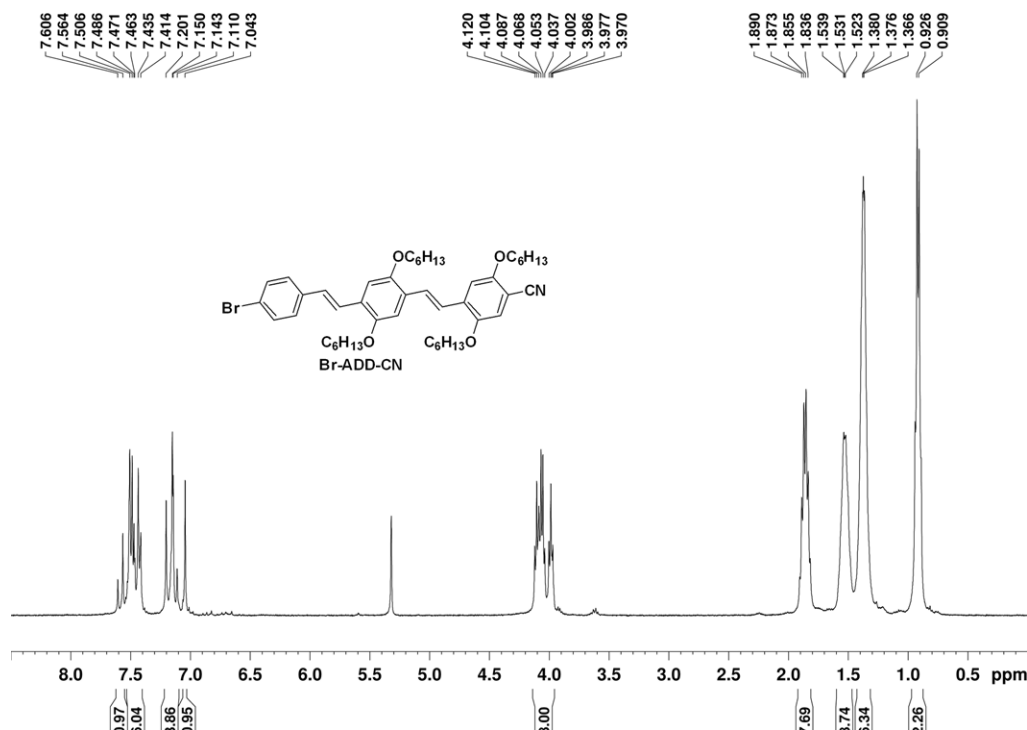


Figure 54. ^1H , ^{13}C , and DEPT 135 NMR spectra of Br-ADD-CN.

bnnvii53a CD₂Cl₂ 400 MHz 9/19/20
BrADD-CN



bnnvii53a CD₂Cl₂ 100 MHz 9/19/20
BrADD-CN

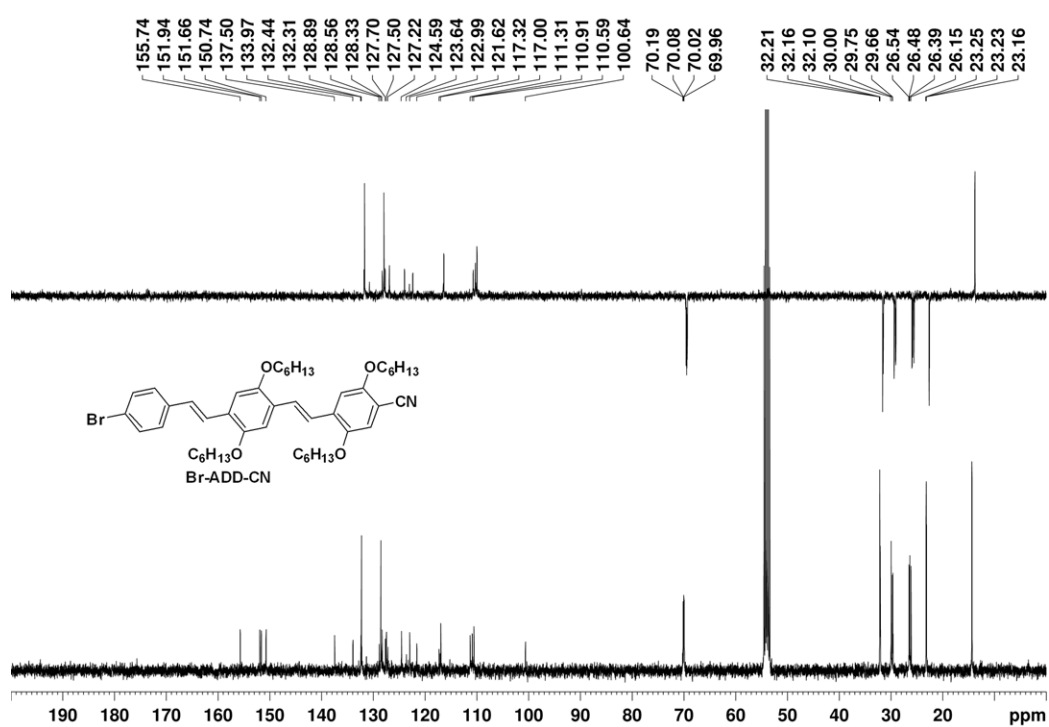


Figure 55. ^1H , ^{13}C , and DEPT 135 NMR spectra of Br-ADA-CN.

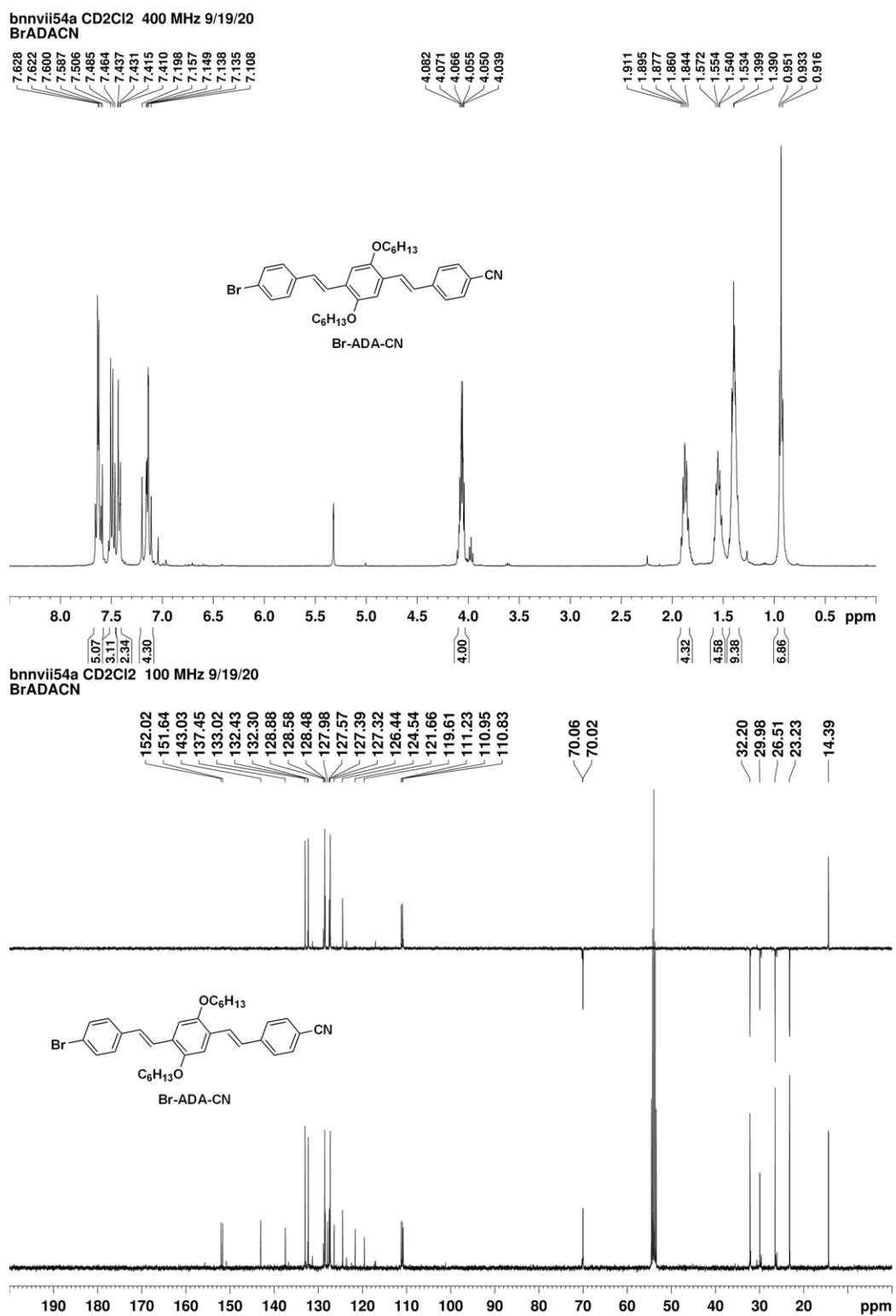


Figure 56. ^1H , ^{13}C , and DEPT 135 NMR spectra of Br-DAA-CN.

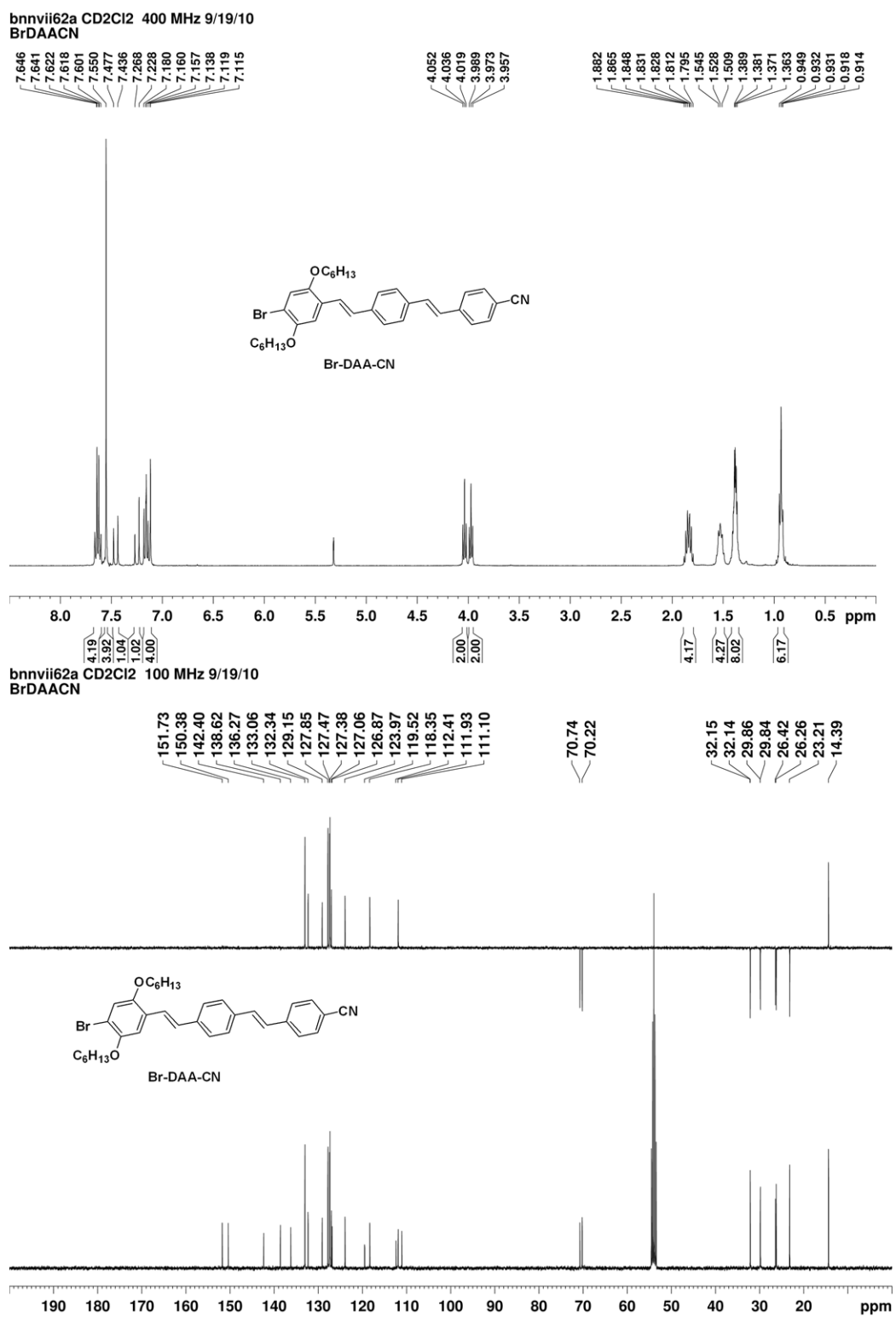
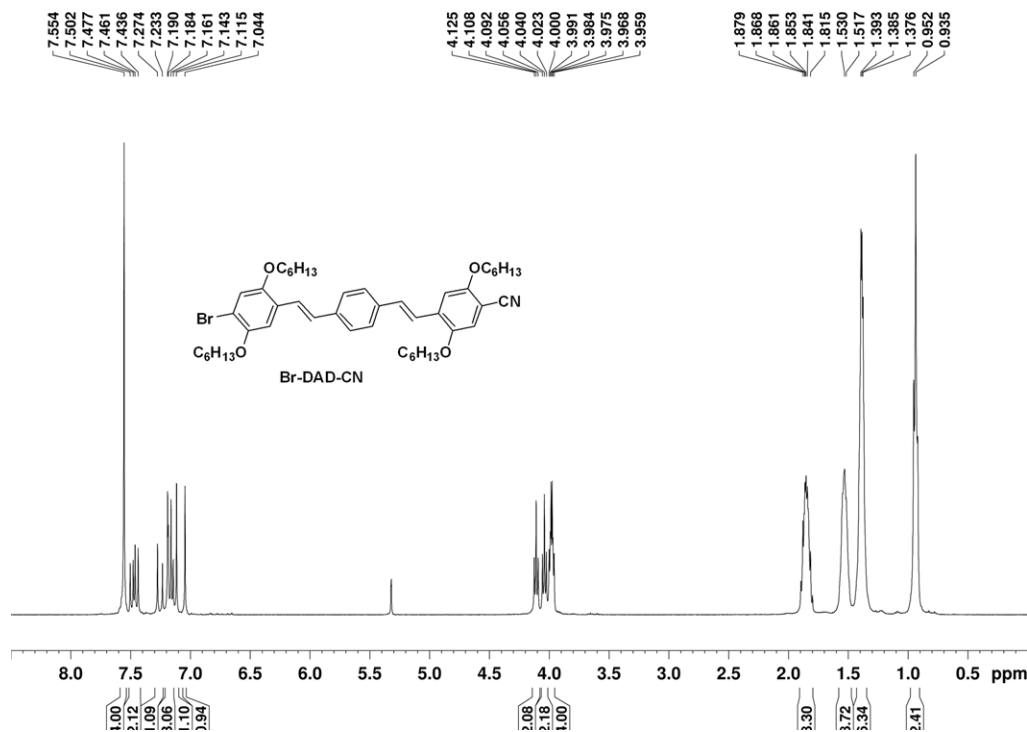


Figure 57. ^1H , ^{13}C , and DEPT 135 NMR spectra of Br-DAD-CN.

bnnvii61a CD₂Cl₂ 400 MHz 9/19/10
BrDADCN



bnnvii61a CD₂Cl₂ 100 MHz 9/19/10
BrDADCN

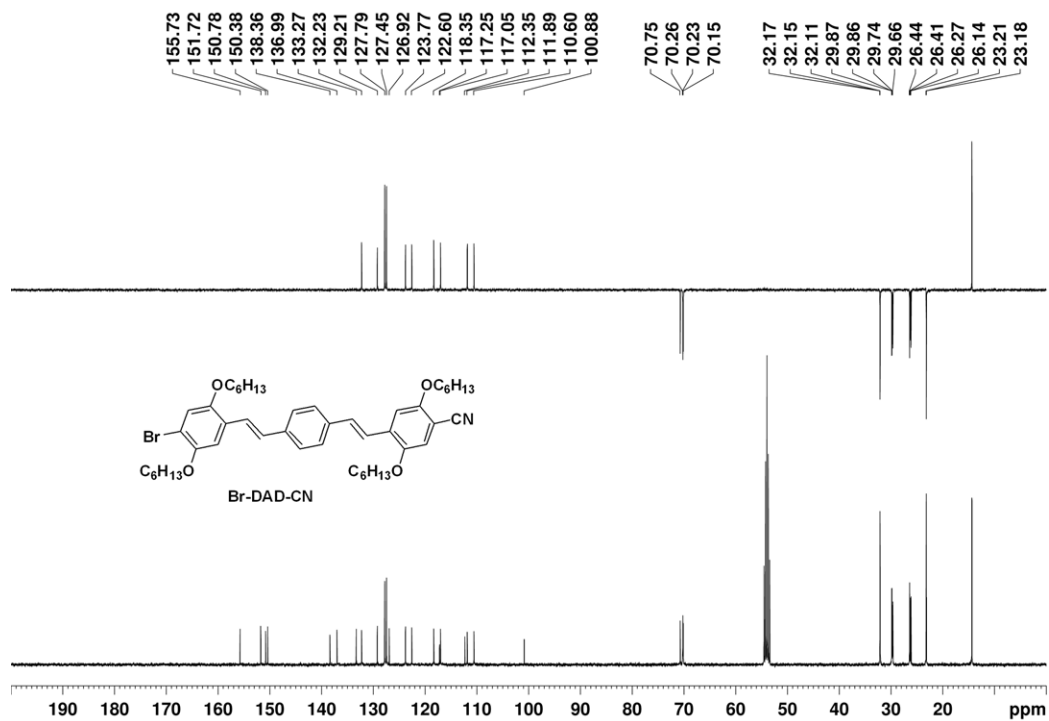
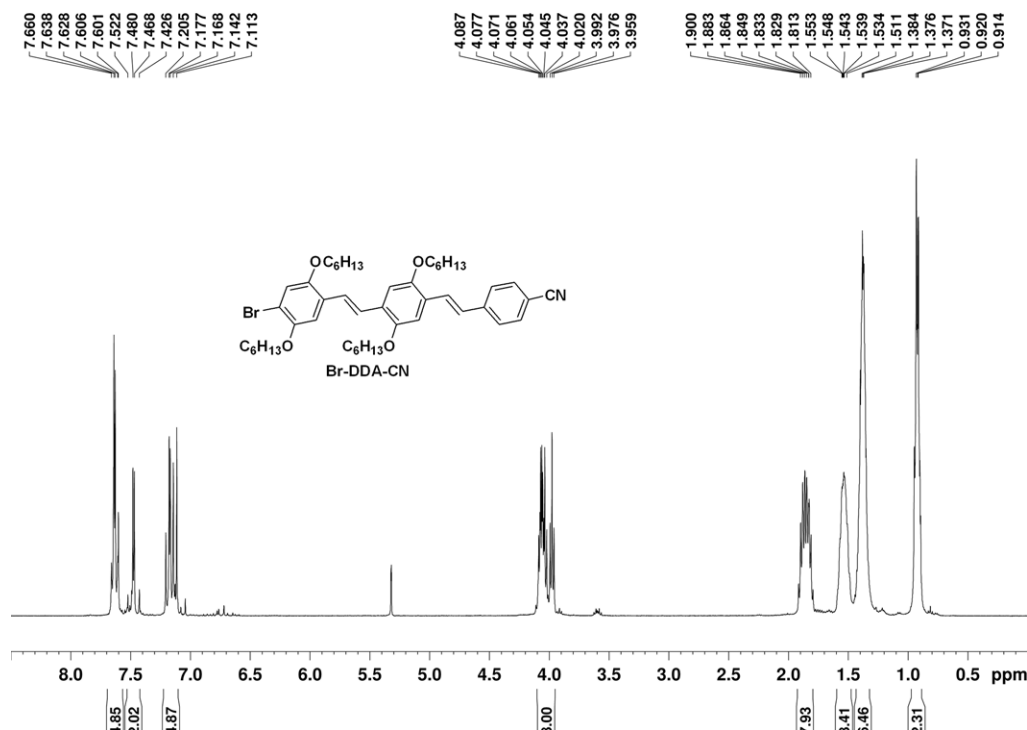


Figure 58. ^1H , ^{13}C , and DEPT 135 NMR spectra of **Br-DDA-CN**.

bnnvii60a CD2Cl2 400 MHz 9/19/10
BrDDACN



bnnvii60a CD2Cl2 100 MHz 9/19/10
BrDDACN

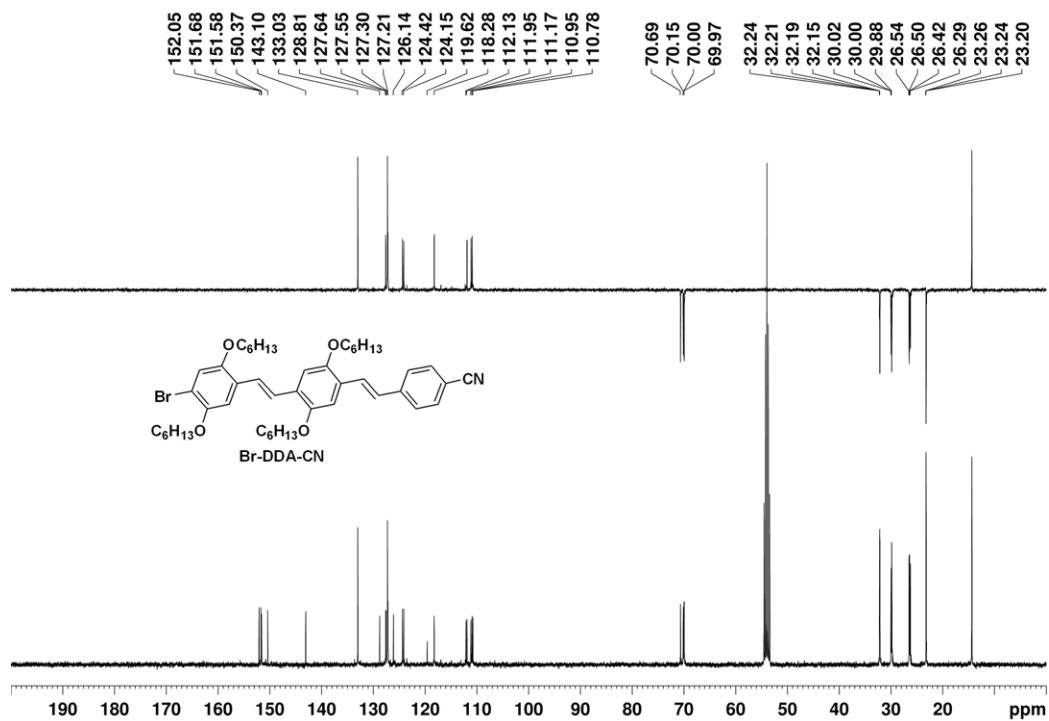


Figure 59. ^1H , ^{13}C , and DEPT 135 NMR spectra of Br-AAD-CHO.

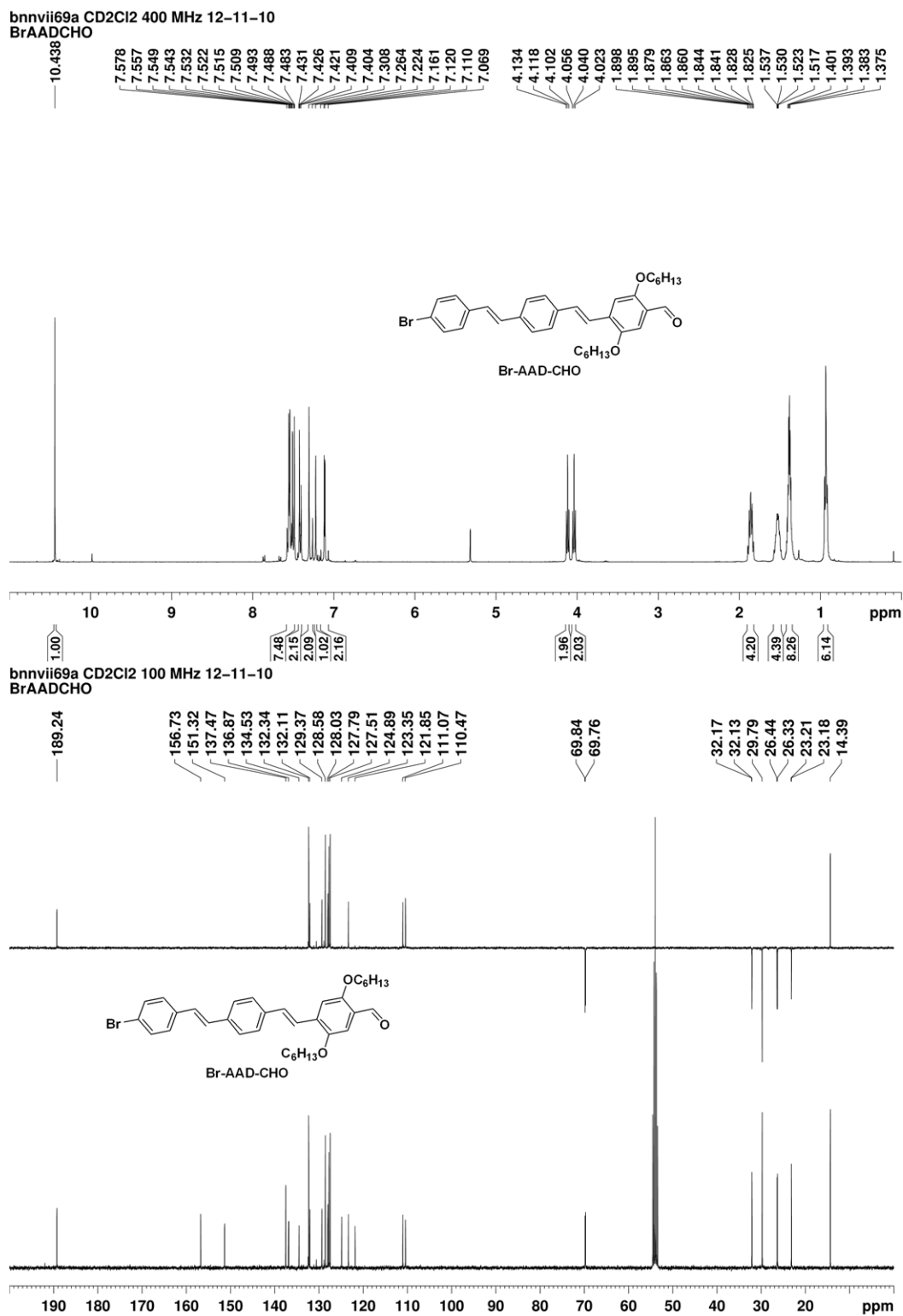
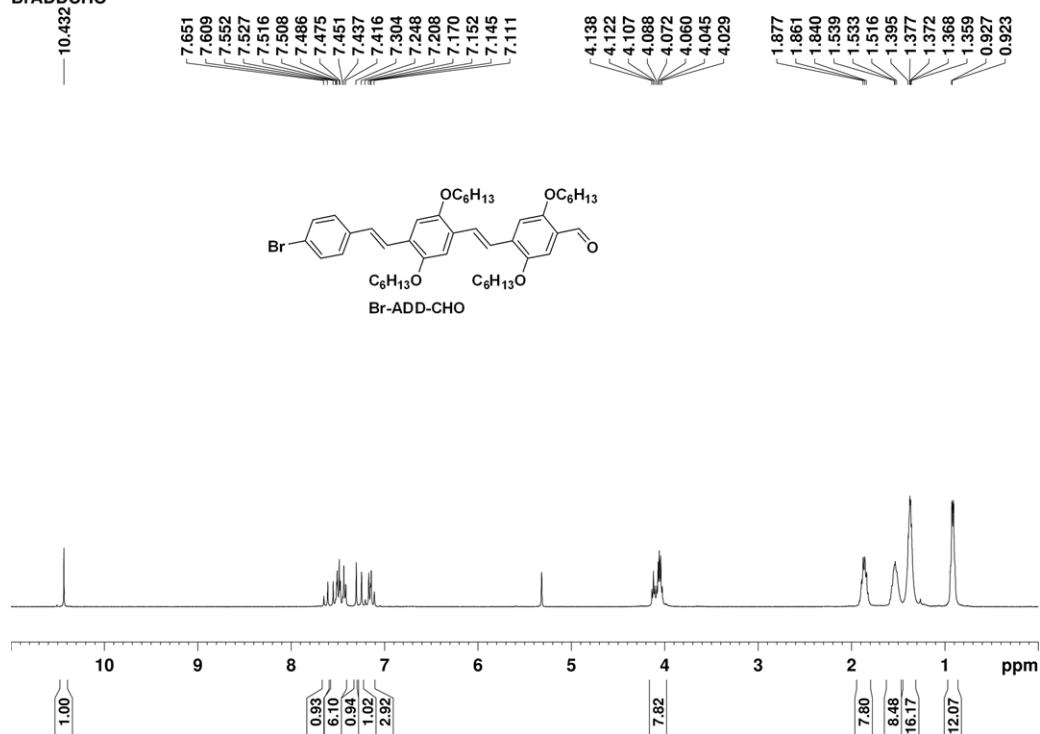


Figure 60. ^1H , ^{13}C , and DEPT 135 NMR spectra of Br-ADD-CHO.

bnnvii68a CD2Cl2 400 MHz 12-11-10
BrADDCHO



bnnvii68a CD2Cl2 100 MHz 12-11-10
BrADDCHO

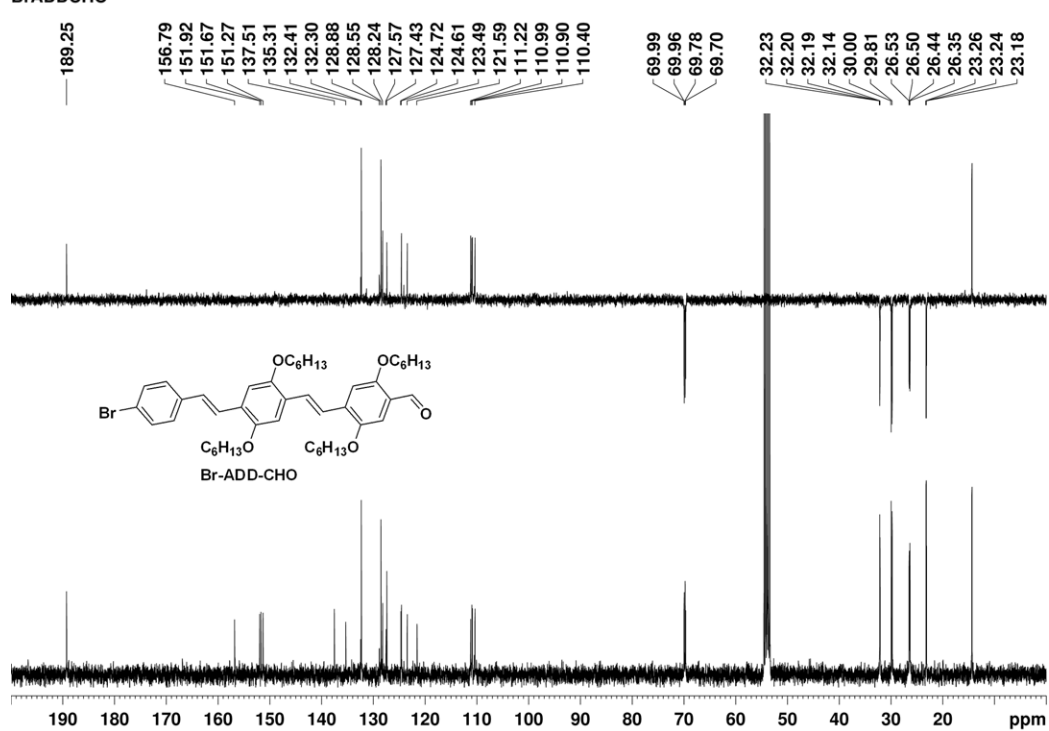


Figure 61. ^1H , ^{13}C , and DEPT 135 NMR spectra of Br-ADA-CHO.

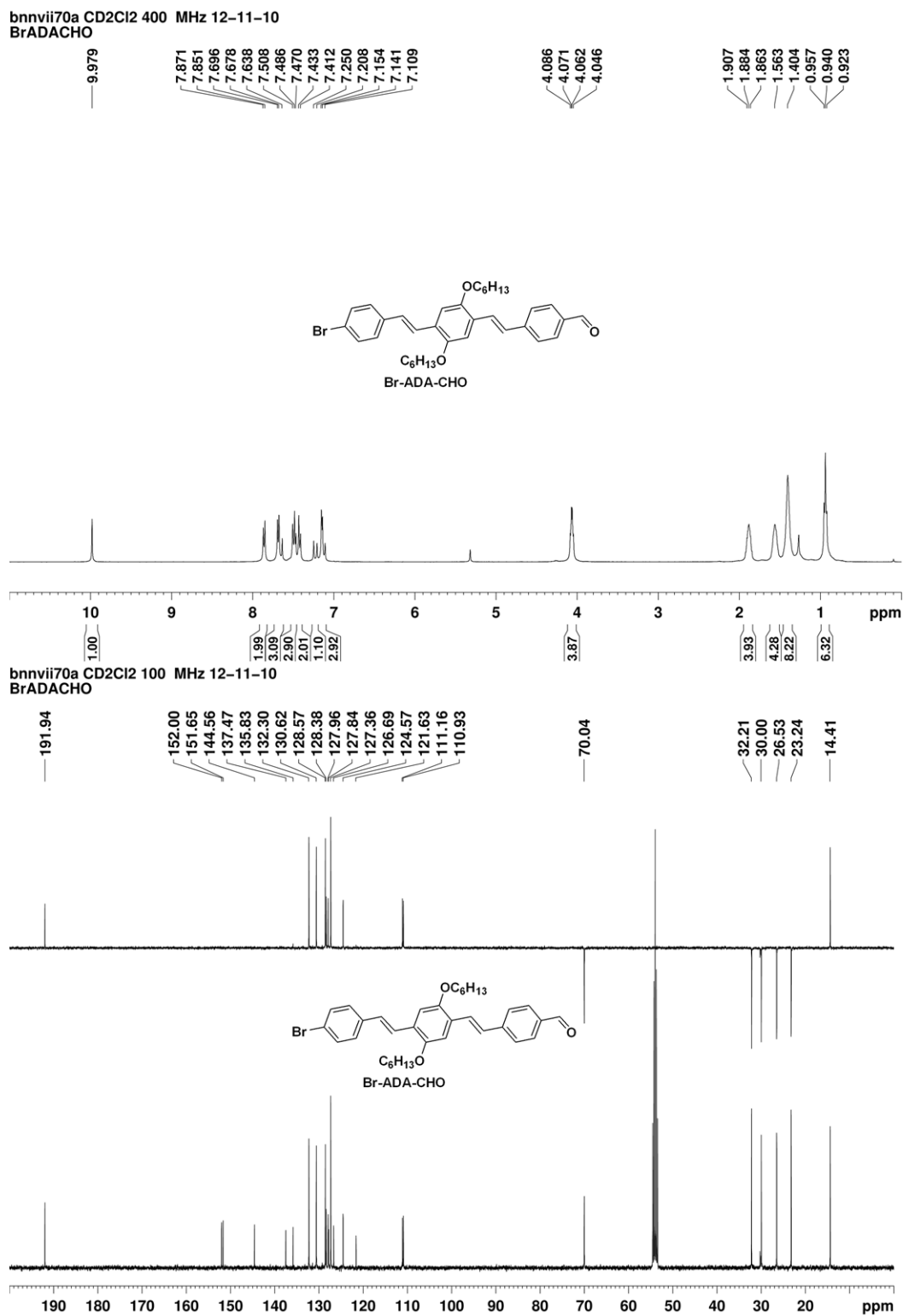


Figure 62. ^1H , ^{13}C , and DEPT 135 NMR spectra of Br-DAA-CHO.

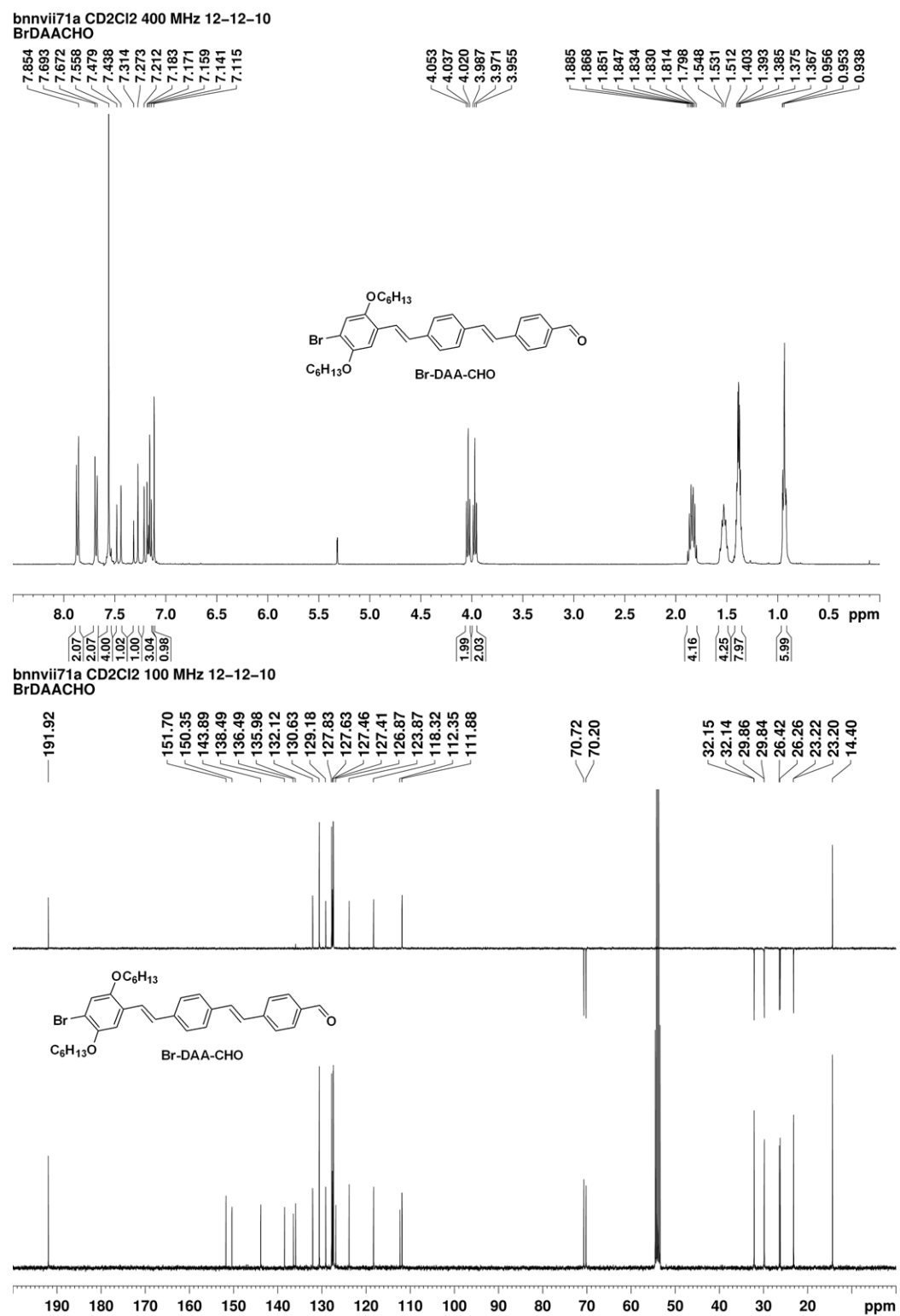
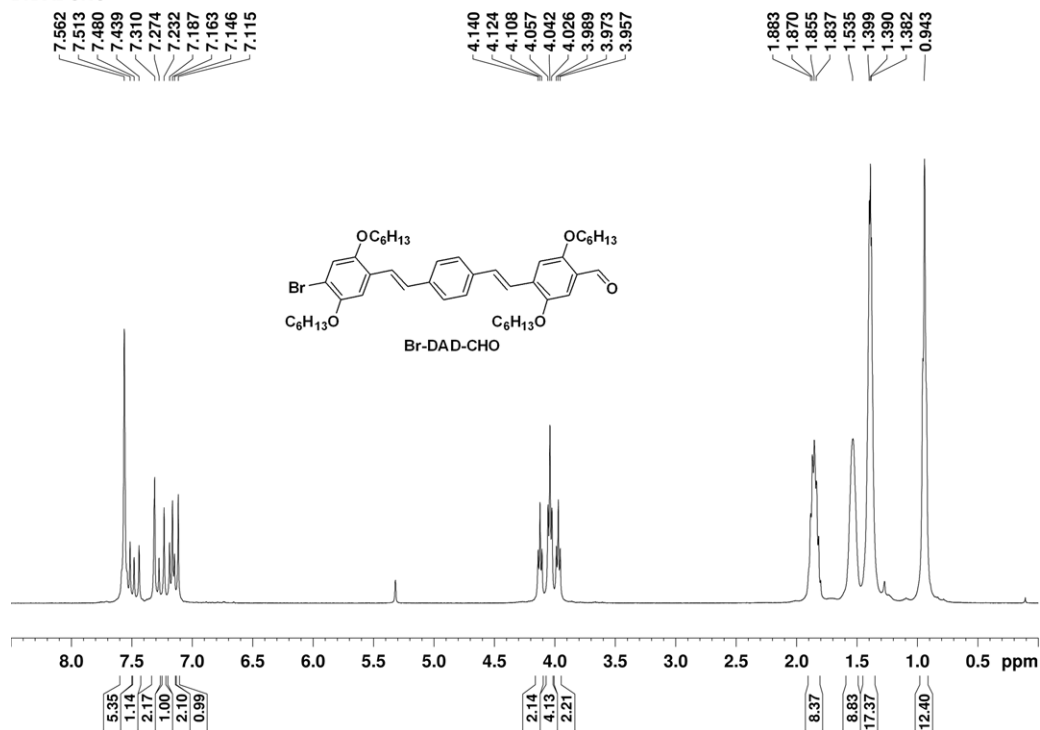


Figure 63. ^1H , ^{13}C , and DEPT 135 NMR spectra of Br-DAD-CHO.

bnnvii67a CD2Cl2 400 MHz 10-23-10
BrDADCHO



bnnvii67a CD2Cl2 100 MHz 10-23-10
BrDADCHO

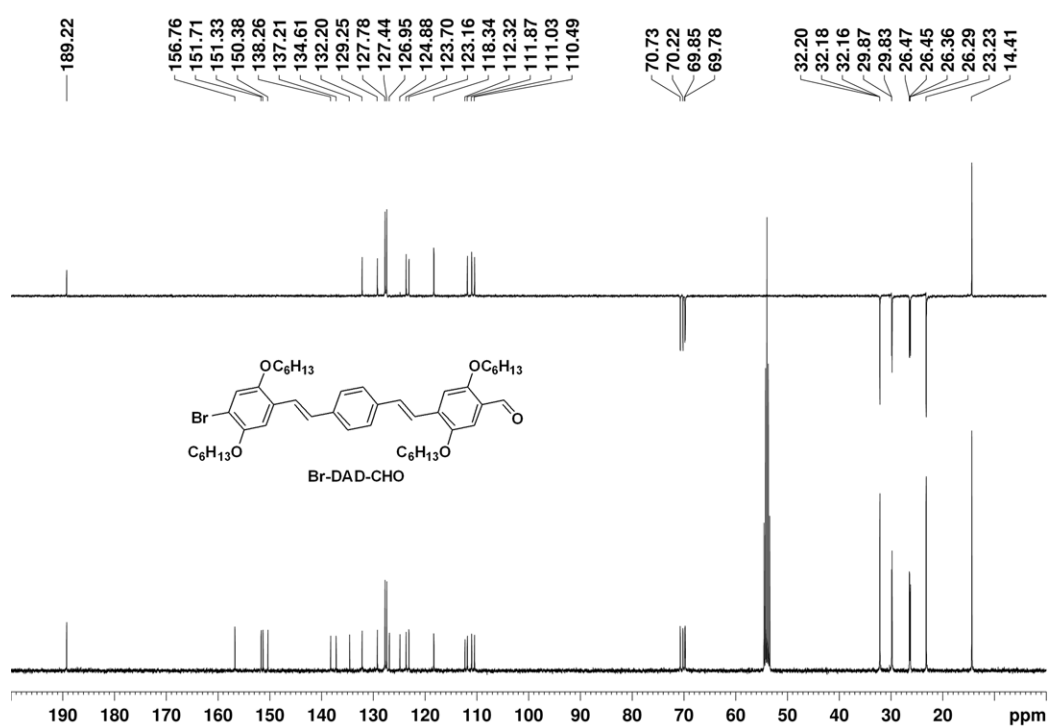


Figure 64. ^1H , ^{13}C , and DEPT 135 NMR spectra of Br-DDA-CHO.

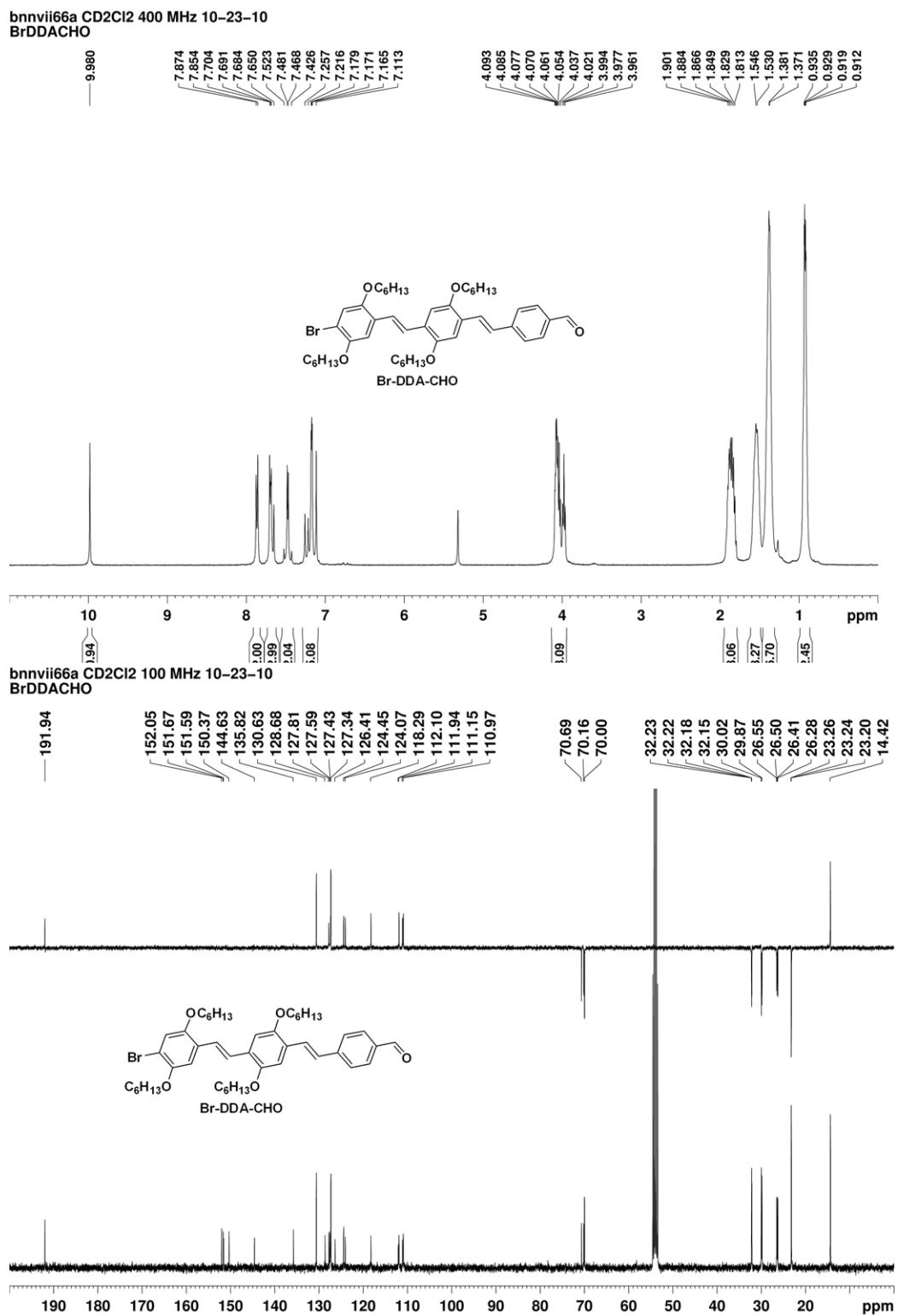


Figure 65. ^1H , ^{13}C , and DEPT 135 NMR spectra of Br-AADD-CN.

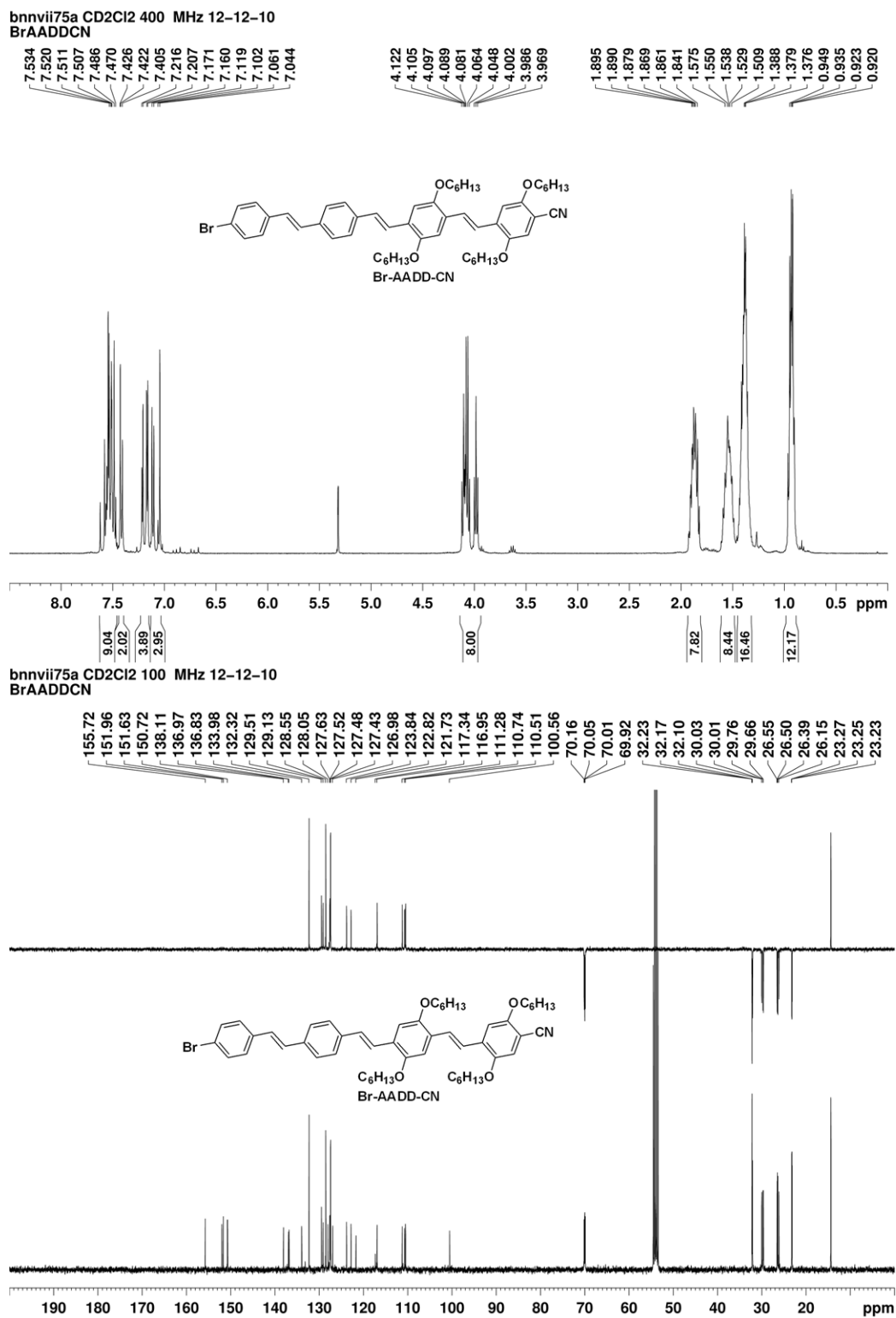
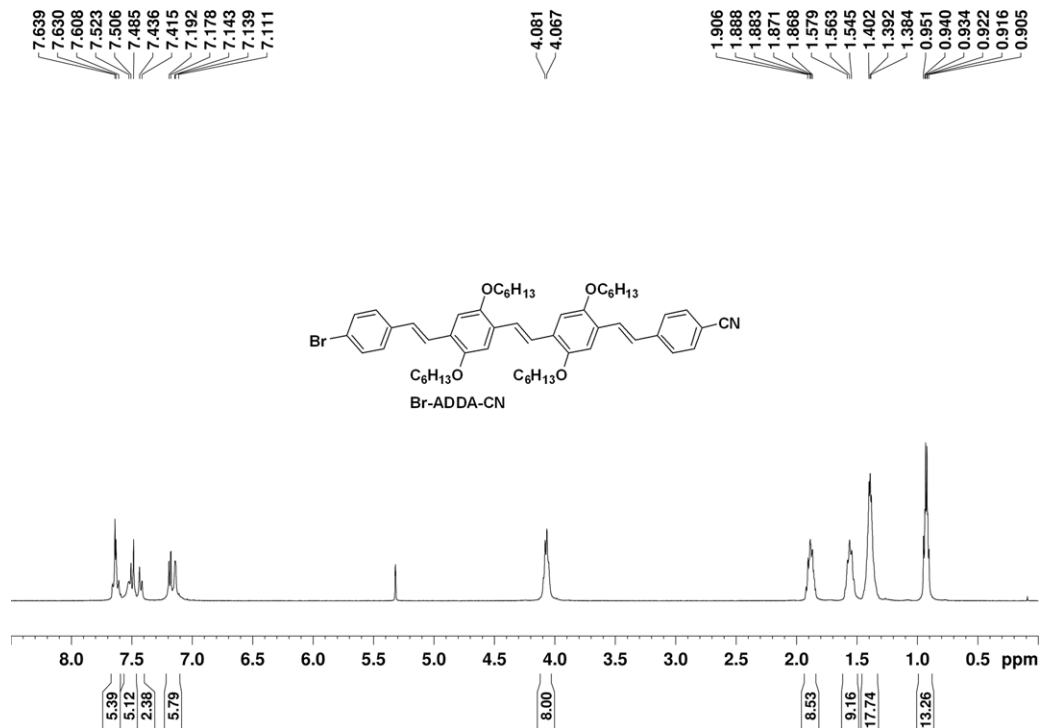


Figure 66. ^1H , ^{13}C , and DEPT 135 NMR spectra of Br-ADDA-CN.

bnnvii74a CD2Cl2 400 MHz 12-5-10
BrADDACN



bnnvii74a CD2Cl2 100 MHz 12-11-10
BrADDACN

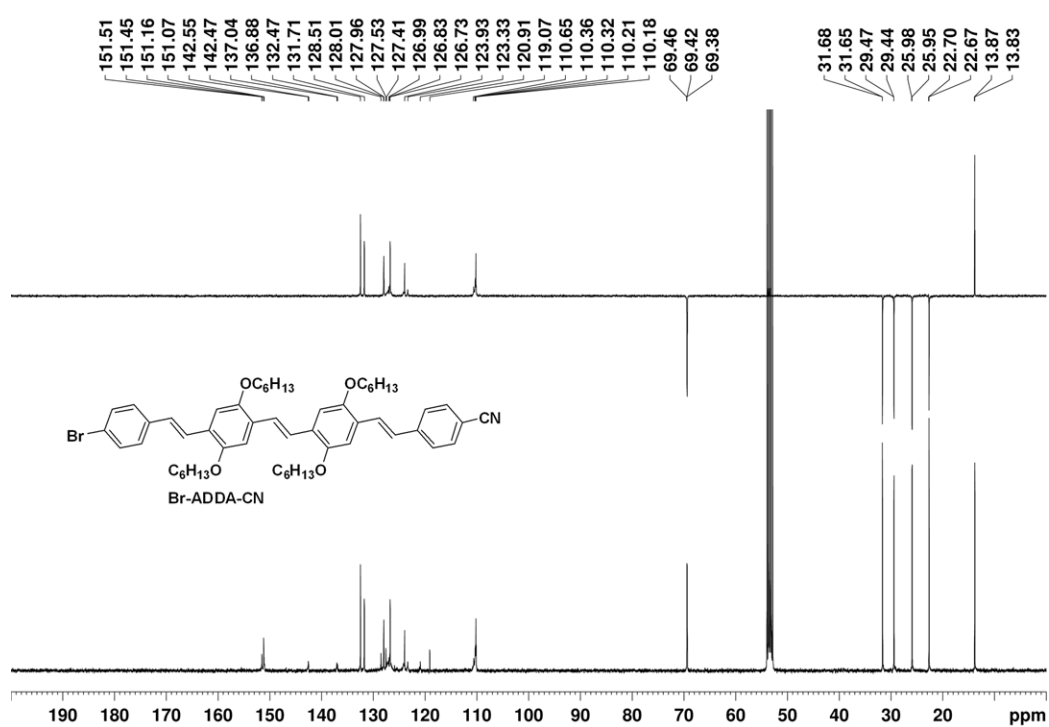


Figure 67. ^1H , ^{13}C , and DEPT 135 NMR spectra of Br-ADAD-CN.

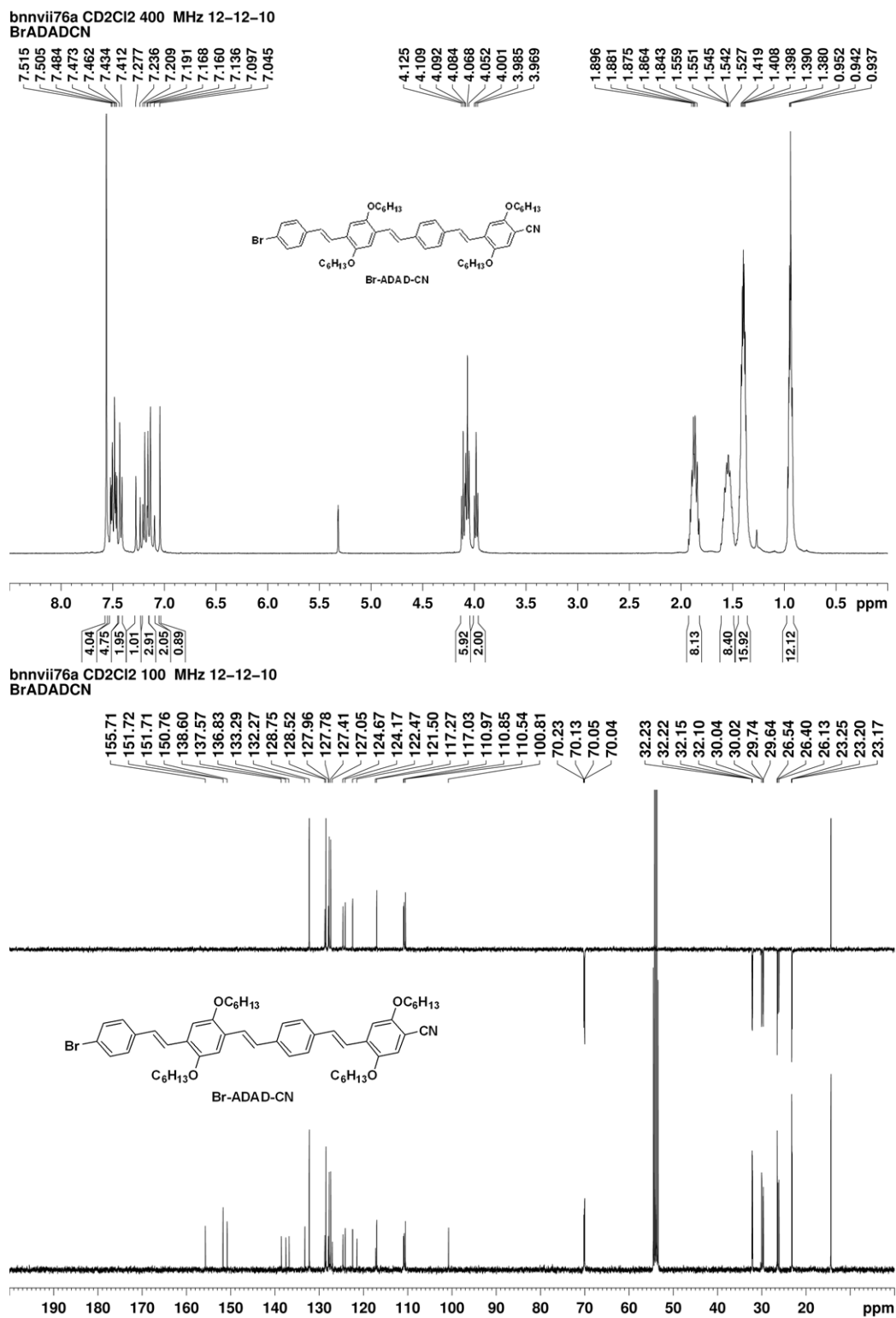


Figure 68. ^1H , ^{13}C , and DEPT 135 NMR spectra of Br-DAAD-CN.

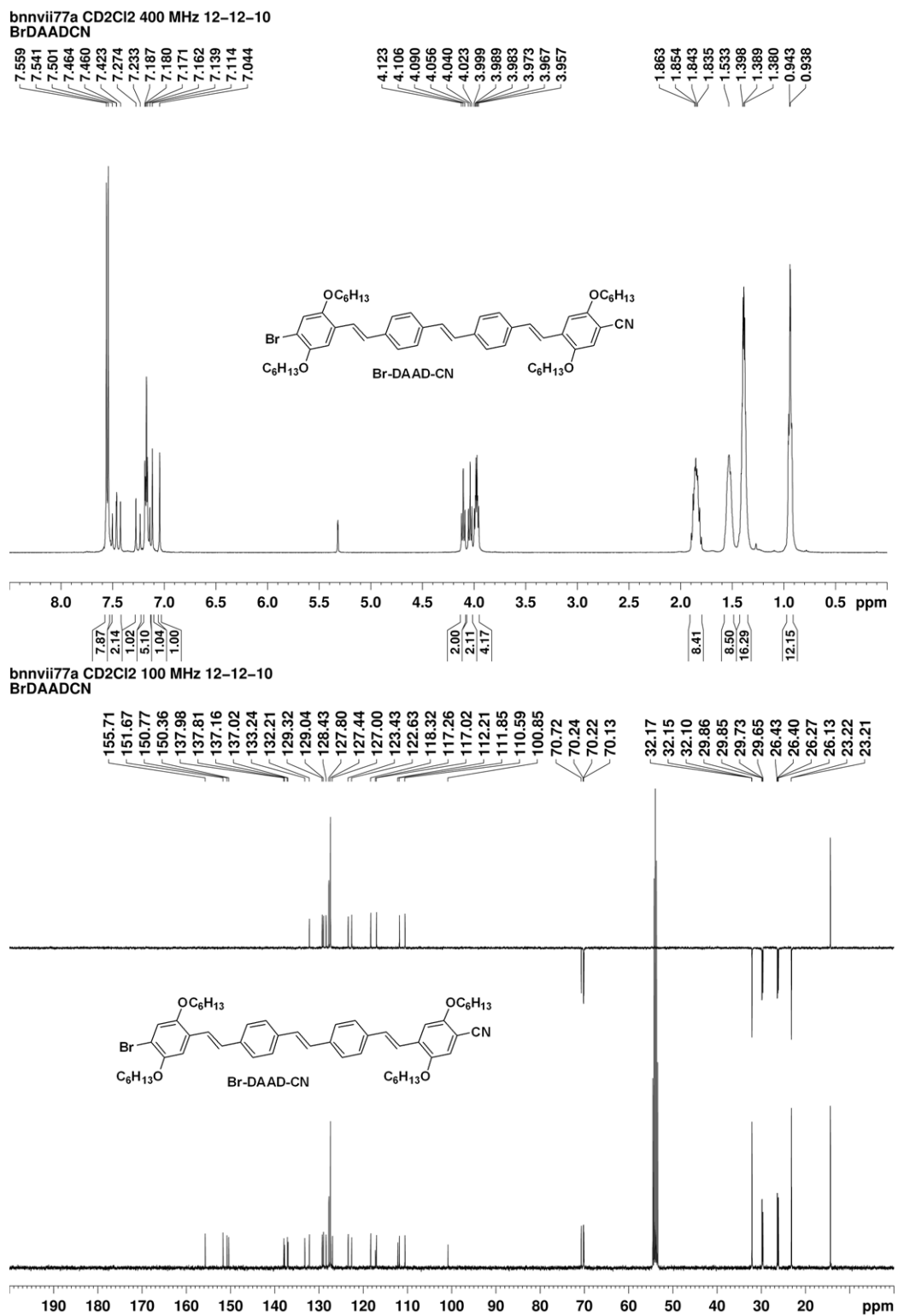


Figure 69. ^1H , ^{13}C , and DEPT 135 NMR spectra of Br-DADA-CN.

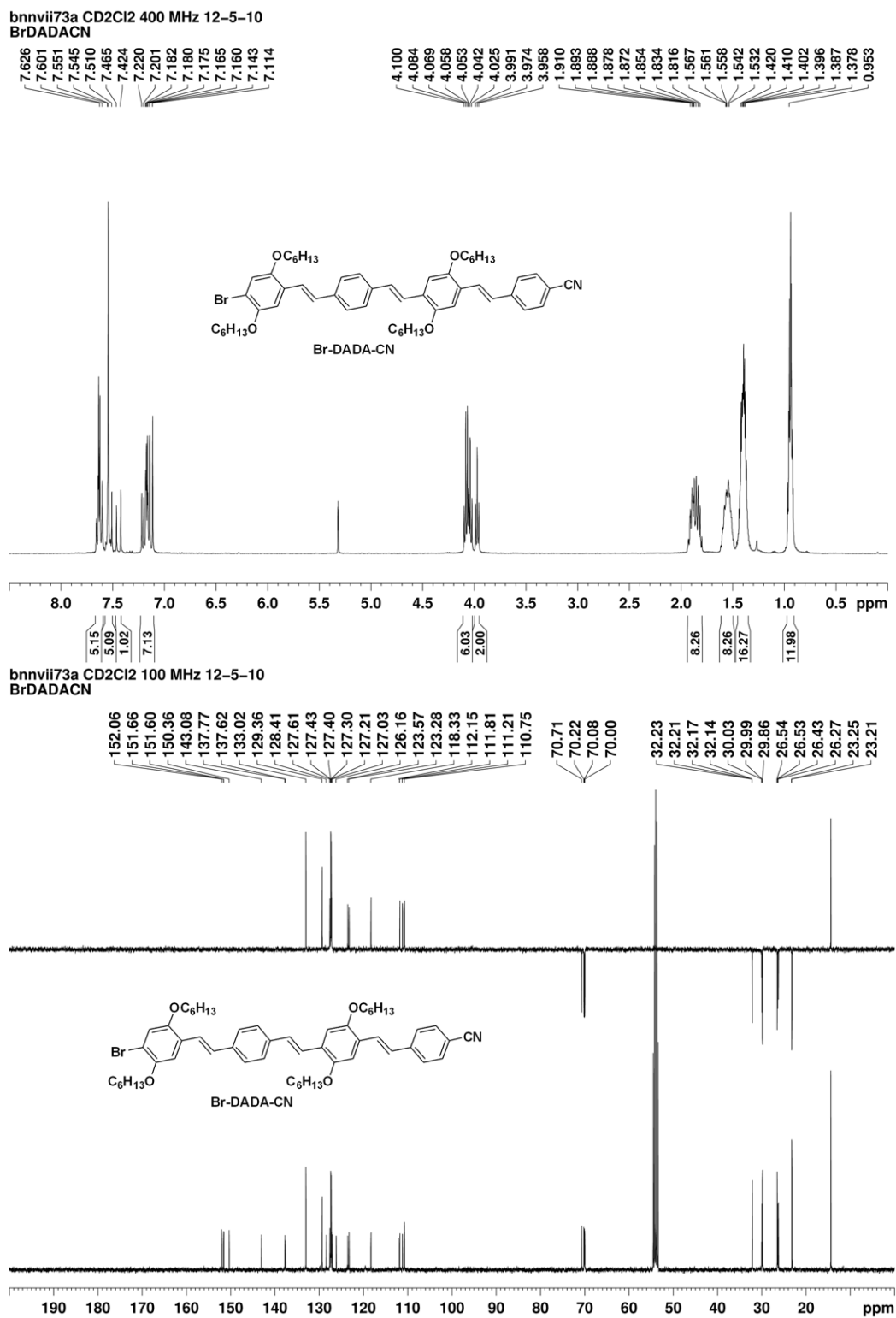
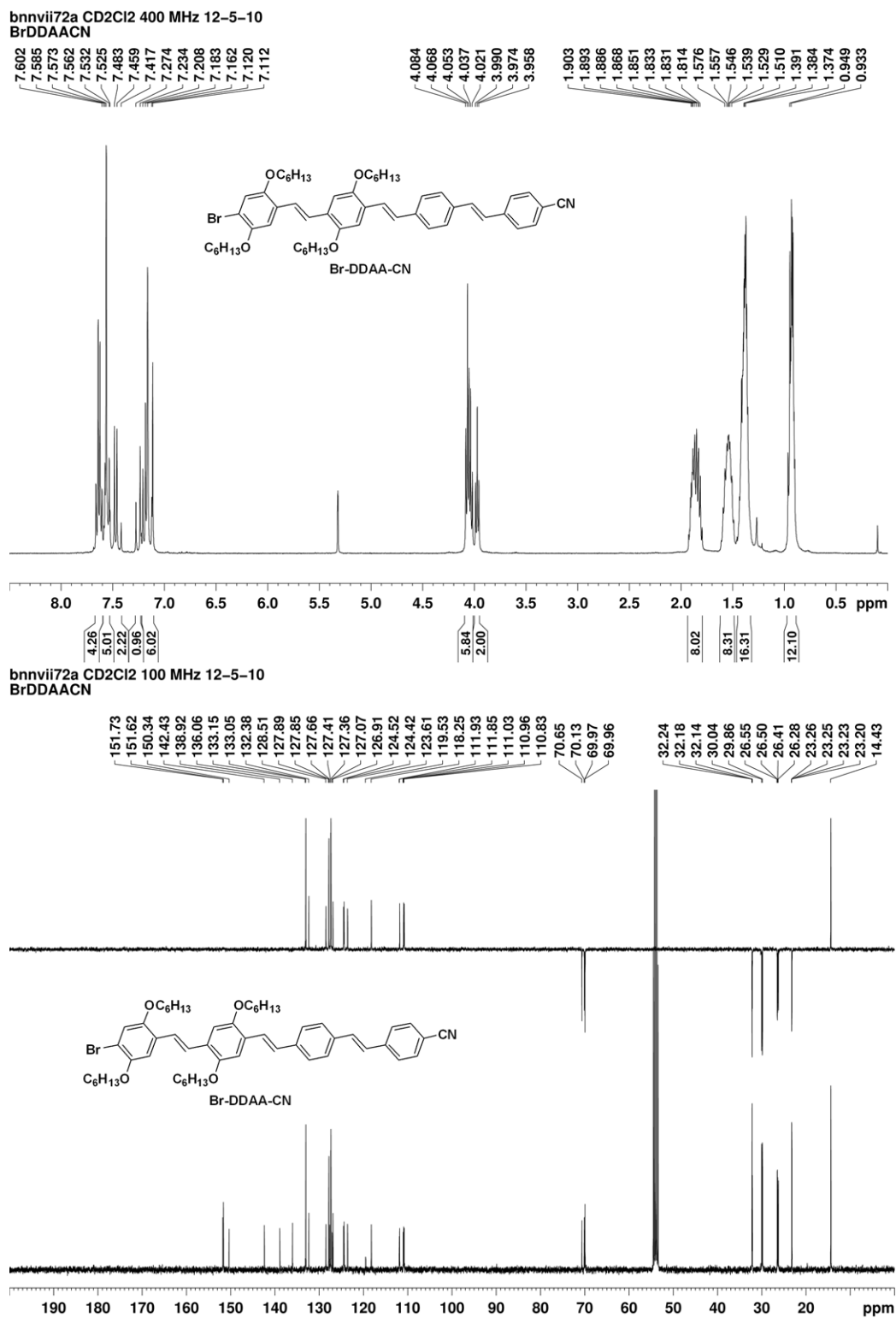


Figure 70. ^1H , ^{13}C , and DEPT 135 NMR spectra of Br-DDAA-CN.



A.2 ABSORPTION AND EMISSION SPECTRA

Figure 71. Absorption and emission spectra of Br-AA-CN.

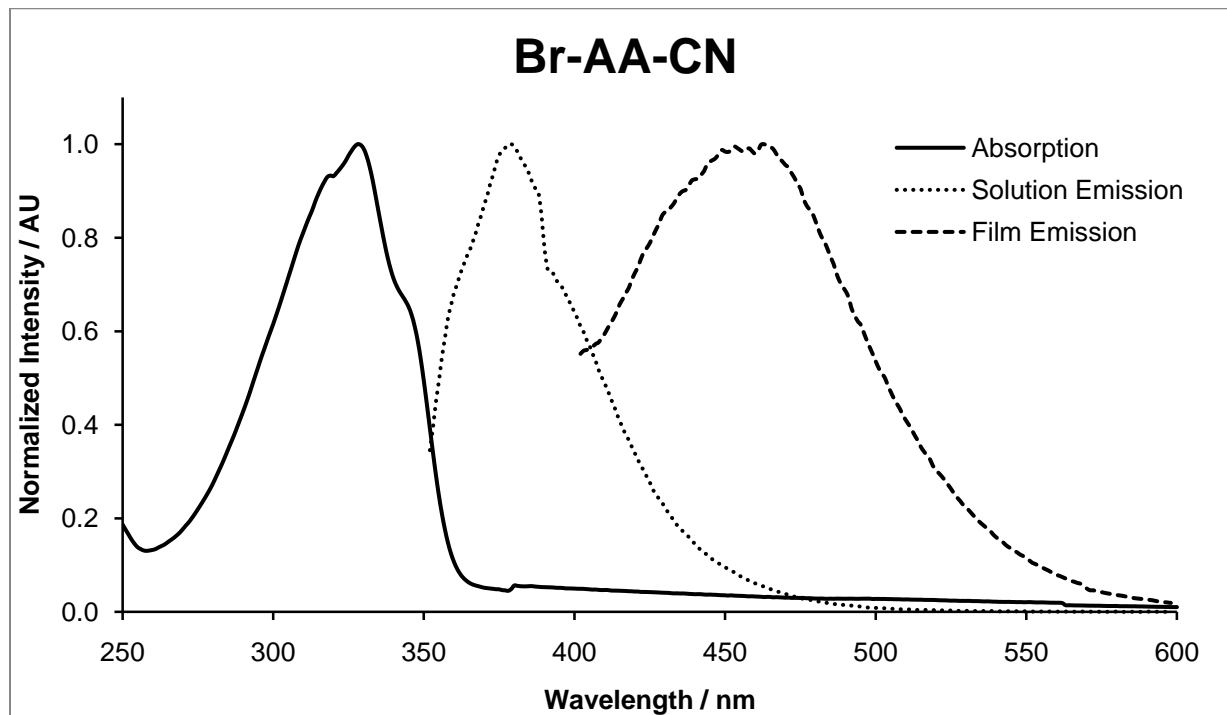


Figure 72. Absorption and emission spectra of Br-DD-CN.

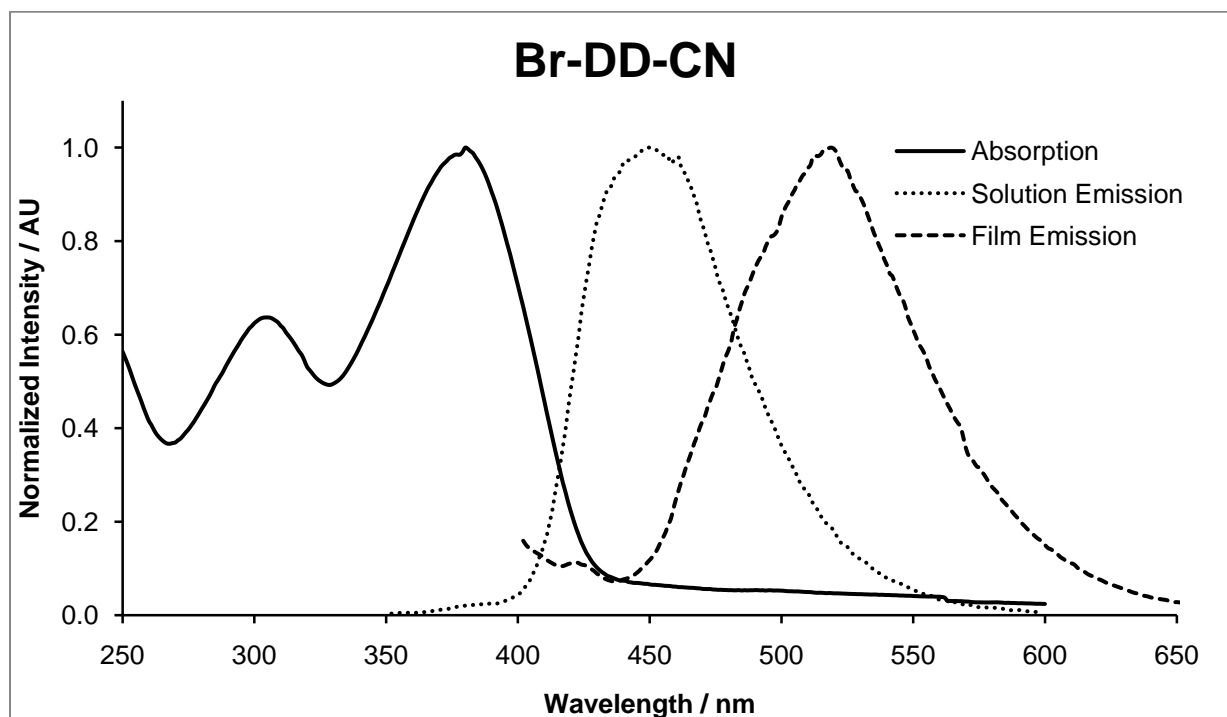


Figure 73. Absorption and emission spectra of Br-AD-CN.

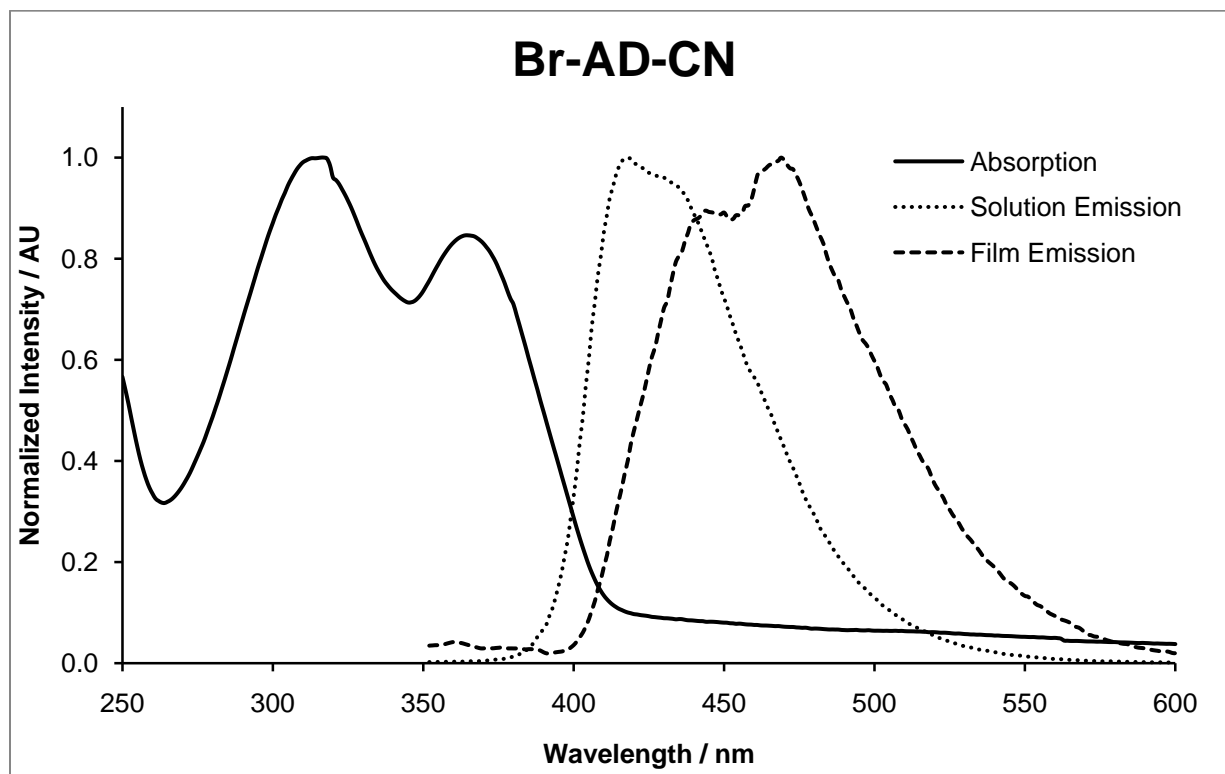


Figure 74. Absorption and emission spectra of Br-DA-CN.

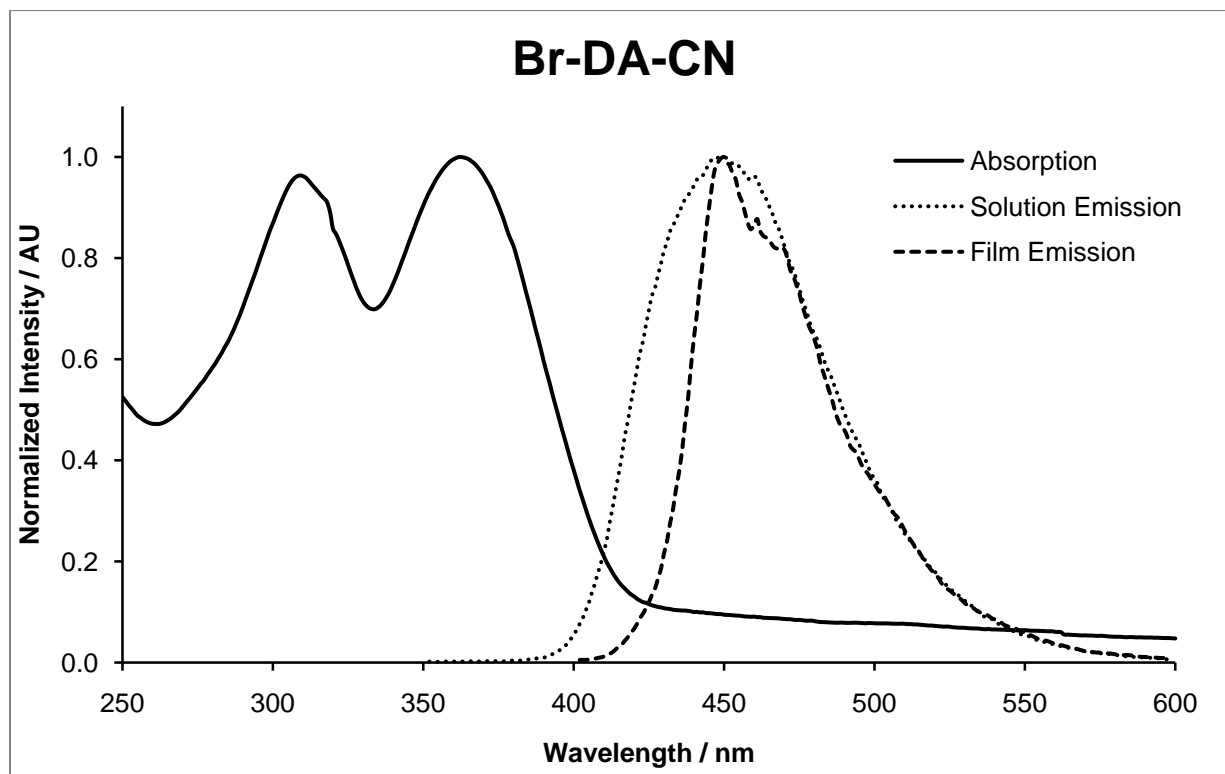


Figure 75. Absorption and emission spectra of Br-AAD-CN.

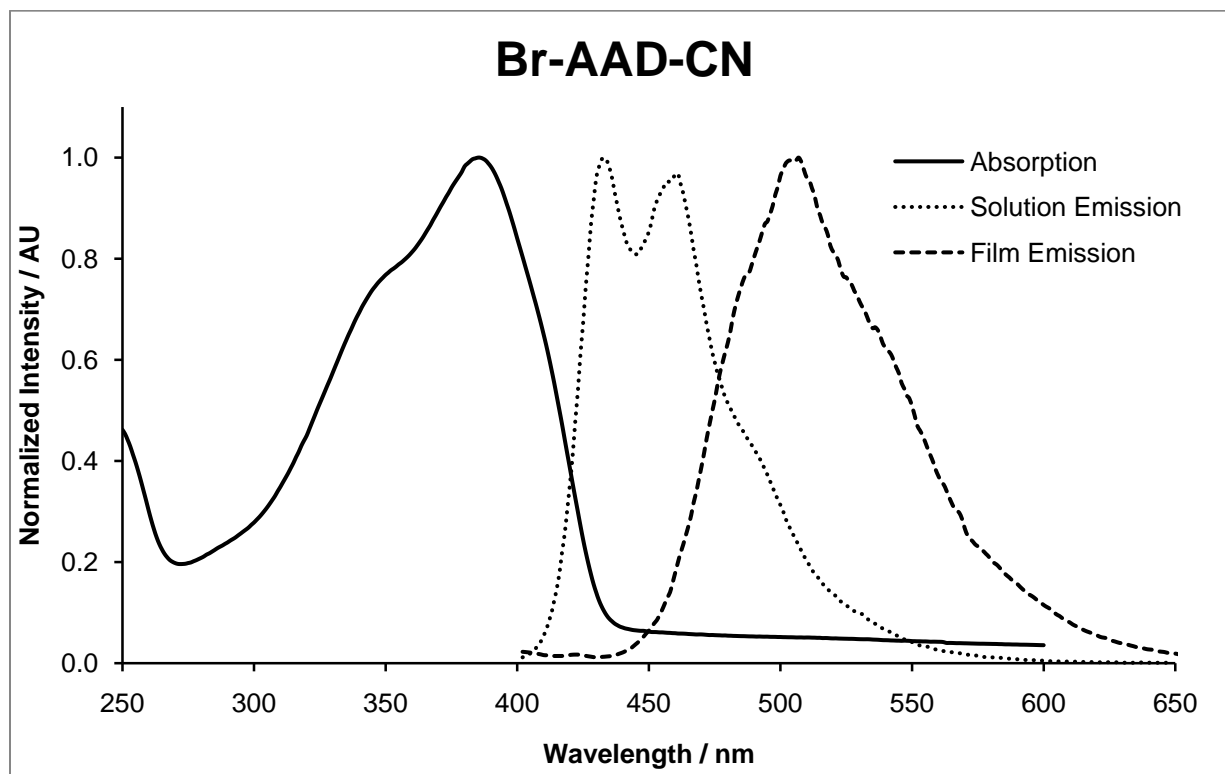


Figure 76. Absorption and emission spectra of Br-DAA-CN.

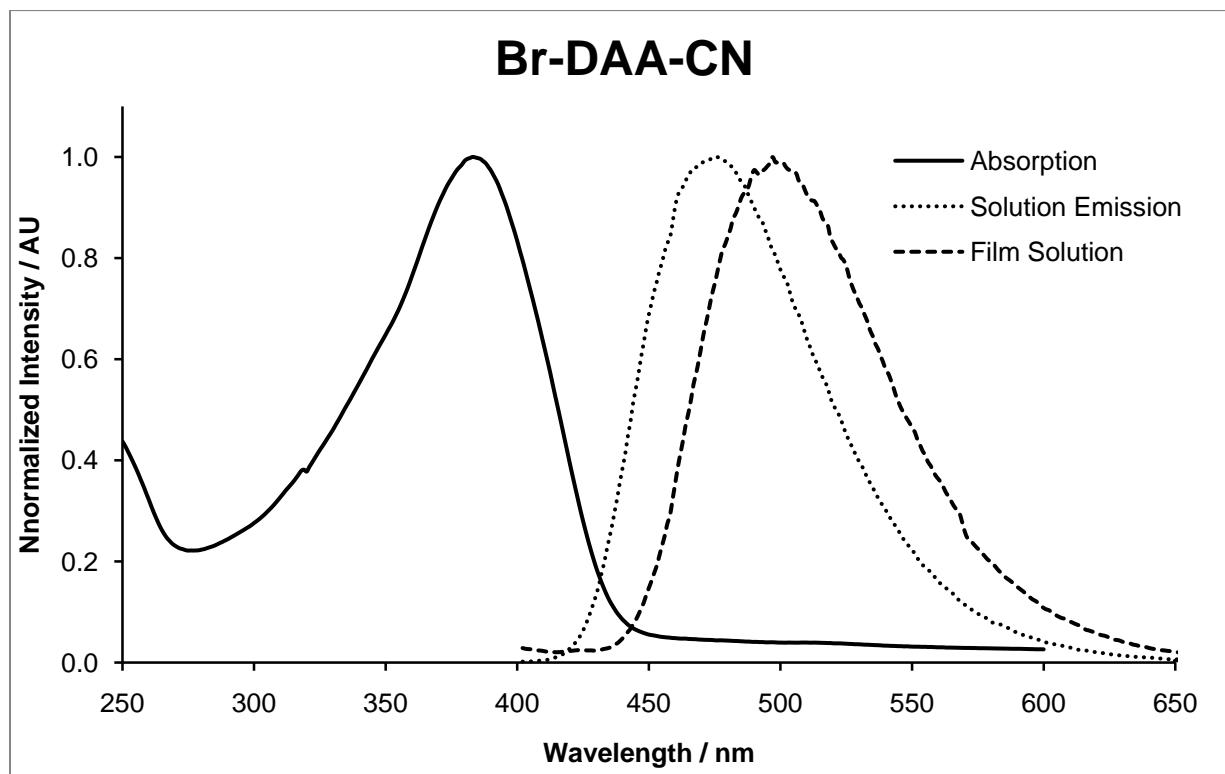


Figure 77. Absorption and emission spectra of Br-ADA-CN.

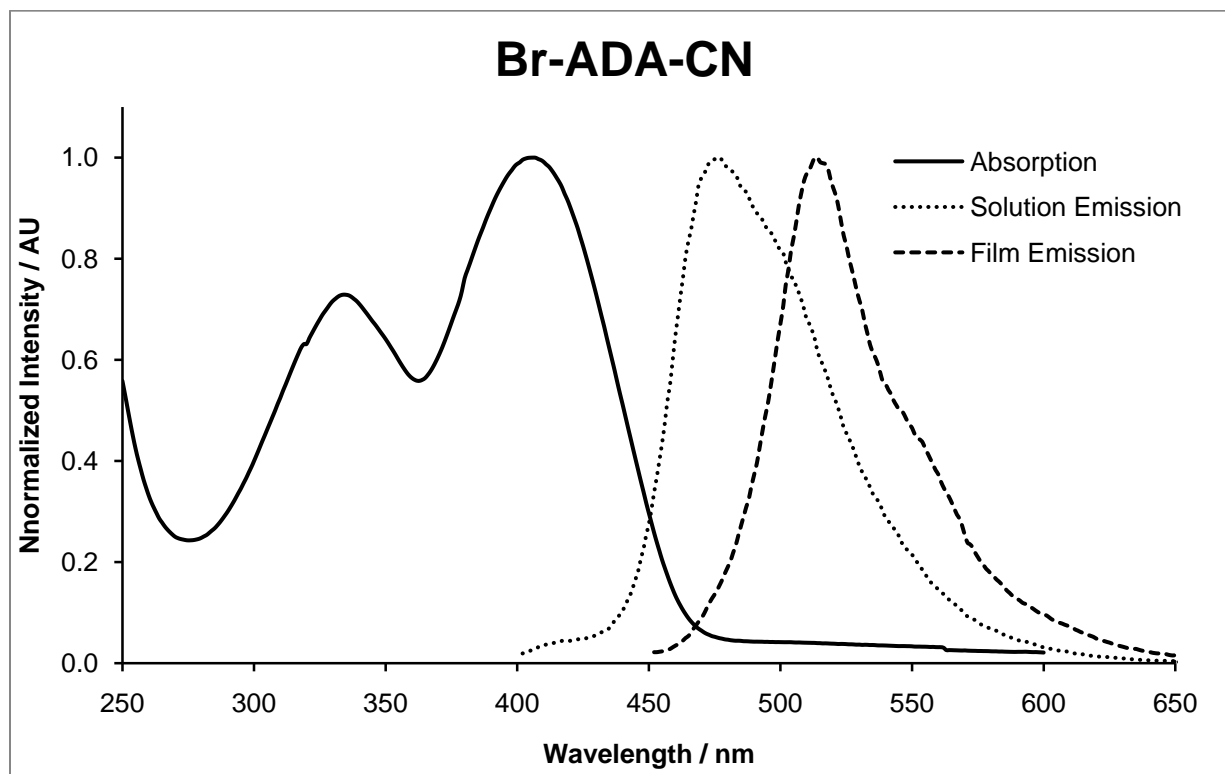


Figure 78. Absorption and emission spectra of Br-DAD-CN.

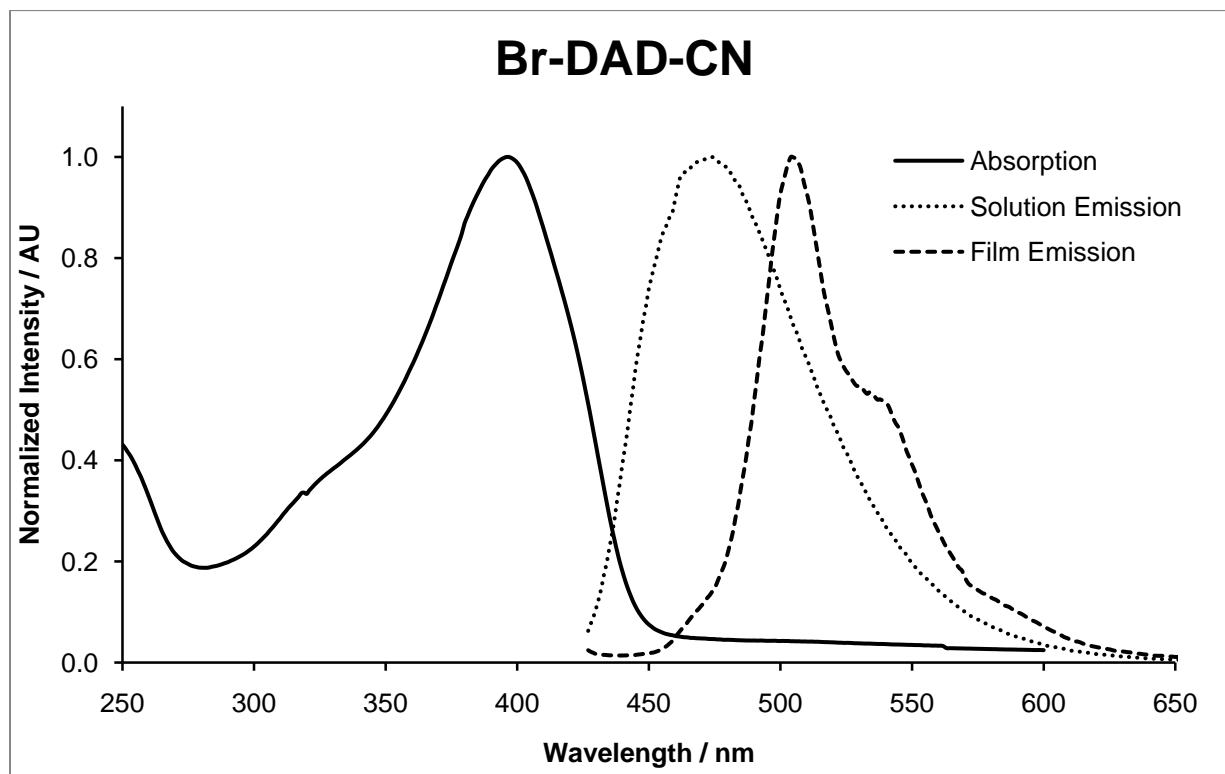


Figure 79. Absorption and emission spectra of Br-ADD-CN.

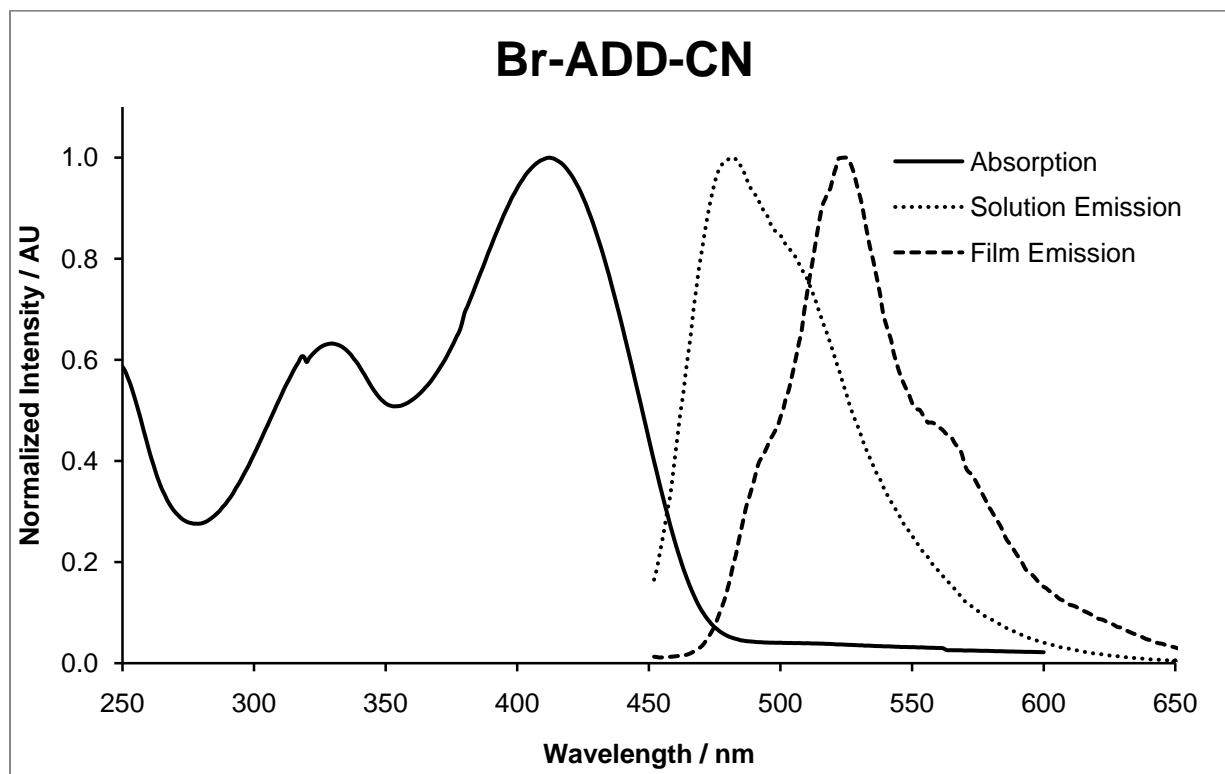


Figure 80. Absorption and emission spectra of Br-DDA-CN.

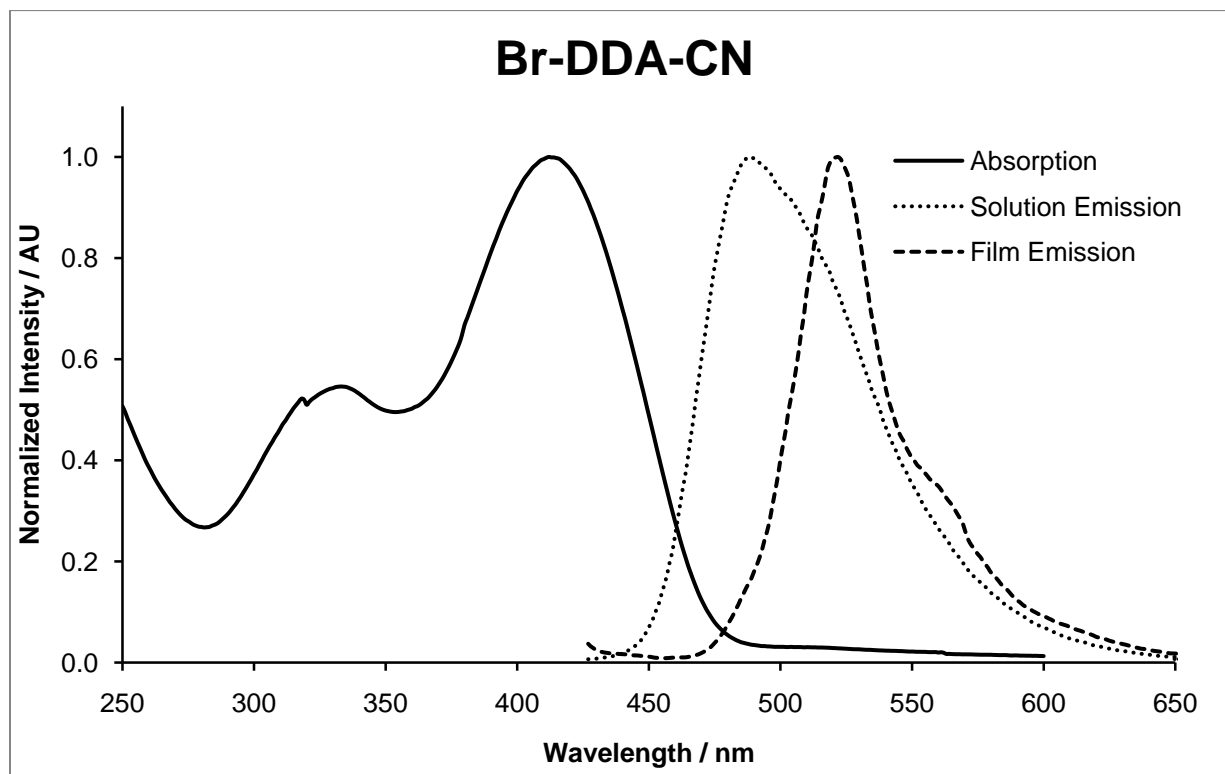


Figure 81. Absorption and emission spectra of Br-AADD-CN.

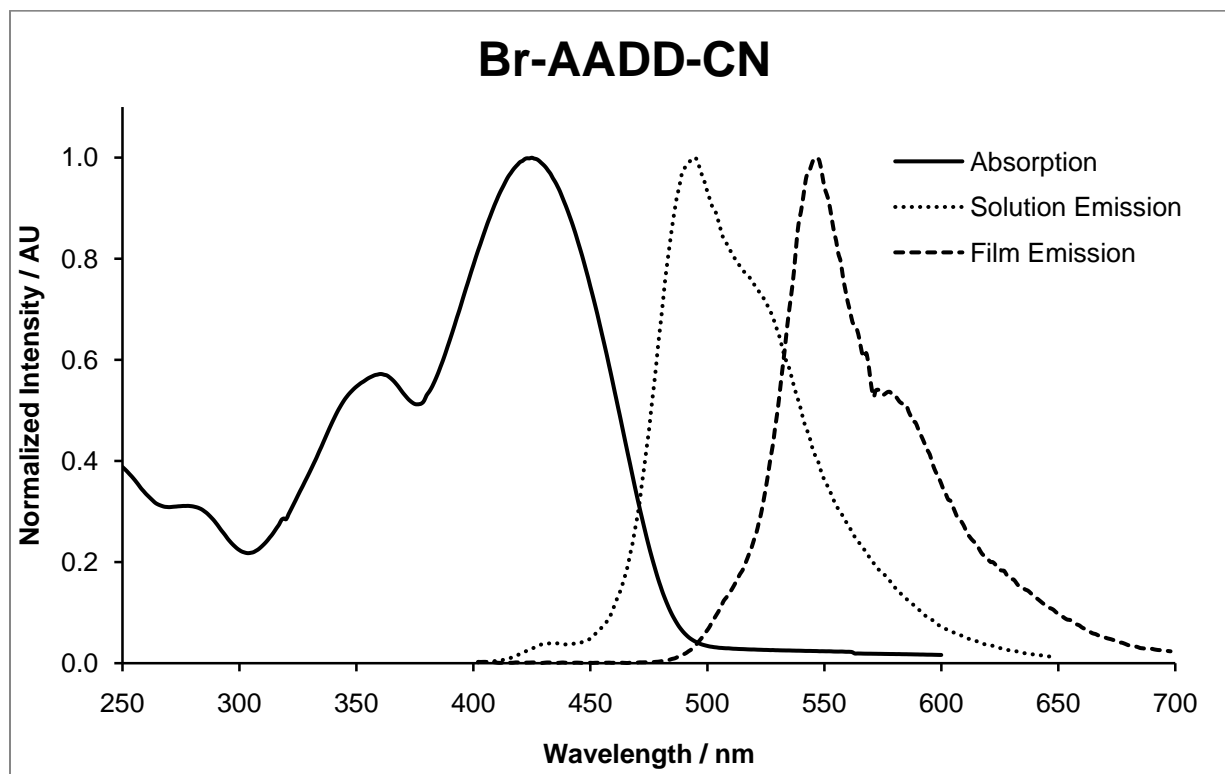


Figure 82. Absorption and emission spectra of Br-AADD-CN.

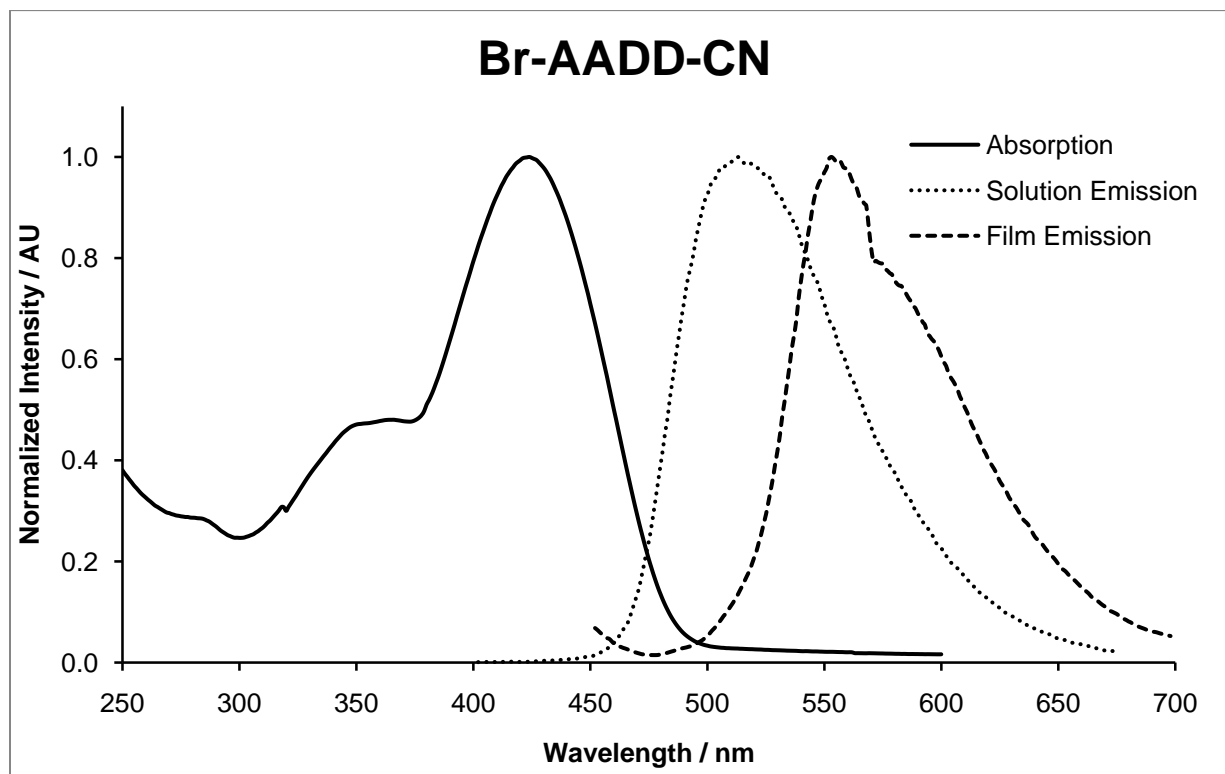


Figure 83. Absorption and emission spectra of Br-ADAD-CN.

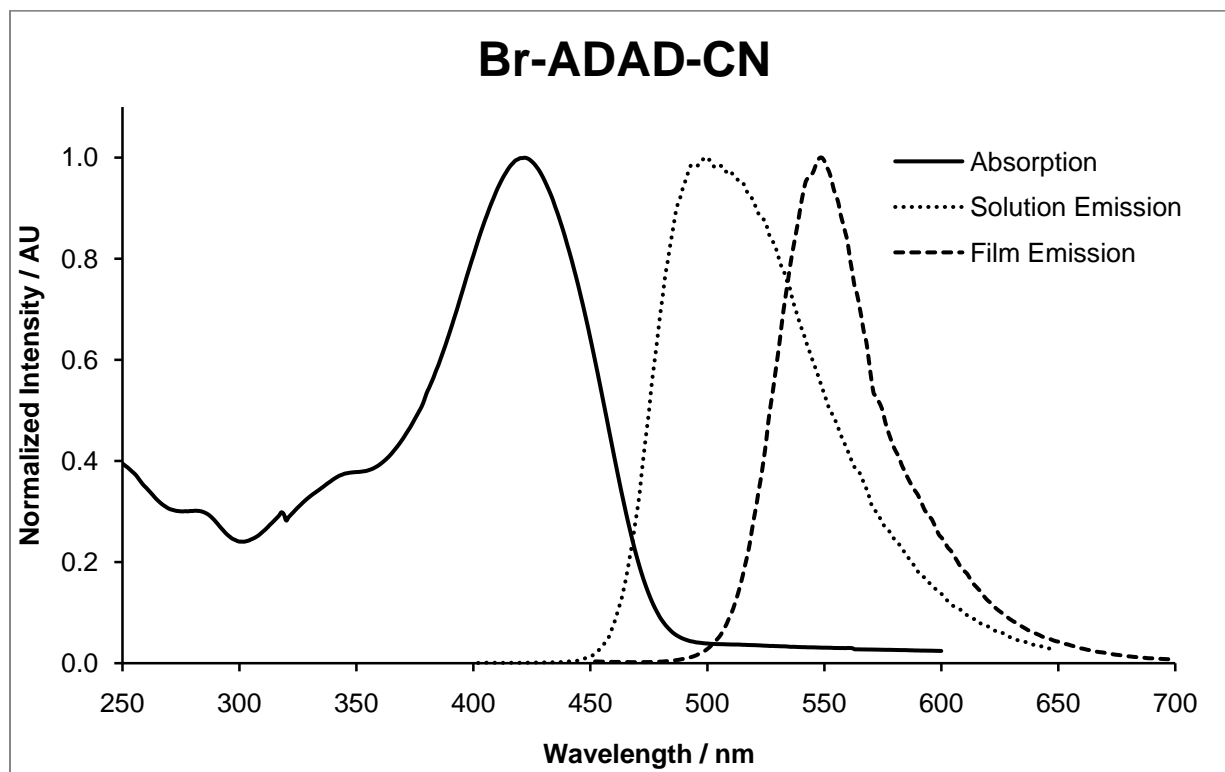


Figure 84. Absorption and emission spectra of Br-DADA-CN.

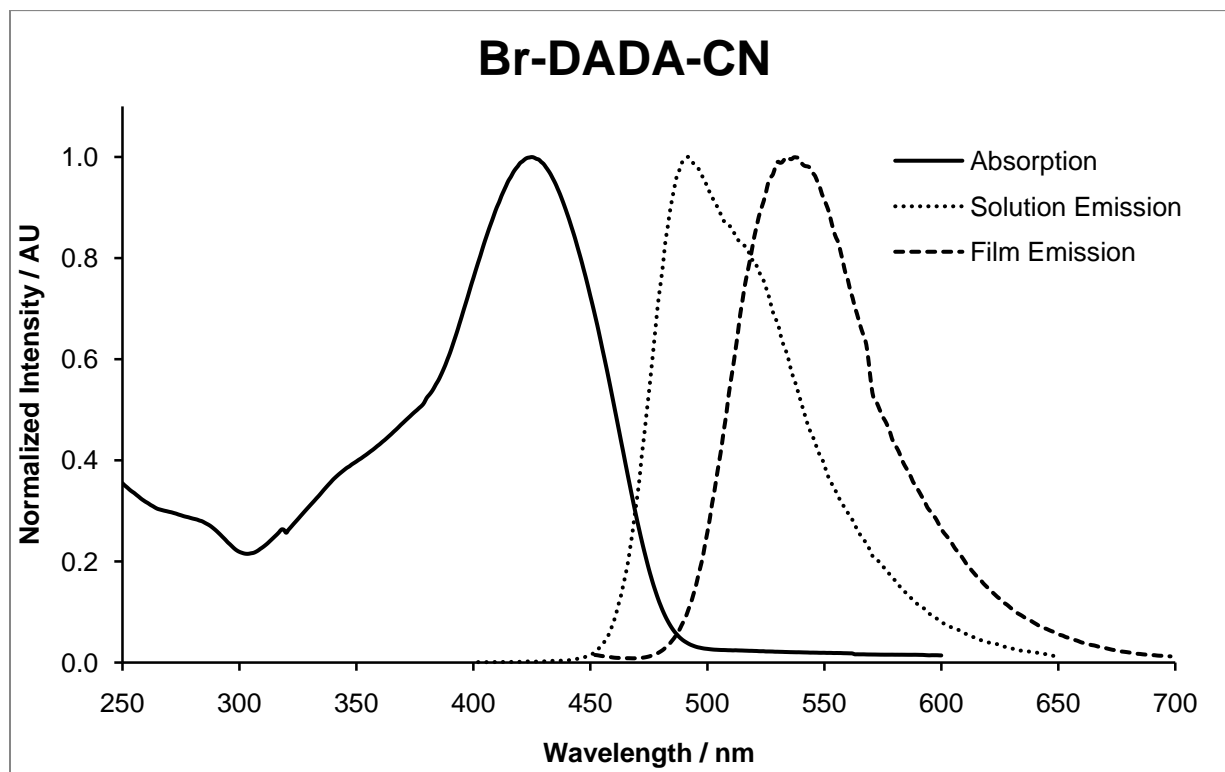


Figure 85. Absorption and emission spectra of Br-ADDA-CN.

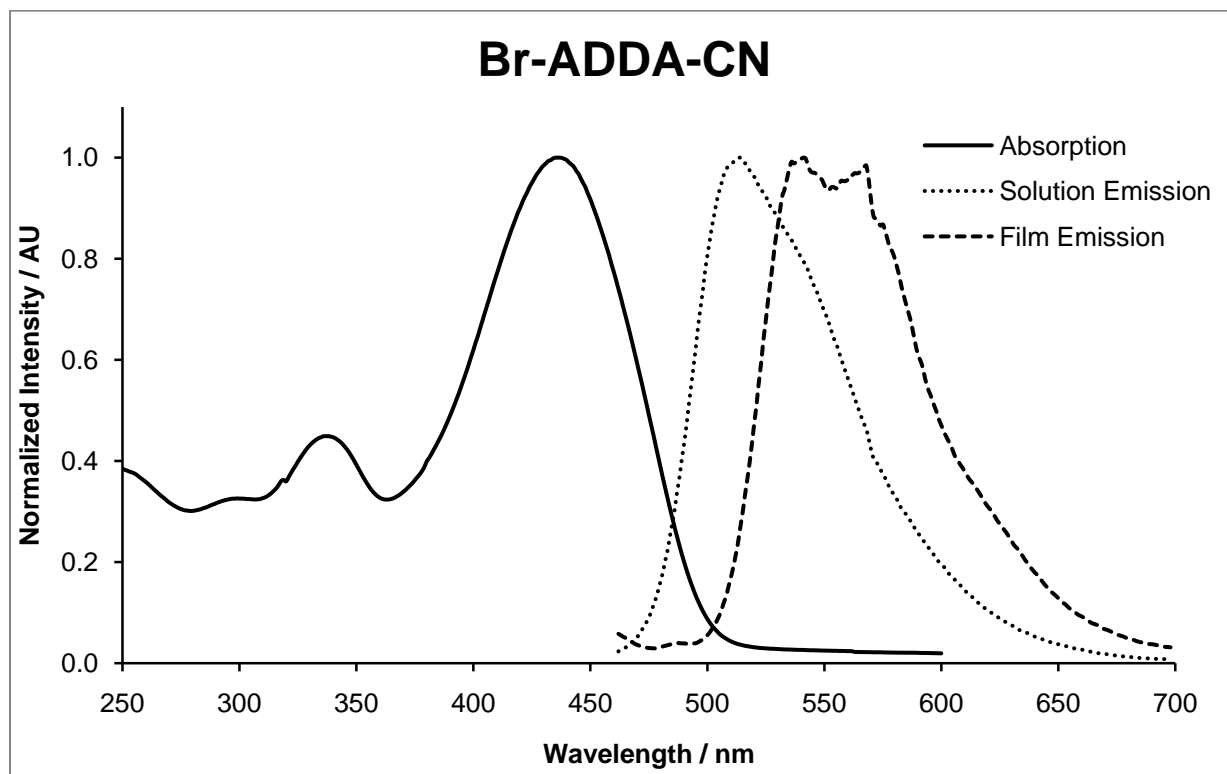
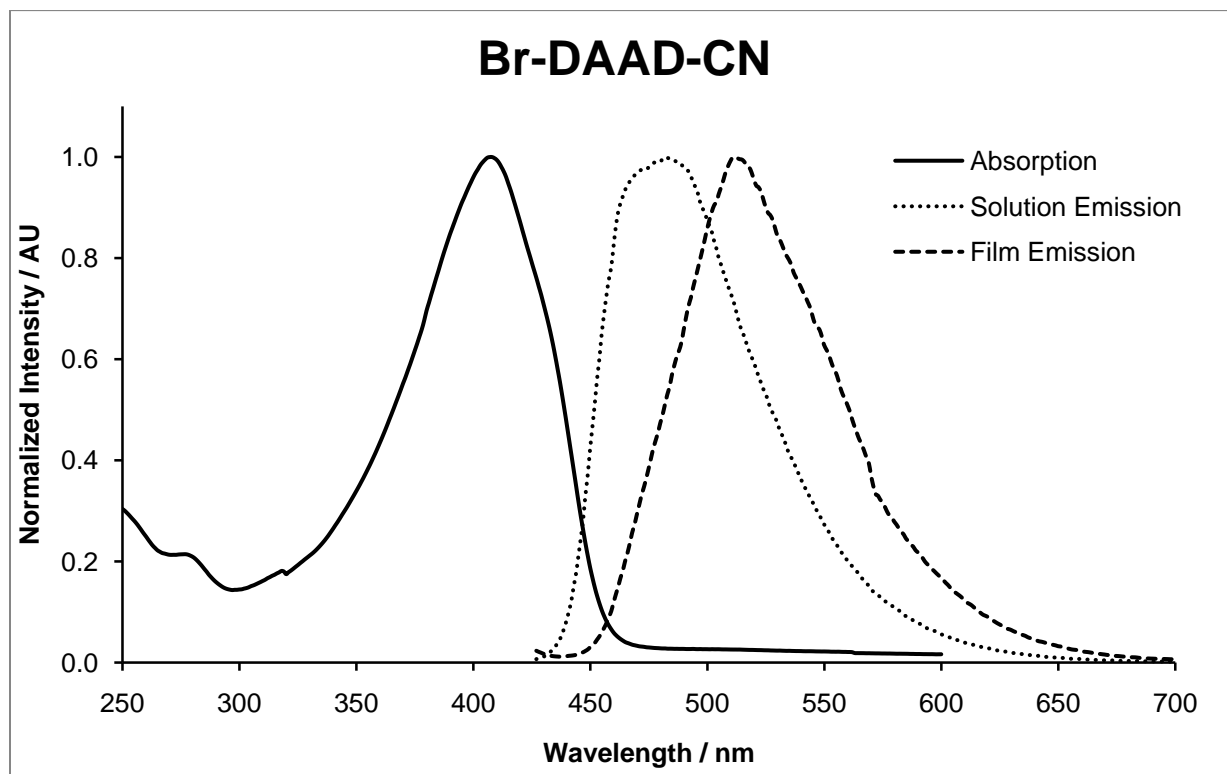


Figure 86. Absorption and emission spectra of Br-DAAD-CN.



A.3 CYCLIC AND DIFFERENTIAL PULSE VOLTAMMOGRAMS

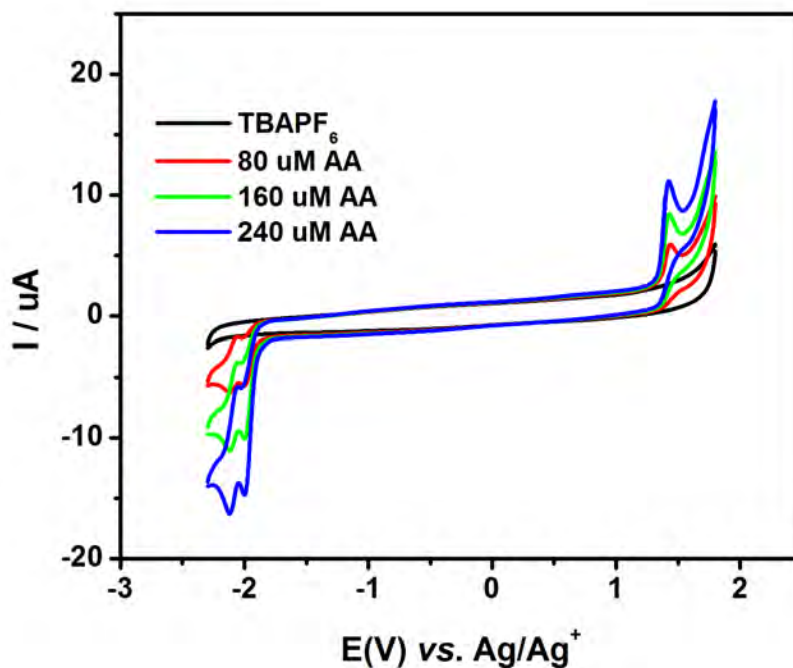


Figure 87. Cyclic voltammograms of Br-AA-CN.

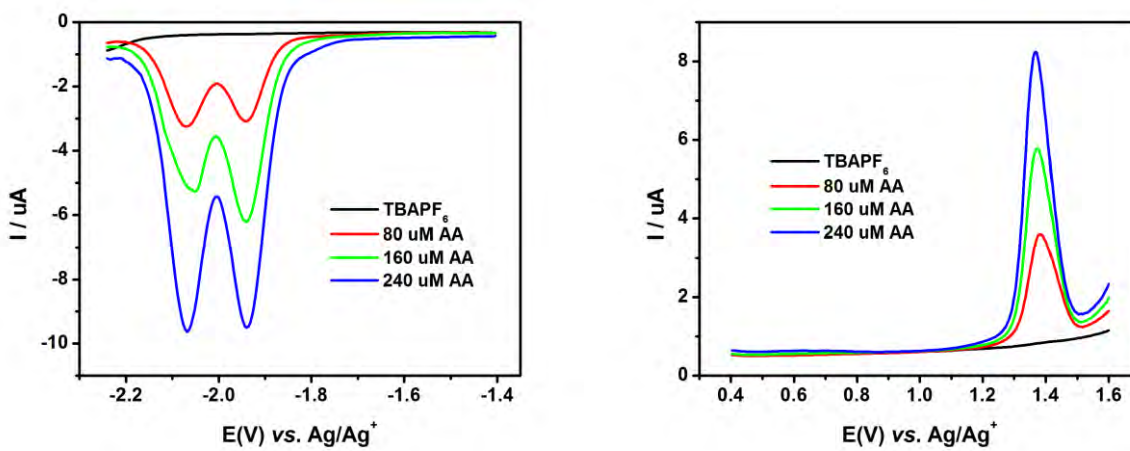


Figure 88. Differential pulse voltammograms of Br-AA-CN. Left: reduction. Right: oxidation.

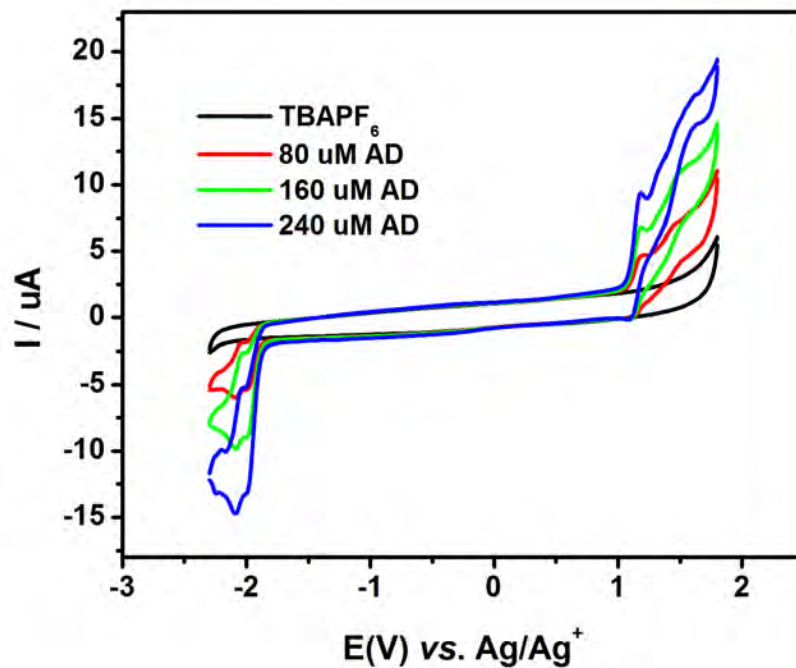


Figure 89. Cyclic voltammograms of Br-AD-CN.

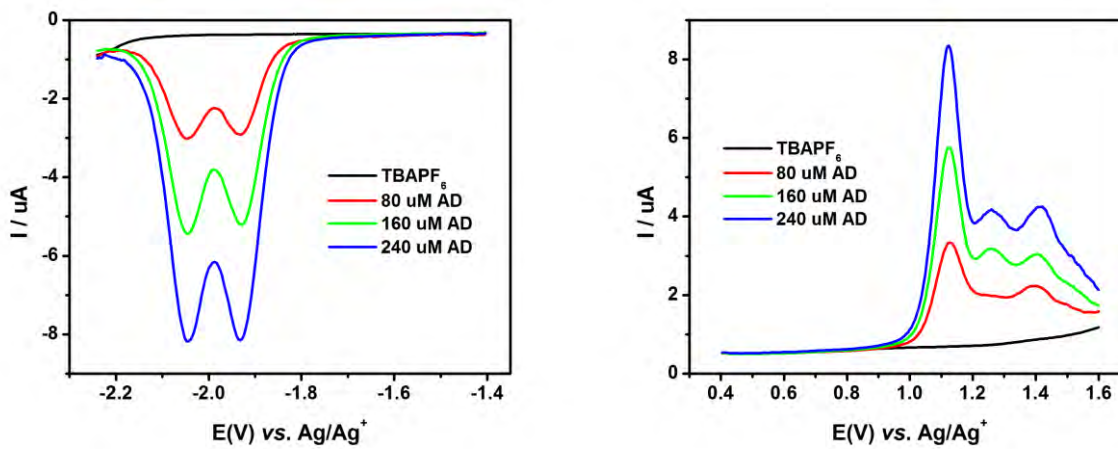


Figure 90. Differential pulse voltammograms of Br-AD-CN. Left: reduction. Right: oxidation.

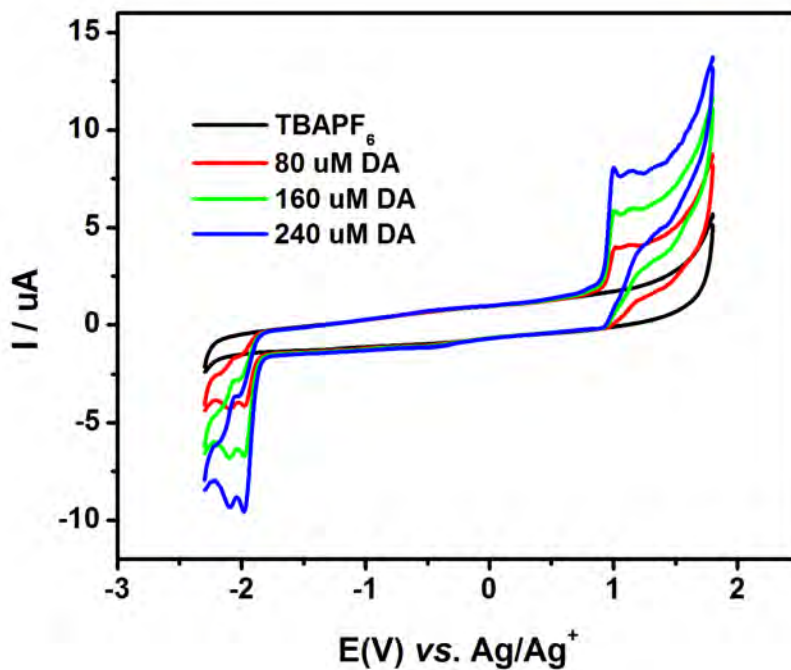


Figure 91. Cyclic voltammograms of Br-DA-CN.

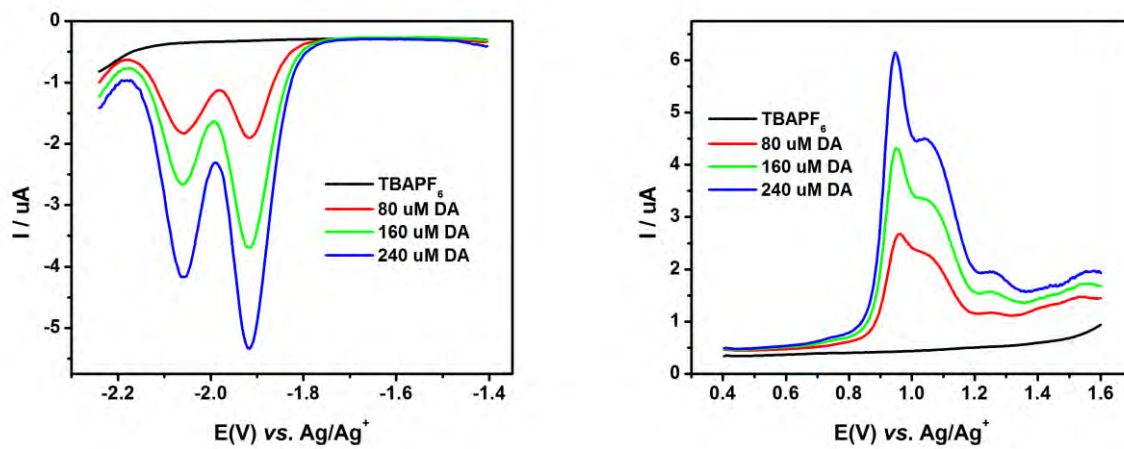


Figure 92. Differential pulse voltammograms of Br-DA-CN. Left: reduction. Right: oxidation.

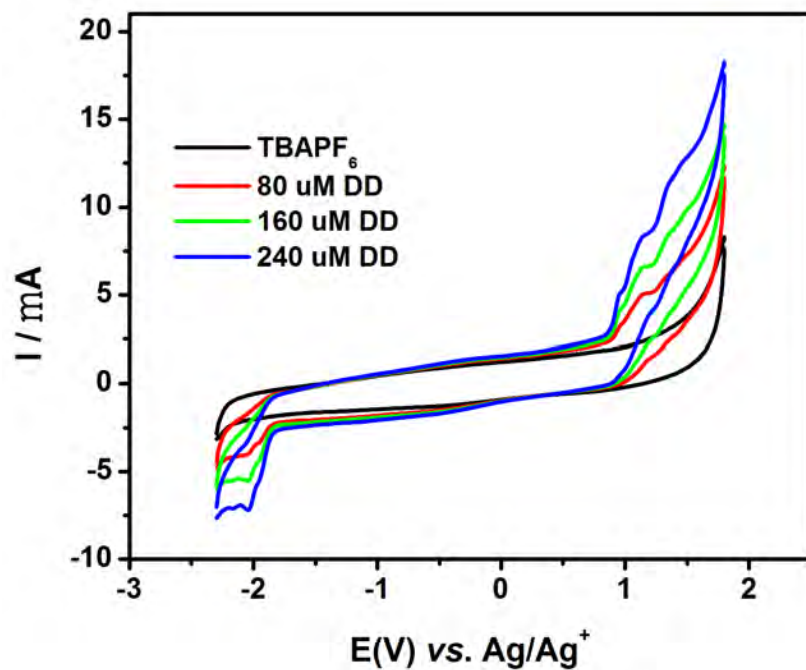


Figure 93. Cyclic voltammograms of Br-DD-CN.

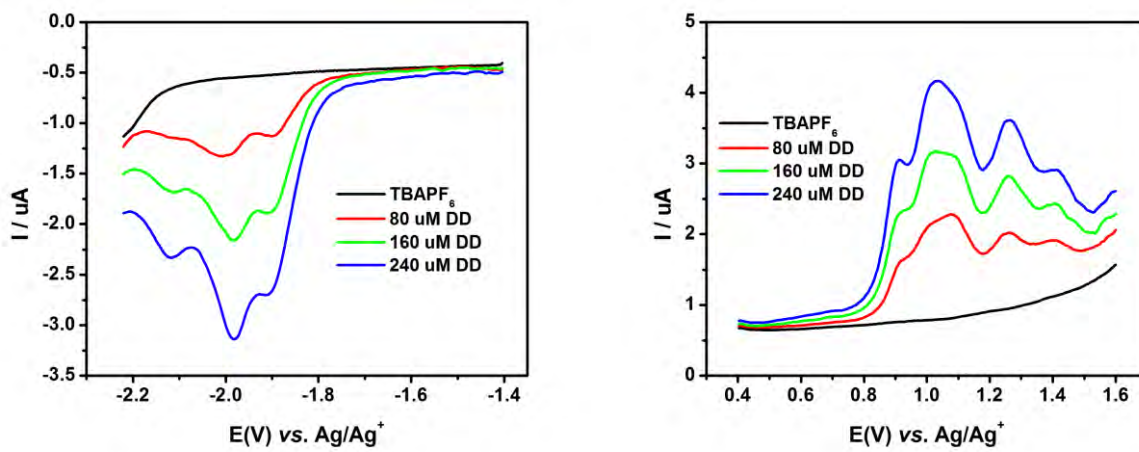


Figure 94. Differential pulse voltammograms of Br-DD-CN. Left: reduction. Right: oxidation.

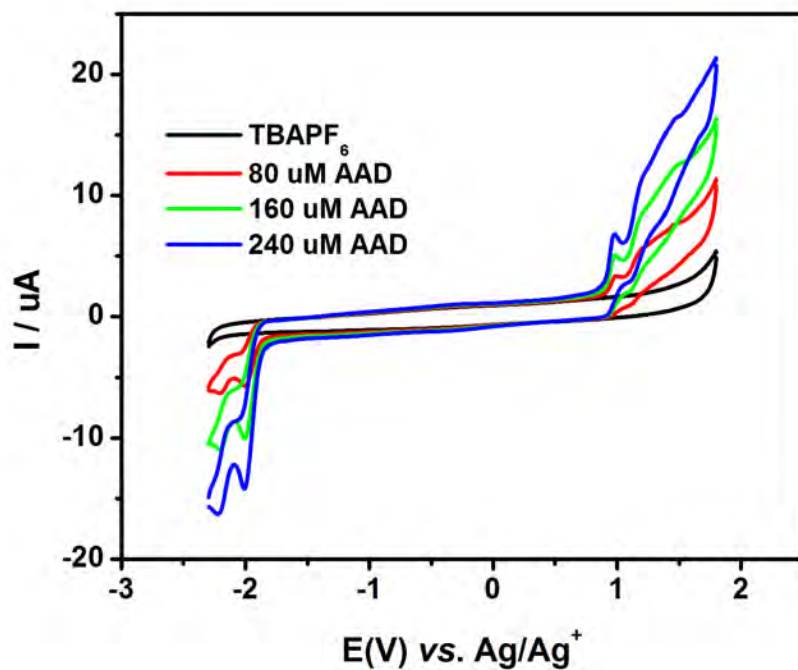


Figure 95. Cyclic voltammograms of Br-AAD-CN.

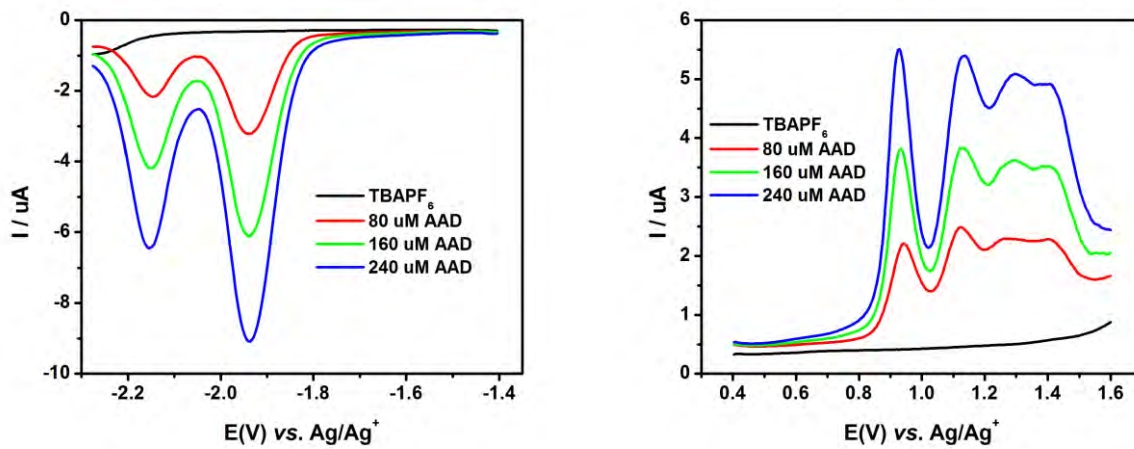


Figure 96. Differential pulse voltammograms of Br-AAD-CN. Left: reduction. Right: oxidation.

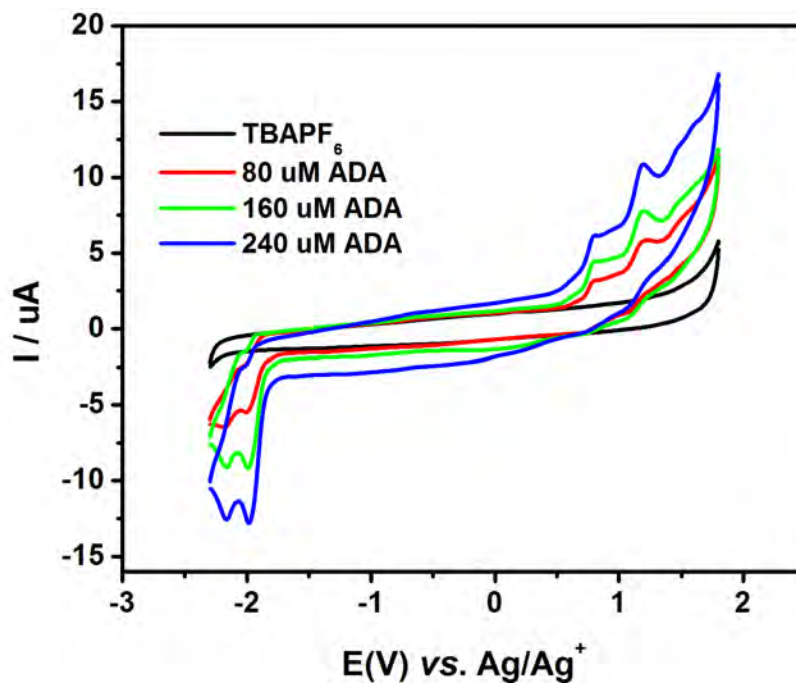


Figure 97. Cyclic voltammograms of Br-ADA-CN.

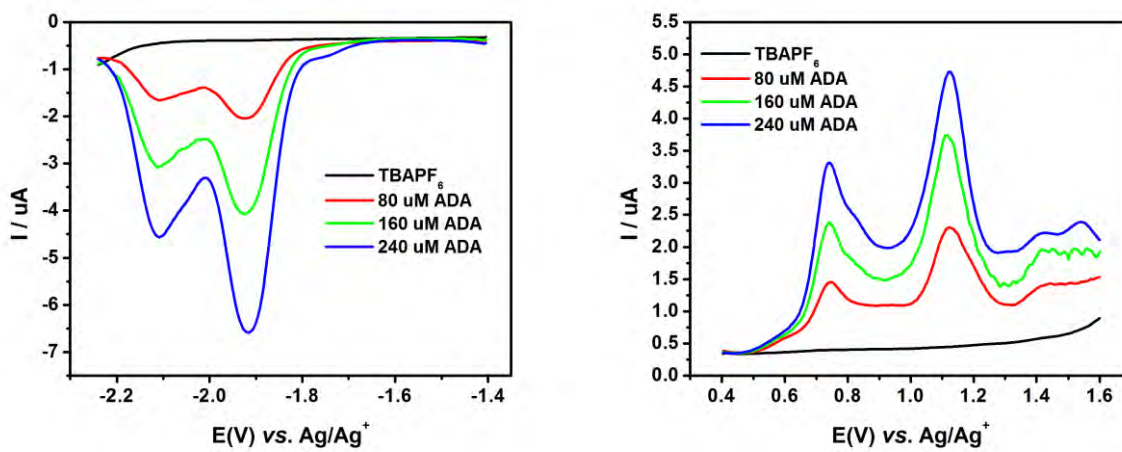


Figure 98. Differential pulse voltammograms of Br-ADA-CN. Left: reduction. Right: oxidation.

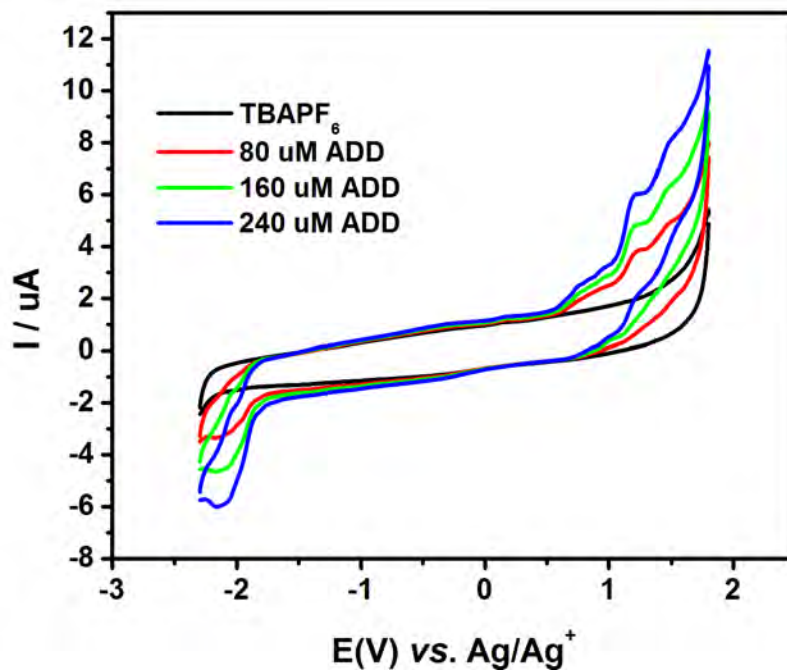


Figure 99. Cyclic voltammograms of Br-AA-CN.

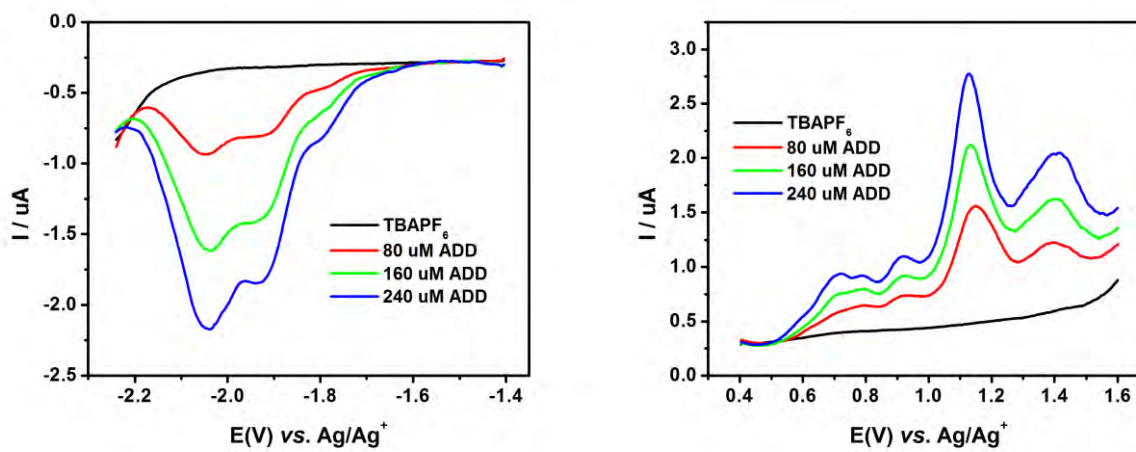


Figure 100. Differential pulse voltammograms of Br-ADD-CN. Left: reduction. Right: oxidation.

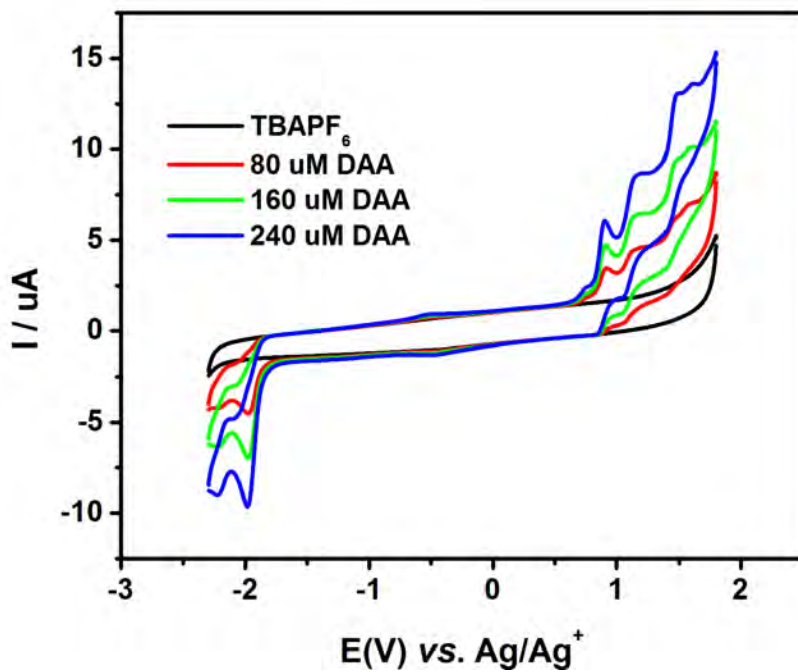


Figure 101. Cyclic voltammograms of Br-DAA-CN.

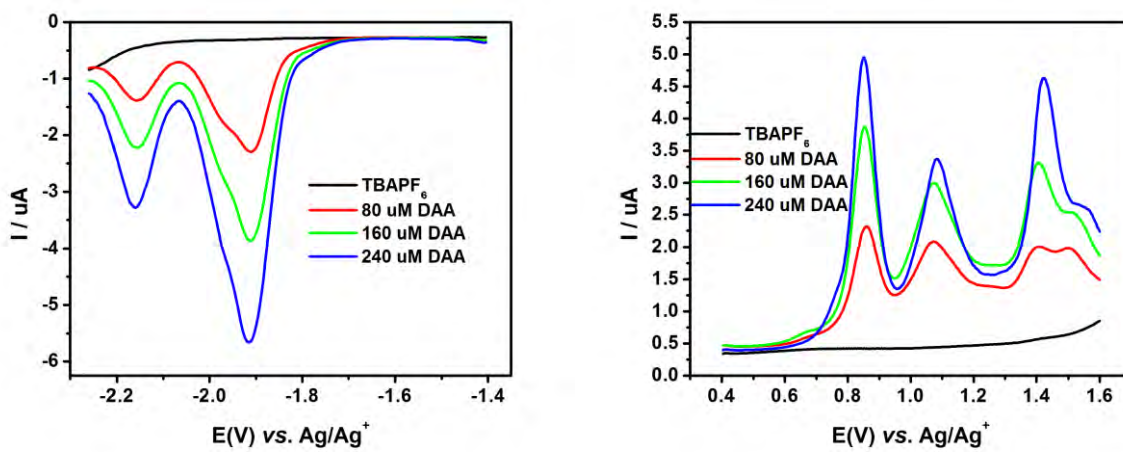


Figure 102. Differential pulse voltammograms of Br-DAA-CN. Left: reduction. Right: oxidation.

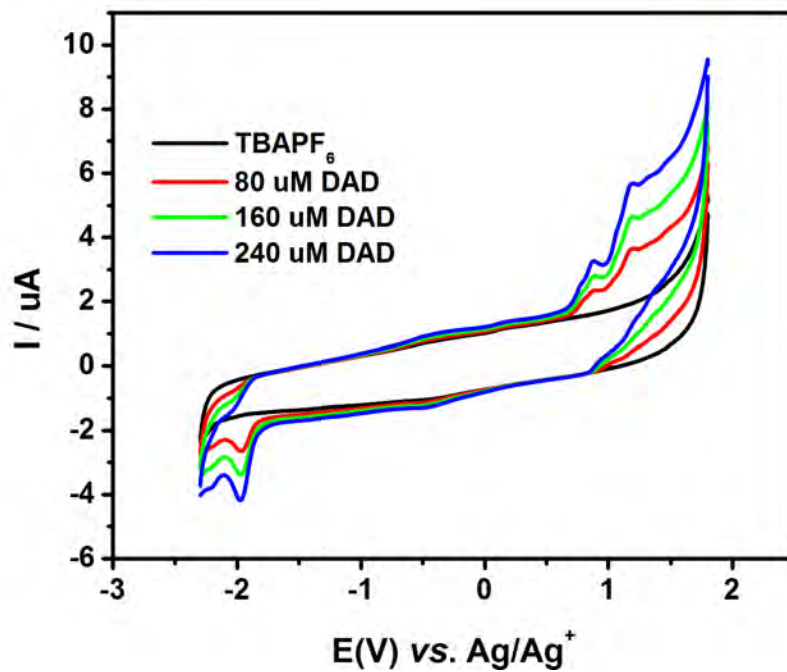


Figure 103. Cyclic voltammograms of Br-DAD-CN.

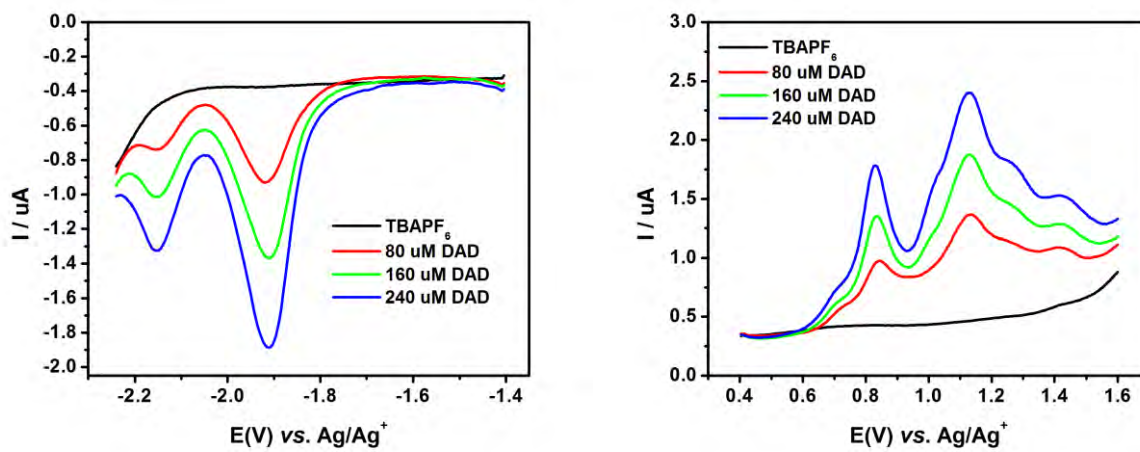


Figure 104. Differential pulse voltammograms of Br-DAD-CN. Left: reduction. Right: oxidation.

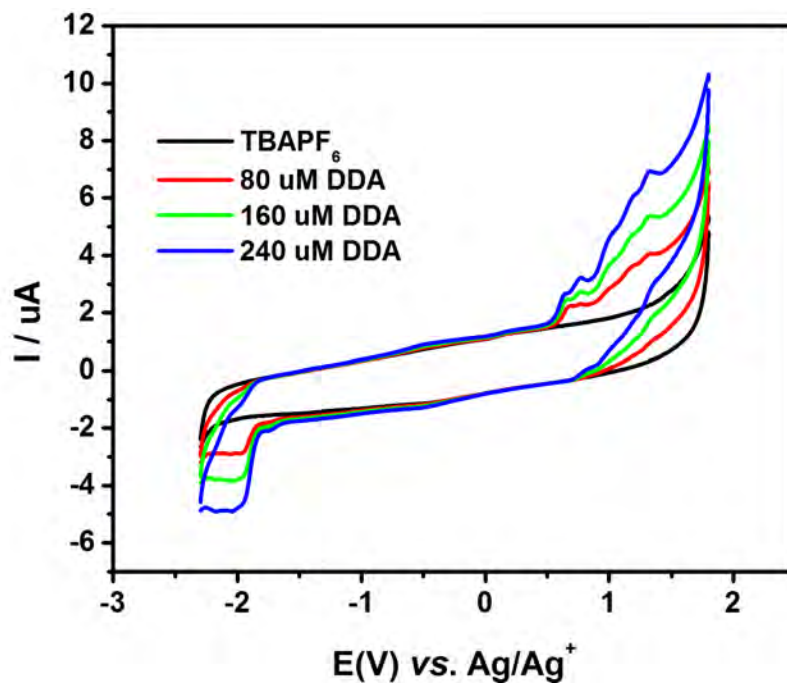


Figure 105. Cyclic voltammograms of Br-DDA-CN.

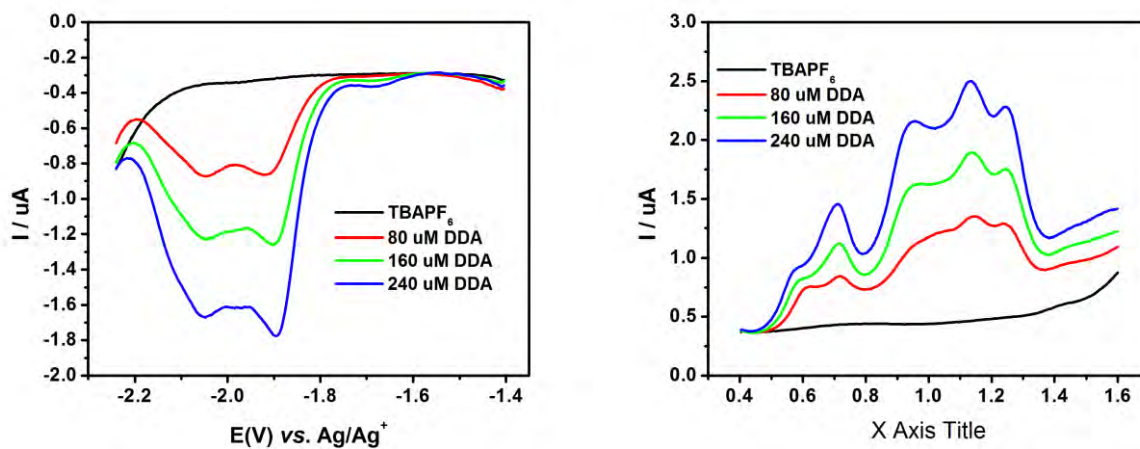


Figure 106. Differential pulse voltammograms of Br-DDA-CN. Left: reduction. Right: oxidation.

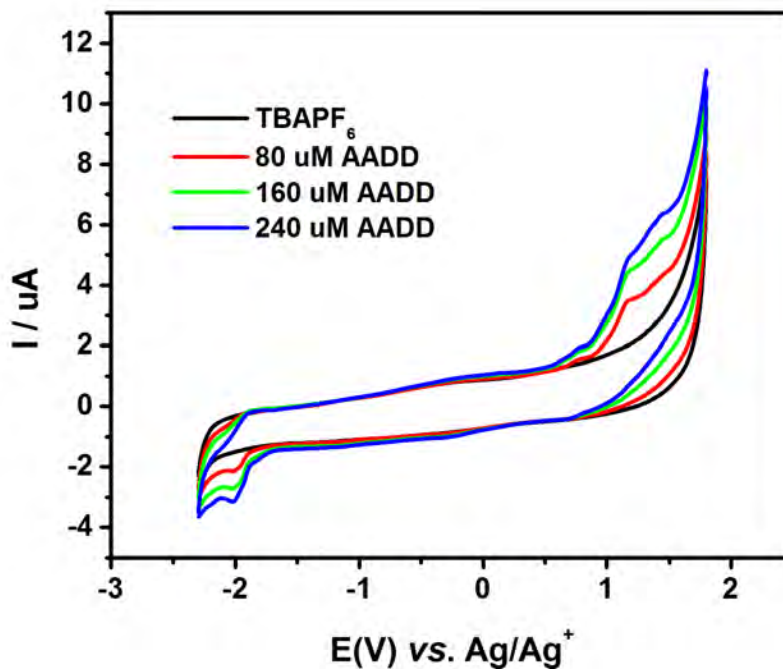


Figure 107. Cyclic voltammograms of Br-AADD-CN.

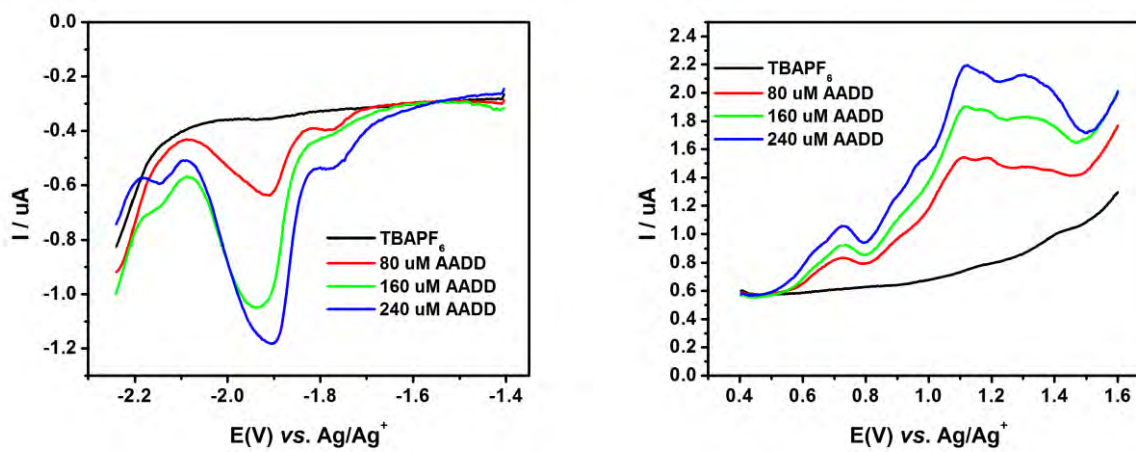


Figure 108. Differential pulse voltammograms of Br-AADD-CN. Left: reduction. Right: oxidation.

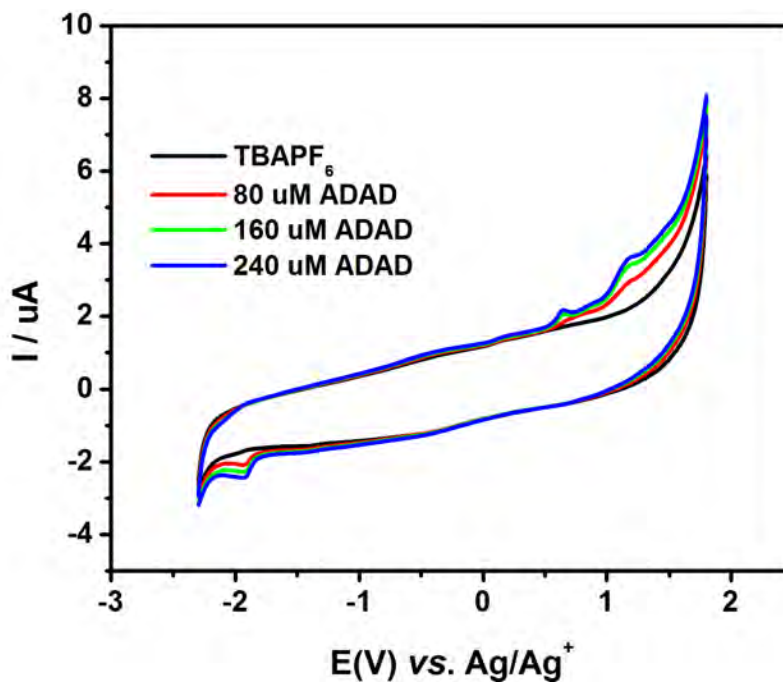


Figure 109. Cyclic voltammograms of Br-ADAD-CN.

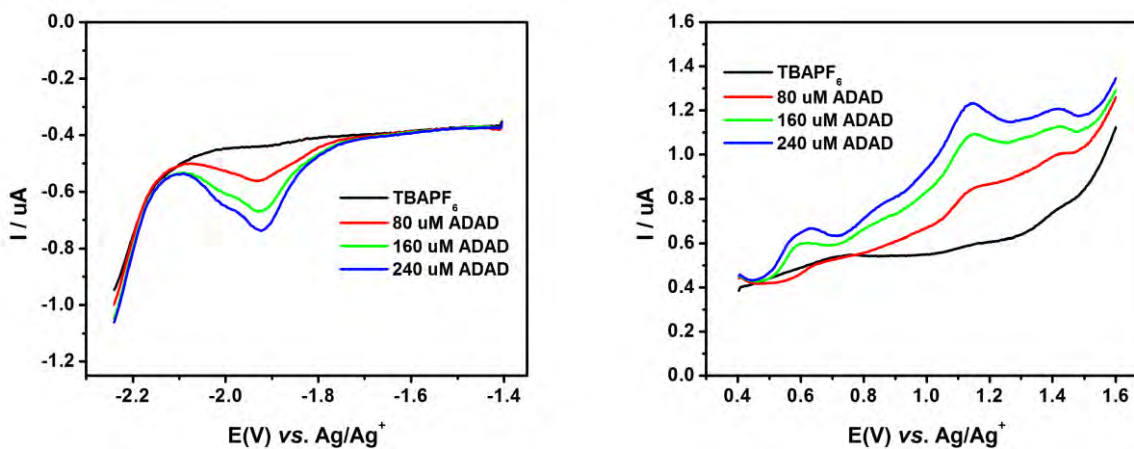


Figure 110. Differential pulse voltammograms of Br-ADAD-CN. Left: reduction. Right: oxidation.

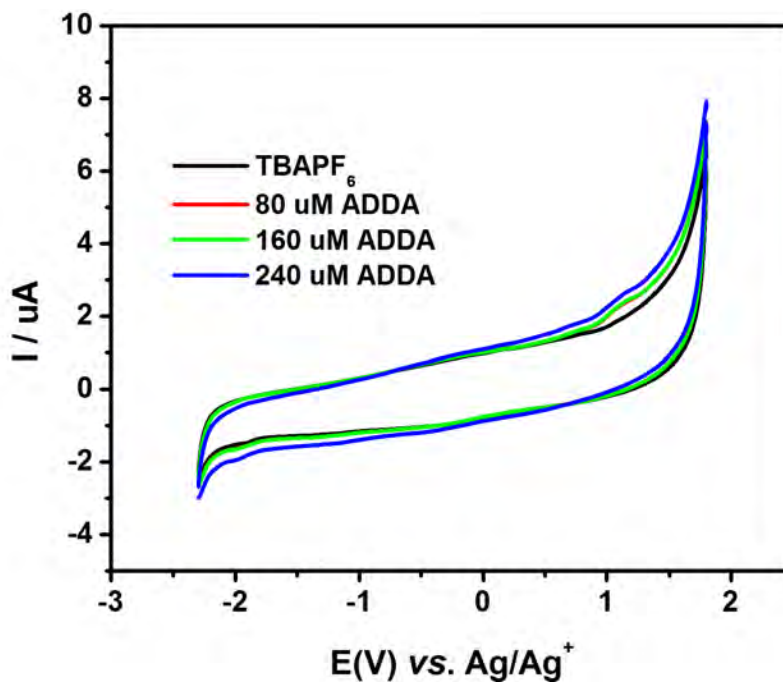


Figure 111. Cyclic voltammograms of Br-ADDA-CN.

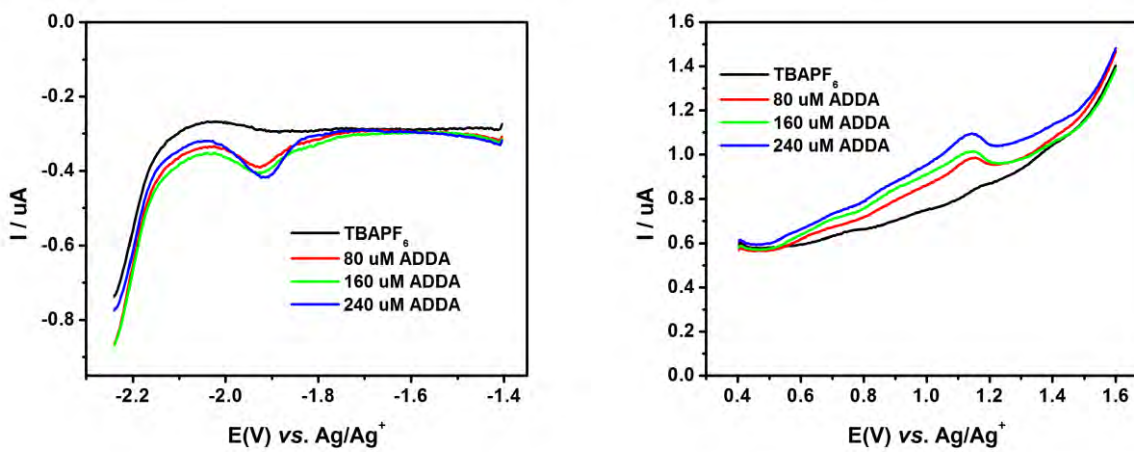


Figure 112. Differential pulse voltammograms of Br-ADAD-CN. Left: reduction. Right: oxidation.

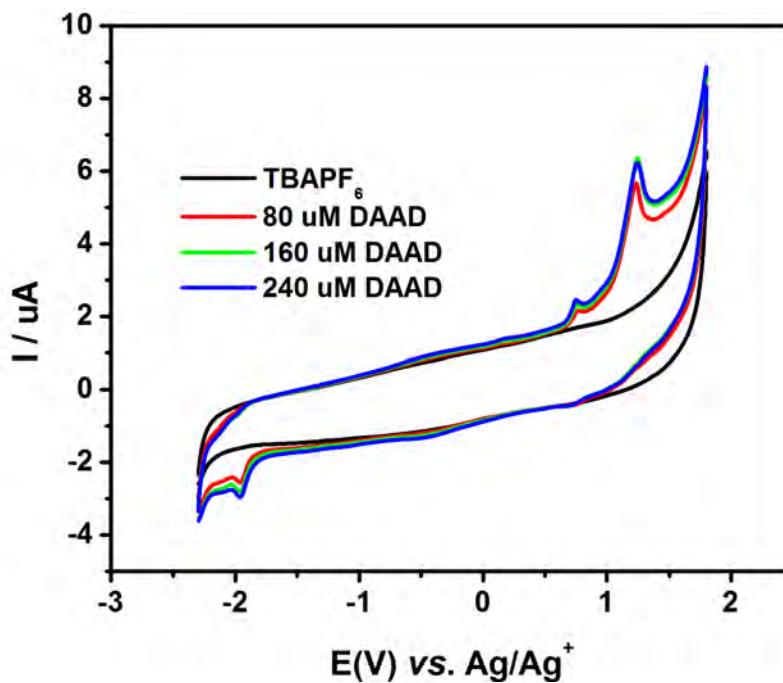


Figure 113. Cyclic voltammograms of Br-DAAD-CN.

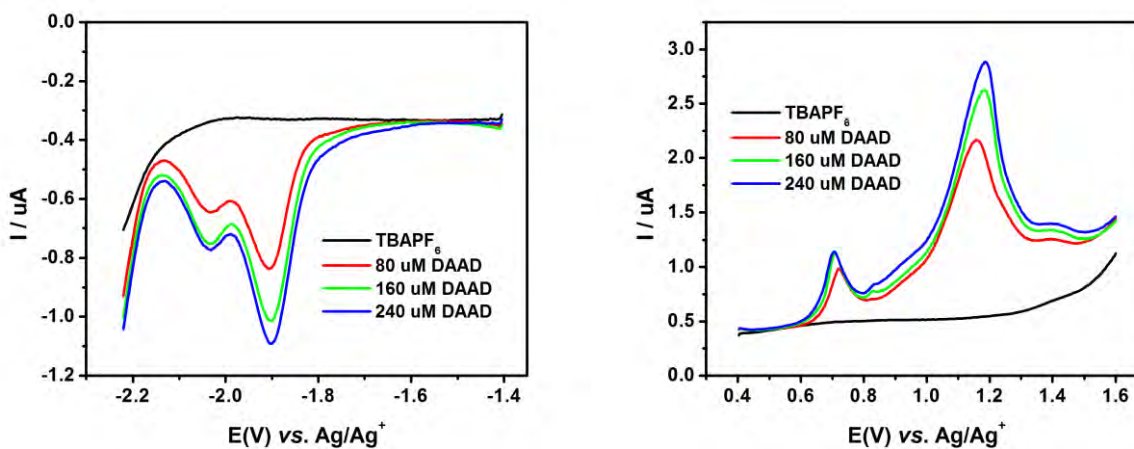


Figure 114. Differential pulse voltammograms of Br-DAAD-CN. Left: reduction. Right: oxidation.

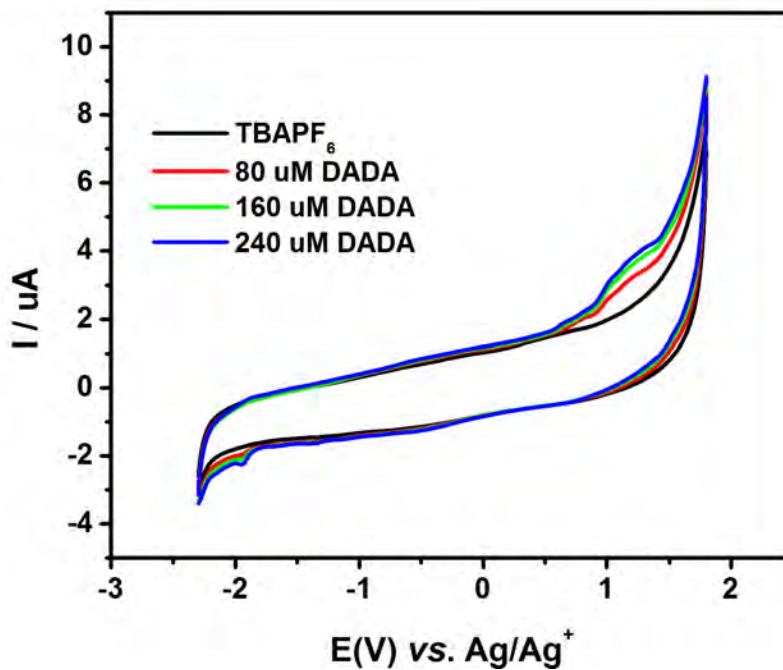


Figure 115. Cyclic voltammograms of Br-DADA-CN.

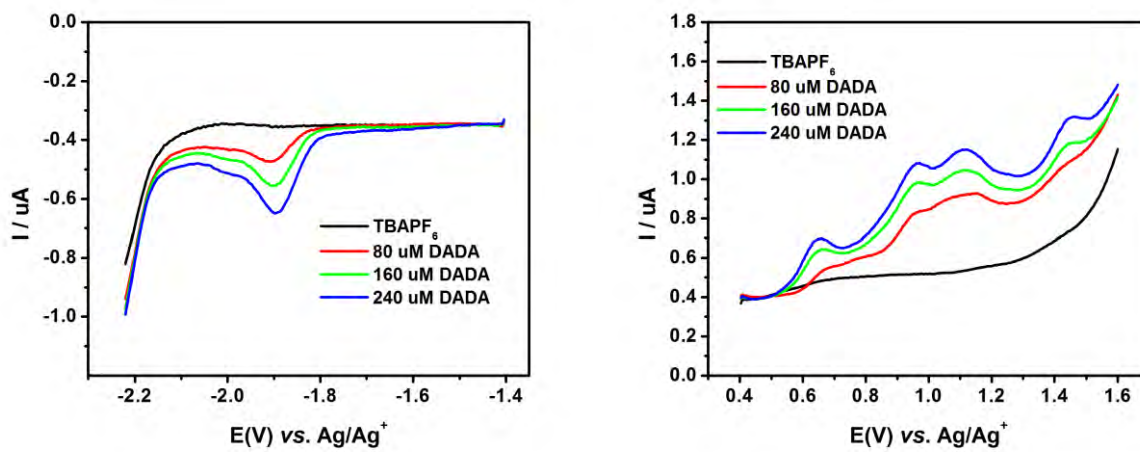


Figure 116. Differential pulse voltammograms of Br-DAAD-CN. Left: reduction. Right: oxidation.

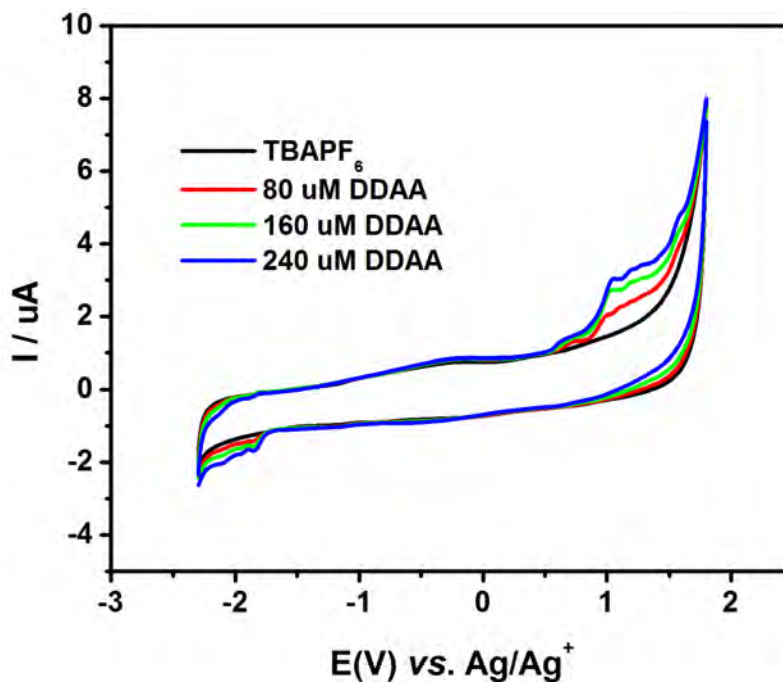


Figure 117. Cyclic voltammograms of Br-DDAA-CN.

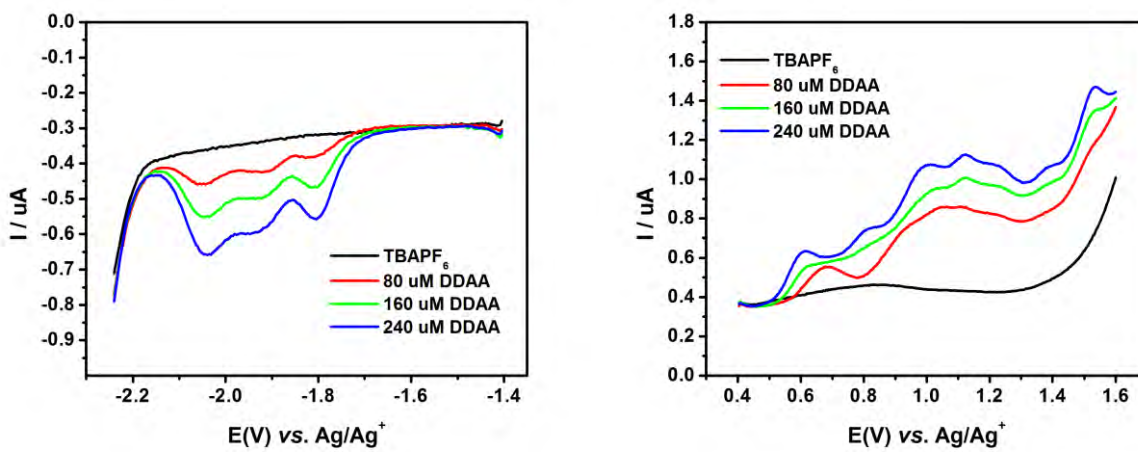


Figure 118. Differential pulse voltammograms of Br-DDAA-CN. Left: reduction. Right: oxidation.

A.4 DIFFERENTIAL SCANNING CALORIMOGRAMS

In all differential scanning calorimograms, the heating curve is plotted in red and the cooling curve in blue.

Figure 119. Differential scanning calorimograms of Br-AA-CN.

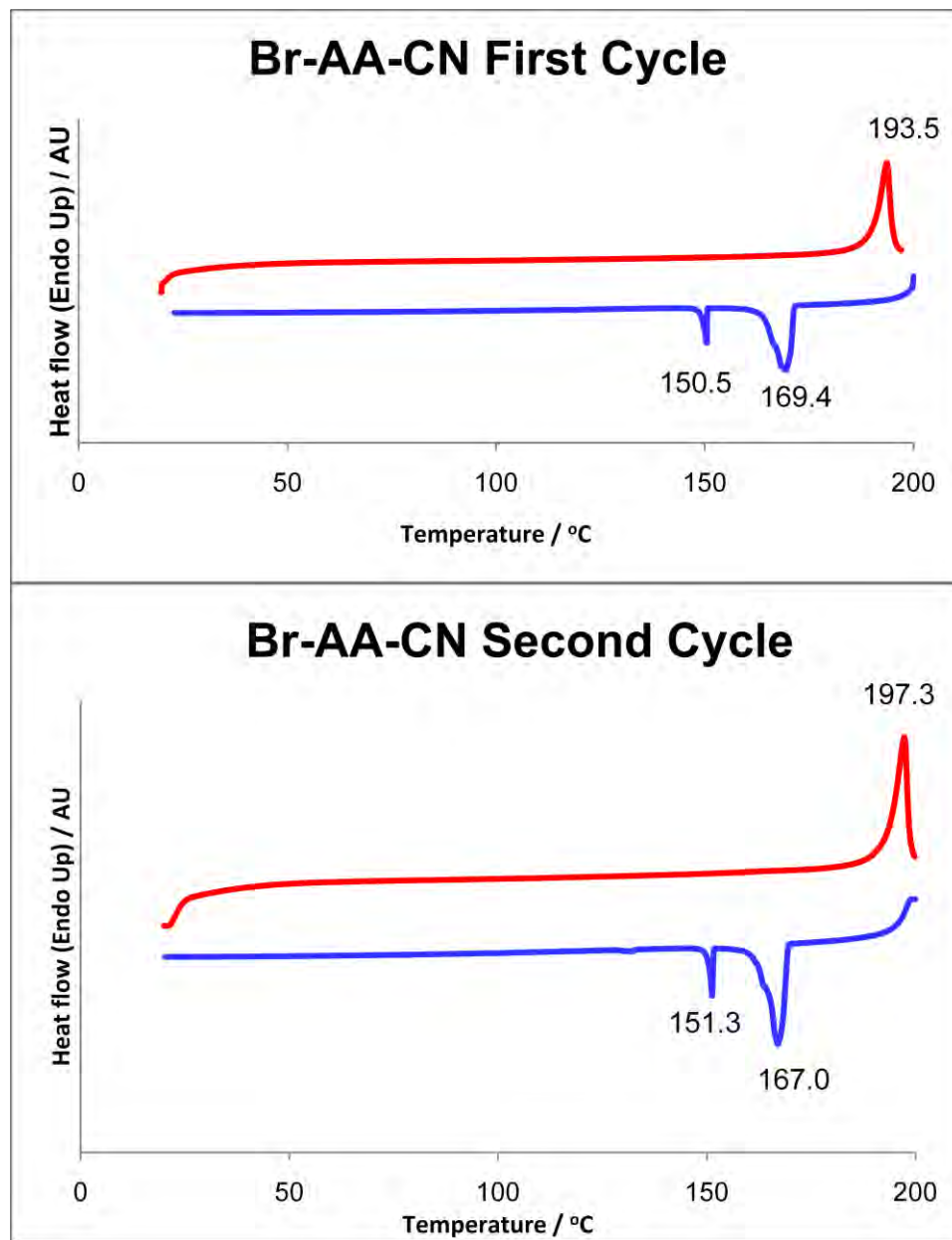


Figure 120. Differential scanning calorimograms of Br-AD-CN.

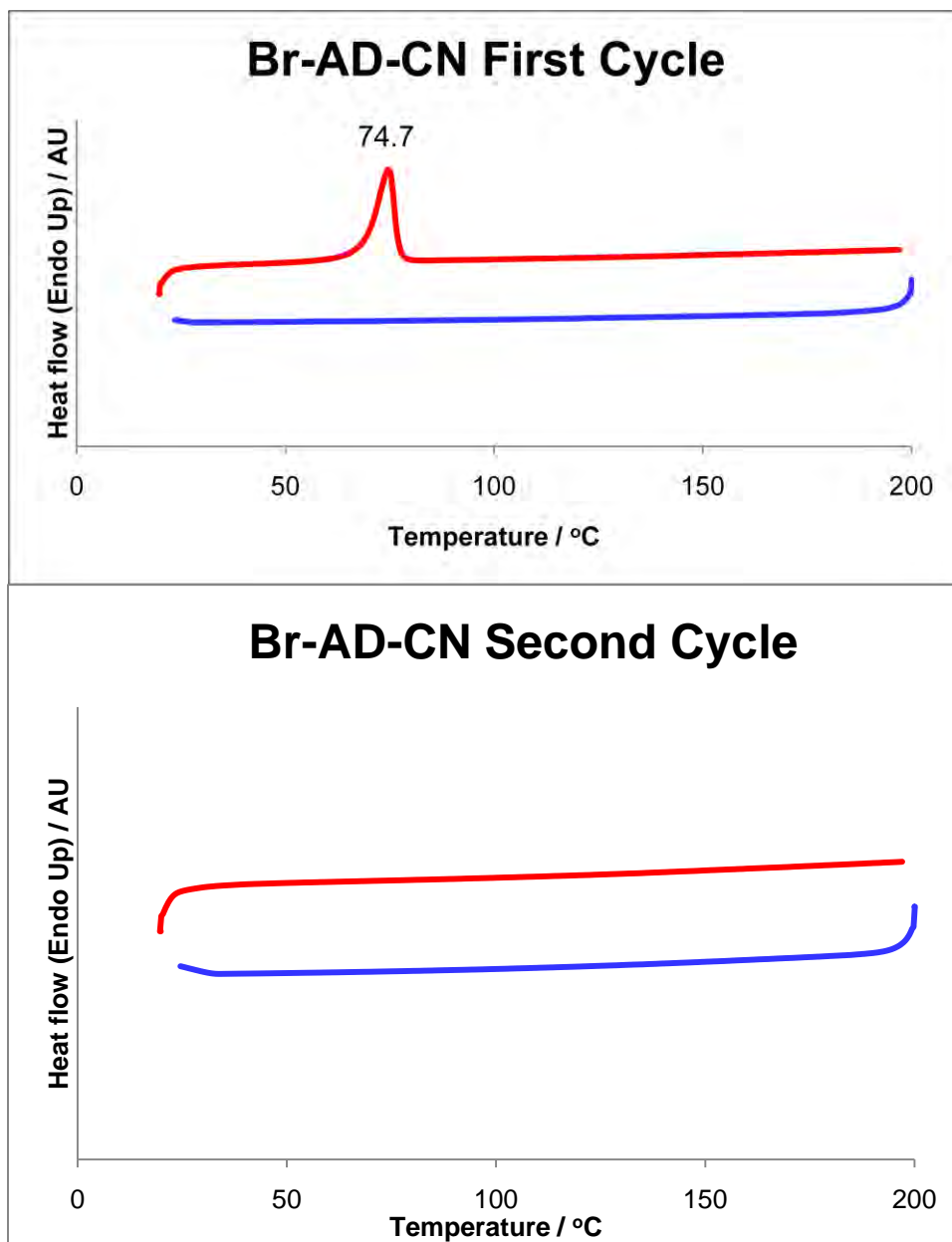


Figure 121. Differential scanning calorimograms of Br-DA-CN.

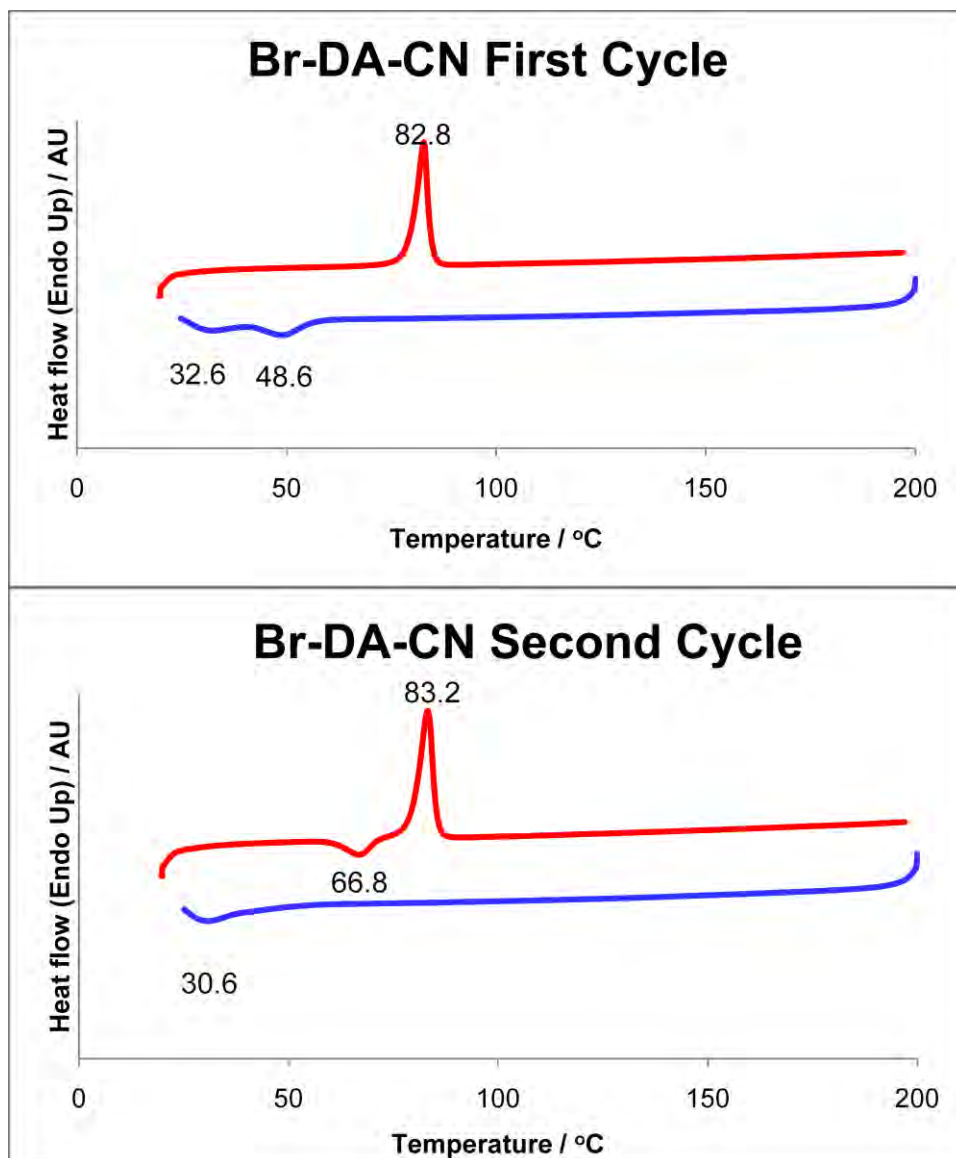


Figure 122. Differential scanning calorimograms of Br-DD-CN.

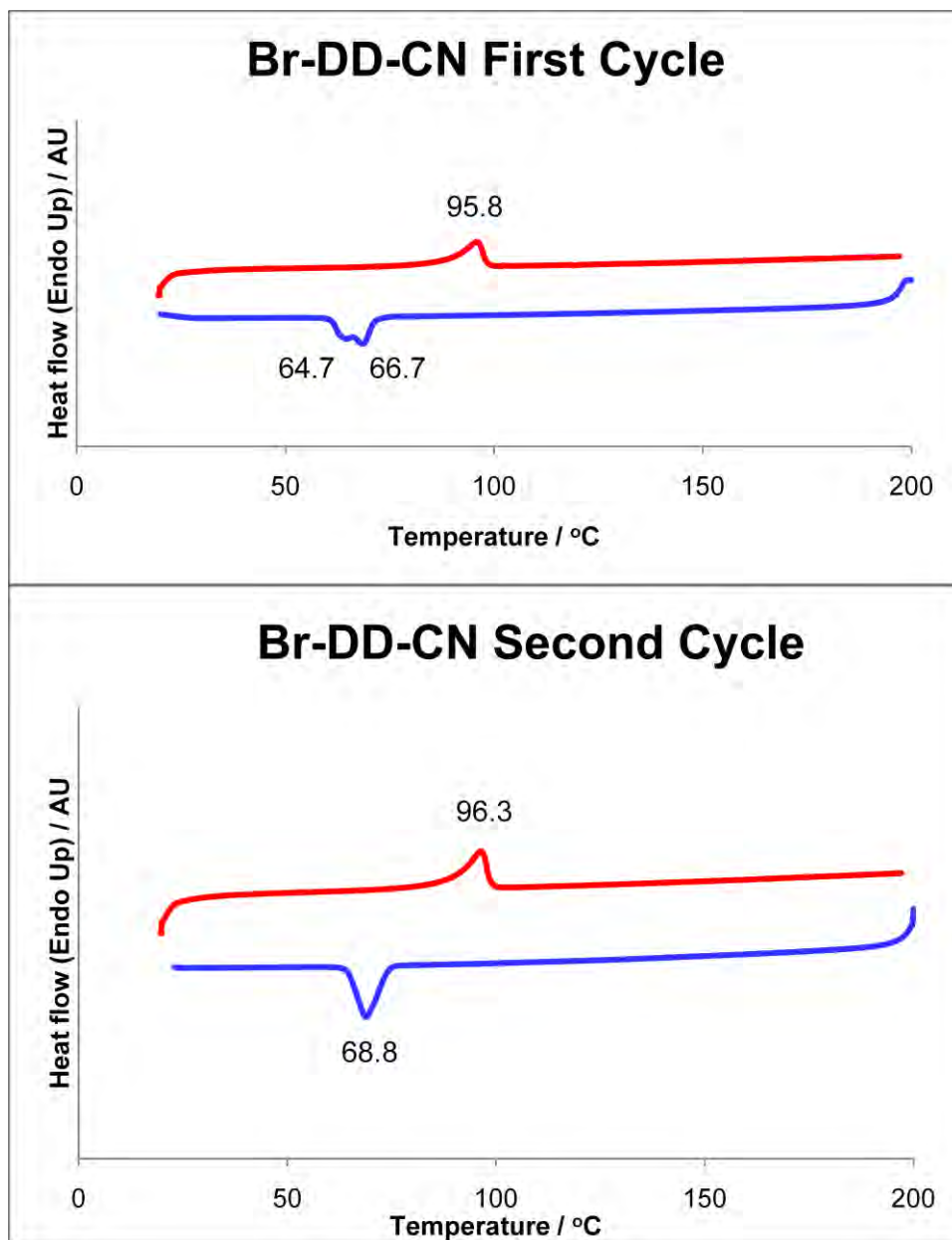


Figure 123. Differential scanning calorimograms of Br-AAD-CN.

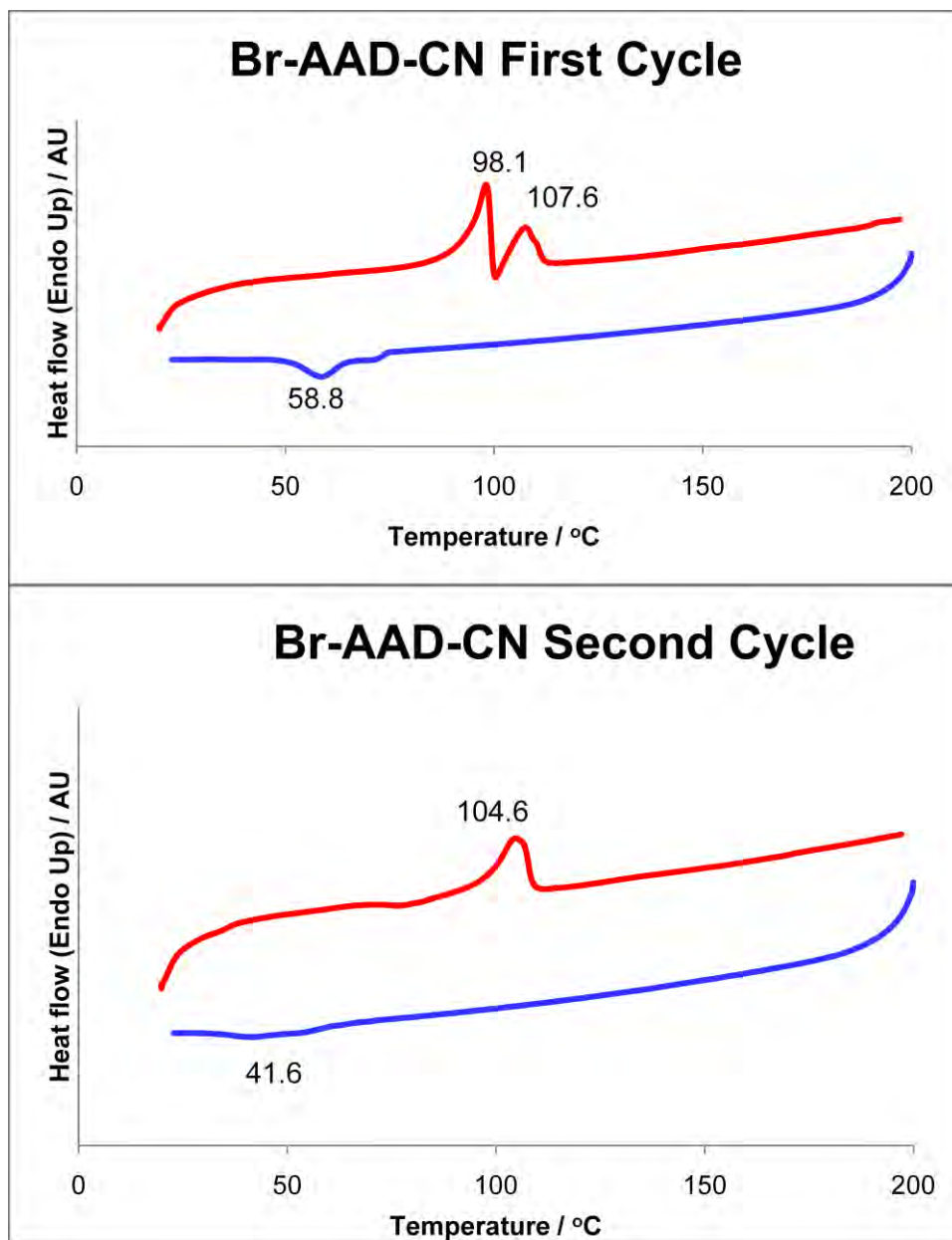


Figure 124. Differential scanning calorimograms of Br-ADA-CN.

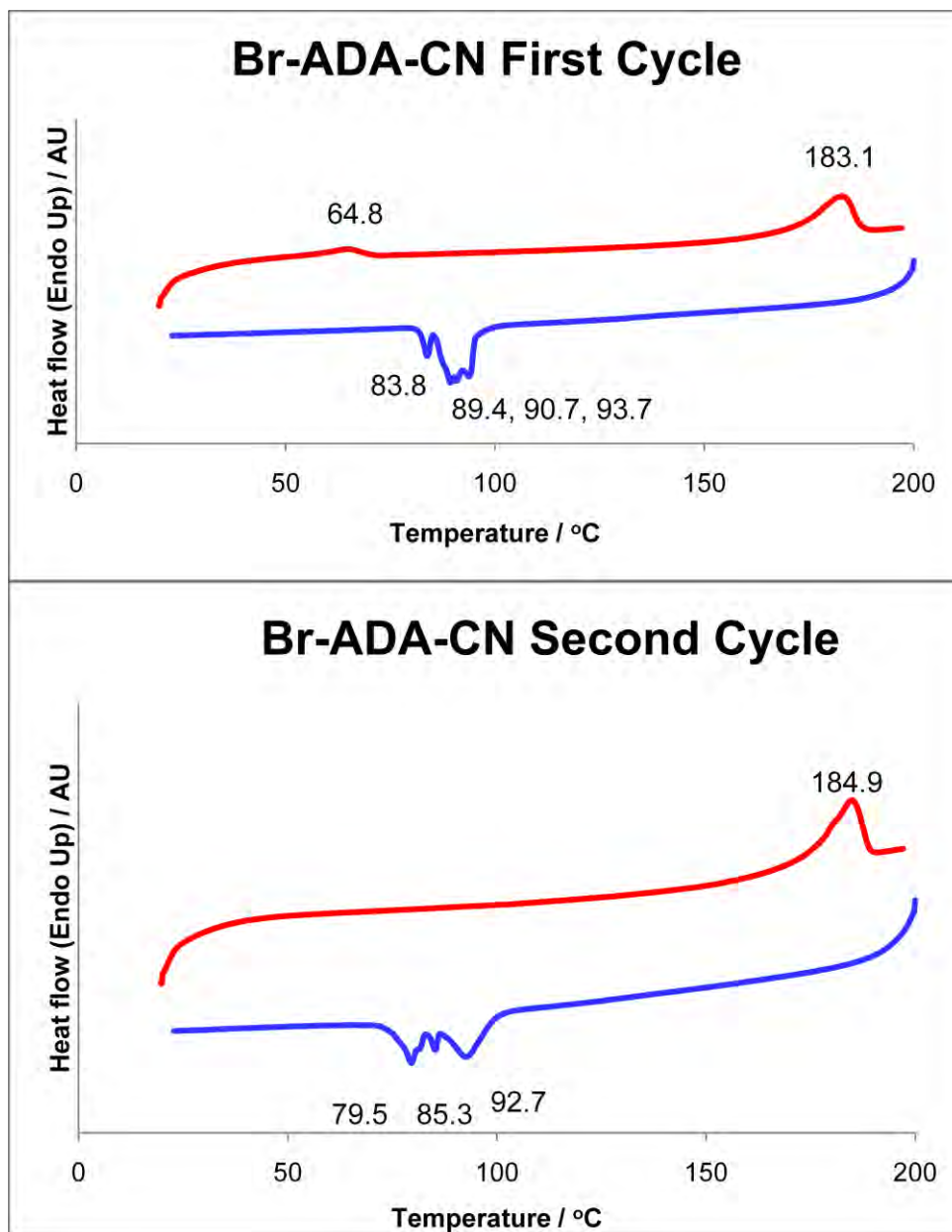


Figure 125. Differential scanning calorimograms of Br-ADD-CN.

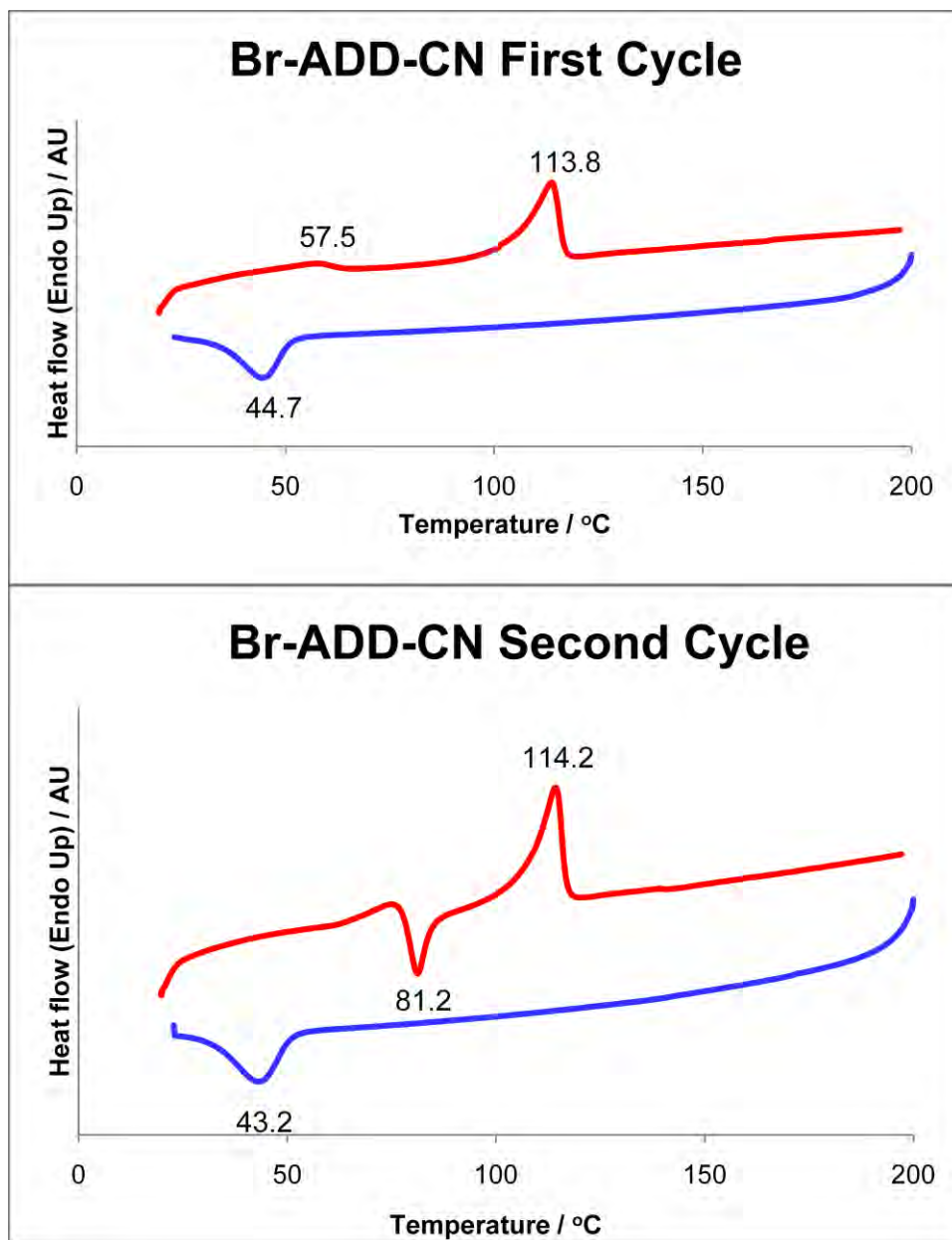


Figure 126. Differential scanning calorimograms of Br-DAA-CN.

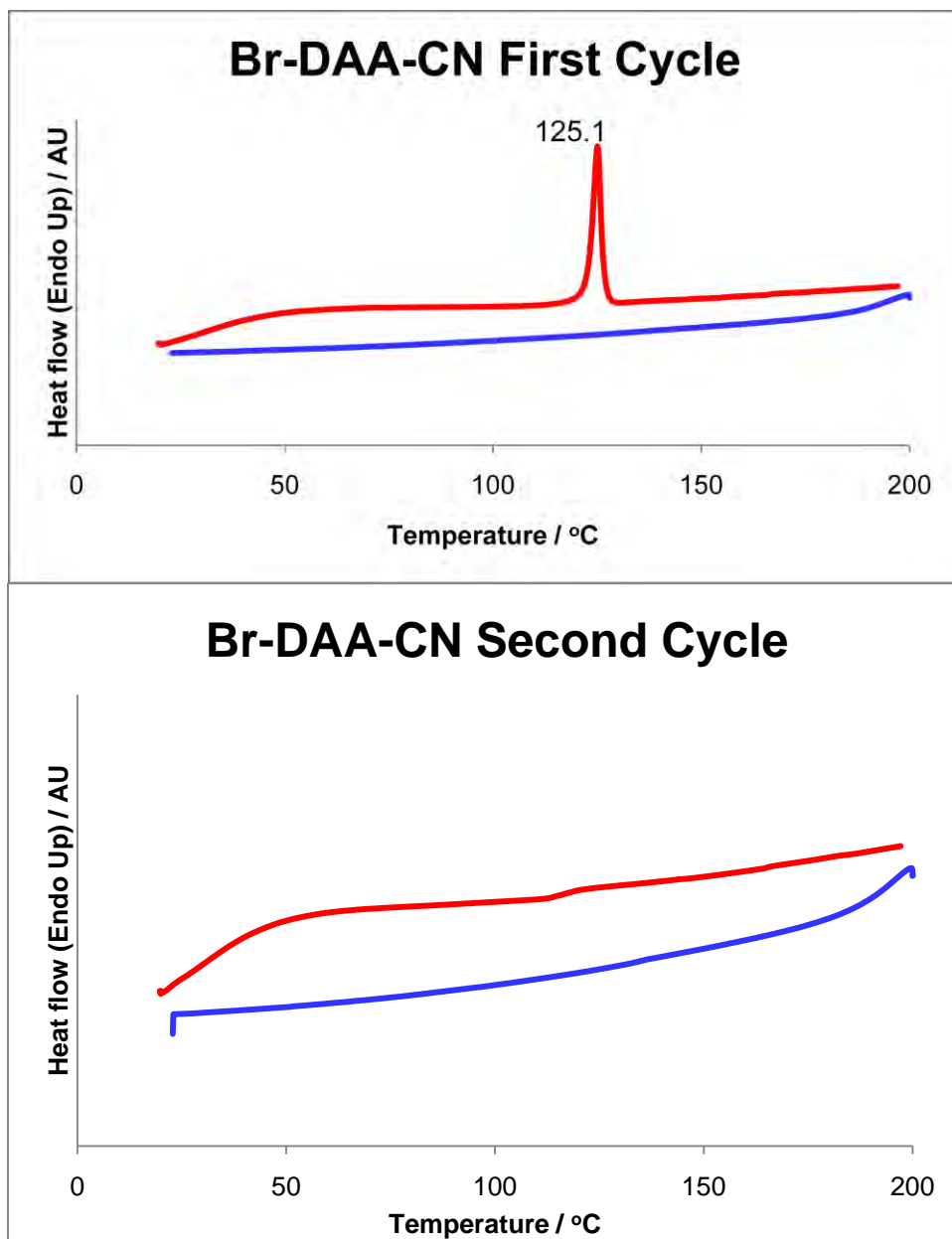


Figure 127. Differential scanning calorimograms of Br-DAD-CN.

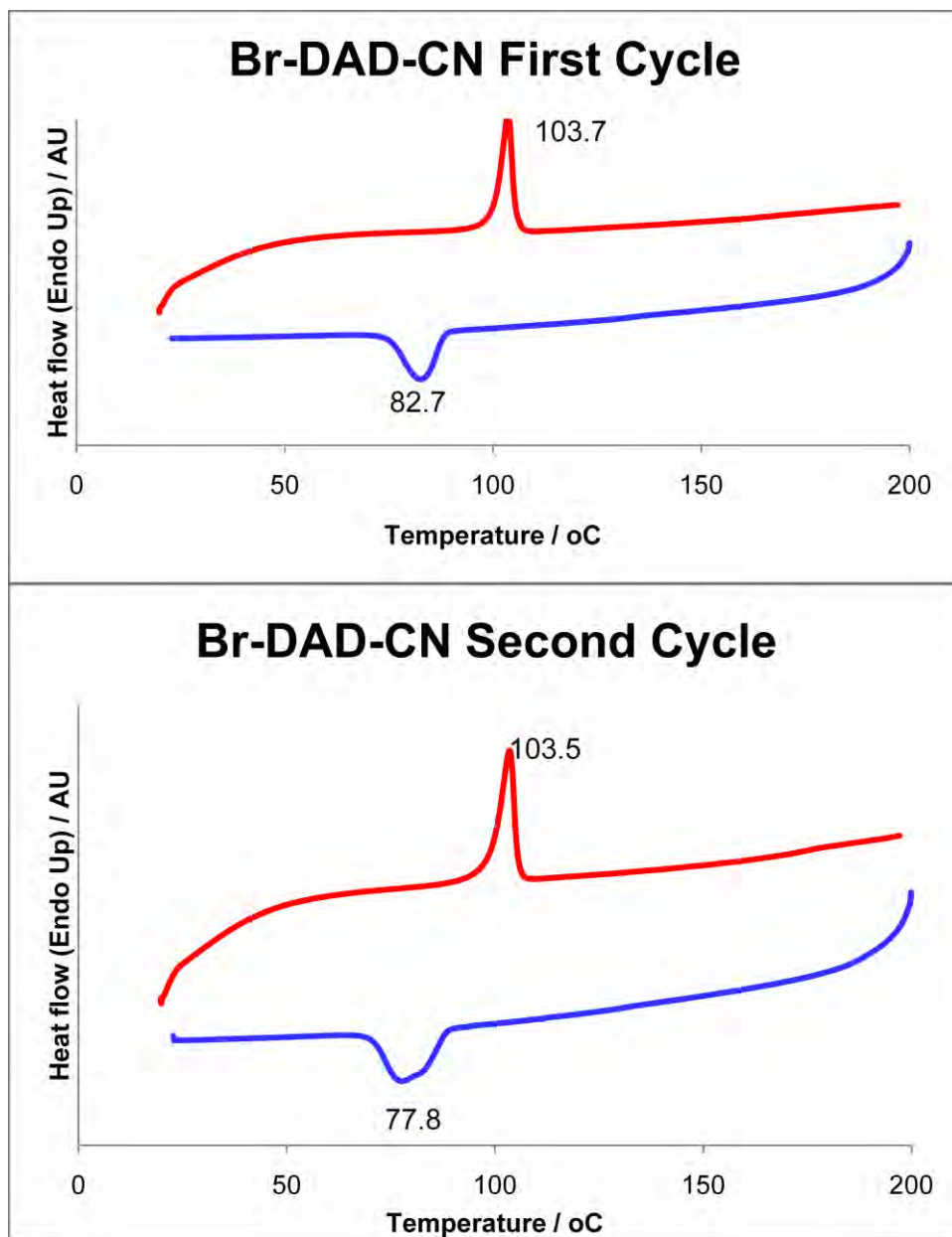


Figure 128. Differential scanning calorimograms of Br-DDA-CN.

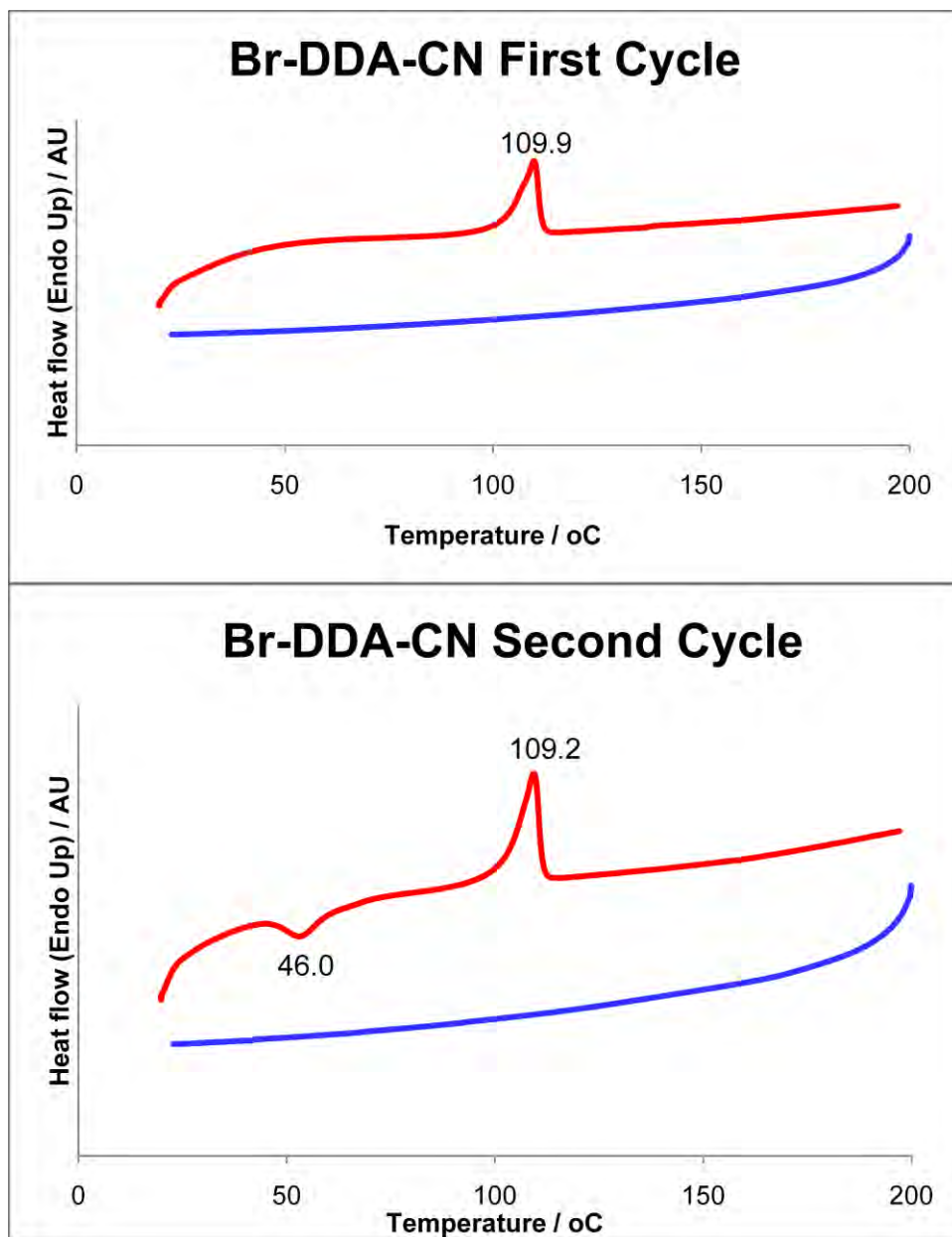


Figure 129. Differential scanning calorimograms of Br-AADD-CN.

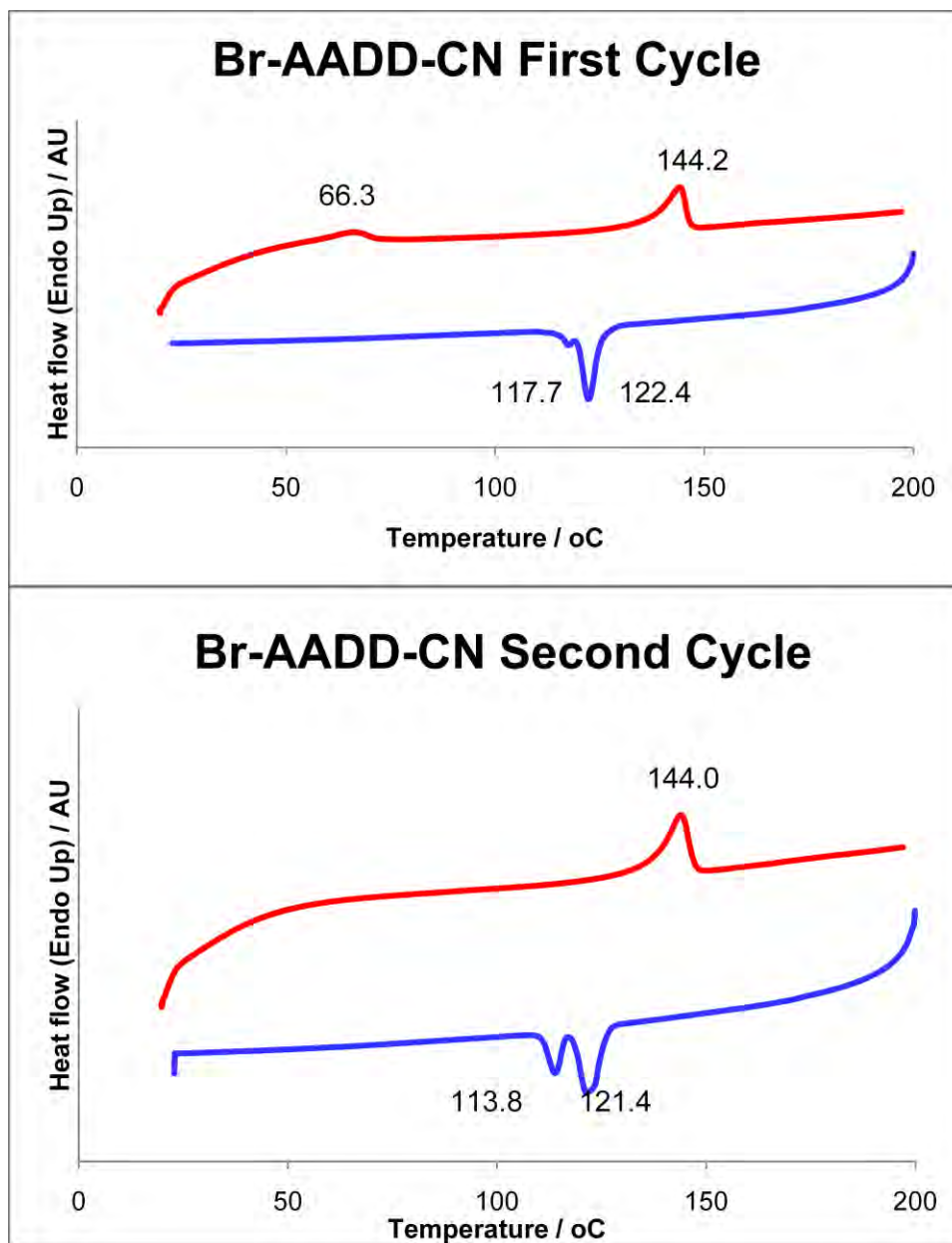


Figure 130. Differential scanning calorimograms of Br-ADAD-CN.

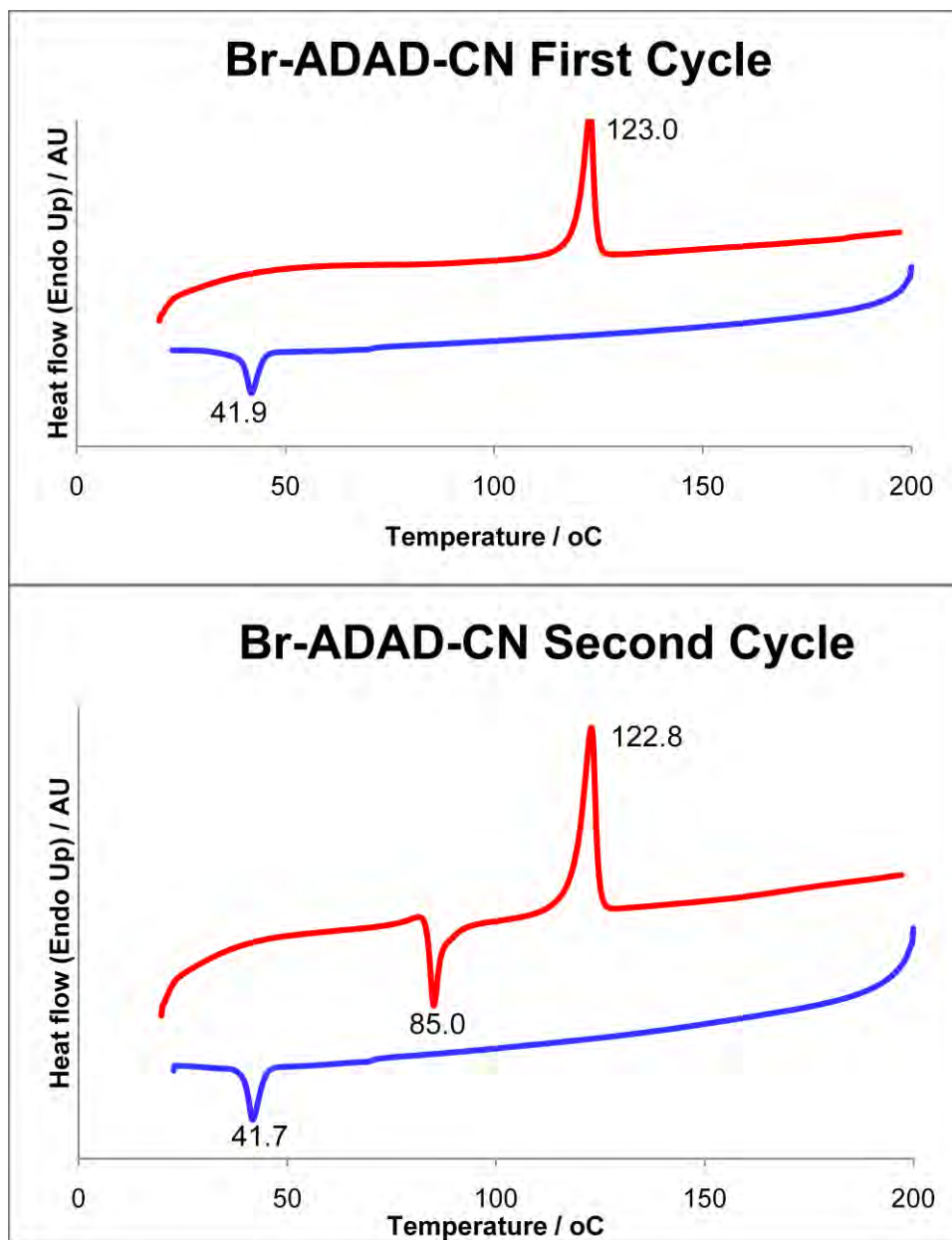


Figure 131. Differential scanning calorimograms of Br-ADDA-CN.

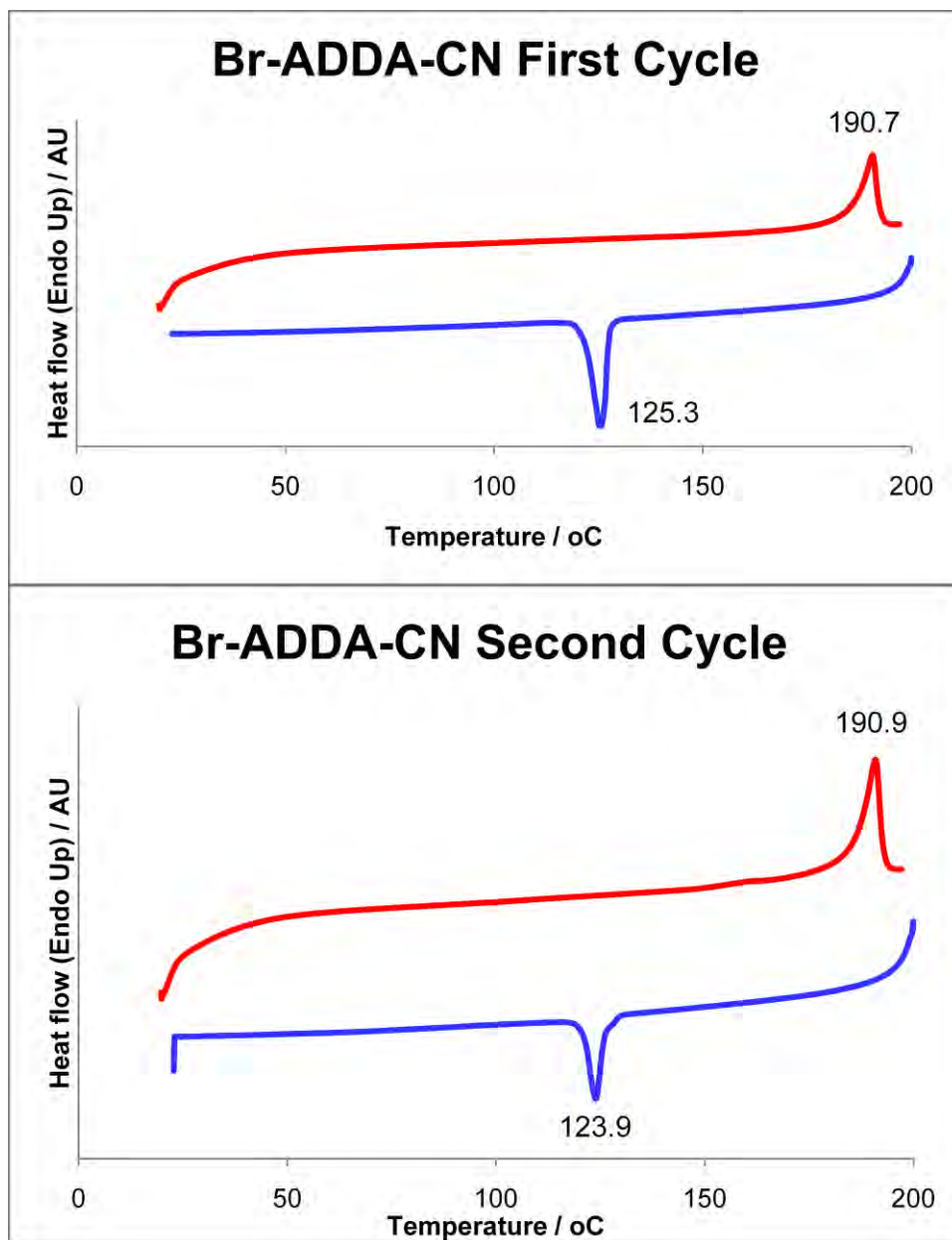


Figure 132. Differential scanning calorimograms of Br-DAAD-CN.

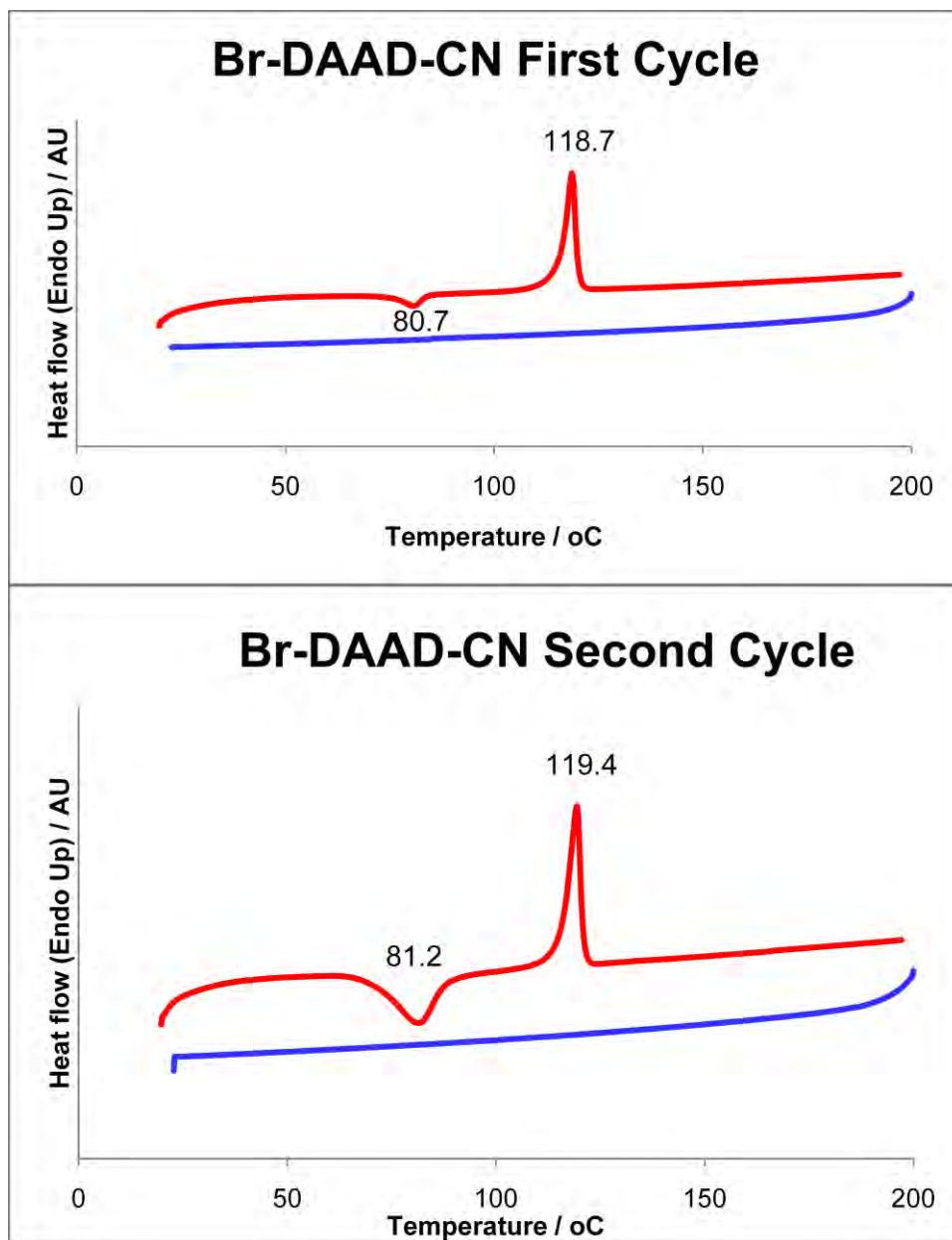


Figure 133. Differential scanning calorimograms of Br-DADA-CN.

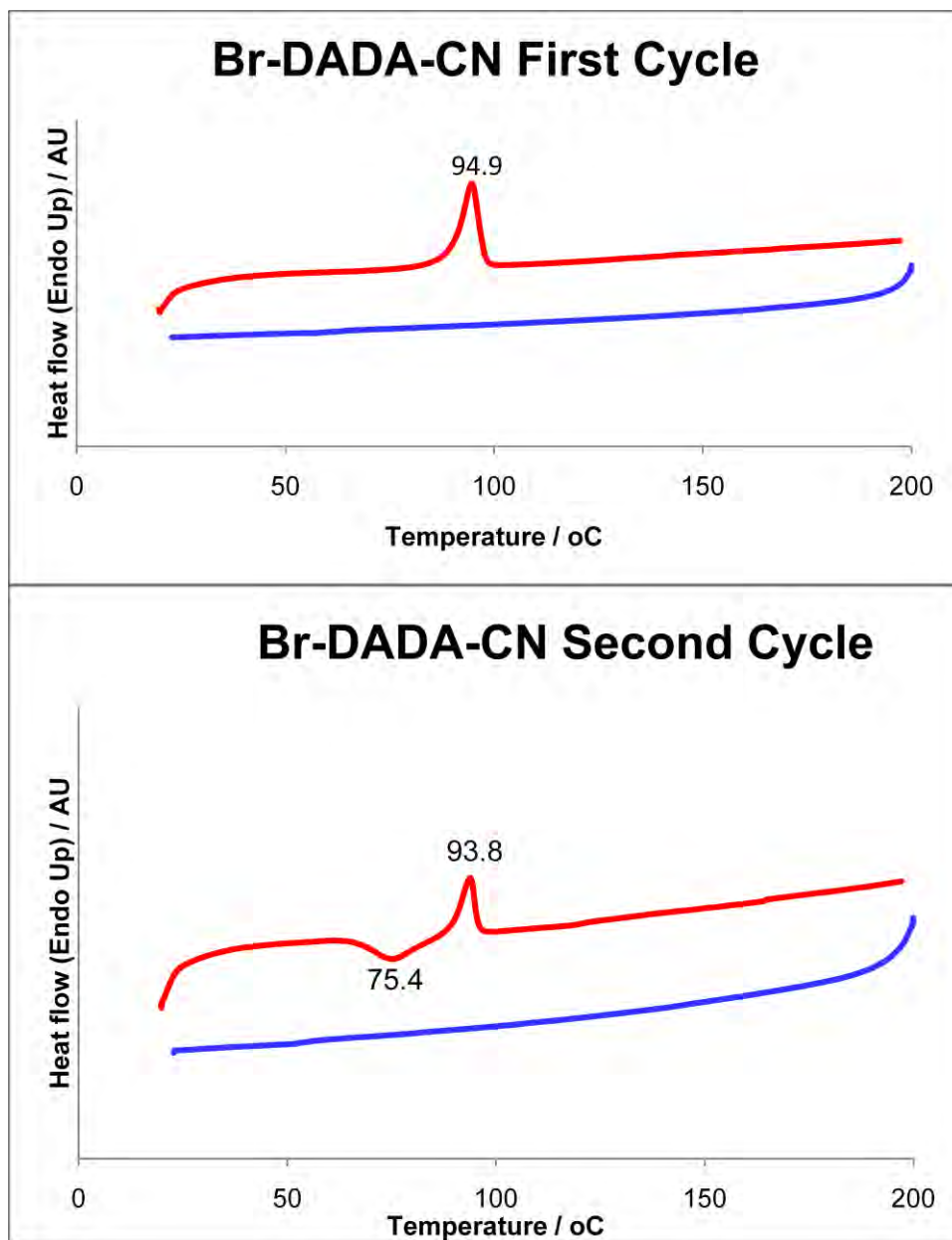
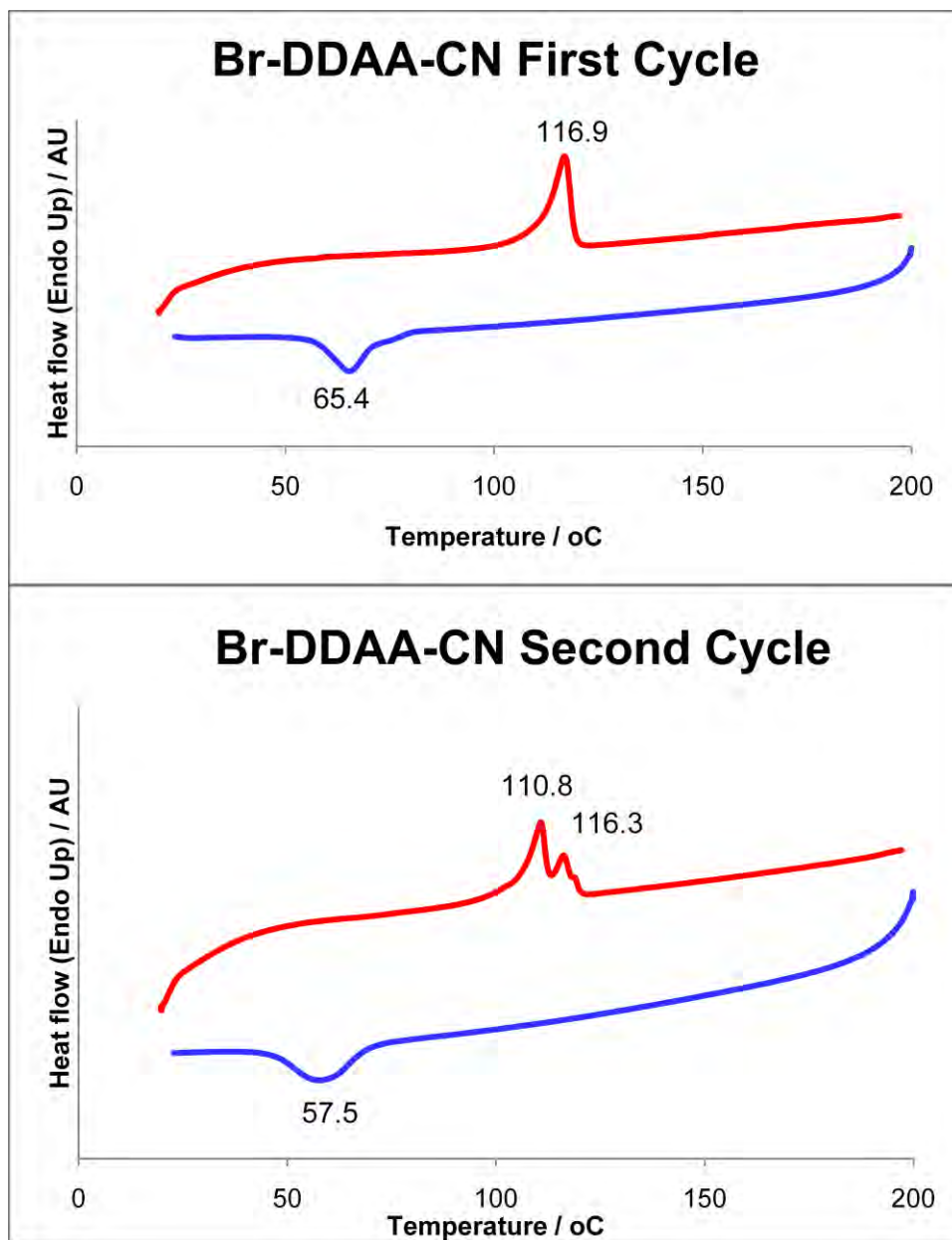


Figure 134. Differential scanning calorimograms of Br-DDAA-CN.



A.5 TRENDS IN OPTOELECTRONIC PROPERTIES

This section contains tables and graphs displaying other methods of organizing the optoelectronic data than the method presented in the main text.

The following tables compare the optoelectronic properties of the various OPVs based on different sequence features. All sequences are listed from (left-to-right) the bromo endgroup to the nitrile endgroup.

Table 16. Sequences with A on the outside.

A outside	$\lambda_{\max}^{\text{abs}}$ nm	$\lambda_{\max}^{\text{em}}$ nm	Δ_g^{opt} eV	Δ_g^{ec} eV
AA	327	381	3.44	3.30
ADA	406	474	2.65	2.65
ADDA	437	511	2.47	2.46

Table 17. Sequences with D on the outside.

D outside	$\lambda_{\max}^{\text{abs}}$ nm	$\lambda_{\max}^{\text{em}}$ nm	Δ_g^{opt} eV	Δ_g^{ec} eV
DD	380	454	2.89	2.81
DAD	396	472	2.77	2.74
DAAD	408	485	2.72	2.60

Table 18. Alternating sequences with A on the bromo end.

Alternating	$\lambda_{\max}^{\text{abs}}$ nm	$\lambda_{\max}^{\text{em}}$ nm	Δ_g^{opt} eV	Δ_g^{ec} eV
A first	nm	nm	eV	eV
AD	364	418	2.99	3.05
ADA	406	474	2.65	2.65
ADAD	422	499	2.58	2.55

Table 19. Alternating sequences with D on the bromo end.

Alternating	$\lambda_{\max}^{\text{abs}}$	$\lambda_{\max}^{\text{em}}$	Δ_g^{opt}	Δ_g^{ec}
D first	nm	nm	eV	eV
DA	362	450	2.97	2.86
DAD	396	472	2.77	2.74
DADA	425	492	2.56	2.54

Table 20. Alternating sequences with A on the nitrile end.

Alternating	$\lambda_{\max}^{\text{abs}}$	$\lambda_{\max}^{\text{em}}$	Δ_g^{opt}	Δ_g^{ec}
A last	nm	nm	eV	eV
DA	362	450	2.97	2.86
ADA	406	474	2.65	2.65
DADA	425	492	2.56	2.54

Table 21. Alternating sequences with D on the nitrile end.

Alternating	$\lambda_{\max}^{\text{abs}}$	$\lambda_{\max}^{\text{em}}$	Δ_g^{opt}	Δ_g^{ec}
D last	nm	nm	eV	eV
AD	364	418	2.99	3.05
DAD	396	472	2.77	2.74
ADAD	422	499	2.58	2.55

Table 22. Blocky sequences with A on the bromo end and D on the nitrile end.

blocky	$\lambda_{\max}^{\text{abs}}$	$\lambda_{\max}^{\text{em}}$	Δ_g^{opt}	Δ_g^{ec}
A first	nm	nm	eV	eV
AD	364	418	2.99	3.05
AAD	385	432	2.86	2.86
ADD	412	479	2.63	2.64
AADD	425	492	2.55	2.49

Table 23. Blocky sequences with D on the bromo end and A on the nitrile end.

blocky	$\lambda_{\max}^{\text{abs}}$	$\lambda_{\max}^{\text{em}}$	Δ_g^{opt}	Δ_g^{ec}
D first	nm	nm	eV	eV
DA	362	450	2.97	2.86
DAA	383	474	2.84	2.77
DDA	412	488	2.62	2.46
DDAA	424	515	2.56	2.41

Table 24. Sequences with two adjacent A units.

AA	$\lambda_{\max}^{\text{abs}}$	$\lambda_{\max}^{\text{em}}$	Δ_g^{opt}	Δ_g^{ec}
	nm	nm	eV	eV
AA	327	381	3.44	3.30
AAD	385	432	2.86	2.86
DAA	383	474	2.84	2.77
AADD	425	492	2.55	2.49
DAAD	408	485	2.72	2.60
DDAA	424	515	2.56	2.41

Table 25. Sequences with two adjacent D units.

DD	$\lambda_{\max}^{\text{abs}}$	$\lambda_{\max}^{\text{em}}$	Δ_g^{opt}	Δ_g^{ec}
	nm	nm	eV	eV
DD	380	454	2.89	2.81
ADD	412	479	2.63	2.64
DDA	412	488	2.62	2.46
AADD	425	492	2.55	2.49
ADDA	437	511	2.47	2.46
DDAA	424	515	2.56	2.41

Table 26. Sequences in the synthesis of Br-AADD-CN.

Build up	$\lambda_{\max}^{\text{abs}}$	$\lambda_{\max}^{\text{em}}$	Δ_g^{opt}	Δ_g^{ec}
AADD	nm	nm	eV	eV
AA	327	381	3.44	3.30
AAD	385	432	2.86	2.86
AADD	425	492	2.55	2.49

Table 27. Sequences in the synthesis of **Br-ADAD-CN**.

Build up	$\lambda_{\max}^{\text{abs}}$	$\lambda_{\max}^{\text{em}}$	Δ_g^{opt}	Δ_g^{ec}
ADAD	nm	nm	eV	eV
AD	364	418	2.99	3.30
ADA	406	474	2.65	2.65
ADAD	422	499	2.58	2.55

Table 28. Sequences in the synthesis of **Br-ADDA-CN**.

Build up	$\lambda_{\max}^{\text{abs}}$	$\lambda_{\max}^{\text{em}}$	Δ_g^{opt}	Δ_g^{ec}
ADDA	nm	nm	eV	eV
AD	364	418	2.99	3.30
ADD	412	479	2.63	2.64
ADDA	437	511	2.47	2.46

Table 29. Sequences in the synthesis of **Br-DDAA-CN**.

Build up	$\lambda_{\max}^{\text{abs}}$	$\lambda_{\max}^{\text{em}}$	Δ_g^{opt}	Δ_g^{ec}
DDAA	nm	nm	eV	eV
DD	380	454	2.89	2.81
DDA	412	488	2.62	2.46
DDAA	424	515	2.56	2.41

Table 30. Sequences in the synthesis of **Br-DADA-CN**.

Build up	$\lambda_{\max}^{\text{abs}}$	$\lambda_{\max}^{\text{em}}$	Δ_g^{opt}	Δ_g^{ec}
DADA	nm	nm	eV	eV
DA	362	450	2.97	2.86
DAD	396	472	2.77	2.74
DADA	425	492	2.56	2.54

Table 31. Sequences in the synthesis of **Br-DAAD-CN**.

Build up	$\lambda_{\max}^{\text{abs}}$	$\lambda_{\max}^{\text{em}}$	$\Delta_{\text{g}}^{\text{opt}}$	$\Delta_{\text{g}}^{\text{ec}}$
DAAD	nm	nm	eV	eV
DA	362	450	2.97	2.86
DAA	383	474	2.84	2.77
DAAD	408	485	2.72	2.60

The following graphs show the trends in optoelectronic data regardless of oligomer length. Of note is the intermingling of the trimers and tetramers in the relative order.

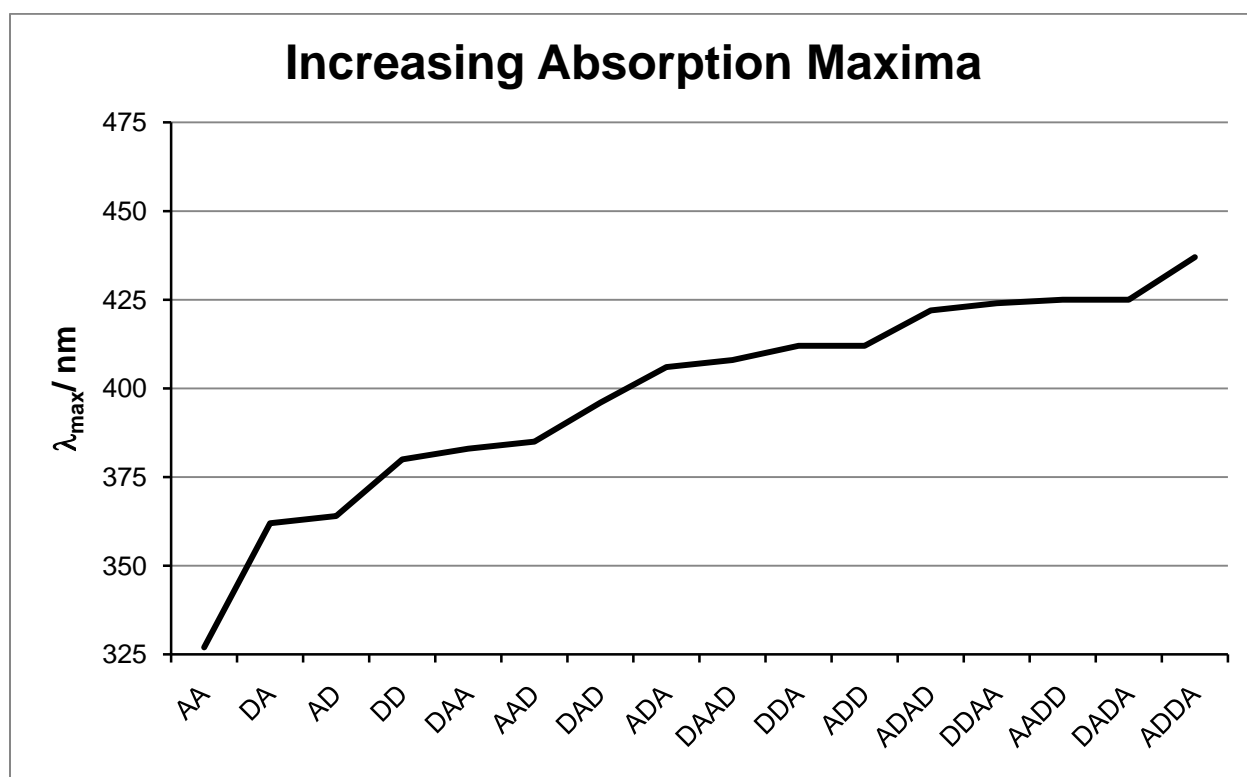


Figure 135. Ordering of the OPVs according to increasing $\lambda_{\max}^{\text{abs}}$, disregarding oligomer length.

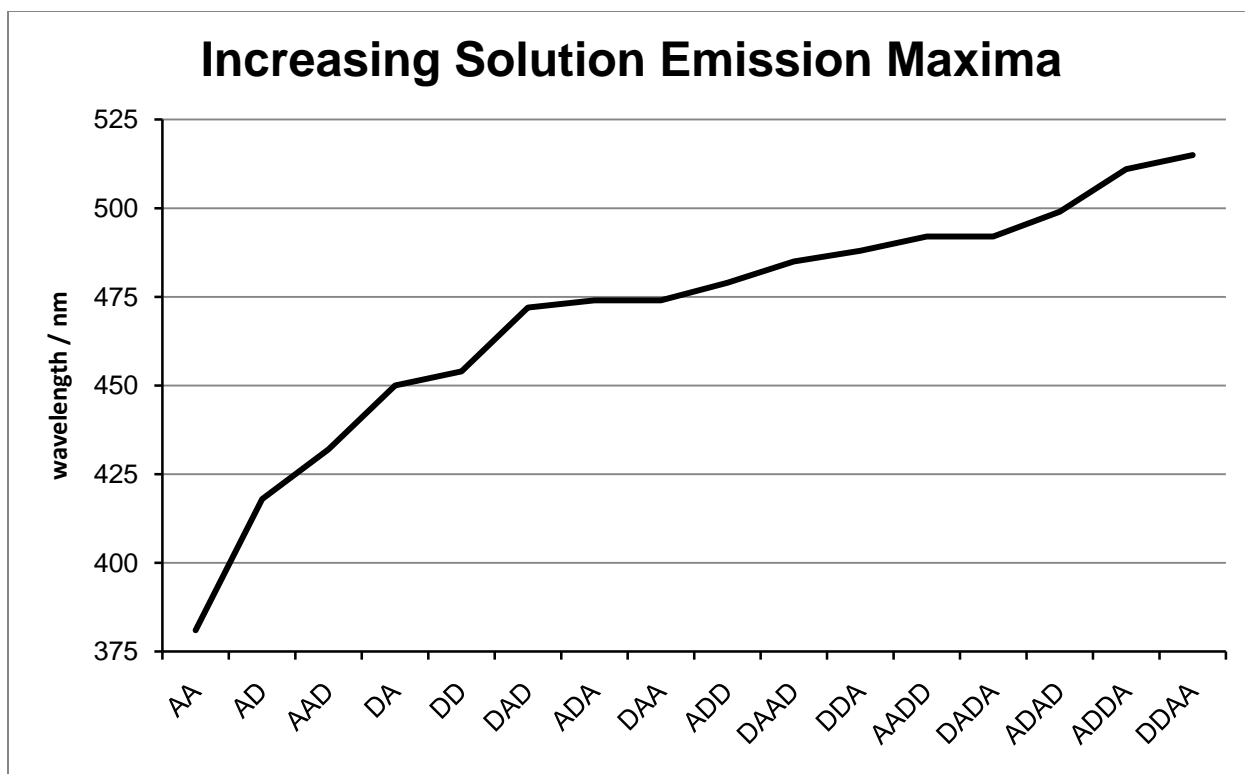


Figure 136. Ordering of the OPVs according to increasing solution $\lambda_{\text{max}}^{\text{em}}$, disregarding oligomer length.

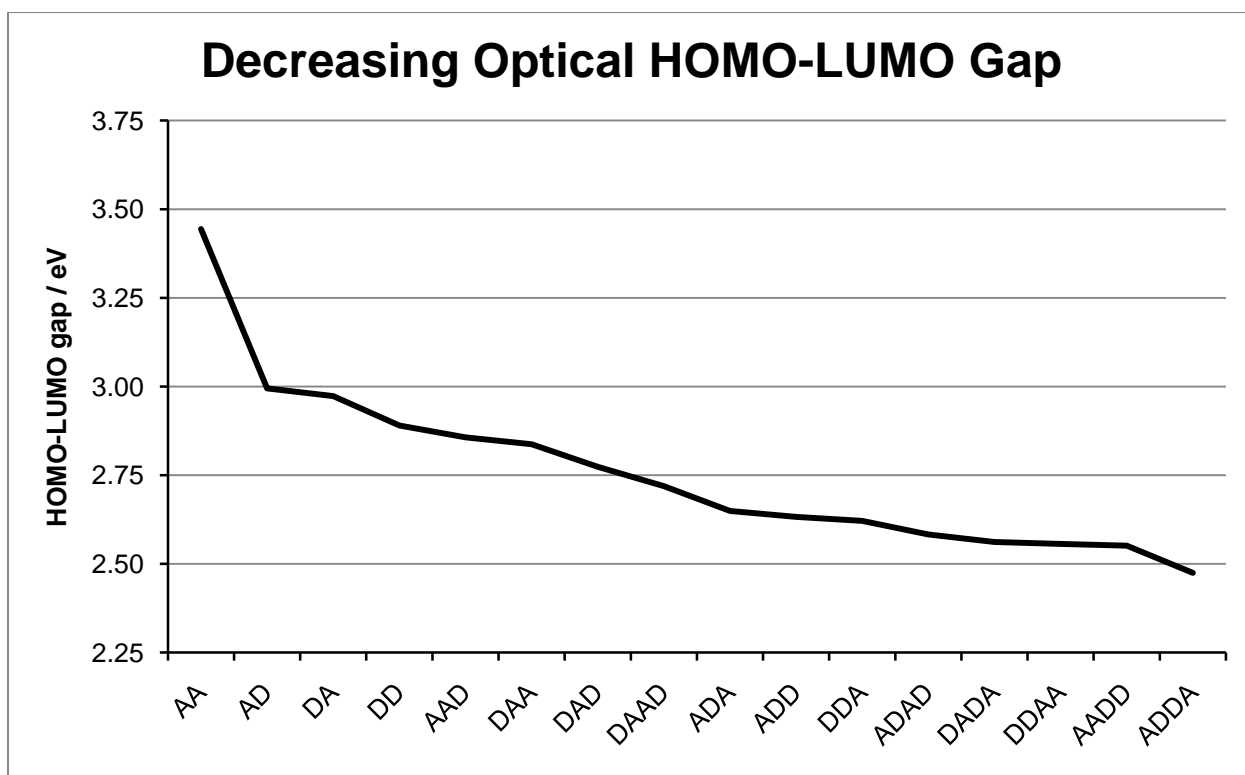


Figure 137. Ordering of the OPVs according to increasing Δ_g^{opt} disregarding oligomer length.

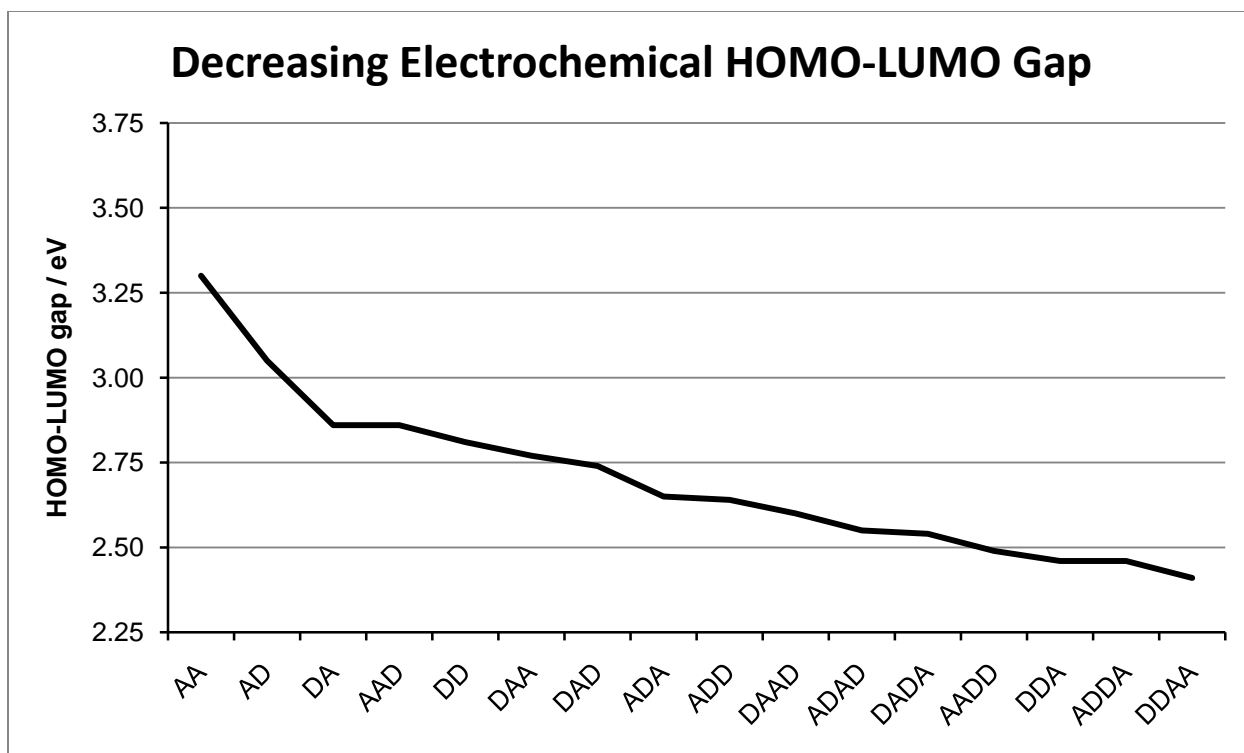


Figure 138. Ordering of the OPVs according to increasing Δ_{eg}^{ec} disregarding oligomer length.

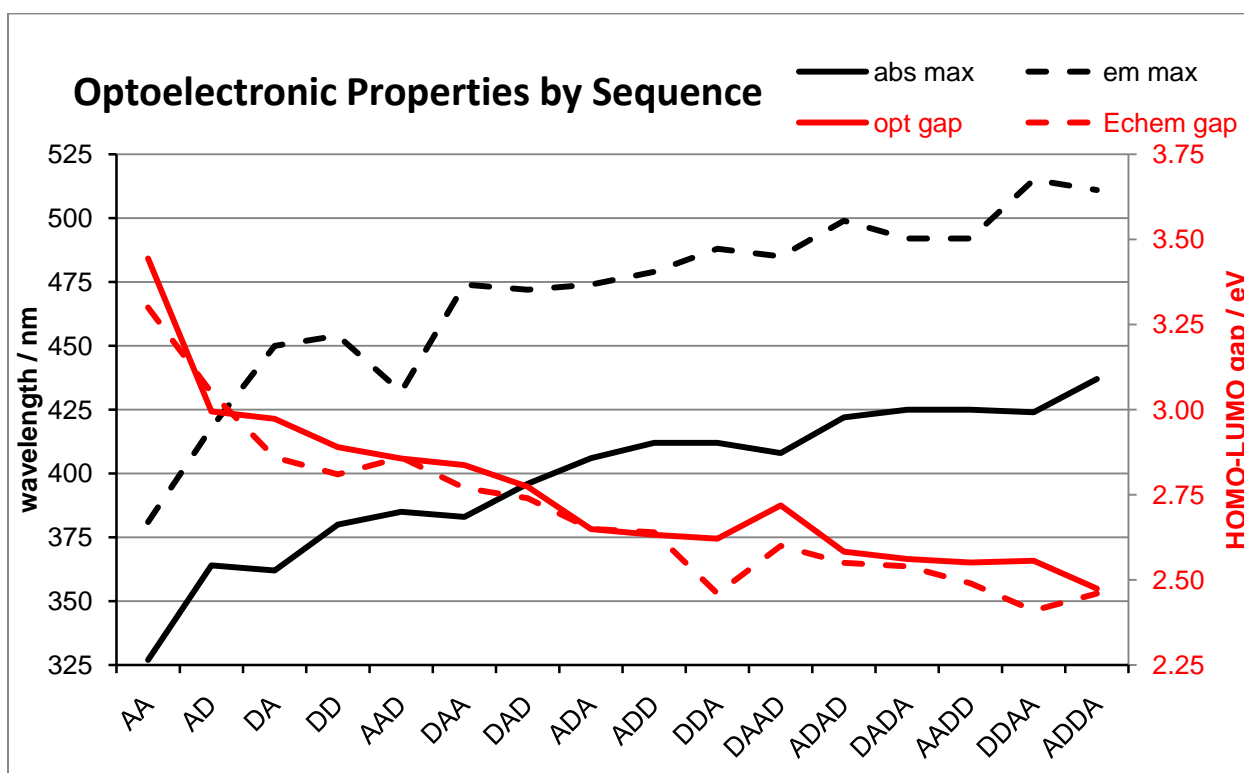


Figure 139. Sequence dependent trends in optoelectronic properties.

APPENDIX B: CHAPTER 3

B.1 ^1H AND ^{13}C NMR SPECTRA OF NEW COMPOUNDS

Figure 140. ^1H and ^{13}C NMR spectra of compound 15.

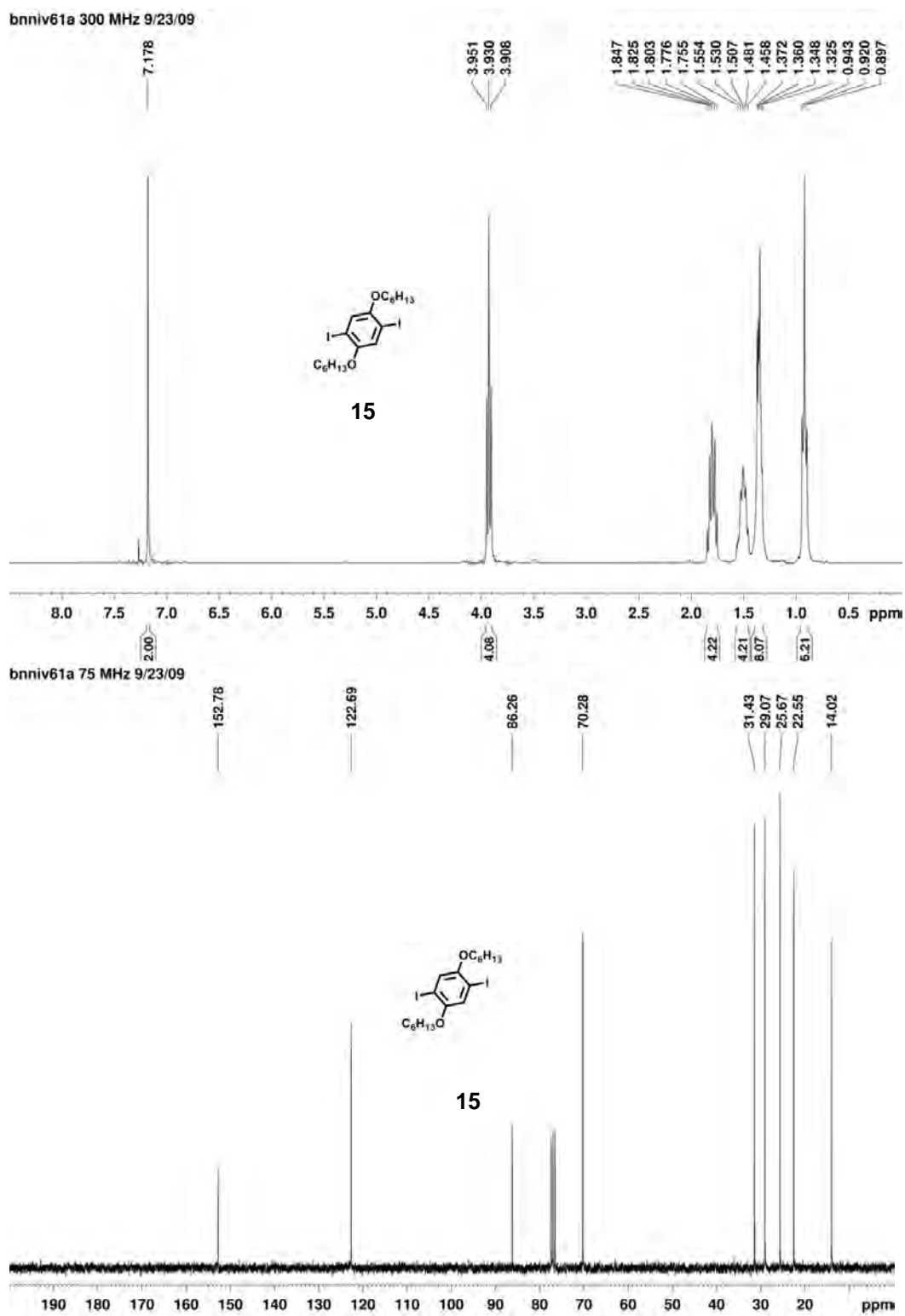
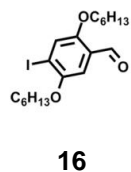
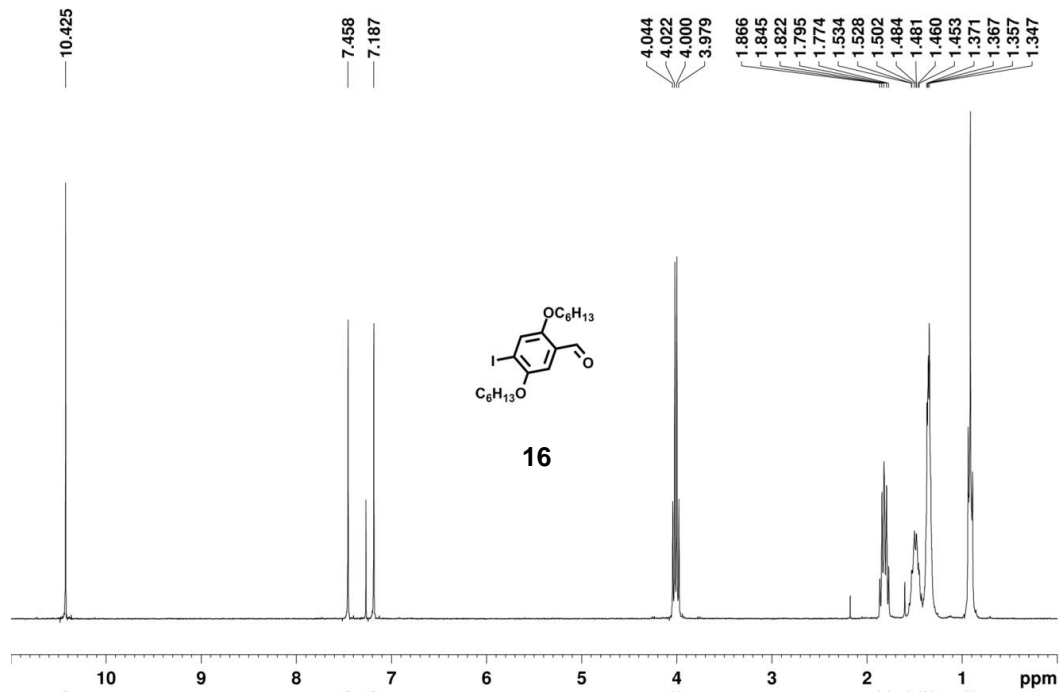


Figure 141. ^1H and ^{13}C NMR spectra of compound 16.

bnnv32b 300 MHz CDCl₃ 9/23/09



bnnv32b 75 MHz CDCl₃ 9/23/09

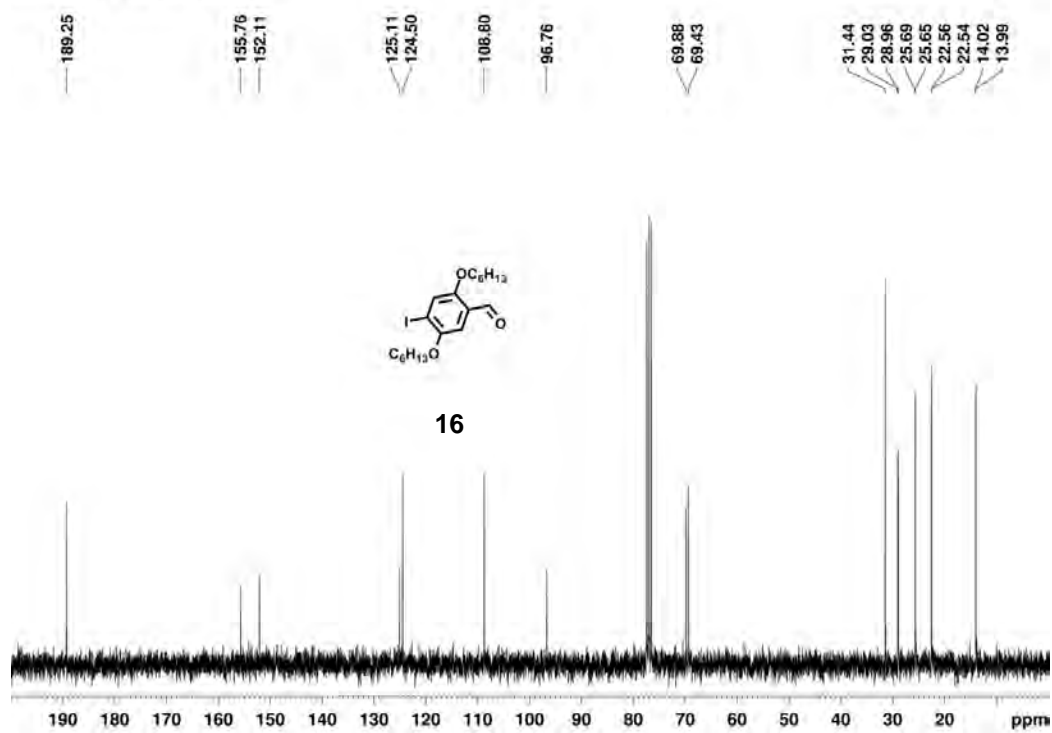
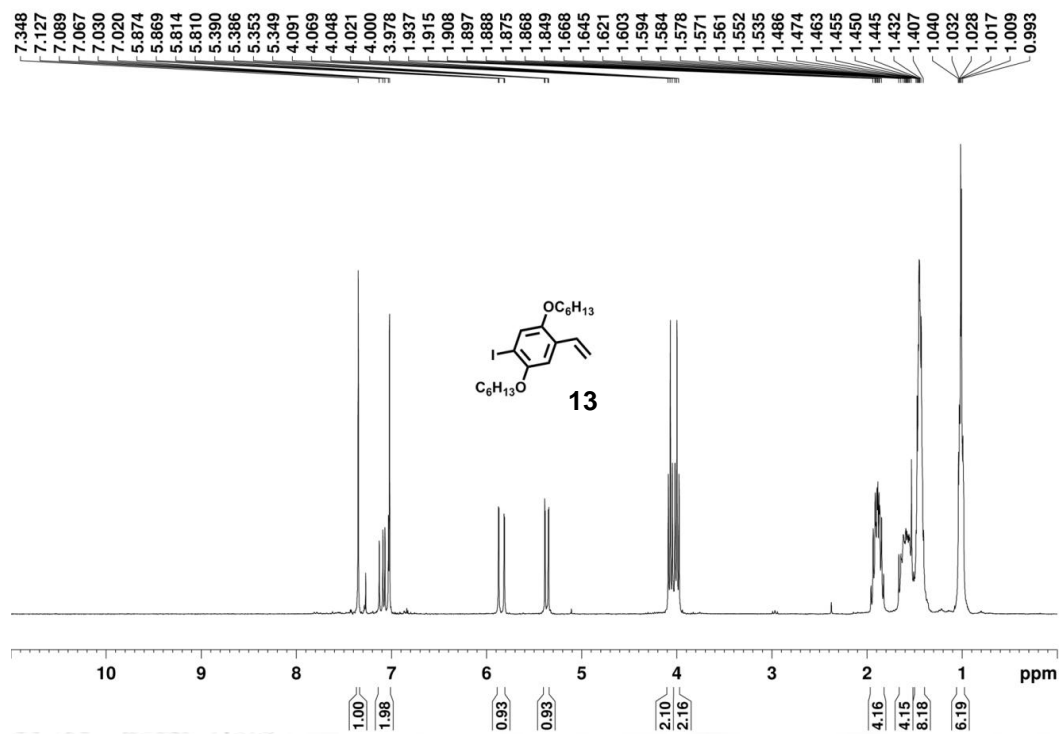


Figure 142. ^1H and ^{13}C NMR spectra of compound 13.

bnniv44a 300 MHz CDCl₃ 9/23/09



bnniv44a 75 MHz CDCl₃ 9/23/09

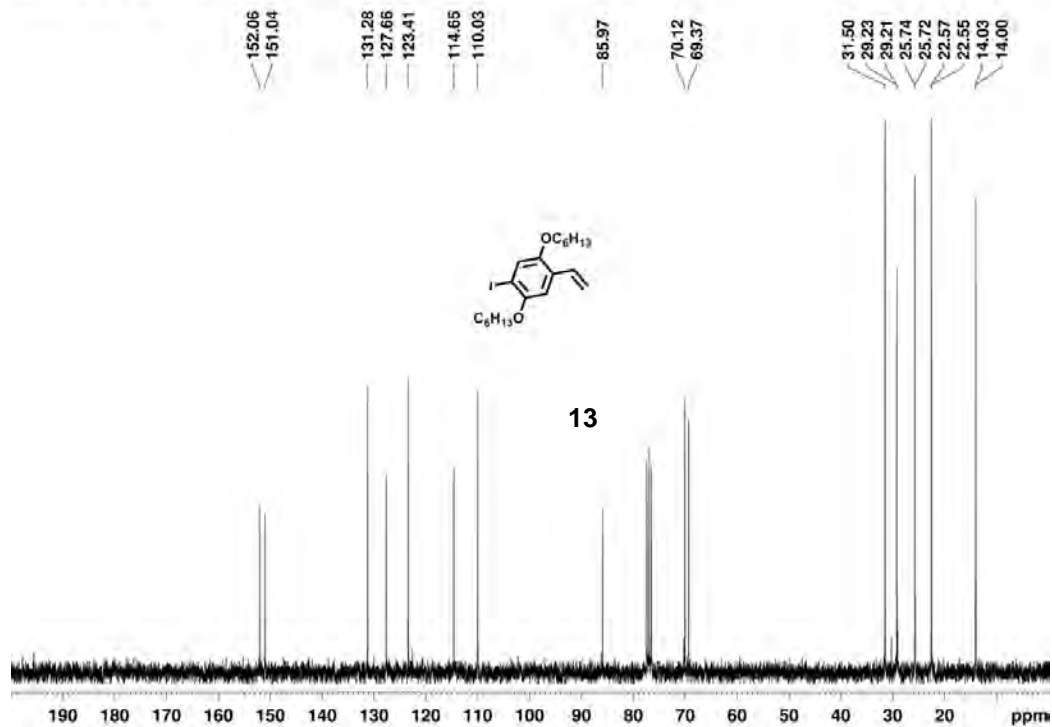


Figure 143. ^1H and ^{13}C NMR spectra of compound 12.

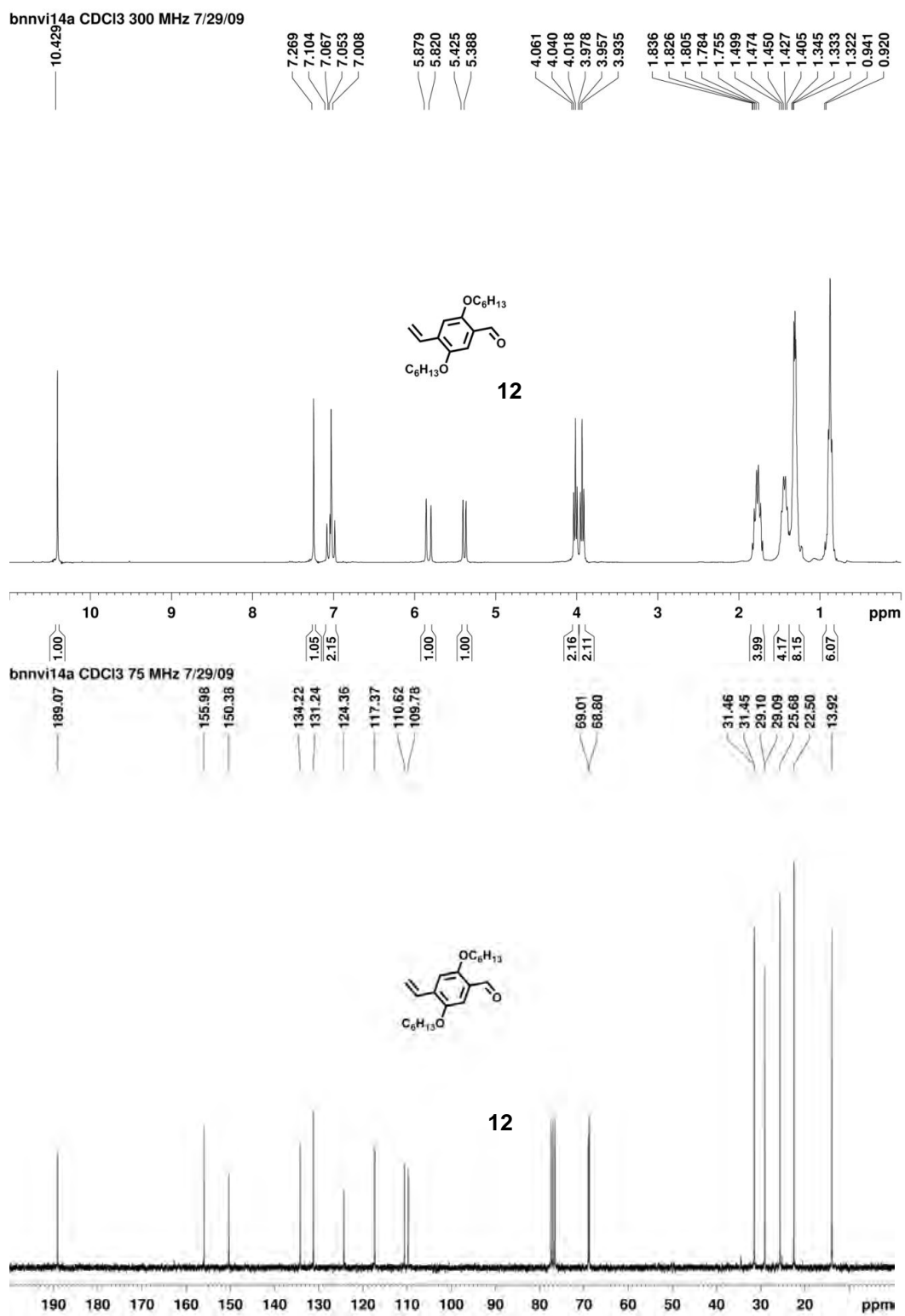


Figure 144. ^1H , ^{13}C , and DEPT 135 NMR spectra of OPV1a.

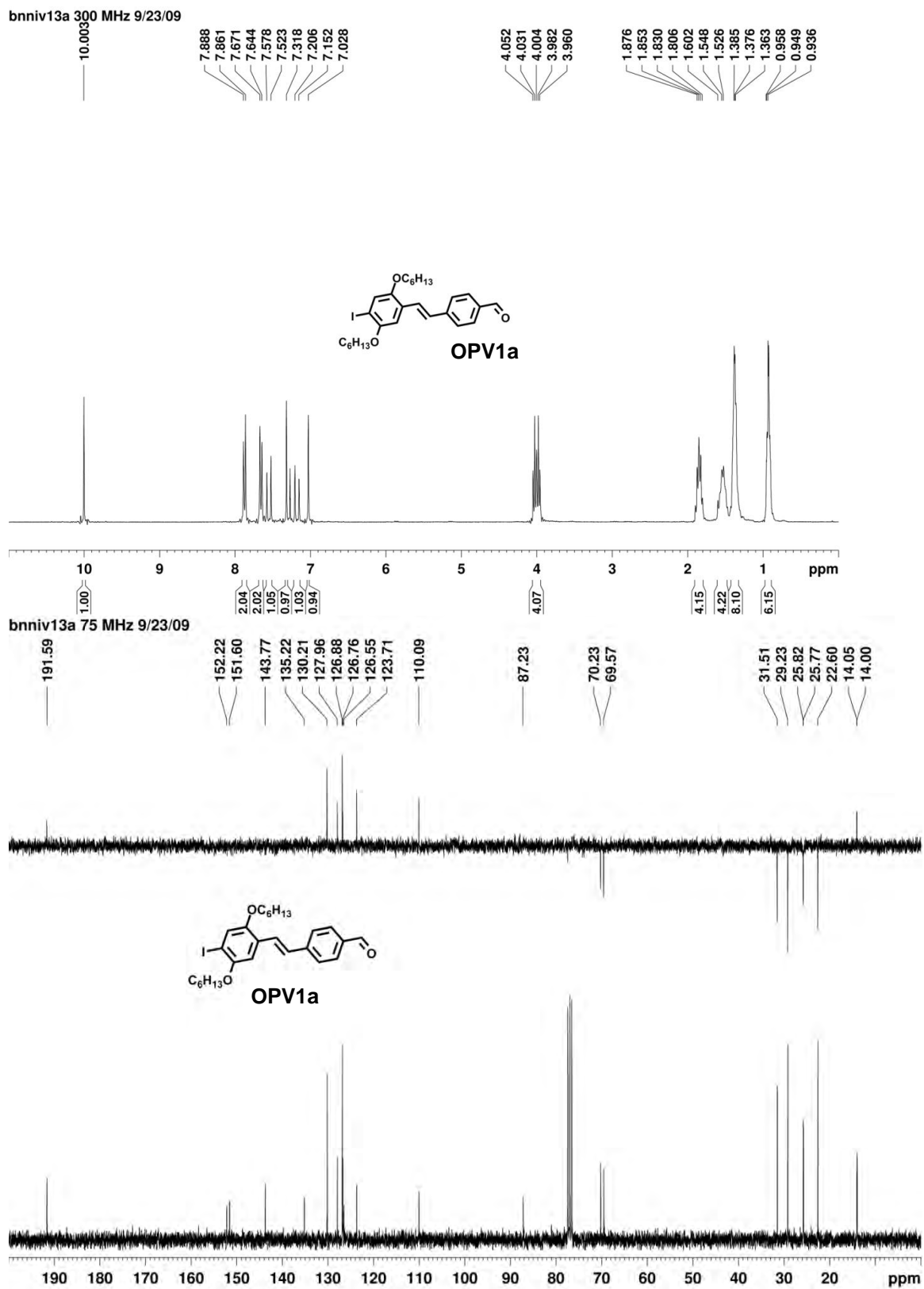
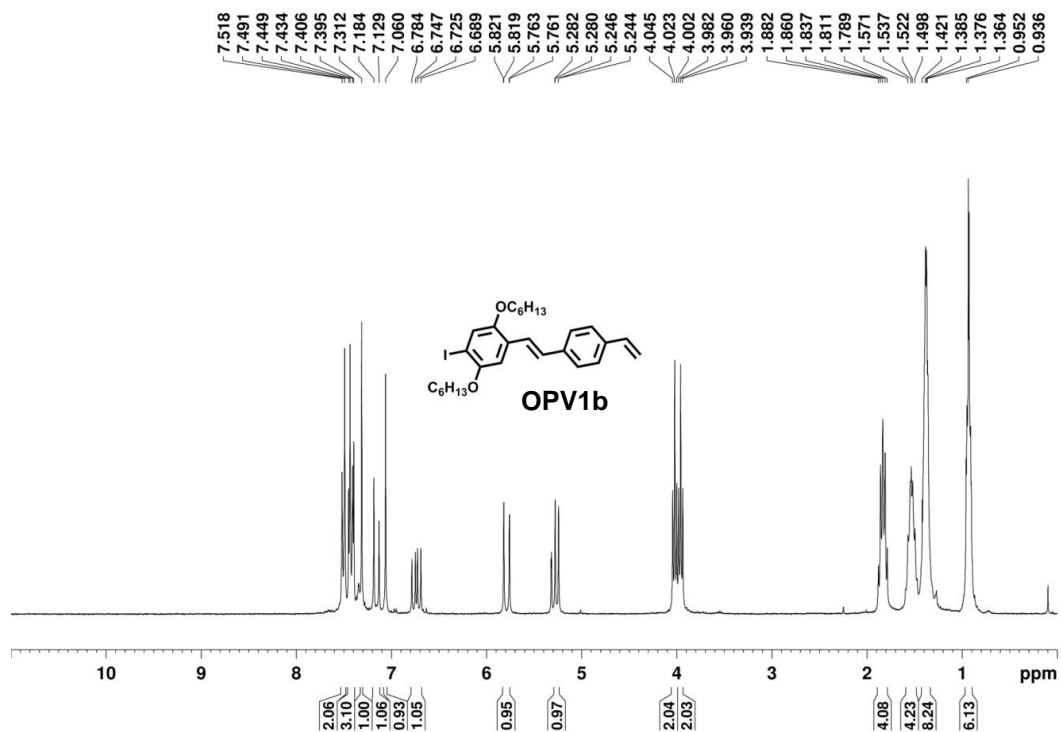


Figure 145. ^1H , ^{13}C , and DEPT 135 NMR spectra of OPV1b.

bnnvi17a 300 MHz CD₂Cl₂ 9/24/09



bnnvi17a DEPT 135 CD₂Cl₂ 9/24/09

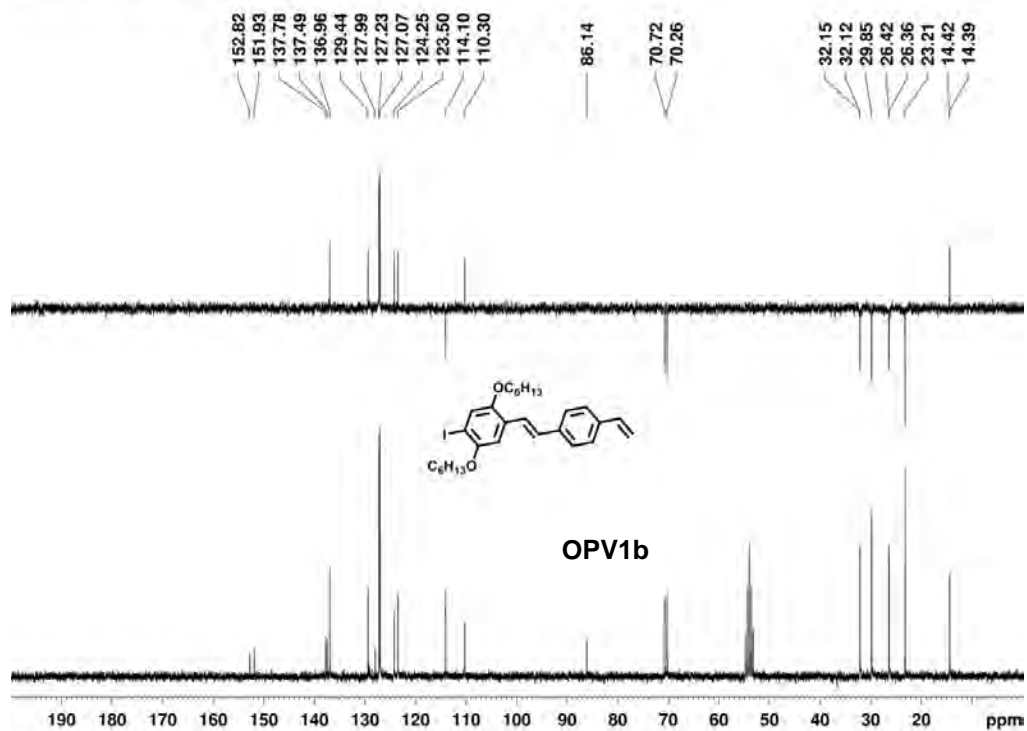


Figure 146. ^1H , ^{13}C , and DEPT 135 NMR spectra of OPV2a.

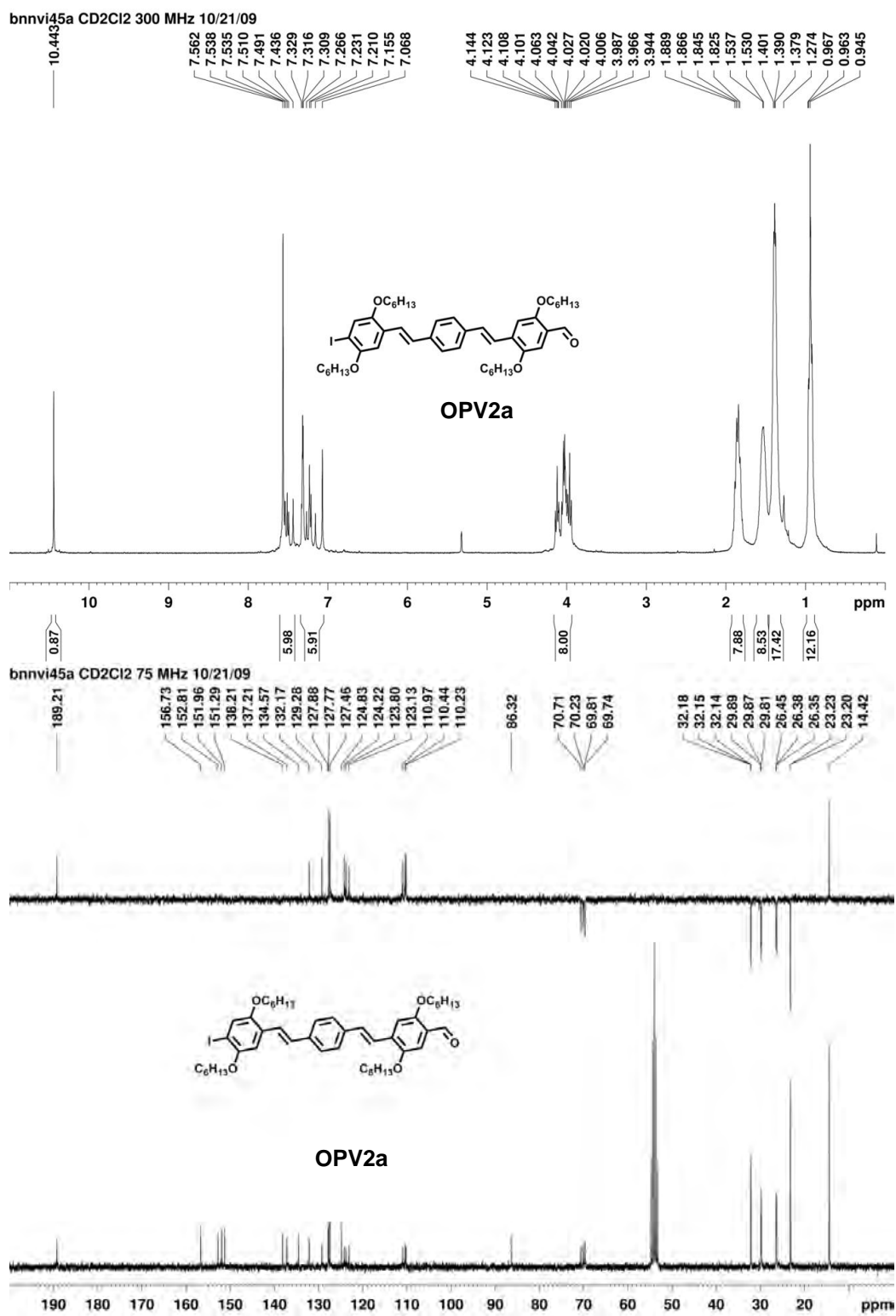
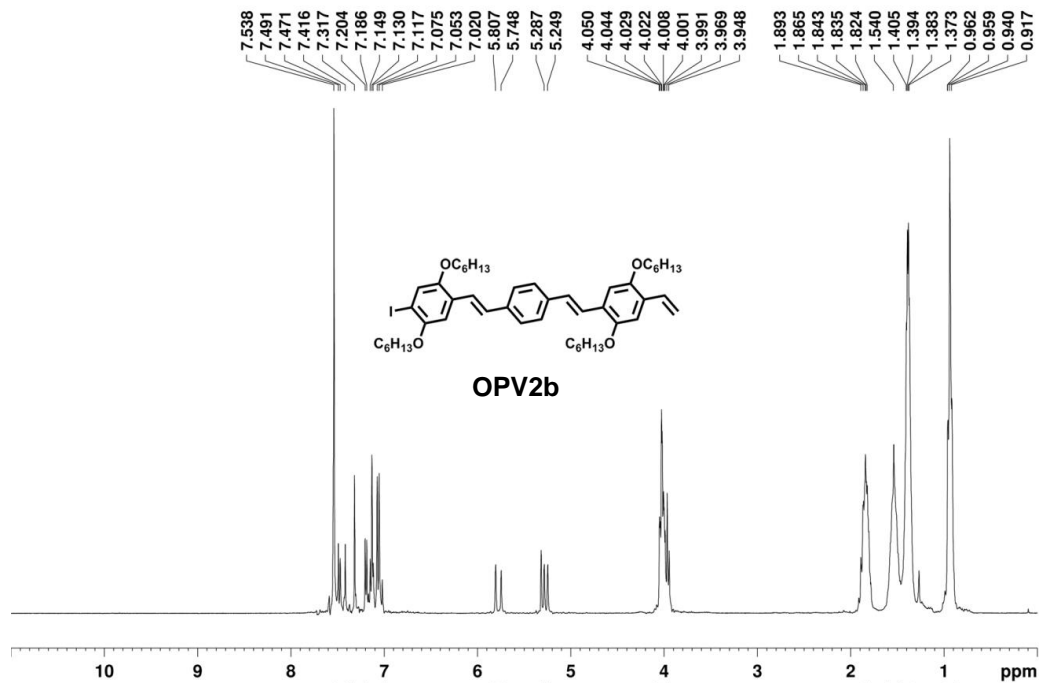


Figure 147. ^1H , ^{13}C , and DEPT 135 NMR spectra of OPV2b.

bnnvi20a 300 MHz CD₂Cl₂ 9/24/09



bnnvi20a DEPT 135 CD₂Cl₂ 9/24/09

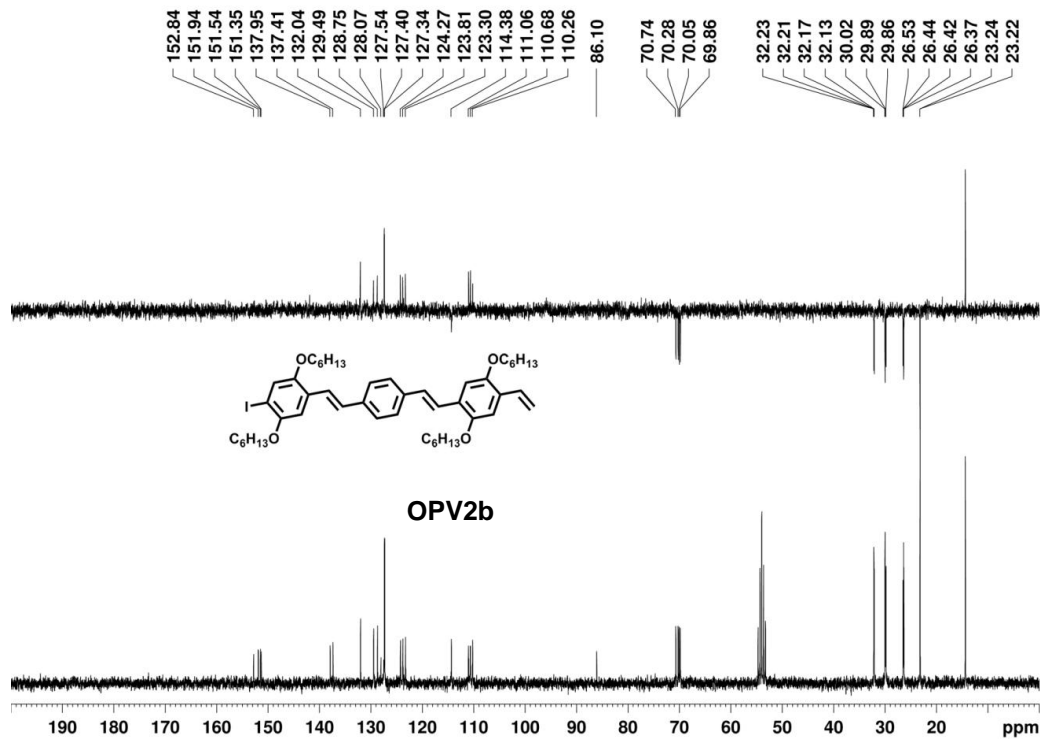


Figure 148. ^1H , ^{13}C , and DEPT 135 NMR spectra of OPV3a.

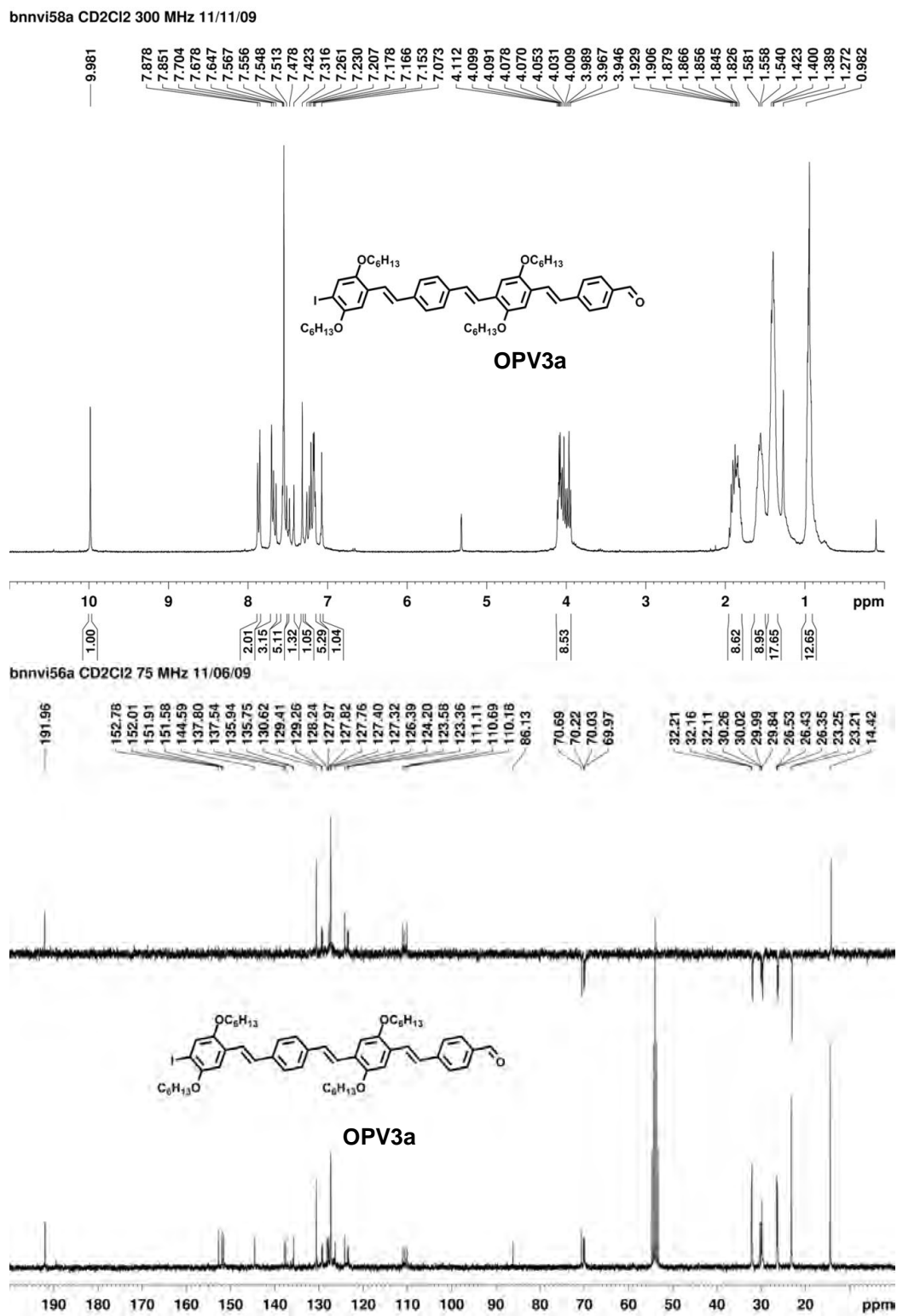


Figure 149. ^1H , ^{13}C , and DEPT 135 NMR spectra of OPV3b.

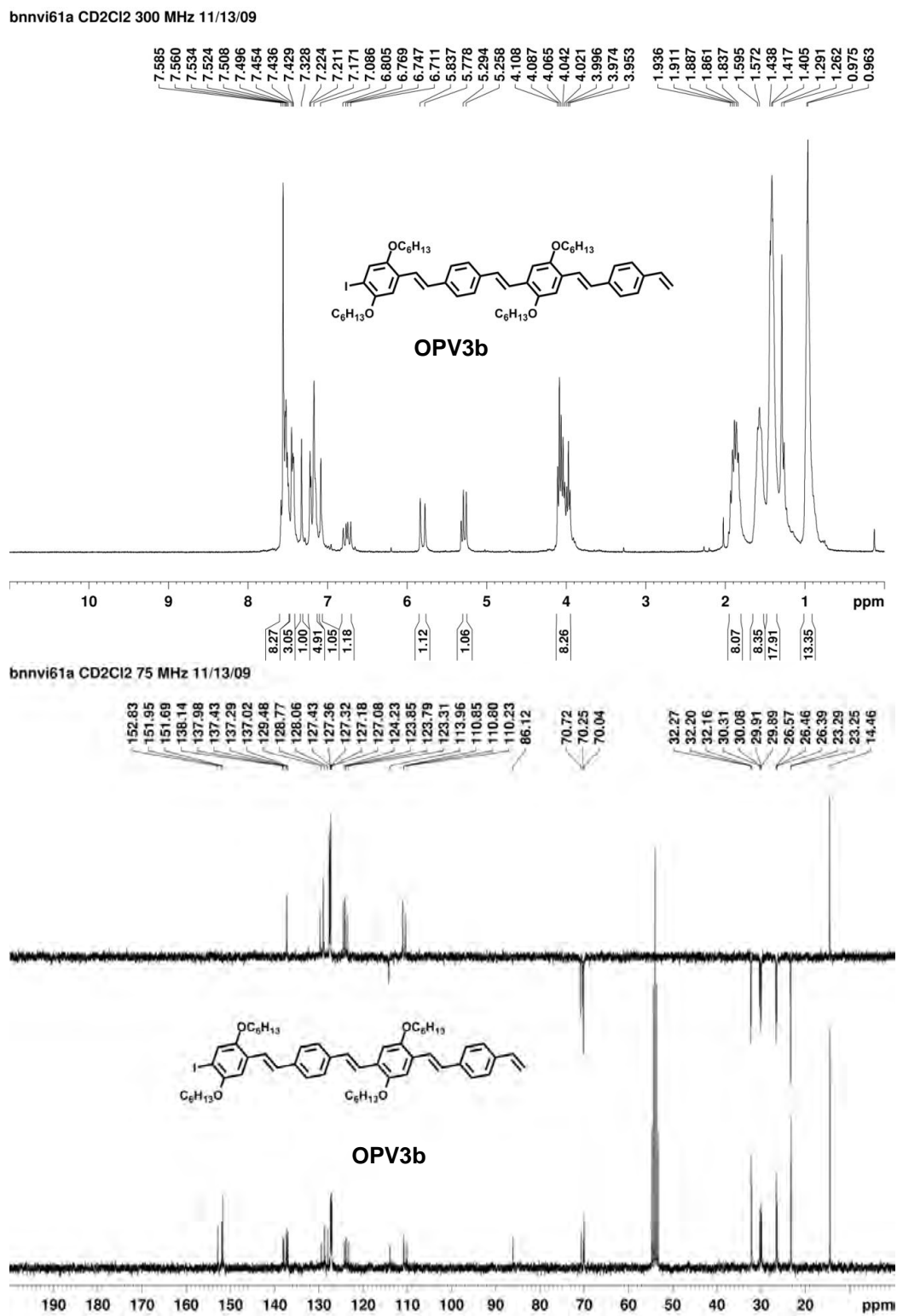


Figure 150. ^1H , ^{13}C , and DEPT 135 NMR spectra of OPV4a.

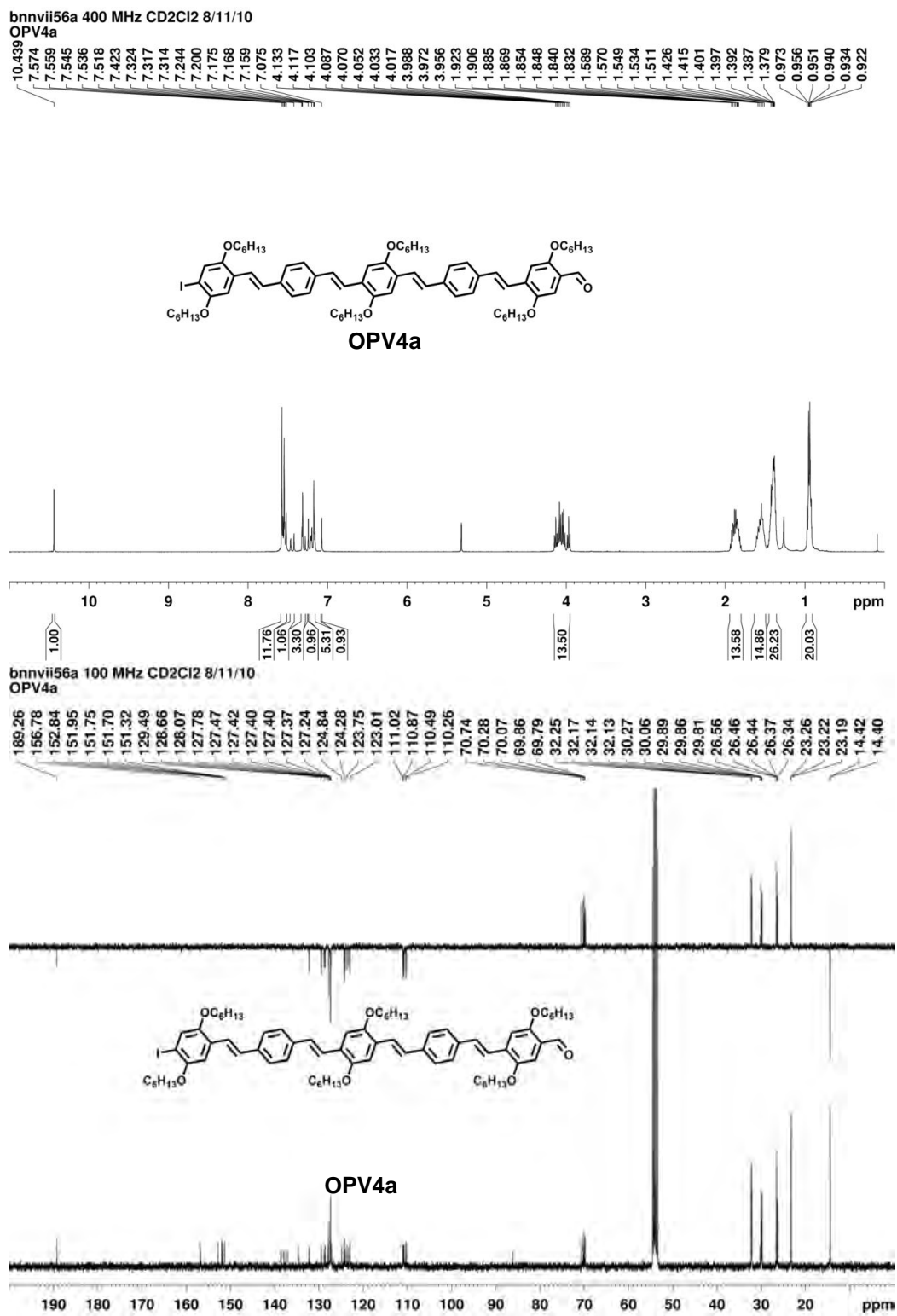


Figure 151. ^1H , ^{13}C , and DEPT 135 NMR spectra of OPV4b.

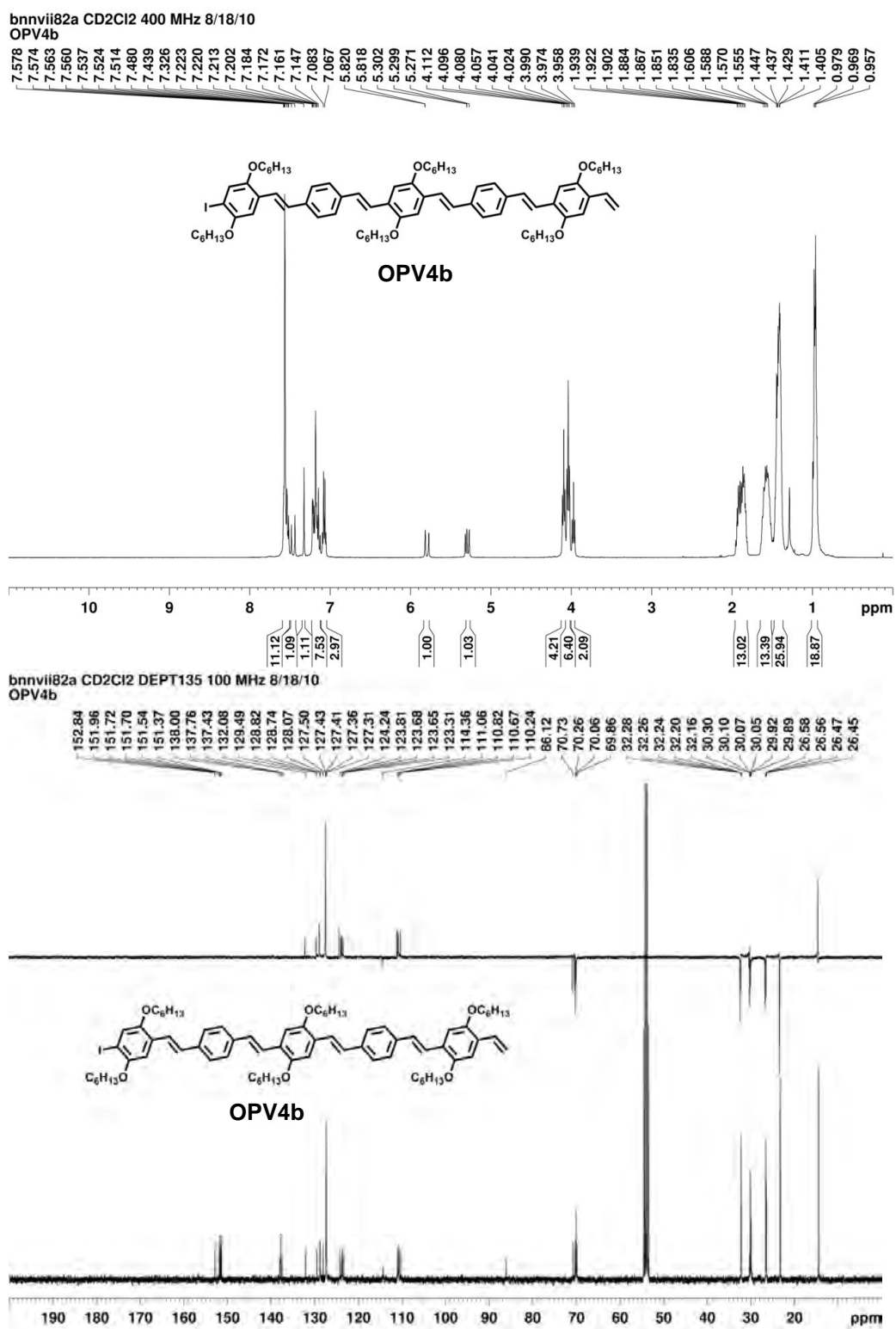


Figure 152. ^1H , ^{13}C , and DEPT 135 NMR spectra of OPV2c.

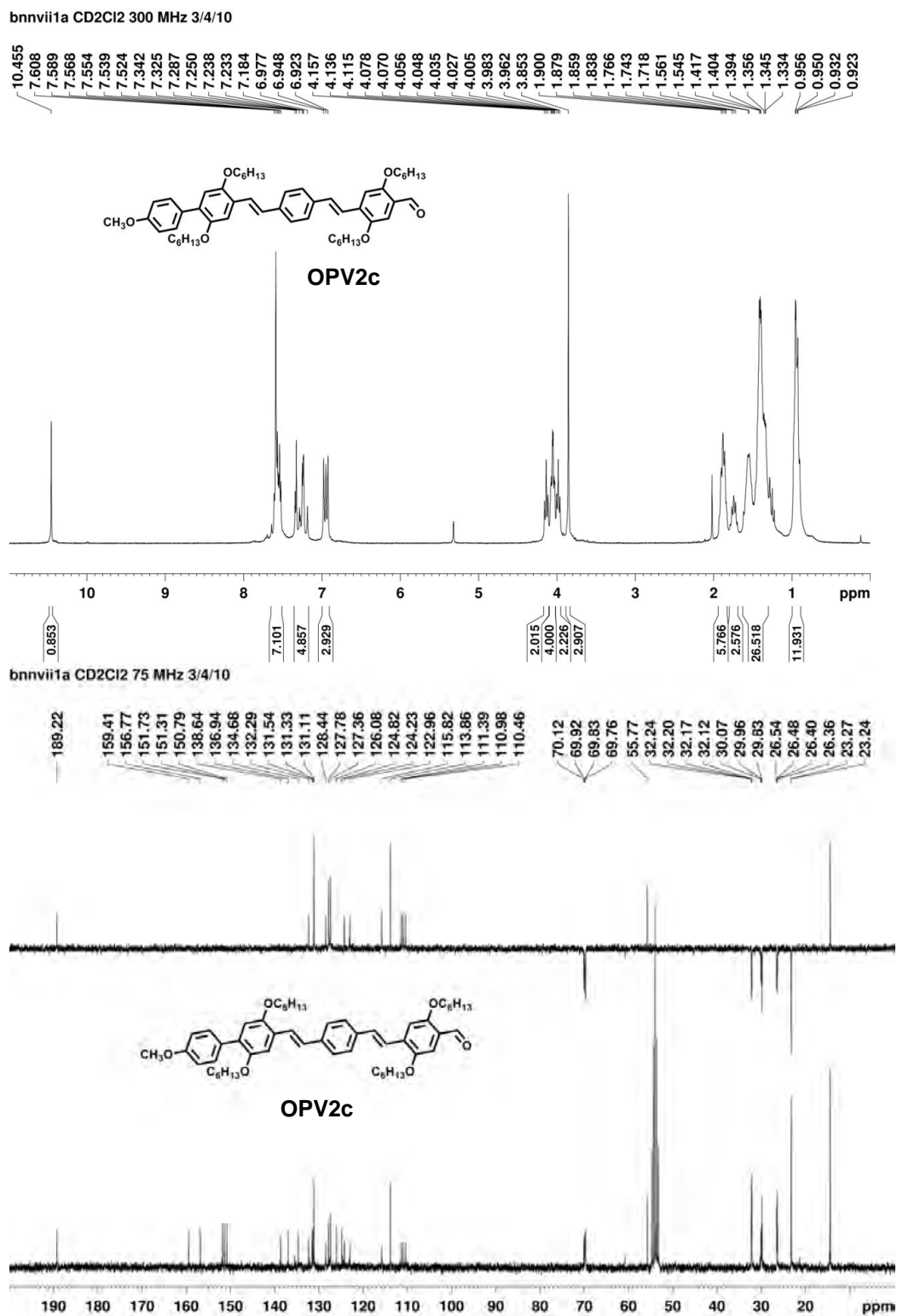


Figure 153. ^1H , ^{13}C , and DEPT 135 NMR spectra of OPV2d.

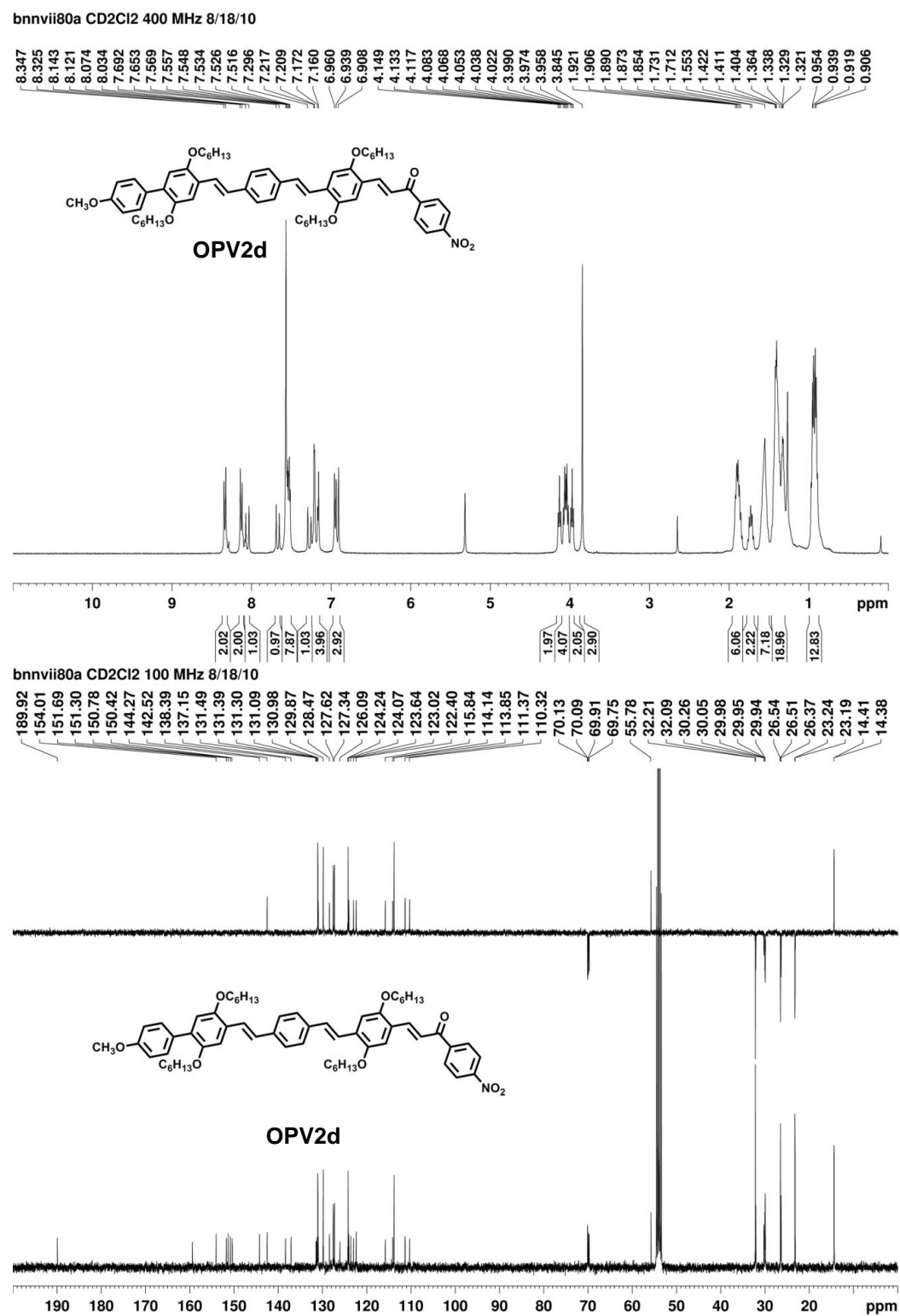
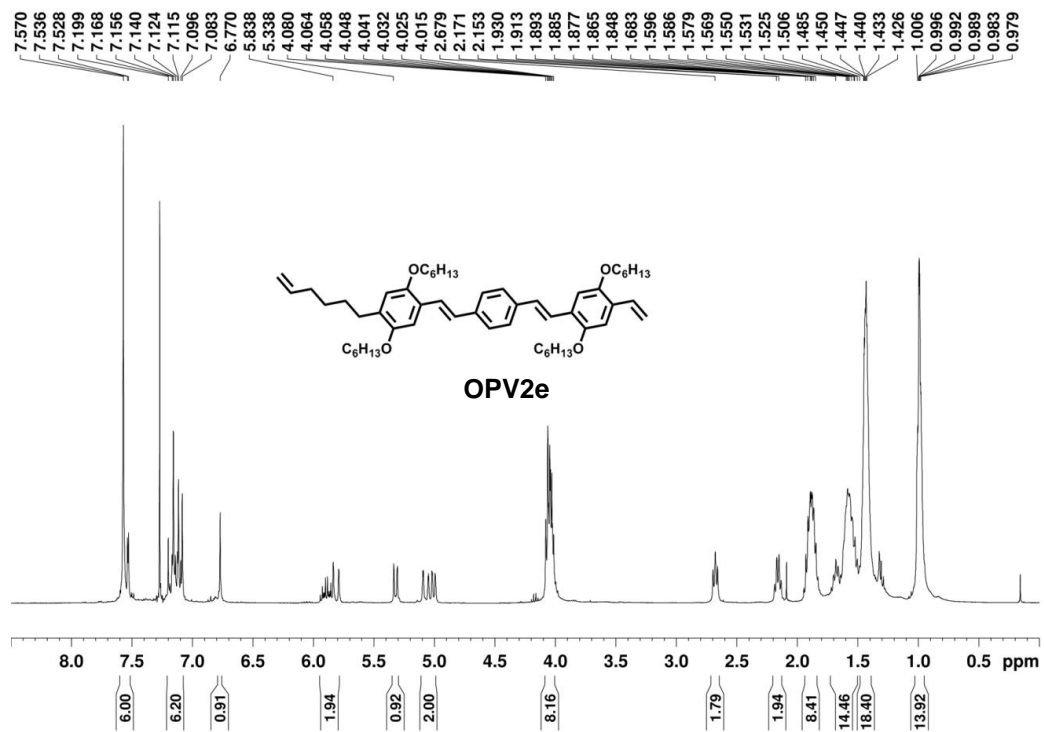


Figure 154. ^1H , ^{13}C , and DEPT 135 NMR spectra of OPV2e.

bnnvii63b CDCl₃ 400 MHz 8/9/10



bnnvii63b CDCl₃ 100 MHz 8/9/10

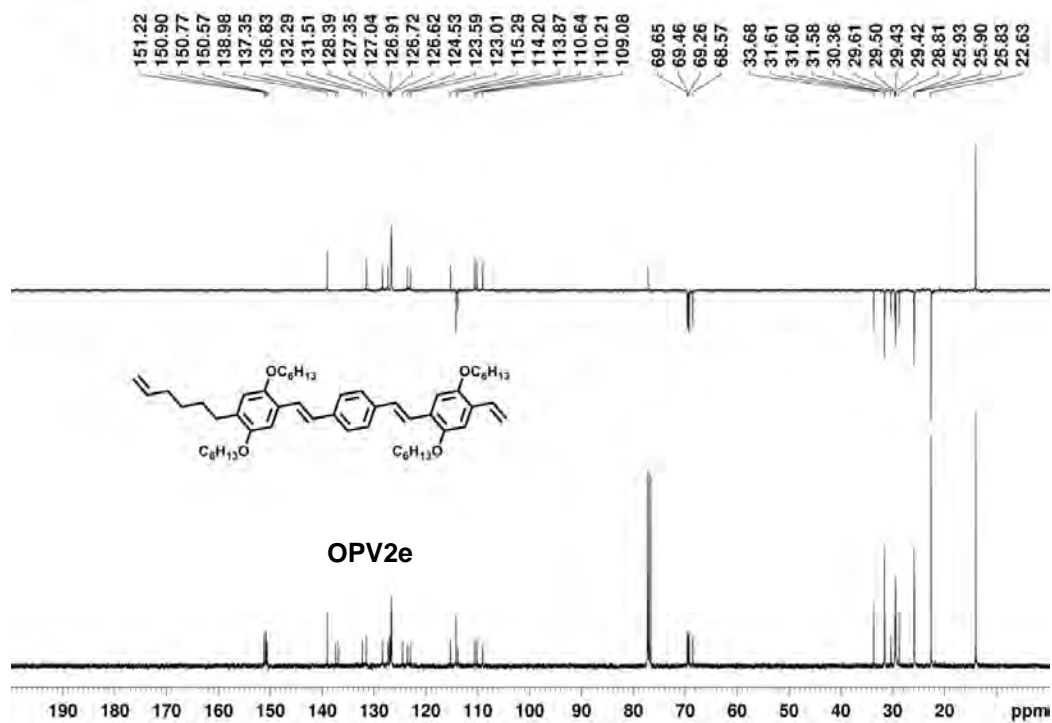


Figure 155. ^1H , and ^{13}C NMR spectra of p(OPV2e).

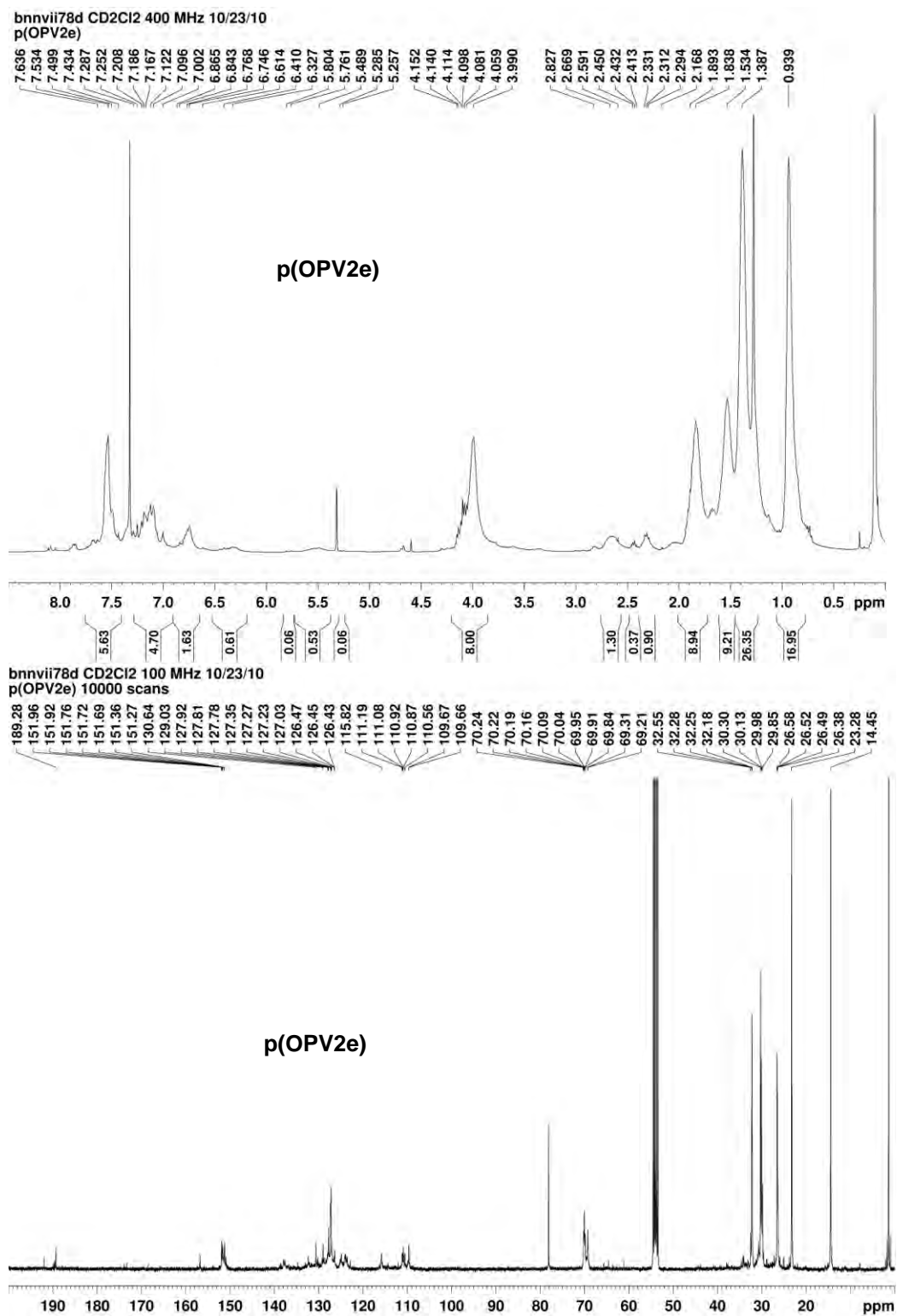
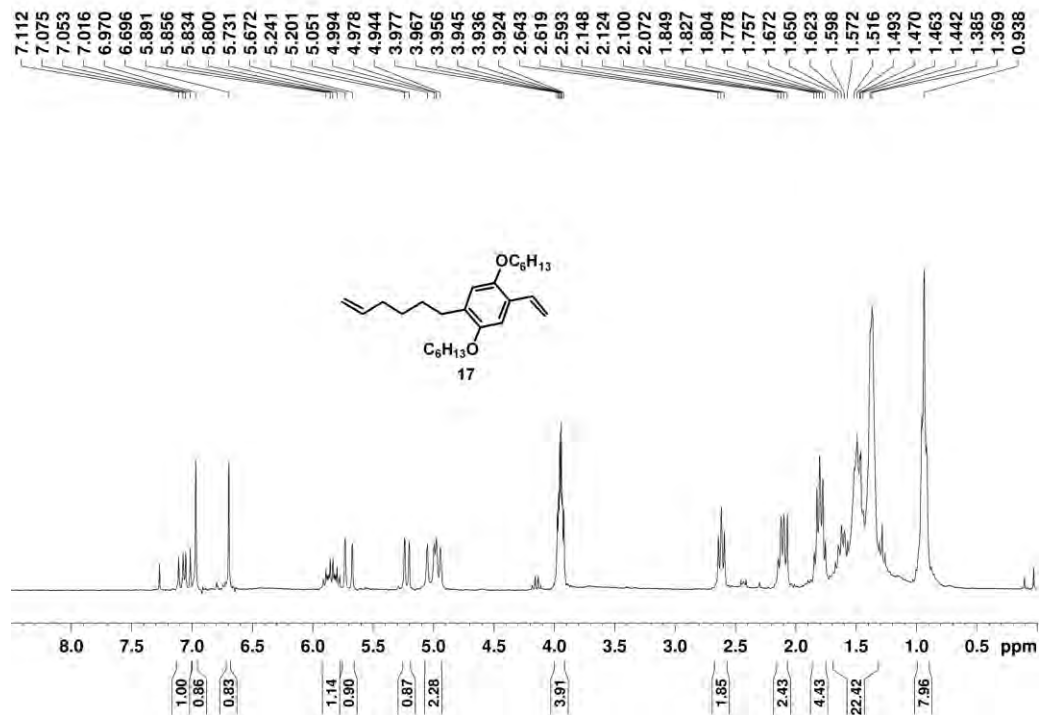


Figure 156. ^1H , ^{13}C , and DEPT 135 NMR spectra of compound 17.

bnnvii3a CDCl₃ 300 MHz 3/3/10



bnnvii3a CDCl₃ 75 MHz 3/4/10

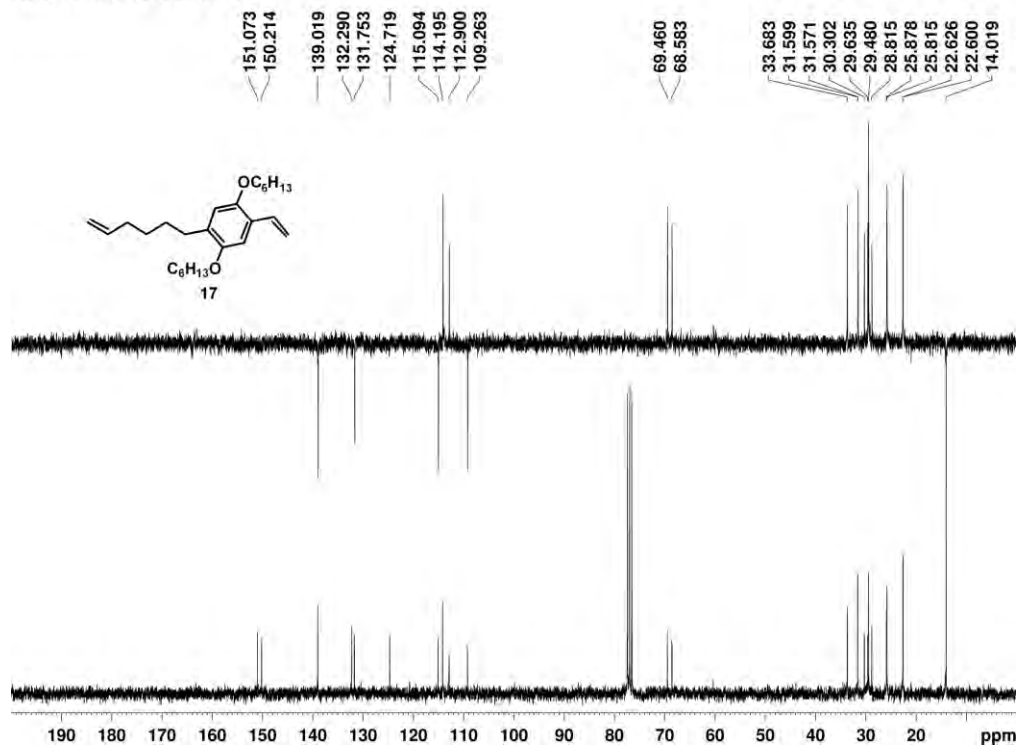


Figure 157. ^1H , ^{13}C , and DEPT 135 NMR spectra of OPV1c.

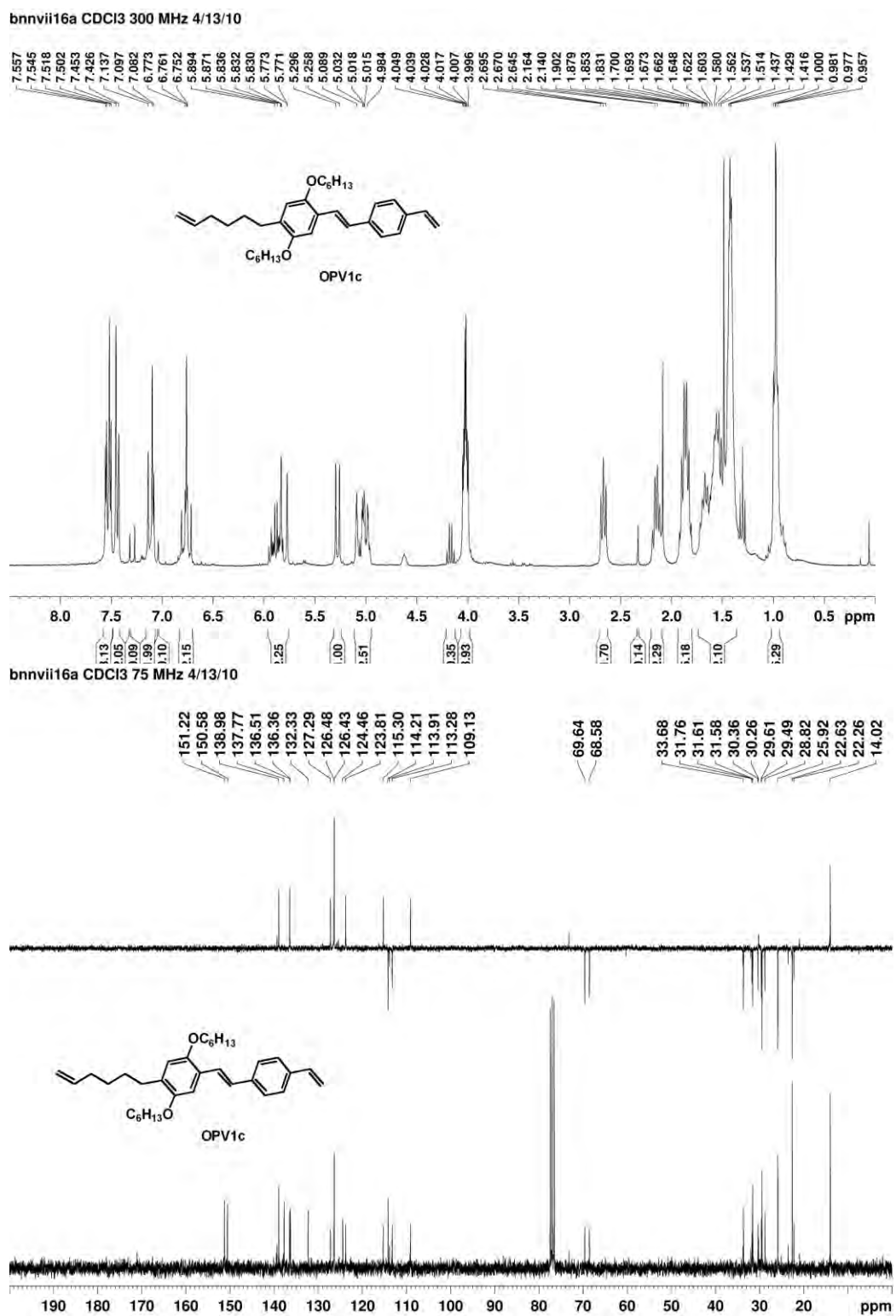


Figure 158. ^1H and ^{13}C NMR spectra of compound 18.

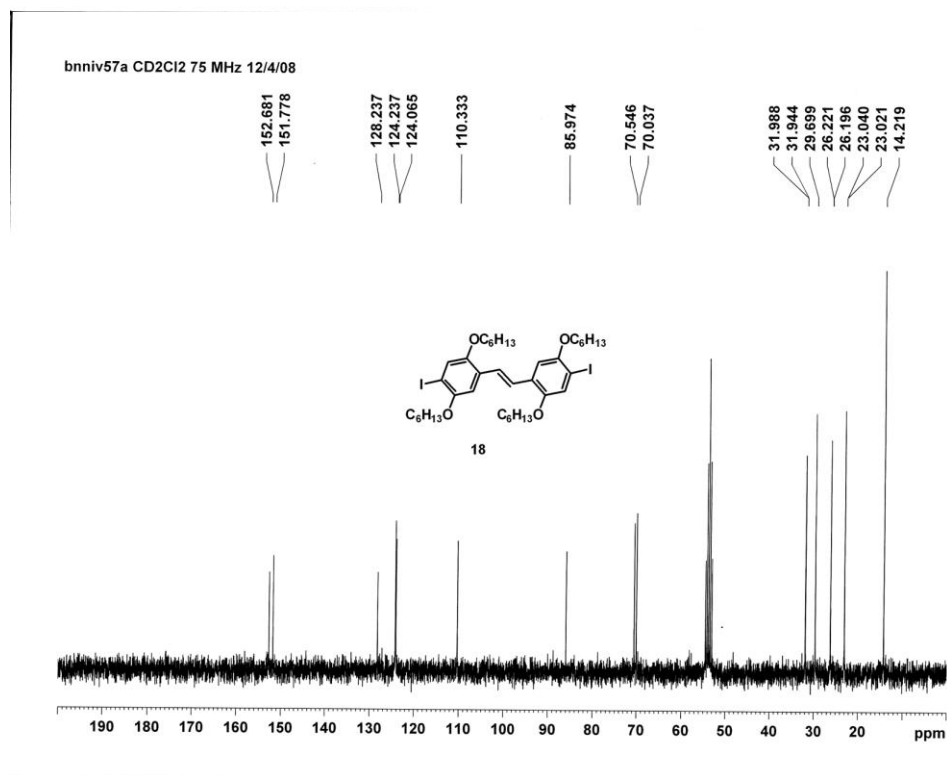
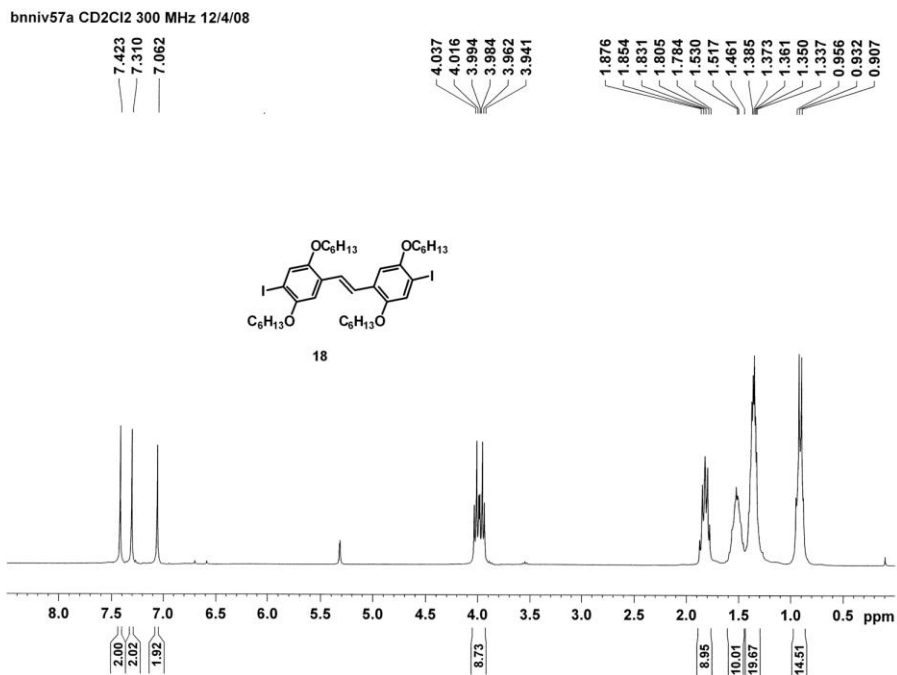
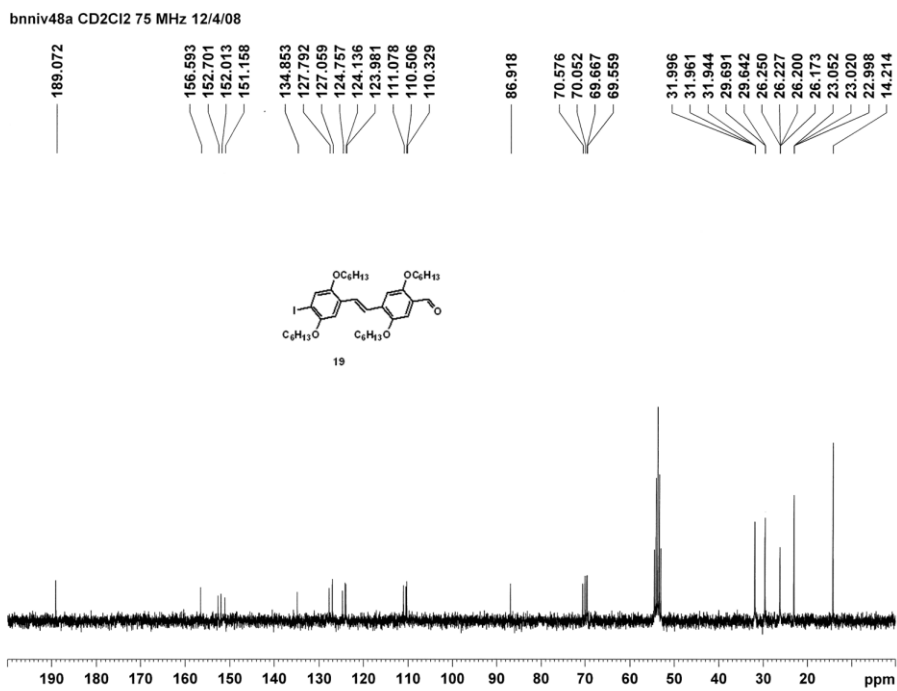
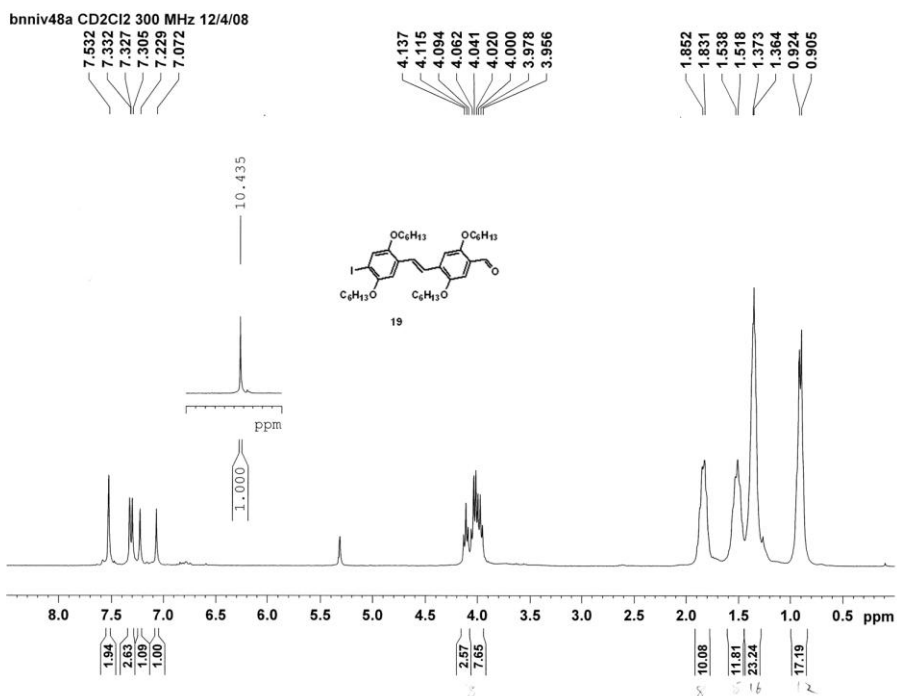


Figure 159. ^1H and ^{13}C NMR spectra of compound 19.



B.2 ABSORPTION AND EMISSION SPECTRA

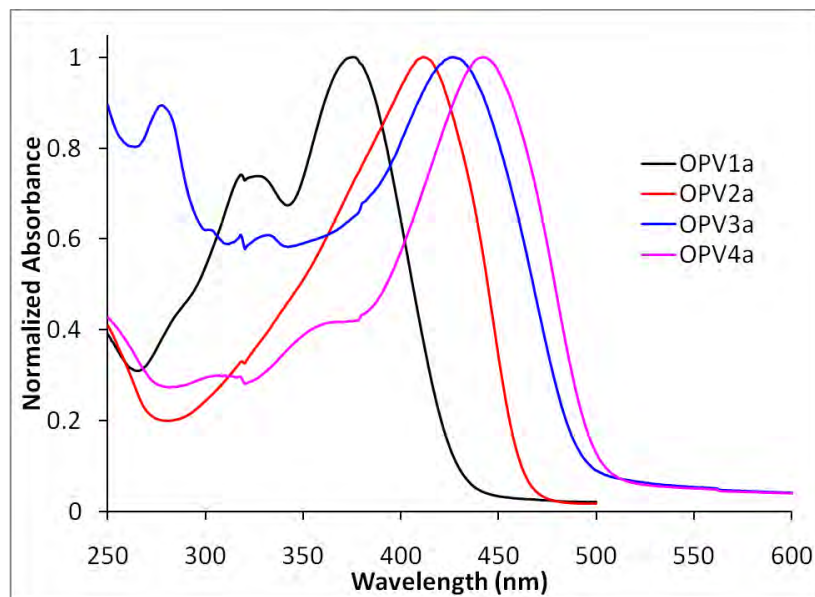


Figure 160. Normalized absorption spectra of **OPV1a**, **OPV2a**, **OPV3a**, and **OPV4a** (10^{-6} M in CHCl_3).

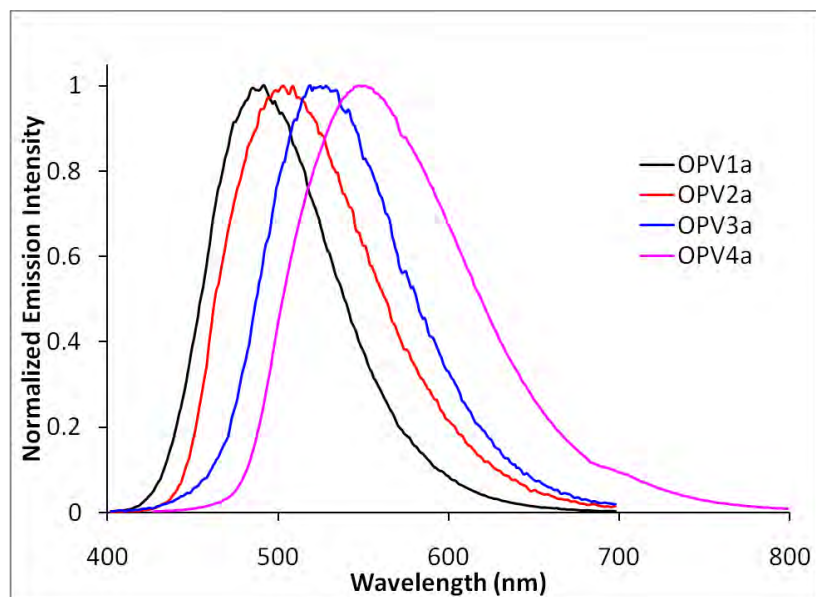


Figure 161. Normalized emission spectra of **OPV1a**, **OPV2a**, **OPV3a**, and **OPV4a** (10^{-6} M in CHCl_3).

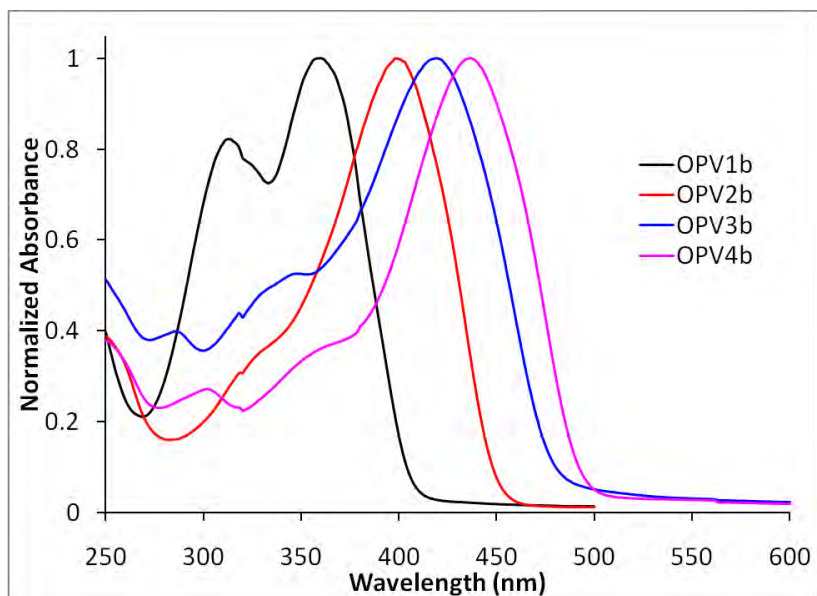


Figure 162. Normalized absorption spectra of **OPV1b**, **OPV2b**, **OPV3b**, and **OPV4b** (10^{-6} M in CHCl_3).

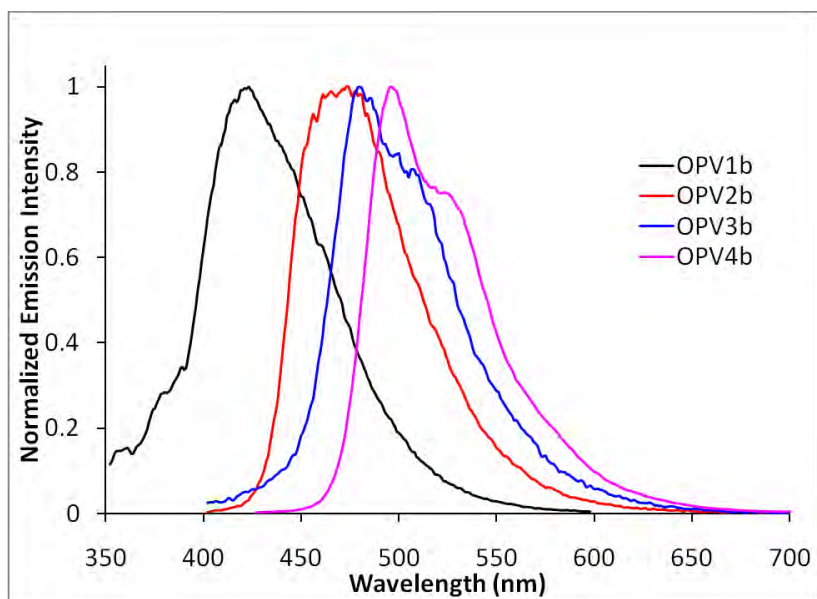


Figure 163. Normalized emission spectra of **OPV1b**, **OPV2b**, **OPV3b**, and **OPV4b** (10^{-6} M in CHCl_3).

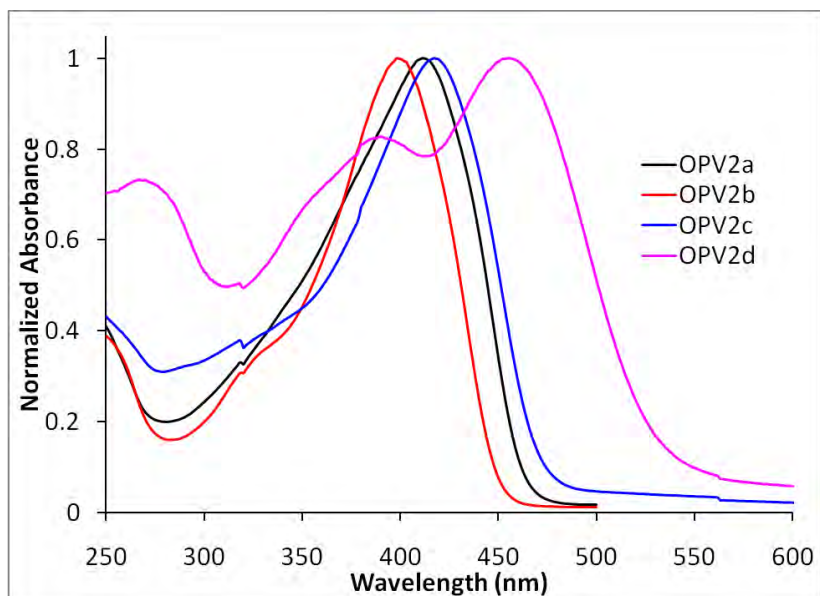


Figure 164. Normalized absorption spectra of **OPV2a**, **OPV2b**, **OPV2c**, and **OPV2d** (10^{-6} M in CHCl_3).

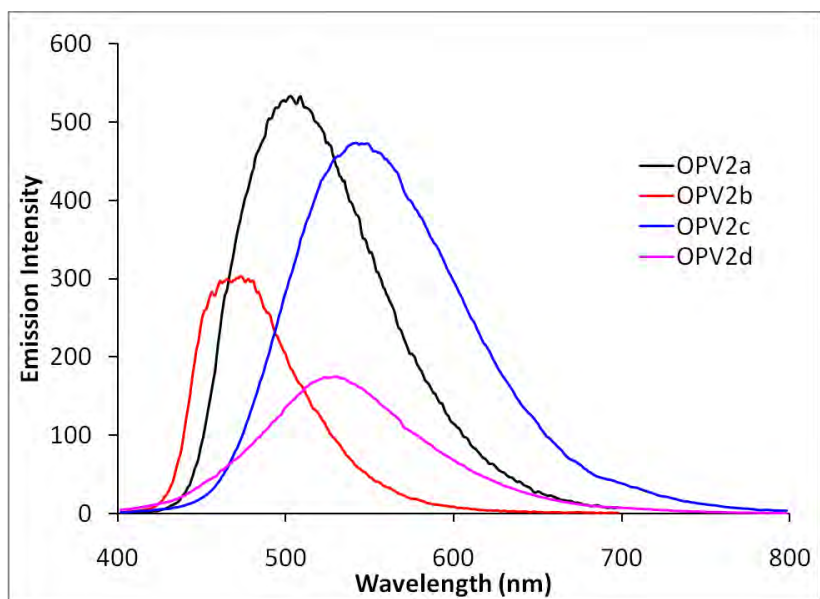


Figure 165. Emission spectra of **OPV2a**, **OPV2b**, **OPV2c**, (10^{-6} M in CHCl_3) and **OPV2d** (10^{-3} M in CHCl_3).

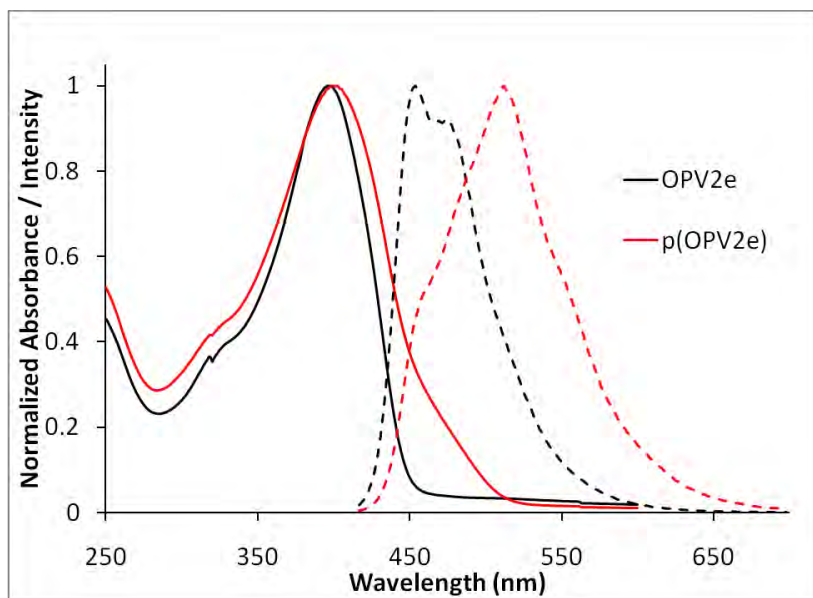


Figure 166. Absorption (solid lines) and emission (dashed lines) spectra of **OPV2e** and **p(OPV2e)** (10^{-5} M in CHCl_3).

APPENDIX C: CHAPTER 4

C.1 ^1H AND ^{13}C NMR SPECTRA OF NEW COMPOUNDS

Figure 167. ^1H and ^{13}C NMR spectra of compound 35.

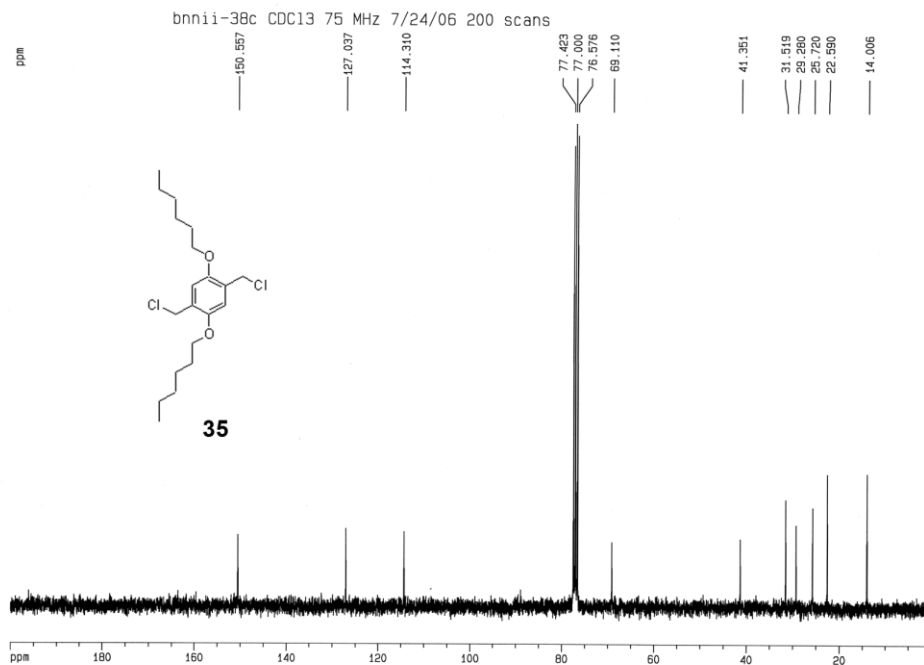
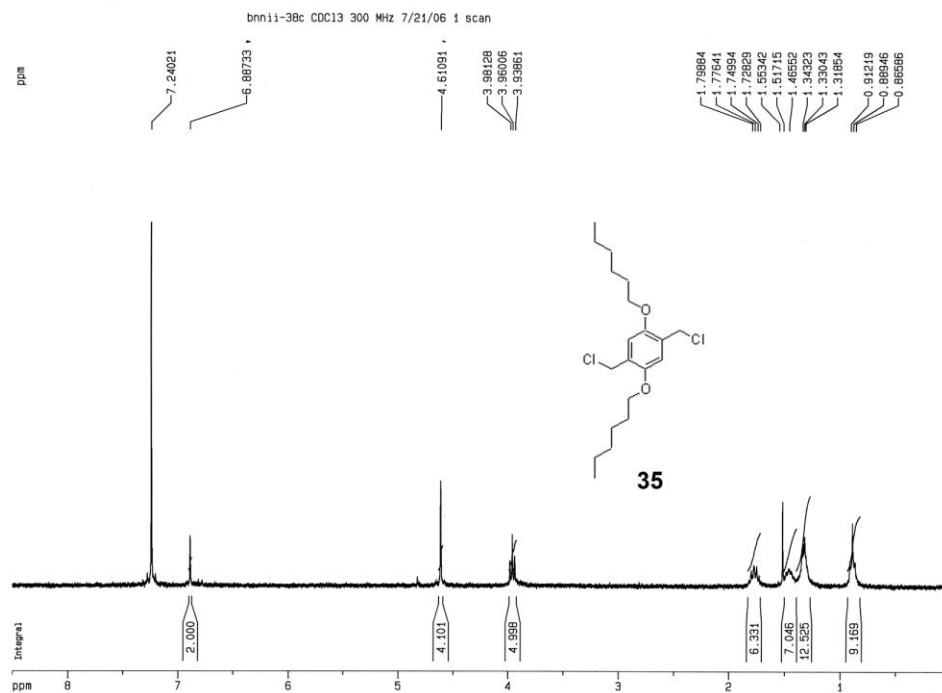


Figure 168. ^1H and ^{13}C NMR spectra of compound **22**.

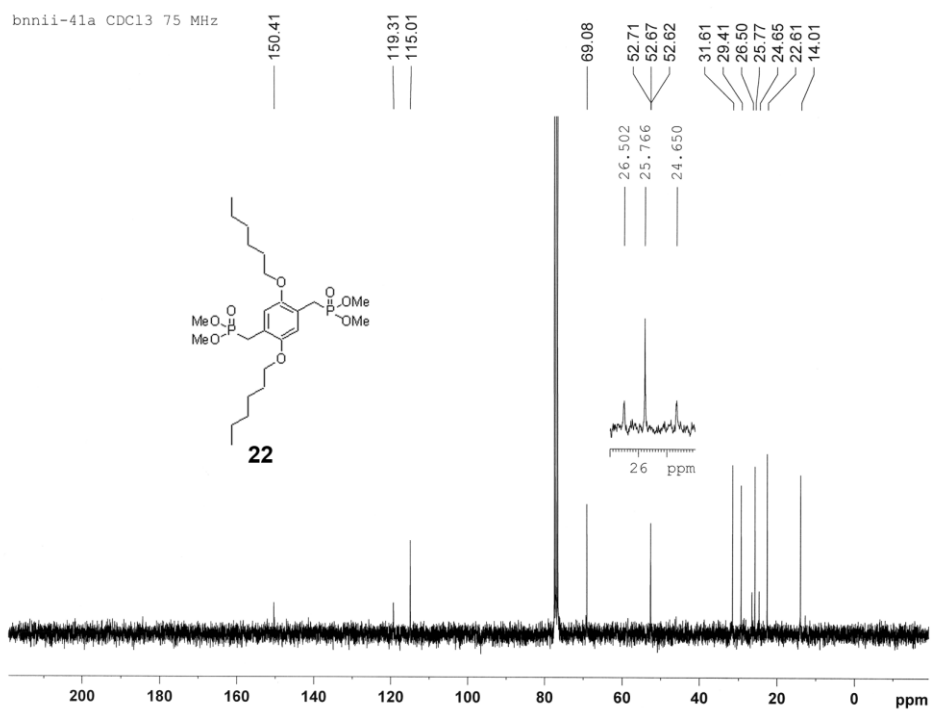
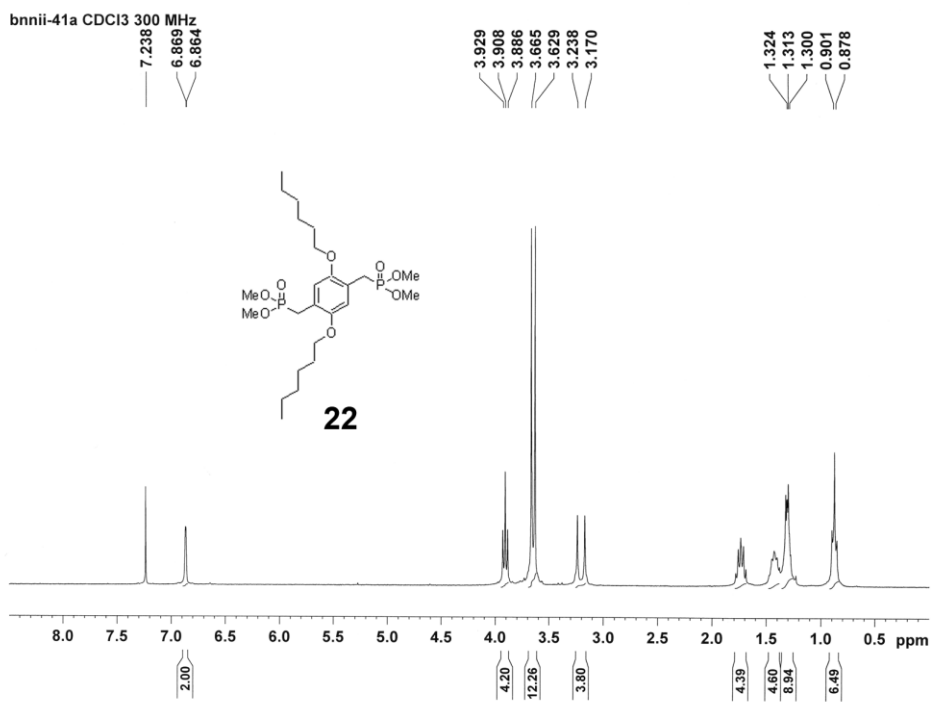


Figure 169. ^1H and ^{13}C NMR spectra of compound 23.

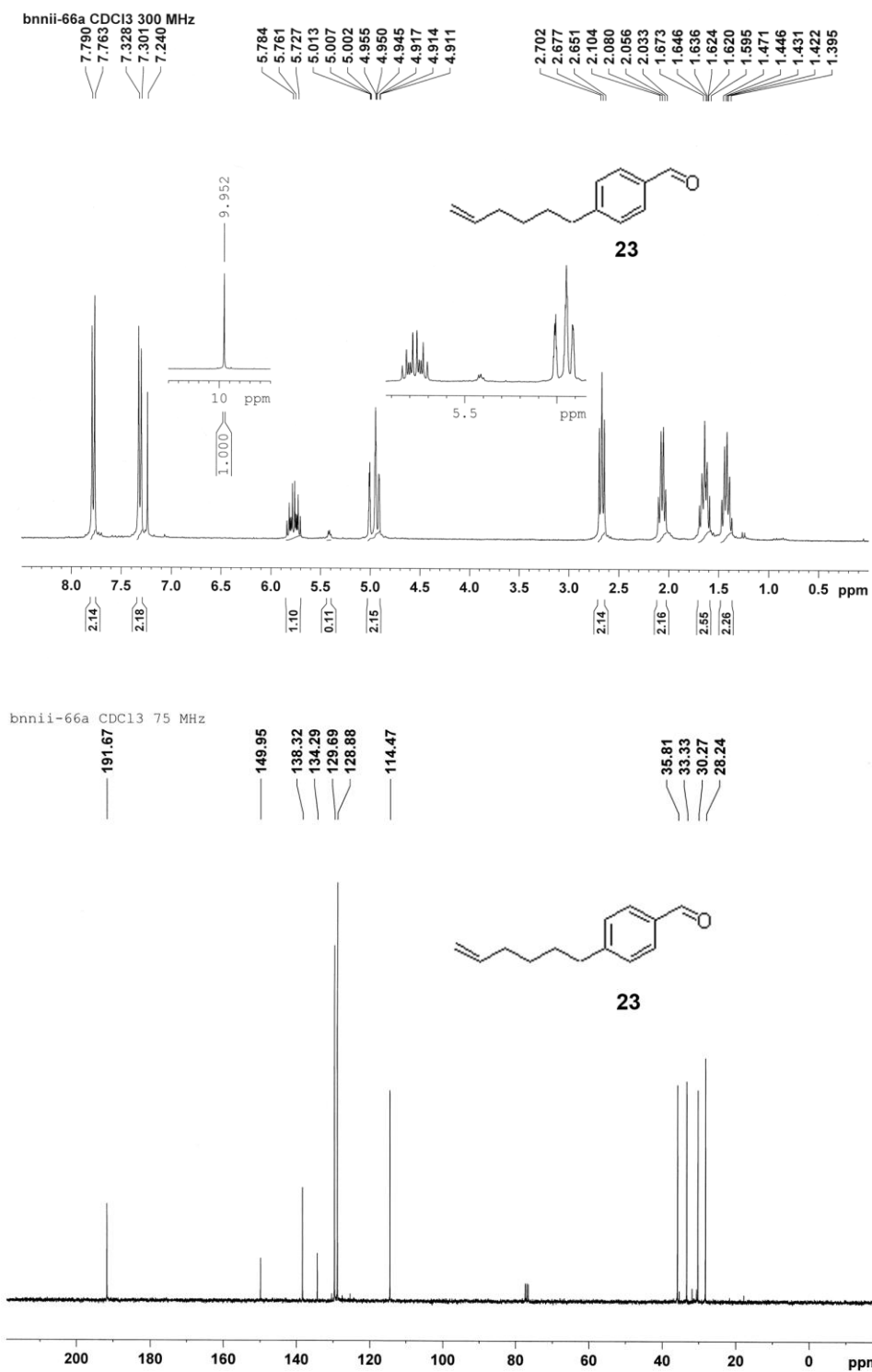


Figure 170. ¹H and ¹³C NMR spectra of compound 24

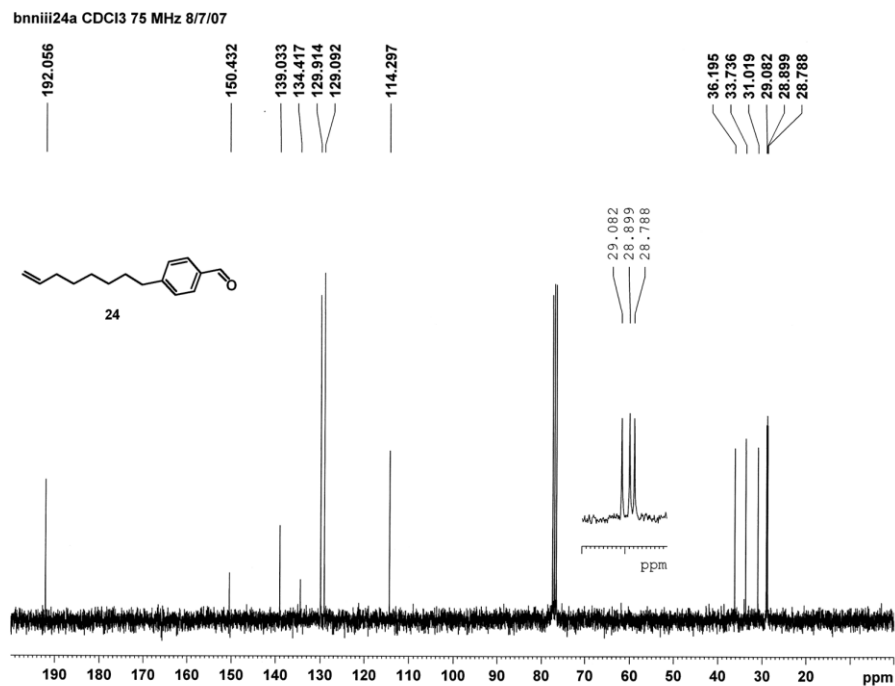
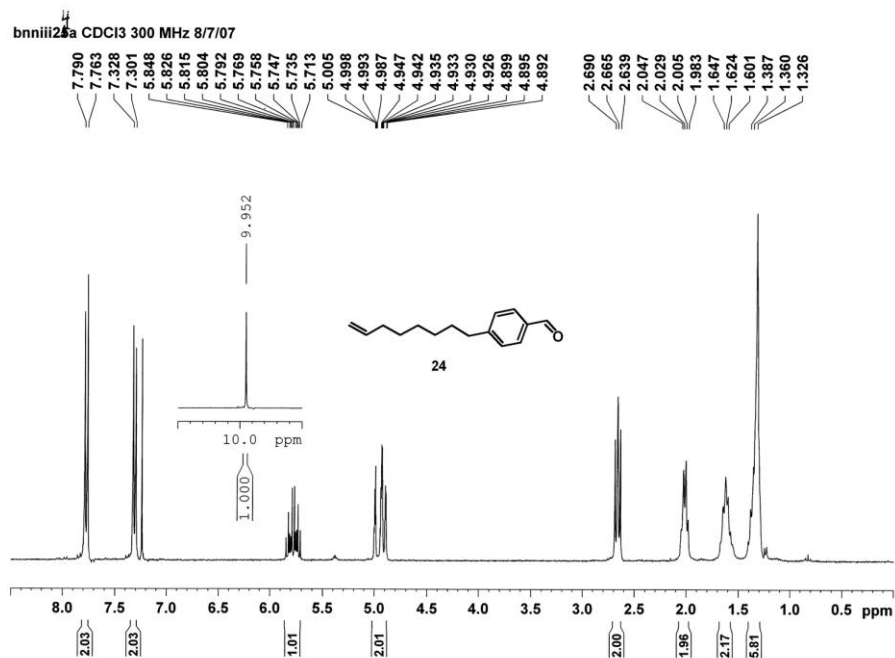


Figure 171. ^1H spectrum of compound 37.

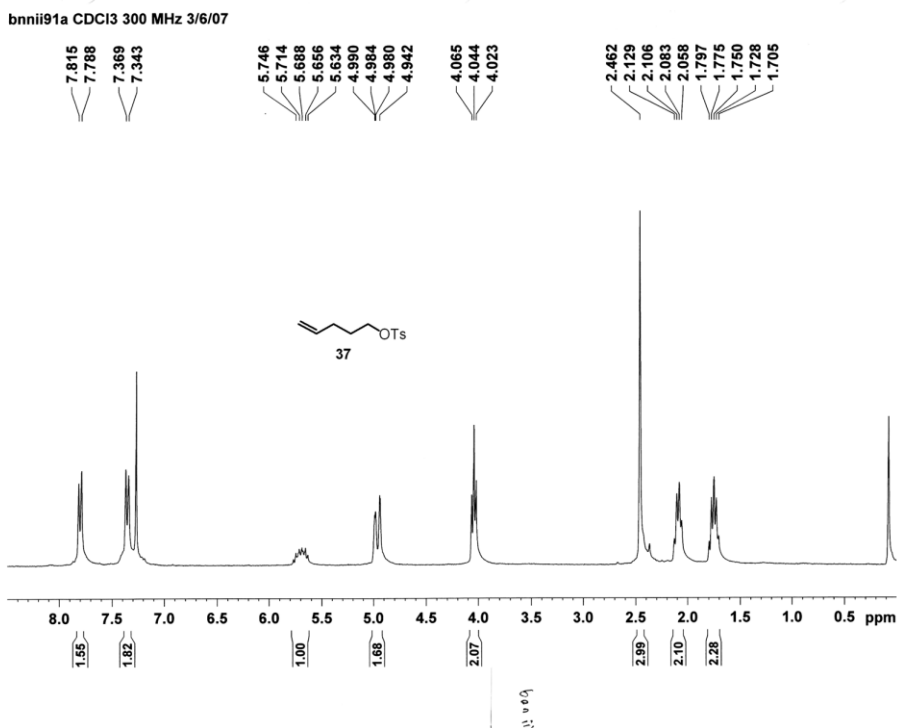


Figure 172. ^1H spectrum of compound 38.

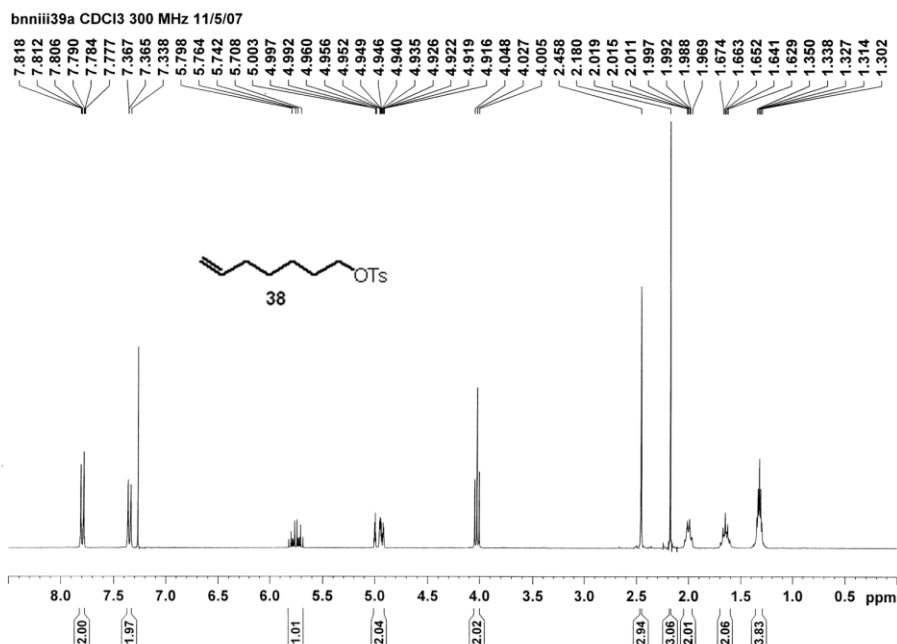


Figure 173. ¹H spectrum of compound 39.

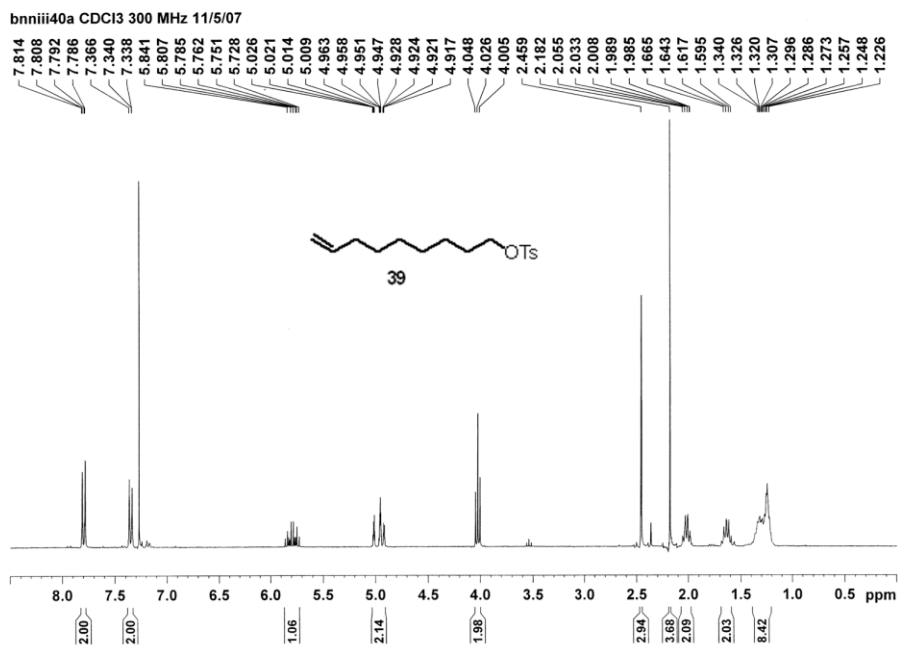


Figure 174. ^1H and ^{13}C NMR spectra of compound 26.

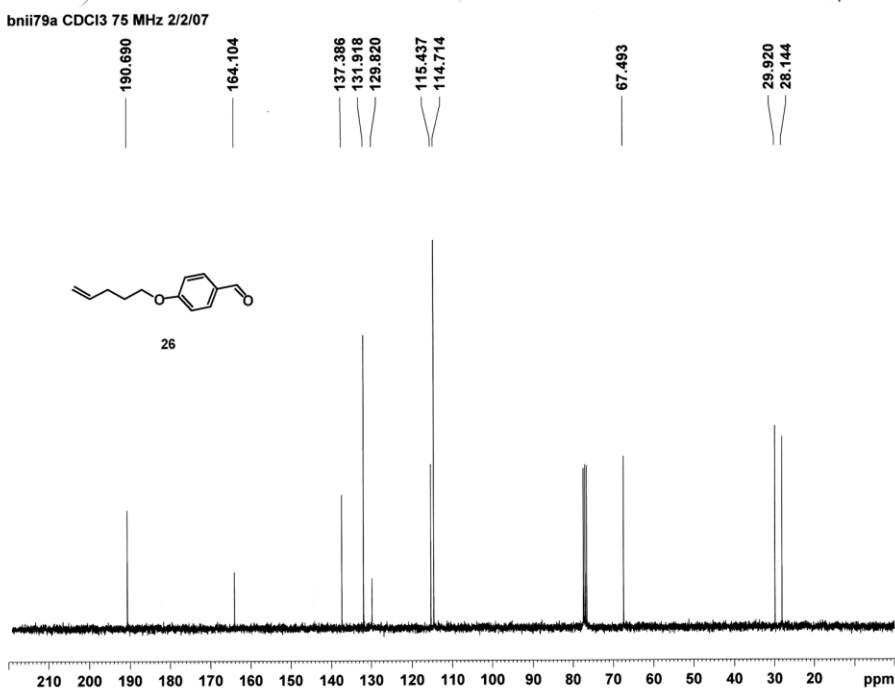
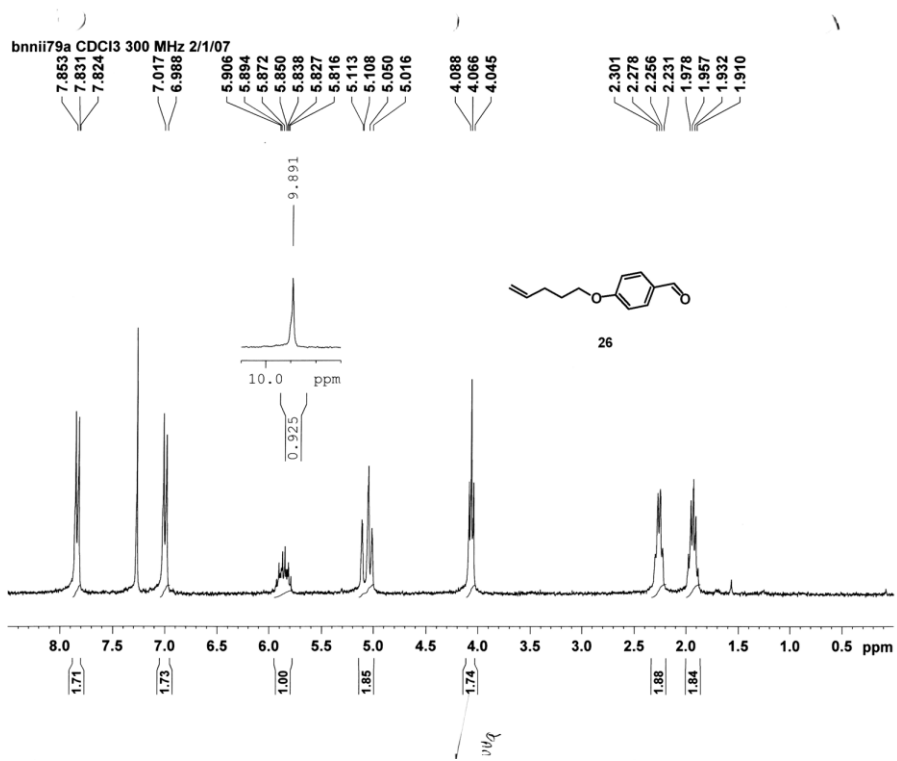


Figure 175. ^1H and ^{13}C NMR spectra of compound 27.

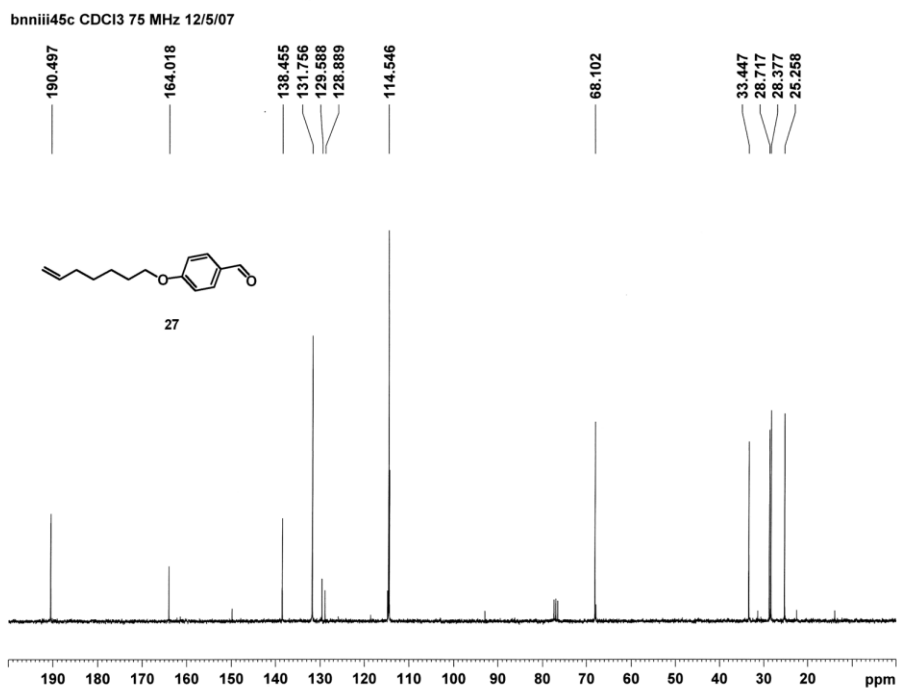
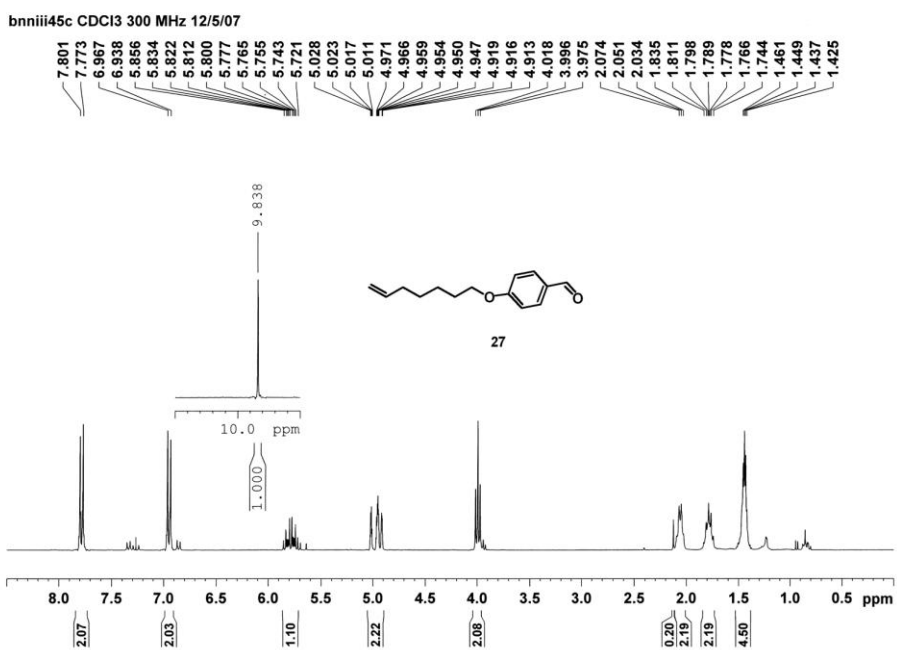


Figure 176. ^1H and ^{13}C NMR spectra of compound 28.

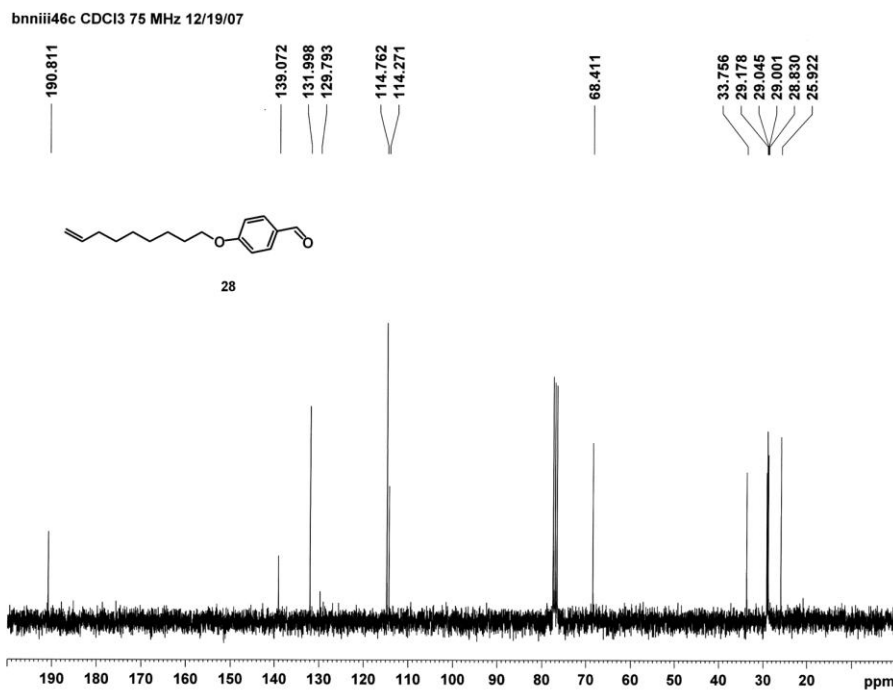
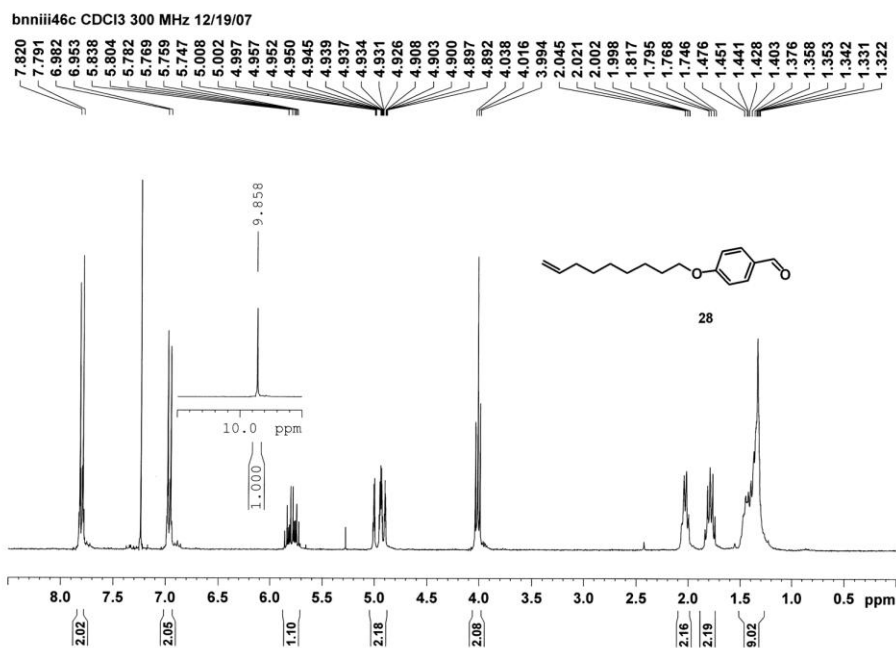


Figure 177. ^1H and ^{13}C NMR spectra of compound 29.

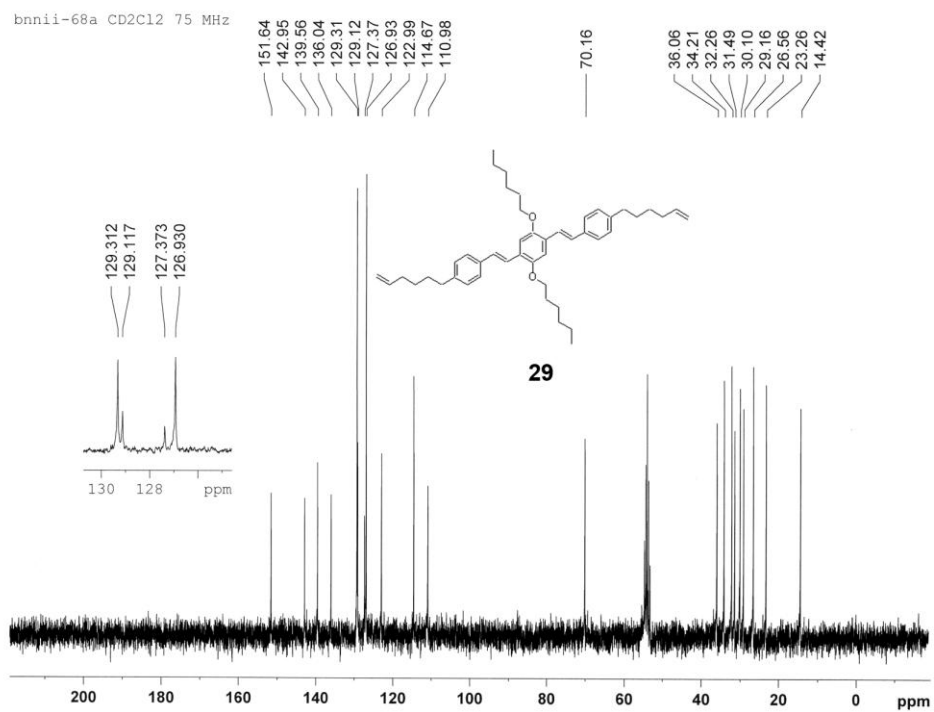
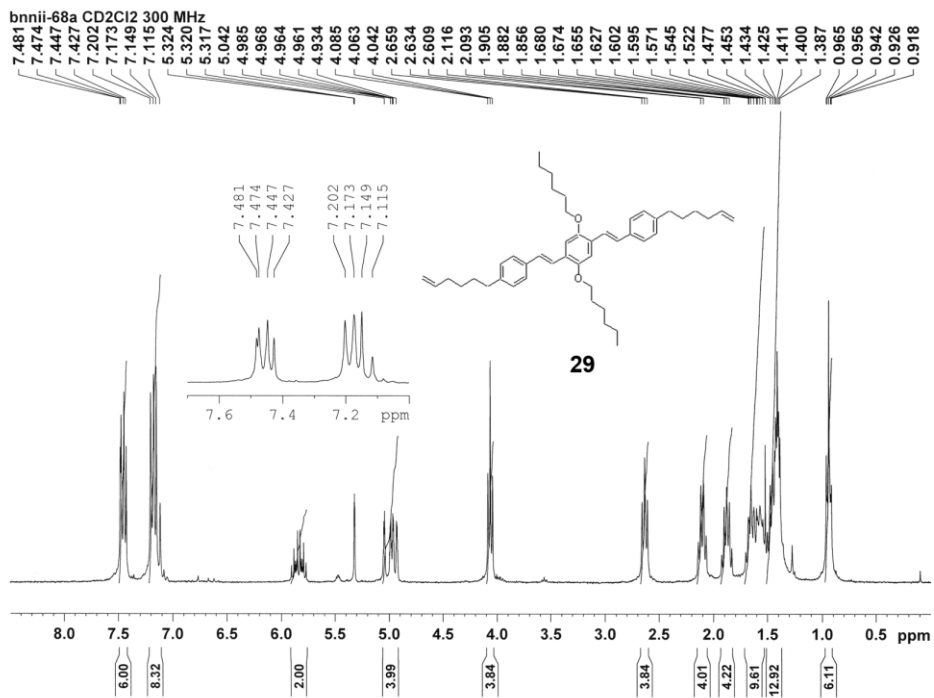


Figure 178. ^1H and ^{13}C NMR spectra of compound 30.

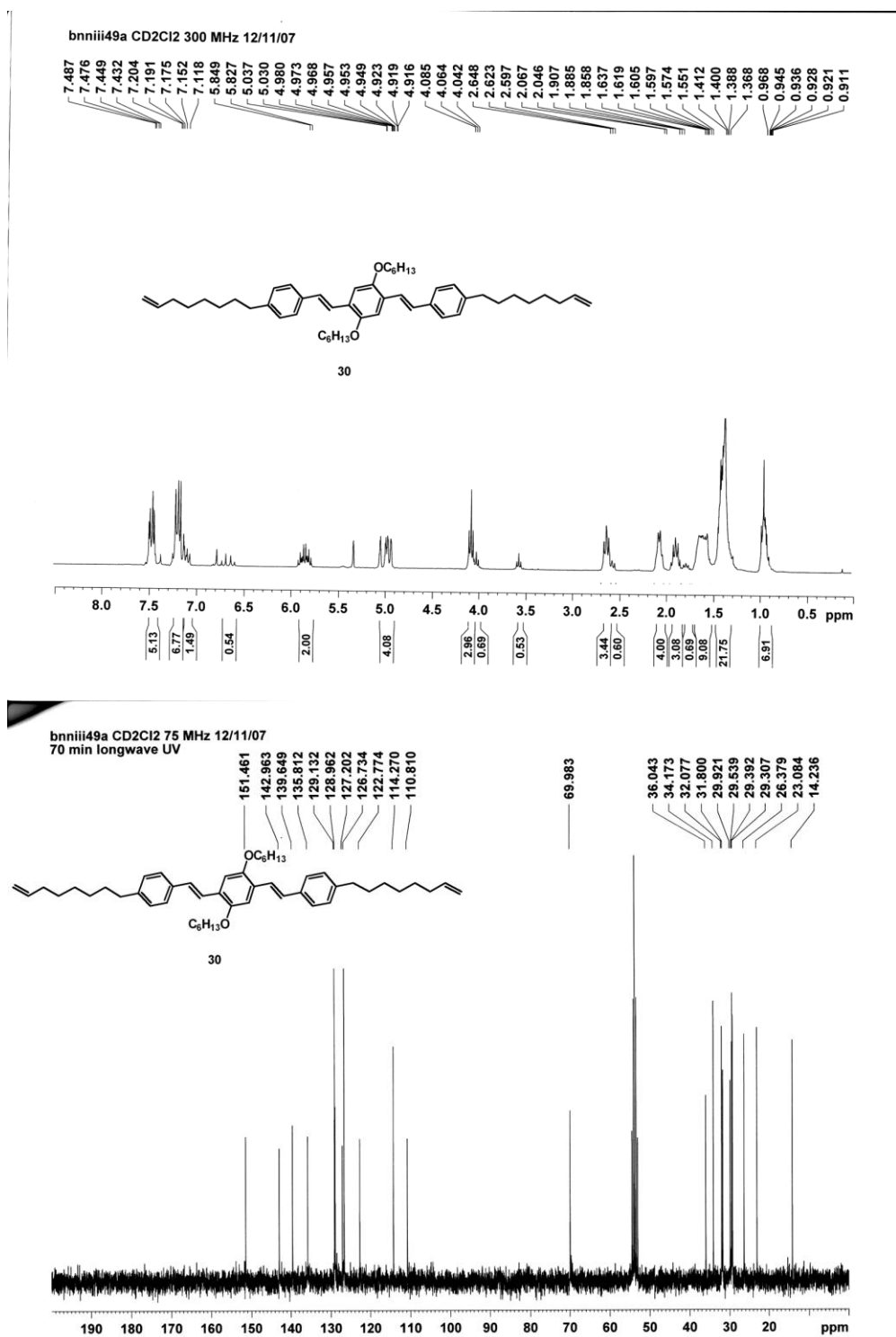


Figure 179. ^1H and ^{13}C NMR spectra of compound 31.

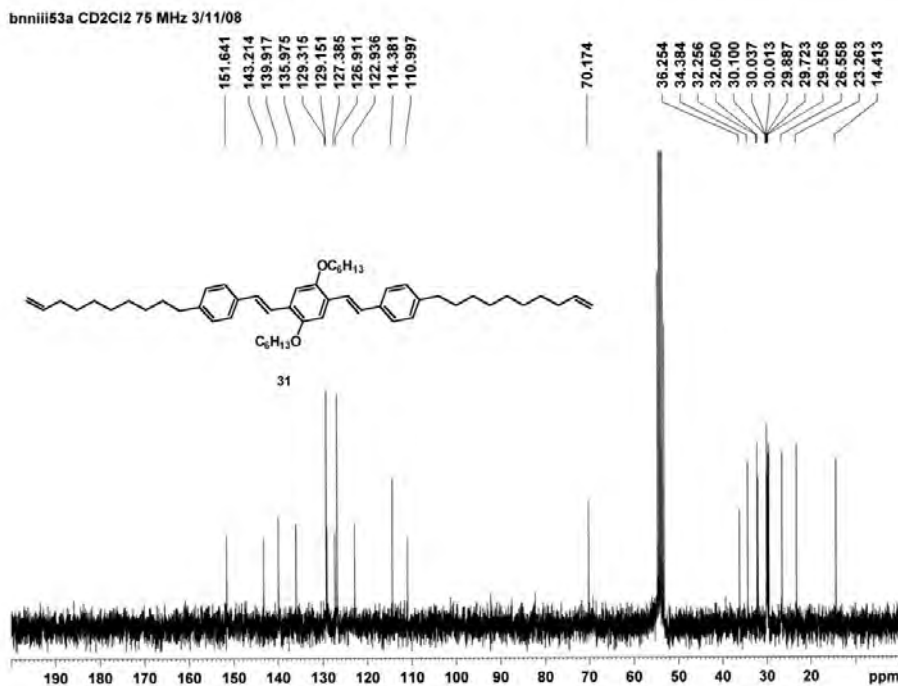
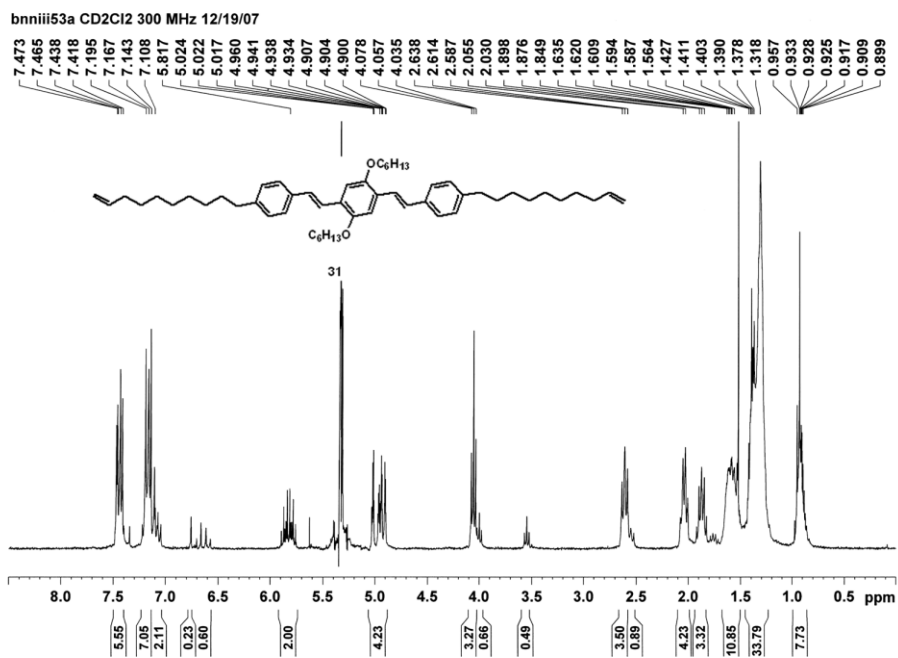


Figure 180. ^1H spectrum of compound 32.

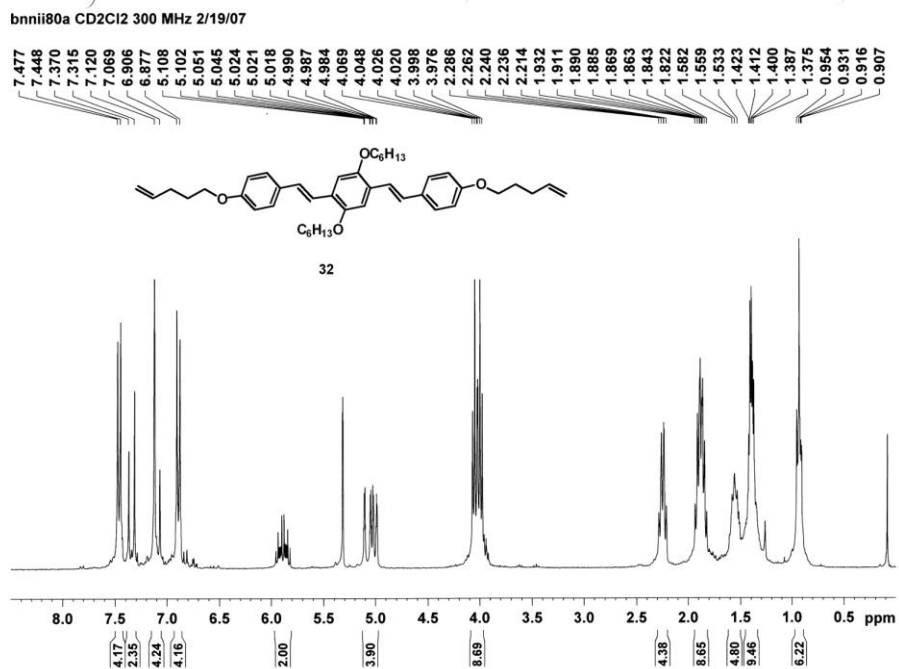


Figure 181. ^1H and ^{13}C NMR spectra of compound 33.

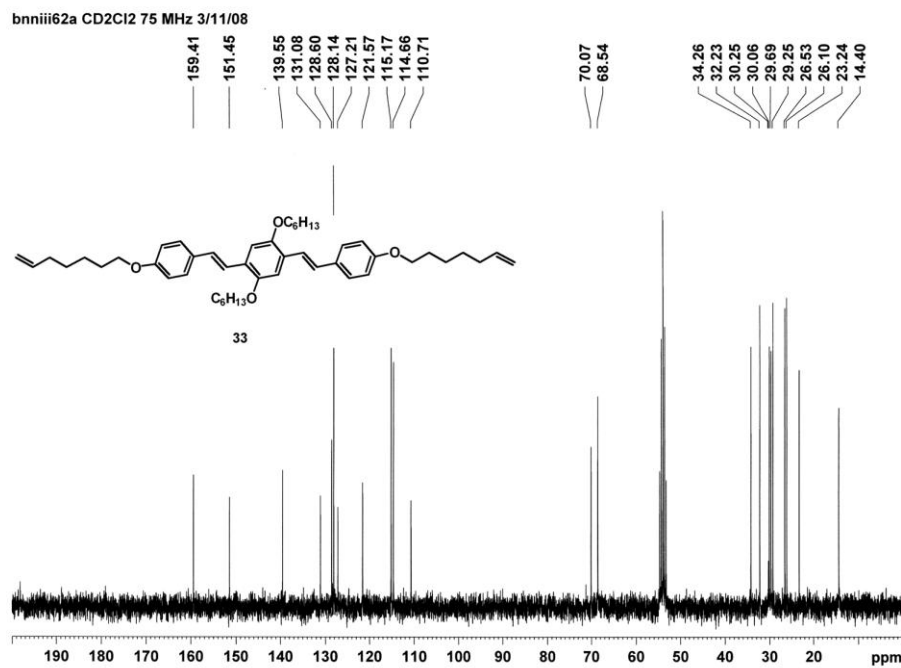
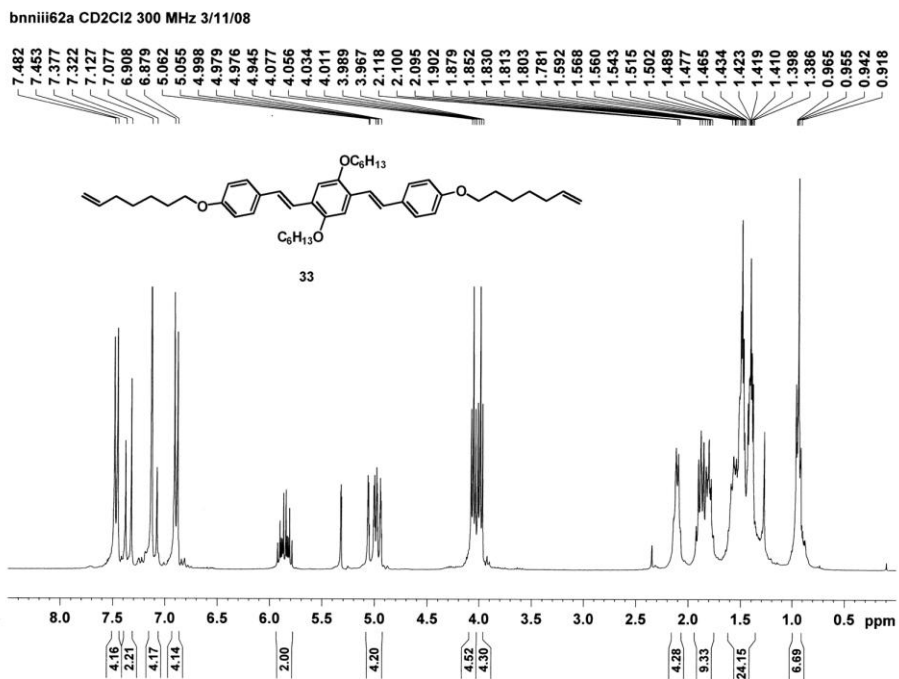


Figure 182. ^1H and ^{13}C NMR spectra of compound 34.

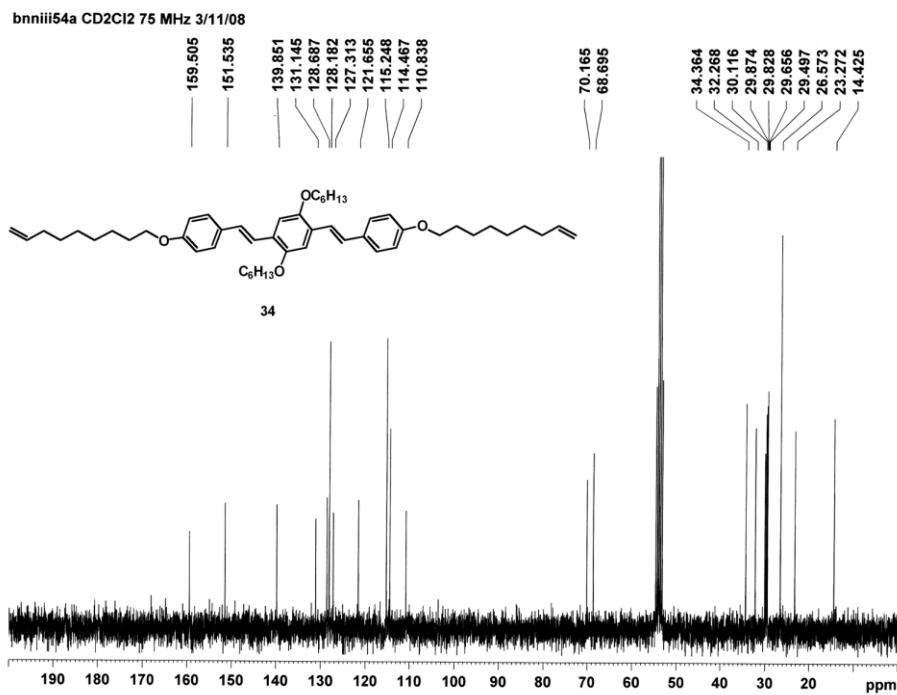
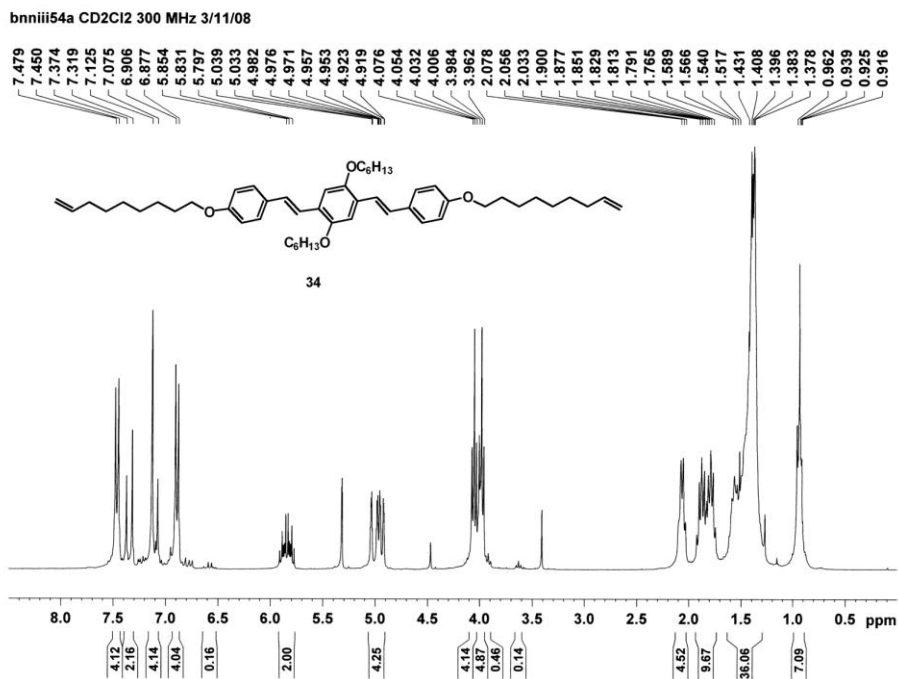


Figure 183. ^1H and ^{13}C NMR spectra of p29.

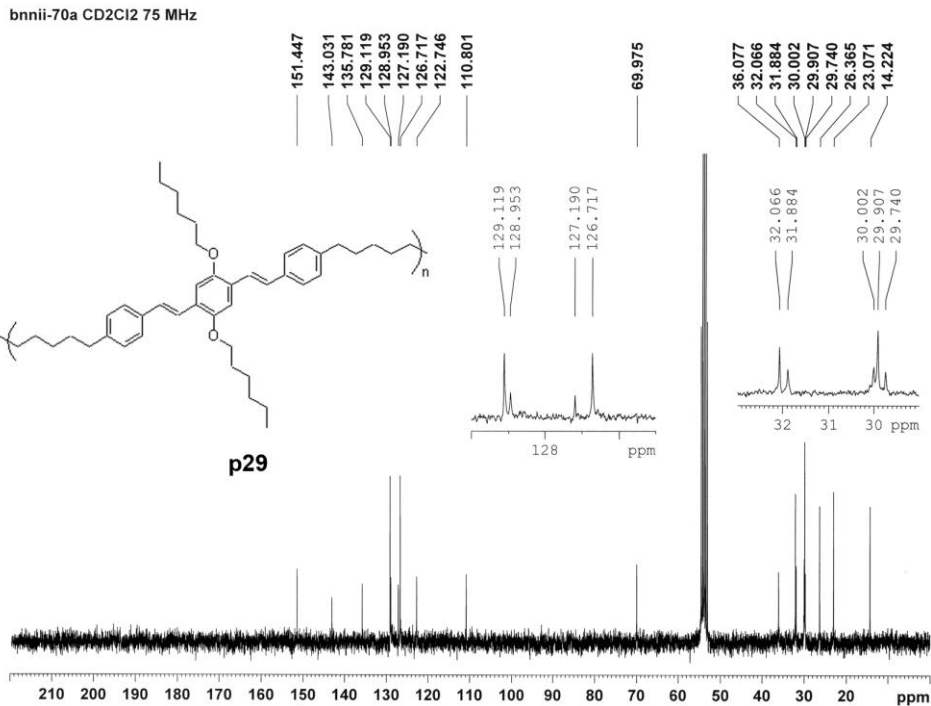
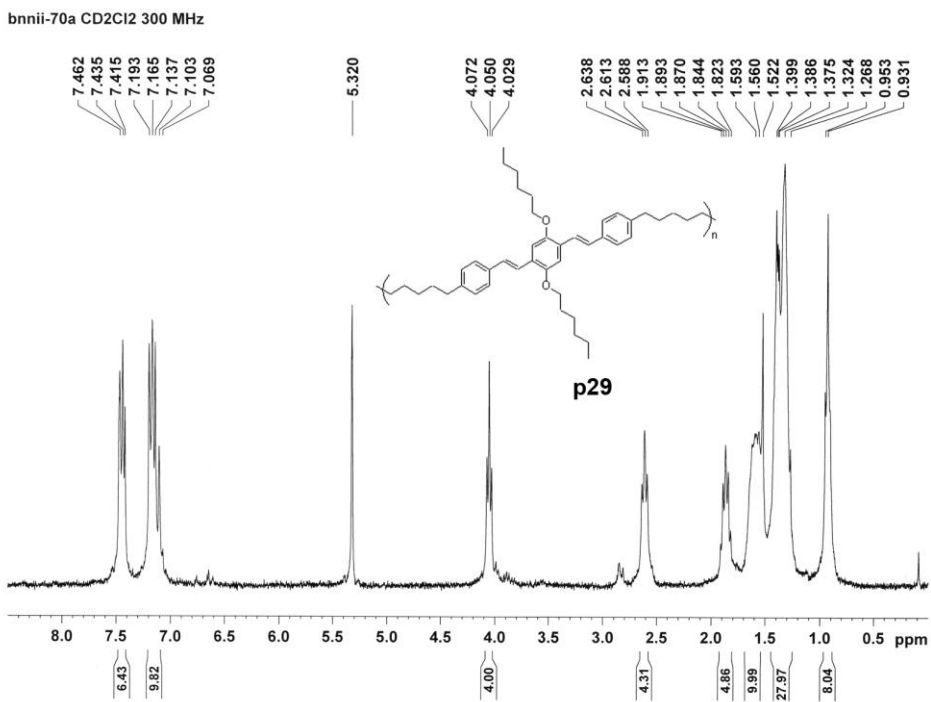
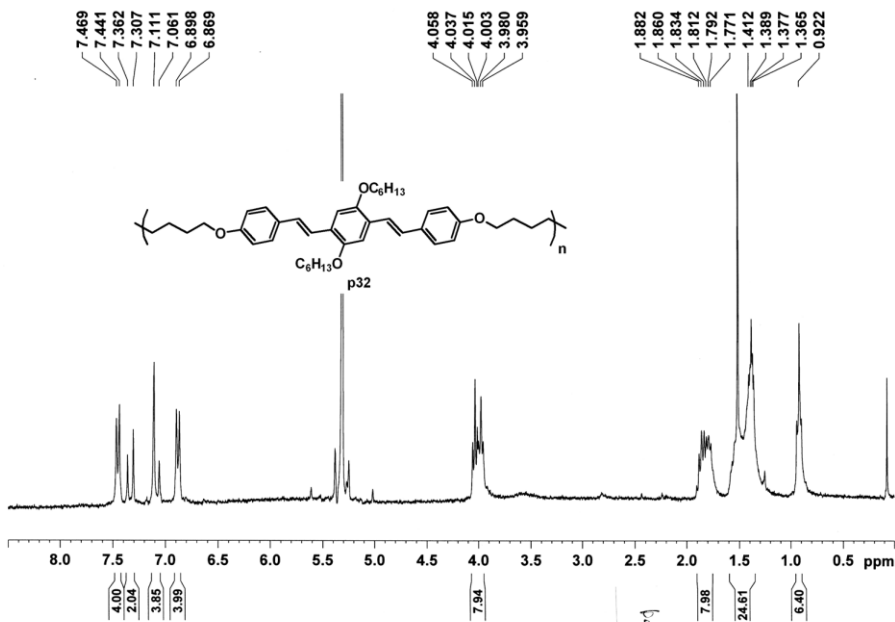


Figure 184. ¹H and ¹³C NMR spectra of p32.

bnnii95b CD2Cl2 300 MHz 3/20/07



bnnii95b CD2Cl2 75 MHz 5-15-07

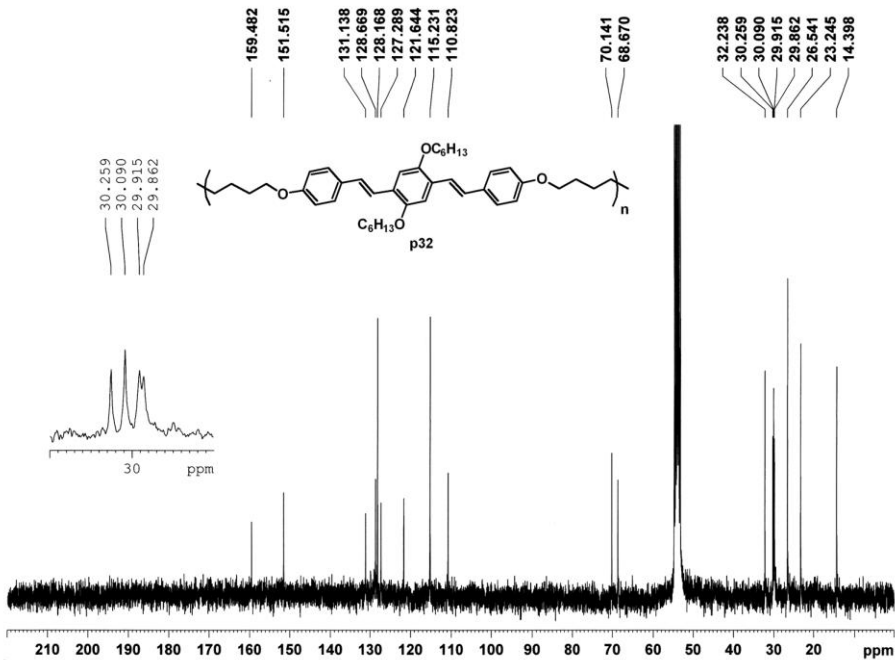


Figure 185. ^1H and ^{13}C NMR spectra of compound O.

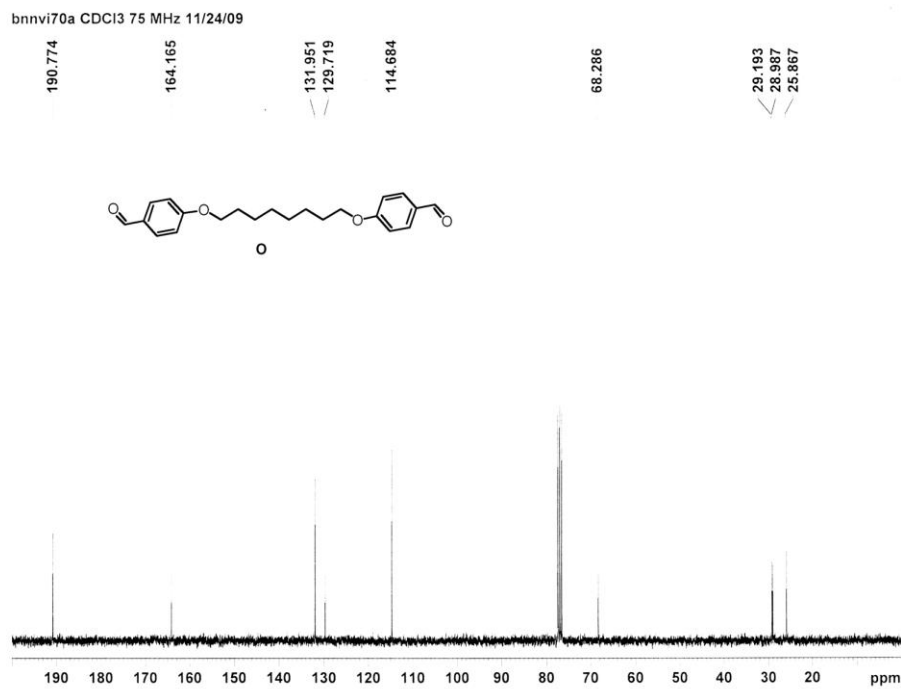
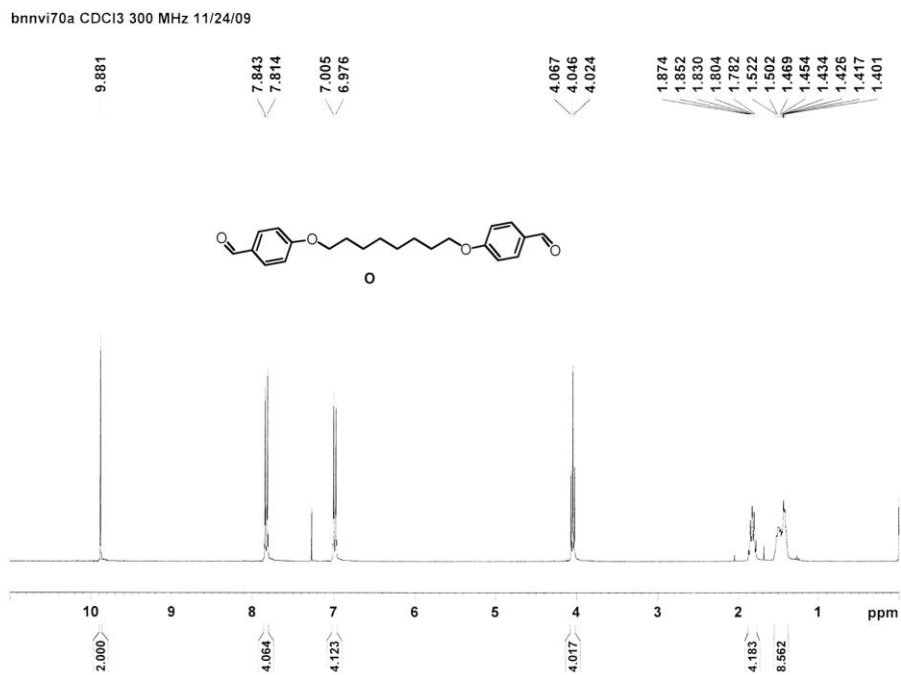
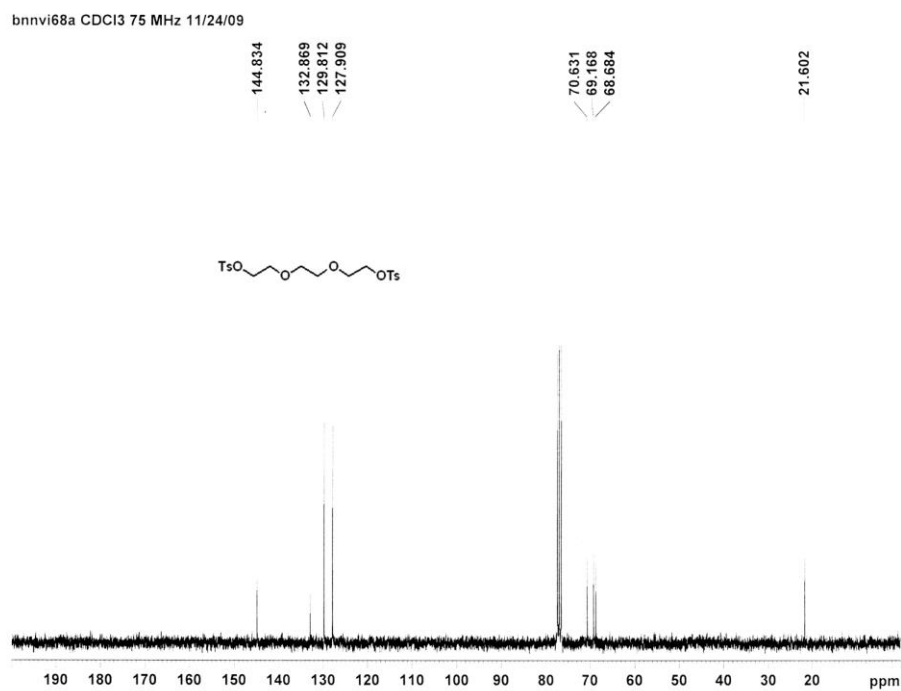
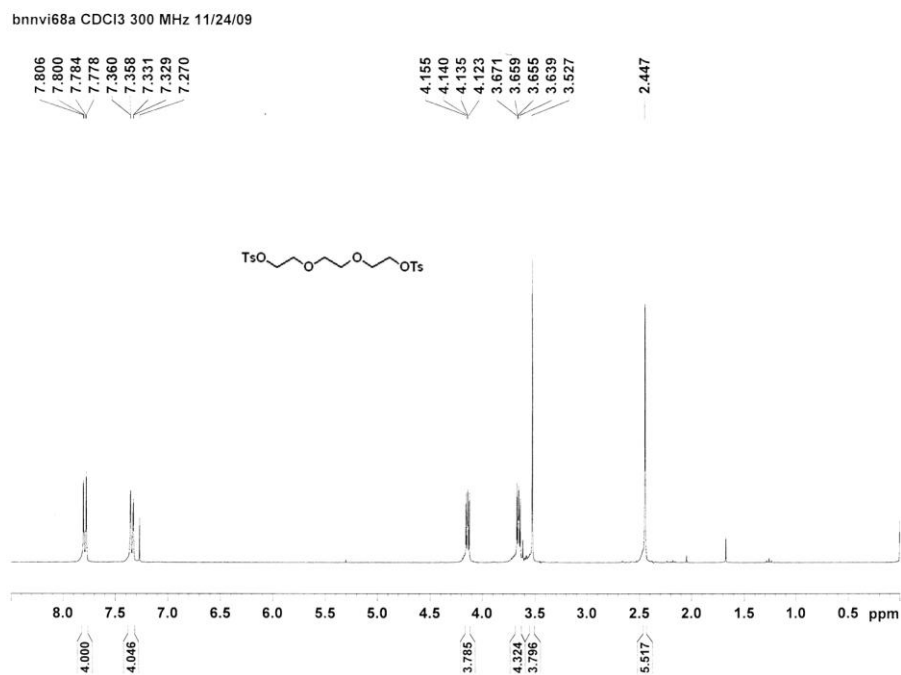


Figure 186. ^1H and ^{13}C NMR spectra of $(\text{TsOCH}_2\text{CH}_2\text{OCH}_2)_2$.



C.2 ABSORPTION AND EMISSION SPECTRA OF 29, 32, P29 AND P32

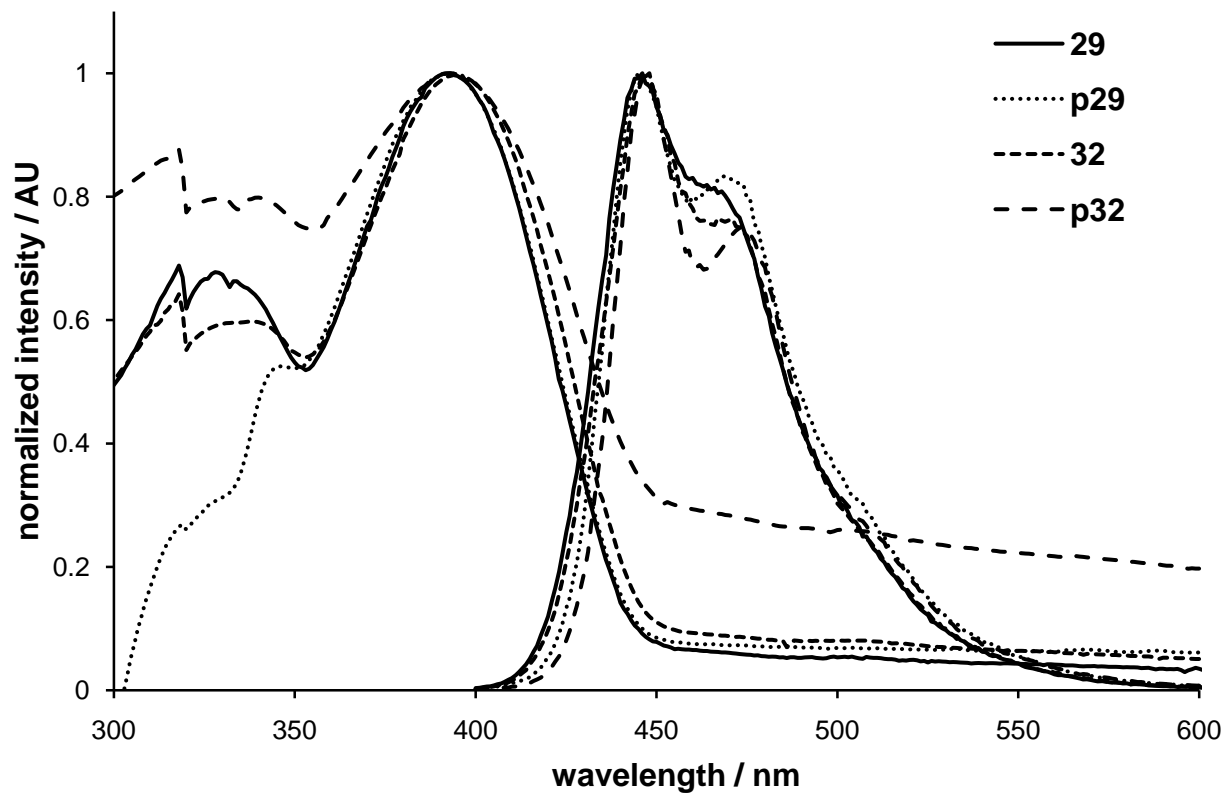


Figure 188. Normalized absorption and emission spectra of 29, 32, p29, p32 (10^{-6} M in CH_2Cl_2)

C.3 DIFFERENTIAL CALORIMOGRAMS OF THE PV-O_XT_Y SERIES

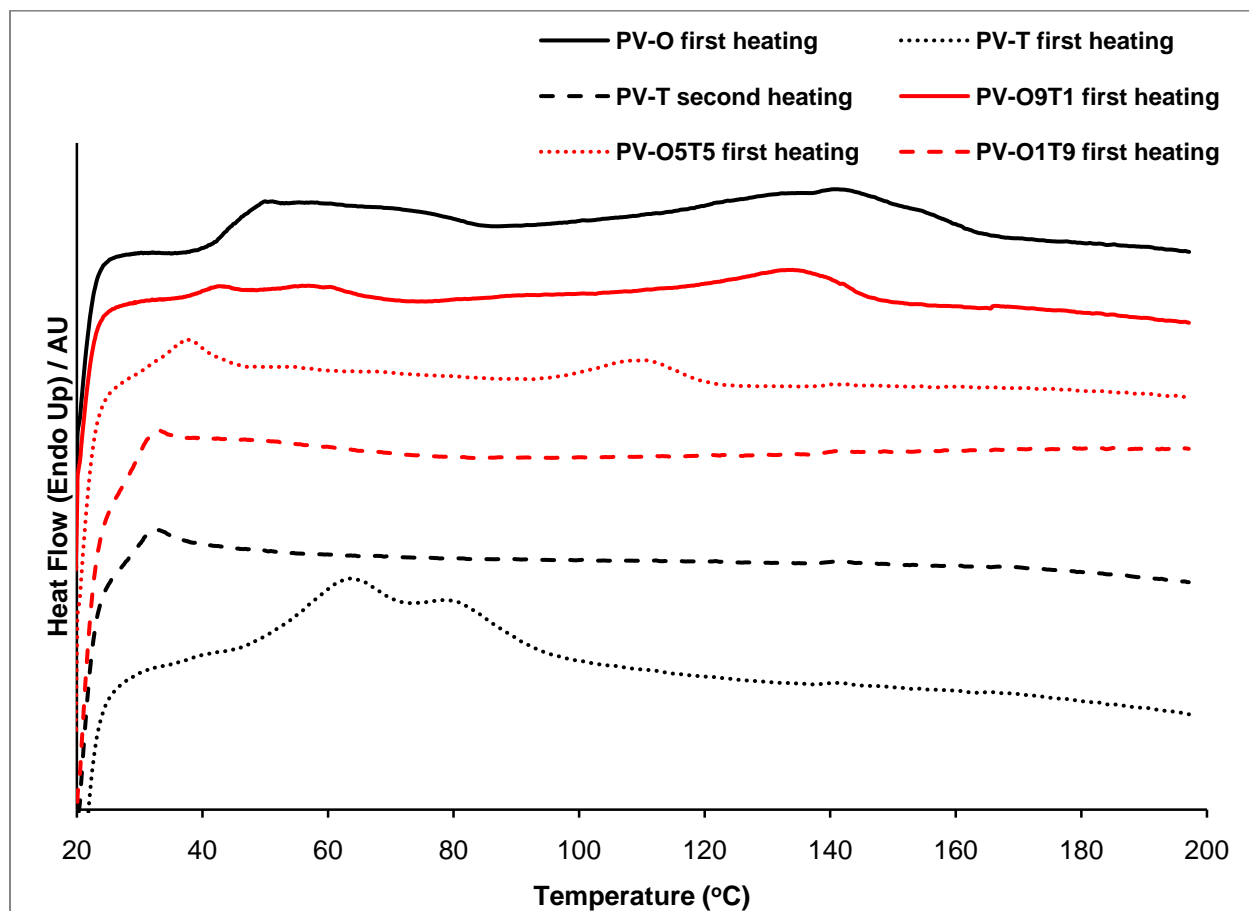


Figure 189. Differential calorimograms of the PV-O_XT_Y series.

REFERENCES

1. Jones, R., "Why nanotechnology needs better polymer chemistry" *Nat. Nanotechnol.* **2008**, *3* (12), 699-700.
2. Lutz, J.-F., "Sequence-controlled polymerizations: the next Holy Grail in polymer science?" *Polym. Chem.* **2010**, *1* (1), 55-62.
3. Hawker, C. J.; Wooley, K. L., "The Convergence of Synthetic Organic and Polymer Chemistries" *Science (Washington, DC, U. S.)* **2005**, *309* (5738), 1200-1205.
4. Badi, N.; Lutz, J.-F., "Sequence control in polymer synthesis" *Chem. Soc. Rev.* **2009**, *38* (12), 3383-3390.
5. Brudno, Y.; Liu, D. R., "Recent Progress Toward the Templated Synthesis and Directed Evolution of Sequence-Defined Synthetic Polymers" *Chem. Biol. (Cambridge, MA, U. S.)* **2009**, *16* (3), 265-276.
6. Polowinski, S., "Template polymerisation and co-polymerisation" *Prog. Polym. Sci.* **2002**, *27* (3), 537-577.
7. Ida, S.; Terashima, T.; Ouchi, M.; Sawamoto, M., "Selective Radical Addition with a Designed Heterobifunctional Halide: A Primary Study toward Sequence-Controlled Polymerization upon Template Effect" *J. Am. Chem. Soc.* **2009**, *131* (31), 10808-10809.
8. Ida, S.; Ouchi, M.; Sawamoto, M., "Template-Assisted Selective Radical Addition toward Sequence-Regulated Polymerization: Lariat Capture of Target Monomer by Template Initiator" *J. Am. Chem. Soc.* **2010**, *132* (42), 14748-14750.

9. Rzaev, Z. M. O., "Complex-radical alternating copolymerization" *Prog. Polym. Sci.* **2000**, *25* (2), 163-217.
10. Lutz, J.-F.; Kirci, B.; Matyjaszewski, K., "Synthesis of well-defined alternating copolymers by controlled/living radical polymerization in the presence of Lewis acids" *Macromolecules* **2003**, *36* (9), 3136-3145.
11. Pfeifer, S.; Lutz, J.-F., "A Facile Procedure for Controlling Monomer Sequence Distribution in Radical Chain Polymerizations" *J. Am. Chem. Soc.* **2007**, *129* (31), 9542-9543.
12. Pfeifer, S.; Lutz, J.-F., "Development of a library of n-substituted maleimides for the local functionalization of linear polymer chains" *Chem. Eur. J.* **2008**, *14* (35), 10949-10957.
13. Satoh, K.; Matsuda, M.; Nagai, K.; Kamigaito, M., "AAB-Sequence Living Radical Chain Copolymerization of Naturally Occurring Limonene with Maleimide: An End-to-End Sequence-Regulated Copolymer" *J. Am. Chem. Soc.* **2010**, *132* (29), 10003-10005.
14. Coates, G. W., "Precise Control of Polyolefin Stereochemistry Using Single-Site Metal Catalysts" *Chem. Rev.* **2000**, *100* (4), 1223-1252.
15. Thomas, C. M., "Stereocontrolled ring-opening polymerization of cyclic esters: synthesis of new polyester microstructures" *Chem. Soc. Rev.* **2010**, *39* (1), 165-173.
16. Ovitt, T. M.; Coates, G. W., "Stereoselective Ring-Opening Polymerization of meso-Lactide: Synthesis of Syndiotactic Poly(lactic acid)" *J. Am. Chem. Soc.* **1999**, *121* (16), 4072-4073.

17. Chamberlain, B. M.; Cheng, M.; Moore, D. R.; Ovitt, T. M.; Lobkovsky, E. B.; Coates, G. W., "Polymerization of Lactide with Zinc and Magnesium β -Diiminate Complexes: Stereocontrol and Mechanism" *J. Am. Chem. Soc.* **2001**, *123*, 3229-3238.
18. Ovitt, T. M.; Coates, G. W., "Stereoselective Ring-Opening Polymerization of *rac*-Lactide with a Single-Site, Racemic Aluminum Alkoxide Catalyst: Synthesis of Stereoblock Poly(Lactic Acid)" *J. Polym. Sci., Part A: Polym. Chem.* **2000**, *38*, 4686-4692.
19. Ovitt, T. M.; Coates, G. W., "Stereochemistry of Lactide Polymerization with Chiral Catalysts: New Opportunities for Stereocontrol Using Polymer Exchange Mechanisms" *J. Am. Chem. Soc.* **2002**, *124*, 1316-1326.
20. Amgoune, A.; Thomas, C. M.; Ilinca, S.; Roisnel, T.; Carpentier, J.-F., "Highly active, productive, and syndiospecific yttrium initiators for the polymerization of racemic beta -butyrolactone" *Angew. Chem. Int. Ed.* **2006**, *45* (17), 2782-2784.
21. Kramer, J. W.; Treitler, D. S.; Dunn, E. W.; Castro, P. M.; Roisnel, T.; Thomas, C. M.; Coates, G. W., "Polymerization of Enantiopure Monomers Using Syndiospecific Catalysts: A New Approach To Sequence Control in Polymer Synthesis" *J. Am. Chem. Soc.* **2009**, *131* (44), 16042-16044.
22. Ueda, M., "Sequence control in one-step condensation polymerization" *Prog. Polym. Sci.* **1999**, *24* (5), 699-730.
23. Hartmann, L.; Boerner, H. G., "Precision Polymers: Monodisperse, Monomer-Sequence-Defined Segments to Target Future Demands of Polymers in Medicine" *Adv. Mater.* **2009**, *21* (32-33), 3425-3431.

24. Antoni, P.; Robb, M. J.; Campos, L.; Montanez, M.; Hult, A.; Malmstrom, E.; Malkoch, M.; Hawker, C. J., "Pushing the Limits for Thiol-Ene and CuAAC Reactions: Synthesis of a 6th Generation Dendrimer in a Single Day" *Macromolecules* **2010**, *43* (16), 6625-6631.
25. Kent, S. B. H., "Total chemical synthesis of proteins" *Chem. Soc. Rev.* **2009**, *38* (2), 338-351.
26. Lutz, J.-F., "1,3-Dipolar cycloadditions of azides and alkynes: a universal ligation tool in polymer and materials science" *Angew. Chem. Int. Ed.* **2007**, *46* (7), 1018-1025.
27. Iha, R. K.; Wooley, K. L.; Nystrom, A. M.; Burke, D. J.; Kade, M. J.; Hawker, C. J., "Applications of Orthogonal "Click" Chemistries in the Synthesis of Functional Soft Materials" *Chem. Rev.* **2009**, *109* (11), 5620-5686.
28. Brzezinska, K.; Wolfe, P. S.; Watson, M. D.; Wagener, K. B., "Acyclic diene metathesis (ADMET) polymerization using a well-defined ruthenium based metathesis catalyst" *Macromol. Chem. Phys.* **1996**, *197* (6), 2065-2074.
29. Tindall, D.; Wagener, K. B., "Acyclic Diene Metathesis (ADMET) Segmented Copolymers" *Macromolecules* **2004**, *37* (9), 3328-3336.
30. Aitken, B. S.; Lee, M.; Hunley, M. T.; Gibson, H. W.; Wagener, K. B., "Synthesis of Precision Ionic Polyolefins Derived from Ionic Liquids" *Macromolecules* **2010**, *43* (4), 1699-1701.
31. Satoh, K.; Ozawa, S.; Mizutani, M.; Nagai, K.; Kamigaito, M., "Sequence-regulated vinyl copolymers by metal-catalyzed step-growth radical polymerization" *Nat. Commun.* **2010**, *1* (April), 1-6, S1-S9.

32. Ward, R. E.; Meyer, T. Y., "*o,p*-Polyaniline: A new form of a classic conducting polymer" *Macromolecules* **2003**, *36* (12), 4368-4373.
33. Copenhafer, J. E.; Walters, R. W.; Meyer, T. Y., "Synthesis and Characterization of Repeating Sequence Copolymers of Fluorene and Methylene Monomers" *Macromolecules* **2008**, *41* (1), 31-35.
34. Stayshich, R. M.; Meyer, T. Y., "Preparation and microstructural analysis of poly(lactic-alt-glycolic acid)" *J. Polym. Sci., Part A: Polym. Chem.* **2008**, *46* (14), 4704-4711.
35. Stayshich, R. M.; Meyer, T. Y., "New Insights into Poly(lactic-co-glycolic acid) Microstructure: Using Repeating Sequence Copolymers To Decipher Complex NMR and Thermal Behavior" *J. Am. Chem. Soc.* **2010**, *132* (31), 10920-10934.
36. Weiss, R. M.; Jones, E. M.; Shafer, D. E.; Stayshich, R. M.; Meyer, T. Y., "Synthesis of Repeating Sequence Copolymers of Lactic, Glycolic and Caprolactic Acids" *J. Polym. Sci., Part A: Polym. Chem.* (Submitted).
37. Stayshich, R. M.; Weiss, R. M.; Li, J.; Meyer, T. Y., "Periodic Incorporation of Pendant Hydroxyl Groups in Repeating Sequence PLGA Copolymers" *Macromol. Rapid Commun.* DOI:10.1002/marc.20100608, Published Online: November 15, 2010.
38. Grimsdale, A. C.; Leok Chan, K.; Martin, R. E.; Jokisz, P. G.; Holmes, A. B., "Synthesis of Light-Emitting Conjugated Polymers for Applications in Electroluminescent Devices" *Chem. Rev.* **2009**, *109* (3), 897-1091.
39. Cheng, Y.-J.; Yang, S.-H.; Hsu, C.-S., "Synthesis of Conjugated Polymers for Organic Solar Cell Applications" *Chem. Rev.* **2009**, *109* (11), 5868-5923.
40. Thompson, B. C.; Frechet, J. M. J., "Polymer-fullerene composite solar cells" *Angew. Chem. Int. Ed.* **2008**, *47* (1), 58-77.

41. Bredas, J.-L.; Beljonne, D.; Coropceanu, V.; Cornil, J., "Charge-Transfer and Energy-Transfer Processes in pi-Conjugated Oligomers and Polymers: A Molecular Picture" *Chem. Rev.* **2004**, *104* (11), 4971-5003.
42. Brabec, C. J.; Gowrisanker, S.; Halls, J. J. M.; Laird, D.; Jia, S.; Williams, S. P., "Polymer-Fullerene Bulk-Heterojunction Solar Cells" *Adv. Mater.* **2010**, *22* (34), 3839-3856.
43. Liang, Y.; Xu, Z.; Xia, J.; Tsai, S.-T.; Wu, Y.; Li, G.; Ray, C.; Yu, L., "For the Bright Future-Bulk Heterojunction Polymer Solar Cells with Power Conversion Efficiency of 7.4%" *Adv. Mater.* **2010**, *22* (20), E135-E138.
44. Havinga, E. E.; ten Hoeve, W.; Wynberg, H., "Alternate donor-acceptor small-band-gap semiconducting polymers; polysquaraines and polycroconaines" *Synth. Met.* **1993**, *55* (1), 299-306.
45. Chen, J.; Cao, Y., "Development of Novel Conjugated Donor Polymers for High-Efficiency Bulk-Heterojunction Photovoltaic Devices" *Acc. Chem. Res.* **2009**, *42* (11), 1709-1718.
46. Inganäs, O.; Zhang, F.; Tvingstedt, K.; Andersson, L. M.; Hellstroem, S.; Andersson, M. R., "Polymer Photovoltaics with Alternating Copolymer/Fullerene Blends and Novel Device Architectures" *Adv. Mater.* **2010**, *22* (20), E100-E116.
47. Roncali, J., "Molecular engineering of the band gap of pi-conjugated systems: facing technological applications" *Macromol. Rapid Commun.* **2007**, *28* (17), 1761-1775.
48. Beaujuge, P. M.; Amb, C. M.; Reynolds, J. R., "Spectral engineering in pi-conjugated polymers with intramolecular donor-acceptor interactions" *Acc. Chem. Res.* **2010**, *43* (11), 1396-1407.

49. Biniek, L.; Fall, S.; Chochos, C. L.; Anokhin, D. V.; Ivanov, D. A.; Leclerc, N.; Leveque, P.; Heiser, T., "Impact of the Alkyl Side Chains on the Optoelectronic Properties of a Series of Photovoltaic Low-Band-Gap Copolymers" *Macromolecules* **2010**, DOI: 10.1021/ma102164c, Published online: November 11, 2010.
50. Zhou, H.; Yang, L.; Price, S. C.; Knight, K. J.; You, W., "Enhanced Photovoltaic Performance of Low-Bandgap Polymers with Deep LUMO Levels" *Angew. Chem. Int. Ed.* **2010**, 49 (43), 7992-7995, S7992/1-S7992/11.
51. Zhou, H.; Yang, L.; Stoneking, S.; You, W., "A Weak Donor-Strong Acceptor Strategy to Design Ideal Polymers for Organic Solar Cells" *ACS Appl. Mater. Interfaces* **2010**, 2 (5), 1377-1383.
52. Zhou, H.; Yang, L.; Xiao, S.; Liu, S.; You, W., "Donor-Acceptor Polymers Incorporating Alkylated Dithienylbenzothiadiazole for Bulk Heterojunction Solar Cells: Pronounced Effect of Positioning Alkyl Chains" *Macromolecules* **2010**, 43 (2), 811-820.
53. Potscavage, W. J., Jr.; Sharma, A.; Kippelen, B., "Critical Interfaces in Organic Solar Cells and Their Influence on the Open-Circuit Voltage" *Acc. Chem. Res.* **2009**, 42 (11), 1758-1767.
54. Rand, B. P.; Burk, D. P.; Forrest, S. R., "Offset energies at organic semiconductor heterojunctions and their influence on the open-circuit voltage of thin-film solar cells" *Phys. Rev. B: Condens. Matter Mater. Phys.* **2007**, 75 (11), 115327/1-115327/11.
55. Heeger, A. J., "Semiconducting polymers: the Third Generation" *Chem. Soc. Rev.* **2010**, 39 (7), 2354-2371.

56. Scharber, M. C.; Muehlbacher, D.; Koppe, M.; Denk, P.; Waldauf, C.; Heeger, A. J.; Brabec, C. J., "Design rules for donors in bulk-heterojunction solar cells-towards 10 % energy-conversion efficiency" *Adv. Mater.* **2006**, *18* (6), 789-794.
57. Pivrikas, A.; Sariciftci, N. S.; Juska, G.; Osterbacka, R., "A review of charge transport and recombination in polymer/fullerene organic solar cells" *Prog. Photovoltaics* **2007**, *15* (8), 677-696.
58. Wurthner, F.; Meerholz, K., "Systems chemistry approach in organic photovoltaics" *Chem. Eur. J.* **2010**, *16* (31), 9366-73.
59. Bredas, J.-L.; Norton, J. E.; Cornil, J.; Coropceanu, V., "Molecular Understanding of Organic Solar Cells: The Challenges" *Acc. Chem. Res.* **2009**, *42* (11), 1691-1699.
60. Kjelstrup-Hansen, J.; Norton, J. E.; da Silva Filho, D. A.; Bredas, J.-L.; Rubahn, H.-G., "Charge transport in oligo phenylene and phenylene-thiophene nanofibers" *Org. Electron.* **2009**, *10* (7), 1228-1234.
61. Mondal, R.; Ko, S.; Norton, J. E.; Miyaki, N.; Becerril, H. A.; Verploegen, E.; Toney, M. F.; Bredas, J.-L.; McGehee, M. D.; Bao, Z., "Molecular design for improved photovoltaic efficiency: band gap and absorption coefficient engineering" *J. Mater. Chem.* **2009**, *19* (39), 7195-7197.
62. Ko, S.; Mondal, R.; Risko, C.; Lee, J. K.; Hong, S.; McGehee, M. D.; Bredas, J.-L.; Bao, Z., "Tuning the Optoelectronic Properties of Vinylene-Linked Donor-Acceptor Copolymers for Organic Photovoltaics" *Macromolecules* **2010**, *43* (16), 6685-6698.
63. Mondal, R.; Becerril, H. A.; Verploegen, E.; Kim, D.; Norton, J. E.; Ko, S.; Miyaki, N.; Lee, S.; Toney, M. F.; Bredas, J.-L.; McGehee, M. D.; Bao, Z., "Thiophene-rich fused-

- aromatic thienopyrazine acceptor for donor-acceptor low band-gap polymers for OTFT and polymer solar cell applications" *J. Mater. Chem.* **2010**, *20* (28), 5823-5834.
64. Oliva, M. M.; Pappenfus, T. M.; Melby, J. H.; Schwaderer, K. M.; Johnson, J. C.; McGee, K. A.; da Silva Filho, D. A.; Bredas, J.-L.; Casado, J.; Lopez Navarrete, J. T., "Comparison of Thiophene-Pyrrole Oligomers with Oligothiophenes: A Joint Experimental and Theoretical Investigation of Their Structural and Spectroscopic Properties" *Chem. Eur. J.* **2010**, *16* (23), 6866-6876, S6866/1-S6866/7.
65. Pingel, P.; Zhu, L.; Park, K. S.; Vogel, J.-O.; Janietz, S.; Kim, E.-G.; Rabe, J. P.; Bredas, J.-L.; Koch, N., "Charge-Transfer Localization in Molecularly Doped Thiophene-Based Donor Polymers" *J. Phys. Chem. Lett.* **2010**, *1* (13), 2037-2041.
66. Sears, J. S.; Chance, R. R.; Bredas, J.-L., "Torsion Potential in Polydiacetylene: Accurate Computations on Oligomers Extrapolated to the Polymer Limit" *J. Am. Chem. Soc.* **2010**, *132* (38), 13313-13319.
67. Viani, L.; Olivier, Y.; Athanasopoulos, S.; da Silva Filho, D. A.; Hulliger, J.; Bredas, J.-L.; Gierschner, J.; Cornil, J., "Theoretical Characterization of Charge Transport in One-Dimensional Collinear Arrays of Organic Conjugated Molecules" *ChemPhysChem* **2010**, *11* (5), 1062-1068.
68. Blouin, N.; Michaud, A.; Gendron, D.; Wakim, S.; Blair, E.; Neagu-Plesu, R.; Belletete, M.; Durocher, G.; Tao, Y.; Leclerc, M., "Toward a Rational Design of Poly(2,7-Carbazole) Derivatives for Solar Cells" *J. Am. Chem. Soc.* **2008**, *130* (2), 732-742.
69. Farinola, G. M.; Babudri, F.; Cardone, A.; Omar, O. H.; Naso, F., "Synthesis of substituted conjugated polymers: tuning properties by functionalization" *Pure Appl. Chem.* **2008**, *80* (8), 1735-1746.

70. Egbe, D. A. M.; Carbonnier, B.; Birckner, E.; Grummt, U.-W., "Arylene-ethynylene/arylene-vinylene copolymers: Synthesis and structure-property relationships" *Prog. Polym. Sci.* **2009**, *34* (10), 1023-1067.
71. Egbe, D. A. M.; Tuerk, S.; Rathgeber, S.; Kuehnlenz, F.; Jadhav, R.; Wild, A.; Birckner, E.; Adam, G.; Pivrikas, A.; Cimrova, V.; Knor, G.; Sariciftci, N. S.; Hoppe, H., "Anthracene Based Conjugated Polymers: Correlation between pi-pi-Stacking Ability, Photophysical Properties, Charge Carrier Mobility, and Photovoltaic Performance" *Macromolecules* **2010**, *43* (3), 1261-1269.
72. Jorgensen, M.; Krebs, F. C., "Stepwise and Directional Synthesis of End-Functionalized Single-Oligomer OPVs and Their Application in Organic Solar Cells" *J. Org. Chem.* **2004**, *69* (20), 6688-6696.
73. Jorgensen, M.; Krebs, F. C., "Stepwise Unidirectional Synthesis of Oligo Phenylene Vinylens with a Series of Monomers. Use in Plastic Solar Cells" *J. Org. Chem.* **2005**, *70* (15), 6004-6017.
74. Xue, C.; Luo, F.-T., "Efficient and Rapid Synthesis of Oligo(p-phenylenevinylene) via Iterative Coherent Approach" *J. Org. Chem.* **2003**, *68* (11), 4417-4421.
75. Krebs, F. C.; Nyberg, R. B.; Jorgensen, M., "Influence of Residual Catalyst on the Properties of Conjugated Polyphenylenevinylene Materials: Palladium Nanoparticles and Poor Electrical Performance" *Chemistry of Materials* **2004**, *16* (7), 1313-1318.
76. Maddux, T.; Li, W.; Yu, L., "Stepwise Synthesis of Substituted Oligo(phenylenevinylene) via an Orthogonal Approach" *J. Am. Chem. Soc.* **1997**, *119* (4), 844-845.

77. Jian, H.; Tour, J. M., "Preparative Fluorous Mixture Synthesis of Diazonium-Functionalized Oligo(phenylene vinylene)s" *J. Org. Chem.* **2005**, *70* (9), 3396-3424.
78. Iwadate, N.; Suginome, M., "Synthesis of B-Protected beta -Styrylboronic Acids via Iridium-Catalyzed Hydroboration of Alkynes with 1,8-Naphthalenediaminatoborane Leading to Iterative Synthesis of Oligo(phenylenevinylene)s" *Org. Lett.* **2009**, *11* (9), 1899-1902.
79. Tour, J. M., "Conjugated macromolecules of precise length and constitution. Organic synthesis for the construction of nanoarchitectures" *Chem. Rev.* **1996**, *96* (1), 537-553.
80. Olah, G. A.; Keumi, T., "Synthetic methods and reactions. 60. Improved one-step conversion of aldehydes into nitriles with hydroxylamine in formic acid solution" *Synthesis* **1979**, (2), 112-13.
81. Brandt, P.; Norrby, P.-O.; Martin, I.; Rein, T., "A Quantum Chemical Exploration of the Horner-Wadsworth-Emmons Reaction" *J. Org. Chem.* **1998**, *63* (4), 1280-1289.
82. Markiewicz, J. T.; Schauer, D. J.; Lofstedt, J.; Corden, S. J.; Wiest, O.; Helquist, P., "Synthesis of 4-Methyldienoates Using a Vinylogous Horner-Wadsworth-Emmons Reagent. Application to the Synthesis of Trichostatic Acid" *J. Org. Chem.* **2010**, *75* (6), 2061-2064.
83. Peng, Z.; Gharavi, A. R.; Yu, L., "Synthesis and characterization of photorefractive polymers containing transition metal complexes as photosensitizer" *J. Am. Chem. Soc.* **1997**, *119* (20), 4622-4632.
84. Norris, B. N.; Pan, T.; Meyer, T. Y., "Iterative synthesis of heterotelechelic oligo(phenylene-vinylene)s by olefin cross-metathesis" *Org. Lett.* **2010**, *12* (23), 5514-5517.

85. Thorn-Csanyi, E.; Narwark, O.; Peetz, R.; Strachota, A., "Diheptyloxy PV oligomers in solution: photoreactivity" *Synth. Met.* **1999**, *101* (1-3), 238.
86. Peetz, R.; Narwark, O.; Herzog, O.; Brocke, S.; Thorn-Csanyi, E., "Ring substituted PV oligomers synthesized via olefin metathesis; fluorescence properties of monodisperse products" *Synth. Met.* **2001**, *119* (1-3), 539-540.
87. Narwark, O.; Meskers, S. C. J.; Peetz, R.; Thorn-Csanyi, E.; Bassler, H., "Spectroscopic characterization of p-phenylene vinylene (PV) oligomers. Part I: A homologous series of 2,5-diheptyloxy substituted PV-oligomers" *Chem. Phys.* **2003**, *294* (1), 1-15.
88. Peetz, R.; Strachota, A.; Thorn-Csanyi, E., "Homologous series of 2,5-diheptyloxy-p-phenylene vinylene (DHepO-PV) oligomers with vinyl or 1-butenyl end groups: Synthesis, isolation, and microstructure" *Macromol. Chem. Phys.* **2003**, *204* (11), 1439-1450.
89. Guerlin, A.; Dumur, F.; Dumas, E.; Miomandre, F.; Wantz, G.; Mayer, C. R., "Tunable Optical Properties of Chromophores Derived from Oligo(p-phenylene vinylene)" *Org. Lett.* **2010**, *12* (10), 2382-2385.
90. Abbel, R.; Grenier, C.; Pouderoijen, M. J.; Stouwdam, J. W.; Leclere, P. E. L. G.; Sijbesma, R. P.; Meijer, E. W.; Schenning, A. P. H. J., "White-Light Emitting Hydrogen-Bonded Supramolecular Copolymers Based on pi-Conjugated Oligomers" *J. Am. Chem. Soc.* **2009**, *131* (2), 833-843.
91. Chatterjee, A. K.; Choi, T.-L.; Sanders, D. P.; Grubbs, R. H., "A General Model for Selectivity in Olefin Cross Metathesis" *J. Am. Chem. Soc.* **2003**, *125* (37), 11360-11370.

92. McKean, D. R.; Parrinello, G.; Renaldo, A. F.; Stille, J. K., "Synthesis of functionalized styrenes via palladium-catalyzed coupling of aryl bromides with vinyl tin reagents" *J. Org. Chem.* **1987**, *52* (3), 422-4.
93. Vundyala, N.; Sun, C.; Sidime, F.; Shi, W.; L'Amoreaux, W.; Raja, K.; Peetz, R. M., "Biotin-functional oligo(p-phenylene vinylene)s synthesized using click chemistry" *Tetrahedron Lett.* **2008**, *49* (45), 6386-6389.
94. Demel, S.; Slugovc, C.; Stelzer, F.; Fodor-Csorba, K.; Galli, G., "Alternating diene metathesis polycondensation (ALTMET) - a versatile tool for the preparation of perfectly alternating AB copolymers" *Macromol. Rapid Commun.* **2003**, *24* (10), 636-641.
95. Choi, T.-L.; Rutenberg, I. M.; Grubbs, R. H., "Synthesis of A,B-alternating copolymers by ring-opening-insertion-metathesis polymerization" *Angew. Chem., Int. Ed.* **2002**, *41* (20), 3839-3841.
96. Cho, M. J.; Choi, D. H.; Sullivan, P. A.; Akelaitis, A. J. P.; Dalton, L. R., "Recent progress in second-order nonlinear optical polymers and dendrimers" *Prog. Polym. Sci.* **2008**, *33* (11), 1013-1058.
97. Ritter, T.; Hejl, A.; Wenzel, A. G.; Funk, T. W.; Grubbs, R. H., "A Standard System of Characterization for Olefin Metathesis Catalysts" *Organometallics* **2006**, *25* (24), 5740-5745.
98. Chung, T. C., "Synthesis of polyalcohols via Ziegler-Natta polymerization" *Macromolecules* **1988**, *21* (4), 865-9.
99. Akcelrud, L., "Electroluminescent polymers" *Prog. Polym. Sci.* **2003**, *28* (6), 875-962.

100. Pasco, S. T.; Lahti, P. M.; Karasz, F. E., "Synthesis of Substituted Poly(p-phenylenevinylene) Copolymers by the Heck Method for Luminescence Studies" *Macromolecules* **1999**, *32* (21), 6933-6937.
101. Yang, Z.; Sokolik, I.; Karasz, F. E., "A soluble blue-light-emitting polymer" *Macromolecules* **1993**, *26* (5), 1188-90.
102. Yang, Z.; Karasz, F. E.; Geise, H. J., "Intrinsically soluble copolymers with well-defined alternating substituted p-phenylenevinylene and ethylene oxide blocks" *Macromolecules* **1993**, *26* (24), 6570-5.
103. Watson, M. D.; Wagener, K. B., "Functionalized Polyethylene via Acyclic Diene Metathesis Polymerization: Effect of Precise Placement of Functional Groups" *Macromolecules* **2000**, *33* (24), 8963-8970.
104. Van Severen, I.; Motmans, F.; Lutsen, L.; Cleij, T. J.; Vanderzande, D., "Poly(p-phenylene vinylene) derivatives with ester- and carboxy-functionalized substituents: a versatile platform towards polar functionalized conjugated polymers" *Polymer* **2005**, *46* (15), 5466-5475.
105. Thiem, H.; Jandke, M.; Hanft, D.; Strohhriegl, P., "Synthesis and orientation of fluorene containing reactive mesogens" *Macromol. Chem. Phys.* **2006**, *207* (4), 370-381.
106. Bongers, K. M.; van den Berg, R. J. B. H. N.; Heitman, L. H.; Ijzerman, A. P.; Oosterom, J.; Timmers, C. M.; Overkleeft, H. S.; van der Marel, G. A., "Synthesis and evaluation of homo-bivalent GnRHR ligands" *Bioorganic & Medicinal Chemistry* **2007**, *15* (14), 4841-4856.